



# 3D FEM Analysis of the Effects of a Ship Collision on a Wind Turbine Support Structure

Definitief Eindrapport (DP1 to DP5)

Client: Rijkswaterstaat Water, Verkeer en Leefomgeving  
Client no.: 31196090  
Document no.: INFR240476-R203-DP5  
Revision: 1  
Date: 21 March 2025

iv-Infra b.v.

Engineering Company with a Passion for Technology



Client: Rijkswaterstaat Water, Verkeer en Leefomgeving  
Project N° client: 31196090  
Project: 3D FEM gevolgschade schip-turbine  
Title document: 3D FEM Analysis of the Effects of a Ship Collision on a Wind Turbine Support Structure

Subtitle document: Final report (DP1 to DP5)  
Revision: 1  
Date: 21 March 2025

Revision	Date	Status	Author(s)	Checked	Approved
0	07-03-2025	Final	GVA; NBU	YYA	WLA
1	21-03-2025	Final	GVA; NBU	YYA	WLA



## Management samenvatting

Het project '3D FEM Analysis of the Effects of a Ship Collision on a Wind Turbine Support Structure' heeft als doel bij te dragen aan de bredere doelstellingen van het Monitorings- en Onderzoeksprogramma Scheepvaartveiligheid Wind op Zee (MOSWOZ) en de maritieme veiligheid te verbeteren naarmate windparken op zee in de Noordzee uitbreiden. In dit project (fase 3) wordt onderzoek gedaan waarbij gebruik wordt gemaakt van realistische modellen van bestaande schepen en windturbines. Het is een vervolg op de eerdere studie, 'Investigation of ship impact against wind turbine foundation in the Dutch part of the North Sea' (fase 1 en 2)', waarbij enkel het bezwijkmechanisme van de windturbine na aanvaring is onderzocht met het Finite Element (FE)-model, zonder gebruik te maken van scheepsmodellen.

De belangrijkste doelstellingen van deze studie, zoals hieronder uiteengezet in de projectscope, zijn:

- **Visualiseren van schade aan kritieke scheepscomponenten:** Evalueren van de structurele impact op de scheepsromp, brandstoftanks en laadruimten na een aanvaring met een windturbine.
- **Categoriseren van scheepsschade:** Classificeren van de omvang van de schade aan de hand van gedefinieerde criteria en het voorspellen van de gevolgen, waaronder risico's voor de structurele integriteit, milieueffecten en de veiligheid van bemanning en passagiers.
- **Vergelijkende analyse:** Vergelijken van 3D FEM-resultaten met eerdere 2D-modellen en soortgelijke scenario's uit fase 2 om de uitkomsten te verifiëren en de betrouwbaarheid van het model te verbeteren.

De volgende scheepstypen worden in deze studie onderzocht: een chemicaliëntanker, een passagiersschip en een containerschip. De simulaties zijn gebaseerd op de volgende informatie.

Nr.	Scheepstype	Romp	GT [-]	DT [ton]	Varend (impact boeg)		Driftend (impact romp)	
					knopen	knopen	knopen	knopen
1	Chemicaliëntanker	Dubbel	10.000	21.000	10	20	2	4
2	Passagiersschip	Enkel	100.000	42.700	20	30	2	4
3	Containerschip	dubbel	200.000	223.000	10	20	2	4

Voor elk scheepstype zijn twee modellen opgesteld: één voor het voorste gedeelte van het schip (boeg) en één voor het midden van het schip (scheepsromp). Om dit te bereiken zijn ontwerpberekeningen voor de verschillende scheepstypen opgesteld. De FE-modellen voor de schepen en de windturbine zijn opgebouwd met Ansys LS-DYNA, waarin materiaaleigenschappen, randvoorwaarden en belastingen zijn meegenomen. Vanwege de rekentijd (en de beperkte bijdrage aan het eindresultaat) is het niet haalbaar om het volledige schip te modelleren. Daarom wordt van elk scheepstype alleen een gedeelte gemodelleerd wat zich beperkt tot het gebied rond de impactzone. De niet-gemodelleerde delen worden gesimuleerd door het toevoegen van een extra massa, een zogenoemde 'added point mass'. Deze puntmassa is verbonden met de buitenrand van het gemodelleerde gedeelte, waardoor de krachtswerking en het gedrag van het gehele schip juist wordt meegenomen in de modellering.



De constructie van de windturbine bestaat uit de fundatie, de substructuur en de toren. De fundatie zelf bestaat uit twee delen: de bodem en de monopile. De interactie tussen de monopile en de bodem wordt gemodelleerd met radiale grondveren. Deze veren worden gedefinieerd aan de hand van p-y-curves, die niet-lineaire stijfheidswaarden bieden aan de hand van niet-lineaire p-y krommen. Bij toepassing van een dynamische amplificatiefactor van 2,5 houden de veren rekening met de verhoogde stijfheid onder dynamische belasting.

In totaal zijn er 12 simulaties uitgevoerd, waarbij 3 verschillende scheepstypen zijn geanalyseerd met 2 verschillende snelheden, zowel voor de varende als driftende scenario's. Het FEM-model en de simulatiemethode zijn zowel gevalideerd als geverifieerd. De resultaten van de frontale aanvaring laten zien dat er grote schade aan de boeg ontstaat bij het voorste deel van de chemicaliëntanker en het passagiersschip. Deze schade beperkt zich echter tot het gebied voor het aanvaringsschot, waardoor de structurele integriteit van het aanvaringsschot behouden blijft en het drijfvermogen van het schip gewaarborgd is. Daarnaast reikt de schade niet tot compartimenten met lading of brandstof, waardoor er geen verlies van lading of lekkage ontstaat. De uitgevoerde analyses tonen echter een kritisch risico voor de windturbineconstructie aan. Door de impact en resulterende krachten is de kans groot dat de constructie bezwijkt in de richting van het schip. Dit wordt veroorzaakt door twee belangrijke factoren: het bezwijken van de constructie van de windturbine op één of meerdere locaties en het feit dat het schip na de aanvaring blijft doorvaren omdat het niet volledig wordt afgeremd door de impact. Deze bevindingen benadrukken dat, hoewel de externe structurele schade aan de schepen aanzienlijk kan zijn, dit niet noodzakelijk leidt tot aanzienlijke gevolgen voor de operationele veiligheid van het schip in deze aanvaarscenario's.

De resultaten van de simulaties met driftende schepen tonen aanzienlijke schade aan de scheepsromp voor alle geanalyseerde scheepstypen. Echter bevindt deze schade zich slechts enkel rond de impactzone en beperkt de schade zich tot de ballasttanks. Deze schade heeft geen invloed op de algehele stabiliteit of drijfvermogen van het schip. Daarnaast vindt er geen verlies van lading of lekkage plaats, omdat de beschadigde gebieden zich buiten de ladingcompartimenten bevinden. De resultaten van de analyses laten zien dat de schade aan de scheepsromp zich beperkt tot enkel plastische vervorming en deuken, waarbij geen scheuren in de romp ontstaan. Verder bezwijkt bij veel analyses de fundatie van de windturbine. Dit leidt tot het bezwijken van de windturbine welke daarbij van het schip af valt en niet op het schip terecht komt, waardoor verdere schade aan het vaartuig wordt voorkomen.

Naast de twaalf aanvaringsanalyses zijn er twee extra simulaties uitgevoerd om de schade te voorspellen die ontstaat wanneer de windturbine bezwijkt en de nacelle (turbine aan de bovenzijde van de toren) op het passagiersschip valt. De valsnelheid van de nacelle in verticale richting (Z-richting) is hierbij afgeleid van de uitgevoerde simulaties waarbij de windturbine instort en richting het schip valt.

De resultaten laten zien dat een verticaal vallende nacelle met een beginsnelheid van 31,55 meter per seconde aanzienlijke schade aan de scheepsconstructie veroorzaakt. Het doorboort in deze analyse zeven opeenvolgende dekken, waarbij het achtste dek aanzienlijke plastische wordt vervormd. Daarentegen toont de impactsimulatie waarbij de nacelle horizontaal valt aan dat de nacelle niet door het bovenste dek gaat, maar terugveert waarbij aanzienlijke vervormingen aan het schip ontstaat. Aan het einde van de simulatie



komt de nacelle bovenop het schip te liggen, waarmee geconcludeerd kan worden dat de horizontale impact resulteert in een andere schade dan bij een verticale impact.

Op basis van de conclusies zijn verschillende aanbevelingen opgesteld. De resultaten van dit project bieden aanvullende inzichten in de effecten van scheepsaanvaringen met windturbines en dragen bij aan een verhoogde scheepvaartveiligheid in de Noordzee.



## Management summary

The project '3D FEM Analysis of the Effects of a Ship Collision on a Wind Turbine Support Structure' aims to contribute to the broader goals of the Monitorings- en Onderzoeksprogramma Scheepvaartveiligheid Wind op Zee (MOSWOZ), enhancing maritime safety as offshore wind farms expand in the North Sea. This project (phase 3) is based on realistic vessels and wind turbines and continues an earlier study 'Investigation of ship impact against wind turbine foundation in the Dutch part of the North Sea' (phase 1 and 2), which did not include the ship structure in the FE model.

The primary objectives of this study, as outlined in the project scope below, include:

- Visualizing damage to critical ship components: Evaluate the structural impact on the ship's hull, fuel tanks, and cargo spaces following a collision with a wind turbine foundation.
- Categorizing ship damage: Classify the extent of damage using defined criteria and predict associated consequences, including risks to structural integrity, environmental impact, and crew/passenger safety.
- Comparative analysis: Compare 3D FEM results with prior 2D models and similar scenarios from phase 2 to verify outcomes and enhance model reliability.

The following vessel types are considered for this study: chemical tanker, passenger vessel and a container ship. Simulations are based on the following information.

Nr.	Ship type	Hull	GT [-]	DT [tonne]	Sailing (impact bow)		Drifting (impact hull)	
					knots	knots	knots	knots
1	Tanker	Double	10,000	21,000	10	20	2	4
2	Passenger Vessel	Single	100,000	42,700	20	30	2	4
3	Container Ship	Double	200,000	223,000	10	20	2	4

Two models have been developed for each vessel type, one for the vessel's forward section (bow) and one for the vessel's midsection (hull structure). Therefore, scantling calculations have been performed for both sections. The FE models for the vessels and monopile are constructed using Ansys LS-DYNA, incorporating material properties, boundary conditions, and loadings. Due to the calculation time and the minimal contribution to the result, it is not feasible to model the entire ship. Therefore, only a section of the ship's hull structure is modeled for each ship type, specifically the area around the impact zone. The parts that are not modeled are simulated with an extra weight, a so-called 'added point mass.' This point mass is connected to the outer boundary of the modelled section so it rotates in the same way the unmodelled section would around. By placing the mass at the correct center of gravity, the ships overall mass moment of inertia (correct resistance to rotational motion around) is properly captured in the analysis.

The structure of the wind turbine consists of the foundation, substructure, and tower. The foundation itself is made up of two parts: one part is soil, and the other is the monopile. The interaction between the wind turbine monopile and the soil is modelled with radial soil springs. These springs are defined using p-y curves, which



provide non-linear stiffness values. When a dynamic amplification factor of 2.5 is applied, the springs account for the increased resistance under dynamic loading conditions.

A total of 12 simulations were conducted, involving 3 different ship types with 2 different velocities for both sailing and drifting. The FEM model and simulation method have been both validated and verified. The results of the head-on sailing impact simulations indicate that while larger areas of damage were observed on the forward sections of the chemical tanker and passenger vessel, this damage is confined to regions outside the critical collision bulkhead. As a result, the structural integrity of the collision bulkhead remains intact, ensuring that the buoyancy of the ship is not compromised. Additionally, no cargo loss or spillage was recorded during these scenarios, highlighting that the damage does not extend to compartments containing cargo or fuel. However, the analysis also indicates a critical risk associated with the wind turbine foundation. Due to the impact velocity and resulting forces, the turbine is likely to collapse toward the ship. This outcome is driven by two key factors: the buckling of the turbine support structure at one or more locations and the fact that the ship continues moving forward after the collision, as it is not halted by the impact. These findings emphasize that while external structural damage to the ships can be significant, it does not necessarily translate to significant outcomes for the ship's operational safety in these collision scenarios.

The drifting impact scenarios reveal significant areas of hull damage for all ship types analysed. However, only localized areas of material failure were observed. This limited material failure primarily affects the ballast tanks, which, despite being compromised, do not impact the ship's overall stability or buoyancy. Additionally, no cargo loss or spillage occurred as the areas of material failure are confined to non-cargo compartments. The results indicate that only plastic deformation and dents were observed on the ship's hull structure, with no cracks present. Furthermore, most of the results indicate buckling failure of the turbine support structure within the soil. This failure causes the turbine support structure to collapse and fall away from the ship, preventing additional damage to the vessel.

Along with the twelve ship collision analyses, two additional simulations were conducted to assess the damage resulting from the failure of the foundation tower and the subsequent landing of the nacelle on the passenger vessel. In the sailing scenarios where a support structure collapses towards the ship, the velocity of the falling nacelle is monitored along its vertical position (Z-direction).

The results indicate that a vertically falling nacelle with an initial velocity of 31.55 meters per second can penetrate through multiple decks, causing extensive damage to the ship's structure. Specifically, the turbine was observed to penetrate seven consecutive decks, with the eighth deck undergoing significant plastic deformation. In contrast, the horizontal impact simulation revealed that the nacelle did not pass through the upper deck, instead causing substantial deformation and rebound. By the end of the simulation, the turbine's nacelle settled on top of the ship, indicating that horizontal impacts result in different types of structural damage compared to vertical impacts.

Based on the conclusions several recommendations are described. The results of this project offer additional insights into the effects of ship collisions with wind turbines and contribute to enhancing shipping safety in the North Sea.



## Table of contents

<b>1</b>	<b>Introduction</b>	<b>11</b>
1.1.	Project introduction	11
1.2.	Scope and objectives	12
1.3.	Report overview	13
<b>2</b>	<b>References</b>	<b>14</b>
2.1.	Documents	14
2.2.	Design standards and guidelines	14
<b>3</b>	<b>Abbreviations and definitions</b>	<b>15</b>
3.1.	Abbreviations	15
3.2.	Units of model	15
<b>4</b>	<b>Ship design Approach (DP1)</b>	<b>16</b>
4.1.	General Approach	16
4.2.	Midship 3D Models	17
4.2.1.	Chemical Tanker	17
4.2.2.	Container Ship	18
4.2.3.	Passenger Vessel	19
4.3.	Fore End 3D Models	23
<b>5</b>	<b>Methodology FEM modelling (DP2 &amp; DP3)</b>	<b>25</b>
5.1.	Applied software	25
5.2.	Steel material model	26
5.2.1.	Material properties	27
5.2.2.	Strain rate effects	28
5.2.3.	Stress-strain curves used in the models	29
5.2.4.	Mesh	30
5.2.5.	Element type and formulation	30
5.2.6.	Constructive components	31
5.3.	Water levels	33
5.4.	Added water mass (ship and foundation)	33
5.4.1.	Ship	33
5.4.2.	Monopile above seabed	33
5.5.	Ship	34
5.5.1.	Chemical Tanker	34
5.5.2.	Container Ship	39
5.5.3.	Passenger Vessel	44
5.5.4.	Boundary conditions	49





5.5.5.	Load conditions static prestressed	49
5.5.6.	Excluded loads on the ship	50
<b>5.6.</b>	<b>Support structure (turbine)</b>	<b>51</b>
5.6.1.	Boundary conditions	54
5.6.2.	Load conditions static prestressed	55
5.6.3.	Excluded loads on the support structure	56
5.6.4.	Soil-structure interaction	56
<b>5.7.</b>	<b>Wind turbine</b>	<b>58</b>
<b>5.8.</b>	<b>Contact between ship and foundation</b>	<b>61</b>
<b>5.9.</b>	<b>Solver setting</b>	<b>61</b>
5.9.1.	Mass scaling	61
5.9.2.	Energy balance	61
<b>5.10.</b>	<b>Model validation and verification</b>	<b>62</b>
<b>6</b>	<b>Simulations</b>	<b>63</b>
<b>6.1.</b>	<b>Ship collision simulations</b>	<b>63</b>
6.1.1.	Sailing	64
6.1.2.	Drifting	66
6.1.3.	Turbine point mass location	67
6.1.4.	Project connections and mesh assemblies	68
6.1.5.	Initial stress and deformation	68
<b>6.2.</b>	<b>Nacelle dropping simulation</b>	<b>69</b>
<b>7</b>	<b>Summary of simulation results (DP4)</b>	<b>71</b>
<b>7.1.</b>	<b>Results Ship Collision</b>	<b>71</b>
7.1.1.	Results Chemical Tanker	72
7.1.2.	Results Container Ship	76
7.1.3.	Results Passenger Vessel	80
7.1.4.	Ship damage results summary	84
7.1.5.	Foundation soil-interaction results summary	85
7.1.6.	General results summary	86
7.1.7.	Comparison of different ship types	87
7.1.8.	Comparison with previous study	88
<b>7.2.</b>	<b>Results nacelle Dropping</b>	<b>90</b>
7.2.1.	Vertical Impact	91
7.2.2.	Horizontal Impact	92
<b>8</b>	<b>Conclusions and recommendations (DP5)</b>	<b>93</b>
<b>8.1.</b>	<b>Conclusion of the ship collisions</b>	<b>93</b>
8.1.1.	Sailing Collision Scenario – Chemical Tanker	94
8.1.2.	Drifting Collision Scenario – Chemical Tanker	94
8.1.3.	Sailing Collision Scenario – Container Ship	94
8.1.4.	Drifting Collision Scenario – Container Ship	95



8.1.5.	Sailing Collision Scenario – Passenger Vessel	95
8.1.6.	Drifting Collision Scenario – Passenger Vessel	95
8.1.7.	Comparison between the ships results	96
8.1.8.	Turbine support structure foundation soil interaction	96
<b>8.2.</b>	<b>Conclusion for the nacelle impact</b>	<b>96</b>
<b>8.3.</b>	<b>Recommendations</b>	<b>97</b>
8.3.1.	Soil modelling	97
8.3.2.	Ship collisions	97
8.3.3.	Nacelle collision	98
<b>APPENDICES</b>		<b>99</b>
<b>A.</b>	<b>R101-DP1 Chemical tanker – Scantling calculation report</b>	<b>99</b>
<b>B.</b>	<b>R102-DP1 Container ship – Scantling calculation report</b>	<b>100</b>
<b>C.</b>	<b>R103-DP1 Cruise ship – Scantling calculation report</b>	<b>101</b>
<b>D.</b>	<b>R104-DP2.3 Memo Steel material model</b>	<b>102</b>
<b>E.</b>	<b>R105-DP2.3 Memo Soil Material Model</b>	<b>103</b>
<b>F.</b>	<b>R106-DP2.3 Memo FE Modelling Approach</b>	<b>104</b>
<b>G.</b>	<b>Drawings Ship’s types</b>	<b>105</b>
G.1.	Chemical tanker	105
G.2.	Container Ship	106
G.3.	Passenger Vessel	107
<b>H.</b>	<b>FEM support structure modal validation</b>	<b>108</b>
<b>I.</b>	<b>FEM Model validation and verification</b>	<b>115</b>
I.1.	Verification model with rigid tower foundation	115
I.2.	Verification model with rigid bow of chemical tanker	120
I.3.	Full mid section vs half midsection validation	128
<b>J.</b>	<b>FEM Model Input and Output</b>	<b>139</b>
J.1.	Results Ship Collision	139
J.2.	Results Turbine dropping	246
<b>K.</b>	<b>Soil spring results</b>	<b>263</b>
K.1.	Chemical tanker	264
K.2.	Container Ship	269
K.3.	Passenger Vessel	273
K.4.	Conclusion and summary	278
<b>L.</b>	<b>Declaration validation team (TNO)</b>	<b>279</b>



# 1 Introduction

---

## 1.1. Project introduction

Offshore wind farms are rapidly expanding in the North Sea. This growth, combined with high maritime traffic in the region, has created increasingly crowded conditions, see *ref. [1]*. As the number of wind turbines and associated infrastructure increases, ensuring the safety of vessels navigating these busy waters and maintaining the structural integrity of the wind farms has become a critical concern, see *ref. [2]*.

This study examines the damage resulting from a collision between a ship and a wind turbine, a scenario that recent events have proven to be realistic. On December 6, 2024, the ship *Valday* drifted off the Dutch coast, highlighting the potential dangers once again. During the stabilization efforts, three crew members aboard the assisting tugs were injured. More recently, on January 12, 2025, the oil tanker *Eventin* also went adrift in the Baltic Sea near the German coast.

By assessing the potential damage from ship-wind turbine collisions, this report provides valuable insights for stakeholders in the maritime and energy sectors, including ship operators and wind farm developers. It also identifies the need for further research to refine collision models and improve mitigation strategies, ensuring the safe operation of both ships and wind turbines in these complex environments. The results aim to contribute to the broader goals of the Monitorings- en Onderzoeksprogramma Scheepvaartveiligheid Wind op Zee (MOSWOZ) executed by Rijkswaterstaat, enhancing maritime safety as offshore wind farms expand in the North Sea.

This research is conducted in multiple phases. This report (Phase 3) builds on the previous study, 'Investigation of Ship Impact Against Wind Turbine Foundation in the Dutch Part of the North Sea' (*ref. [4 & 5]*), which covered Phases 1 and 2. In that study, ship structures were not included in the FE model, whereas they are incorporated in this phase.

The document '3D FEM Analysis to Determine the Effects of a Ship Collision Against a Wind Turbine Monopile Foundation' (*ref. [6]*) highlights that running simulations with detailed ship models will enhance the research by providing deeper insights into the impact of such collisions. Additionally, it outlines the requirements for the follow-up study, specifying the necessary properties and conditions to be considered.



## 1.2. Scope and objectives

Among the extended objectives of this study, as described in the project specifications, the most important ones have been identified and prioritized to properly define the project scope and outcomes. The primary objectives of this study, as outlined in the project scope below, include:

- Visualizing damage to critical ship components: Evaluate the structural impact on the ship's hull, fuel tanks, and cargo spaces following a collision with a wind turbine foundation.
- Categorizing ship damage: Classify the extent of damage using defined criteria and predict associated consequences, including risks to structural integrity, environmental impact, and crew/passenger safety.
- Comparative analysis: Compare 3D FEM results with prior 2D models and similar scenarios from phase 2 to verify outcomes and enhance model reliability.



### 1.3. Report overview

This document includes a comprehensive analysis of various collision scenarios, assessment of ship types and sizes, and evaluation of their interactions with offshore wind turbine structures. Specifically, there are five sub-tasks for this study, which are (DP in Dutch is the abbreviation for DeelProduct, meaning sub-task):

- ship design approach (DP1)
- methodology FEM modelling (DP2 & DP3)
- summary of simulation results (DP4)
- conclusions and recommendations (DP5)

The second chapter, References, lists the primary documents, standards, and guidelines used in the study. It includes references from Rijkswaterstaat (RWS) and design standards critical to ensuring compliance with maritime and structural regulations.

The third chapter, Abbreviations and definitions, introduces key terminology, abbreviations, and units used throughout the report. This chapter ensures clarity and consistency, providing a solid foundation for understanding the technical content.

The fourth chapter, Ship design Approach (DP1), delves into the selection and modeling of the reference ships. It discusses the general approach for creating midship and fore-end 3D models of a chemical tanker, container ship, and passenger vessel, offering detailed descriptions and justifications for their inclusion.

The fifth chapter, Methodology FEM modelling (DP2 & DP3), explains the methods and tools used to build and analyze the finite element models. This includes material properties, mesh settings, boundary conditions, water levels, and the inclusion of added water mass. Separate sections detail the modeling of ships, support structures, wind turbines, and their interactions during collisions. It also describes solver settings and validation techniques to ensure accuracy and reliability.

The sixth chapter, Simulations, presents the collision scenarios studied, including ship collision simulations during sailing and drifting, and turbine collision simulations.

The seventh chapter, Summary of simulation results (DP4), compiles the findings from the simulations. It analyzes the outcomes based on different collision scenarios, including cases with no hull damage, hull damage with cargo or bunker leakage, and damage affecting accommodations.

The eighth chapter, Conclusions and recommendations (DP5), synthesizes the key insights from the study, providing conclusions and actionable recommendations. This includes design considerations for wind turbines and safety measures for ships to mitigate collision risks.

The appendices provide additional documentation and support for the main report, including detailed scantling calculation reports for the selected ships, memos on material and soil models, FEM modeling approaches, validation results, and verification reports.

## 2 References

### 2.1. Documents

Documents that are used during this study, are provided in *Table 1*.

Table 1. Reference documents

Ref.	Document	Title	Date
1.	--	Programma Noordzee 2022-2027	March 2022
2.	31132-3-MSCN-rev.1.0	WIND OP ZEE 2030: Gevolgen voor scheepvaartveiligheid en mogelijk mitigerende maatregelen	May 2019
3.	31196090 Bijlage K versie 2	Vraagspecificatie 3D FEM gevolgschade schip-turbine.pdf	May 2024
4.	Bijlage K Annex 01-01 081R030M006-Rev4	Investigation of ship impact against wind turbine foundation in Dutch NS.pdf	March 2024
5.	Bijlage K Annex 01-02 081R030M011-Rev2	Investigation of ship impact against wind turbine foundation Dutch NS.pdf	March 2024
6.	Bijlage K Annex 01-03 081R030M010-Rev5	3D FEM analysis effects ship collision against wind turbine monopile.pdf	January 2024
7.	Bijlage K Annex 01-05 081R030M010-App-A - Properties Windfarm 2 - Foundation 'WD 34.6m PD 28.75m'.xlsx	Excel file containing information and data about Wind Farm 2	-

### 2.2. Design standards and guidelines

The design standards and guidelines are provided in *Table 2*.

Table 2. Design standards and guidelines

Ref.	Document	Title	Date
8.	DNV-RP-C208	Determination of structural capacity by non-linear finite element analysis methods.	October 2022
9.	DNV-RP-C204	Structural design against accidental loads.	September 2019
10.	NEN-EN 10025-2	Hot-rolled products of structural steels – Part 2	Augustus 2019

## 3 Abbreviations and definitions

### 3.1. Abbreviations

The abbreviations used in this report are provided in *Table 3*.

Table 3. List of abbreviations

Abbreviation	Definition
CAD	Computer-aided design
DP	Deelproduct
DT	Displacement Tonnage
etc.	Et cetera
FE	Finite elements
FEM	Finite element method
GT	Gross Tonnage
LAT	Lowest Astronomical Tide
MSL	Mean Sea Level
MW	Mega Watt
ROTX	Rotation about X-axis
ROTY	Rotation about Y-axis
ROTZ	Rotation about Z-axis
SB	Starboard
Uy	Displacement in the Y-direction
Uz	Displacement in the Z-direction
vs.	versus
3D	Three-dimensional

### 3.2. Units of model

The units used in this report are provided in *Table 4*.

Table 4. Units

Parameter	Unit
Dimensions	Millimeter [mm]
Force/Weight	Newton [N]
Mass	Tonne [T]
Deformation	Millimeter [mm]
Stress	Megapascal [MPa] (1MPa = 1 N/mm <sup>2</sup> )
Energy	Megajoule [MJ]
Time	Second [s]

## 4 Ship design Approach (DP1)

### 4.1. General Approach

The information regarding each vessel type considered for this study is sourced from the Plan of Approach and is presented in *Table 5* below:

Table 5. Chosen ship types and main properties

Ship Type	Tanker	Passenger Vessel	Container Ship
GT [-]	10,000	100,000	200,000
DT [tonne]	21,000	42,700	223,000
Length [m]	135	242	379.4
Breadth [m]	23	36	59

In order to develop representative models for each vessel type, the following steps have been followed:

- Finding similar existing vessels to be used as reference for the 3D models based on the input information presented in the Plan of Approach;
- Performing scantling calculations in accordance with Bureau Veritas NR467 Rules for the Classification of Steel Ships, January 2023 edition.

All six ship models described in *Section 4.2 & 4.3* are based on real existing ships.

Scantling calculations have been conducted using the data from the Plan of Approach as input. Any missing information, such as structural layout and block coefficient, has been derived from similar existing vessels mentioned earlier. The following tools have been used for this evaluation:

- **MARS 2000** (Bureau Veritas software) to calculate the local and global strength of typical sections for the 3D models;
- **DNV Nauticus Hull spreadsheets** for determining the primary supporting members.

Two models have been developed for each vessel type, one for the vessel's fore peak and one for the vessel's mid part. Therefore, scantling calculations have been performed for both areas. Extensive information regarding the scantling calculation performed for each vessel type is presented in *Appendix A* to *Appendix C*. Information regarding the structural layout, scantling sizes and materials considered for each vessel type are presented in the same appendices.



## 4.2. Midship 3D Models

### 4.2.1. Chemical Tanker

Most of the input used for the scantling calculations has been taken from the Plan of Approach. Furthermore, real existing tankers have been used as reference for any missing input for the structural evaluation and 3D modeling. The figure below shows the structural layout used as reference for the midship 3D model. An enlarged version of *Figure 1* is included in *Appendix G.1*.

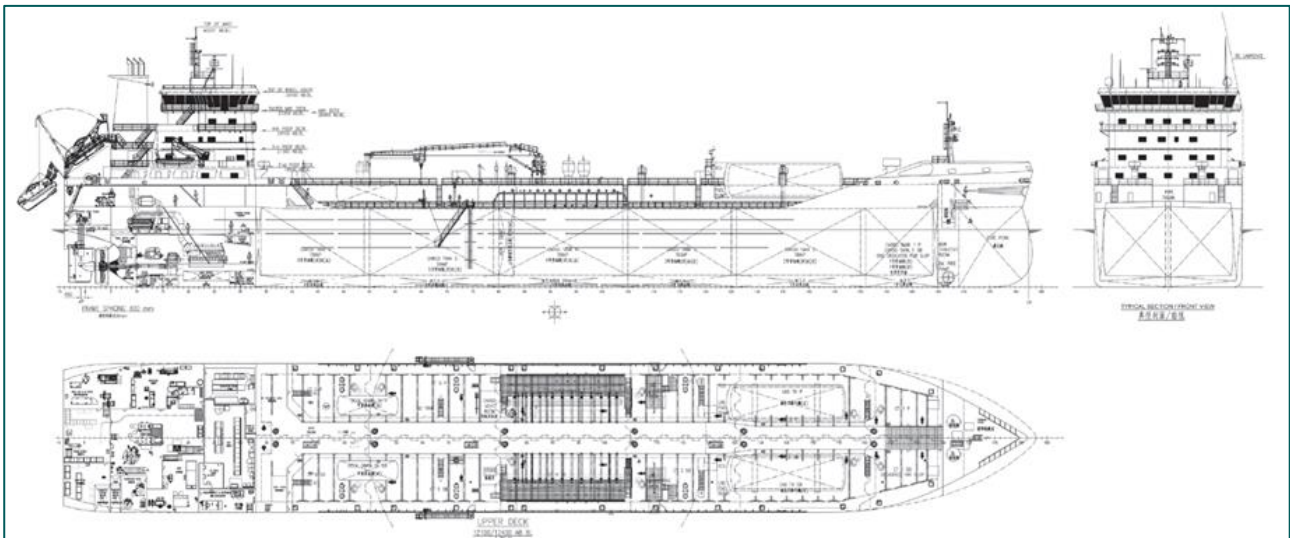


Figure 1. General arrangement plan – reference tanker

#### 4.2.2. Container Ship

Most of the input used for the scantling calculations has been taken from the Plan of Approach. Furthermore, real existing container ships have been used as reference for any missing input for the structural evaluation and 3D modeling. The figure below shows the structural layout used as reference for the midship 3D model. An enlarged version of *Figure 2* is included in *Appendix G.2*.

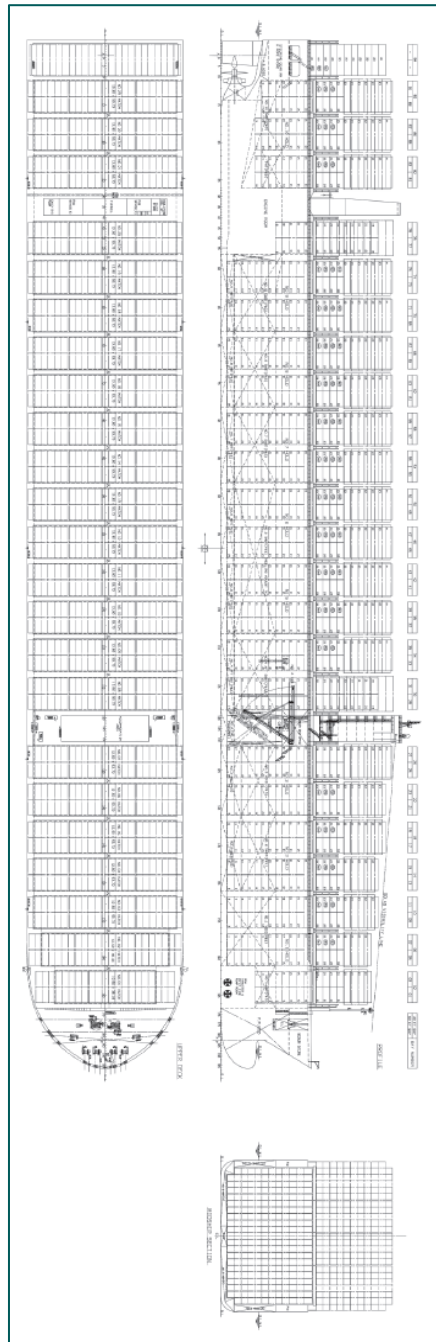


Figure 2. General arrangement plan – reference container ship

#### 4.2.3. Passenger Vessel

Most of the input used for the scantling calculations has been taken from the Plan of Approach. Furthermore, real existing passenger vessels have been used as reference for any missing input for the structural evaluation and 3D modelling. *Figure 3 & 4* below shows the structural layout used as reference for the midship 3D model. An enlarged version of *Figure 3* is included in Appendix G.3.

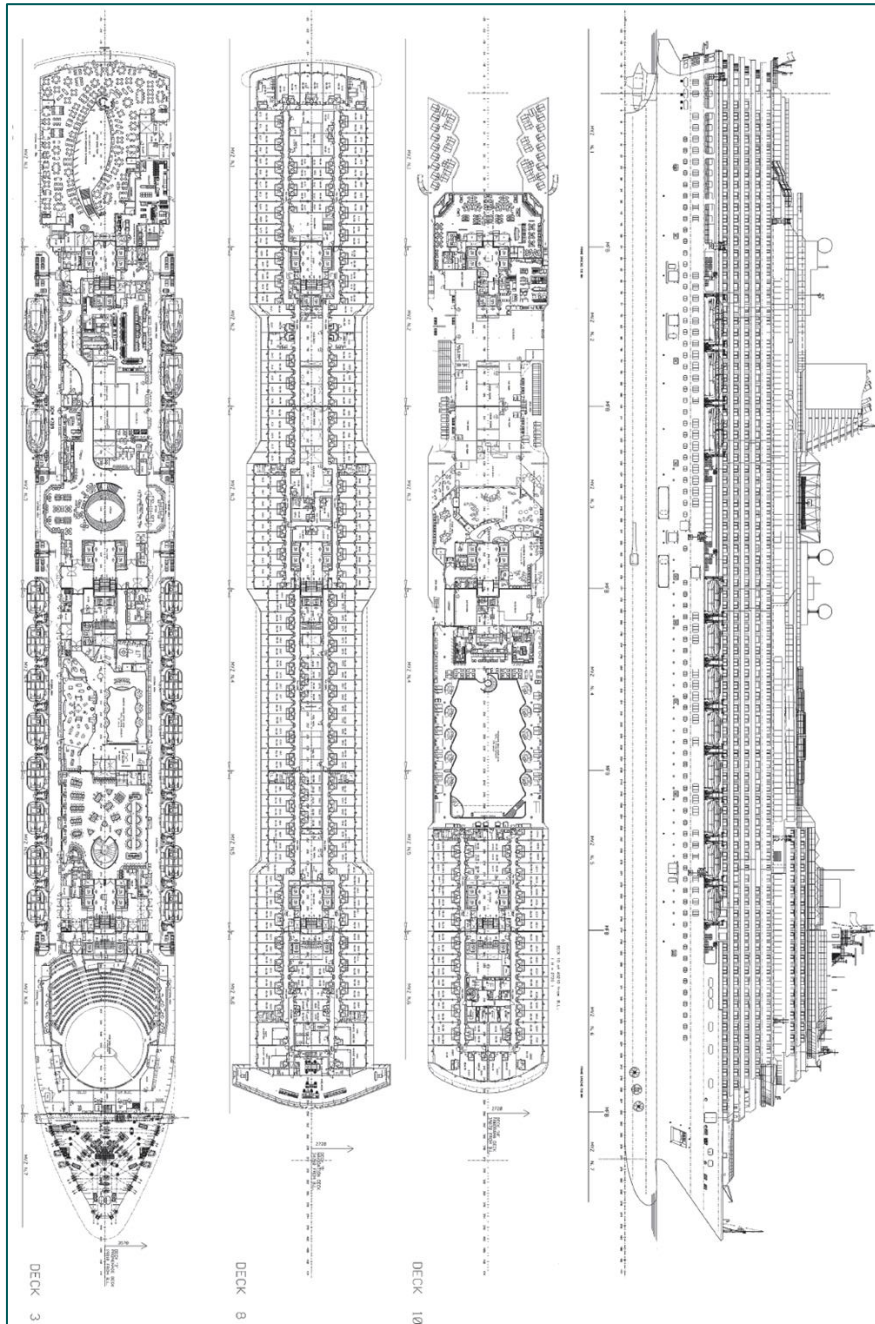


Figure 3. General arrangement plan – reference passenger vessel

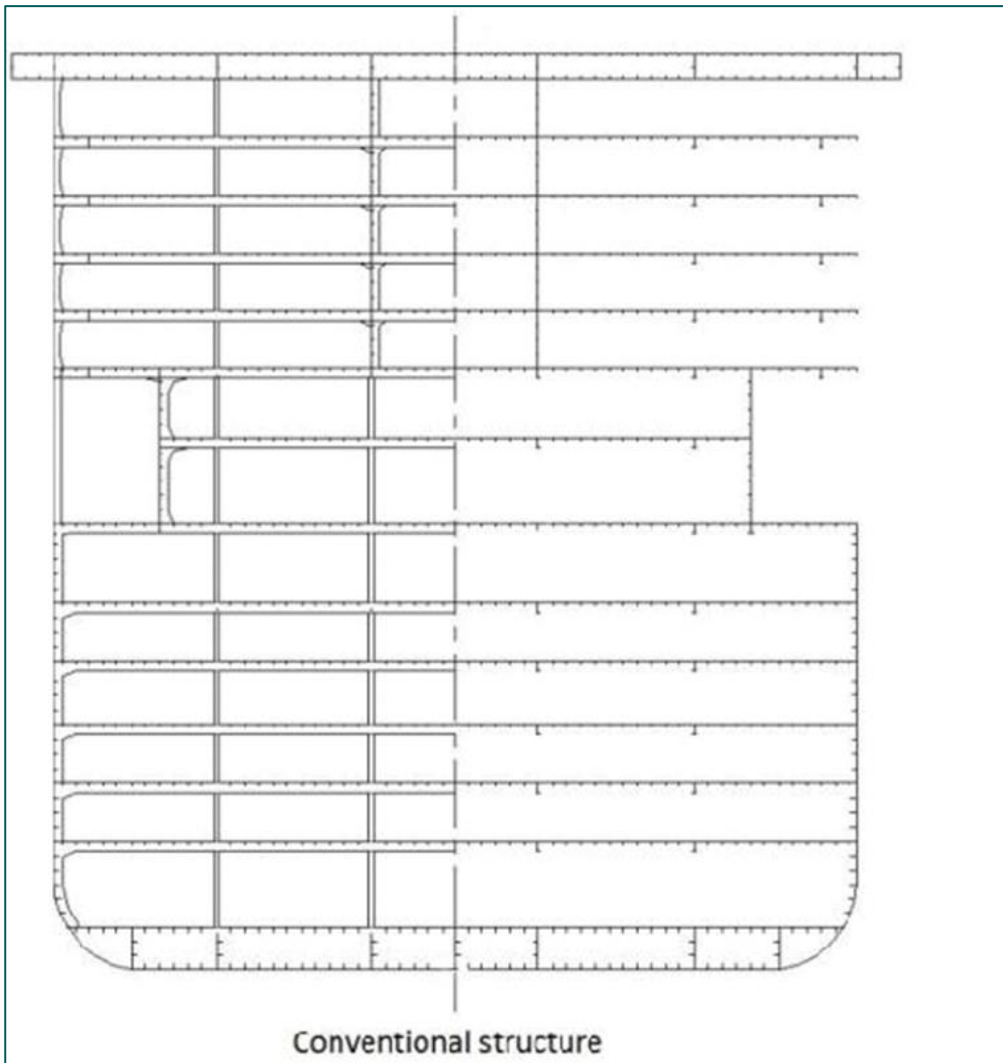


Figure 4. Typical structural layout – passenger vessel

The considered mid section for each ship type is shown in the *Figure 5, 6 & 7* below.

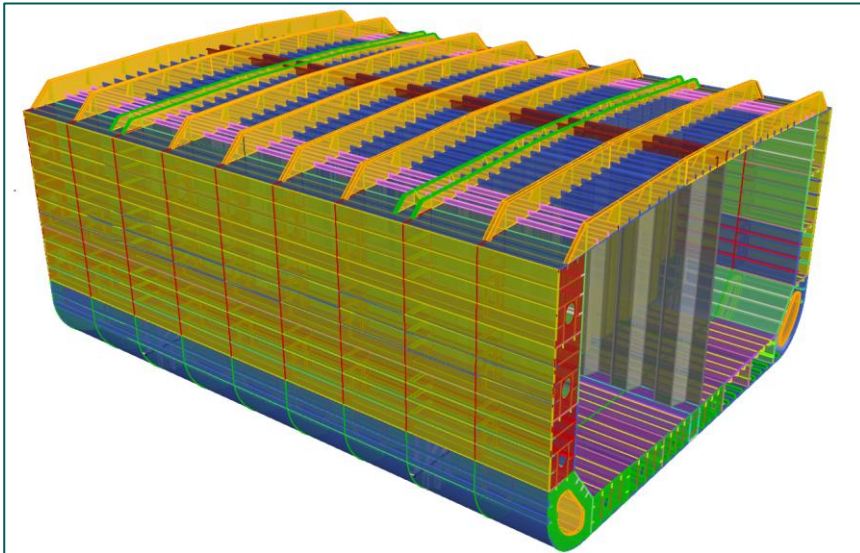


Figure 5. Chemical tanker – Mid section

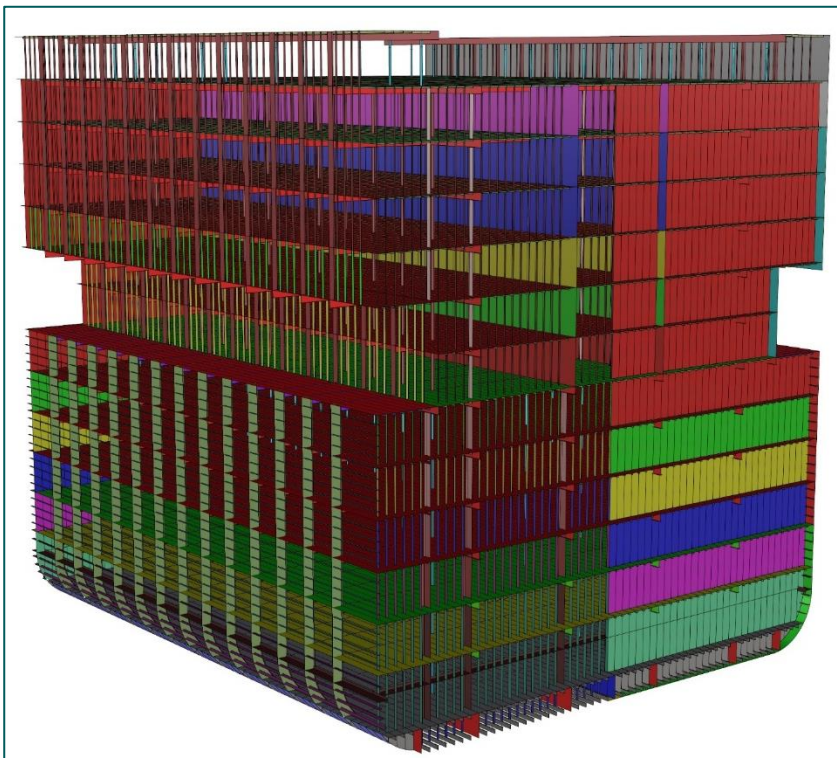


Figure 6. Passenger vessel – Mid section

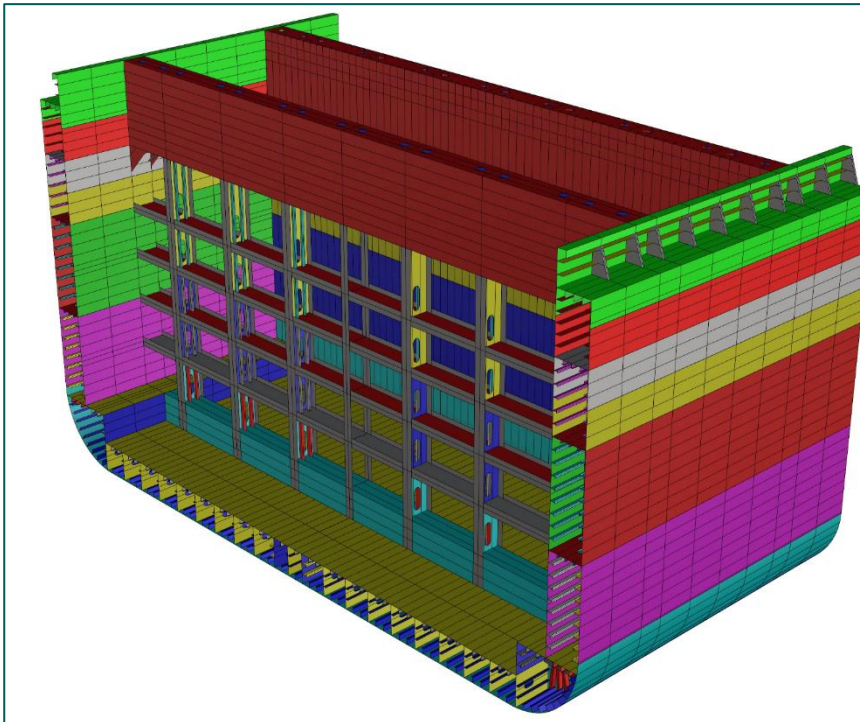


Figure 7. Container ship – Mid section

### 4.3. Fore End 3D Models

The fore end structural layout philosophy of the assessed vessel types is considered to be similar, see *Figure 8*. The only significant difference between them is due to the overall dimensions of the vessels.

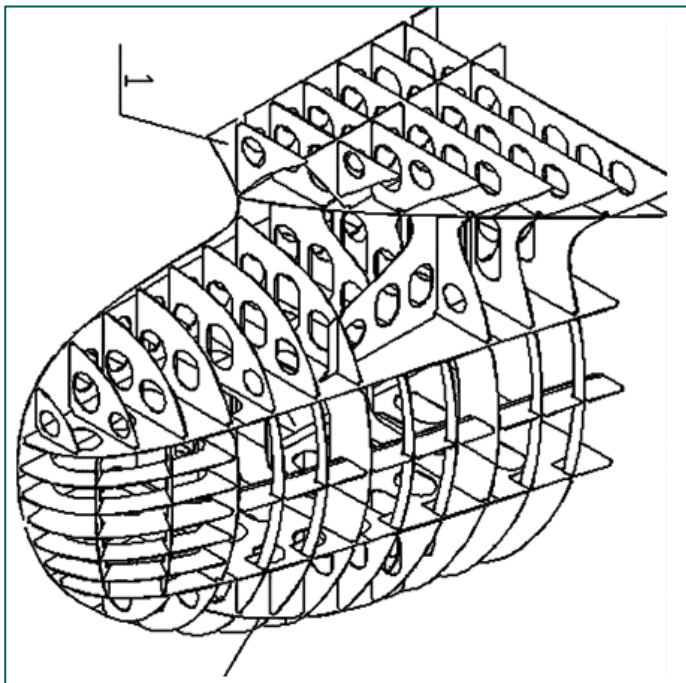


Figure 8. Fore end structural layout

In order to provide more depth to this study, it was decided to assess 3 different fore end configurations as described below:

- Bulwark extended further forward of the ship compared with the bulb – Passenger vessel;
- Bulb extended further forward of the ship compared with the bulwark - Tanker;
- Bulb and bulwark forward extremities to be at similar longitudinal location – Container ship.

In this way, the first impact of the bow end with the monopile will take place at different elevations for both the vessel and the turbine support structure. The considered fore end profile for each ship type is shown in *Figure 9, 10 & 11* below.

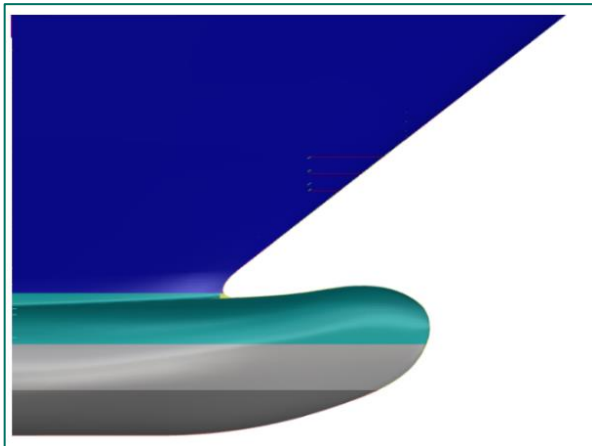


Figure 9. Passenger vessel – Fore end



Figure 10. Chemical tanker – Fore end

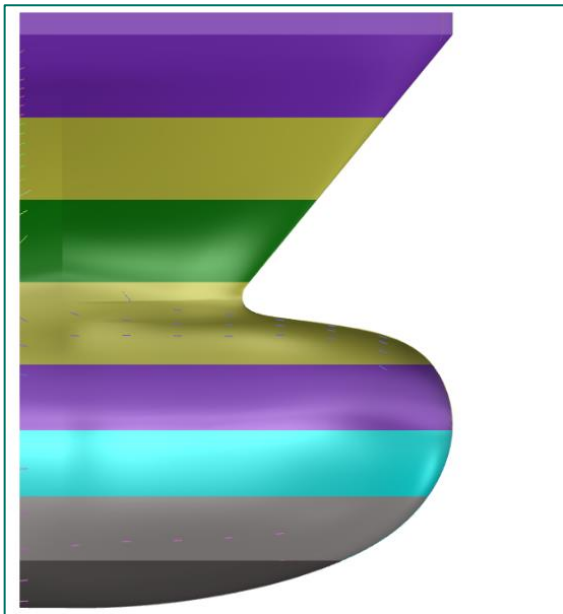


Figure 11. Container ship – Fore end



## 5 Methodology FEM modelling (DP2 & DP3)

The FE models are constructed using Ansys LS-DYNA, incorporating material properties, boundary conditions, and loadings. These models provide a robust foundation for assessing structural performance under specified loads and predicting potential areas for failure.

This chapter contains a detailed description of the FE model configured for the loading scenarios. This includes information on the geometry, material properties, boundary conditions, and applied loads.

### 5.1. Applied software

The software used during this study is presented in *Table 6*.

Table 6. Applied software

Software name	Purpose	Description	Version used
Nauticus Hull 64	Primary Supporting Members – Hand Calculation Evaluation	Nauticus Hull is a complete structural analysis package, developed by naval architects for naval architects	20.30 – January 2024
Mars2000	Scantling Calculations	to perform the assessment of 2D prescriptive requirements for over twenty different types of ships	2.9m
Rhinoceros	3D modelling	Is a 3d CAD modeling modeler for design and fabrication	8.7
Ansys Mechanical (Workbench)	Integrates various Ansys simulation tools	Ansys Mechanical is a finite element analysis (FEA) software for simulating structural, thermal, and dynamic responses of materials and assemblies.	2024 R2
LS-DYNA	Collision simulation	LS-DYNA is a nonlinear finite element analysis (FEA) software specialized in dynamic, impact, and crash simulations.	2024 R14

## 5.2. Steel material model

The ship and the wind turbine are built up with steel grade list in *Table 7*. LS-DYNA material model \*MAT\_024 (\*MAT\_PIECEWISE\_LINEAR\_PLASTICITY) is used to model the steel material, which describes the non-linear, elastic-plastic behavior of different steel grades and plate thicknesses. It uses a piecewise linear approach to define the stress-strain curve. Additionally, failure effective plastic strain is set, so that the element will be deleted from the calculation when the plastic strain reaches this value, see below *Figure 12*.

Table 7. Steel material grades used in the design of the ship and wind turbine of Wind farm 2

Steel material grade	Ship	Wind turbine
S235	×	
S355	×	×

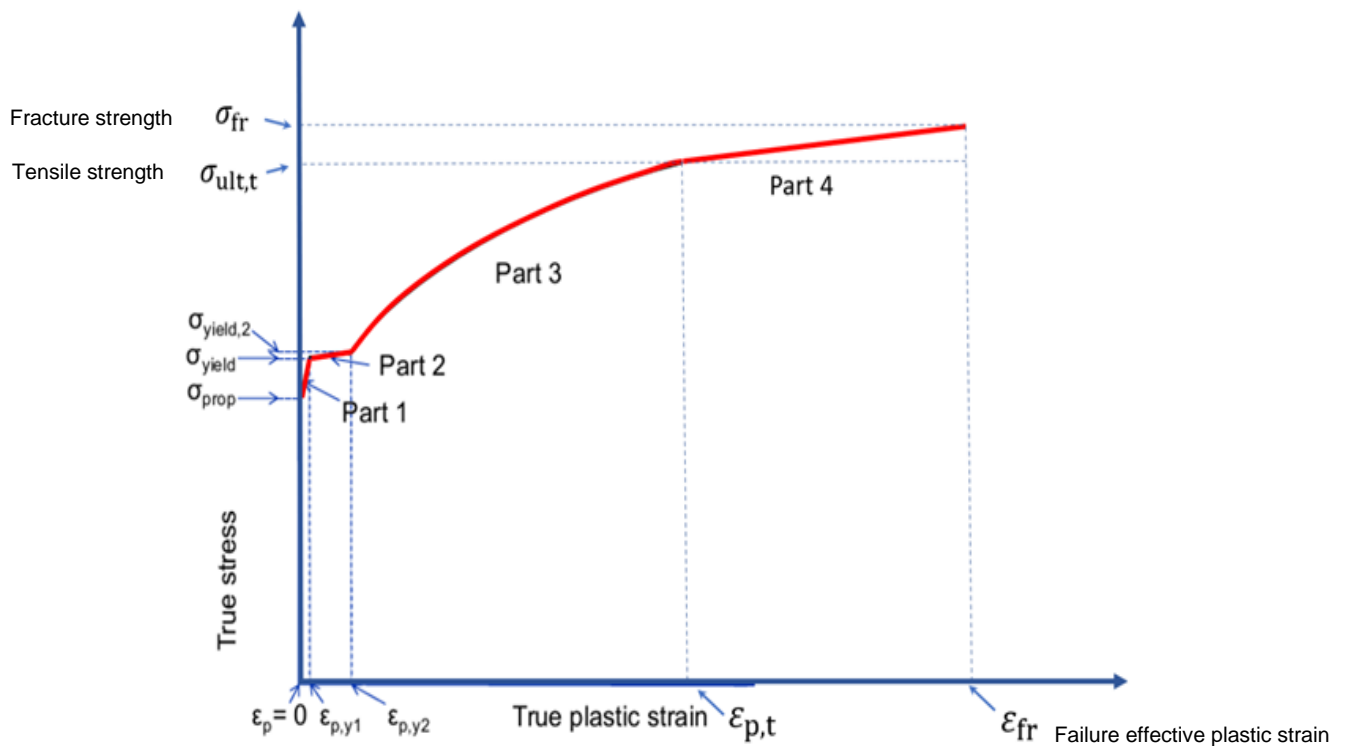


Figure 12 – Applied plastic stress-strain curve based on ref. [8] and [10] in LS-DYNA material model \*MAT\_024

### 5.2.1. Material properties

The material properties used to define the stress-strain curve in *Figure 14 & 15* for S235 and S355 with different thicknesses are given in *Table 8 & 9*. More detailed elaboration of these properties can be referred to *Appendix D*.

Table 8. Material properties of S235 steel for various thickness ranges

Parameter	Unit	Thickness $t \leq 16$ mm	Thickness $16 < t \leq 40$ mm	Thickness $40 < t \leq 63$ mm	Thickness $63 < t \leq 100$ mm
E (Young's modulus)	[MPa]	210,000	210,000	210,000	210,000
$\sigma_{prop}$ (Proportional limit)	[MPa]	211.7	202.7	193.7	193.7
$\epsilon_{prop}$	[-]	0.00101	0.00097	0.00092	0.00092
$\sigma_{yield}$ (Yield point)	[MPa]	236.2	226.1	216.1	216.1
$\epsilon_{p\_y1}$	[-]	0.004	0.004	0.004	0.004
$\sigma_{yield,2}$ (Yield point 2)	[MPa]	243.4	233.2	223	223
$\epsilon_{p\_y2}$	[-]	0.020	0.020	0.020	0.020
$\sigma_{ult,t}$ (Ultimate tensile strength)	[MPa]	360	359	358	358
$\epsilon_{p,t}$	[-]	0.11779	0.11783	0.11788	0.11788
$\sigma_{fr}$ (Fracture strength)	[MPa]	362.3	361.0	360.0	360.0
$\epsilon_{fr}$	[-]	0.23	0.23	0.23	0.23
$\epsilon_{fail}$ (Failure effective plastic strain, $= \epsilon_{fr} - \epsilon_{prop}$ )	[-]	0.22899	0.22903	0.22908	0.22908
K (parameter used in curve part 3)	[MPa]	520	520	520	520
n (parameter used in curve part 3)	[-]	0.166	0.166	0.166	0.166
Tang. modulus (parameter used in curve part 4)	[MPa]	21	21	21	21

Table 9. Material properties of S355 steel for various thickness ranges

Parameter	Unit	Thickness $t \leq 16$ mm	Thickness $16 < t \leq 40$ mm	Thickness $40 < t \leq 63$ mm	Thickness $63 < t \leq 100$ mm	Thickness $t > 100$ mm
E (Young's modulus)	[MPa]	210,000	210,000	210,000	210,000	<b>210,000</b>
$\sigma_{prop}$ (Proportional limit)	[MPa]	320	311	301.9	283.9	<b>256.2</b>
$\epsilon_{prop}$	[-]	0.00152	0.00148	0.00144	0.00135	<b>0.00122</b>
$\sigma_{yield}$ (Yield point)	[MPa]	357	346.9	336.9	316.7	<b>275</b>
$\epsilon_{p\_y1}$	[-]	0.004	0.004	0.004	0.004	<b>0.004</b>
$\sigma_{yield,2}$ (Yield point 2)	[MPa]	366.3	353.1	342.9	322.5	<b>277.3</b>
$\epsilon_{p\_y2}$	[-]	0.015	0.015	0.015	0.015	<b>0.015</b>
$\sigma_{ult,t}$ (Ultimate tensile strength)	[MPa]	470	467	456	452	<b>446</b>
$\epsilon_{p,t}$	[-]	0.064	0.06406	0.06410	0.06419	<b>0.06432</b>
$\sigma_{fr}$ (Fracture strength)	[MPa]	472.7	469.2	459.0	454.7	<b>448.7</b>
$\epsilon_{fr}$	[-]	0.19	0.19	0.19	0.19	<b>0.19</b>
$\epsilon_{fail}$ (Failure effective plastic strain, = $\epsilon_{fr} - \epsilon_{prop}$ )	[-]	0.188	0.18852	0.18856	0.18865	<b>0.18878</b>
K (parameter used in curve part 3)	[MPa]	740	740	725	725	<b>725</b>
n (parameter used in curve part 3)	[-]	0.166	0.166	0.166	0.166	<b>0.166</b>
Tang. modulus (parameter used in curve part 4)	[MPa]	21	21	21	21	<b>21</b>

### 5.2.2. Strain rate effects

Strain rate effects become significant above  $0.1 \text{ s}^{-1}$ , leading to increased strength and reduced ductility, particularly at small strains near the yield point, see *Figure 13* out of *ref. [8]*. These effects are less pronounced at higher strains. If included in simulations, it is essential to select appropriate strain rate hardening models and parameters and to document that they produce the expected response to ensure accuracy. The strain rate effect is not considered for the material in the simulations to ensure a conservative approach (*ref [8]*). By neglecting the material's enhanced strength under high strain rates, the analysis captures a worst-case scenario, providing a more cautious assessment of the structure's response.

For strain rates above  $0.1 \text{ s}^{-1}$  increased strength and reduced ductility will be experienced. In most cases it will be safe to exclude the effect.

Strain rate hardening is sensitive to the strain magnitude, and this must be accounted for when selecting the models and model parameters to simulate strain rate effects. Generally the relative increase in flow stress is less for large strains than for small strains, i.e. at the yield point. See [\[7.10\]](#).

If strain-rate hardening effects are included in a simulation, it should be documented that the selected strain-rate hardening model and corresponding parameters result in the expected response.

Figure 13. Material response without strain rate effects for a conservative assessment (Chapter 4.6.8, *ref [8]*)

### 5.2.3. Stress-strain curves used in the models

Figure 14 & 15 present the stress-strain curves for the two mentioned steel grades, with different curves representing the material behavior across various material thickness ranges.

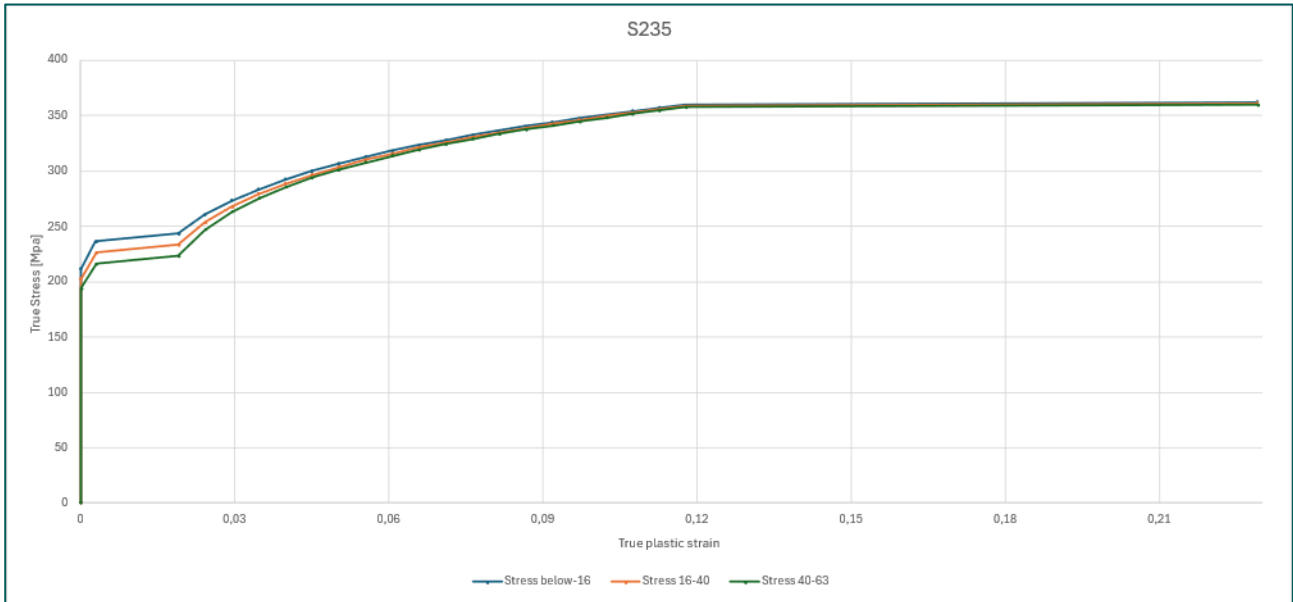


Figure 14 Stress-strain curves for steel grade S235

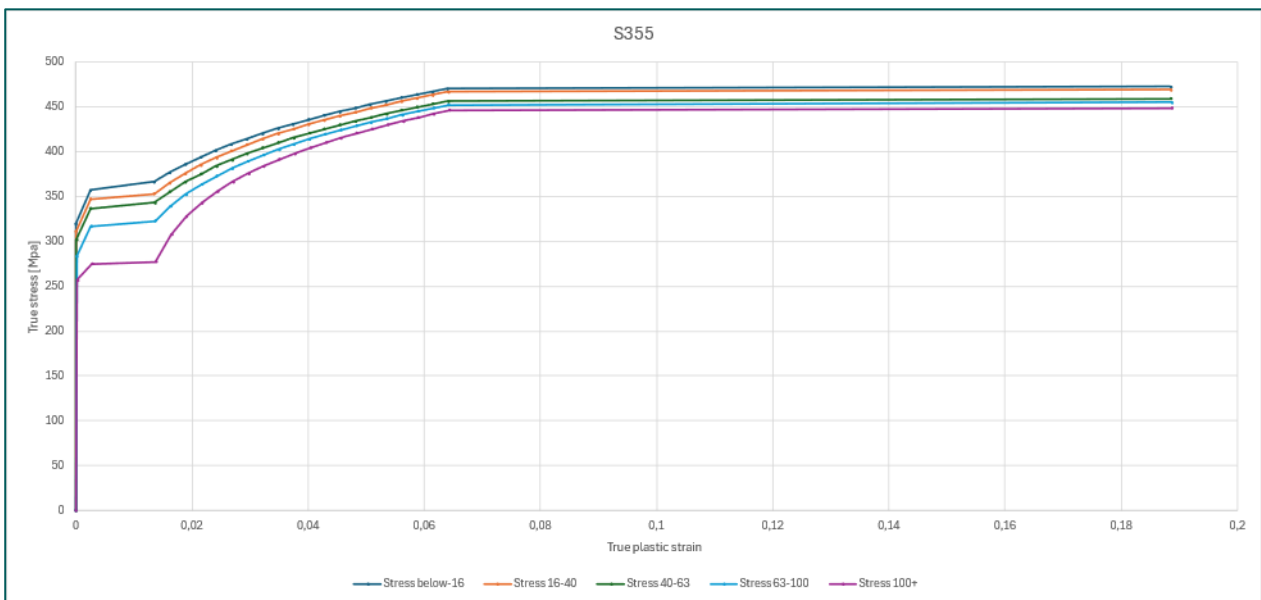


Figure 15. Stress-strain curves for steel grade S355

#### 5.2.4. Mesh

The mesh of the ship section and turbine support structure is generated using the Prime Mesh method in Ansys, ensuring seamless integration across different element types. As outlined in *Appendix F*, it is advised that for areas outside the collision zone, modelling the plate stiffeners as beam-only elements with an element size of 150 mm is an effective approach to reduce simulation computation time. Within the collision zone, using a shell-beam model with an element size of at most 100 mm and preferably six integration points is recommended for achieving accurate results.

The size of the impact zone is determined based on preliminary simulations, ensuring that the refined mesh and detailed modeling are focused on the regions experiencing the most significant deformation and stress. These initial analyses help identify the critical areas where higher resolution is necessary. By refining the mesh specifically in these zones, the simulation maintains computational efficiency while improving the accuracy of force distribution and internal energy conversion.

#### 5.2.5. Element type and formulation

In the simulation, linear shell elements are combined with beam elements to model the structural components, ensuring proper connectivity between the shell and beam elements, see *Table 10*. The plate thicknesses of the shell elements are assigned based on the Scantling reports: [*Appendix A*], [*Appendix B*] and [*Appendix C*].

Table 10. Applied elements

Nr.	Element	Description	Element size	Collision zone	Used for
1	Shell	4-nodes / 3-nodes shell element, Hughes-Liu, integration points: 6	$\leq 100$	inside	Plate and stiffeners
		4-nodes / 3-nodes shell element, Hughes-Liu, integration points: 6	$\geq 100$	outside	Plate
2	Beam	2-nodes beam element, Hughes-Liu with cross section integration	$\geq 100$	outside	Stiffeners

### 5.2.6. Constructive components

The primary structure of the ship consists of plates, T-profiles and bulb flats. The FEM model primarily employs shell elements, with exceptions for bulb flats and flanges of certain T-profiles narrower than the thresholds listed in *Table 11 & 12*, which are modelled as beam elements. This approach ensures a high-quality mesh and reduces computation time.

Component names in the mid-section align with the Scantling reports ([*Appendix A*], [*Appendix B*], [*Appendix C*]).

Table 11. Constructive components mid section

Element	Components Chemical Tanker	Components Container Ship	Components Passenger Ship
Shell	Keel plate	Keel plate	Keel plate
	Bottom	Bottom	Bottom
	Bilge	Bilge	Bilge
	Side shell	Side shell	Side shell
	Sheer strake	Upper strength deck (weather)	Upper strength deck (weather)
	Upper strength deck (weather)	Inner bottom	Upper strength deck (no weather)
	Inner bottom	Double bottom girder	Lower deck
	Double bottom girder	Inner hull	Inner bottom
	Inner hull	Double hull girder	Double bottom girder
	Double hull girder	Tank and watertight bulkhead	Miscellaneous
	Hopper well bulkhead		
	Vertical corrugation		
Beam	Bulb flats	Flanges (width < 300mm)	Bulb flats
			Flanges (width < 300mm)
			Pipes



For the forward section, the component names are also derived from the Scantling reports: [Appendix A], [Appendix B] and [Appendix C].

Table 12. Constructive components forward section

Element	Components Chemical Tanker	Components Container Ship	Components Passenger Ship	
Shell	Keel plate	Keel plate	Bottom	
	Side shell	Bottom	Side shell	
	Upper strength deck (weather)	Side shell	Upper strength deck (weather)	
	Lower deck	Sheer strake	Lower deck	
	Double bottom girder		Upper strength deck (weather)	Miscellaneous
			Lower deck	
			Inner bottom	
		Miscellaneous		
Beam	Bulb flats	Pipes	Bulb flats	
		Flanges (width < 200mm)	Flanges (width < 300mm)	
			Pipes	



### 5.3. Water levels

As mentioned in section 3.3.4 of document *ref.[6]* the water level at the moment of impact is assumed to be equal to Mean Sea Level (MSL) in which the MSL is located at 1.72m above the LAT, as specified in Table 2.2 of document *ref.[6]*.

### 5.4. Added water mass (ship and foundation)

Added mass represents the additional inertia experienced by an object when it accelerates in a fluid due to the mass of the water being displaced and set in motion around it. For ships, the added mass is primarily applied to the wetted surfaces of the hull, accounting for the hydrodynamic effects of water during collision. Similarly, for the monopile, the added mass is considered on the submerged surfaces. In the simulations, added water mass is modeled to be active only during the collision event and will act in the direction of the collision.

#### 5.4.1. Ship

The added mass factors of the ships are given in Chapter 3.3.10. of *ref.[6]*. During a collision while the ship is sailing (Surge) the added mass factor is 1.05. During a collision while the ship is drifting (Sway), the added mass factor is 1.85. *Figure 16* describes the different movements.

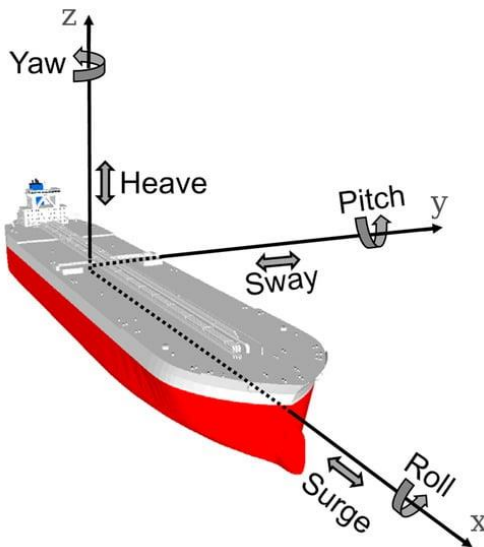


Figure 16. Vessels motions along the three axes (from: <https://www.mdpi.com/2077-1312/9/8/800>)

The added water mass expressed in kilos is shown for the chemical tanker, Container ship and Passenger vessel in *Table 14, 18 & 22* respectively. The added water mass of the modelled sections has been added to the FEM model and is placed on the outer hull of the ship for each model.

#### 5.4.2. Monopile above seabed

Conform Chapter 3.3.6. of *ref.[6]* the water mass at the foundation at the moment of impact is as follows:

- The water level inside of the foundation is the same as outside of the foundation and is equal to MSL. The mass of the water has been added to the mass of the pile
- The water level outside of the foundation is equal to MSL with an added water mass factor of 1.2.

## 5.5. Ship

This paragraph explains the structure of the FEM ship models. Due to the calculation time, it is not feasible to model the entire ship. Therefore, only a portion of the ship is modeled for each ship type, specifically the area around the impact zone. The parts that are not modeled are simulated with a so-called 'added point mass.' This point mass is rigidly connected to the outer edge of the section and will follow the same displacement and rotations as the point mass acting at the center of gravity of the omitted part. This method of implementation drastically reduces the calculation time, but the results remain reliable.

### 5.5.1. Chemical Tanker

Table 13 & 14 below provide an overview of the dimensions and masses that are used in the ship section and also the masses of the omitted ship sections, conform reference [5]. DT stands for displacement tonnage and is the mass of the water the ship displaces, which is equal to the ship's total mass, including the mass of the hull, cargo, fuel and any other components on board. It is assumed the ship is fully loaded.

Table 13. Global information

Total length [m]	Width [m]	Draught [m]	DT [ton]	DT [kg]
135	23.0	8.3	21,000	21,000,000

The added water mass coefficients in Table 14, sourced from reference [6], apply to the surge and sway motions of the vessels.

Table 14. Ship masses and velocities

Section	Ship movements	Coefficient Added Mass Water [-]	Added Mass Water [kg]	Total Mass [kg]	Velocity [knots]	Velocity [m/s]
Fore	Surge	0.05	1,050,000	22,050,000	10	5.14
Fore	Surge	0.05	1,050,000	22,050,000	20	10.29
Mid	Sway	0.85	17,850,000	38,850,000	2	1.03
Mid	Sway	0.85	17,850,000	38,850,000	4	2.06

Table 15 displays the masses incorporated into the model of the section. The additional mass is added to ensure that the mass of the modelled section matches the theoretical DT of the modelled section. The added water mass is placed around the hull of the section and corresponds to the mass of the attached water, as described in Table 14. The point masses represent the not modelled parts of the ship, including the self-weight of the steel, additional weights, and the added water masses. The omitted part in the analysis for the vessel's fore end is modelled with a single point mass. For the analysis with the midsection, both omitted sides are simulated with one point mass each (two point masses in total). The point masses are constrained in all directions, except the direction of the impact, to simulate their structural influence accurately.

Table 15. Section masses and properties

Section	Section Length [m]	Section steel mass [kg]	Additional mass [kg]	Added Mass Water section [kg]	Number of point mass	Point mass [kg]	Total mass [kg]
Fore	15.9	214,410	2,025,590	112,000	1	19,698,000	22,050,000
Mid	35.2	807,370	4,668,186	4,654,222	2	14,360,111	38,850,000

The global coordinates of the point masses representing the omitted parts are shown in *Table 16*. In a horizontal plane, the point mass is located at the center of the omitted section for the simulation with mid-section, while one point mass is located at the end of the modelled forward section, and the z-coordinate corresponds to half of the ship's draught. The added masses for the mid section forward section are shown in *Figure 18 & 20*, respectively.

Table 16. Global coordinates added point masses chemical tanker

		X [m]	Y [m]	Z [m LAT]
Mid section	Left	15.3	-42.55	-2.45
	Right	15.3	42.55	-2.45
forward section		19.41	1.50	-2.45

### 5.5.1.1. Mid Section

The chemical tanker section features a design with a double-plated hull, two bulkheads, and one transverse structure, see *Figure 17*. Its global dimensions are 35.2 meters in length, 23 meters in width, and approximately 13 meters in height.

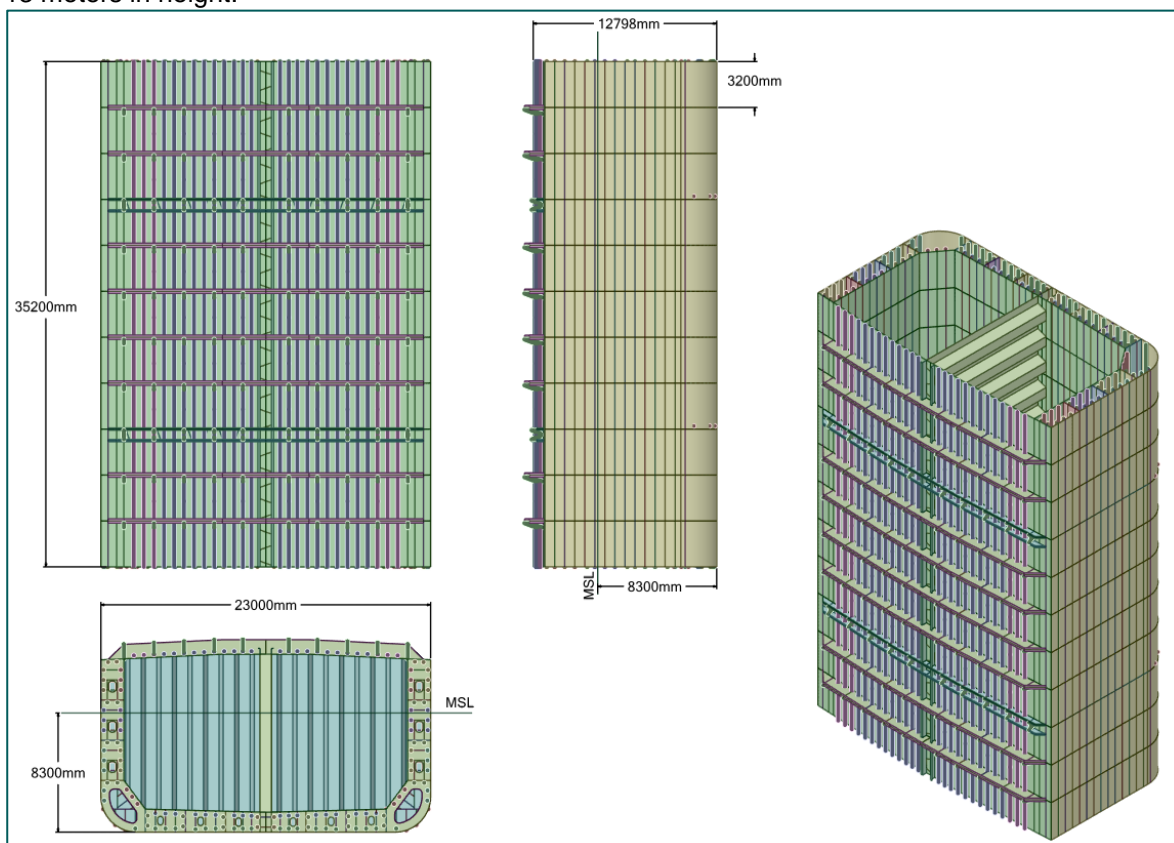


Figure 17. Chemical Tanker - Mid section – dimension

Figure 18 shows the modelled mid section including the two point masses which are placed at each end of the chemical tanker section and are used to represent the displacement tonnage of the not modelled part of the tanker. The point masses for the chemical tanker section are positioned according to the full ship's dimensions, with the assumption of an even mass distribution along the tanker's length. An even mass distribution serves as a baseline providing a practical way to compute and offer initial insights into the ship's structural behavior.

The point masses are rigidly (MPC,RBE2) connected to the left and right outer edges of the section.

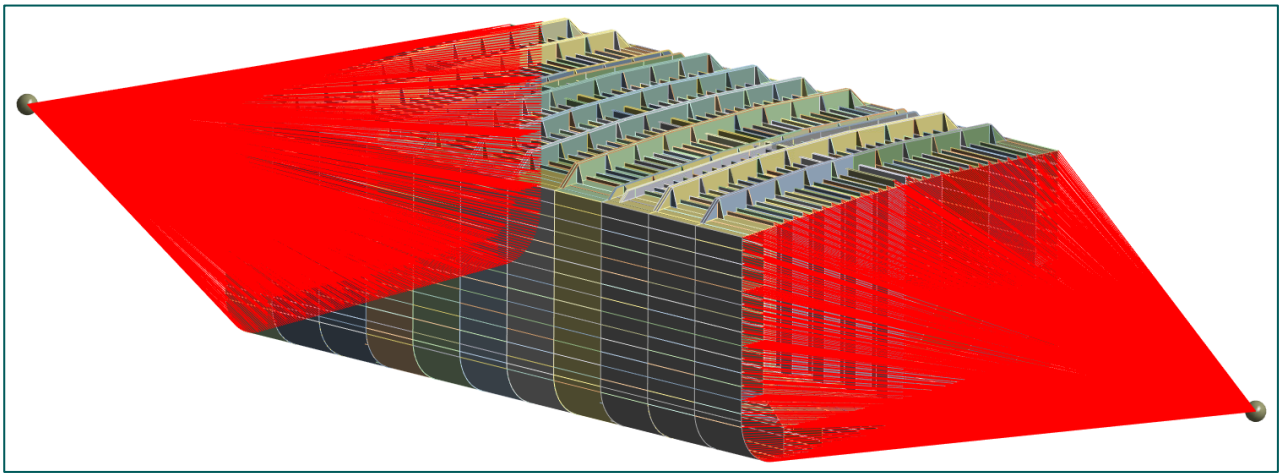


Figure 18. Chemical Tanker - Mid section point masses

### 5.5.1.2. Forward section

Figure 19 shows the forward section of the chemical tanker which features multiple decks and a protruding bow, with global dimensions of 22 meters in width, 16 meters in length, and 12 meters in height. A single point mass is used to represent the omitted section of the chemical tanker.

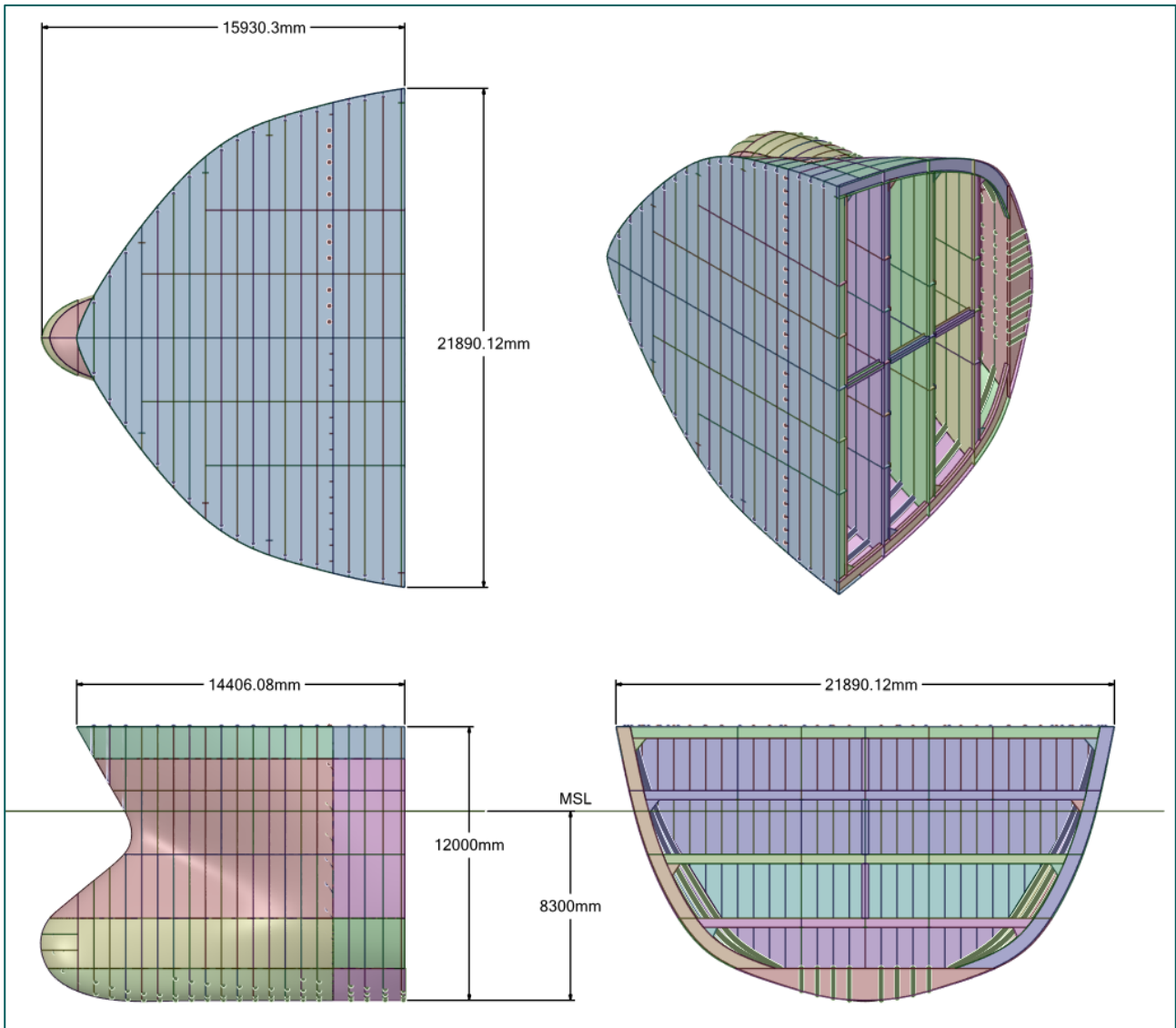


Figure 19. Chemical Tanker- Forward section - Global dimensions

The point mass shown in *Figure 20* represents the omitted part of the chemical tanker.

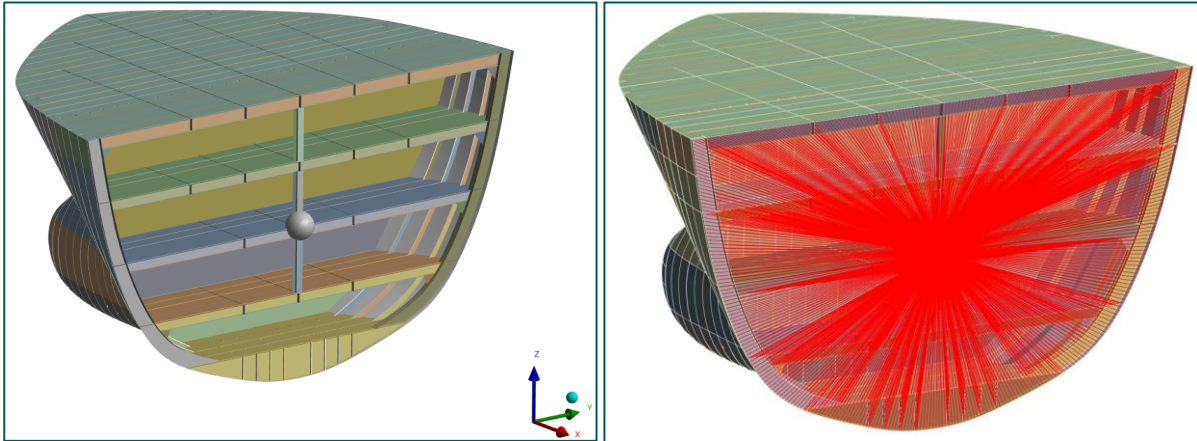


Figure 20. Chemical Tanker – Forward section - point mass

## 5.5.2. Container Ship

The tables below provide an overview of the dimensions and masses that are used in the ship section and also the masses of the omitted ship sections, conform reference [5]. It is assumed that the ship is fully loaded and that the containers themselves do not include any stiffness and therefore are not modelled.

Table 17. Global dimensions

Total length [m]	Width [m]	Draught [m]	DT [ton]	DT [kg]
397.4	59.0	16.0	223,000	223,000,000

The added water mass coefficients in *Table 18*, sourced from reference [6], apply to the surge and sway of the vessels.

Table 18. Ship masses and velocities

Section	Ship movements	Coefficient Added Mass Water [-]	Added Mass Water [kg]	Total Mass [kg]	Velocity [knots]	Velocity [m/s]
Fore	Surge	0.05	11,150,000	234,150,000	10	5.14
Fore	Surge	0.05	11,150,000	234,150,000	20	10.29
Mid	Sway	0.85	189,550,000	412,550,000	2	1.03
Mid	Sway	0.85	189,550,000	412,550,000	4	2.06

*Table 19* displays the masses incorporated into the model of the section. The additional mass is added to ensure that the mass of the modelled section matches the theoretical DT of the modelled section. The added water mass is placed around the hull of the section and corresponds to the mass of the attached water, as described in *Table 18*. The point masses represent the uncalculated portion of the ship, including the self-weight of the steel, additional weights, and the added water masses. The omitted part in the analysis for the vessel's fore end is modelled with a single point mass. For the analysis with the midsection, both omitted sides are simulated with one point mass each. The point masses are constrained in all directions, except the direction of the impact, to simulate their structural influence accurately.

Table 19. Section masses and properties

Section	Section Length [m]	Section steel mass [kg]	Addition mass [kg]	Added Mass Water section [kg]	Number of point mass	Point mass – omitted part [kg]	Total mass [kg]
Fore	23.6	1,129,300	12,226,010	667,765	1	220,126,925	234,150,000
Mid	41.8	5,362,800	18,093,164	19,937,569	2	184,578,234	412,550,000



The global coordinates of the point masses representing the omitted parts are shown in *Table 20*. In a horizontal plane, the point mass is located at the center of the omitted section for the simulation with mid-section, while one point mass is located at the end of the modelled forward section, and the z-coordinate corresponds to half of the ship's draught. The added masses for the mid section and forward section are shown in *Figure 22 & 24*, respectively.

Table 20. Global coordinates added point masses container ship

		X [m]	Y [m]	Z [m LAT]
Mid section	Left	33.25	102.15	-6.3
	Right	33.25	-102.15	-6.3
Forward section		27.33	1.50	-6.3

#### 5.5.2.1. Mid Section

The container ship's midsection includes two distinct bulkheads and is shown in *Figure 21*. The full section's global dimensions are 60 meters in width, 42 meters in length, and 34 meters in height. Two point masses are applied: at each end to represent the omitted parts of the vessel.

The half of the midsection near the impact location is modeled in detail with shells and beams. The half midsection opposite the impact location is modeled in a simplified manner without the beam stiffeners and small shell stiffeners. Care was taken to ensure that the structural stiffness remained the same after this simplification. Further details can be found in *Appendix H*.



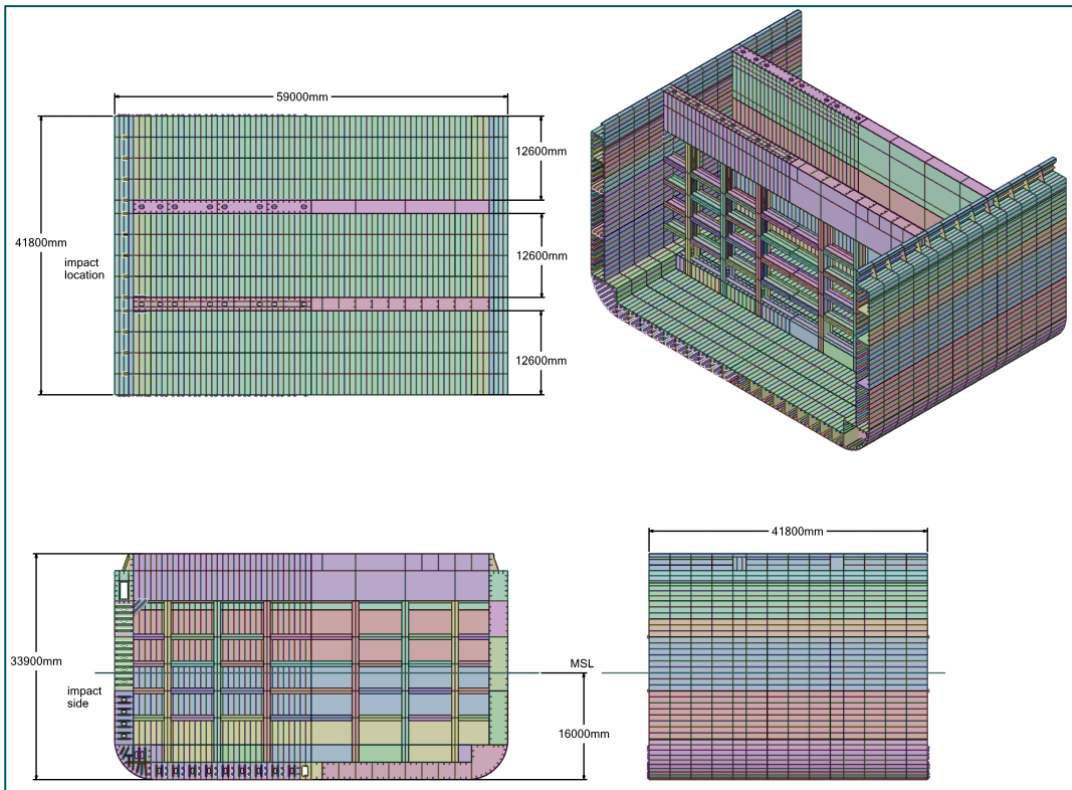


Figure 21. Container Ship - Mid section - Global dimensions

In *Figure 22*, the 2 point masses are shown, each representing an omitted section of the vessel. The point masses are rigidly (MPC,RBE2) connected to the left and right outer edges of the section.

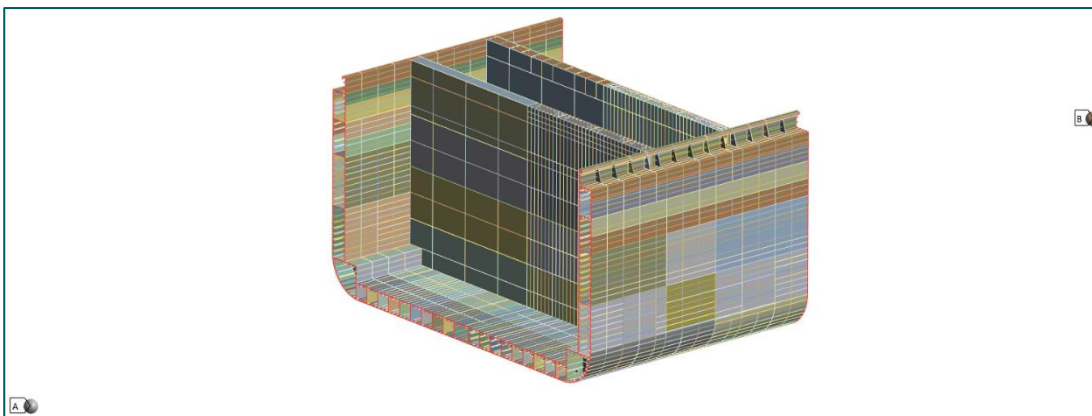


Figure 22. Container Ship - Mid section - point masses

### 5.5.2.2. Forward section

Figure 23 shows the forward section of the container ship which features a bow aligned with the deck level, with global dimensions of 31 meters in width, 24 meters in length, and 32.5 meters in height. A single point mass is used to represent the omitted section of the container ship.

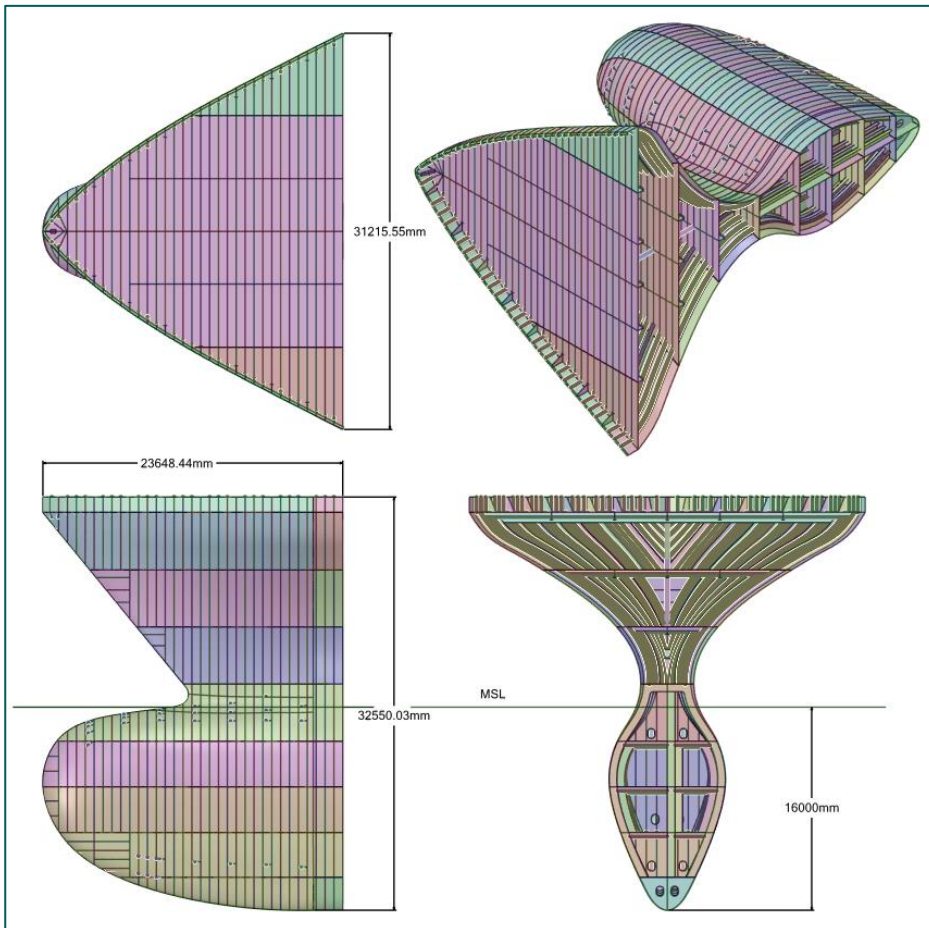


Figure 23. Container Ship – Forward section - Global dimensions

The point mass shown in *Figure 24* represents the omitted part of the container ship.

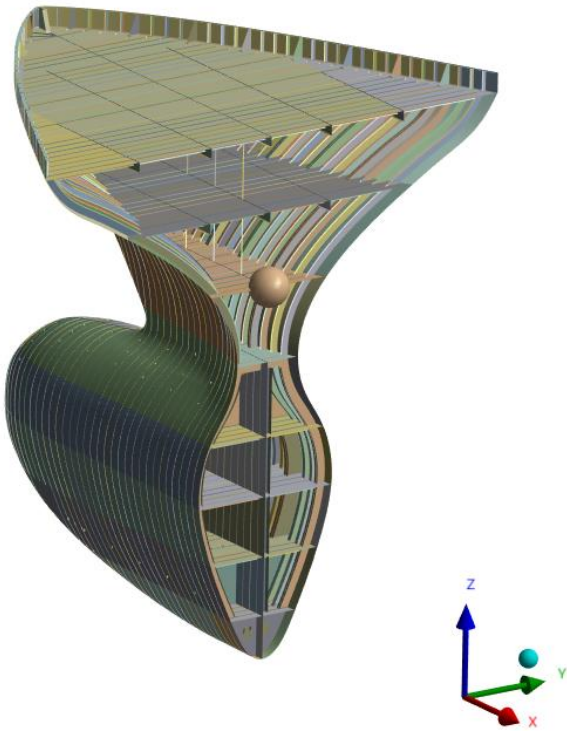


Figure 24. Container Ship – Forward section - point mass

### 5.5.3. Passenger Vessel

The tables below provide an overview of the dimensions and masses that are used in the ship section and also the masses of the omitted ship sections, conform reference [5].

Table 21. Global dimensions

Total length [m]	Width [m]	Draught [m]	DT [ton]	DT [kg]
242	36.0	8.3	42,700	42,700,000

The added water mass coefficients in Table 22, sourced from reference [6], apply to the surge and sway motions of the vessels.

Table 22. Ship masses and velocities

Section	Ship movements	Coefficient Added Mass Water [-]	Added Mass Water [kg]	Total Mass [kg]	Velocity [knots]	Velocity [m/s]
Fore	Surge	0.05	2,135,000	44,835,000	20	10.29
Fore	Surge	0.05	2,135,000	44,835,000	30	15.43
Mid	Sway	0.85	36,295,000	78,995,000	2	1.03
Mid	Sway	0.85	36,295,000	78,995,000	4	2.06

Table 23 displays the masses incorporated into the model of the section. The additional mass is added to ensure that the mass of the modelled section matches the theoretical DT of the modelled section. The added water mass is placed around the hull of the section and corresponds to the mass of the attached water, as described in Table 22. The point masses represent the not modelled part of the ship, including the self-weight of the steel, additional weights, and the added water masses. The omitted part in the analysis for the vessel's fore end is modelled with a single point mass. For the analysis with the midsection, both omitted sides are simulated with one point mass each. The point masses are constrained in all directions, except the direction of the impact, to simulate their structural influence accurately.

Table 23. Section masses and properties

Section	Section Length [m]	Section steel mass [kg]	Addition mass [kg]	Added Mass Water section [kg]	Number of point mass	Point mass – omitted part [kg]	Total mass [kg]
Fore	23.6	753,220	3,410,912	208,207	1	40,462,661	44,835,000
Mid	39.2	2,254,200	4,662,494	5,879,190	2	33,099,558	78,995,000



The global coordinates of the point masses representing the omitted parts are shown in *Table 24*. In a horizontal plane, the point mass is located at the center of the omitted section for the simulation with mid-section, while one point mass is located at the end of the modelled forward section, and the z-coordinate corresponds to half of the ship's draught. The added masses for the mid section and forward section are shown in *Figure 26 & 28*, respectively.

Table 24. Global coordinates added point masses passenger vessel

		X [m]	Y [m]	Z [m LAT]
Mid section	Left	21.75	71.00	-2.45
	Right	21.75	-69.6	-2.45
Forward section		35.21	1.5	-2.45

### 5.5.3.1. Mid Section

The passenger vessel's midsection includes 13 decks and is shown in *Figure 25*. The full section's global dimensions are 36 meters in width, 39.2 meters in length, and 40 meters in height. Two point masses are applied: two at each end to represent the omitted parts of the vessel.

The half of the midsection near the impact location is modeled in detail with shells and beams. The half midsection opposite the impact location is modeled in a simplified manner without the beam stiffeners and small shell stiffeners. Care was taken to ensure that the structural stiffness remained the same after this simplification. Further details can be found in *Appendix H*.

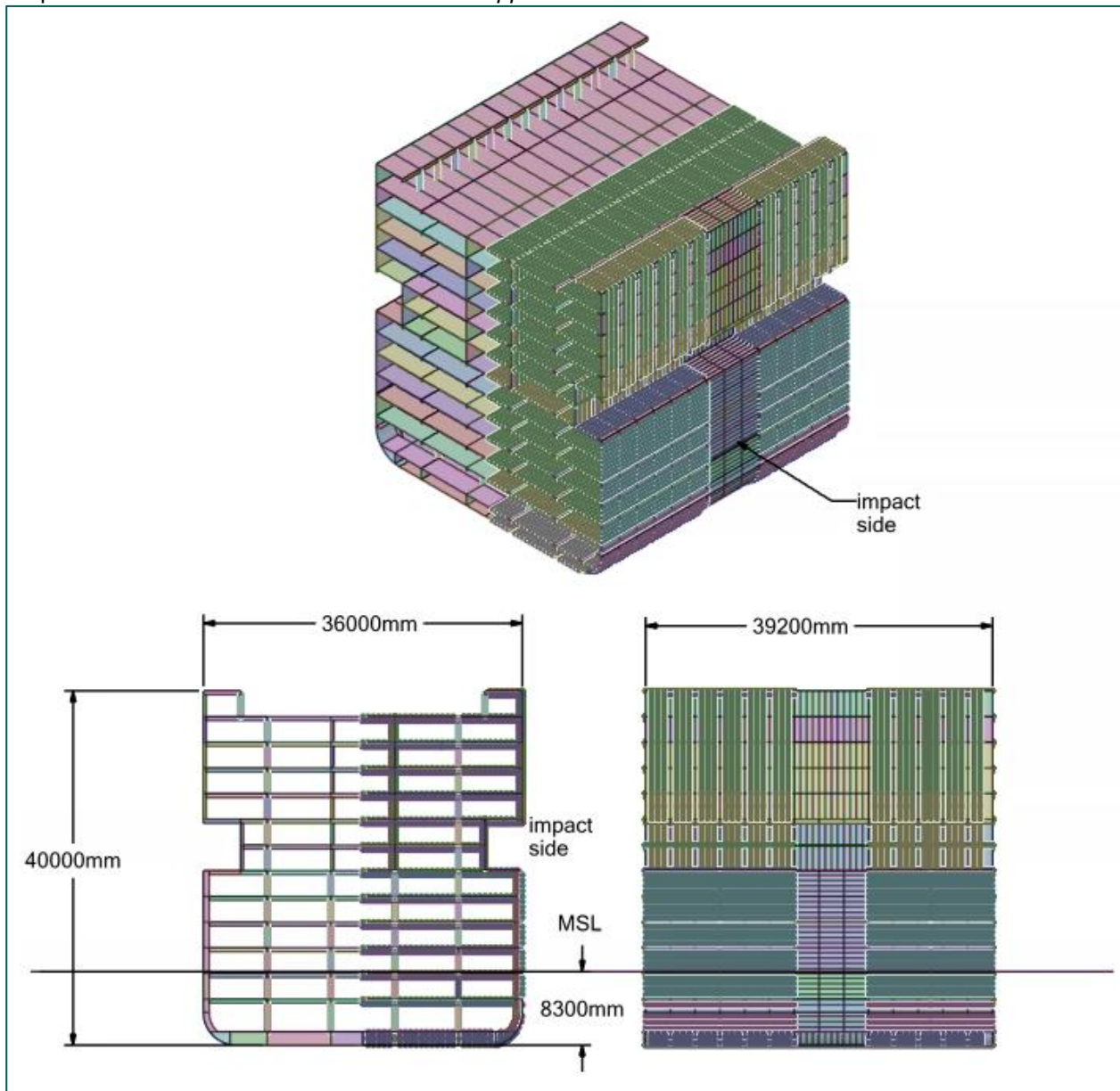


Figure 25. Passenger Vessel - Mid section - Global dimensions

In *Figure 26*, the 2 point masses are shown, each representing an omitted section of the vessel. The point masses are rigidly (MPC,RBE2) connected to the left and right outer edges of the section.

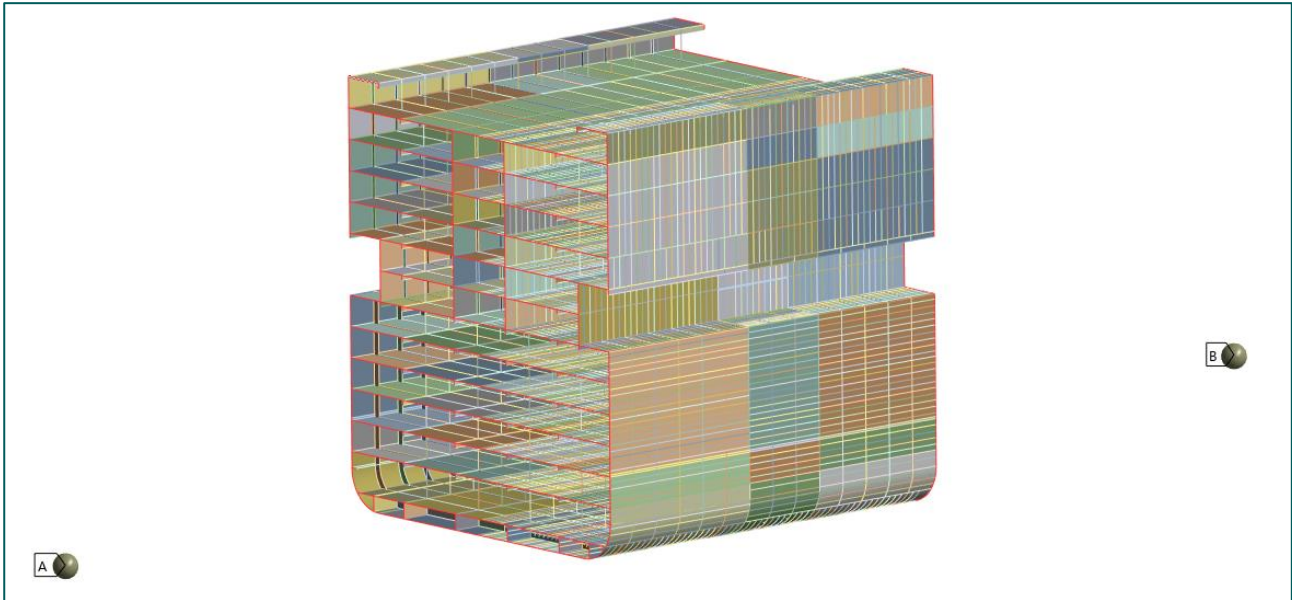


Figure 26. Passenger vessel - Mid section - point masses

### 5.5.3.2. Forward section

Figure 27 shows the forward section of the passenger vessel which features a bow aligned with the deck level, with global dimensions of 31 meters in width, 31.5 meters in length, and 24 meters in height. A single point mass is used to represent the omitted section of the passenger vessel.

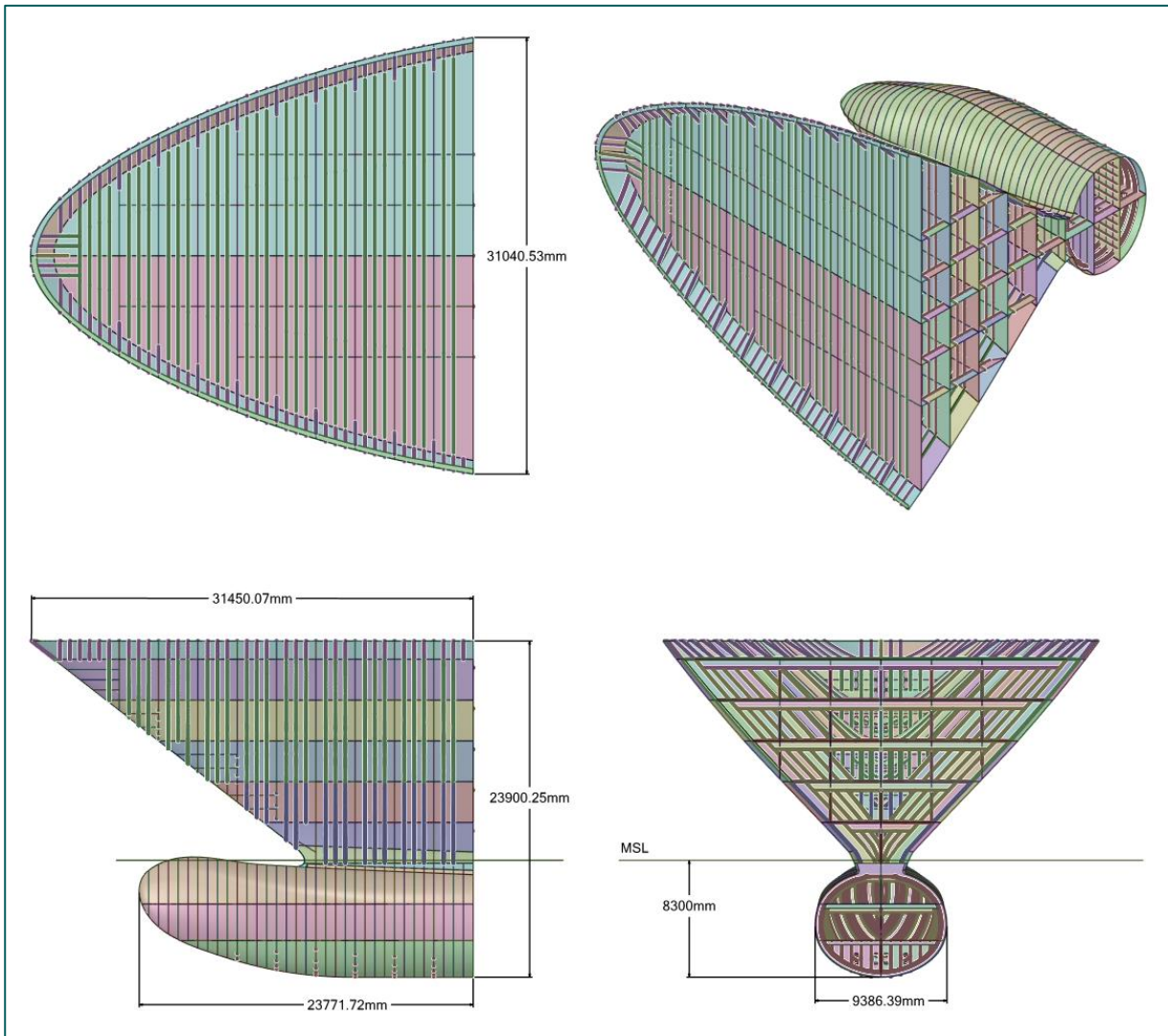


Figure 27. Passenger vessel – Forward section - Global dimensions



The point mass shown in *Figure 28* represents the omitted part of the passenger vessel.

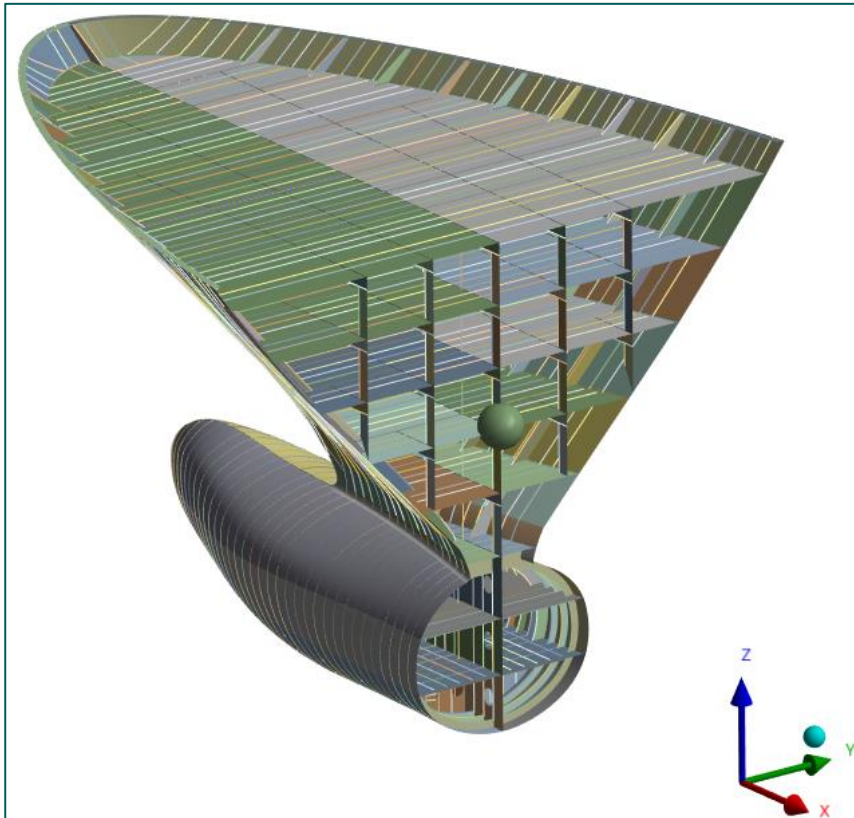


Figure 28. Passenger vessel – Forward section - point mass

#### 5.5.4. Boundary conditions

Establishing 3D FEM ship models in LS-Dyna is essential for accurately simulating impact scenarios between ships and other structures. The models incorporate hydrostatic pressure, velocity, added mass, and constraints in five degrees of freedom ( $U_z$ ,  $U_y$ ,  $ROT_x$ ,  $ROT_y$  and  $ROT_z$ ). During the impact simulation, no wind, wave, or current loading acting on the ship are considered, and propulsion loading is excluded. Water damping is also neglected to simplify the analysis.

#### 5.5.5. Load conditions static prestressed

In this simulation, an implicit prestressed approach is used to simulate the stress state within a ship under various environmental loads, including hydrostatic pressures. The prestressing is achieved through a static structural analysis in ANSYS Mechanical, where all relevant loads are applied to ensure a realistic initial stress state.

The load conditions for the ship section include:

- Hydrostatic pressure
- Lightweight tonnage (framing, machinery, decking, etc.)
- Deadweight tonnage (cargo, fuel, supplies, etc.)



#### **5.5.6. Excluded loads on the ship**

As described in Chapter 3.3.12 of reference [6], the wind, wave, and propulsion loads acting on the ship types are significantly smaller than the maximum impact loads. As a result, the influence of wind, current, and propulsion loads on the impact results is minimal. Therefore, these loads are not included in the impact analysis.

## 5.6. Support structure (turbine)

In *Figure 29*, there is an illustration of the details of the support structure. The support structure consists of the foundation, substructure, and tower. The foundation itself is made up of two parts: one part is soil, and the other is the monopile. The foundation spans from -63.35 m LAT to -34.60 m LAT. The penetration length of the monopile is 28.75 m. The substructure starts at -34.60 m LAT and extends to 19.15 m LAT. The tower extends from 19.15 m LAT to 105.81 m LAT. The details of the turbine blades are not included here, as they are not considered in the simulations. The information and dimensions are copied from reference [6].

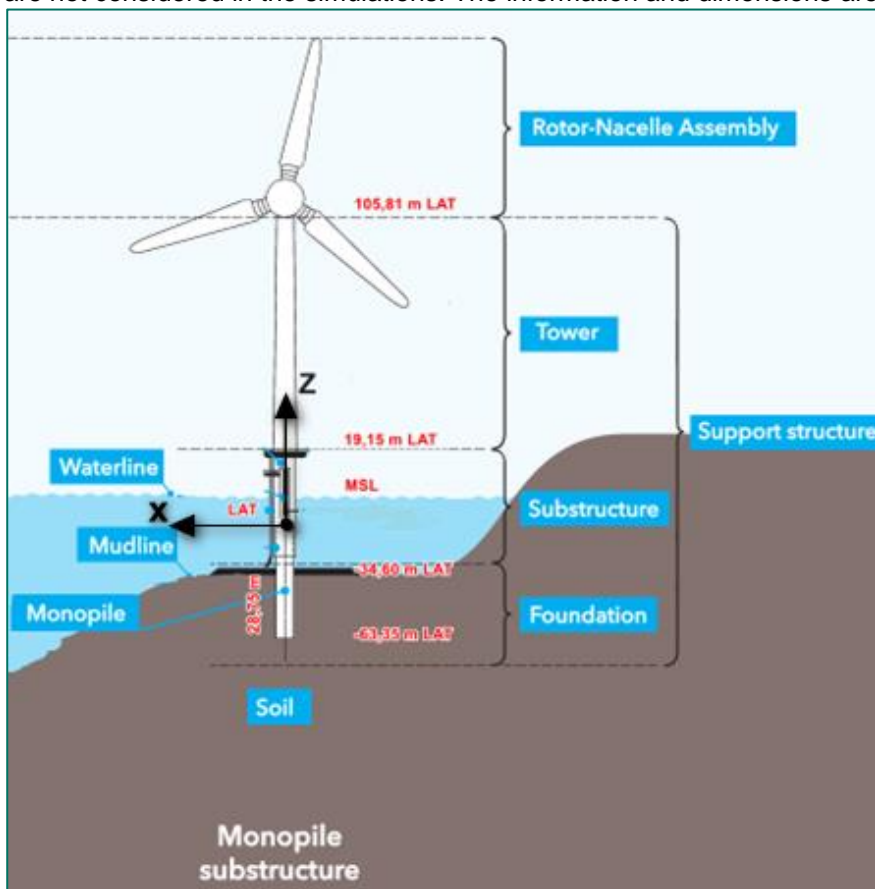


Figure 29. Definition and key elevations of Wind farm 2 (Figure made/created based on definition in Figure 1-1 of DNV-ST-0126)

In the simulations, the ship is always moving in the negative (in *Figure 29* shown) x-direction towards the support substructure. In one of the scenarios related to the collision simulation of the falling turbine on the ship, the turbine falls in the negative z-direction.



Wind farm 2 is chosen for this study and the details of the wind turbine used in Wind farm 2 are provided in ref. [7], as shown in *Table 25*.

Table 25. Wind farm 2 main data (ref. [7])

Identification			Wind farm 2
<b>Turbine</b>	Nacelle plus rotor mass	[tonnes]	478.4
	Hub height	[m LAT]	108.85
	Lower position of blade tip	[m LAT]	26.85
<b>Tower</b>	Top elevation	[m LAT]	105.81
	Bottom elevation	[m LAT]	19.15
<b>Pile</b>	Top elevation	[m LAT]	19.15
	Bottom elevation	[m LAT]	-63.35
	Water depth	[m]	34.60
	Pile penetration	[m]	28.75
	Steel quality		S355
<b>Water level</b>	MSL	[m LAT]	1.72

The turbine tower & foundation is designed as a steel tube with varying diameters, with its lower section embedded in the seabed for stability. The turbine tower, substructure and turbine foundation are made of S355 steel. The wall thicknesses vary over multiple sections as shown in *Figure 30* (right), according to the foundation properties (reference [7]).

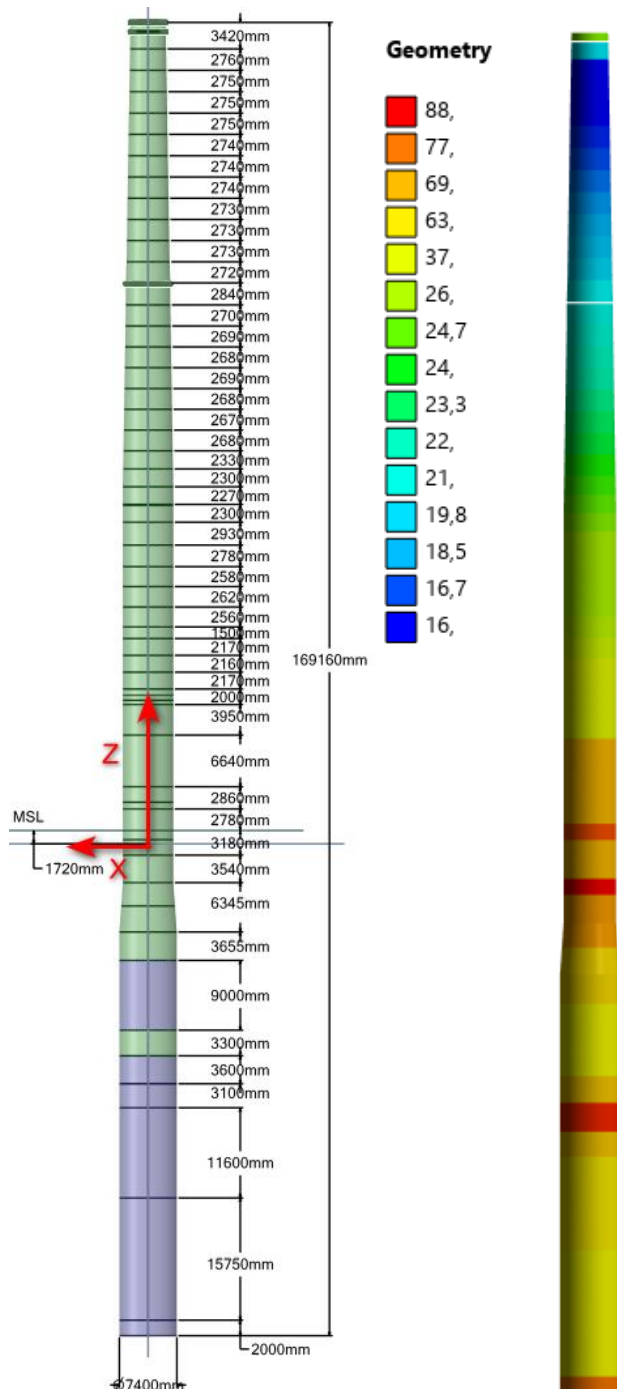


Figure 30. The turbine foundation's dimensions and material (left), and shell thickness (right)

### 5.6.1. Boundary conditions

The load on the foundation model includes the following: the steel mass of all tubulars, concentrated masses such as flanges, platforms, tower equipment, the nacelle and rotor, and the water inside and outside the pile. The precise values of these loads on the foundation and tower are taken from the 'Masses Input Sheet' of reference [7]. These loads are applied as distributed loads on the respective shells in the FEM model.

The bottom edge of the turbine foundation is modelled with a hinge boundary condition. This boundary constraint restricts the vertical displacement and axial rotation, while allowing other degrees of freedom. *Figure 31* below shows this hinged location.

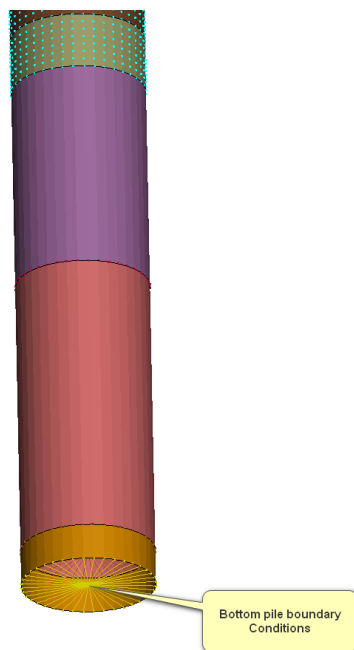


Figure 31. Turbine foundation - bottom boundary condition

### 5.6.2. Load conditions static prestressed

The turbine support structure is subjected to wind, wave, and current loads using data from the previous project phase (*ref.[6]*). Wind loads from the turbine blades are applied at the top of the support structure. Additionally, wind load is applied to the tower, and the upper part of the substructure. Wave and current loads are applied to the submerged part of the substructure, see *Figure 32*. The direction of these loads is aligned with the collision direction in drifting scenarios and perpendicular to the collision direction in the sailing scenarios. Within each scenario the wind and water loads are applied in the same direction.

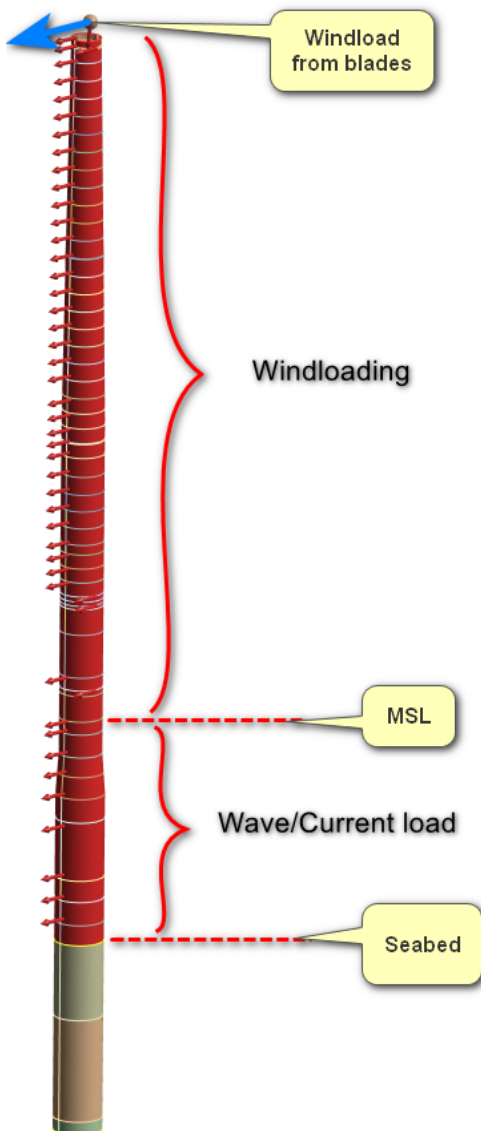


Figure 32 - Wind, wave and current load

### 5.6.3. Excluded loads on the support structure

Turbine blade dynamics, nacelle-induced vibrations, and thermal loads are excluded from the simulation.

### 5.6.4. Soil-structure interaction

To describe the modelling approach for soil-structure interaction between the wind turbine monopile and the soil, a memo titled 'INFR240476-R105-DP2.3 Memo Soil Material Model rev.1c' [Appendix E] has been prepared. This serves as the soil boundary condition for the monopile in the 3D FEM ship collision simulations for this project.

In turbine foundation modeling, radial soil springs are applied in layers from a depth of -34.6 m LAT down to -63.6 m LAT, with each layer representing 0.5 m LAT in depth, see *Figure 33*. These springs are defined using p-y curves, which provide stiffness values in N/m depth. Since the springs are applied for each 0.5-meter layer, the p-value from the p-y curves is divided by 2 to correctly distribute the stiffness across the layers. With a dynamic amplification factor of 2.5, the springs account for the increased response under dynamic loading conditions. Each spring, set as compression-only and extending 15 meters in length, is configured to resist loading when compressed, closely simulating the natural behavior of soil. With 59 in depth layers and 40 springs in the radial direction per layer, this model ensures detailed and realistic soil behavior surrounding the turbine foundation. More details can be found in the Memo soil material [Appendix E]. The reaction forces and deformation of each soil layer can be found in Soil spring results [Appendix J].

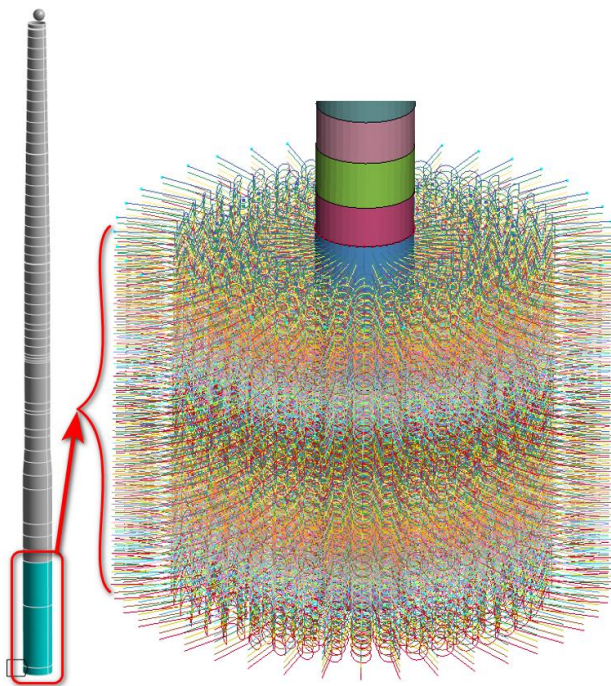


Figure 33. Turbine foundation - soil structure interaction



The monopile is a hollow steel tube, and soil accumulates inside the structure during installation. This soil affects the radial stiffness of the steel tube. To accurately represent this effect, a rigid radial connection is introduced. This connection models the load transfer from the steel structure to the enclosed soil. As shown in *Figure 34*, the rigid connection is applied to several soil layers at various depths. These locations were chosen because preliminary simulations indicated that the monopile buckle in the upper layers, suggesting that soil failure was more likely in those areas. However, adding too many radial rigid connections along the soil depth can make the monopile excessively stiff. Therefore, the final choice was made to coincide with an existing transition in the tube, balancing realism in the simulation with structural efficiency.

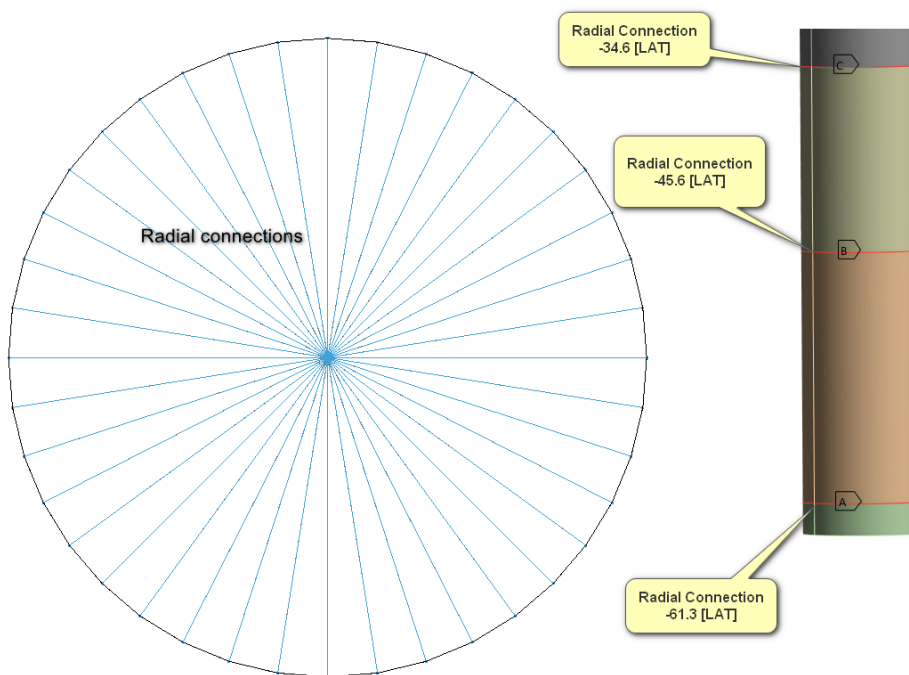


Figure 34 - Internal soil layer rigid connection - top view [left] locations [right]

## 5.7. Wind turbine

One of the simulations being considered is for a situation in which a wind turbine falls onto a ship. In order to accurately model this scenario in Ansys (LS-DYNA), it is essential to first create a model of the turbine itself. This allows for a realistic simulation of the interaction between the turbine and the ship during the collision. *Figure 35* provides an overview of the details of the turbine components. As shown, the nacelle contains various mechanical and electrical part, each part with its own mass and stiffness. The nacelle itself functions as a protective casing that houses all of these components. Modelling each individual part inside the nacelle does not lead to more accurate results of the impact simulation, but it is time-consuming and computationally inefficient. Therefore, only the overall nacelle is modelled as a simple block, representing the external structure of the turbine without detailing its internal components.

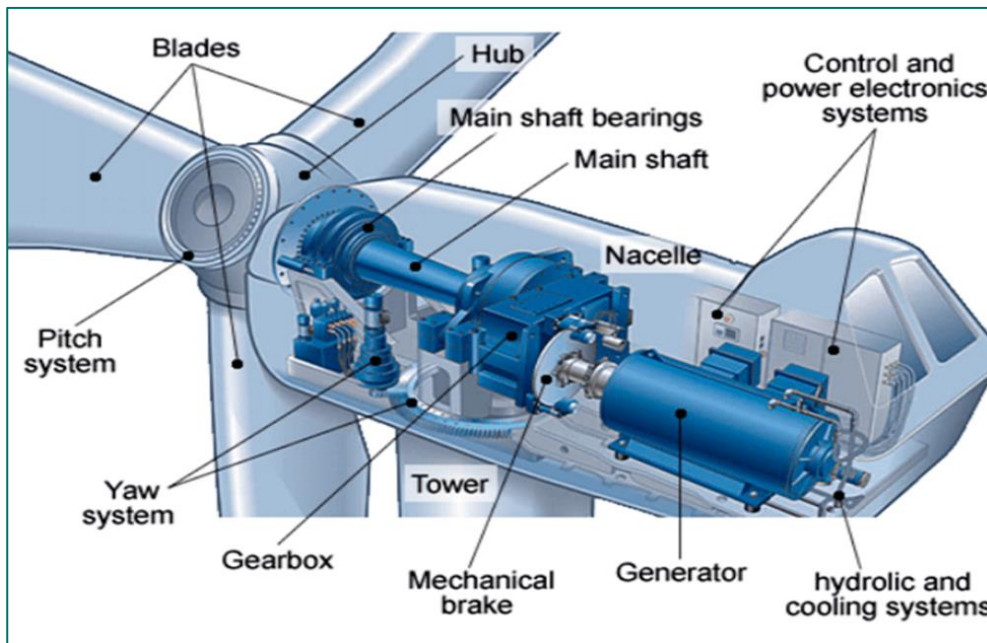


Figure 35. Details of the nacelle and hub (reference: <https://kpenenergy.in>)

The details of the wind turbine used in Wind farm 2 are provided in ref. [7], as shown in *Table 26*. However there's no detailed information about the shape of the nacelle and hub, as these can vary across various sources depending on the turbine and its MW rating. Based on the MW rating of Wind farm 2, two references are found including the dimensions and mass of the nacelle.

Table 26. Wind turbine information from ref. [7]

Parameter	Unit	Wind farm 2
Rated power	[MW]	9.5
Nacelle plus rotor mass	[tonnes]	478.4
Hub height	[m LAT]	108.85
Rotor diameter	[m]	164
Lower position of blade tip	[m LAT]	26.85

The first reference provided detailed information about the nacelle, including its dimensions and mass. This information was based on publicly available data on the MHI Vestas V174-9.5 MW turbine, a reliable and well-documented offshore wind turbine. According to this source, the nacelle is approximately 21 m in length, 9 m in width, and 9 m in height, with a total mass of around 390 tons. *Figure 36 & 37* give an impression of the MHI Vestas V174-9.5 MW turbine.



Figure 36. V174-9.5 MW (reference: [www.vestas.com](http://www.vestas.com))



Figure 37. MHI Vestas Offshore V174-9.5 MW offshore turbine (reference: [wind-turbine-models.com](http://wind-turbine-models.com))

The second [reference](#) focused on the hub, providing the necessary dimensions for our modelling (see [Figure 38](#)). Specifically, details from the LEANWIND 8 MW reference turbine (LW) were included to approximate the hub in our model.

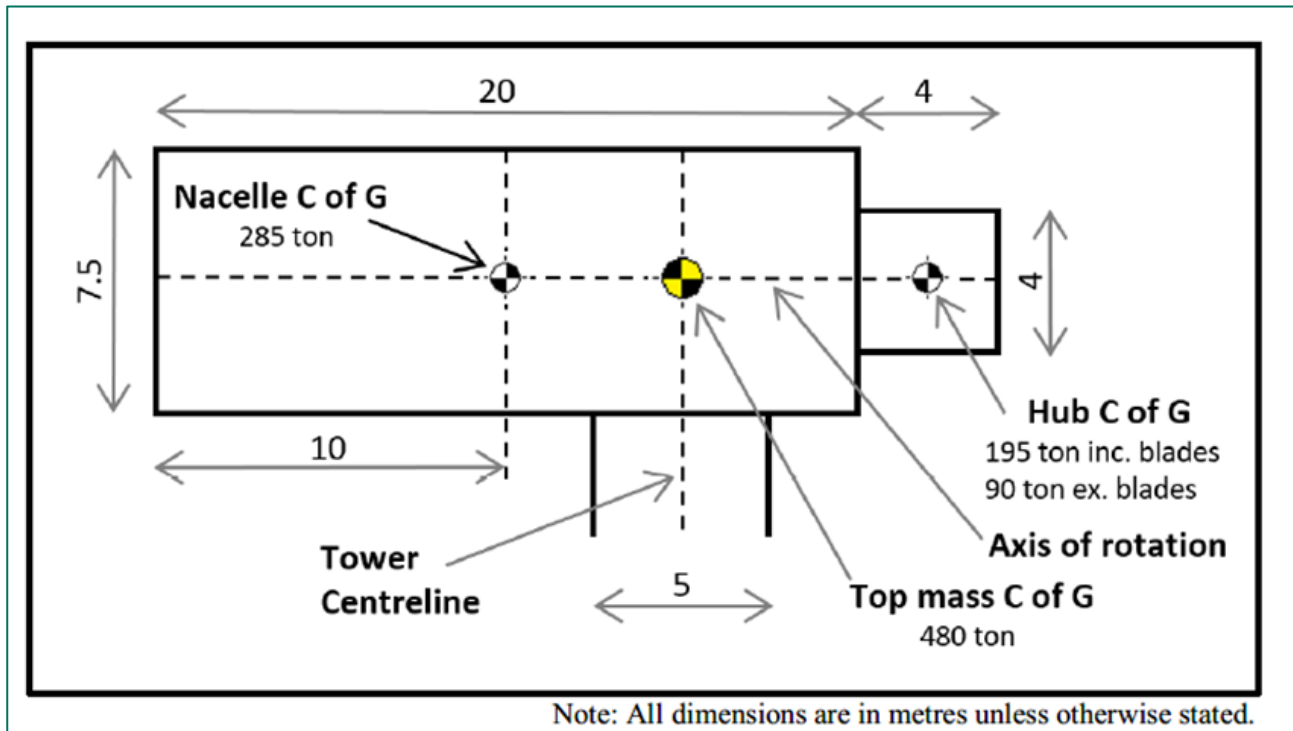


Figure 38. Top mass distribution for the 8 MW LW turbine

As mentioned in *ref. [7]*, the rotor mass, which includes the hub and three blades, is 184.502 tonnes. The nacelle mass is 293.882 tonnes, resulting in a total mass of 478.384 tonnes (the sum of the nacelle and rotor). It is important to note that the blades were not included in our model. This simplification was made to focus on the structural behavior of the tower and its foundation, as the blades primarily influence aerodynamic performance rather than the structural interactions being analyzed in this study. However, since no specific information about the blade mass is provided, a mass of 105 tonnes for the blades has been defined based on [Figure 38](#).

Based on the information obtained, the key parameters incorporated into the model were identified as follows:

- Nacelle dimensions: Approximately 20 m in length, 8 m in width, and 8 m in height.
- Hub dimensions: The hub is modelled as a cylinder with a height of 4 m and a diameter of 4 m.
- Total mass: 478.374 tonnes - 105 tonnes = 372.374 tonnes



## 5.8. Contact between ship and foundation

The simulation incorporates a frictionless (dynamic and static friction coefficient are 0) contact between the ship and the turbine support structure, which is a conservative approach. By neglecting tangential resistance, this assumption focuses solely on normal forces, ensuring that the analysis captures a worst-case scenario for the collision. This is consistent with the methodology used in *ref [6]* paragraph 3.3.11, aligning the analysis with established practices.

## 5.9. Solver setting

The analysis was conducted using Ansys 2024 R2 (Workbench) with a 3D Shell-Beam-Springs model. The material was modelled using piecewise nonlinear plastic behavior, and the geometry was treated as non-linear. The analysis type employed was Explicit Dynamic using the LS-DYNA solver, which is suitable for simulating large deformations and impact scenarios.

### 5.9.1. Mass scaling

Mass scaling in LS-Dyna is a technique used to reduce the computation time of explicit dynamic analyses. In the simulations, mass scaling is employed with a minimum allowed timestep of 1e-6 seconds to ensure computational efficiency while maintaining numerical stability. This approach artificially increases element mass on small element where necessary, enabling larger timesteps for explicit time integration without significantly affecting the accuracy of the results. It is important to note that this only happens on elements that are small and therefore force a small timestep. The added mass due to this option is very small and doesn't have a significant effect on the total mass.

### 5.9.2. Energy balance

In the LS-Dyna impact simulation between a ship and a support structure, the energy balance is tracked by recording key energy components, including kinetic energy, internal energy, hourglass energy, and contact energy. It is essential to ensure that the total energy of the system - the sum of all energy components - remains consistent throughout the simulation. Since the contact is frictionless, no sliding energy is considered.

For all simulations, the hourglass energy method with Flanagan-Belytschko stiffness form is selected. This method is used for shell elements to ensure robust numerical integration while minimizing hourglass modes. It is commonly applied for simulating thin-walled structures under large deformations and dynamic loading conditions. A factor of 0.1 is used for a balance between minimizing artificial stiffness (to avoid overly rigid behavior) and controlling numerical instabilities caused by hourglass modes. This value is typically selected for dynamic simulations to maintain stability without compromising accuracy. For each simulation the energy balance is plotted and shown in the results.



### 5.10. Model validation and verification

Achieving an optimal balance between simulation accuracy and computational efficiency presents a significant challenge in FEM modelling, particularly when dealing with large-scale structural models. A memo (*Appendix F*) has been provided to address this as a verification. Calculation time is heavily influenced by factors such as the mesh size, the quantity of elements, and the types of elements used, including shell, beam, or combinations of shell and beam elements.

Model validation was performed on the support structure using the results from the previous phase of this project (Phase 2), as detailed in *Appendix G*.

## 6 Simulations

In total, 14 collision simulations will be performed. 12 simulations involve impacts between various ship sections and the turbine support structure, while 1 simulation focuses on the dropping of the nacelle on the deck of a passenger vessel. This comprehensive approach ensures a detailed assessment of different impact scenarios and their effects on both the ships and the turbine foundation.

### 6.1. Ship collision simulations

A total of 12 distinct collision scenarios were simulated involving the three ship types (see *Table 5*) and the monopile foundation. For each ship type, one simulation involved a head-on collision with the monopile (while sailing), and another simulated a sideways impact with the monopile (while drifting). For each scenario, two different analyses were performed at varying speeds, providing a clearer understanding of the trends in the results. The analyses are presented per ship type in *Table 27, 29 & 28* below. The X and Y coordinate provided correspond to the point where the ship collides with the monopile and the Z coordinate corresponds to the bottom of the section. The values GT and DT represent the size of the ship types: GT stands for Gross Tonnage, a measure of the ship's overall internal volume, while DT stands for Displacement Tonnage, which refers to the weight of the volume of water displaced by the vessel.

Table 27. Collision simulations – Chemical Tanker

No.	Ship side	Hull	GT [-]	DT [tonne]	Ship status	Speed [knots]	X [m]	Y [m]	Z [m LAT]
1	Chemical Tanker Bow	Double	10,000	21,000	Sailing	10	3.4	1.5	-6.6
2	Chemical Tanker Bow	Double	10,000	21,000	Sailing	20	3.4	1.5	-6.6
3	Chemical Tanker SB side	Double	10,000	21,000	Drifting	2	3.7	0.0	-6.6
4	Chemical Tanker SB side	Double	10,000	21,000	Drifting	4	3.7	0.0	-6.6

Table 28. Collision simulations – Container ship

No.	Ship side	Hull	GT [-]	DT [tonne]	Ship status	Speed [knots]	X [m]	Y [m]	Z [m LAT]
5	Container ship Bow	Single	200,000	223,000	Sailing	10	3.6	0.7	-14.3
6	Container ship Bow	Single	200,000	223,000	Sailing	20	3.6	0.7	-14.3
7	Container ship SB side	Single	200,000	223,000	Drifting	2	3.7	0.0	-14.3
8	Container ship SB side	Single	200,000	223,000	Drifting	4	3.7	0.0	-14.3

Table 29. Collision simulations – Passenger vessel

No.	Ship side	Hull	GT [-]	DT [tonne]	Ship status	Speed [knots]	X [m]	Y [m]	Z [m LAT]
9	Passenger vessel Bow	Single	100,000	42,700	Sailing	20	3.6	0.8	-6.6
10	Passenger vessel Bow	Single	100,000	42,700	Sailing	30	3.6	0.8	-6.6
11	Passenger vessel SB side	Single	100,000	42,700	Drifting	2	3.7	0.0	-6.6
12	Passenger vessel SB side	Single	100,000	42,700	Drifting	4	3.7	0.0	-6.6

### 6.1.1. Sailing

In the sailing impact scenario, the forward section of the ship is offset by 1.5 meters, with the impact directed head-on, accurately simulating a direct collision. In *Figure 39*, it can be seen that the wind load direction is applied perpendicular to the impact directions. With this scenario the turbine foundation is most likely to fail toward the ship.

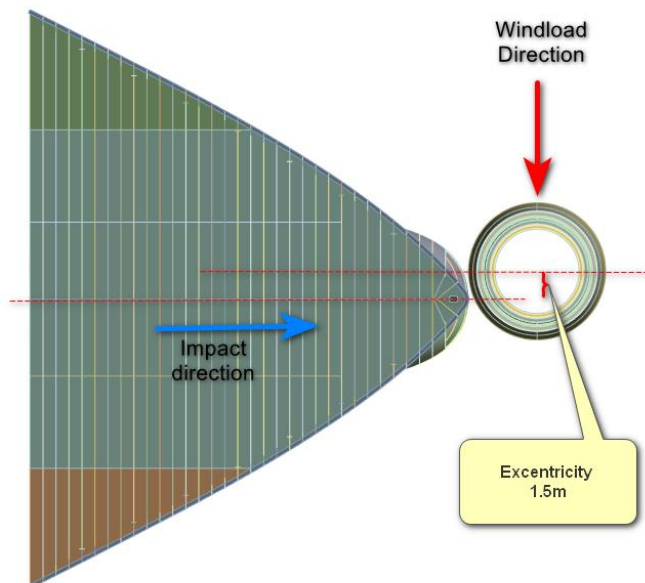


Figure 39. Eccentricity vs wind load direction



The vertical (z-axis) location of the impact is carefully positioned based on the ship's draft and the water level at the turbine foundation, ensuring that the simulation reflects realistic conditions. This setup (see *Figure 40*) provides a detailed assessment of collision effects at the precise height where the ship would contact the turbine structure, allowing for accurate impact analysis that incorporates vessel-specific and environmental conditions.

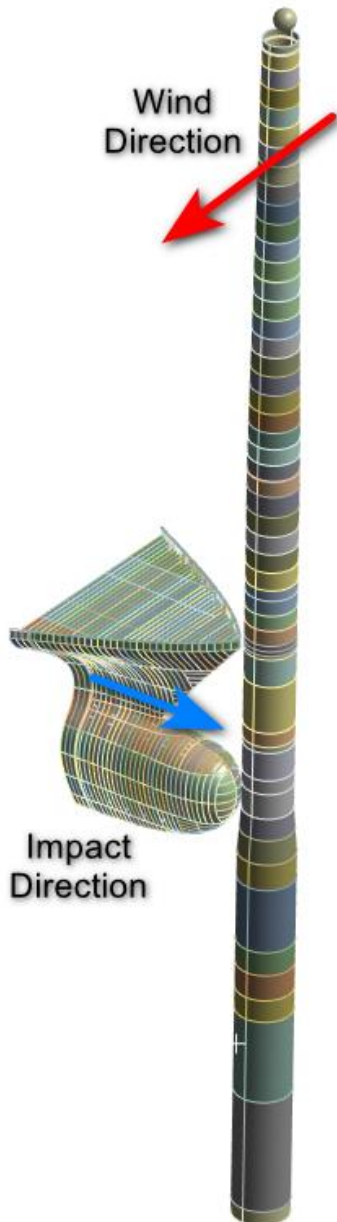


Figure 40. Sailing impact direction vs. wind load direction

### 6.1.2. Drifting

In the drifting impact scenario, the ship's midsection impacts a critical area between the bulkhead and stiffeners, representing a worst-case collision scenario. This location, chosen for its structural vulnerability, highlights the maximum potential damage from a lateral drift. The vertical impact point is determined by the ship's draft and the water level at the turbine foundation, ensuring the simulation accurately represents real-world conditions. This setup (see *Figure 41*) provides insights into the structural resilience of both the ship and turbine foundation under severe impact conditions, emphasizing the effects on the turbine structure where it's most exposed.

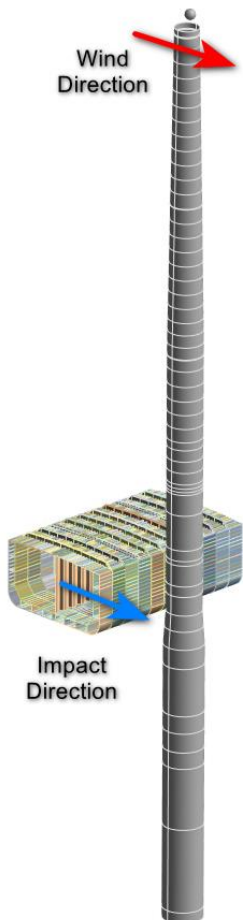


Figure 41. Drifting impact direction vs wind direction

### 6.1.3. Turbine point mass location

The turbine's point mass on top of the turbine foundation has an offset of 781 mm. This offset reflects the asymmetric positioning of the turbine's hub, nacelle, and rotor relative to the foundation. In *Figure 42* it can be seen that the offset of the mass is opposite to the direction of the wind loading. So for the drifting scenario's the offset is applied toward the ships and for the sailing scenario's the offset is perpendicular to the ship.

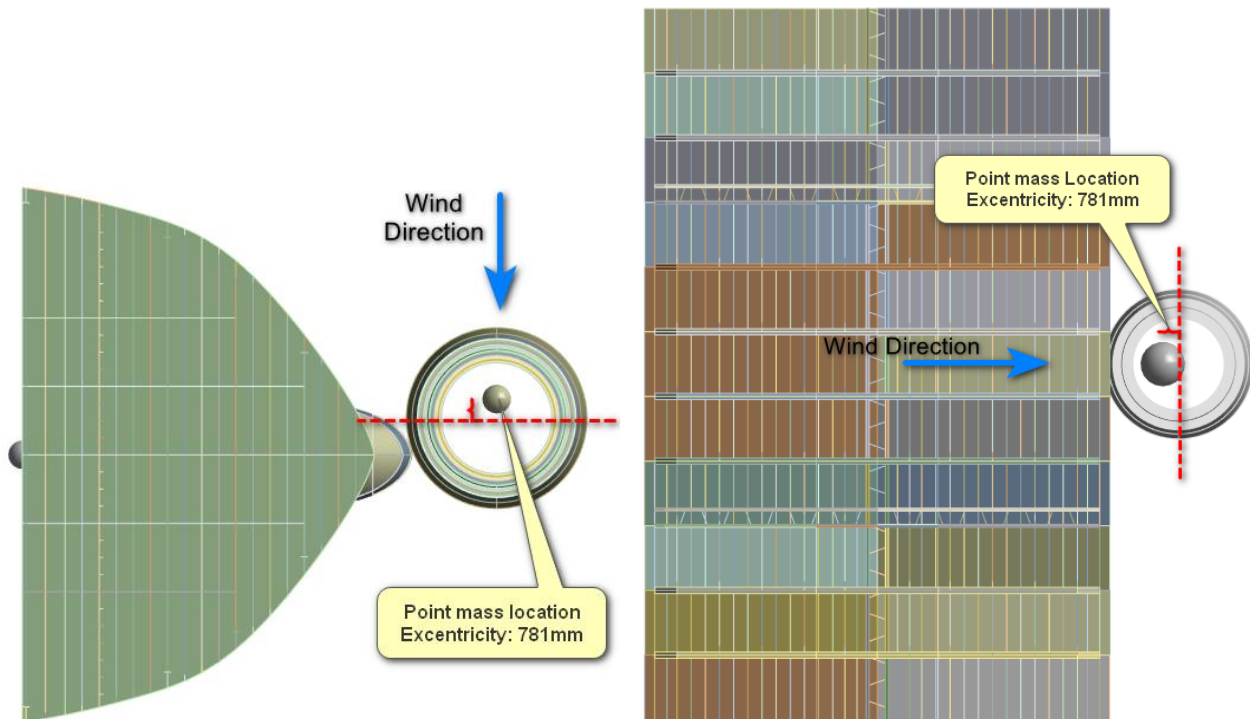


Figure 42. Turbine mass point eccentricity for sailing[left] and drifting [right]

#### 6.1.4. Project connections and mesh assemblies

In Ansys Workbench, assembling the ship sections and turbine foundation meshes into a single simulation enables a detailed impact analysis while allowing for the reuse of the turbine foundation's mesh and certain loading conditions. This approach streamlines the setup and ensures consistency across simulations. This is explained in *Figure 43*. In red the mesh assembly is shown of the chemical tanker mid-section with the turbine foundation. And in yellow the mesh assembly is shown of the chemical tanker fore-part and the turbine foundation.

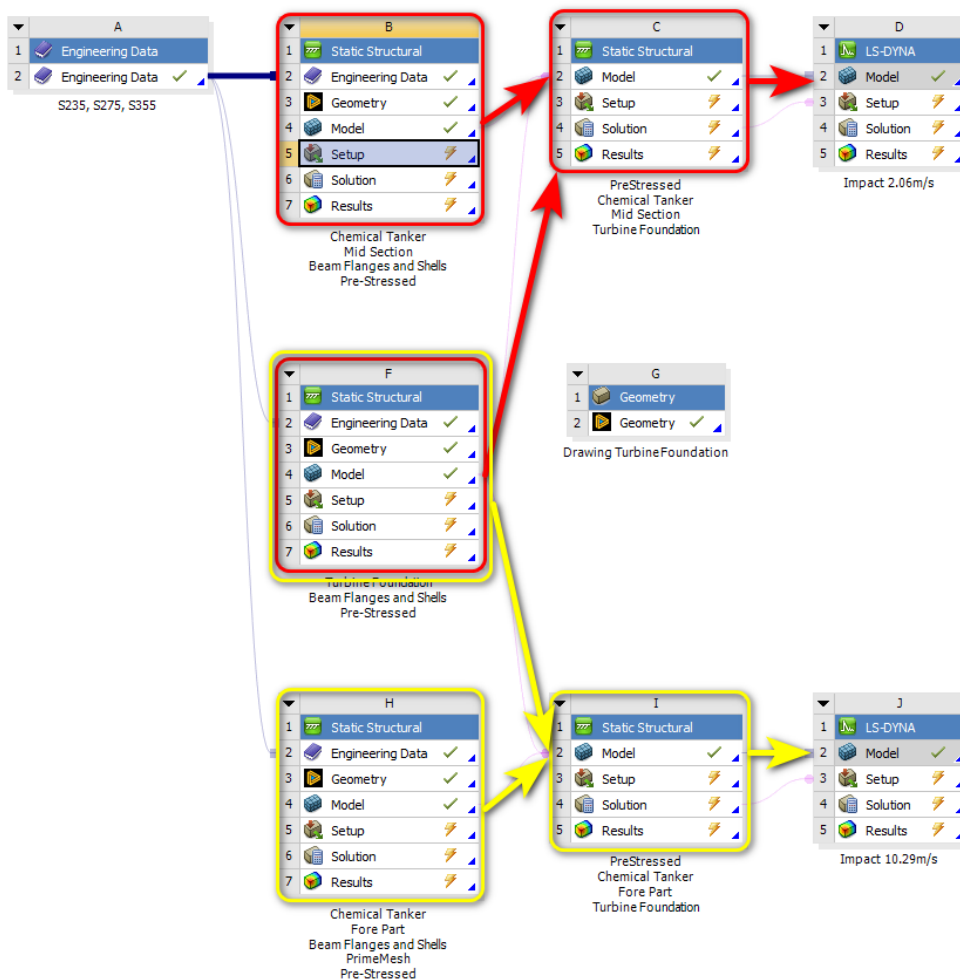


Figure 43. Model connections and mesh assemblies

#### 6.1.5. Initial stress and deformation

The stress state and deformations described in *Paragraph 5.5.5* is imported as initial conditions into an explicit LS-DYNA simulation. Dynamic relaxation is employed within the explicit analysis to maintain stability and accurately reflect the preloaded conditions. After 0.1 seconds, the ship section is subjected to an impact velocity, allowing for a clear separation between the initial stress application and the collision.

## 6.2. Nacelle dropping simulation

In the sailing scenarios where a support structure collapses towards the ship, the velocity of the falling nacelle is monitored along its position in the Z-direction. This allows us to determine the nacelle's velocity at the moment of collision. Using the Z-location (height) of the passenger vessel's upper deck, the collision velocity at that height is derived and used as the initial velocity for the simulation.

To further simplify the modelling process, the nacelle and hub were modelled as solids (Nacelle is modelled as a block). The detailed internal configuration of the nacelle, such as the rotor and other internal components, is not expected to significantly affect the impact dynamics under consideration. For our purposes, the shape is not critical. Instead, the key parameters influencing the simulation are the mass, dimensions, and velocity during the impact simulation with a ship. This simplified representation enables an accurate evaluation of the nacelle assembly's impact behavior while minimizing unnecessary computational complexity.

As mentioned in *Paragraph 5.7*, the modelled nacelle has a mass of 372 Tons. The initial fall velocity is derived from the nacelle's fall speed when the foundation tower is collapsing, based on the collision analyses conducted. Further details are provided in *Section 7.2*.

*Figure 44* shows the model defined in Ansys as the nacelle for the collision simulation. As previously mentioned, the nacelle is modeled as a fully rigid component. The ship's decks are modeled with a finer mesh compared to the other elements to ensure accurate results. It is important to note that simulation time plays an important role in this process.

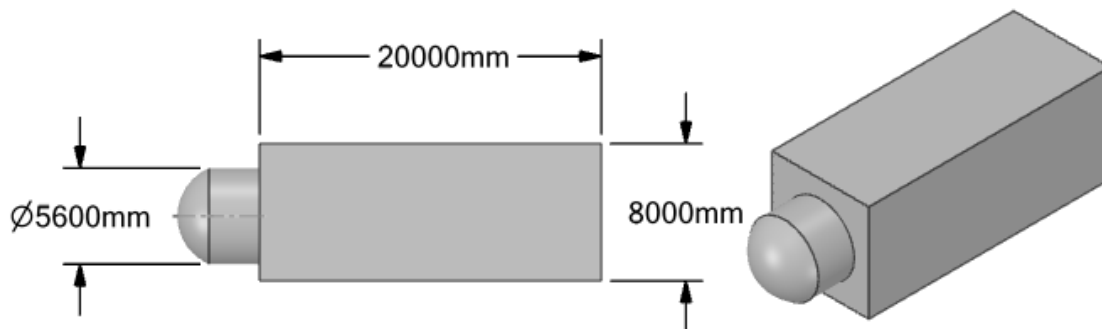


Figure 44. Nacelle dimensions in Ansys

The passenger vessel was selected for the collision simulation with the nacelle due to the following reasons:

- The number of decks,
- The size and area of the ship,
- The higher likelihood of the turbine falling onto the ship given its size, and
- For the container ship, detailed information about the containers themselves is unavailable.

For the turbine collision scenario, the nacelle falls directly onto the ship in the vertical (z) direction as illustrated, in *Figure 45*.

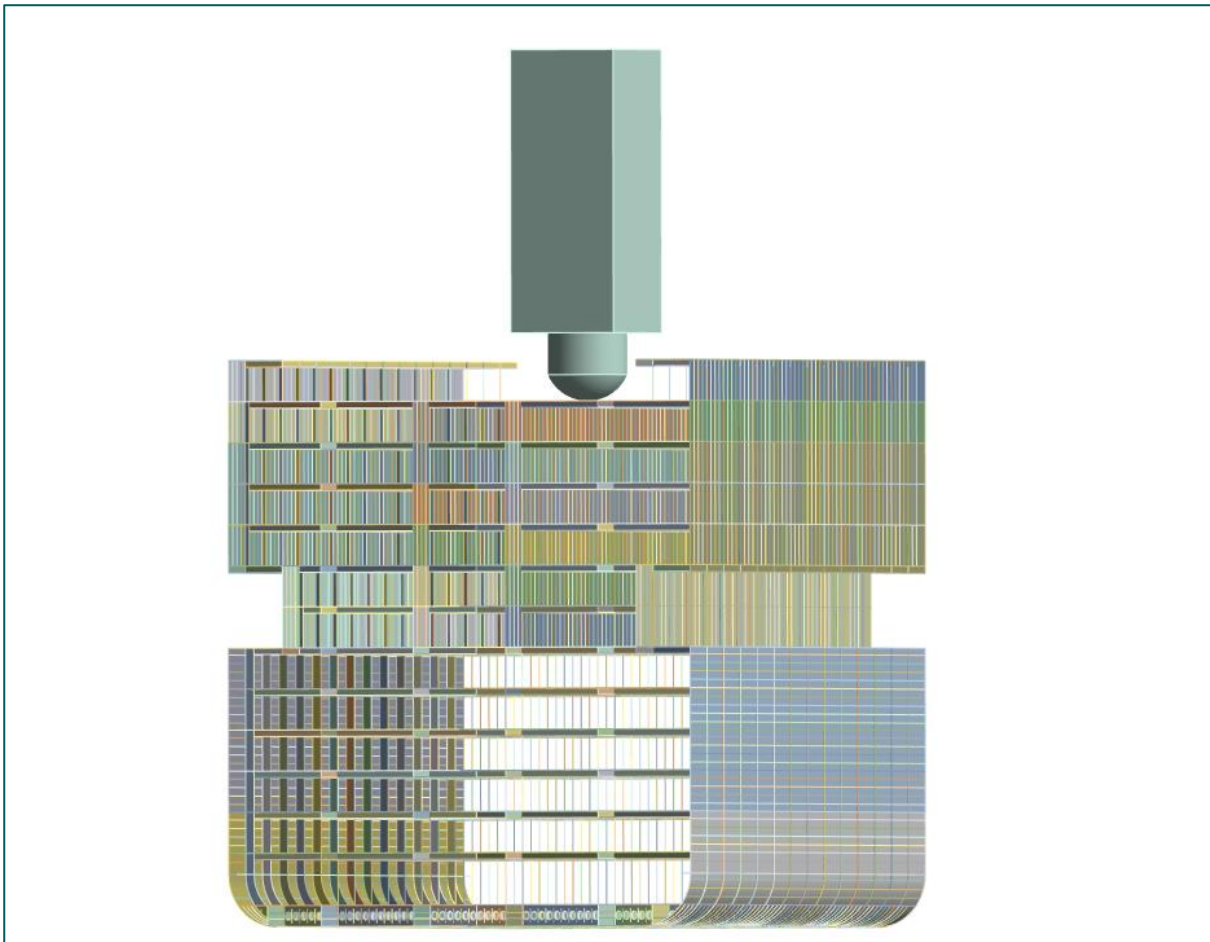


Figure 45. The Ansys model setup for the collision simulation between the nacelle and the passenger vessel

Given the uncertainty of the impact angle, a conservative approach was adopted for this simulation. In the case of a vertical impact, it is anticipated that the nacelle could penetrate the ship. Additionally, an extra simulation was performed where the nacelle impacted the ship in a horizontal position. This was necessary because the results from the head-on sailing scenario indicated that a horizontal impact was a plausible and critical condition to consider.



## 7 Summary of simulation results (DP4)

### 7.1. Results Ship Collision

This paragraph summarizes the results from all ship collision simulations. A total of 12 simulations were conducted, involving 3 different ship types, as outlined in *Paragraph 6.1*. An overview of these simulations is provided in *Table 30*.

Each simulation is analyzed for the Chemical Tanker, Container Ship, and Passenger Vessel in Paragraphs 7.1.1 to 7.1.3, respectively. For each simulation, a detailed explanation is given, accompanied by a figure depicting the simulation at its final time step. This illustrates the resulting damage to both the ship and the wind turbine foundation. The FEM model and simulation method have been both validated and verified, with additional details provided in *Appendix I*.

The damage outcomes for the ships are consolidated in *Section 7.1.4*, while the damage to the turbine foundation is discussed in *Section 7.1.5*. A summary of the overall results from all simulations is presented in *Section 7.1.6*. All results, along with a visual timeline for each analysis, are provided in *Appendices J.1.1* to *J.1.12*.

Table 30. Overview all ship collision simulations

No.	Ships Type		Speed [knots]	DT [Tonne]
1	Chemical Tanker	Bow	10	21,000
2	Chemical Tanker	Bow	20	21,000
3	Chemical Tanker	SB side	2	21,000
4	Chemical Tanker	SB side	4	21,000
5	Container Ship	Bow	10	223,000
6	Container Ship	Bow	20	223,000
7	Container Ship	SB side	2	223,000
8	Container Ship	SB side	4	223,000
9	Passenger Vessel	Bow	20	42,700
10	Passenger Vessel	Bow	30	42,700
11	Passenger Vessel	SB side	2	42,700
12	Passenger Vessel	SB side	4	42,700

### 7.1.1. Results Chemical Tanker

This paragraph presents the results of the four analyses conducted with the chemical tanker. For each simulation, a brief explanation is provided, accompanied by figures that illustrate the damage observed at the end of the simulation.

#### 7.1.1.1. Simulation 1 – Bow chemical tanker, 10 knots

In this simulation, the chemical tanker approaches the turbine foundation with an initial speed of 5.14 m/s. Following the collision, the ship's speed reduces to 1.76 m/s. The impact causes the upper layers of the soil to fail, leading the foundation tower to fail below the seabed. This is the only point where the tower fails by the end of the simulation. At the location of the bulbous bow, where the initial contact occurs, plastic deformation is observed, but the tower does not collapse at this stage. If the tower were to fail, it would fall off the ship, and there would be no risk of the nacelle dropping onto the ship. *Figure 46* illustrates the damage to the bow of the chemical tanker, with the bulbous bow experiencing the most significant impact. However, this damage does not present a threat of environmental harm or compromise the ship's stability, as it is confined to the area forward of the first bulkhead (also known as the collision bulkhead). All simulation results can be found in *Appendix J.1.1*.

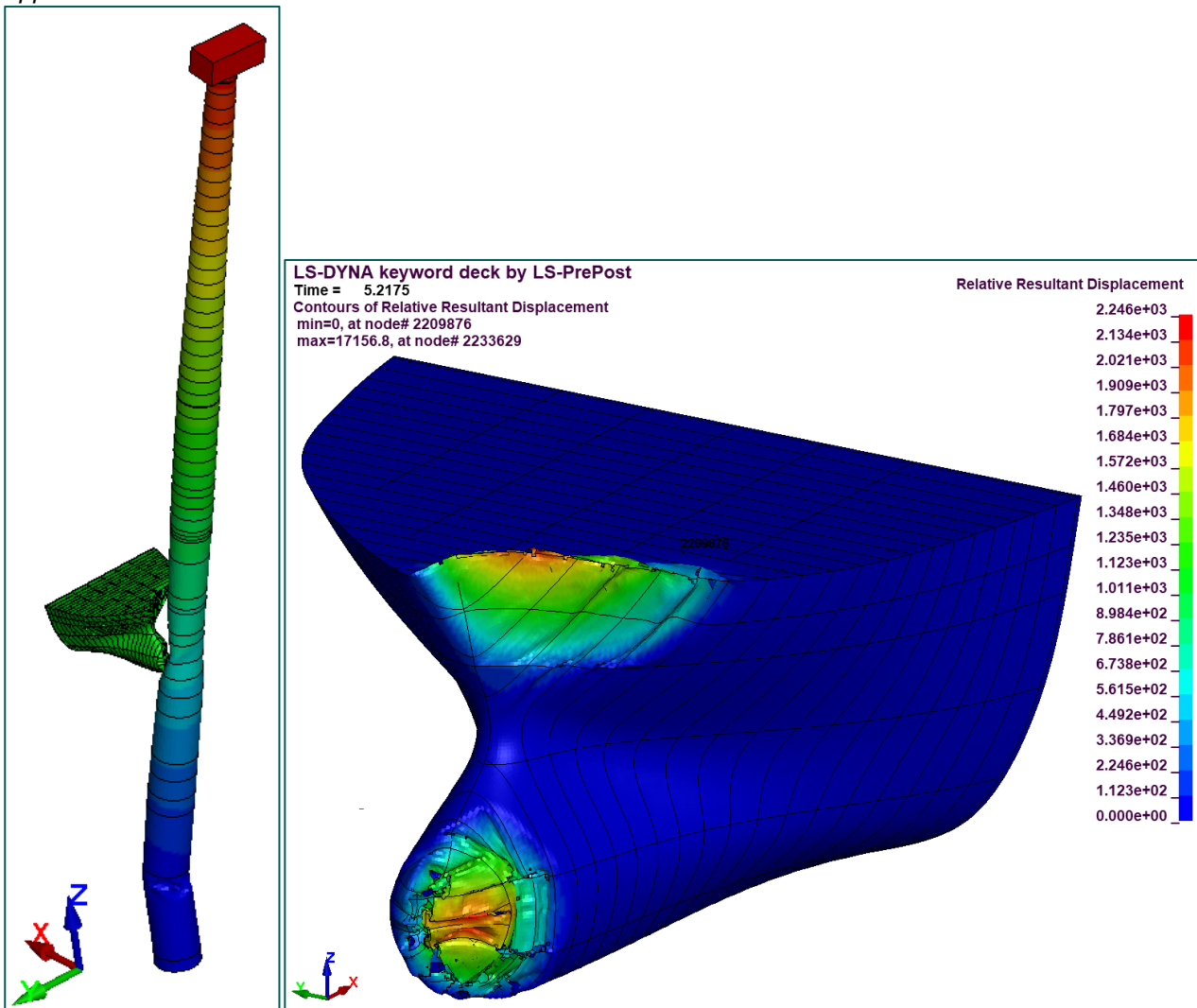


Figure 46. Global displacement (left) and deformation of ship [mm] (right) at end of simulation 1



### 7.1.1.2. Simulation 2 - Bow chemical tanker, 20 knots

Figure 47 shows the displacement at the end of the simulation. Table 51 in Appendix J.1.2 presents the full visual timelapse of the collision analysis, illustrating the bow of the chemical tanker colliding with the wind turbine foundation at a speed of 10.29 m/s. As shown, the monopile foundation experiences failure at three distinct locations, as detailed in Table 34 and Figure 47. Additionally, the nacelle tilts towards the ship, with a high likelihood of falling onto the moving vessel. The damage to the vessel is shown in Figure 96, where the failed elements are highlighted. As observed, the damage is confined to the area forward of the first bulkhead, causing no leakage and posing no risk of instability. Following the collision, the chemical tanker's speed decreases from 10.29 m/s to 8.12 m/s. Since the vessel sails away from the wind turbine, the remaining energy and speed might possibly cause a potential subsequent impact. All results of the simulation can be found in Appendix J.1.2.

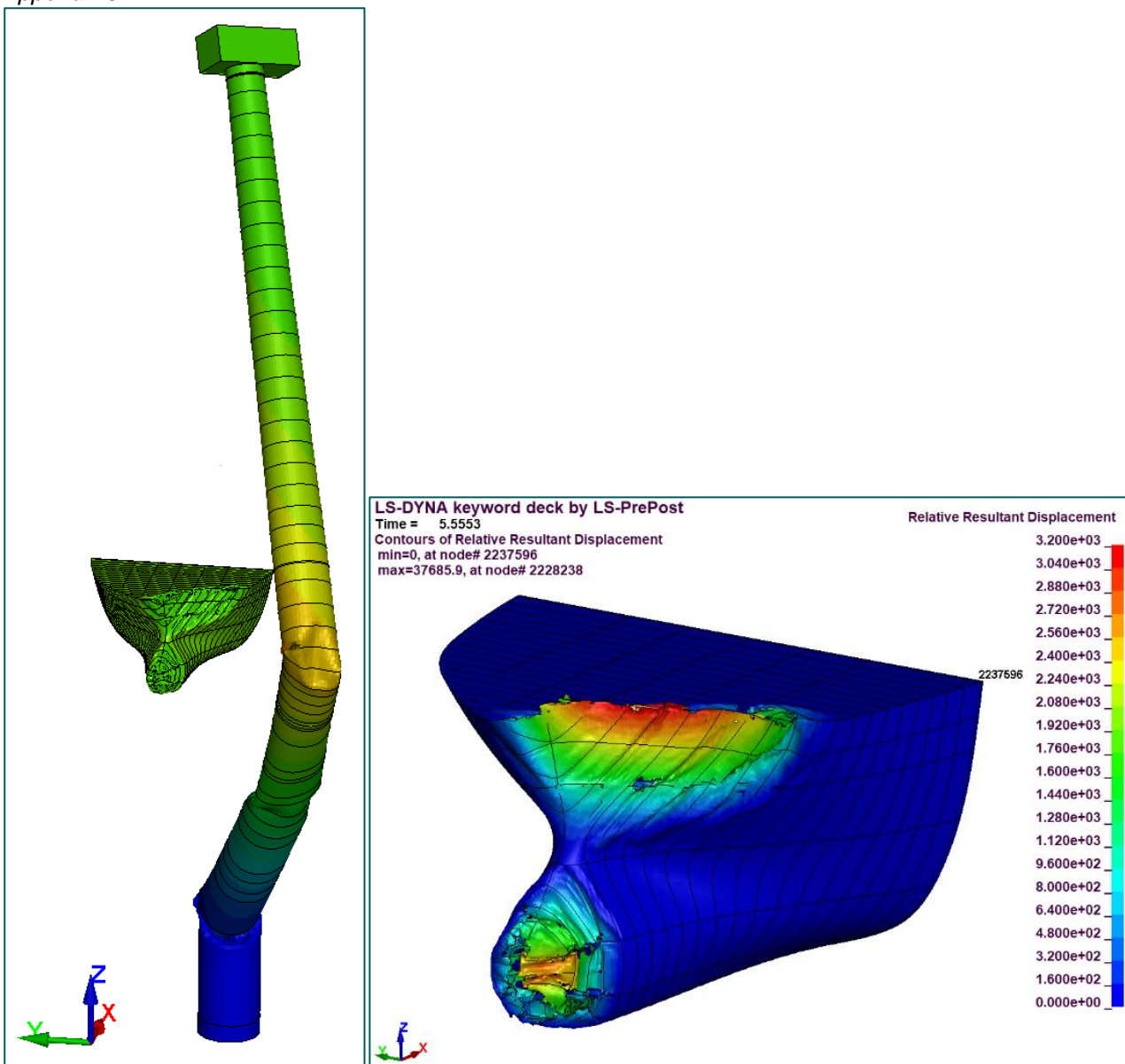


Figure 47. Global displacement (left) and deformation of ship [mm] (right) at end of simulation 2

### 7.1.1.3. Simulation 3 – SB side chemical tanker, 2 knots

In Simulation 3, the starboard (SB) side of the chemical tanker impacts the turbine tower at a speed of 1.03 m/s. The ship comes to a standstill due to the collision and will gradually drift away from the tower due to its elasticity. The damage to both the turbine foundation and the ship is limited to plastic deformation, with no effective plastic strain failure reached. *Figure 48* shows the displacement at the end of the simulation. All simulation results can be found in *Appendix J.1.3*.

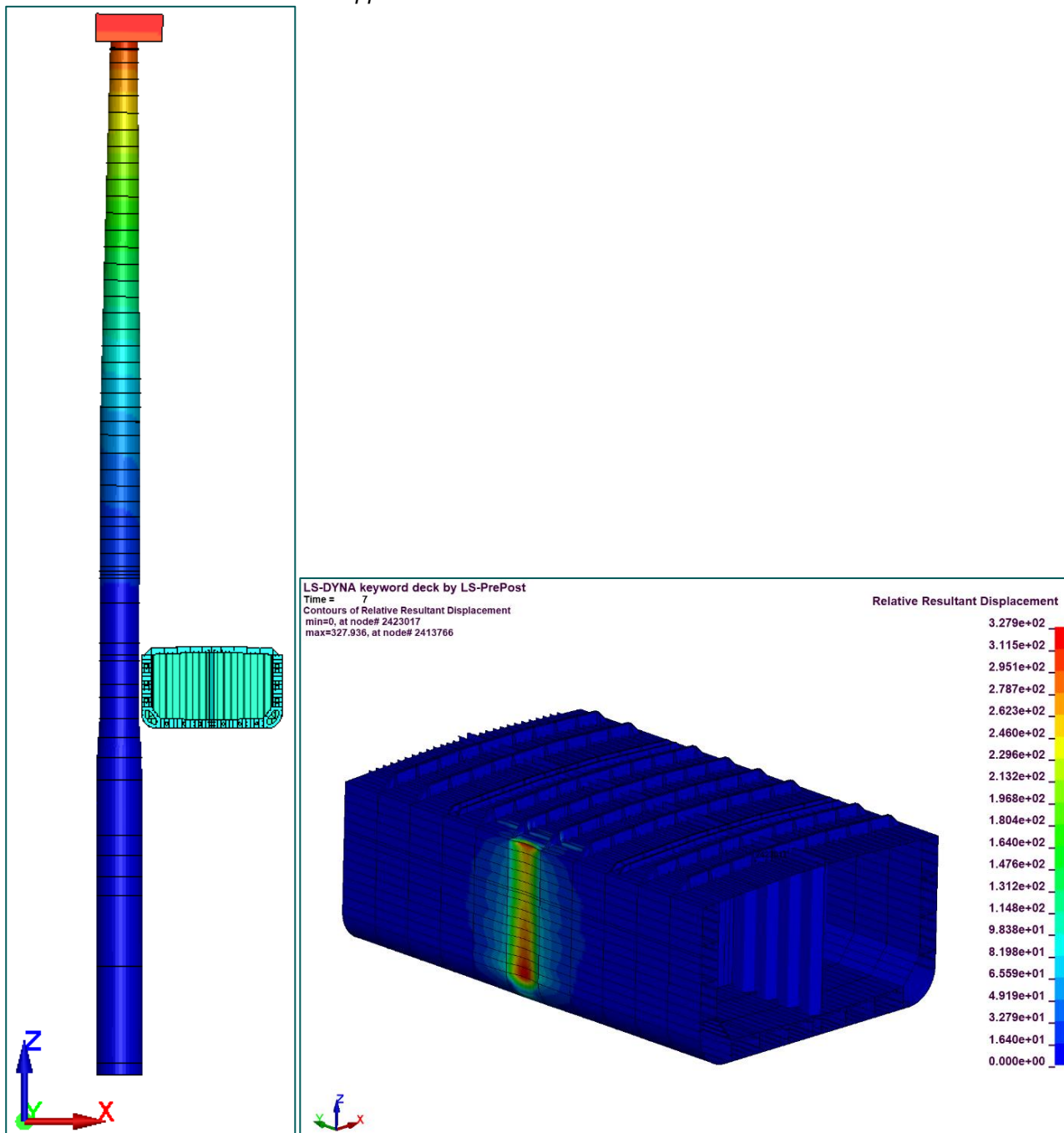


Figure 48. Global displacement (left) and deformation of ship [mm] (right) at end of simulation 3

#### 7.1.1.4. Simulation 4 – SB side chemical tanker, 4 knots

In simulation 4, the chemical tanker drifts with its SB side towards the turbine foundation at an initial speed of 2.06 m/s. Throughout the simulation, all kinetic energy from the ship is converted into internal energy, bringing the ship to a complete stop. By the end of the simulation, the turbine tower begins to collapse, as shown in *Figure 49*, left. The full visual timeline of the simulation is available in *Table 53* of *Appendix J.1.4*. The damage to the ship is confined to plastic deformations of both the outer and inner hull, with the maximum deformation of the outer hull reaching 0.74 meters, as depicted in *Figure 49*, right. The damage to both the turbine foundation and the ship is limited to plastic deformation, with no effective plastic strain failure reached.

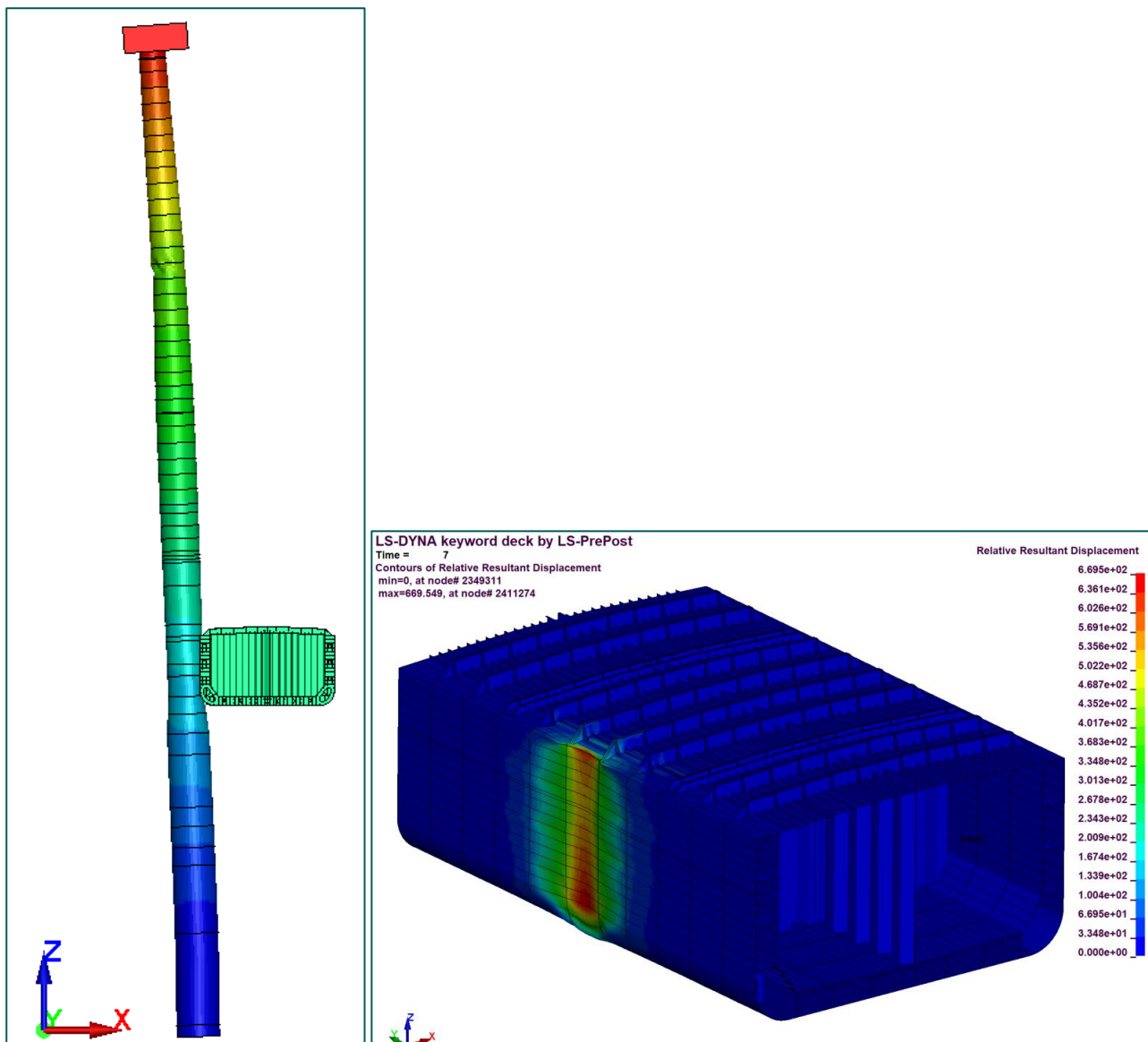


Figure 49. Global displacement (left) and deformation of ship [mm] (right) at end of simulation 4

### 7.1.2. Results Container Ship

This paragraph summarizes the findings from the four analyses carried out on the container ship. Each simulation is briefly explained, and illustrations are included to highlight the damage observed at the end of each simulation.

#### 7.1.2.1. Simulation 5 – Bow container ship, 10 knots

In this simulation, the container ship's bow collides with the turbine foundation at a speed of 5.14 m/s, resulting in the tower failing in three locations, as shown in *Figure 49* (left). The nacelle falls toward the ship, with a high likelihood that it will land on the ship. After the collision, the ship's speed decreases to 4.85 m/s. The damage to the bow is limited to plastic deformation, with no cracks observed, as seen in *Figure 49* (right). All analysis results are presented in *Appendix J.1.5*.

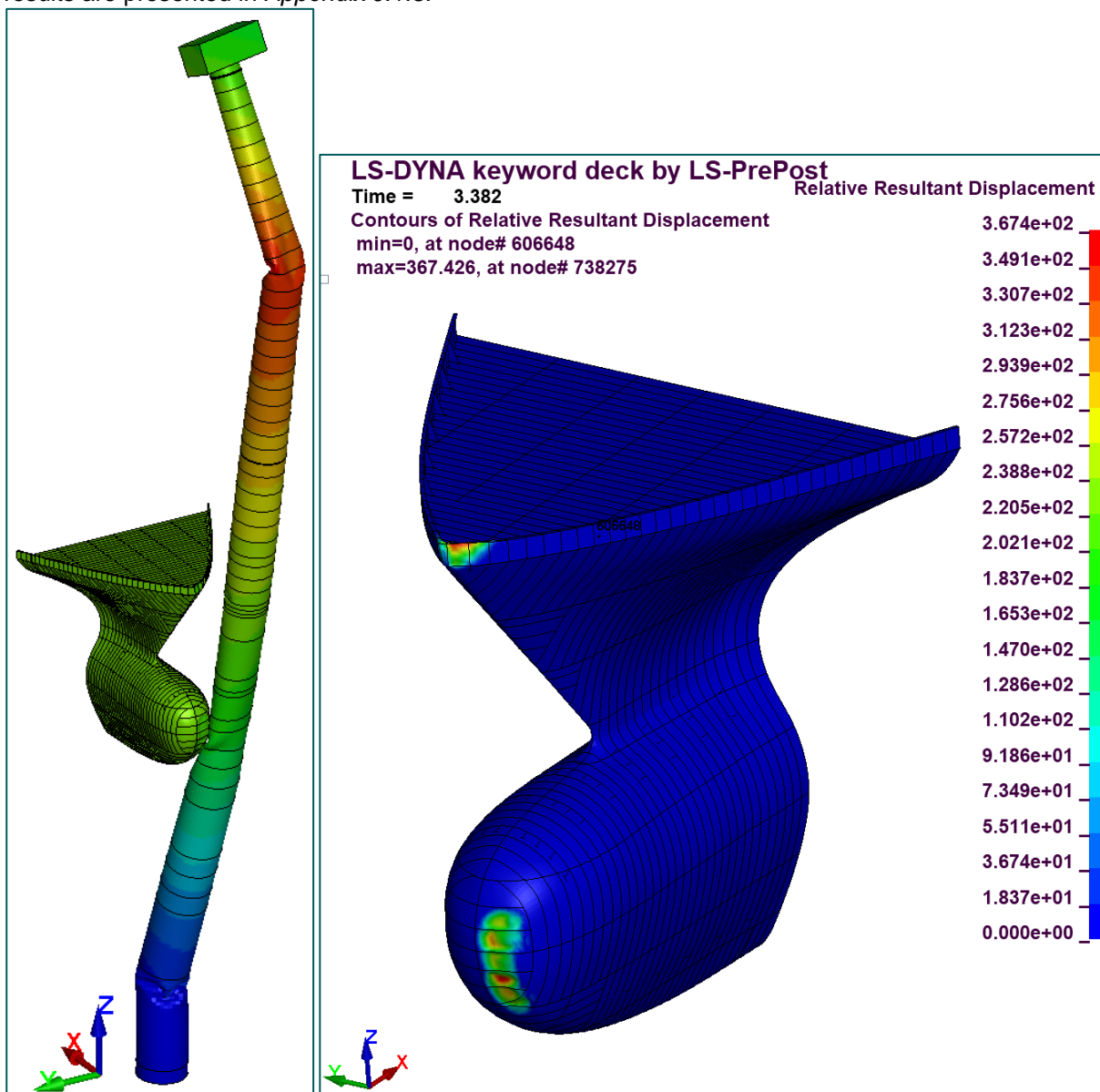


Figure 50 Global displacement (left) and deformation of ship [mm] (right) at end of simulation 5

### 7.1.2.2. Simulation 6 – Bow container ship, 20 knots

In simulation 6, the turbine tower is struck by the bow of the container ship at a speed of 10.29 m/s. As shown in *Figure 51* (left), the foundation tower fails at three distinct locations. The lowest location is at the ground level, while the other two points are at the height of the bulbous bow and the bow, which are in one line as described in *Paragraph 5.5.2.2*. As the tower collapses, the nacelle falls toward the ship, with a high likelihood of landing on it. A complete visual timelapse of the collision simulation is provided in *Table 55* of *Appendix J.1.6*.

The damage to the ship from the collision is minimal, consisting of small dents in the outer hull, as seen in *Figure 51*, right. Additionally, the ship's speed decreases from an initial value of 10.29 m/s to 10.1 m/s due to the impact, suggesting that the ship retains enough energy to continue sailing and potentially cause multiple subsequent impacts. All results from the simulation are available in *Appendix J.1.6*.

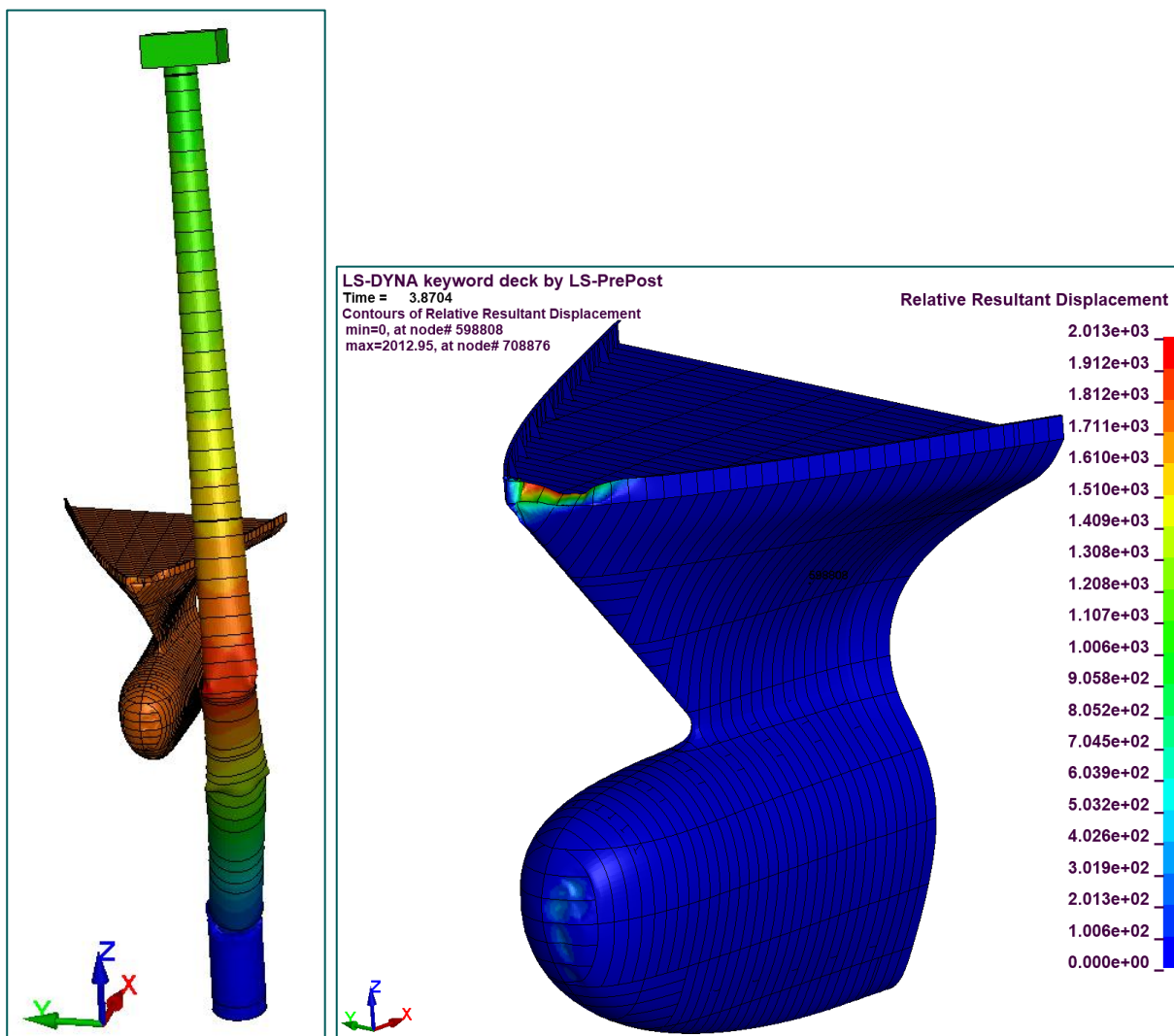


Figure 51 Global displacement (left) and deformation of ship [mm] (right) at end of simulation 6

### 7.1.2.3. Simulation 7 – SB side container ship, 2 knots

In Simulation 7, the SB side of the container ship impacts the turbine tower at a speed of 1.03 m/s. The ship gradually pushes the tower over, causing the upper soil layers to fail and the tower to break off beneath the seabed. This is the only location where the turbine foundation fails, resulting in the turbine falling off the ship. After the collision, the ship's speed is reduced to 0.73 m/s. The damage to the ship is limited to a small dent, see *Figure 52*. All simulation results are available in *Appendix J.1.7*.

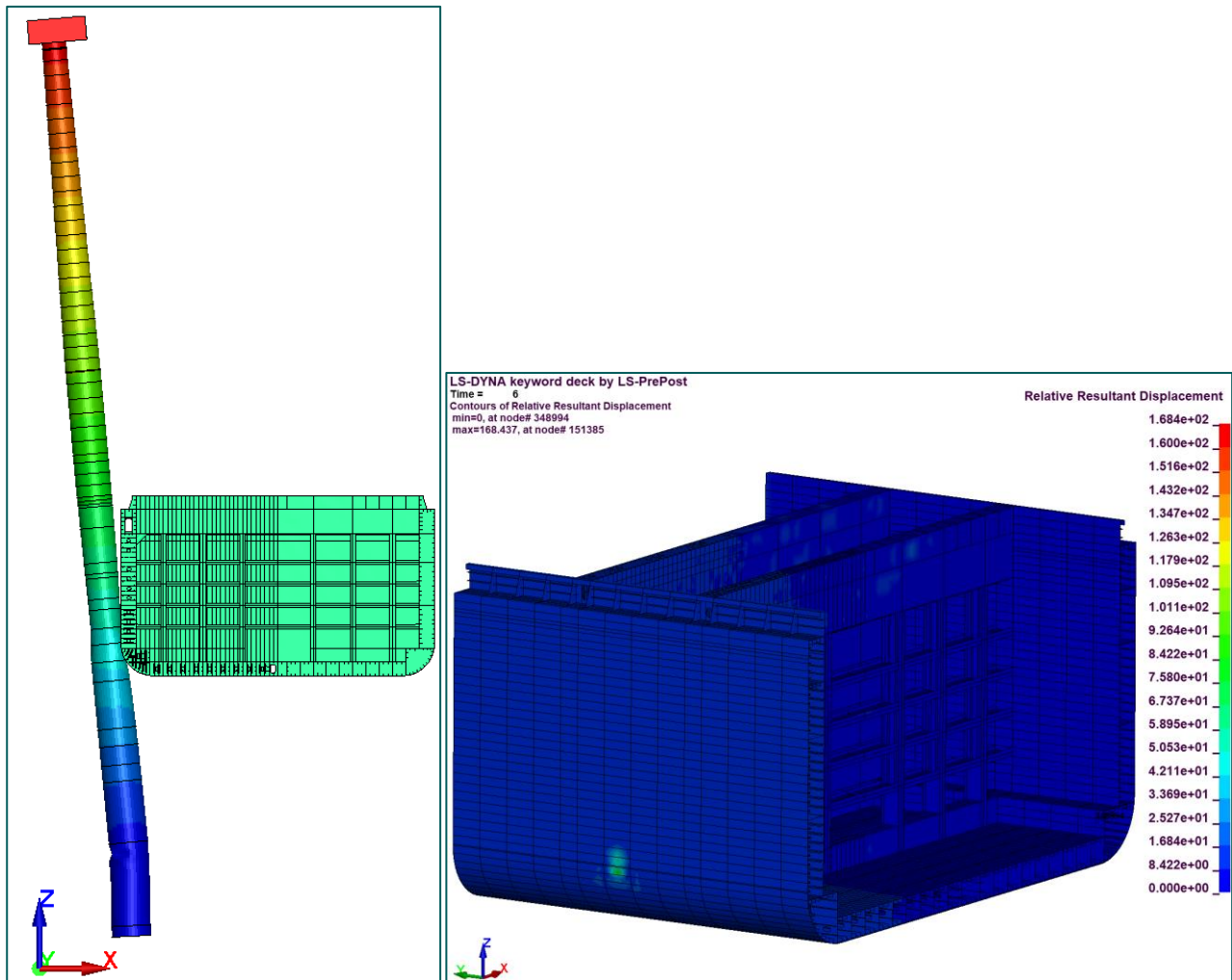


Figure 52. Global displacement (left) and deformation of ship [mm] (right) at end of simulation 7

#### 7.1.2.4. Simulation 8 – SB side container ship, 4 knots

In simulation 8, the SB side of the container ship impacts the turbine tower with a velocity of 2.06 m/s. Due to the high rigidity of the lower soil layers in the foundation, the impact force is sufficiently intense to cause the foundation tower to break at both the top and bottom, with the upper portion falling towards the ship, see *Figure 53*, left. By the end of the simulation, the tower foundation moves away from the ship at a speed greater than the final speed of the ship, resulting in no further contact between the two components. However, it is likely that the turbine will eventually land on the ship, as it falls in its direction.

The damage to the ship's hull is limited to a few dents in the outer surface, with no structural failure occurring, as shown in *Figure 53*, right. All simulation results can be found in *Appendix J.1.8*.

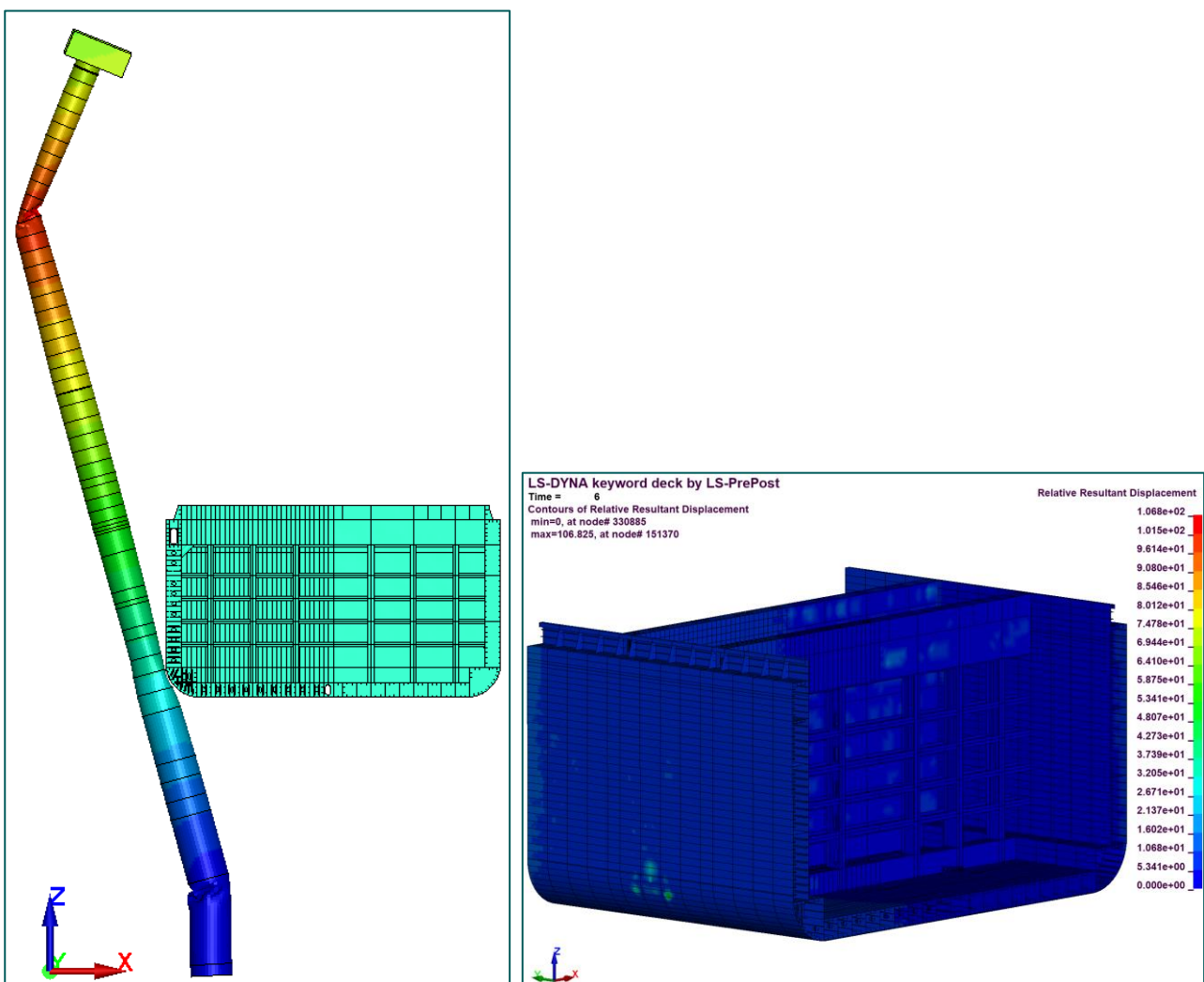


Figure 53. Global displacement (left) and deformation of ship [mm] (right) at end of simulation 8

### 7.1.3. Results Passenger Vessel

This paragraph outlines the outcomes of the four analyses performed on the passenger vessel. A brief description is provided for each simulation, accompanied by images that show the damage at the end of the simulation.

#### 7.1.3.1. Simulation 9 – Bow passenger vessel, 20 knots

In this simulation, the passenger vessel's bow collides with the turbine foundation at a speed of 10.29 m/s, causing the tower to fail in two locations, as shown in *Figure 54* (left). The nacelle falls toward the ship, with a high likelihood of landing on the ship. After the collision, the ship's speed decreases to 9.05 m/s.

The bow sustains significant damage, with the collision causing upward deformation, as seen in *Figure 54* (right). The bow tip, which is the initial point of contact, extends beyond the bulbous bow. The damage to the bow occurs above the waterline and ahead of the first bulkhead, meaning there is no environmental impact and no risk to the ship's stability. All analysis results are presented in *Appendix J.1.9*.

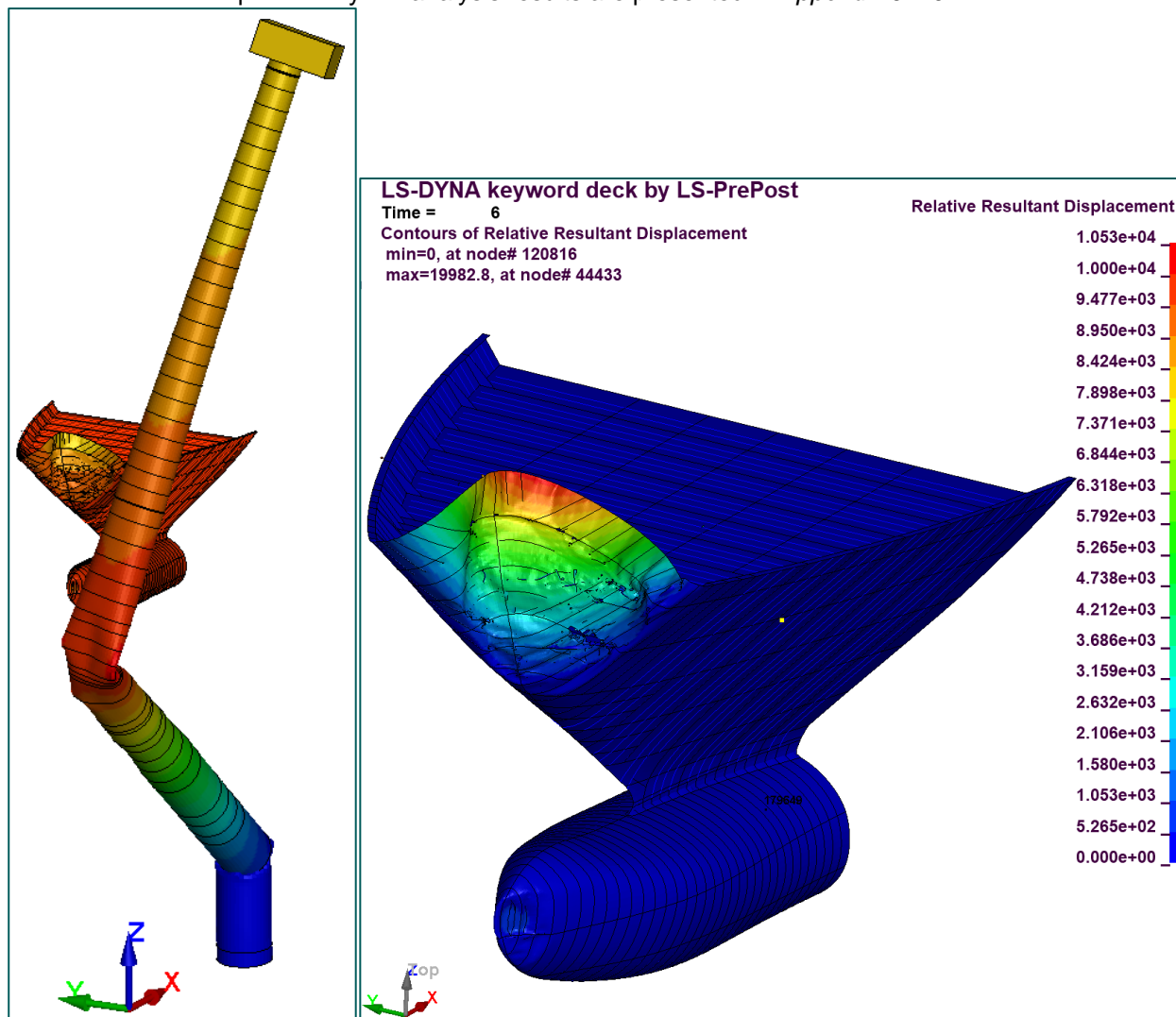


Figure 54. Global displacement (left) and deformation of ship [mm] (right) at end of simulation 9



### 7.1.3.2. Simulation 10 – Bow passenger vessel, 30 knots

In simulation 10, the bow of the passenger vessel collides with the turbine tower at a speed of 15.43 m/s. This impact leads to the failure of the turbine foundation at two locations and resulting in significant damage to the bow tip, as shown in *Figure 55*. However, this damage does not pose any risks to the ship or the environment. As the tower collapses, the turbine falls toward the ship, with a high likelihood of landing on it. Following the collision, the ship's speed has decreased to 14.6 meters per second. More simulation results are available in *Appendix J.1.10*.

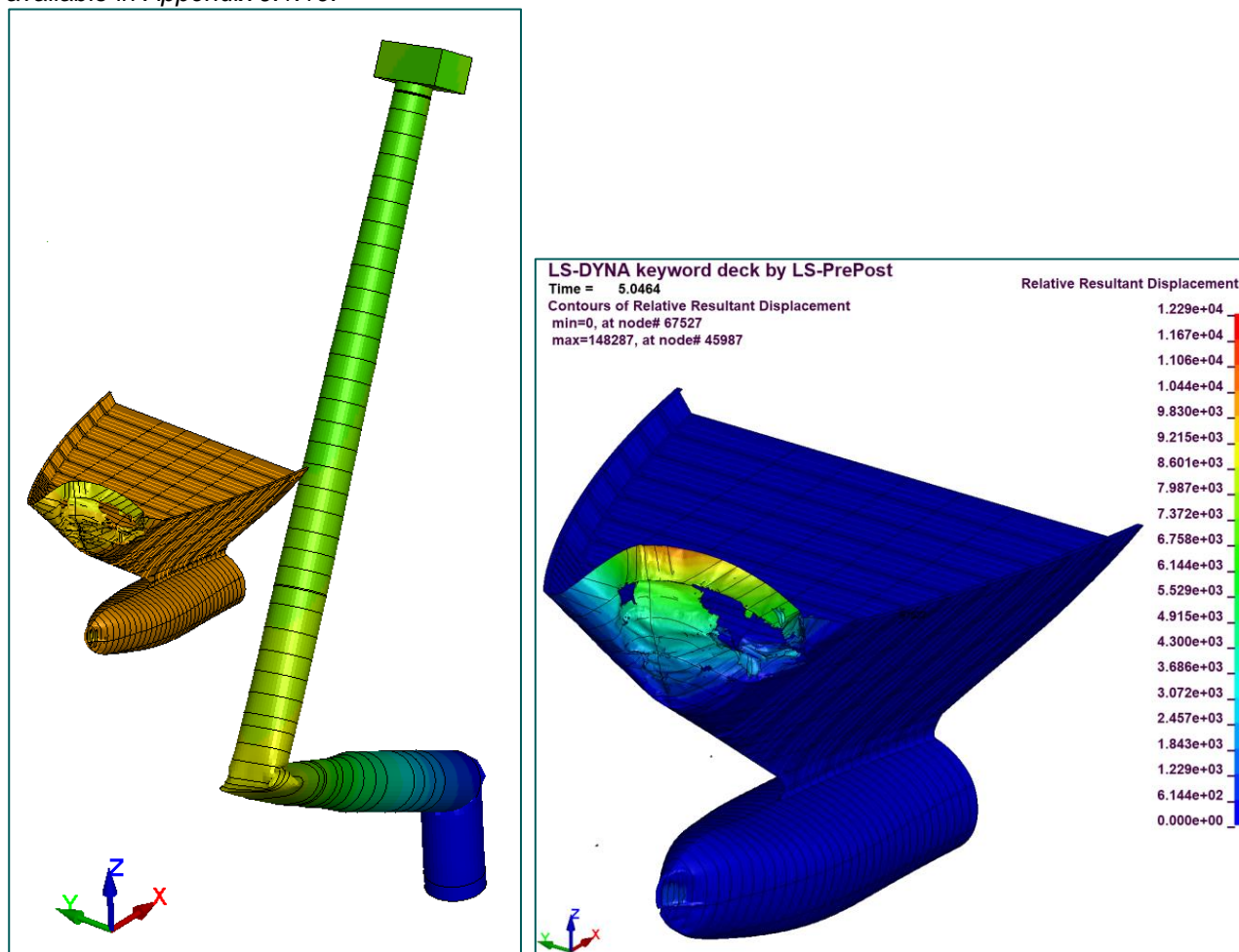


Figure 55. Global displacement (left) and deformation of ship [mm] (right) at end of simulation 10

### 7.1.3.3. Simulation 11 – SB side passenger vessel, 2 knots

In Simulation 11, the passenger vessel drifts with its SB side towards the turbine foundation at an initial speed of 1.03 meters per second. Throughout the simulation, all of the ship's kinetic energy is converted into internal energy, bringing the ship to a complete stop. The damage to the ship at the end of the simulation is limited to plastic deformation only, see *Figure 56*. All analysis results are presented in *Appendix J.1.11*.

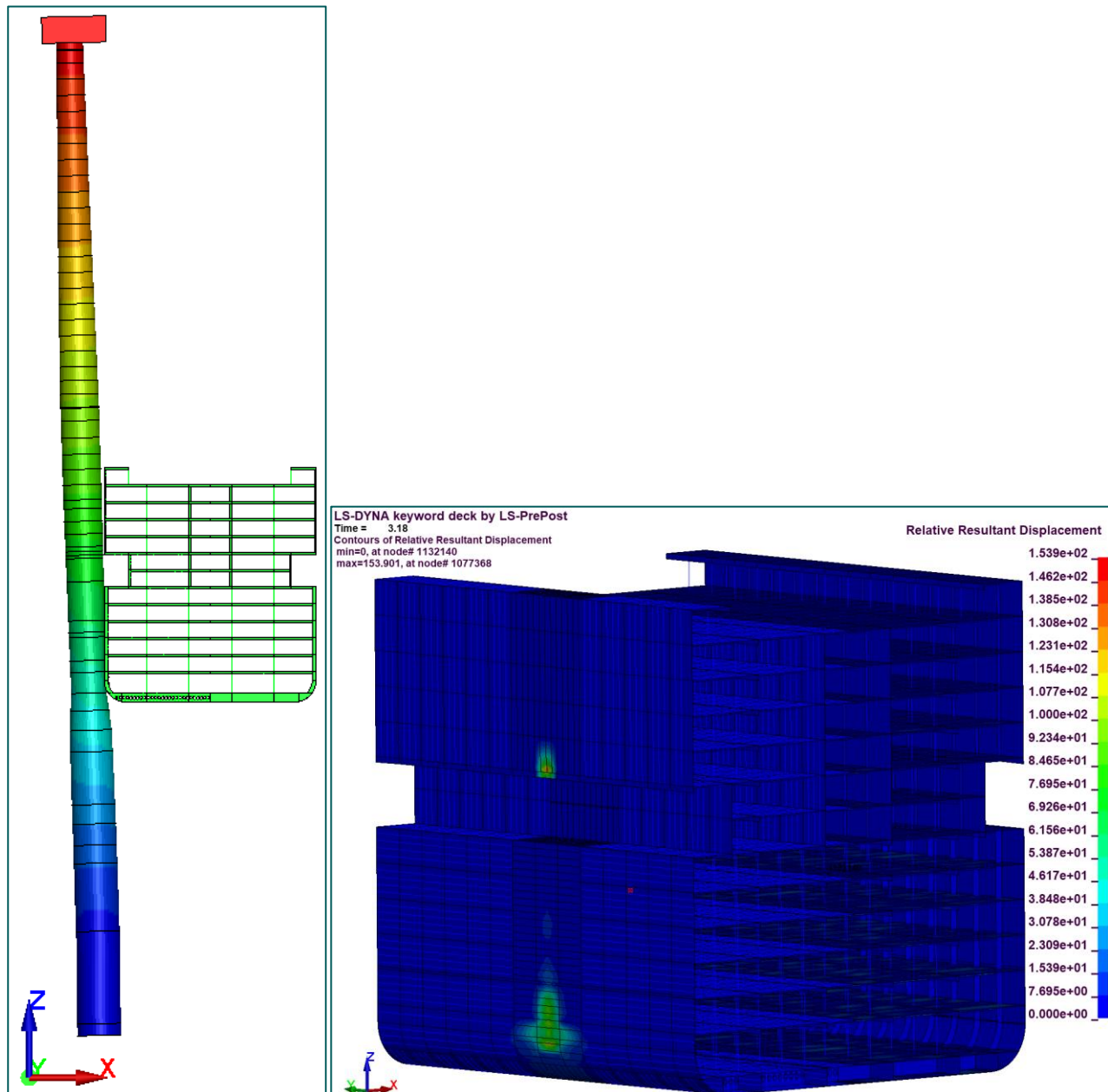


Figure 56. Global displacement (left) and deformation of ship [mm] (right) at end of simulation 11

#### 7.1.3.4. Simulation 12 – SB side passenger vessel, 4 knots

In simulation 12, the SB side of the passenger vessel impacts the turbine tower, causing it to break off at the ground level. As a result, the tower falls off the ship and does not land on it. After the collision, the vessel's remaining velocity is 0.8 meters per second. The damage to the ship is minimal, consisting of a few dents in the outer surface, as shown in *Figure 57*. Additional simulation results can be found in *Appendix J.1.12*.

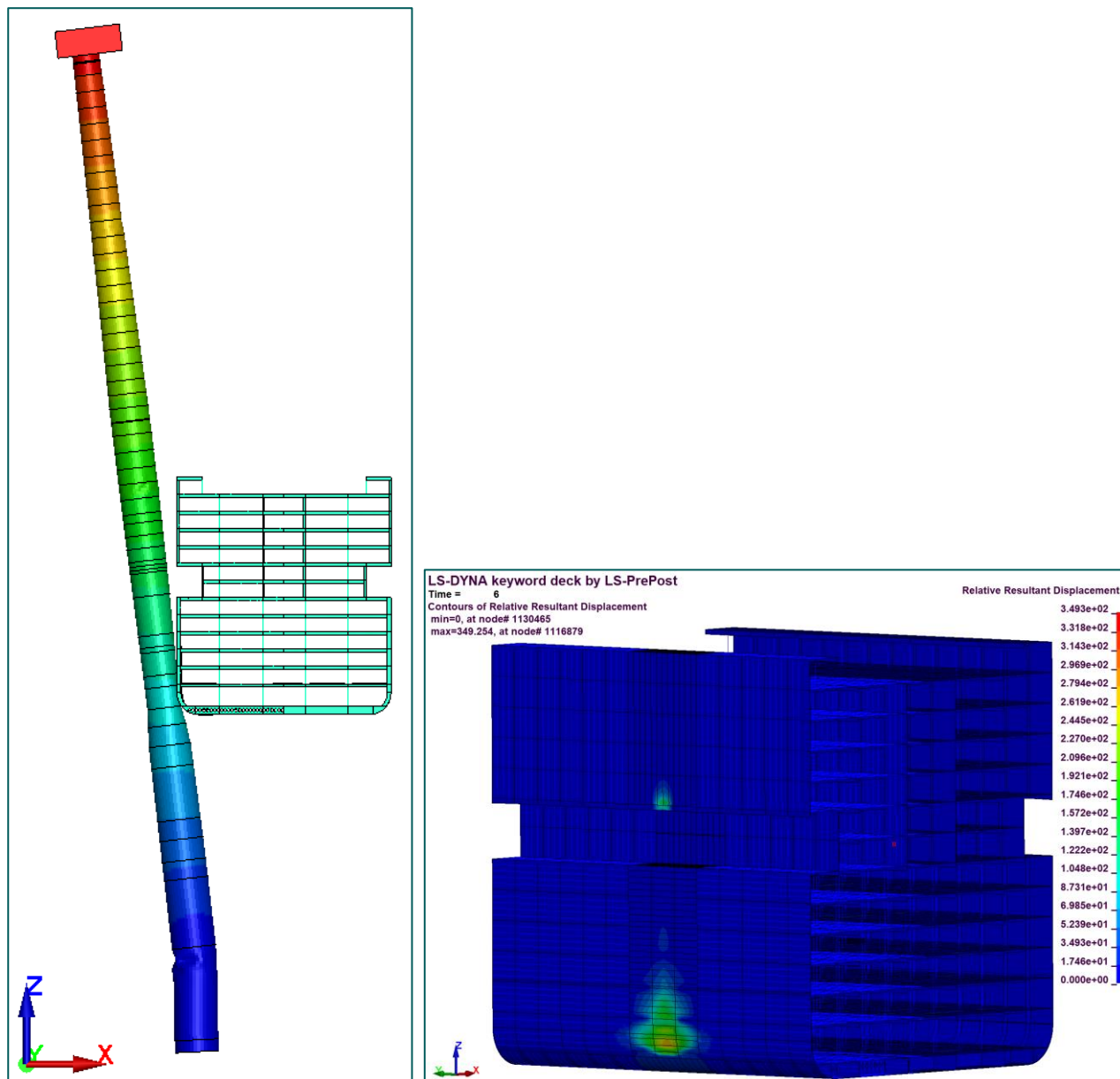


Figure 57. Global displacement (left) and deformation of ship [mm] (right) at end of simulation 12

#### 7.1.4. Ship damage results summary

This section summarizes the damage results for each simulation. *Table 31, 32 & 33* present the results for the chemical tanker, container ship, and passenger vessel, respectively. Additional details on the results for each simulation are available in the corresponding *Appendices J.1.1 to J.1.12*.

Table 31. Damage summary Chemical Tanker Simulation

Chemical Tanker							
#	Ship motion	Initial Speed [knots]	Initial Speed [m/s]	Speed at end time [m/s]	Wind	Impact part	Damage
1	Sailing	10	5.14	1.8	Perpendicular direction	Bow	Yes, but no leakage or risk of instability
2	Sailing	20	10.29	8.1	Perpendicular direction	Bow	Yes, but no leakage or risk of instability
3	Drifting	2	1.03	0.0	Drifting direction	SB side	Yes, but effective plastic strain failure not reached in the outer hull
4	Drifting	4	2.06	0.0	Drifting direction	SB side	Yes, but effective plastic strain failure not reached in the outer hull

Table 32. Damage summary Container Ship Simulation

Container Ship							
#	Ship motion	Initial Speed [knots]	Initial Speed [m/s]	Speed at end time [m/s]	Wind	Impact part	Damage
5	Sailing	10	5.14	4.85	Perpendicular direction	Bow	Yes, small dent in outer hull
6	Sailing	20	10.29	10.1	Perpendicular direction	Bow	Yes, small dent in outer hull
7	Drifting	2	1.03	0.7	Drifting direction	SB side	Yes, small dent in outer hull
8	Drifting	4	2.06	1.82	Drifting direction	SB side	Yes, small dent in outer hull

Table 33. Damage summary Passenger Vessel Simulation

Passenger Vessel							
#	Ship motion	Initial Speed [knots]	Initial Speed [m/s]	Speed at end time [m/s]	Wind	Impact part	Damage
9	Sailing	20	10.29	9.1	Perpendicular direction	Bow	Yes, but no leakage or risk of instability
10	Sailing	30	15.43	14.6	Perpendicular direction	Bow	Yes, but no leakage or risk of instability
11	Drifting	2	1.03	0.0	Drifting direction	SB side	Yes, small dent in outer hull
12	Drifting	4	2.06	0.8	Drifting direction	SB side	Yes, small dent in outer hull

### 7.1.5. Foundation soil-interaction results summary

This section presents an overview of the foundation soil interaction results for each simulation. The results for the chemical tanker, container ship, and passenger vessel are shown in *Table 34*, *35* & *36*, respectively. The tables also indicate the failure modes of the turbine foundation (third column), which are explained in further detail in *Section 7.1.7*. The fall velocity is the velocity in z direction of the nacelle at the end of the simulation. More information on the results for each simulation can be found in *Appendices J.1.1* to *J.1.12*. *Appendix J* illustrates the deformation of soil springs and their reaction forces.

Table 34. Summary Foundation Chemical Tanker Simulations

#	Ship motion	Foundation failure / Failure mode	Failure location [m LAT]	Collapse direction	Impact force [MN]	Fall velocity nacelle [m/s]
1	Sailing	Yes (5)	-45.6	Away from ship	43	1.9
2	Sailing	Yes (7)	-45.6 -5.0 +30.51	Towards the ship	54	22.9
3	Drifting	No (1)	0	Doesn't collapse	22	-
4	Drifting	Yes (2)	+69.41	Simulation too short to say	31	-

Table 35. Summary Foundation Container Ship Simulations

#	Ship motion	Foundation failure / Failure mode	Failure location [m LAT]	Collapse direction	Impact force [MN]	Fall velocity nacelle [m/s]
5	Sailing	Yes (7)	-45.6 -5.0 +77.7	Towards the ship	15	8.4
6	Sailing	Yes (7)	-45.6 -5.0 +19.95	Towards the ship	25	13.1
7	Drifting	Yes (6)	-45.6	Away from ship	29	0.3
8	Drifting	Yes (8)	-45.6 +77.7	Towards the ship	37	4.3

Table 36. Summary Foundation Passenger Vessel Simulation

#	Ship motion	Foundation failure / Failure mode	Failure location [m LAT]	Collapse direction	Impact force [MN]	Fall velocity nacelle [m/s]
9	Sailing	Yes (7)	-45.6 +19.95	Towards the ship	66	18.9
10	Sailing	Yes (7)	-45.6 +19.95	Towards the ship	69	26.6
11	Drifting	No (1)	-	Simulation too short to say	25	-
12	Drifting	Yes (8)	-45.6	Away from ship	31	0.4



### 7.1.6. General results summary

This paragraph provides a summary of the overall results from the simulations. The tables below offer insight into the energy levels from the analyses, as well as the maximum deformation observed in both the foundation tower and the ship. The simulations vary in duration, depending on when the ship model detaches from the turbine foundation and no further energy is transferred. *Table 37, 38 & 39* present the results for the chemical tanker, container ship, and passenger vessel, respectively. Additional details on the results for each simulation are available in the corresponding *Appendices J.1.1 to J.1.12*.

Table 37. Summary Chemical Tanker Simulation

Chemical Tanker Simulation	1	2	3	4
Ship Motion	Sailing	Sailing	Drifting	Drifting
Total simulation time [sec]	5.2	5.5	7	7
Initial kinetic energy ship [MJ]	292	1167	21	82
Kinetic energy ship at end time [MJ]	36	727	-	-
Max. internal energy ship [MJ]	38	69	5	15
Internal energy ship at end time [MJ]	37	66	4	15
Max. deformation ship [m]	2.2	3.2	0.33	0.74
Max. deformation foundation [m]	32.2	64.0	0.9	8.2

Table 38. Summary Container Ship Simulation

Container Ship Simulation	5	6	7	8
Ship Motion	Sailing	Sailing	Drifting	Drifting
Total simulation time [sec]	3.4	3.9	6	6
Initial kinetic energy ship [MJ]	3098	12396	218	873
Kinetic energy ship at end time [MJ]	2754	11943	101	683
Max. internal energy ship [MJ]	8	13	-	-
Internal energy ship at end time [MJ]	8	13	-	-
Max. deformation ship [m]	0.4	2.0	0.2	0.1
Max. deformation foundation [m]	28.0	44.6	14.9	34.8

Table 39. Summary Passenger Vessel Simulation

Passenger Vessel Simulation	9	10	11	12
Ship Motion	Sailing	Sailing	Drifting	Drifting
Total simulation time [sec]	5.55	5.05	5.55	6
Initial kinetic energy ship [MJ]	2373	5340	42	167
Kinetic energy ship at end time [MJ]	1856	4779	-	25
Max. internal energy ship [MJ]	-	-	-	-
Internal energy ship at end time [MJ]	-	-	-	-
Max. deformation ship [m]	10.5	12.29	0.2	0.3
Max. deformation foundation [m]	62.3	70.0	5	23.5

For results of plastic strains, see *Appendices J.1.1 to J.1.12*.



### 7.1.7. Comparison of different ship types

In this section the damage of the different ship types is compared. The comparison of ship collisions can be divided into a ship's bow and the ship's SB sidel. For all ship types, more damage occurs in a collision at high speed than at low speed.

#### 7.1.7.1. Ship's bow

As outlined in *Section 4.3*, the bow shapes of the three ship types vary. On the chemical tanker, the bulb extends further than the bulwark. In contrast, the bulwark of the passenger ship extends farther forward than the bulb. On the container ship, the bulb and bulwark protrude equally, leading to two initial contact points at the collision impact.

In addition to the differences in bow shape and the number of initial contact points between the ship and the monopile, the size of the bow also varies across ship types. *Section 5.5* provides the overall dimensions for each ship, with the chemical tanker's bow having a height of 12 meters, the container ship's bow measuring 32.6 meters, and the passenger ship's bow at 24 meters. These geometric differences result in variations in plate thickness and the number of internal stiffeners. Naturally, larger bow dimensions results in thicker plates.

The previous paragraphs clearly show that the Chemical Tanker's bulb sustains the most severe damage compared to the bulbs of the other ships, with a deformation exceeding 3 meters. Additionally, some elements fail in this simulation. The deformation at the bulb of the passenger ship and container vessel measures 0.8 meters and 0.3 meters, respectively. Furthermore, the damage to the container vessel is limited to a dent where no elements fail.

Among the various ship types, the passenger vessel's bulwark sustains the most damage, with a displacement of 8.3 meters. This is due to the bow design, which makes it the first point of contact in a collision and because this type of ship has a higher velocity. The bulwark deformation measures 3.2 meters for the chemical tanker and less than 1 meter for the container ship. Additionally, when looking at the stiffness of the different bulwarks, it can also be concluded that the container ship has the most stiffness and the passenger ship has the least stiffness.

#### 7.1.7.2. Ship's SB side

In the simulations of the starboard side, the chemical tanker experiences the most deformation, followed by the passenger vessel and the container ship. For all ship types, the damage remains limited to a dent without any element failures, avoiding significant consequences. The smallest ship sustains the most damage, while the largest ship sustains the least. This is due to the increased stiffness and larger contact surface of bigger ships, which help distribute the force over a bigger area.

### 7.1.8. Comparison with previous study

In this paragraph a comparison is do between the results from this study and the previous study preformed by HVR [ref. 4]. In this previous study several failure mode are determined that are shown in *Figure 58 & 59*.

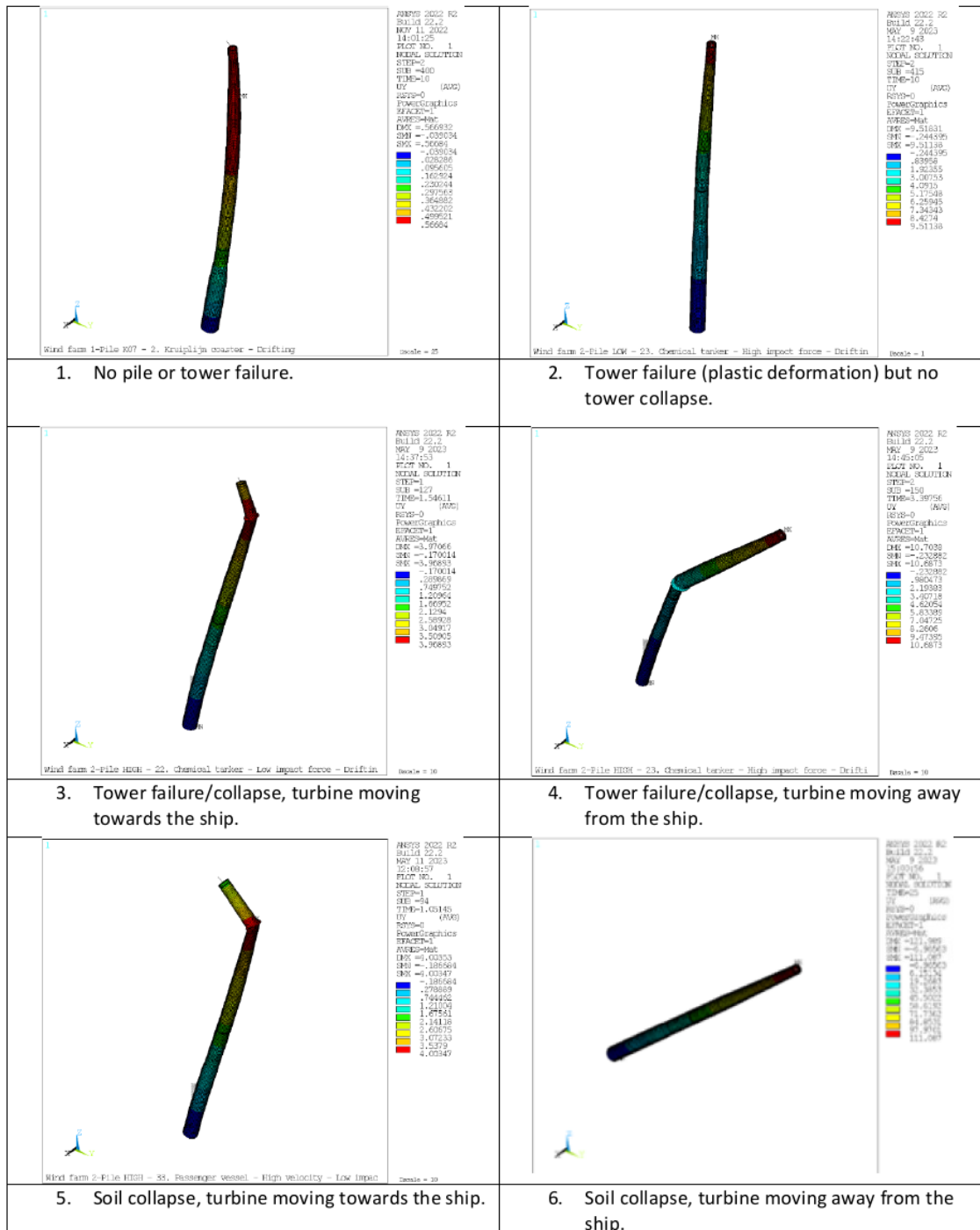


Figure 58 - Failure modes table 2.3 previous study HVR [ref. 4]



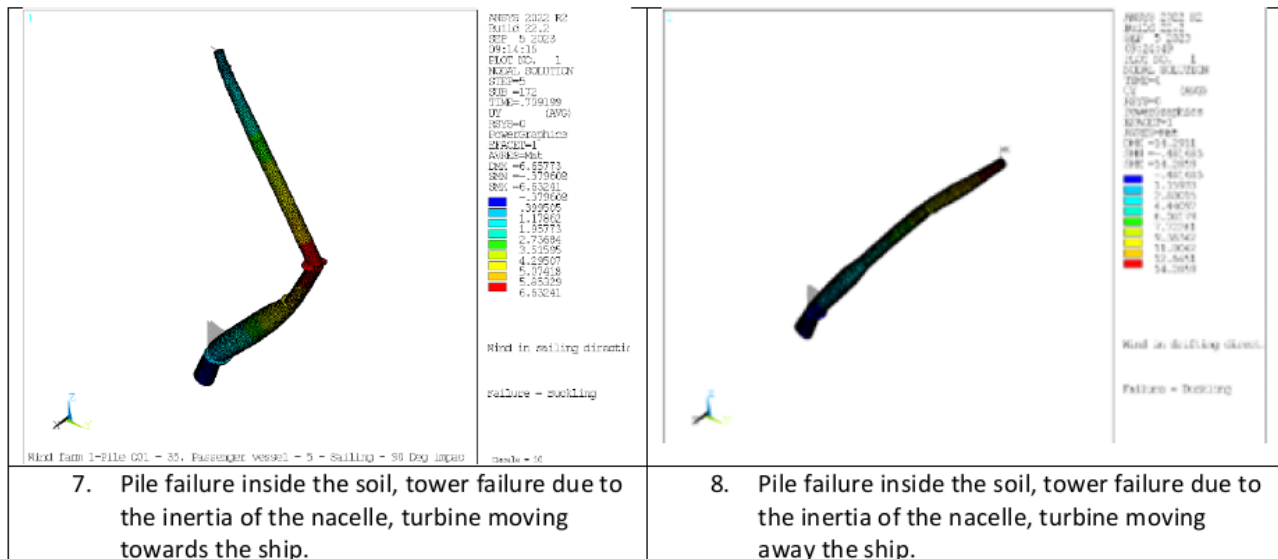


Figure 59- Failure modes table 2.4 previous study HVR [ref. 4] (continue)

In Table 40 for each ship collision the result is expressed in one of the failure modes. In the 3rd column of the table the failure modes are shown from the previous study in the last column the failure mode is shown of this study.

Table 40 - Failure modes comparison

Ship type	Ship Motion	Failure mode from Previous study HVR	Failure mode from this study
Chemical Tanker	Sailing	4 (Tower failure)	7 (Pile failure)
	Drifting	5 (Soil collapse)	2 (Tower failure)
Container Shipp	Sailing	4 (Tower failure)	7 (Pile failure)
	Drifting	5 (Soil collapse)	8 (Pile failure)
Passenger Vessel	Sailing	6 (Soil collapse)	7 (Pile failure)
	Drifting	5 (Soil collapse)	8 (Pile failure)

The result comparison in Table 40 shows differences between the failure modes, with the largest variations attributed to soil stiffness. In this study, a dynamic amplification factor has been applied to taking into account the increased stiffness of the soil springs during collision. This results in different failure modes of the wind turbine under the same collision condition, that soil collapse was mainly observed in the previous study, while pile failure is mostly the failure mode resultant from this study.

An additional comparison was performed between this study and the previous one, with results provided in *Appendix H*. The results indicate minor differences, demonstrating the global stiffness and mass of the support structure remain identical in both studies and thus verified.

## 7.2. Results nacelle Dropping

Along with the twelve ship collision analyses, two additional simulations were conducted to assess the damage resulting from the failure of the foundation tower and the subsequent landing of the nacelle on the ship. Due to the nacelle's elongated shape, two separate analyses were performed, which are described in *Paragraphs 7.2.1 & 7.2.2*. The first simulation evaluates the damage caused when the nacelle falls vertically onto the ship ('nose down'), while the second analysis examines the impact of the nacelle falling horizontally onto the ship (nacelle falling on its side). The principles for this simulation are outlined in *Section 6.2*.

The nacelle drop simulation was selected to be conducted in conjunction with the passenger vessel for the following reasons:

- Containers were not modeled, making the container ship unrealistic and yielding unreliable results.
- In an earlier stage of the investigation, the nacelle appeared to fall off the ship when hit by the chemical tanker.
- The impact with the passenger ship would result in the highest number of casualties, making it the most critical scenario to analyze.

The initial velocity of the nacelle at the moment of impact was based on the fall velocity observed during the ship collision simulations with the bow of the three ship types. *Figure 60* illustrates the velocity of the nacelle for each analysis, plotted against height, and includes the trend line of these velocities. The upper deck of the passenger ship is located at a height of 30.5 m LAT, where the nacelle has a theoretical fall velocity of 31.55 meters per second.

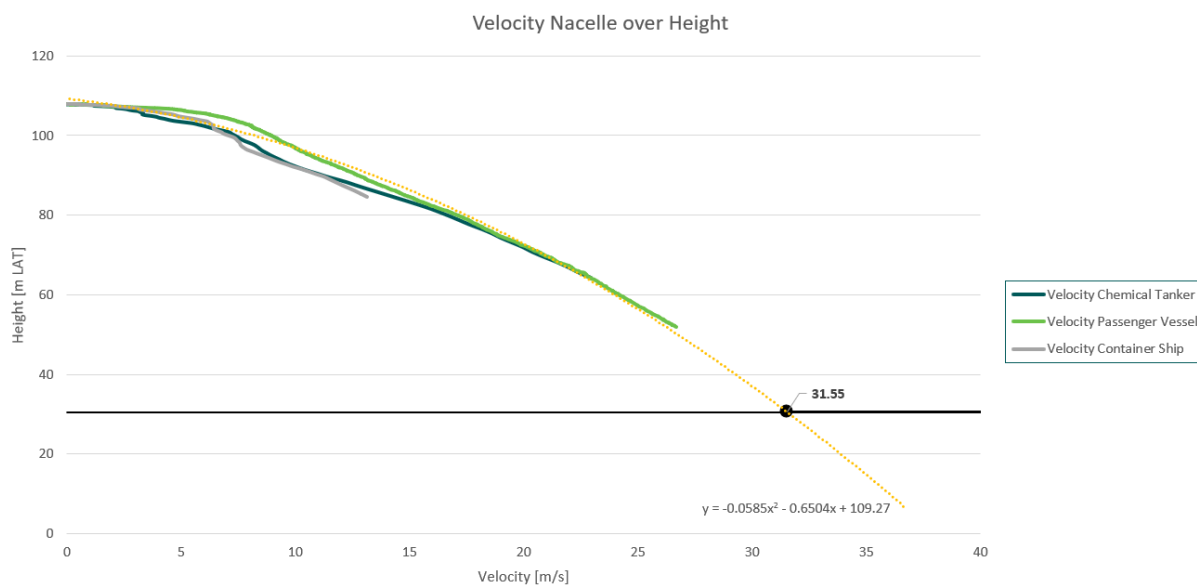


Figure 60. Fall velocity nacelle over height compared to passenger upper deck height

It is important to note that the assumed rigid constraints on the outer end of the mid-section play a significant role in these results. Additionally, the presumed rigid nacelle geometry is a crucial factor in determining the extent of the damage. These assumptions influence both the vertical and horizontal impact simulations, affecting the penetration depth and deformation patterns observed in the passenger ship.

### 7.2.1. Vertical Impact

This section presents the results of the simulation in which the nacelle falls vertically onto the upper deck of the passenger ship with an initial velocity of 31.55 meters per second. After 1.5 seconds, the nacelle stops and penetrates more than half depth of the passenger vessel as illustrated in *Figure 61*. A complete visual timelapse is provided in *Table 62* of *Appendix J.2.1*. As shown, the nacelle penetrates the ship, passing through seven consecutive decks, while the eighth deck experiences significant plastic deformation.

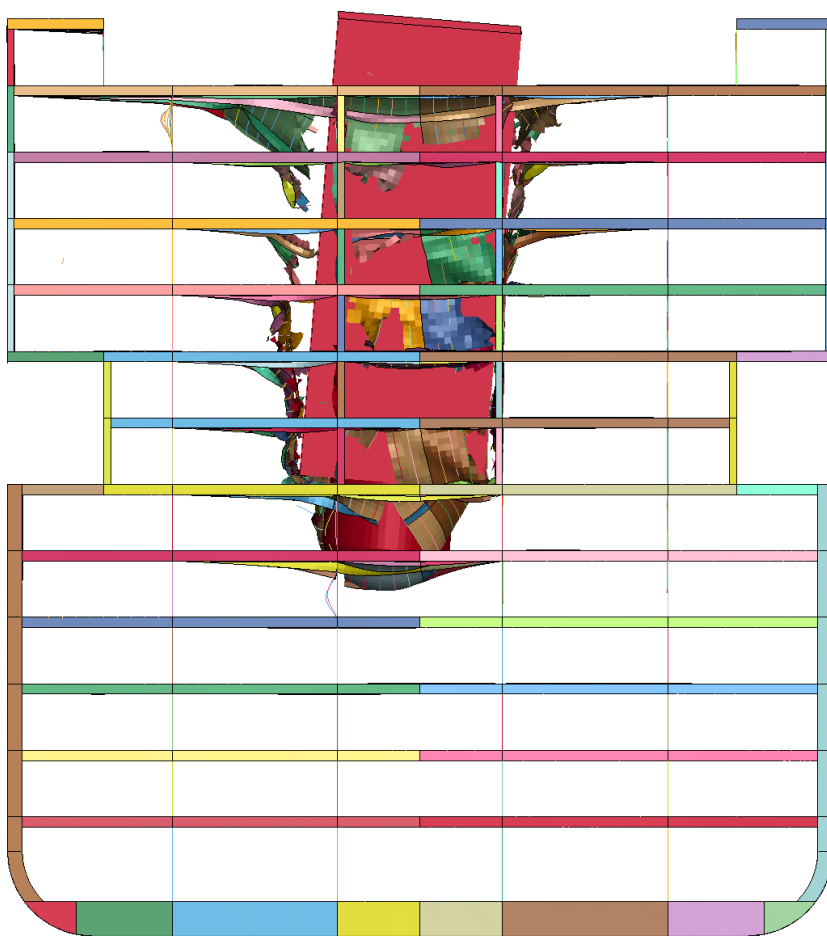


Figure 61. Displacement at end of simulation

### 7.2.2. Horizontal Impact

Figure 62 illustrates the impact at the end of the simulation. The complete visual timelapse can be found in Table 63 in Appendix J.2.2. As shown, the nacelle does not pass through the upper deck. Instead, the upper deck of the passenger vessel deforms, causing the nacelle to rebound upward. By the end of the simulation, the nacelle settles on top of the ship, while the upper two decks undergo significant deformation.

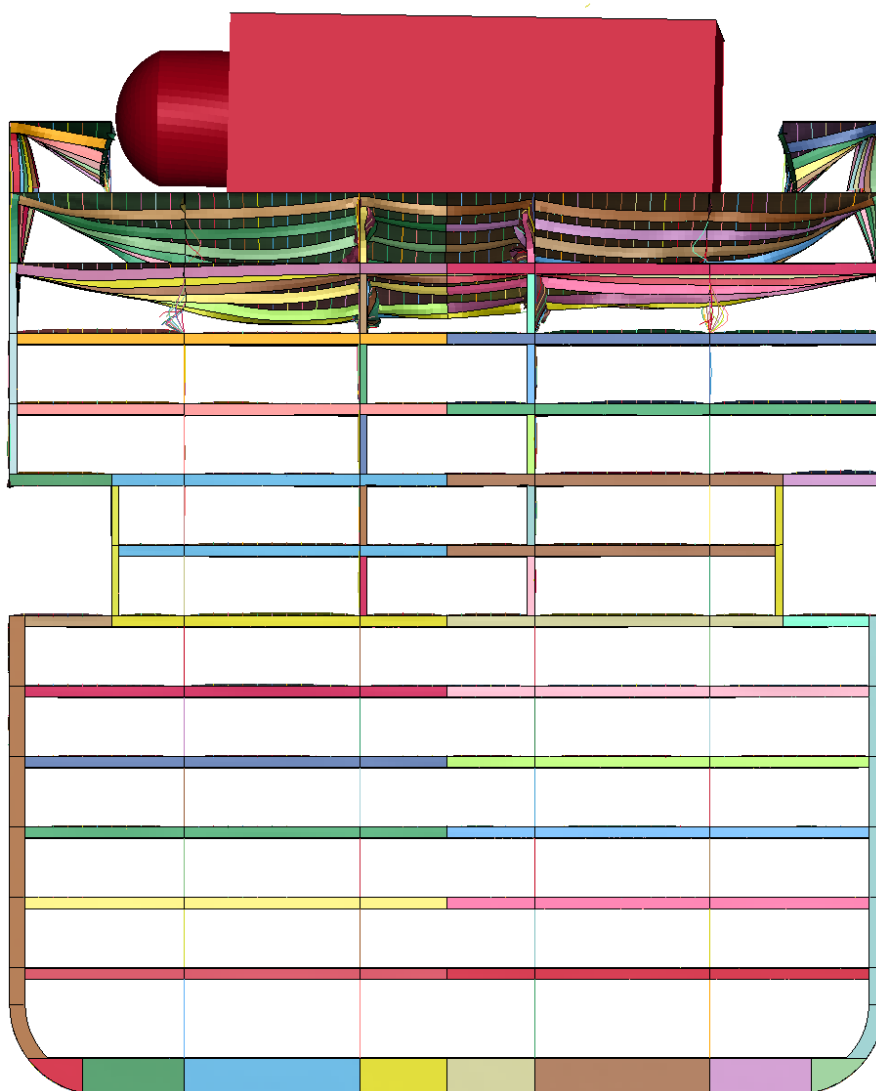


Figure 62. Displacement at end of simulation



## 8 Conclusions and recommendations (DP5)

---

The study comprehensively analyzed the effects of ship collisions on wind turbine support structures using explicit dynamic analysis with 3D Finite Element Modeling (FEM). By simulating various collision scenarios, including impacts from chemical tankers, container ships, and passenger vessels with different velocities and impact directions, the research identified limited damage to the ships. However, the turbine support structure exhibited different failure modes depending on the impact scenario, highlighting the structural response variations under different loading conditions.

Key findings revealed that the severity of damage depends on the ship type, collision orientation, and velocity. Sailing collisions posed a greater risk to turbine stability, while drifting impacts highlighted vulnerabilities in the ships' structural integrity. In drifting collisions, large areas of damage were observed, but the results remained below the effective plastic strain limits. Only localized small areas of material failure were detected, which did not compromise the ship's structural integrity or buoyancy. In sailing collisions, ships exhibited large areas where the effective plastic strain failure threshold was reached; however, the damage did not extend to the collision bulkhead, preserving both structural integrity and buoyancy. Additionally, damage to the forepart in these scenarios did not compromise ship stability or buoyancy. Among the analyzed ship types, the chemical tanker and the passenger vessel sustained the most damage in sailing impacts.

For falling nacelle scenarios, the results indicate that a vertically falling nacelle can penetrate multiple decks, causing extensive structural damage. In contrast, the horizontal impact simulation showed that the nacelle did not penetrate the first deck but instead caused substantial plastic deformation and the first deck crushed onto the second deck.

Since this study builds on a previously conducted study[ref. 4] , several comparisons were made to ensure consistency between the results. These comparisons confirm overall agreement while also highlighting differences due to variations in complexity. More details can be found in paragraph 7.1.8.

### 8.1. Conclusion of the ship collisions

The result of ship collisions in *Paragraph 7.1* with wind turbine support structure provides critical insights into the structural behavior of both ships and turbine foundations under various impact scenarios.

The difference in damage resulting from the collision of the chemical tanker and the container ship can be attributed to several factors:

1. **Bow Plate Thickness:** The chemical tanker's bow has a plate thickness of 13-15 mm, whereas the container ship's bow is significantly thicker, measuring 25-30 mm at the point of initial impact.
2. **Internal Stiffening:** The container ship features a greater number of internal stiffeners, which are also thicker and more robust compared to those in the chemical tanker, enhancing its structural resistance to impact.
3. **Impact Force Distribution:** The container ship's larger bow distributes the impact force over a greater surface area, reducing localized damage. The container ship's bow height is 32.5 meters, while the chemical tanker's is only 12 meters, leading to different energy dissipation patterns during collision.



### 8.1.1. Sailing Collision Scenario – Chemical Tanker

The results of the head-on sailing impact scenarios (*Paragraph 7.1.1*) show that while large areas of damage occur on the forward sections of the chemical tanker, this damage remains confined forward of the collision bulkhead. As a result, the collision bulkhead remains intact, ensuring that the ship's buoyancy is not compromised. Additionally, no cargo loss or spillage is recorded, as the damage does not extend to compartments containing cargo or fuel.

The analysis identifies a risk to the wind turbine support structure, particularly in a 20-knot impact scenario, where the turbine is likely to collapse toward the ship. This outcome is primarily due to buckling in one or more locations of the support structure and the fact that the ship continues moving forward after the collision, as it is not halted by the impact.

For a 10-knot collision, damage to the ship is less severe compared to the 20-knot scenario. While the turbine support structure still experiences buckling, the results suggest that in this case, the structure collapses away from the ship, indicating a different failure progression due to lower impact energy.

Across all sailing impact simulations, not all of the ship's kinetic energy is transferred during the collision. Consequently, the ships do not come to a complete stop after the collision and continue moving forward.

### 8.1.2. Drifting Collision Scenario – Chemical Tanker

The drifting impact scenarios results (*Paragraph 7.1.1*) reveal hull damage, but only localized small areas of material failure are observed. This damage primarily affects the ballast tanks, which, despite being compromised, do not impact the ship's overall stability or buoyancy. Additionally, no cargo loss or spillage occurs, as the damage is confined to non-cargo compartments.

The 4-knot collision scenario results in greater hull damage than the 2-knot scenario. In the 2-knot impact, the turbine support structure remains intact, showing no signs of failure. However, in the 4-knot scenario, buckling occurs in the upper levels of the support structure, indicating an increased risk of structural failure, with the turbine falling away from the ship.

Across all drifting impact simulations, it was observed that the ship's kinetic energy is fully transferred during the collision. As a result, the ship comes to a complete stop after the collision.

### 8.1.3. Sailing Collision Scenario – Container Ship

The head-on sailing impact scenarios results (*Paragraph 7.1.2*) indicate that only small areas of damage occur on the forward sections of the container ship. Despite this damage, the structural integrity of the bow remains intact, ensuring that the ship's buoyancy is not compromised. Additionally, no cargo loss or spillage occurs, as the damage does not extend beyond the collision bulkhead to compartments containing cargo or fuel.

The analysis identifies a risk to the wind turbine support structure in a 20-knot impact scenario, where the turbine is likely to collapse toward the ship. This is primarily due to buckling in one or more locations of the support structure and the fact that the ship continues moving forward post-collision, as it is not halted by the impact.

For a 10-knot impact, damage to the ship is less severe compared to the 20-knot scenario. While the turbine support structure also experiences buckling, in this case, the structure collapses toward the ship, suggesting a different failure pattern due to the lower impact energy.

Across all sailing impact simulations, only a small part of the ship's kinetic energy is transferred during the collision. Consequently, the ship does not stop completely and continues its forward motion after the collision.



#### **8.1.4. Drifting Collision Scenario – Container Ship**

The drifting impact scenarios results (*Paragraph 7.1.2*) reveal areas of hull damage, but only localized small areas of plastic deformation occur, without cracks. Additionally, no cargo loss or spillage is recorded, as the damaged areas remain confined to non-cargo compartments.

The 4-knot collision scenario results in greater hull damage compared to the 2-knot scenario. In the 2-knot impact, the turbine support structure remains intact, showing no signs of failure. However, in the 4-knot scenario, buckling occurs in the upper levels of the support structure, indicating an increased risk of structural failure, with the turbine collapsing away from the ship.

Across all drifting impact simulations, not all of the ship's kinetic energy is absorbed during the collision. As a result, the ships do not come to a complete stop after the collision and continue moving forward.

#### **8.1.5. Sailing Collision Scenario – Passenger Vessel**

The head-on sailing impact scenarios results (*Paragraph 7.1.3*) show that large areas of damage occur on the forward section of the passenger vessel. However, the structural integrity of the bow remains intact, ensuring that the ship's buoyancy is not compromised. Additionally, no cargo loss or spillage occurs, as the damage does not extend beyond the collision bulkhead to compartments containing cargo or fuel.

The analysis highlights a risk to the wind turbine support structure in a 30-knot impact scenario, where the turbine is likely to collapse toward the ship. This is primarily due to buckling at one or more locations of the support structure and the fact that the ship continues moving forward after the collision, as it is not halted by the impact.

For a 20-knot impact, damage to the ship is less severe compared to the 30-knot scenario. While the turbine support structure still experiences buckling, the results suggest that also in this case, the structure collapses toward the ship.

Across all sailing impact simulations, only a small part of the ship's kinetic energy is transferred during the collision. As a result, the ship does not come to a stop completely and continues its forward motion.

#### **8.1.6. Drifting Collision Scenario – Passenger Vessel**

The drifting impact scenarios results (*Paragraph 7.1.3*) reveal areas of hull damage, but only localized small areas of plastic deformation occur. Additionally, no cargo loss or spillage is recorded, as the damaged areas remain confined to non-cargo compartments.

The 4-knot collision scenario results in greater hull damage compared to the 2-knot scenario. In the 2-knot impact, the turbine support structure remains intact, showing no signs of failure. However, in the 4-knot scenario, buckling occurs in the upper levels of the turbine support structure, indicating an increased risk of structural failure, with the turbine collapsing away from the ship.

Across all drifting impact simulations, not all of the ship's kinetic energy is absorbed during the collision. As a result, the ships do not come to a complete stop after the collision and continue moving sideways.



### 8.1.7. Comparison between the ships results

The bow shapes and sizes of the three ship types significantly influence the collision impact, with variations in bulb and bulwark protrusion, plate thickness, and internal stiffening. The chemical tanker's bulb sustains the most severe damage, with deformations exceeding 3 meters, while the passenger ship's bulwark suffers the most displacement at 8.3 meters due to its bow, bulwark design and higher velocity. The container ship experiences the least damage, with only a minor dent and no element failures, demonstrating its superior structural stiffness. Overall, the container ship has the stiffest bulwark, while the passenger ship has the least stiffness, contributing to different deformation patterns in a collision. A more detailed comparison can be found in *Paragraph 7.1.7*.

### 8.1.8. Turbine support structure foundation soil interaction

The simulation results in *Paragraph 7.1.5* emphasize the soil-structure interaction for the turbine foundation during ship collisions. In the head-on sailing collision scenarios, the upper soil layers fail, reducing the structural support around the turbine support structure. Additionally, buckling occurs in the lower soil layers, indicating deformation progression as the collision force penetrates deeper into the foundation. In the drifting impact scenario involving the chemical tanker, the soil exhibits sufficient resistance, with only the first soil layers failing, preventing further deformation. However, for the passenger vessel and container ship impacts, the soil also experiences failure, and the turbine support structure buckles at the mid-depth, suggesting that different ship types and impact conditions influence foundation stability in varying ways.

## 8.2. Conclusion for the nacelle impact

The simulations conducted in *Paragraph 7.2* have demonstrated insights into the structural impact of a nacelle falling onto a passenger vessel. The results indicate that a vertically falling nacelle ('nose down') with an initial velocity of 31.55 meters per second can penetrate through multiple decks, causing extensive damage to the ship's structure. Specifically, the nacelle was observed to penetrate seven consecutive decks, with the eighth deck undergoing significant plastic deformation and material failure.

In contrast, the horizontal impact simulation (nacelle falling on its side) revealed that the nacelle did not penetrate through the first deck but instead caused substantial plastic deformation. By the end of the simulation, the turbine's nacelle settled on top of the ship, indicating that horizontal collision result in a different structural damage compared to vertical impact. This difference is primarily due to the larger contact area between the nacelle and the ship in a horizontal impact, which leads to greater energy dissipation into the first levels of the ship's decks. As a result, the upper deck is crushed down to the lower deck level, and large areas of plastic deformation occur.

These two scenarios have the limitations of impact angles, impact location (centrally to the ship cross-section), not taking into account other components of the turbine, etc. But the given boundary conditions form the worst-case scenario's and give the conservative results which can be used to evaluate similar impacts on other types of ship.





### 8.3. Recommendations

Based on the findings of the study, the following recommendations are proposed to enhance the safety and structural resilience of offshore wind turbine support structures and maritime operations in the Dutch North Sea.

#### 8.3.1. Soil modelling

The radial P-y soil curves on the outer side of the monopile indicated that buckling was likely to occur in the upper soil layers. To improve accuracy, adding soil springs inside the tube to account for the compressed soil would provide a more realistic representation of the load transfer. Further investigation is recommended to validate this approach.

P-y curves are employed to represent the surrounding soil, but this method is only applicable for smaller deformations. Utilizing a solid material model for the soil both inside and outside of the monopile will yield more detailed results.

#### 8.3.2. Ship collisions

- The simulations did not include the main platform of the turbine support structure, even though the impact occurs at the same position as this platform, potentially affecting local damage to the ship. It is recommended to further investigation to assess its influence on ship damage.
- It is recommended to investigate other collision eccentricities that may alter the impact response.
- Further investigation is recommended on additional load cases that were not considered in the current simulations.
- Finer mesh and improved element formulations for increased accuracy.
- Alternative boundary conditions for the ship, as the current setup (only Ux free) may be too conservative and does not account for global bending effects.
- Different material curves for both the turbine and ship, considering upper and lower boundary conditions.
- A reversible soil model to better represent soil behavior post-impact.
- Impact with other wind turbines, as stronger turbines could result in greater damage to the ship.
- Currently, the ships can only move in the collision direction. It is recommended to further investigate scenarios where they can also rotate and shift post-impact, as this may affect impact forces and structural response.
- The strain rate effect is excluded in these simulations. Strain rate effect: Under quick deformation, metals become stronger but less ductile. Slower deformation keeps metals more ductile and closer to their normal properties. Further investigation is recommended to assess its impact on structural response and damage during the collision.



### 8.3.3. Nacelle collision

- The conducted simulations do not include effect related to the water surrounding the ship. To get more detailed result the hydrodynamic effects is recommended to included. A method to incorporate this is to use fluid-structure interaction.
- The nacelle's larger dimensions relative to the passenger vessel's mid-section make boundary conditions crucial in the simulation. To reduce the influence of rigid constraints, increasing the mid-section dimensions is recommended for more accurate results.
- The nacelle is currently modeled as a rigid box, but in reality, it contains flexible components such as the rotor shaft, bearings, hub, and outer shell. To improve accuracy, it is recommended to model the nacelle in more detail, incorporating flexible parts to better represent its structural behavior.
- Two nacelle orientations have been analyzed, but it is recommended to investigate additional orientations to better assess the nacelle's fall behavior on the ship.
- The impact location is currently applied at the center of the mid-section. It is recommended to investigate the effects of an eccentric impact, as a nacelle striking off-center could introduce stability issues, especially if it impacts the edge of the deck. For instance, if the nacelle falls on the deck edge of the chemical tanker, it may lead to serious stability concerns.
- It is recommended to conduct impact simulations for the chemical tanker as well. If the nacelle falls onto the vessel, it could penetrate the structure, potentially causing spillage or midsection failure, depending on whether the impact occurs vertically or horizontally.
- It is recommended to investigate scenarios where the nacelle falls with blades attached, to assess the impact of increased weight and potential damage caused by the blades.



## APPENDICES

### A. R101-DP1 Chemical tanker – Scantling calculation report



# 3D FEM gevolgschade schip-turbine

Chemical Tanker – Scantling Calculations Report

Client: Rijkswaterstaat  
Document nr: 001  
Revision: 2  
Date: 24 February 2025

**Iv-Infra b.v.**

Engineering Company with a Passion for Technology



Client: Rijkswaterstaat

Document title: 3D-FEM gevolgschade schip-turbine

Document subtitle: Chemical Tanker – Scantling Calculations Report

Revision: 2

Date: 24 February 2025

Revision	Status	Date	Author(s)	Checked	Approved	Description
0	TI	24-09-2024	IZ	GV, MMI	WL	Ter informatie
1	TI	25-10-2024	IZ	GV, MMI	WL	Ter informatie
2	TI	24-02-2024	IZ	GV, MMI	WL	Ter informatie

The only difference between revision 2 and revision 1 is the removal of the ship names that the ship model is based on.

## Summary

In this report is presented the scantling evaluation of the midship and fore area of a chemical tanker with the following main dimensions and characteristics:

<b>Vessel Characteristics</b>		<b>Unit</b>
<b>GT</b>	10000	t
<b>Lpp</b>	135	m
<b>B</b>	23	m
<b>D</b>	12	m
<b>T</b>	8.3	m
<b>Displacement</b>	21000	t
<b>Speed</b>	14	kn

This section was designed with Mars 2000 and checked according to the following rules:

- BV NR467 Rules for the Classifications of steel ships, January 2023 edition.

DNV Nauticus Hull - Primary Supporting Members spreadsheets were used for the design of PSM in midship cargo area and fore area.

The profiles used in the scantling definition are according to DIN Standard.

## TABLE OF CONTENTS

---

<b>1</b>	<b>Assumptions</b>	<b>5</b>
<b>2</b>	<b>Abbreviations</b>	<b>6</b>
<b>3</b>	<b>Scantling Design</b>	<b>7</b>
3.1.	Basic Ship Data	7
3.2.	Midship Section	10
3.3.	Transverse Bulkhead Midship	18
3.4.	Primary Supporting Members Midship	21
3.5.	Fore Section	22
3.6.	Transverse Bulkhead Fore	31
3.7.	Primary Supporting Members Fore	34
<b>4</b>	<b>Scantling Results</b>	<b>35</b>
4.1.	Transverse Section	35
4.2.	Transverse Bulkhead Midship	40
4.3.	Primary Supporting Members Midship	42
4.4.	Fore Section	45
4.5.	Transverse Bulkhead Fore	49
4.6.	Primary Supporting Members Fore	51
<b>5</b>	<b>Conclusion</b>	<b>53</b>

# 1 Assumptions

In this memo, a scantling design of a chemical tanker is provided, which will be used during the ship impact simulations for project INF240746 RWS WV.L.

Considering similar vessels and the input “INFR240476 - Plan van Aanpak rev.0 – definitief”, the following technical particulars were assumed for the scantling calculation:

- Scantling Length: 135 m
- Depth: 12 m
- Breadth: 23 m
- Scantling Draught: 8.3 m
- Minimum Draught at ballast: 4 m
- Service Speed: 14 kn
- Block coefficient: 0.795
- Double bottom: 1.4/1.6 m
- Double Hull: 1.6 m
- Frame spacing: 0.8 m (mid area), 0.7 (fore and aft area)
- Webframe spacing: 3.2 m

The ship model is based on similar existing ships.

The following frame spacing was considered:

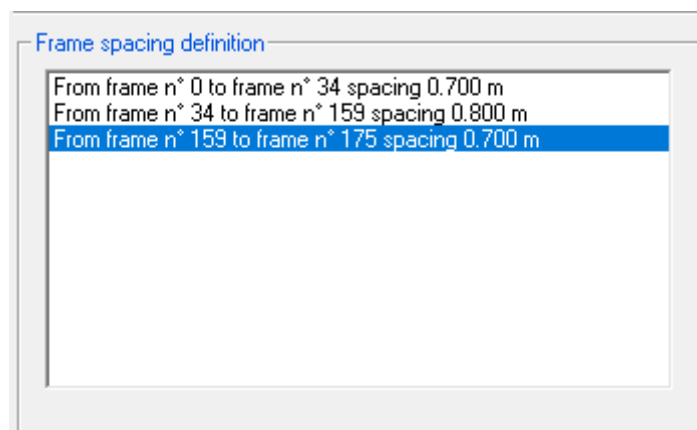


Figure 1 – Frame Spacing

The materials have been assumed to be Grade A steel with a yield stress of 235 MPa and high tensile strength steel (Grade HT36) with a specific minimum yield strength of 355 MPa. The Youngs modulus for both materials has been considered as 206000 N/mm<sup>2</sup>.





## 2 Abbreviations

---

BL	Base Line	
CL	Center Line	
FR	Frame	
PSM	Primary Supporting Member	

### 3 Scantling Design

#### 3.1. Basic Ship Data

The following input has been used for the Basic ship data module (BSD).

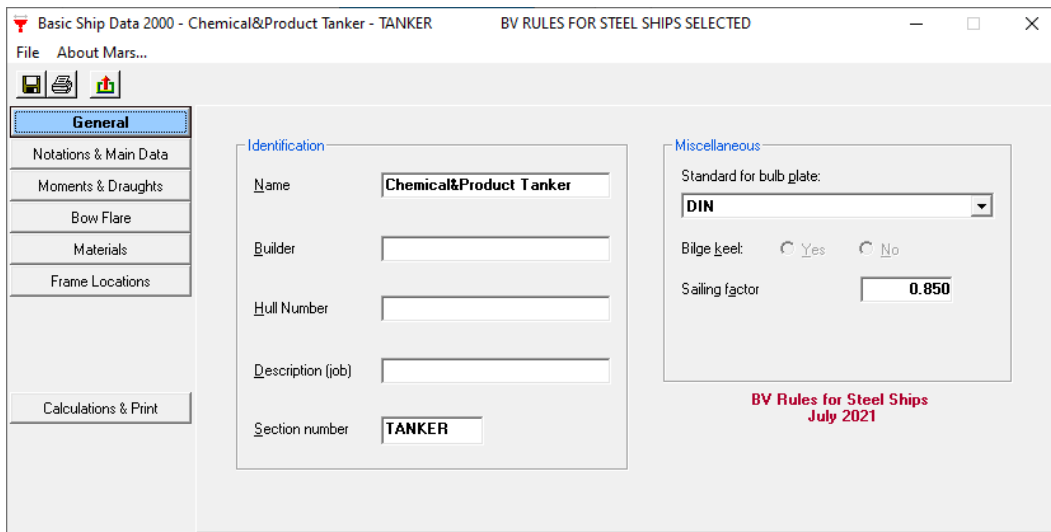


Figure 2 – Basic Ship Data – General

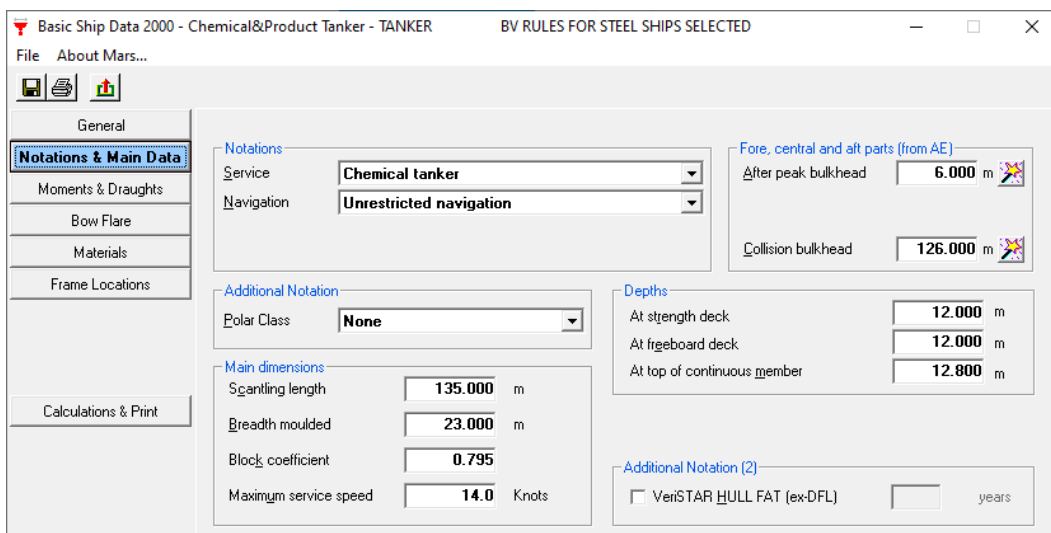


Figure 3 – Basic Ship Data – Class Notation and Main Data

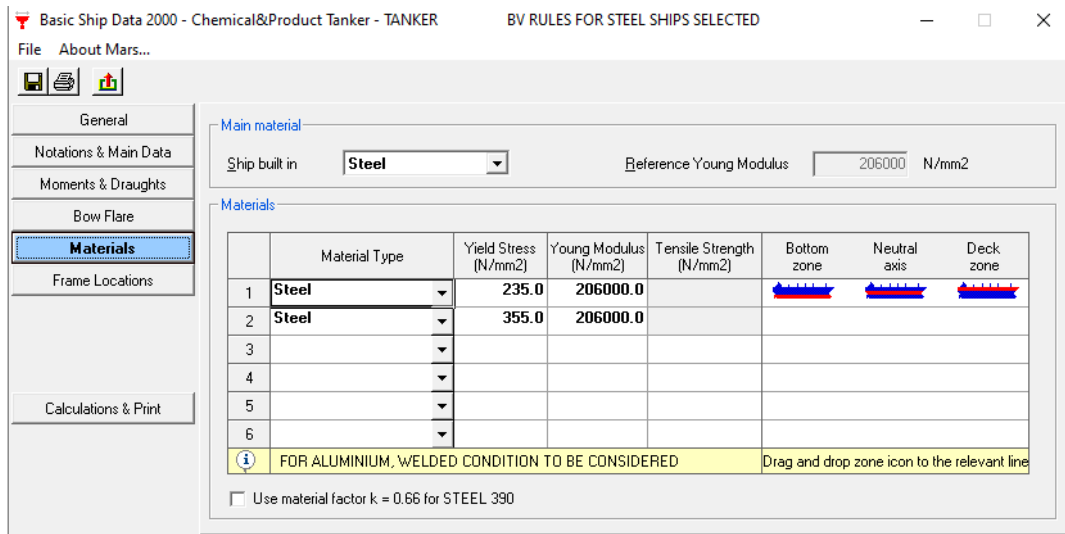


Figure 4 – Basic Ship Data - Materials

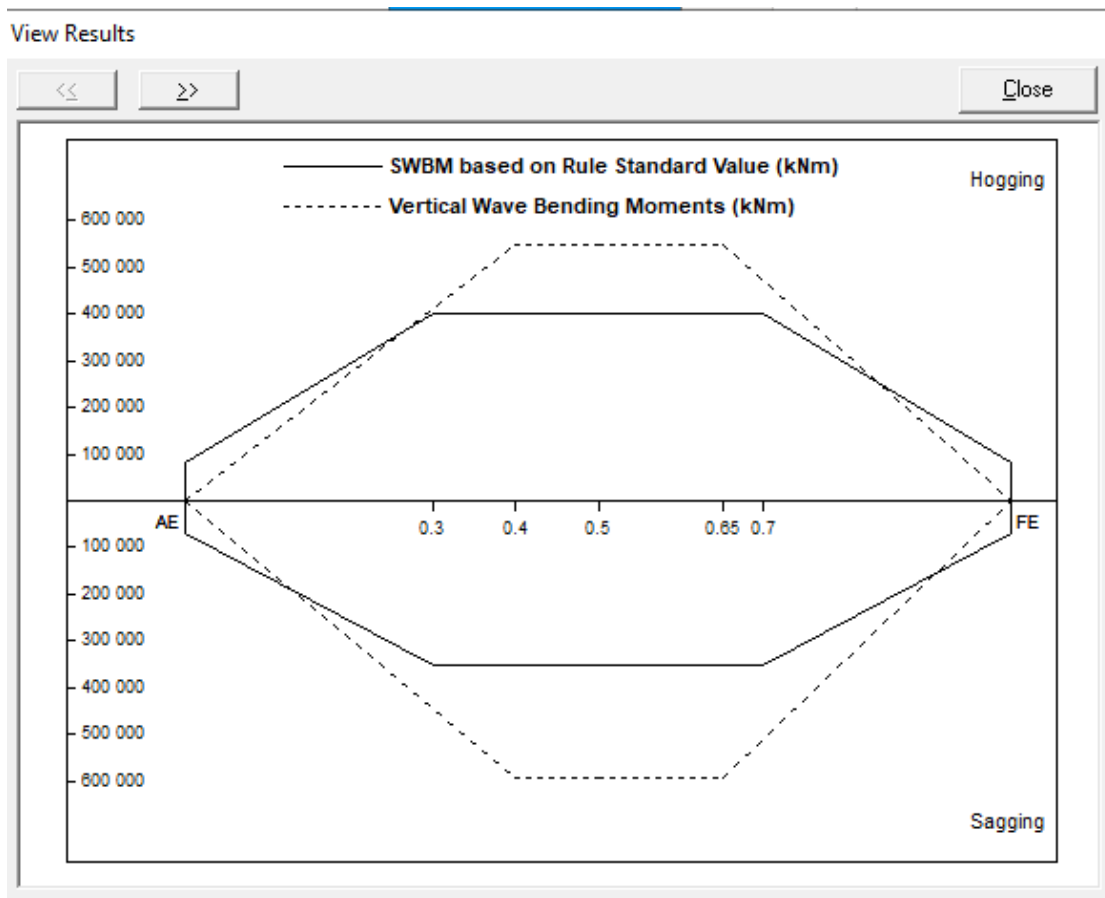


Figure 5 – SWBM and VWBM



View Results

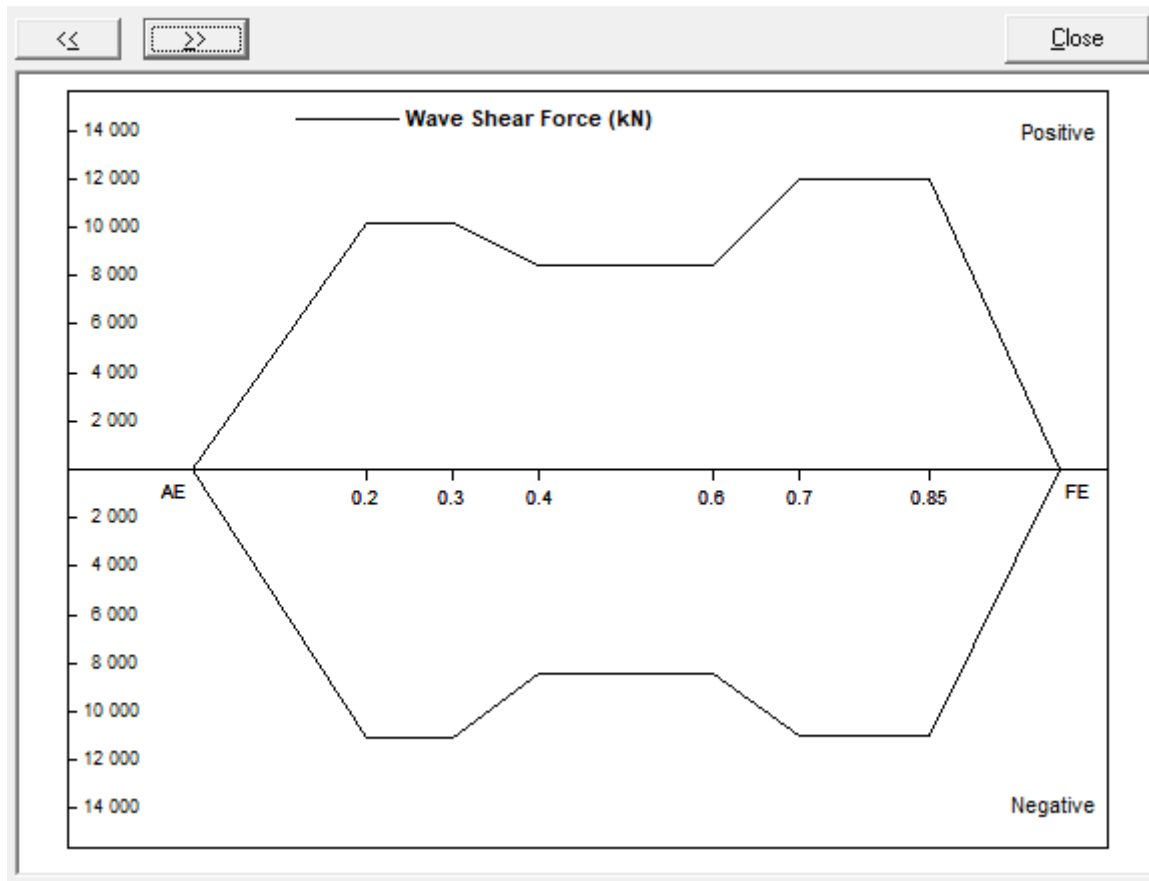


Figure 6 – Wave Shear Force

### 3.2. Midship Section

The location of the assessed cross section is FR 91+0.13 m, at 67.63 m from the aft end. The frame spacing for this area is 0.8 m, the webframe spacing is 3.2 m.

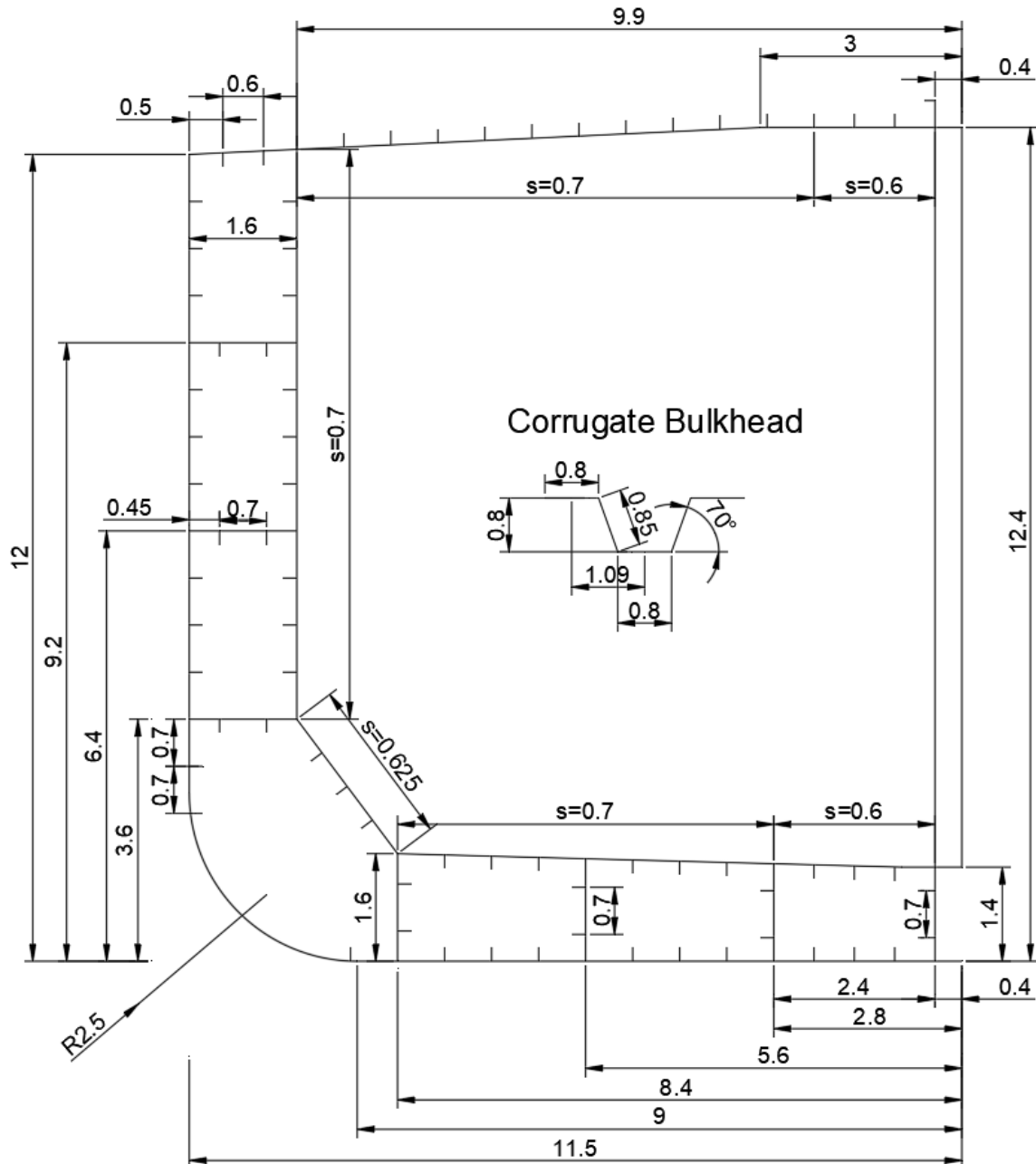



Figure 7 – Midship Section – Spacing (meters)

**Main Section Data**

Main | SW | Fatigue | Ship State | Wave | Flooding

Name Location Dimensions

Name: Midship Section

Longitudinal Location (from AE): 67.630 m 

Breadth moulded: 23.000 m

Depth moulded: 12.000 m

Depth at top of continuous member: 12.800 m

Materials

ST235 in neutral axis

ST235 in deck Extension heights: 0.000 m

ST235 in bottom 0.000 m

Input of: Half section Default (BSD)

Ok Cancel

Figure 8 – Midship Section – Main Section Data

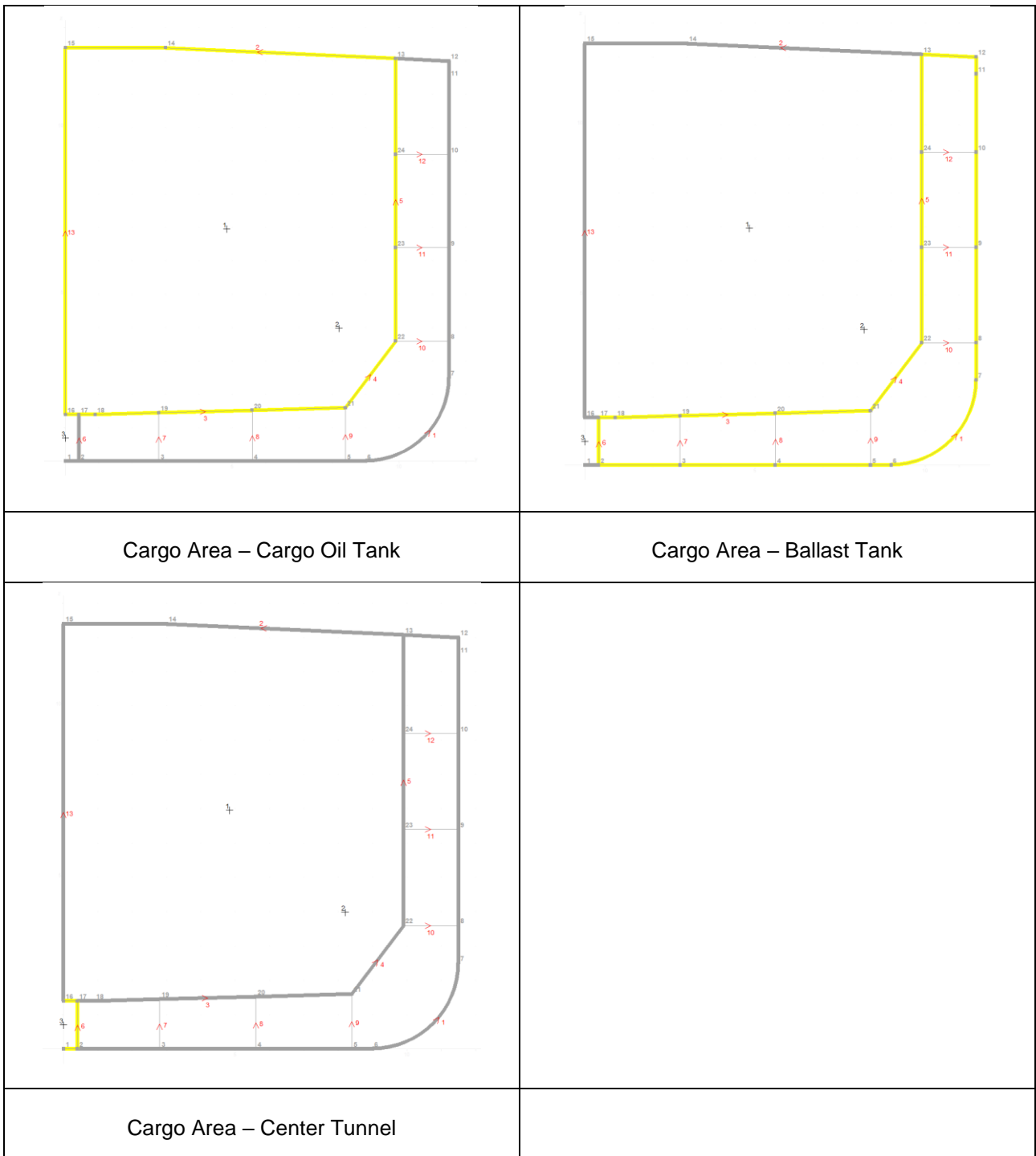


Figure 9 – Midship Section – Compartments

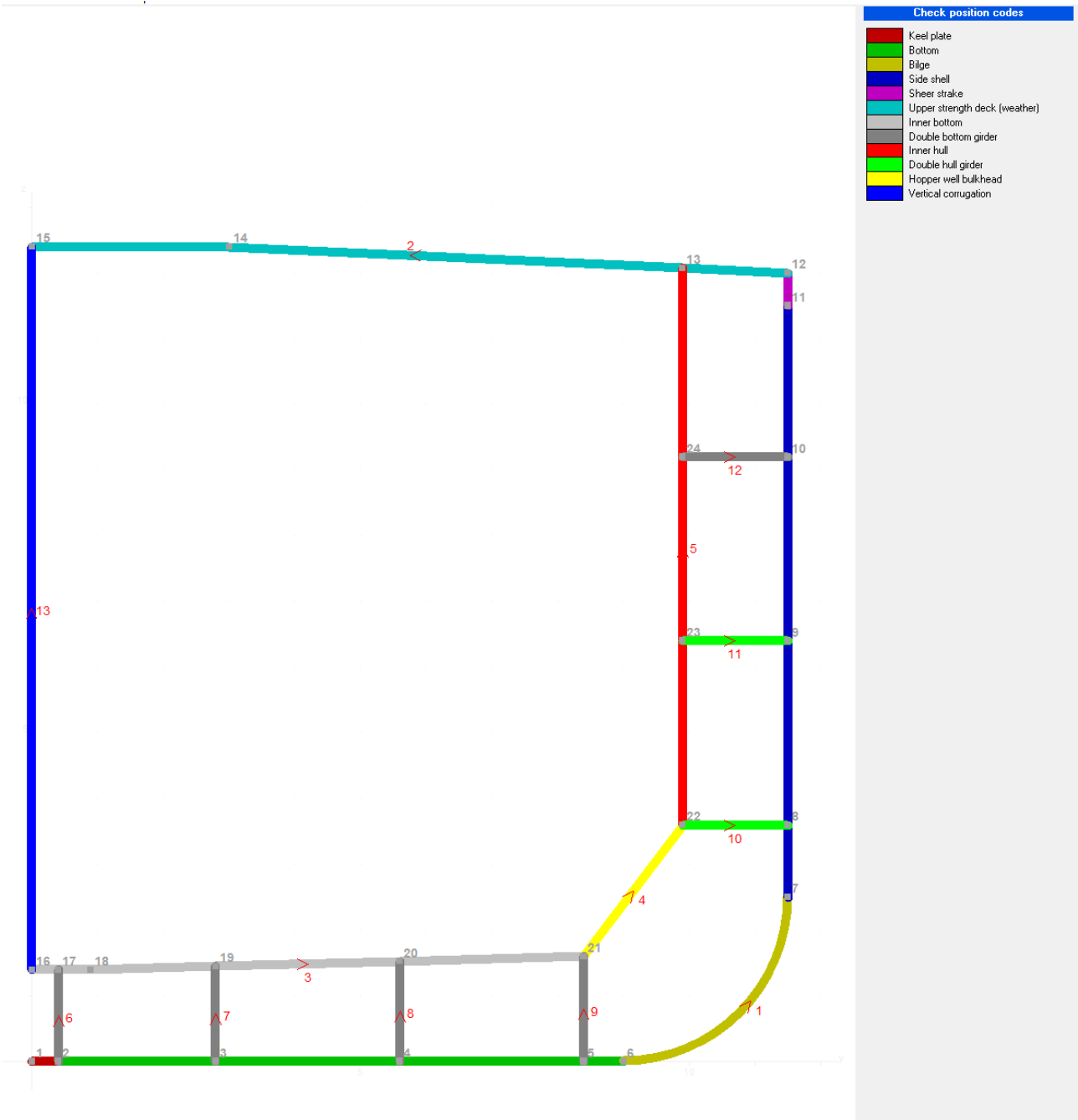


Figure 10 – Midship Section – Position Codes



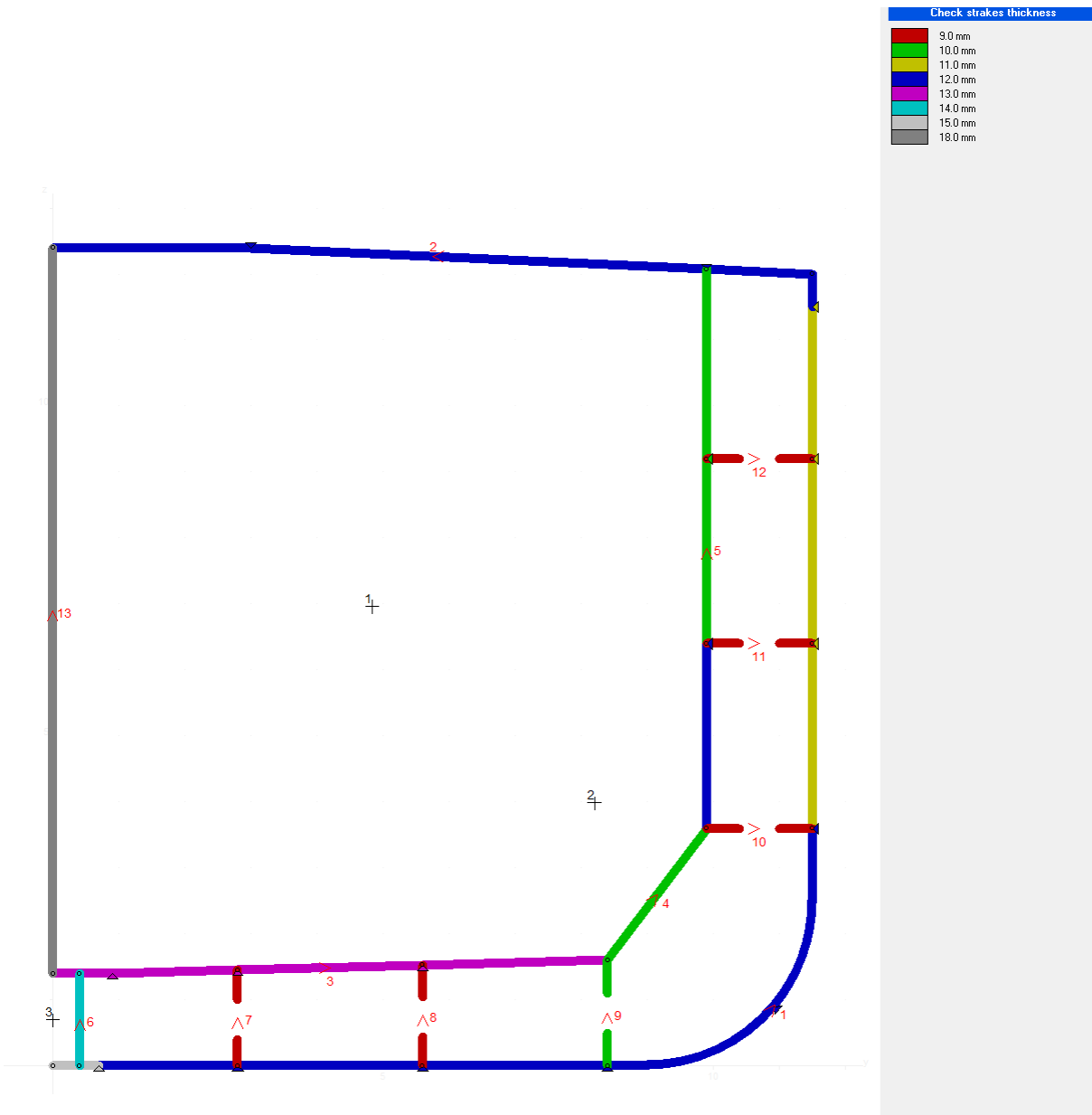


Figure 11 – Midship Section – Plate thickness

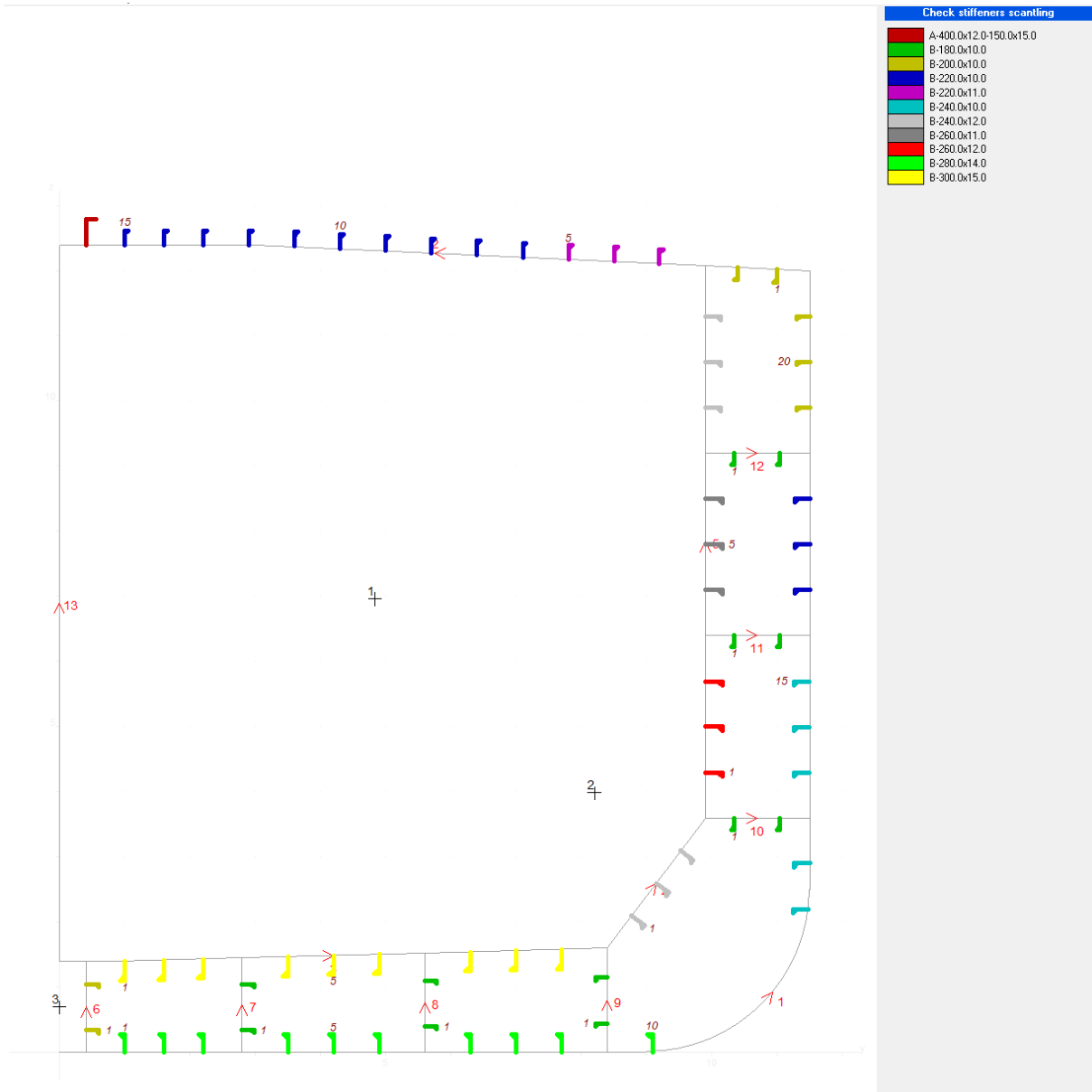


Figure 12 – Midship Section – Stiffeners Scantling

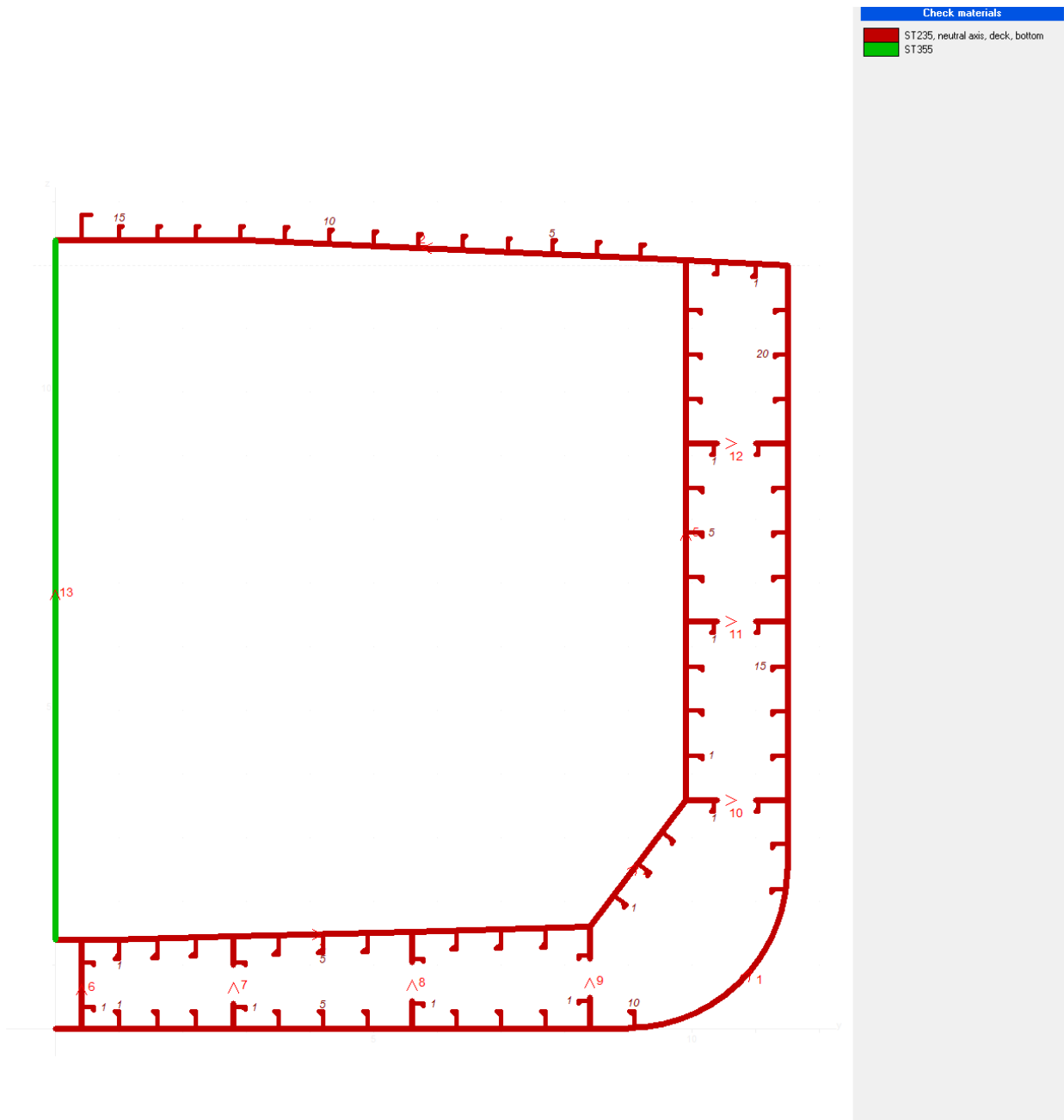


Figure 13 – Midship Section – Materials

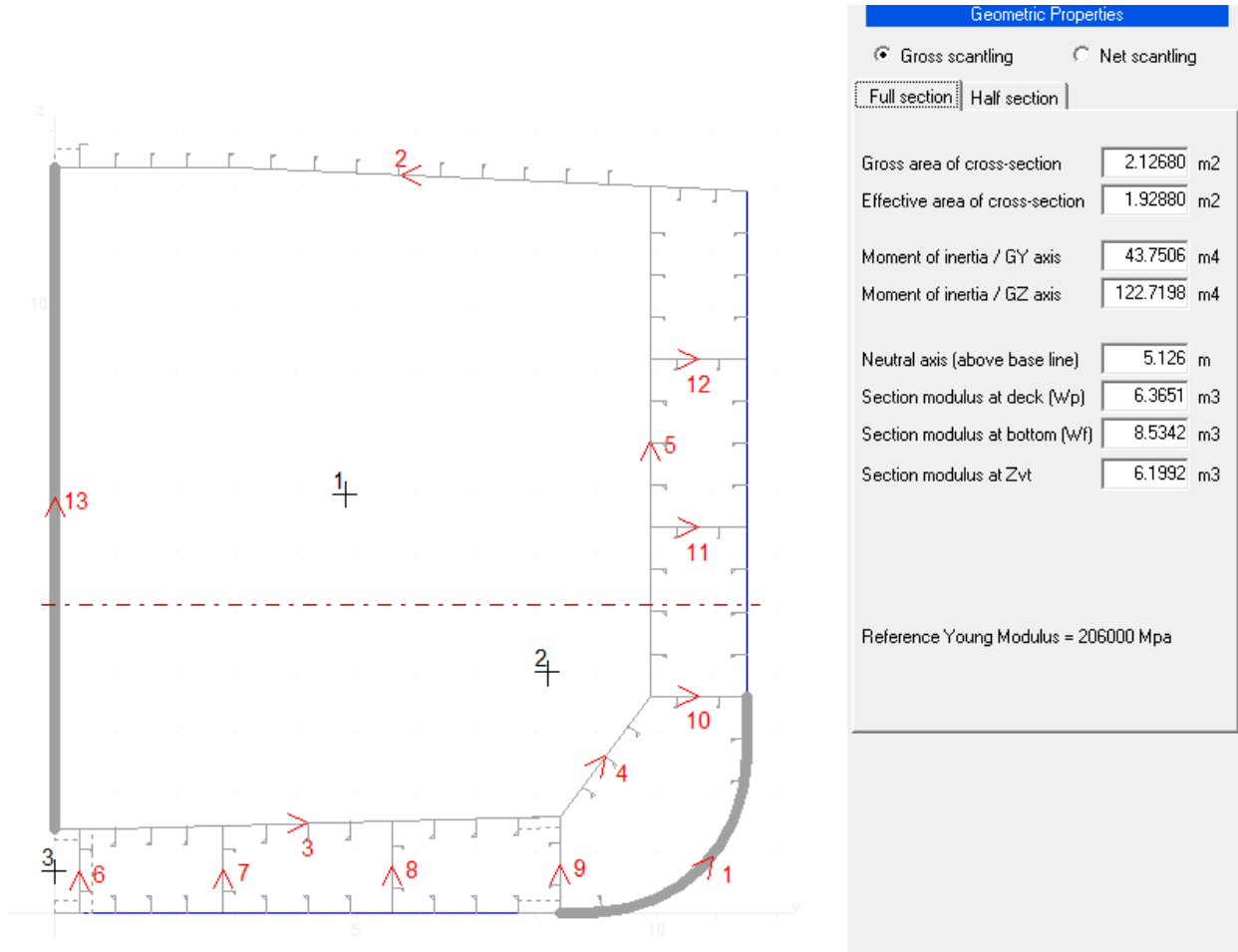


Figure 14 – Midship Section – Geometric Properties

### 3.3. Transverse Bulkhead Midship

The location of the assessed transverse bulkhead is FR 79, at 57.9 m from the aft end.

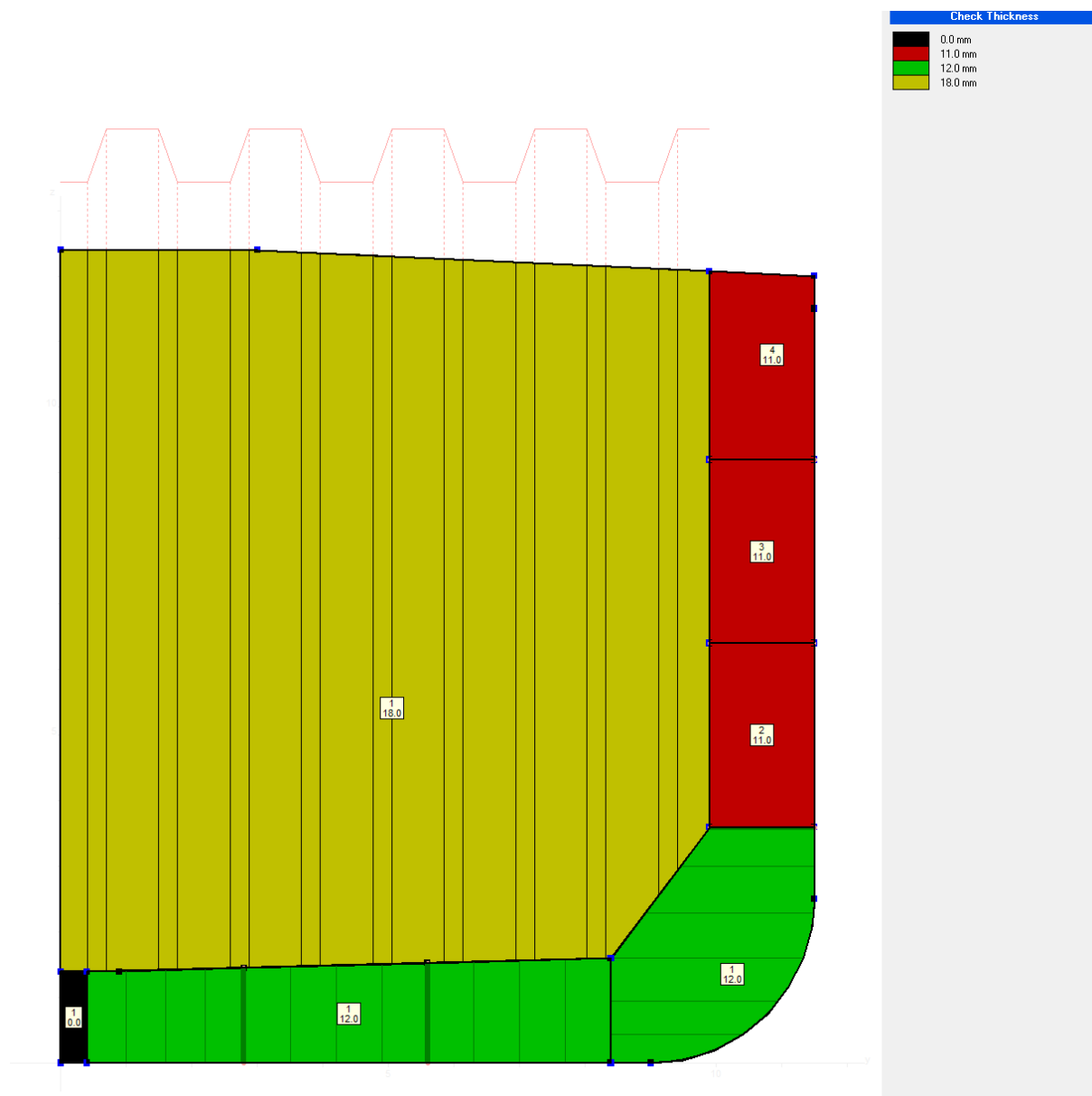


Figure 15 – Transverse Bulkhead – Plate thickness

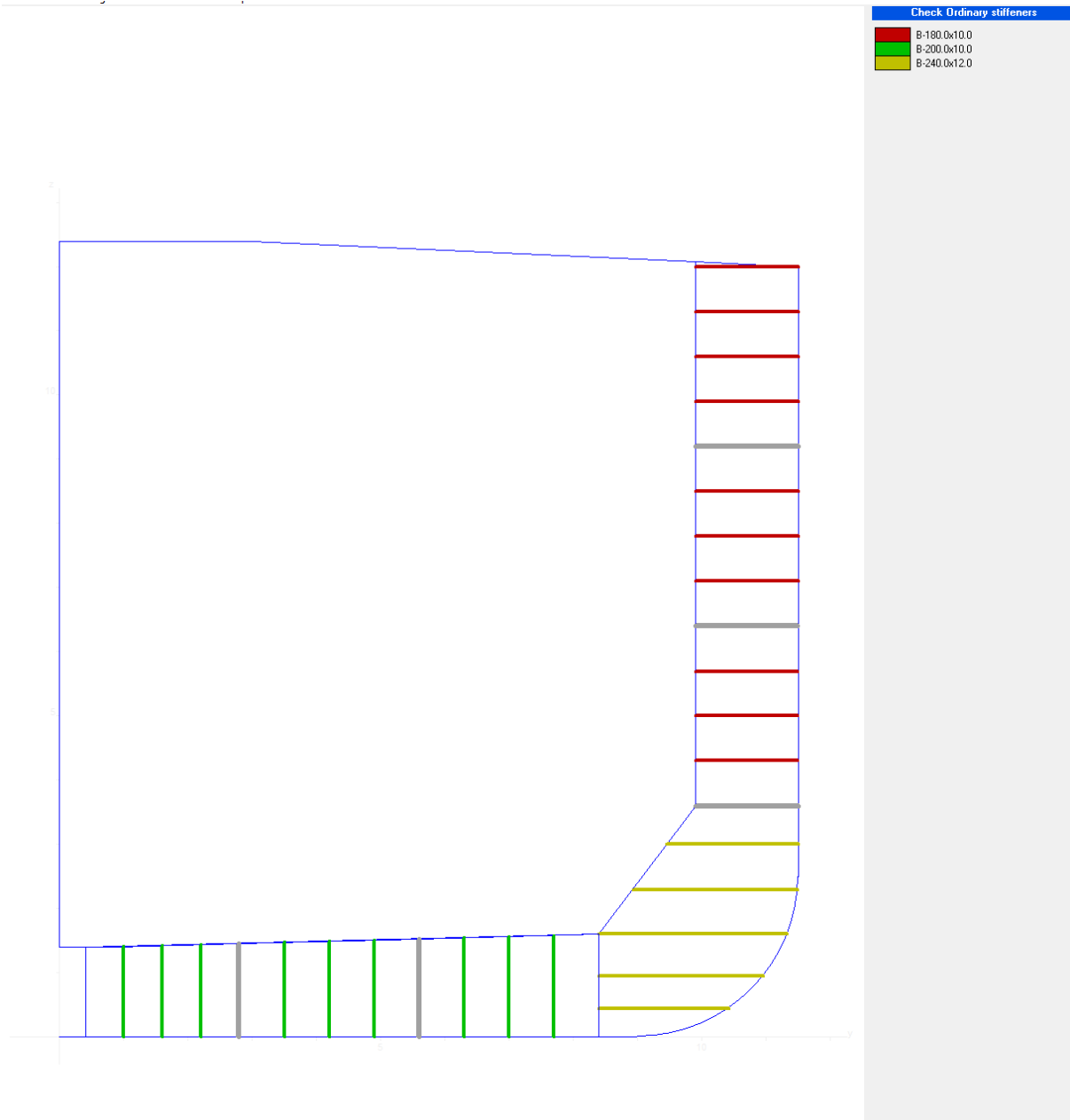


Figure 16 – Transverse Bulkhead – Stiffeners Scantling

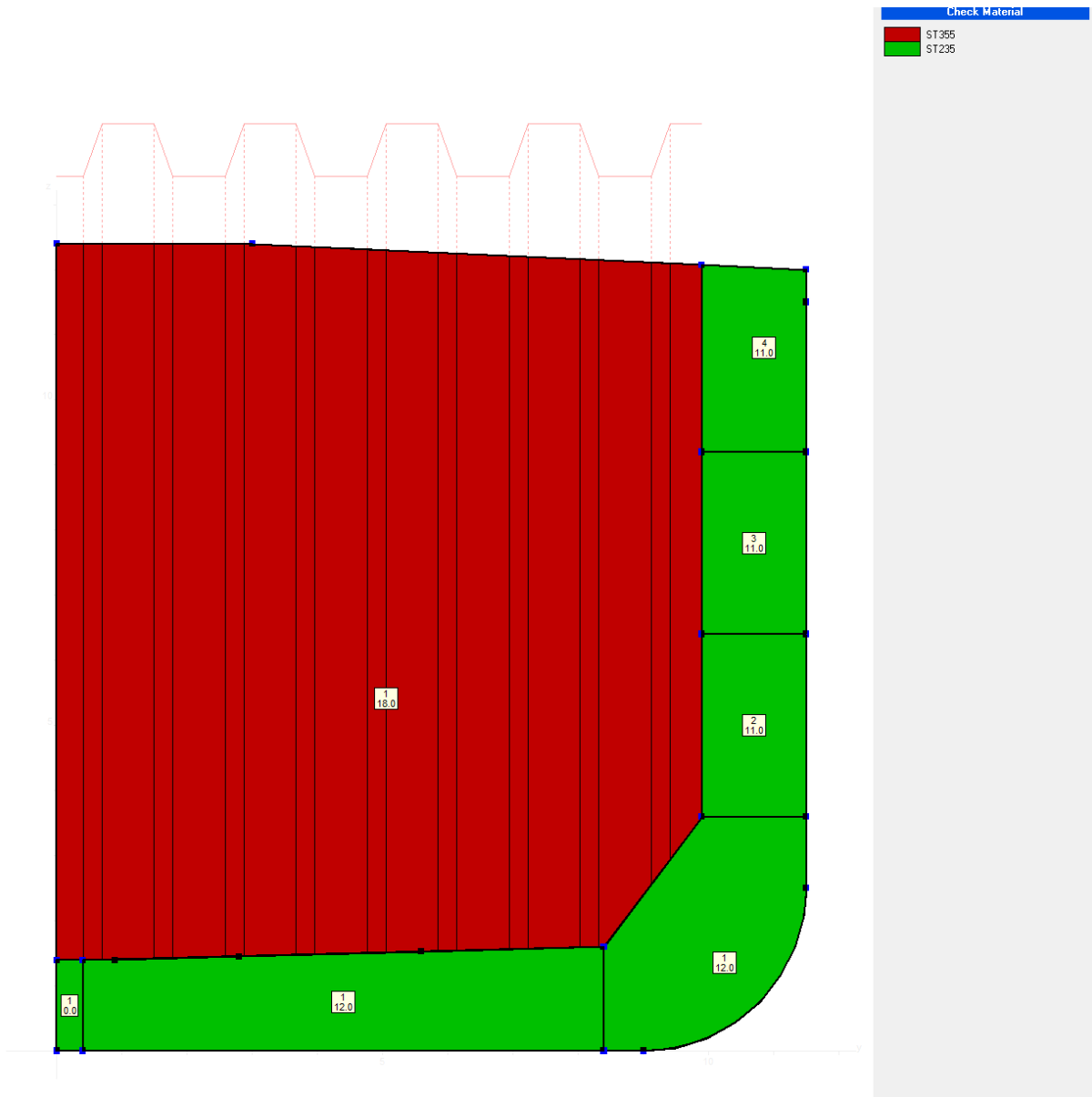


Figure 17 – Transverse Bulkhead – Materials

### 3.4. Primary Supporting Members Midship

The web frame spacing for the midship area is 3.2m.

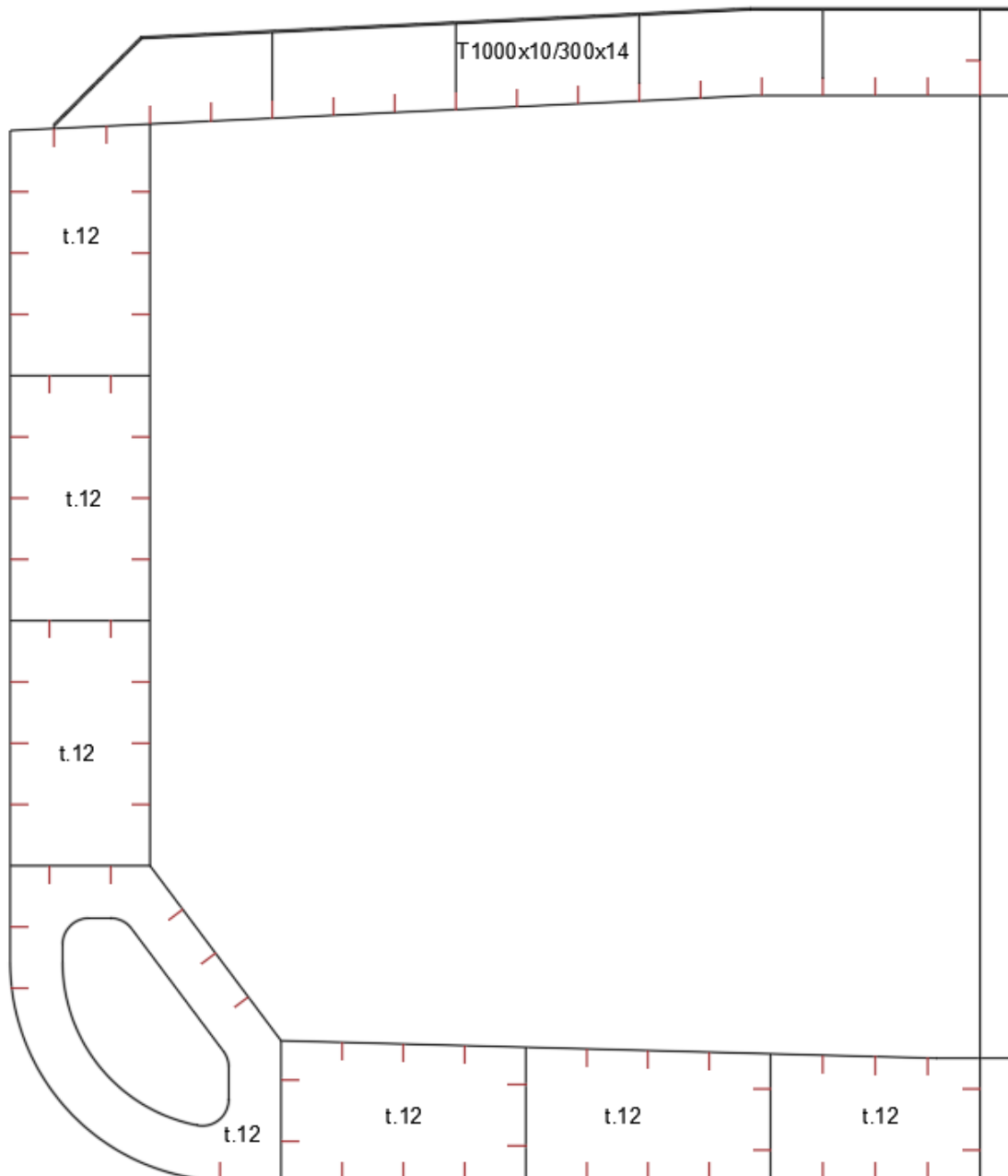


Figure 18 – Primary Supporting Members Sketch



### 3.5. Fore Section

The location of the assessed cross section is FR 170, at 129.6 m from the aft end.  
 The frame spacing for this area is 0.7m, the webframe spacing is 2.8 m.

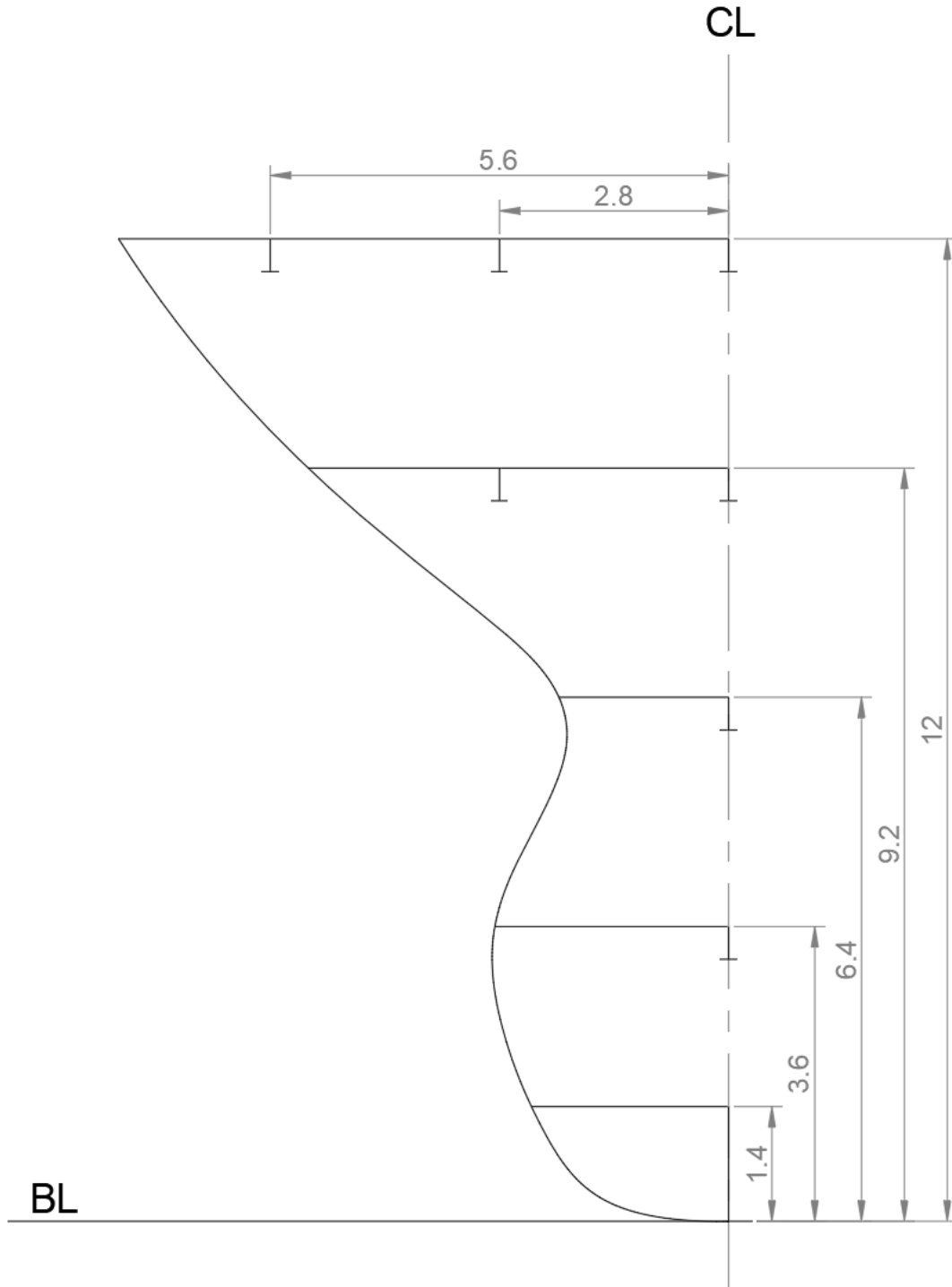



Figure 19 – Fore Section – Spacing (meters)

**Main Section Data**

Main	SW	Fatigue	Ship State	Wave	Flooding
------	----	---------	------------	------	----------

**Name Location Dimensions**

Name:

Longitudinal Location (from AE):  m 

Breadth moulded:  m

Depth moulded:  m

Depth at top of continuous member:  m

**Materials**

<input type="text" value="ST235"/>	in neutral axis	Extension heights:
<input type="text" value="ST235"/>	in deck	<input type="text" value="0.000"/> m
<input type="text" value="ST235"/>	in bottom	<input type="text" value="0.000"/> m

Input of:

Figure 20 – Fore Section – Main Section Data

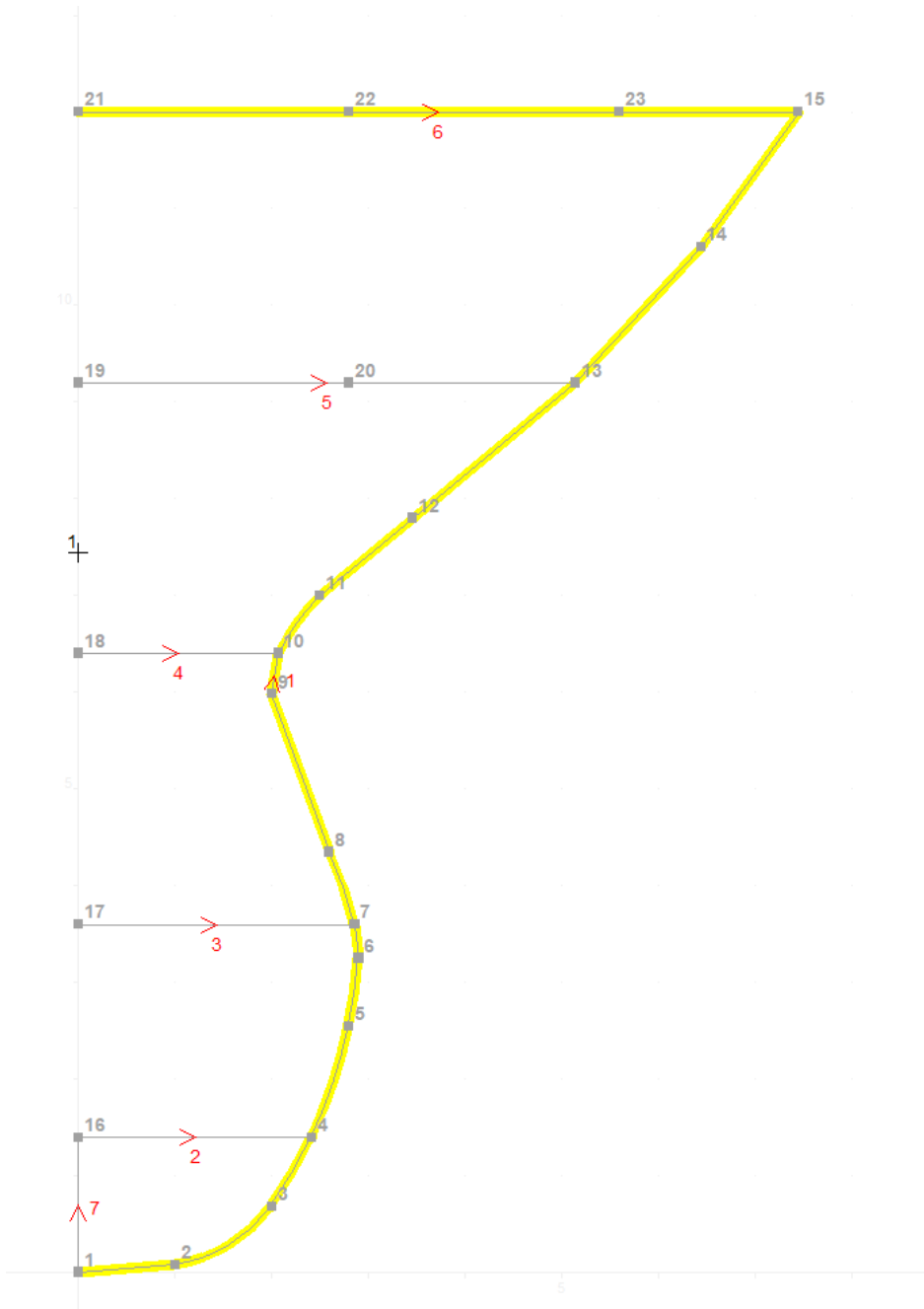


Figure 21 – Fore Section – Compartments

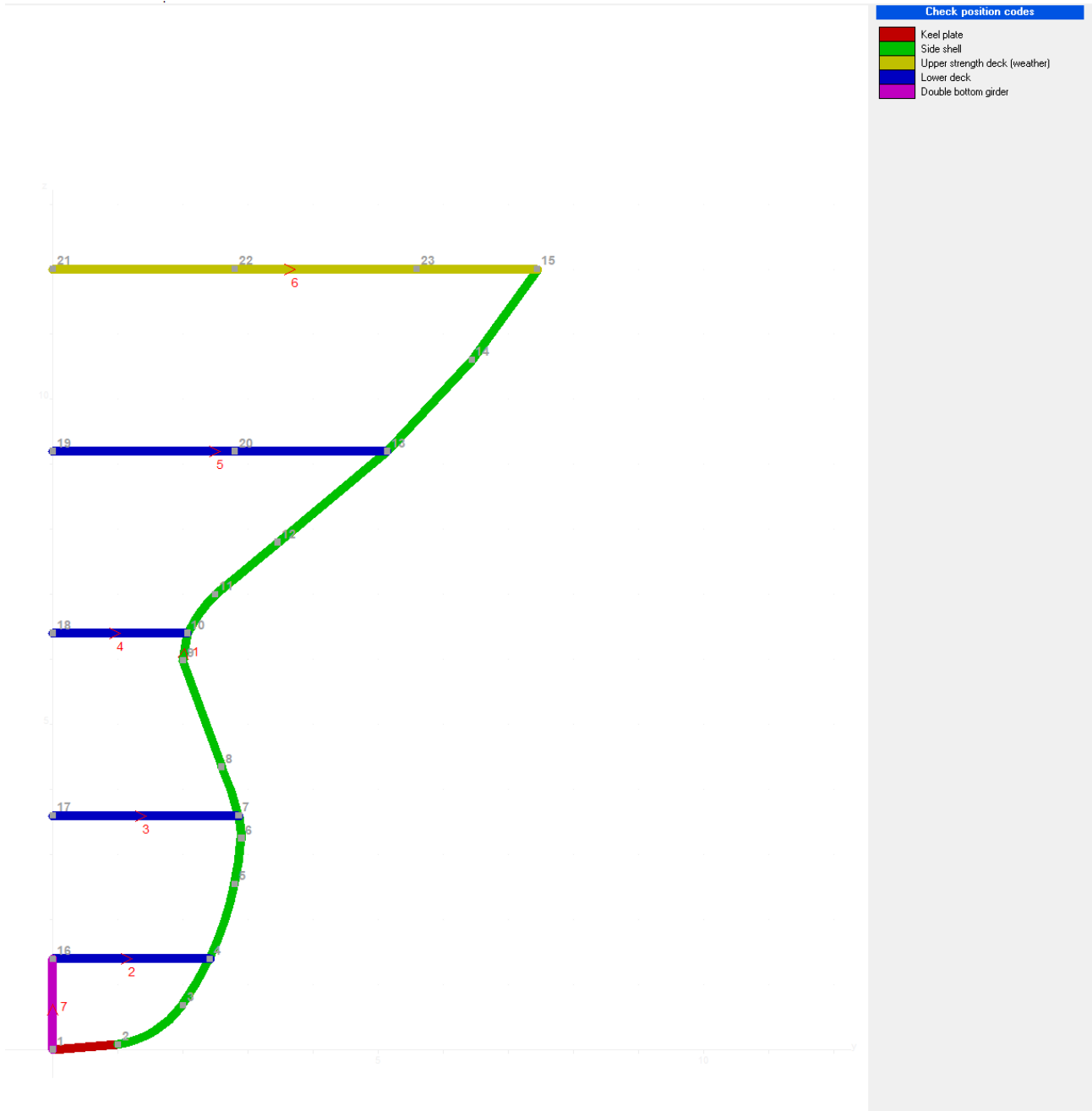


Figure 22 – Fore Section – Position Codes

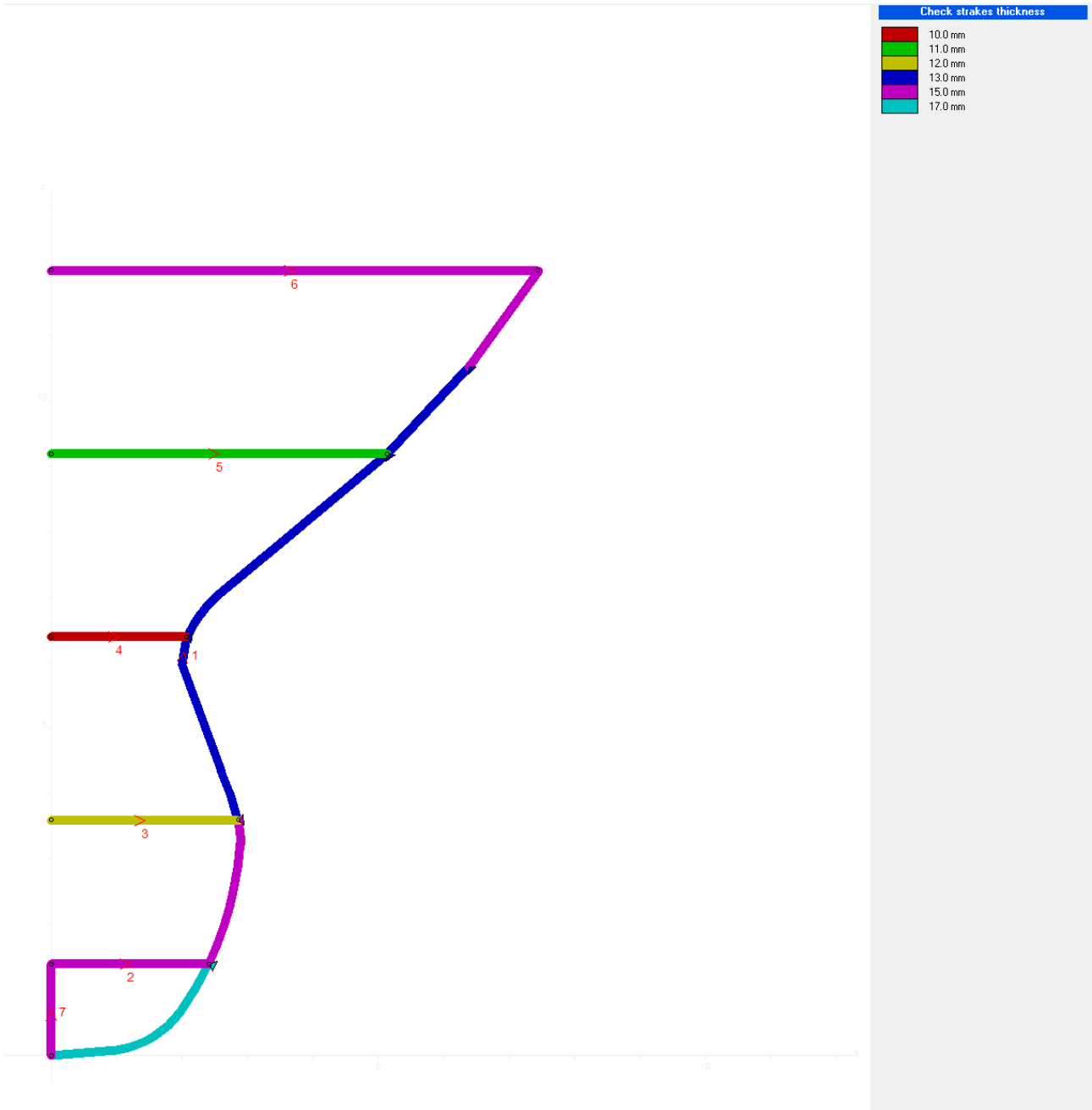


Figure 23 – Fore Section – Plate thickness

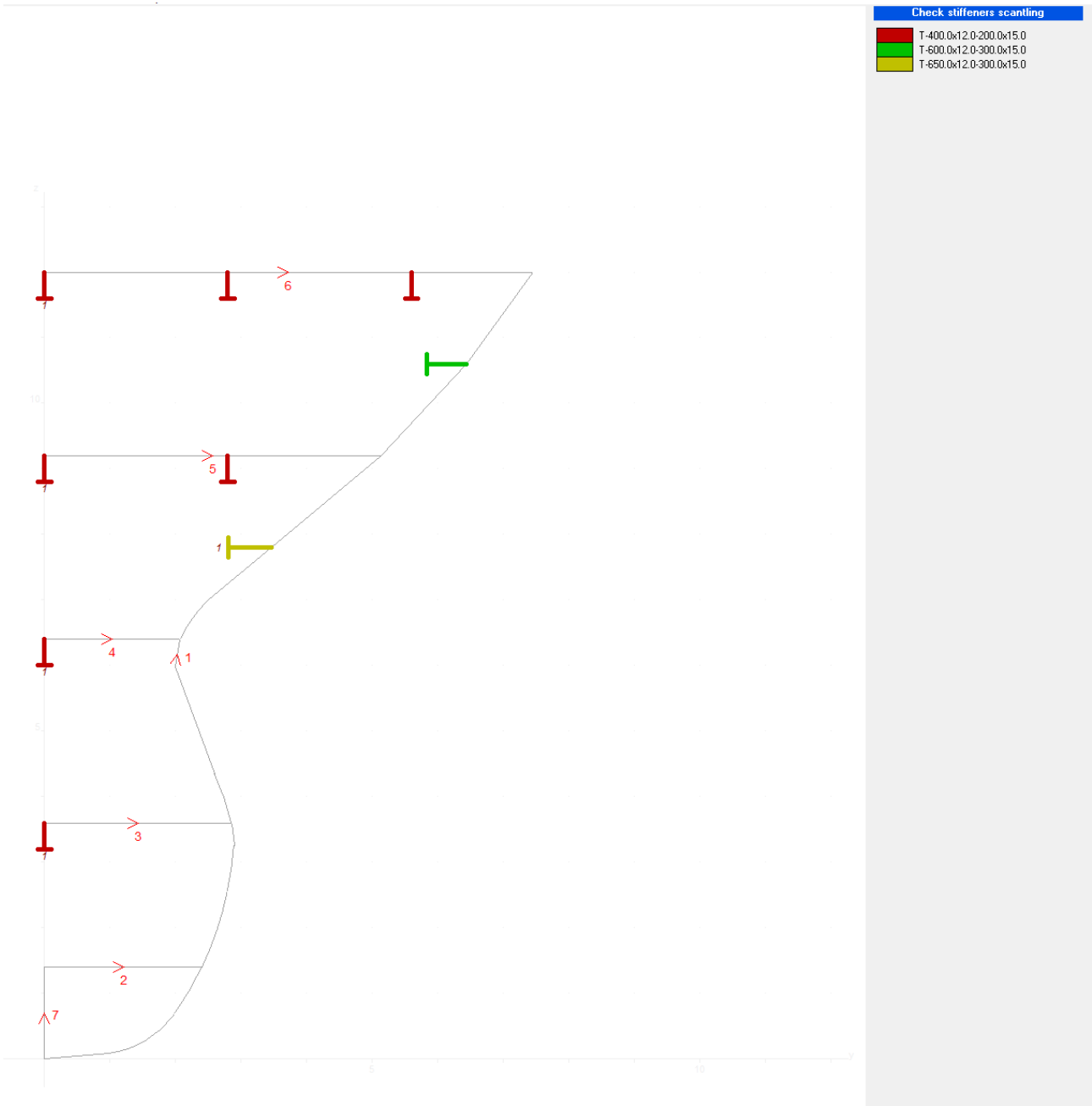


Figure 24 – Fore Section – Stiffeners Scantling

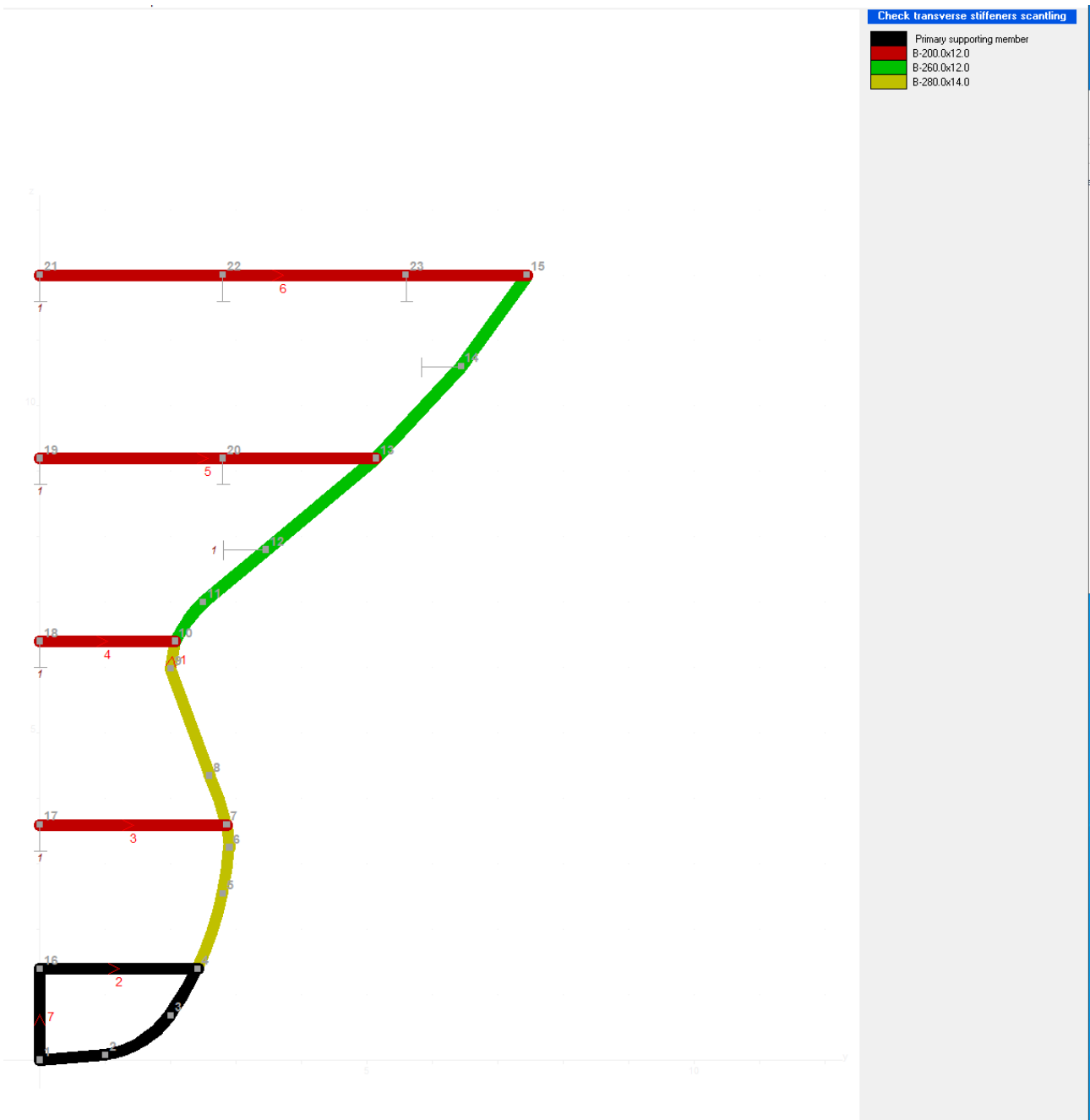


Figure 25 – Fore Section – Transverse Stiffeners Scantling

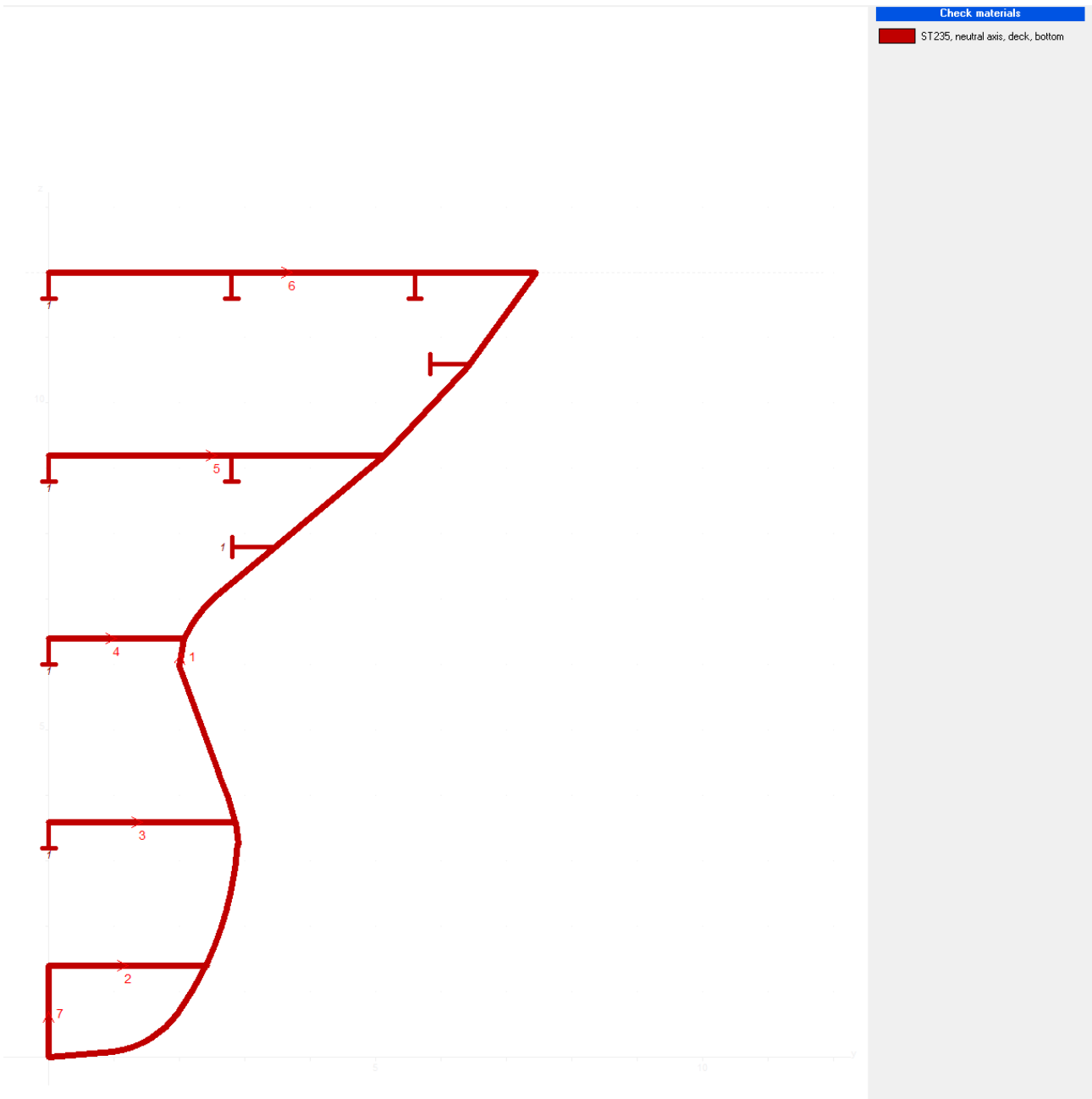


Figure 26 – Fore Section – Materials



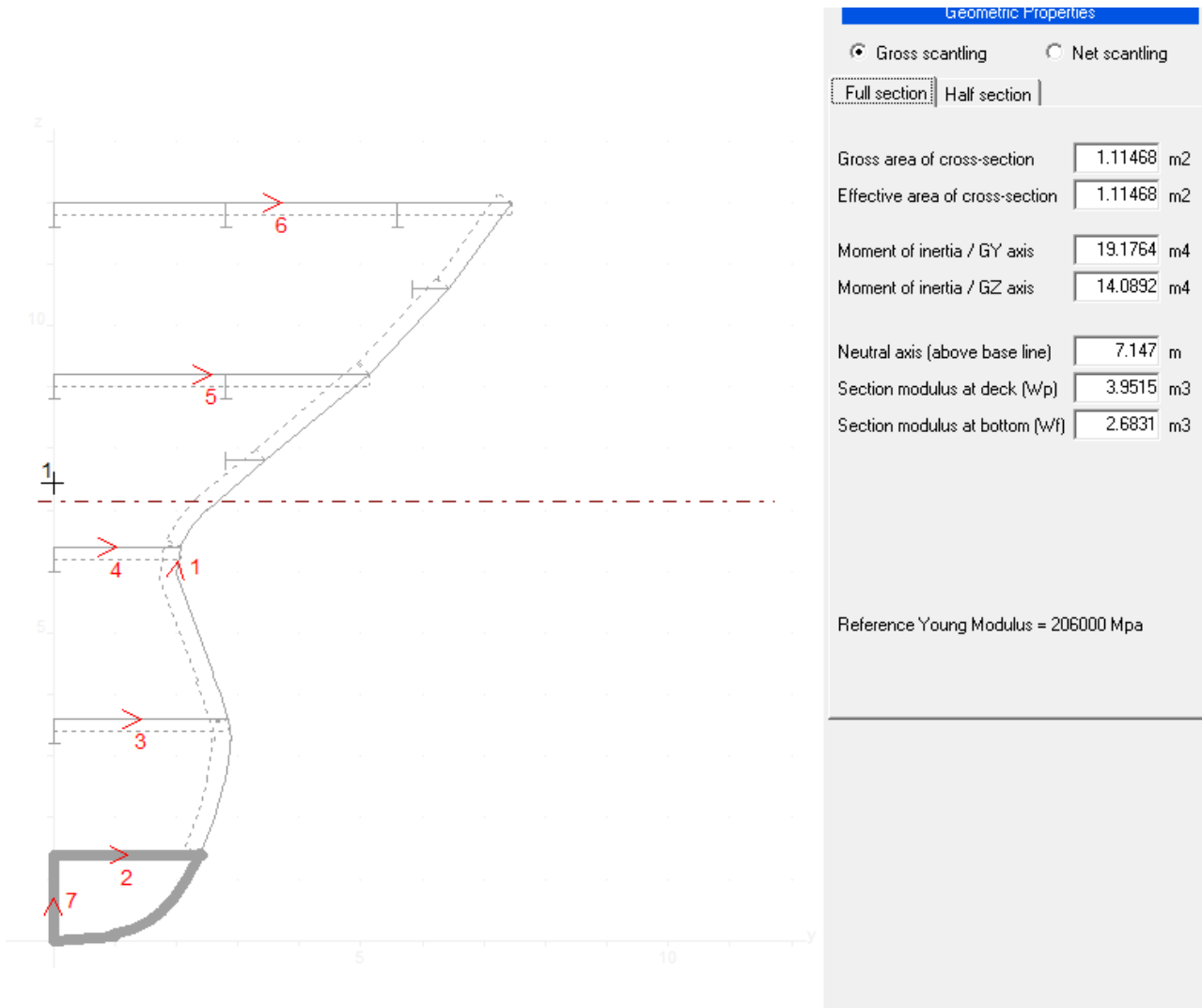


Figure 27 – Fore Section – Geometric Properties

### 3.6. Transverse Bulkhead Fore

The location of the assessed transverse bulkhead is FR 167, at 127.5 m from the aft end.

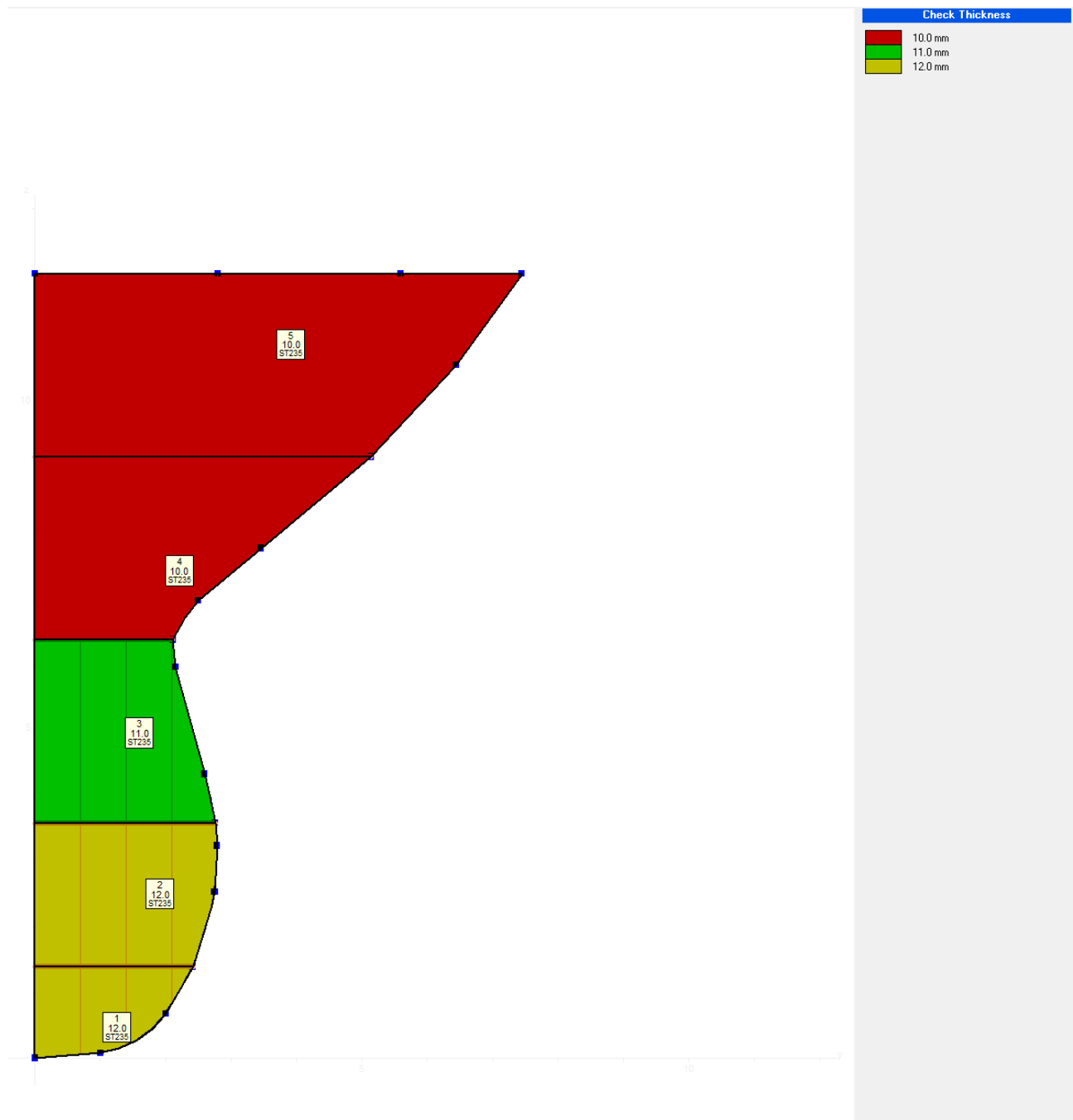


Figure 28 – Transverse Bulkhead Fore – Plate thickness

stiffener arrangements - cross - 1992 - 1.jpg

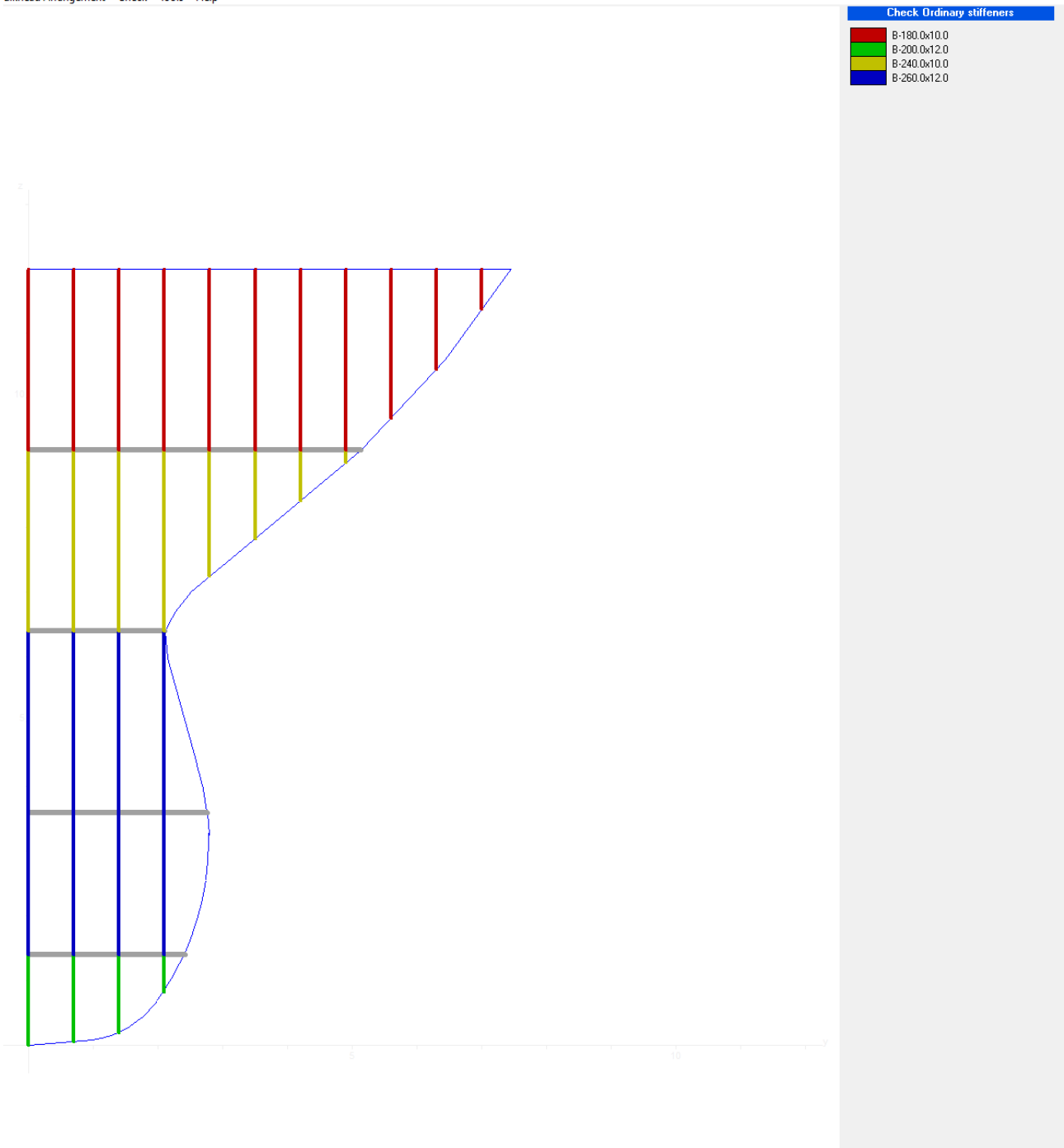


Figure 29 – Transverse Bulkhead Fore – Stiffeners Scantling

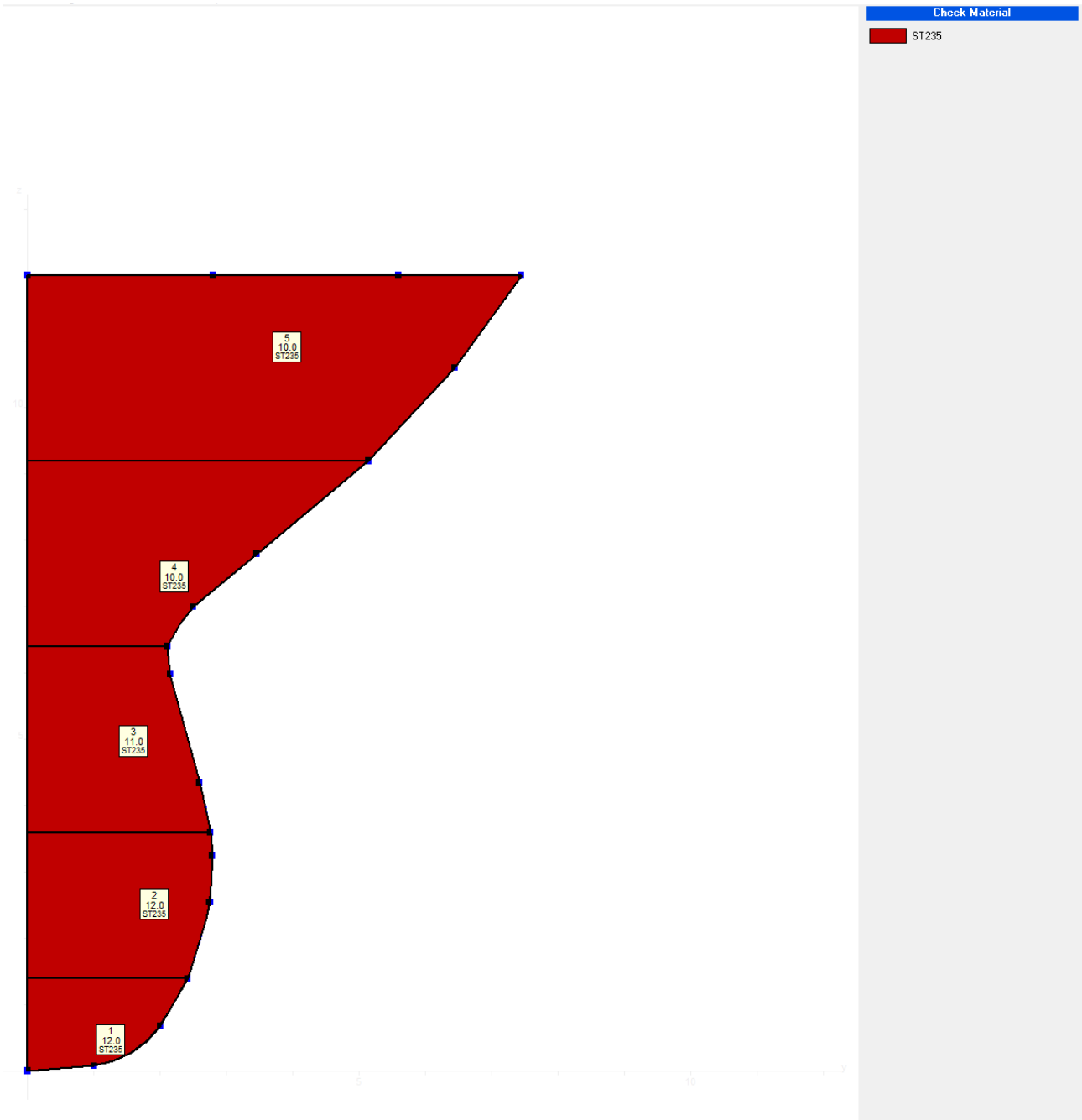


Figure 30 – Transverse Bulkhead Fore – Materials

### 3.7. Primary Supporting Members Fore

The web frame spacing for the fore area is 2.8m.

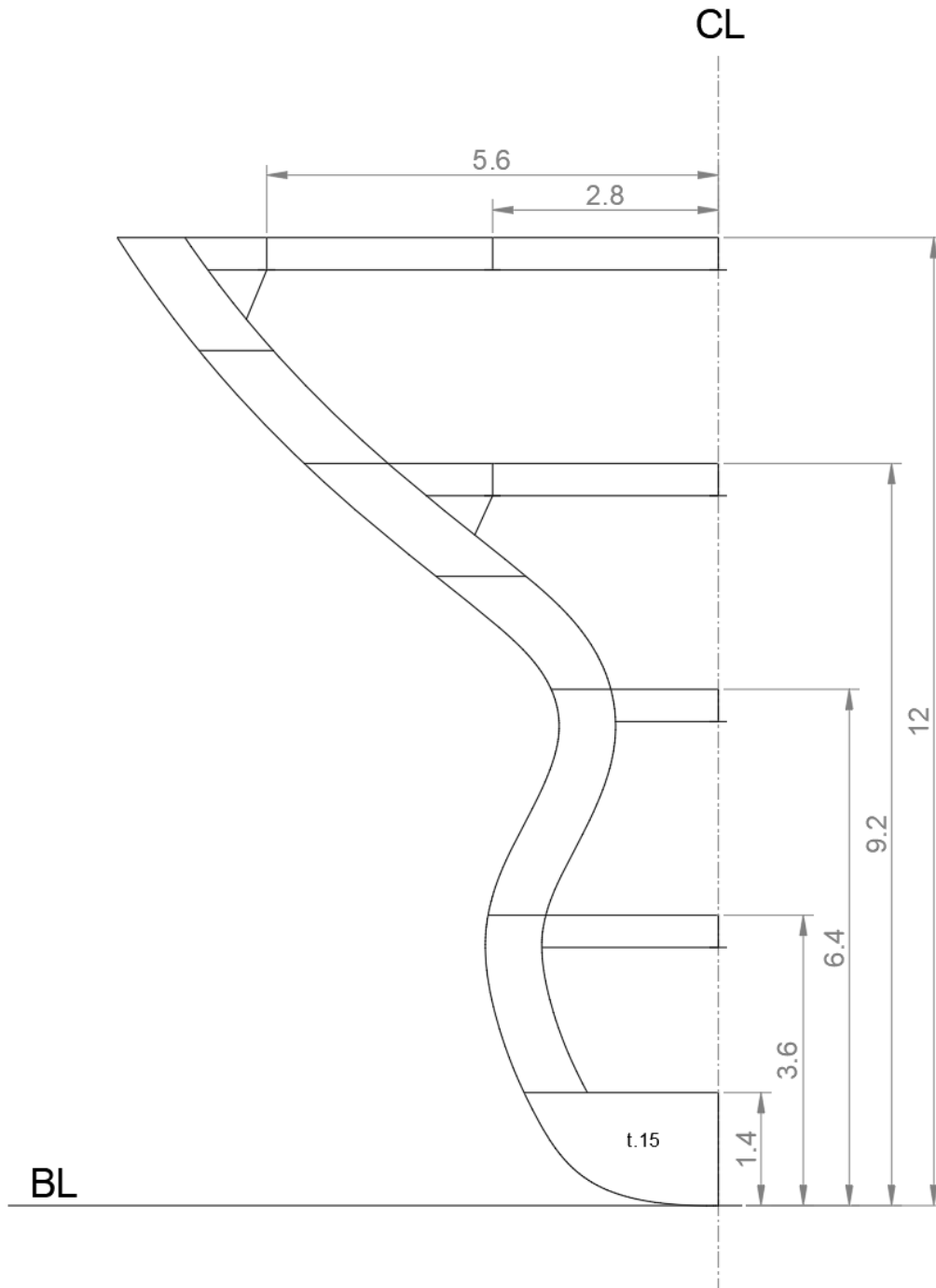


Figure 31 – Primary Supporting Members Fore Sketch

## 4 Scantling Results

### 4.1. Transverse Section

According to the calculation performed in BV Mars 2000, the designed cross section meets the BV Rules requirements.

Hull girder strength criteria			
Hull Girder Loads	Section Moduli	Ultimate Strength	Net/Gross Moduli
		Hogging	Sagging
Design S.W.B.M. (still water bending moment)	400 028.	- 351 551.	(kNm)
Design vertical wave bending moment (Rule)	546 454.	- 594 932.	(kNm)
Design horizontal wave bending moment (Rule)	313 397.		(kNm)
		Positive	Negative
Design vertical shear force	1.		(kN)
Rule vertical wave shear force	8 413.	- 8 413.	(kN)

Close

Figure 32 – Midship Section – Hull Girder Loads

Hull girder strength criteria				
Hull Girder Loads	Section Moduli	Ultimate Strength	Net/Gross Moduli	
	Rule	Actual	at z / BL	k
Modulus at deck	5.40847	6.36510 (m3)	12.000 (m)	1.00
Modulus at bottom	5.40847	8.53423 (m3)	0.000 (m)	1.00
Modulus at Zvt	5.40847	6.19920 (m3)	12.184 (m)	1.00
Inertia	21.90430	43.75059 (m4)	(for information only)	

Close

Figure 33 – Midship Section – Section Modulus and Inertia Check

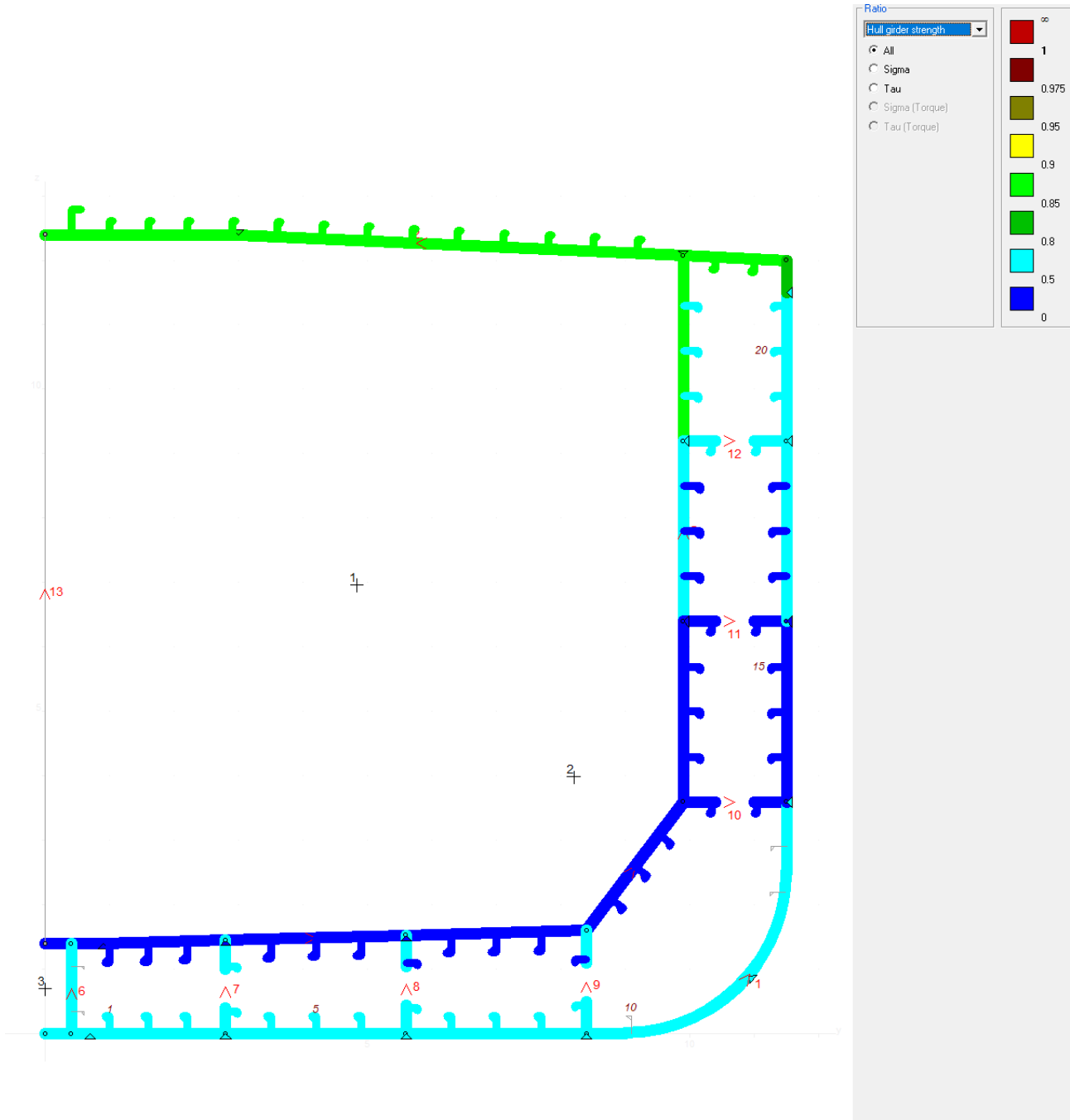


Figure 34 – Midship Section – Hull Girder Strength Check

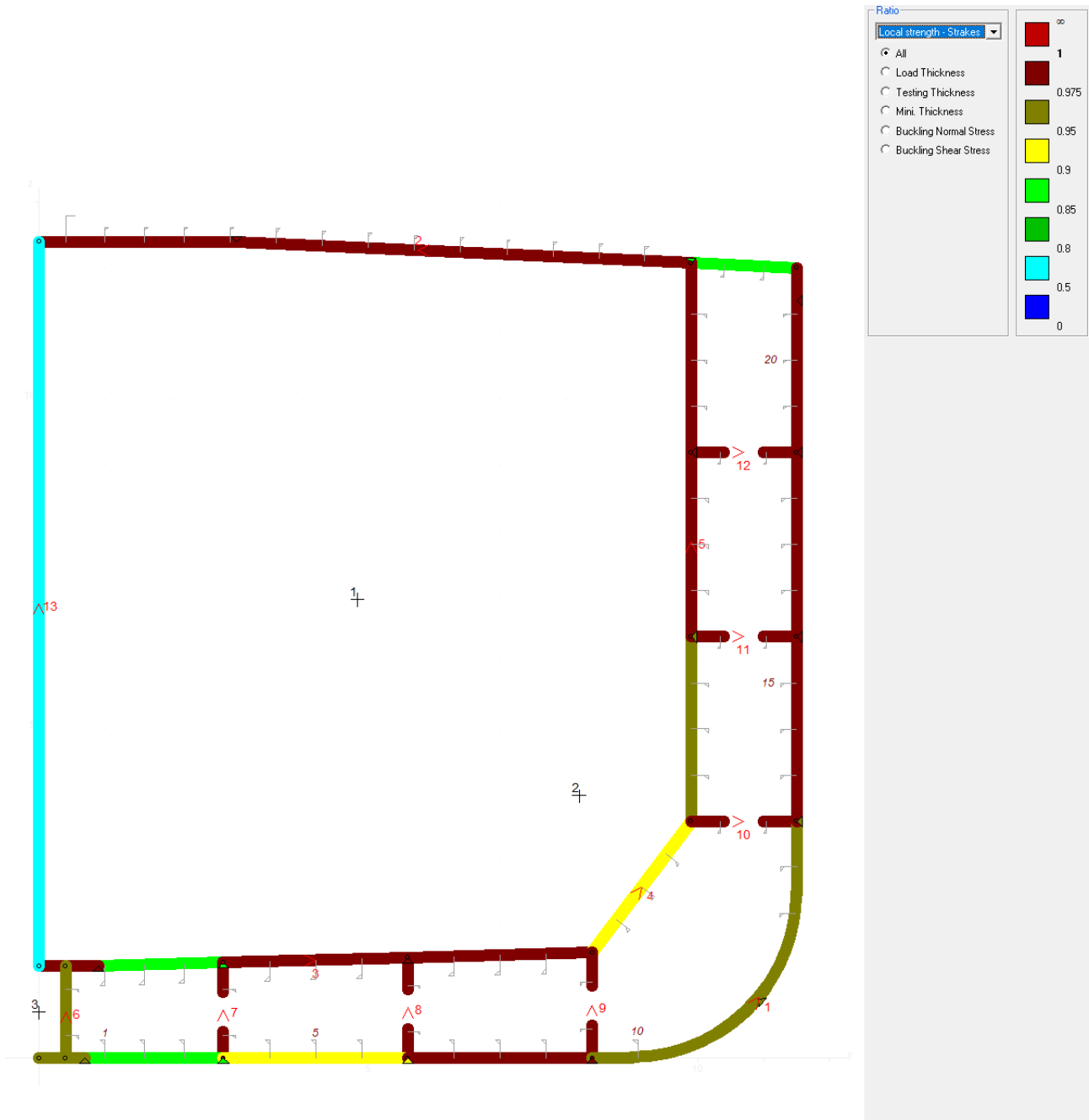


Figure 35 – Midship Section – Local Strength Check – Plates



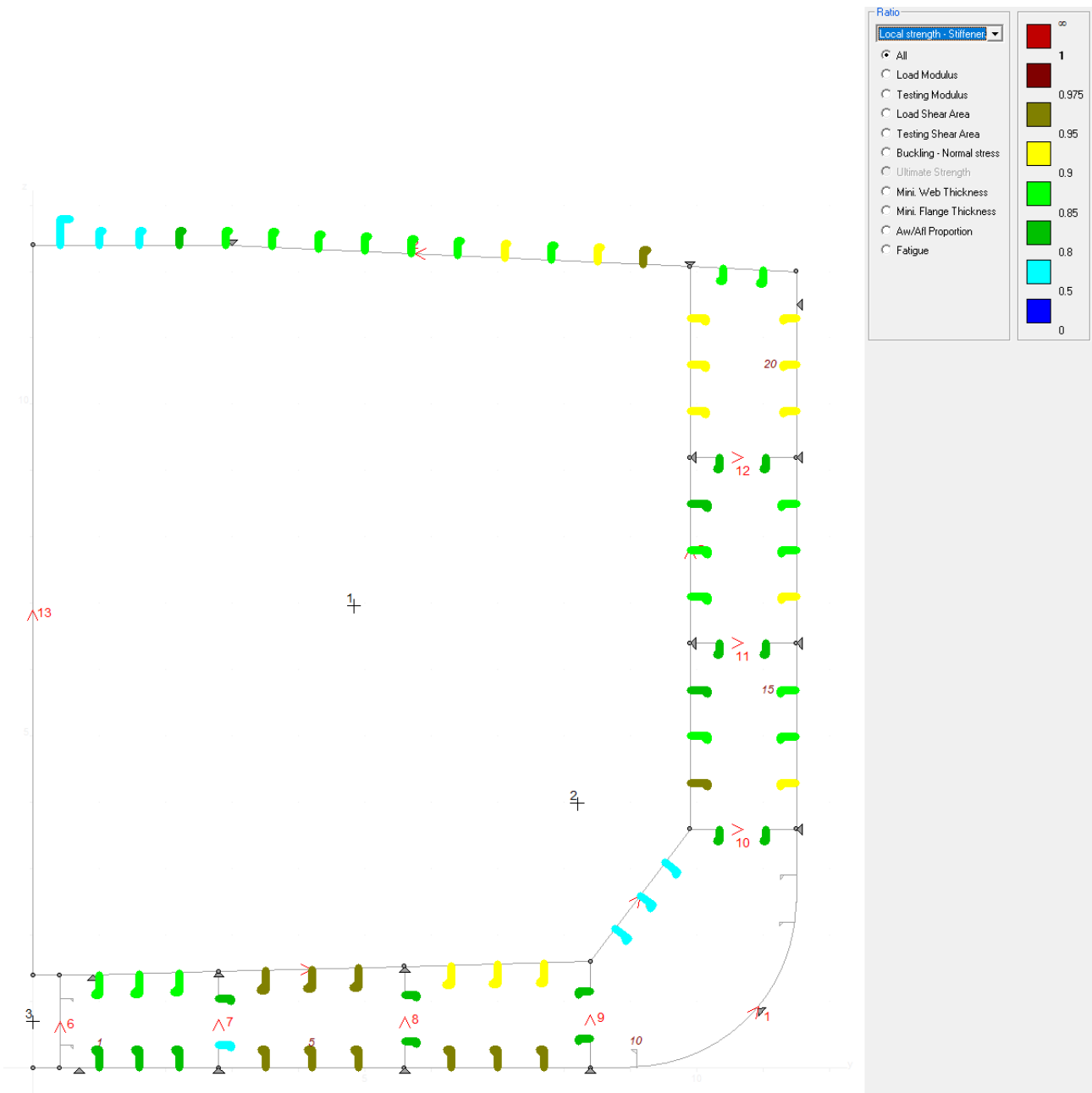


Figure 36 – Midship Section – Local Strength Check – Longitudinal Stiffeners

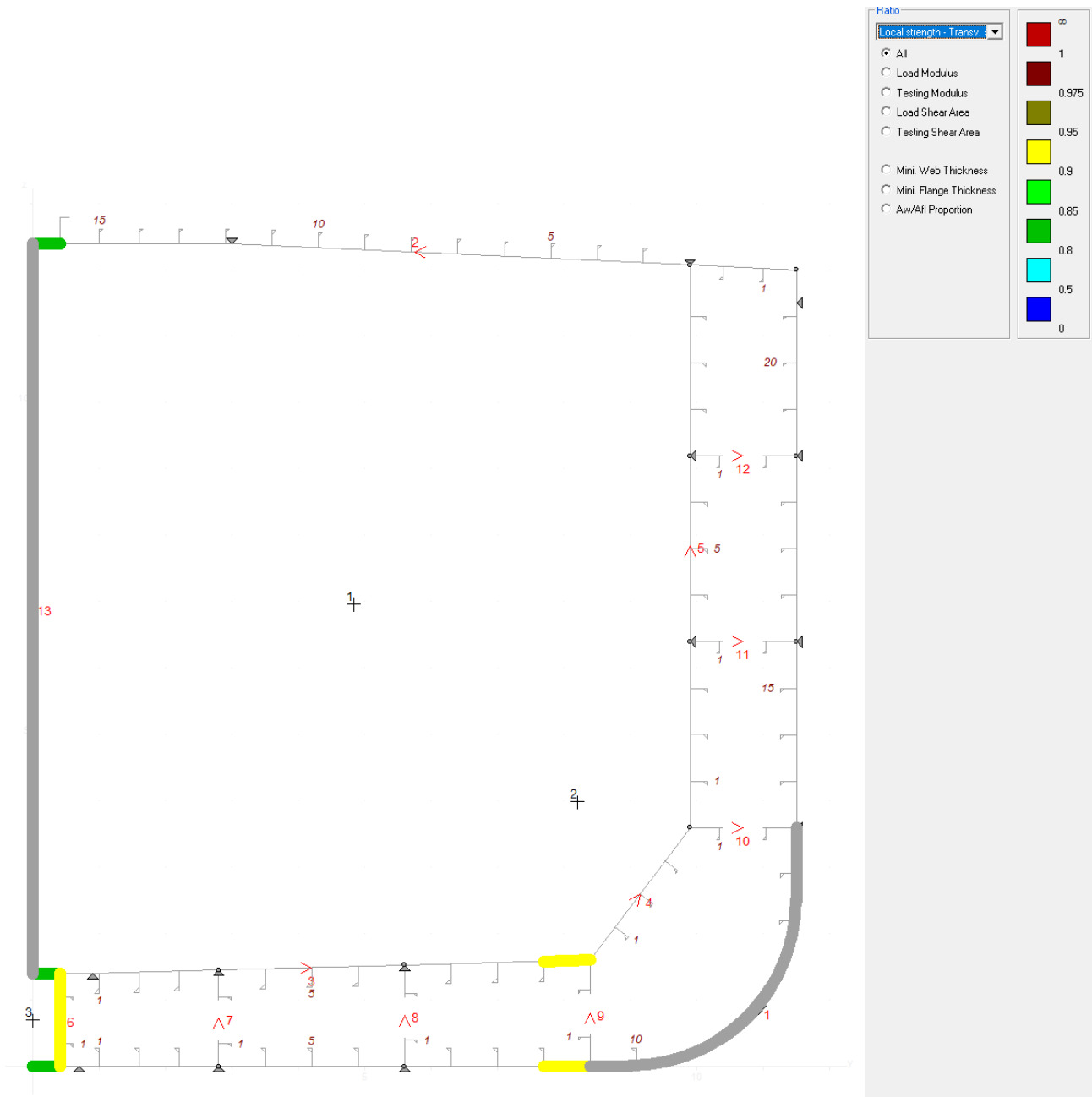
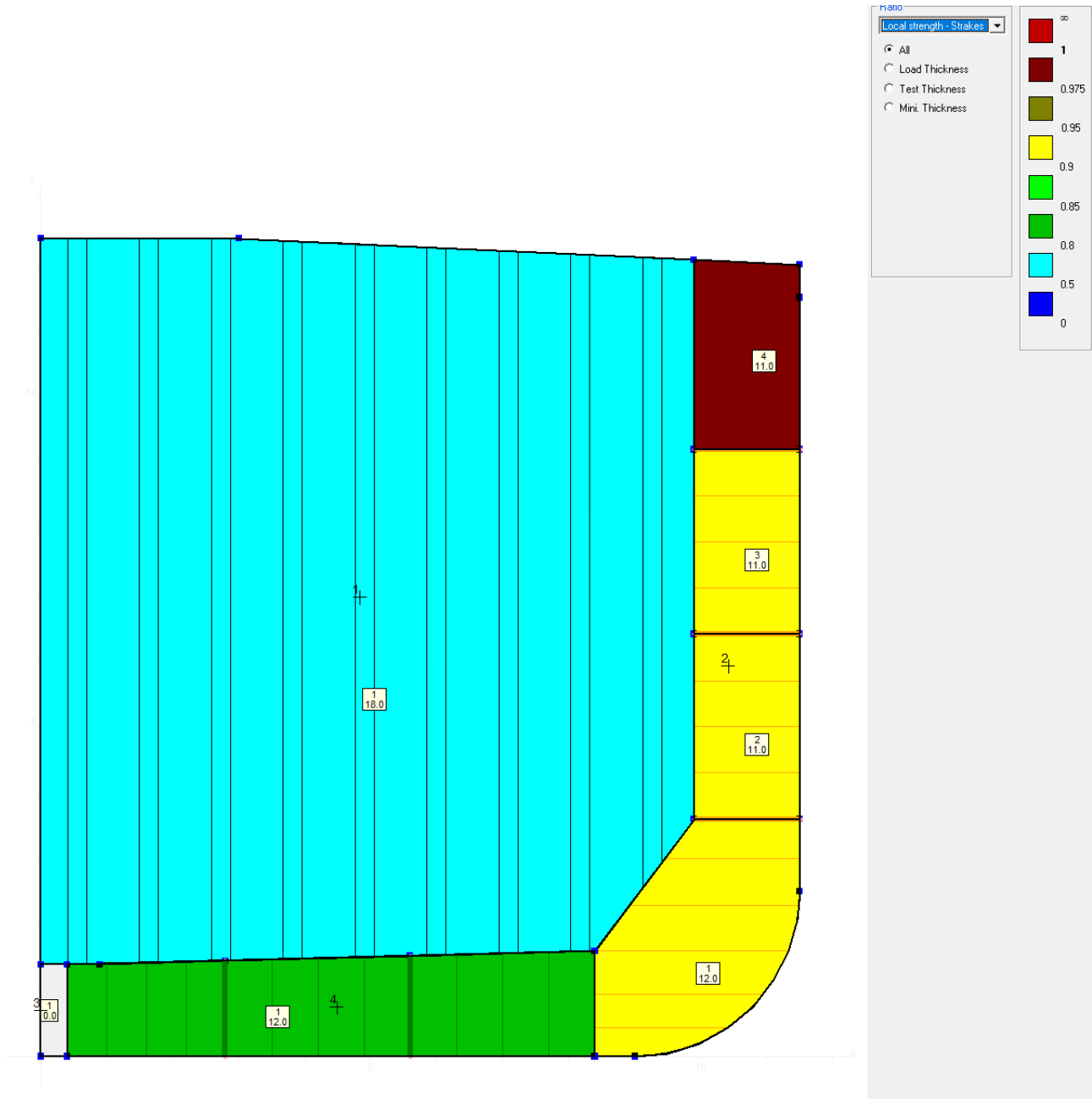


Figure 37 – Midship Section – Local Strength Check – Transverse Stiffeners

## 4.2. Transverse Bulkhead Midship

According to the calculation performed in BV Mars 2000, the designed transverse bulkhead meets the BV Rules requirements.



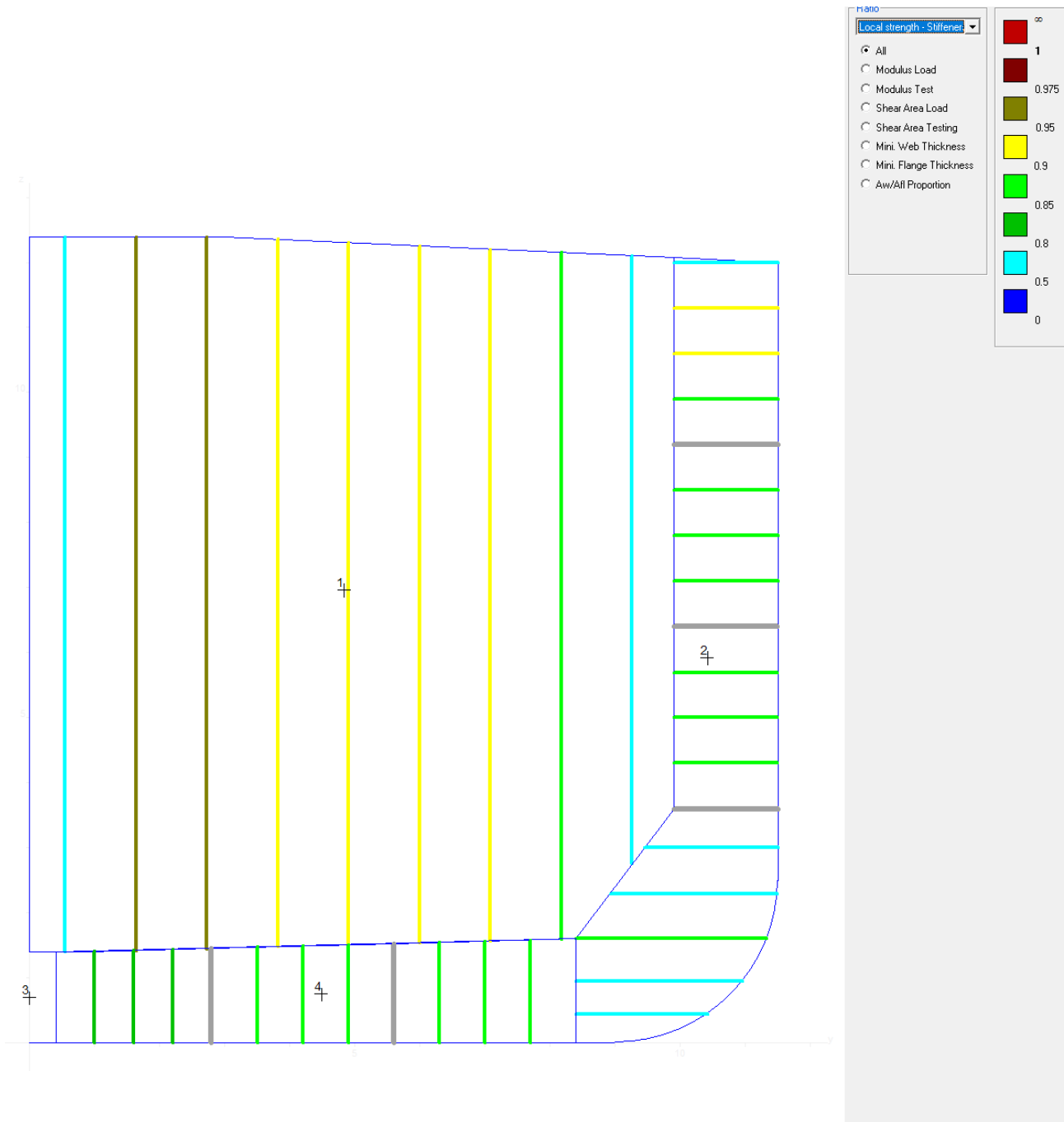



Figure 39 – Transverse Bulkhead – Local Strength Check – Stiffeners

### 4.3. Primary Supporting Members Midship

According to the calculation performed with DNV Nauticus Hull-Primary Supporting Members, the designed PSM meets the Rules requirements.

- Deck Transverse T1000x10/300x14


NAUTICUS™  
HULL

Program: **Primary Supporting Members**  
 Rule ref: **DNV rules Pt.3. Ch.6 Sec.6 July 2015**  
 Rev: 2015-05-29

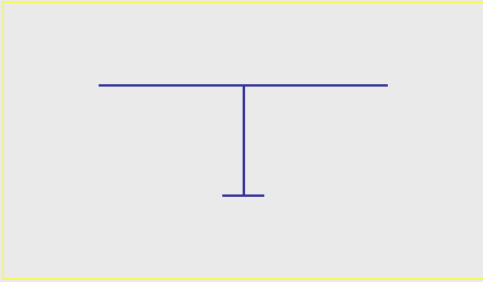
Select/ edit profile
Dim. Help...
Copy to Profile stack
Print
Results>>
Stack->>

Position: Deck Transverse

Name / Id # BuiltUpTbar 1000 x 200 x 10 x 14

Total plate Width:	2118.5	[mm]
Plate Thickness, pT:	14.0	[mm]
Web Height, hw:	1000.0	[mm]
Web Thickness, t:	10.0	[mm]
Flange width (incl. web), bf:	300.0	[mm]
Flange thickness, tf:	14.0	[mm]
Angle Between Profile & Plate:	90.0	[Degrees]

Corrosion addition, plate  $t_c$  0.0 [mm]  
 Corrosion addition, girder 0.0 [mm]



**PROFILE PROPERTIES:**

Total Area: $A_{tot\_n50}$	438.59	[cm2]
Effective Area: $A_{e\_n50}$	438.59	[cm2]
Shear Area in Y-dir.: $A_{yshr\_n50}$	372.80	[cm2]
Shear Area in Z-dir.: $A_{zshr\_n50}$	88.01	[cm2]
Torsional resistance: $Z_{t\_n50}$	180.2	[cm3]
Section modulus: $Z_{yTop\_n50}$	26120.0	[cm3]
Section modulus: $Z_{yBot\_n50}$	7099.5	[cm3]
Section modulus, z-axis: $Z_{z\_n50}$	10501.9	[cm3]

Req. net section mod.  $Z_{n50} >=$  6731.9 [cm3]  
 Req. net shear area:  $A_{shr\_n50} >=$  47.1 [cm2]  
 Web stiff. inertia req.:  $I_{st} >=$  -60.3 [cm4]

OK

Distance to Neutral axis: Yna =	0.00	[mm]
Distance to Neutral axis: Zna =	808.30	[mm]
Shear center offset: eY =	0.00	[mm]
Shear center offset: eZ =	209.83	[mm]
Torsional mom. of inertia: Ix =	252.3	[cm4]
Moment of inertia: Iy =	573856.6	[cm4]
Moment of inertia: Iz =	1112415.4	[cm4]
Centrifugal mom. of in.: Iyz =	0.0	[cm4]
Web and Flange min thick.: t >=	6.0	[mm]
Web pl. slenderness req.: tw >=	6.5	[mm]
Flange slenderness req.: tf >=	12.5	[mm]
Max unsupp. flange length: S <sub>b</sub> <=	5.1	[m]

OK

**BEAM DATA:**

Effective bending span: $l_{bdg}$	9.9	[m]
Effective shear span: $l_{shr}$	9.9	[m]
Load breadth / PSM Spacing: S	3.2	[m]
Yield stress: $R_{eH}$	235.0	[MPa]
Pem. bending stress coeff.: $C_1$	0.85	[-]
Pem. combined str. coeff.: $C_{11}$	0.95	[-]
Pem. bending stress coeff.: $C_{12}$	0.85	[-]
Pem. shear stress coeff.: $C_1$	0.85	[-]
Young's modulus: E	206.0	[GPa]
Cross contraction: $\nu$	0.3	[-]
Shear Modulus: $G=E/(2(1+\nu))$	79.23	[GPa]
Density of material: $\rho$	7.8	[kg/dm3]

Bending moment and shear force distribution factors

Position	1	2	3	Select....
$f_{bdg}$	-	8.00	-	
$f_{shr}$	0.50	-	0.50	

**DESIGN LOAD SET:** LS1 AC-II

Distributed pressure: [kN/m2] Load intensity: [kN/m] At point (x-distance from A)

At Left end: $P_A$	34.3	$q_A$	109.76	$X_A$	0	[m]
Intern. Point: $P_1$		$q_1$	0	$X_{q1}$		[m]
At Right end: $P_B$	34.3	$q_B$	109.76	$X_B$	9.9	[m]

Concentrated loads: Force: [kN] Moment: [kNm] Location: [m]

Load no. 1	$F_1$	$M_1$	$X_1$
Load no. 2	$F_2$	$M_2$	$X_2$
Load no. 3	$F_3$	$M_3$	$X_3$
Load no. 4	$F_4$	$M_4$	$X_4$
Load no. 5	$F_5$	$M_5$	$X_5$
Load no. 6	$F_6$	$M_6$	$X_6$

**Axial load and end moments:**

Hull girder stress, Axial Load:  $\sigma_{hg}$  [Mpa]  $F_z$  = 0.0 [kN]  
 Left end moment: (when  $f_{bdg1}=0$ )  $M_A$  [kNm]  
 Right end moment: (when  $f_{bdg2}=0$ )  $M_B$  [kNm]

Figure 40 – PSM – Deck Transverse Check

- Floor plate 12mm.



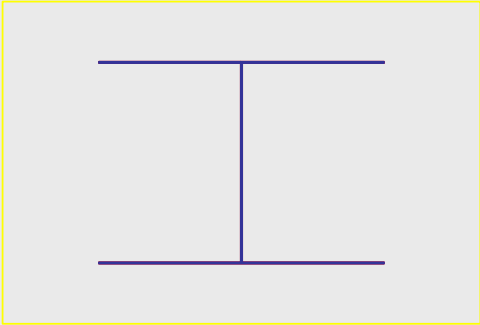
NAUTICUS<sup>™</sup>  
HULL

Program: **Primary Supporting Members**  
 Rule ref: **DNV rules Pt.3. Ch.6 Sec.6 July 2015**  
 Rev: 2015-05-29

Select/ edit profile
Dim. Help...
Copy to Profile stack
Print
Results>>
Stack>>

Position:  
Name / Id #

DoubleSkin 1400 x 10	
PSM spacing, S:	1886.0 [mm]
Web Height between plates:	1400.0 [mm]
Thickness of top/inner plate:	13.0 [mm]
PSM Web plate Thickness:	12.0 [mm]
Thickness of bottom/outer plate:	12.0 [mm]
Corrosion addition, plate $t_c$ :	0.0 [mm]
Corrosion addition, girder:	0.0 [mm]



**PROFILE PROPERTIES:**

Total Area: $A_{tot\_n50} =$	639.50 [cm2]	Distance to Neutral axis: $Y_{na} =$	0.00 [mm]
Effective Area: $A_{x\_n50} =$	639.50 [cm2]	Distance to Neutral axis: $Z_{na} =$	733.01 [mm]
Shear Area in Y-dir.: $A_{yshr\_n50} =$	314.34 [cm2]	Shear center offset: $eY =$	0.00 [mm]
Shear Area in Z-dir.: $A_{zshr\_n50} =$	160.84 [cm2]	Shear center offset: $eZ =$	7.49 [mm]
Torsional resistance: $Z_{x\_n50} =$	1838611.6 [cm3]	Torsional mom. of inertia: $I_x =$	2390195.1 [cm4]
Section modulus: $Z_{yTop\_n50} =$	37912.5 [cm3]	Moment of inertia: $I_y =$	2623495.4 [cm4]
Section modulus: $Z_{yBot\_n50} =$	35790.6 [cm3]	Moment of inertia: $I_z =$	1397623.2 [cm4]
Section modulus, z-axis: $Z_{z\_n50} =$	14821.0 [cm3]	Centrifugal mom. of in.: $I_{yz} =$	[cm4]
Req. net section mod. $Z_{n50} >=$	7563.1 [cm3]	Web and Flange min thick.: $t >=$	7.0 [mm]
Req. net shear area: $A_{shr\_n50} >=$	93.6 [cm2]	Web pl. slenderness req.: $tw >=$	7.0 [mm]
Web stiff. inertia req.: $I_{st} >=$	-75.1 [cm4]	! Flange slenderness req.: $tf >=$	78.5 [mm]
	OK	Max unsupp. flange length: $S_b <=$	37.3 [m]

Copy to Profile stack
Floors
Other area

**BEAMDATA:**

Effective bending span: $l_{bdg} =$	8.4 [m]
Effective shear span: $l_{shr} =$	8.4 [m]
Load breadth / PSM Spacing: $S =$	3.2 [m]
Yield stress: $R_{eH} =$	235.0 [MPa]
Perm. bending stress coeff.: $C_s =$	0.85 [-]
Perm. combined str. coeff.: $C_{s1} =$	0.95 [-]
Perm. bending stress coeff.: $C_{s2} =$	0.85 [-]
Perm. shear stress coeff.: $C_t =$	0.85 [-]
Young's modulus: $E =$	206.0 [GPa]
Cross contraction: $v =$	0.3 [-]
Shear Modulus: $G = E / (2(1+v)) =$	79.23 [GPa]
Density of material: $\rho =$	7.8 [kg/dm3]

Bending moment and shear force distribution factors:

Position	1	2	3	Select....
$f_{bdg}$	12.00	24.00	12.00	
$f_{shr}$	0.50	-	0.50	

**DESIGN LOAD SET:** LS1 AC-II

**Distributed pressure:** [ kN/m<sup>2</sup> ] [ kN/m ]

At Left end: $P_A =$	80.29	$q_A =$	256.928	$X_A =$	0 [m]
Interm. Point: $P_1 =$		$q_1 =$	0	$X_{q1} =$	[m]
At Right end: $P_B =$	80.29	$q_B =$	256.928	$X_A =$	8.4 [m]

**Concentrated loads:** Force: [ kN ] Moment: [ kNm ] Location: [ m ]

Load no. 1	$F_1 =$	$M_1 =$	$X_1 =$
Load no. 2	$F_2 =$	$M_2 =$	$X_2 =$
Load no. 3	$F_3 =$	$M_3 =$	$X_3 =$
Load no. 4	$F_4 =$	$M_4 =$	$X_4 =$
Load no. 5	$F_5 =$	$M_5 =$	$X_5 =$
Load no. 6	$F_6 =$	$M_6 =$	$X_6 =$

**Axial load and end moments:**

Hull girder stress, Axial Load:  $\sigma_{hg} =$  [Mpa]  $F_x =$  0.0 [kN]

Left end moment: (when  $f_{bdg1}=0$ )  $M_A =$  [kNm]

Right end moment: (when  $f_{bdg3}=0$ )  $M_B =$  [kNm]

Figure 41 – PSM – Floor Check

- Side webframe plate 12mm.



NAUTICUS<sup>®</sup>  
HULL

Program: **Primary Supporting Members**

Rule ref: **DNV rules Pt.3. Ch.6 Sec.6 July 2015**

Rev: 2015-05-29

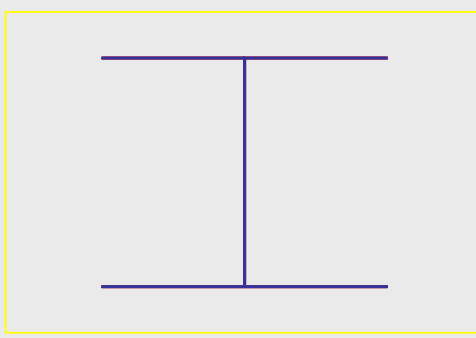
<input type="button" value="Select/ edit profile"/> <input type="button" value="Dim. Help..."/> <input type="button" value="Copy to Profile stack"/> <input type="button" value="Print"/> <input type="button" value="Results&gt;&gt;"/> <input type="button" value="Stack&gt;&gt;"/>	
Position: <b>Side Webframe</b> Name / Id # <b>DoubleSkin 1600 x 10</b> PSM spacing, S: 1886.0 [mm] Web Height between plates: 1600.0 [mm] Thickness of top/inner plate: 13.0 [mm] PSM Web plate Thickness: 12.0 [mm] Thickness of bottom/outer plate: 12.0 [mm]	
Corrosion addition, plate $t_c$ 0.0 [mm] Corrosion addition, girder 0.0 [mm]	
<b>PROFILE PROPERTIES:</b> ?	
Total Area: $A_{tot\_n50} = 663.50$ [cm <sup>2</sup> ] Effective Area: $A_{x\_n50} = 663.50$ [cm <sup>2</sup> ] Shear Area in Y-dir.: $A_{yshr\_n50} = 314.34$ [cm <sup>2</sup> ] Shear Area in Z-dir.: $A_{zshr\_n50} = 182.46$ [cm <sup>2</sup> ] Torsional resistance: $Z_{x\_n50} = 2390843.9$ [cm <sup>3</sup> ] Section modulus: $Z_{yTop\_n50} = 43943.7$ [cm <sup>3</sup> ] Section modulus: $Z_{yBot\_n50} = 41565.7$ [cm <sup>3</sup> ] Section modulus, z-axis: $Z_{z\_n50} = 14821.1$ [cm <sup>3</sup> ]  Req. net section mod. $Z_{n50} >= 10407.9$ [cm <sup>3</sup> ] Req. net shear area: $A_{shr\_n50} >= 128.8$ [cm <sup>2</sup> ] Web stiff. inertia req.: $I_{st} >= -69.3$ [cm <sup>4</sup> ]  OK	Distance to Neutral axis: $Y_{na} = 0.00$ [mm] Distance to Neutral axis: $Z_{na} = 835.10$ [mm] Shear center offset: $eY = 0.00$ [mm] Shear center offset: $eZ = 9.40$ [mm] Torsional mom. of inertia: $I_x = 3108097.1$ [cm <sup>4</sup> ] Moment of inertia: $I_y = 3471133.1$ [cm <sup>4</sup> ] Moment of inertia: $I_z = 1397626.1$ [cm <sup>4</sup> ] Centrifugal mom. of in.: $I_{yz} =$ [cm <sup>4</sup> ] Web and Flange min thick: $t >= 7.0$ [mm] Floors Web pl. slenderness req.: $tw >= 7.0$ [mm] ! Flange slenderness req.: $tf >= 78.5$ [mm] Max unsupp. flange length: $S_b <= 36.8$ [m] Other area  Not OK!
<b>BEAMDATA:</b> ? <input type="button" value="Copy to Beam"/>	<b>DESIGN LOAD SET:</b> L51 AC-II
Effective bending span: $l_{bdg} = 8.4$ [m] Effective shear span: $l_{shr} = 8.4$ [m] Load breadth / PSM Spacing: $S = 3.2$ [m] Yield stress: $R_{eH} = 235.0$ [MPa] Perm. bending stress coeff.: $C_s = 0.85$ [-] Perm. combined str. coeff.: $C_{s1} = 0.95$ [-] Perm. bending stress coeff.: $C_{s2} = 0.85$ [-] Perm. shear stress coeff.: $C_t = 0.85$ [-] Young's modulus: $E = 206.0$ [GPa] Cross contraction: $\nu = 0.3$ [-] Shear Modulus: $G = E / (2(1+\nu)) = 79.23$ [GPa] Density of material: $\rho = 0.0$ [kg/dm <sup>3</sup> ]  Bending moment and shear force distribution factors Position 1 2 3 Select.... $f_{bdg}$ 12.00 24.00 12.00 $f_{shr}$ 0.50 - 0.50	Load intensity: At point (x-distance from A) Distributed pressure: [kN/m <sup>2</sup> ] ? [kN/m] At Left end: $P_A = 110.49$ $q_A = 353.568$ $X_A = 0$ [m] Interm. Point: $P_1 =$ $q_1 = 0$ $X_{q1} =$ [m] At Right end: $P_B = 110.49$ $q_B = 353.568$ $X_A = 8.4$ [m]  Concentrated loads: Force: [kN] ? Moment: [kNm] Location: [m] Load no. 1 $F_1 =$ $M_1 =$ $X_1 =$ Load no. 2 $F_2 =$ $M_2 =$ $X_2 =$ Load no. 3 $F_3 =$ $M_3 =$ $X_3 =$ Load no. 4 $F_4 =$ $M_4 =$ $X_4 =$ Load no. 5 $F_5 =$ $M_5 =$ $X_5 =$ Load no. 6 $F_6 =$ $M_6 =$ $X_6 =$  Axial load and end moments: Hull girder stress, Axial Load: $\sigma_{hg} =$ [Mpa] $F_x = 0.0$ [kN] Left end moment: (when $f_{bdg1}=0$ ) $M_A =$ [kNm] Right end moment: (when $f_{bdg3}=0$ ) $M_B =$ [kNm]

Figure 42 – PSM – Side Webframe Check

#### 4.4. Fore Section

According to the calculation performed in BV Mars 2000, the designed cross section meets the BV Rules requirements.

Hull girder strength criteria

Hull Girder Loads | Section Moduli | Net/Gross Moduli

	Hogging	Sagging	
Design S.W.B.M. (still water bending moment)	122 675.	- 107 809.	(kNm)
Design vertical wave bending moment (Rule)	62 452.	- 67 992.	(kNm)
Design horizontal wave bending moment (Rule)	35 817.		(kNm)

	Positive	Negative	
Design vertical shear force	1.		(kN)
Rule vertical wave shear force	3 207.	- 2 945.	(kN)

Close

Figure 43 – Fore Section – Hull Girder Loads

Hull girder strength criteria

Hull Girder Loads | Section Moduli | Net/Gross Moduli

	Rule	Actual	at z / BL	k
Modulus at deck	1.48102	3.95155 (m <sup>3</sup> )	12.000 (m)	1.00
Modulus at bottom	1.48102	2.68309 (m <sup>3</sup> )	0.000 (m)	1.00

Inertia	21.90430	19.17637 (m <sup>4</sup> ) (for information only)		
---------	----------	---	--	--

Close

Figure 44 – Fore Section – Section Modulus and Inertia Check



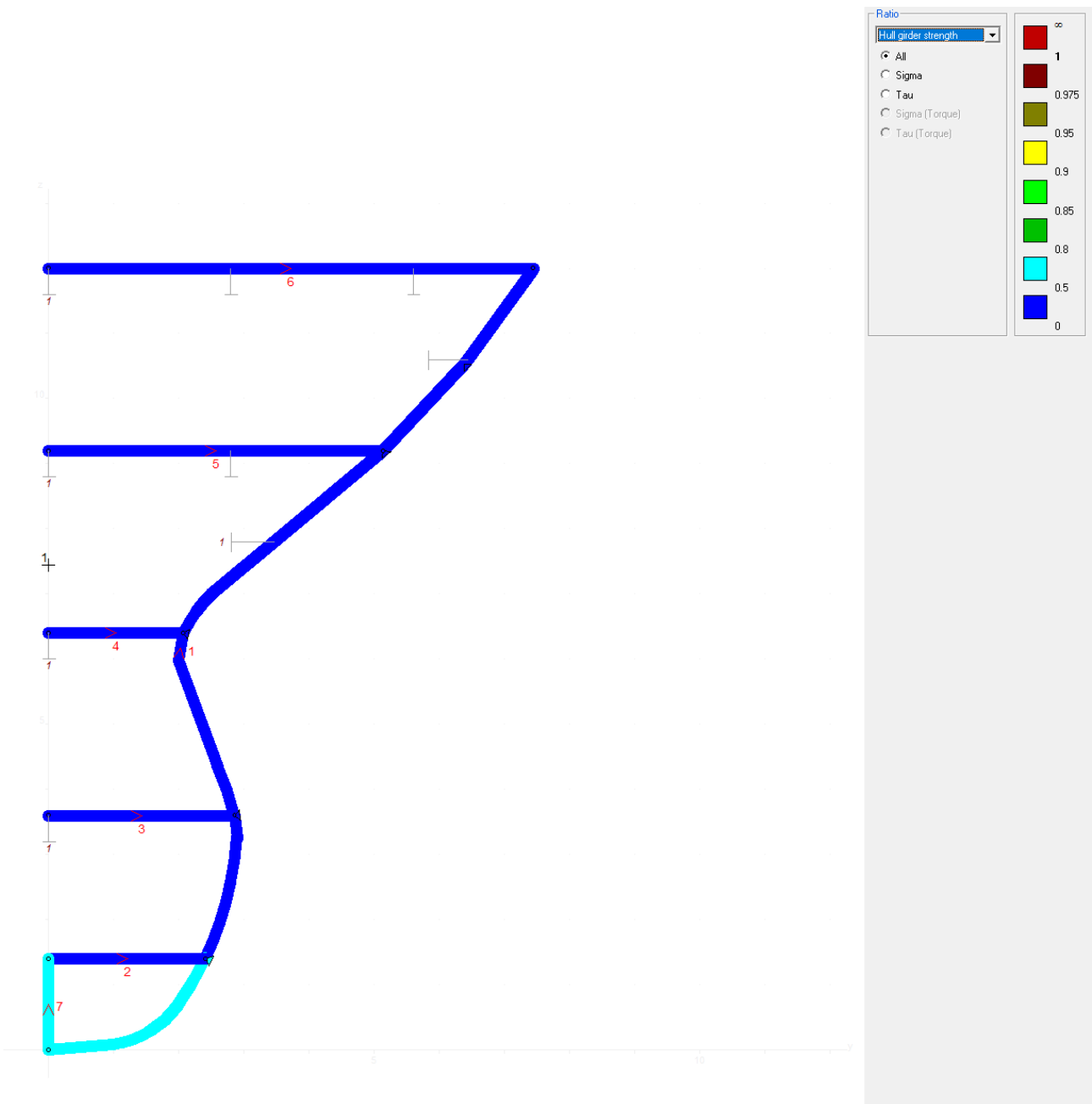


Figure 45 – Fore Section – Hull Girder Strength Check

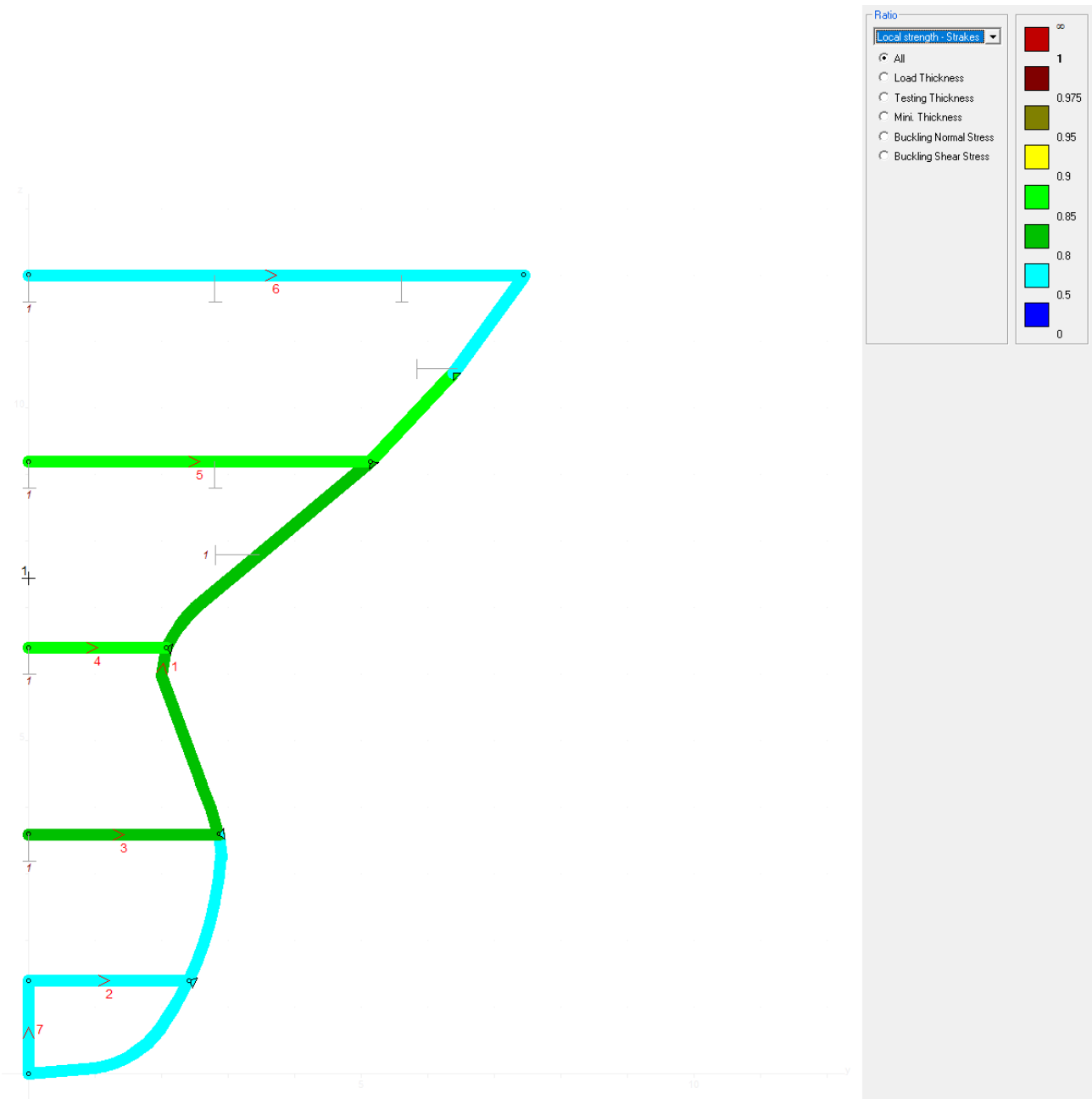


Figure 46 – Fore Section – Local Strength Check – Plates

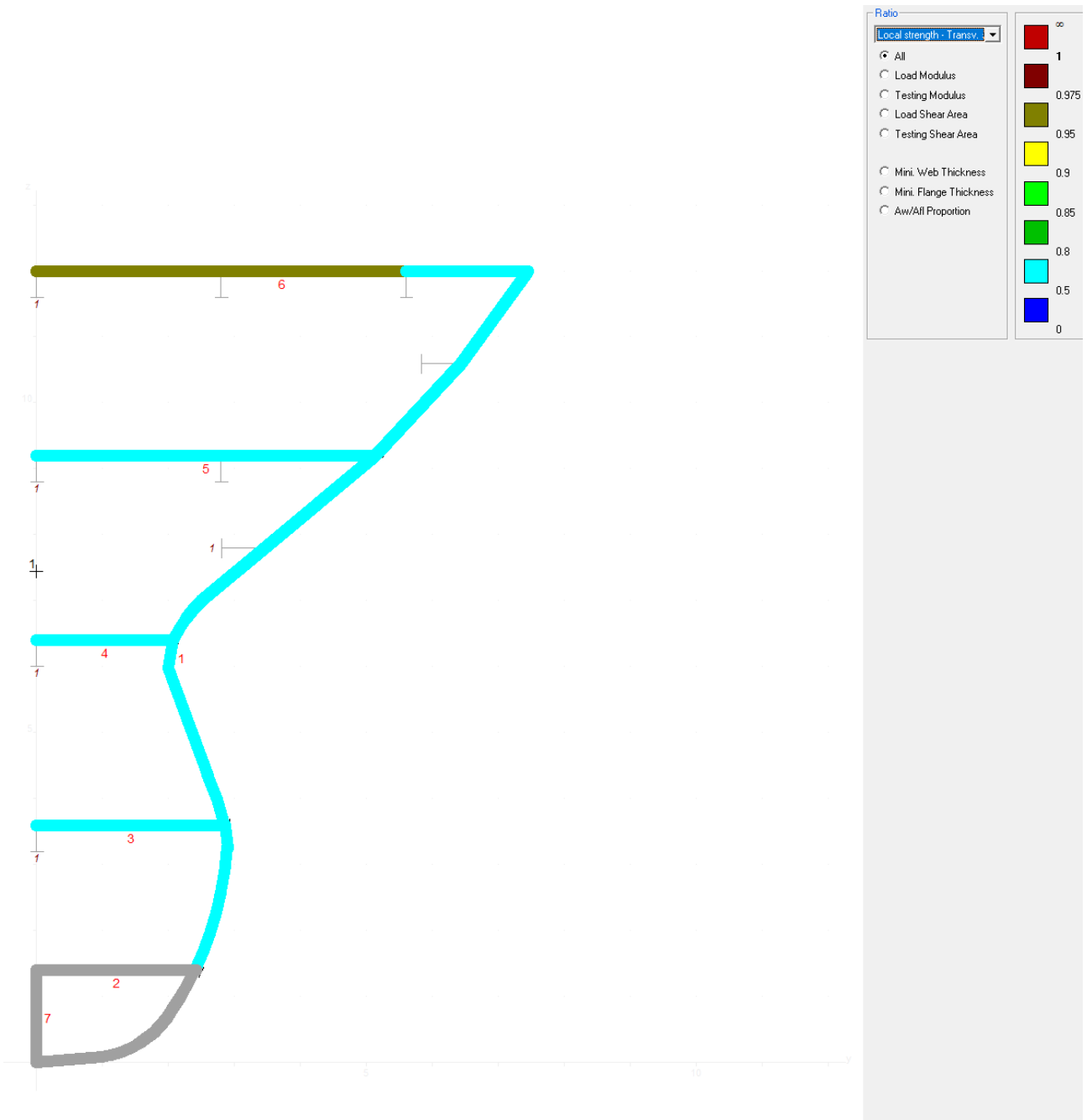


Figure 47 – Fore Section – Local Strength Check – Transverse Stiffeners

#### 4.5. Transverse Bulkhead Fore

According to the calculation performed in BV Mars 2000, the designed transverse bulkhead meets the BV Rules requirements.

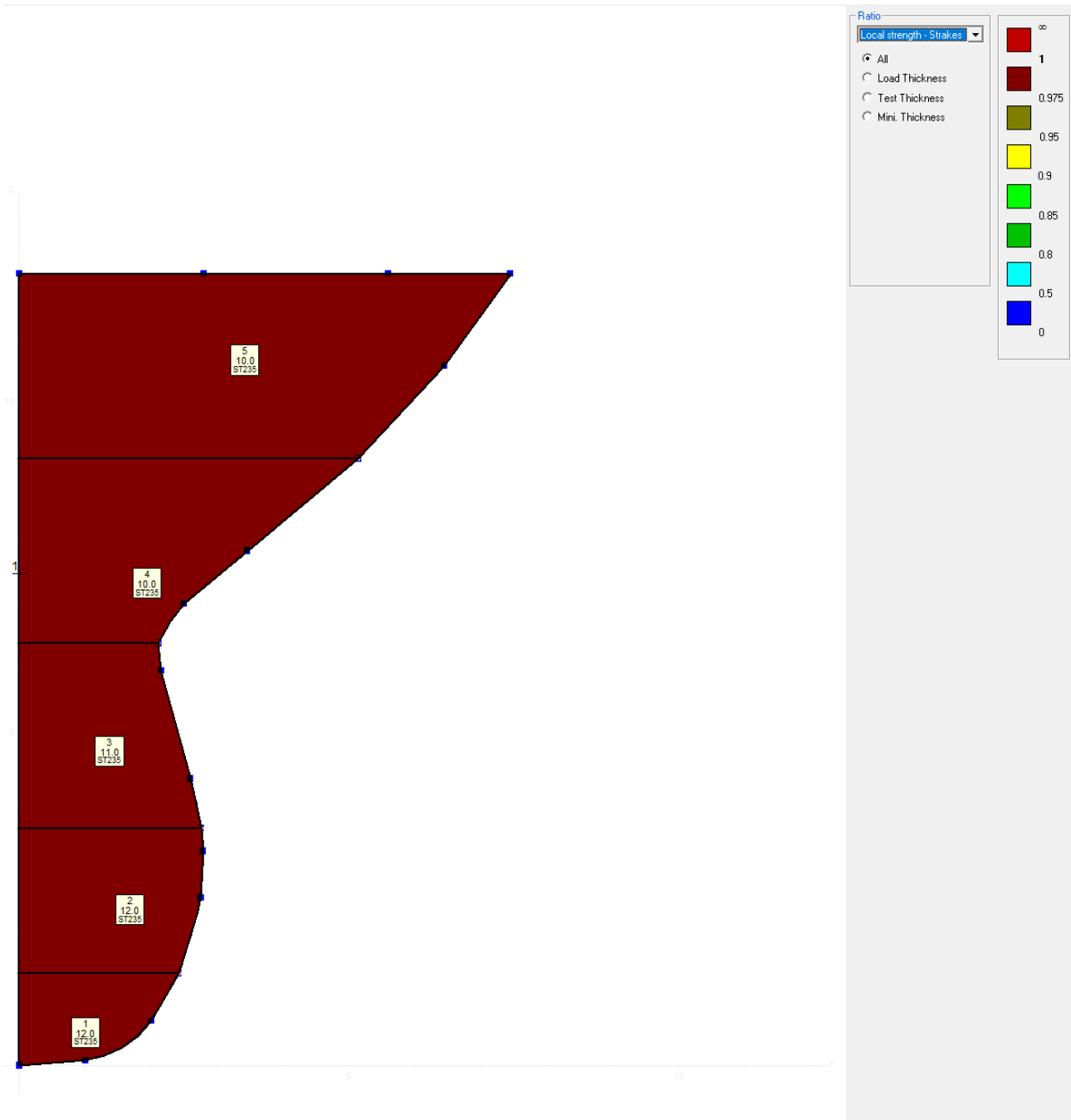


Figure 48 – Transverse Bulkhead Fore – Local Strength Check – Plates

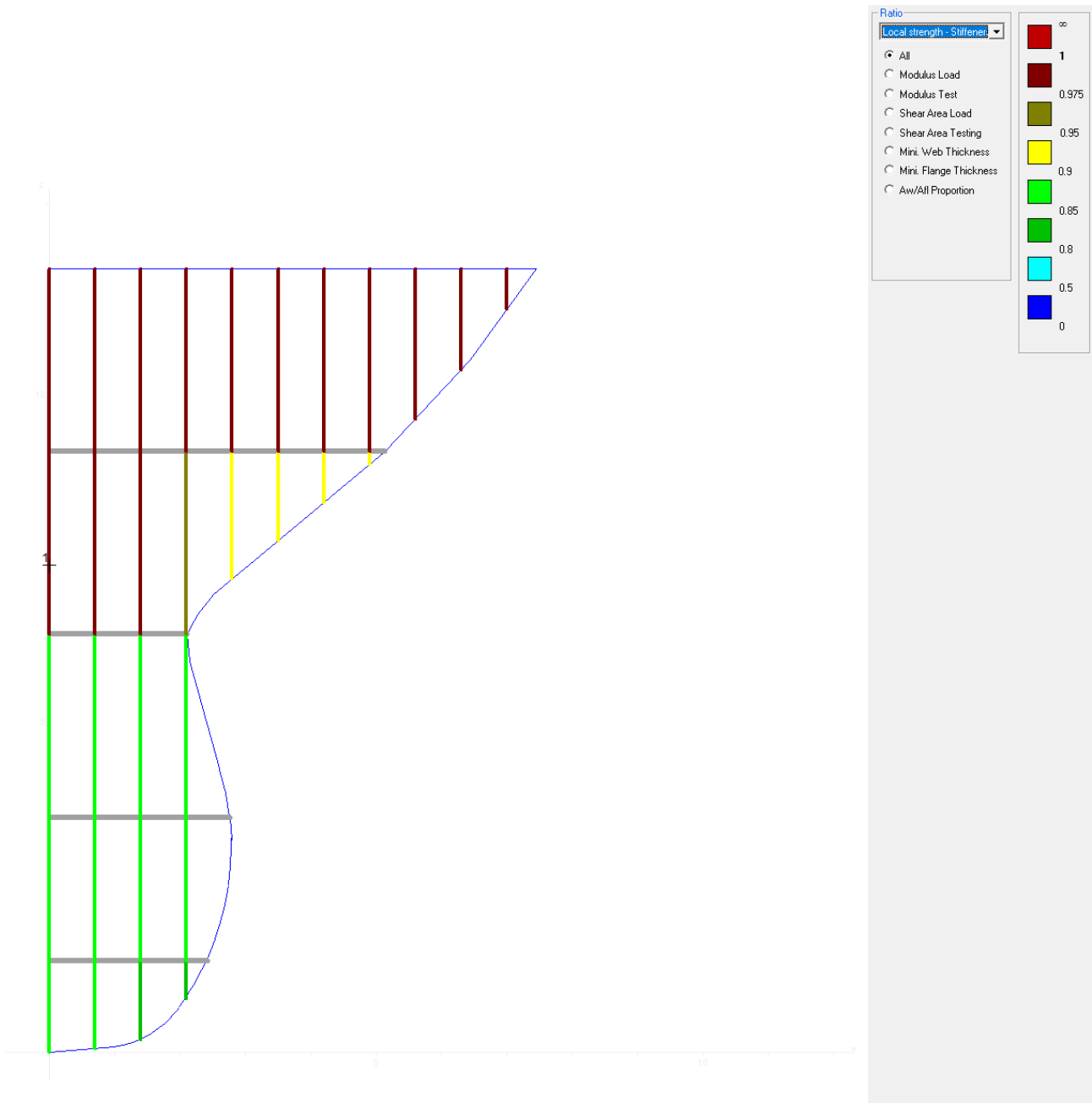



Figure 49 – Transverse Bulkhead Fore – Local Strength Check – Stiffeners

## 4.6. Primary Supporting Members Fore

According to the calculation performed with DNV Nauticus Hull-Primary Supporting Members, the designed PSM meets the Rules requirements.

- Main Deck Transverse and Girders T500x14/300x16


NAUTICUS™  
HULL

Program: **Primary Supporting Members**  
 Rule ref: **DNV rules Pt.3. Ch.6 Sec.6 July 2015**  
 Rev: 2015-05-29

Select/ edit profile
Dim. Help...
Copy to Profile stack
Print
Results>>
Stack>>

Position: **Deck Transverse**

Name / Id # **BuiltUpTbar 600 x 300 x 14 x 16**

Total plate Width: 1746.2 [mm]

Plate Thickness, pT: 10.0 [mm]

Web Height, hw: 500.0 [mm]

Web Thickness, t: 14.0 [mm]

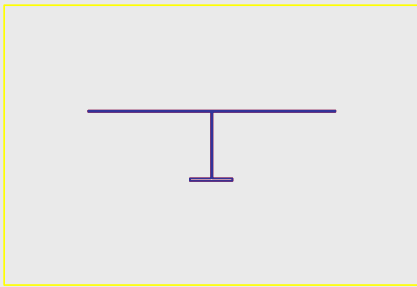
Flange width (incl. web), bf: 300.0 [mm]

Flange thickness, tf: 16.0 [mm]

Angle Between Profile & Plate: 90.0 [Degrees]

Corrosion addition, plate: 0.0 [mm]

Corrosion addition, girder: 0.0 [mm]



**PROFILE PROPERTIES:**

Total Area: A <sub>tot_n50</sub> =	292.62 [cm2]	Distance to Neutral axis: Yna =	0.00 [mm]
Effective Area: A <sub>x_n50</sub> =	292.62 [cm2]	Distance to Neutral axis: Zna =	375.85 [mm]
Shear Area in Y-dir.: A <sub>yshr_n50</sub> =	248.73 [cm2]	Shear center offset: eY =	0.00 [mm]
Shear Area in Z-dir.: A <sub>zshr_n50</sub> =	65.38 [cm2]	Shear center offset: eZ =	141.02 [mm]
Torsional resistance: Z <sub>x_n50</sub> =	100.6 [cm3]	Torsional mom. of inertia: Ix =	140.9 [cm4]
Section modulus: Z <sub>yTop_n50</sub> =	8311.3 [cm3]	Moment of inertia: Iy =	124795.4 [cm4]
Section modulus: Z <sub>yBot_n50</sub> =	3320.4 [cm3]	Moment of inertia: Iz =	447323.0 [cm4]
Section modulus, z-axis: Z <sub>z_n50</sub> =	5123.4 [cm3]	Centrifugal mom. of in.: Iyz =	0.0 [cm4]
Req. net section mod. Z <sub>n50</sub> >=	3262.9 [cm3]	Web and Flange min thick.: t >=	6.0 [mm]
Req. net shear area: A <sub>shr_n50</sub> >=	56.5 [cm2]	Web pl. slenderness req.: tw >=	4.0 [mm]
Web stiff. inertia req.: I <sub>st</sub> >=	-19.3 [cm4]	Flange slenderness req.: tf >=	12.5 [mm]
	OK	Max unsp. flange length: S <sub>b</sub> <=	5.5 [m]

**BEAM DATA:**

Effective bending span: l <sub>bdg</sub> =	6.0 [m]
Effective shear span: l <sub>shr</sub> =	6.0 [m]
Load breadth / PSM Spacing: S =	2.8 [m]
Yield stress: R <sub>eH</sub> =	235.0 [MPa]
Perm bending stress coeff.: C <sub>s</sub> =	0.85 [-]
Perm combined str. coeff.: C <sub>s1</sub> =	0.95 [-]
Perm bending stress coeff.: C <sub>s2</sub> =	0.85 [-]
Perm shear stress coeff.: C <sub>t</sub> =	0.85 [-]
Young's modulus: E =	206.0 [GPa]
Cross contraction: v =	0.3 [-]
Shear Modulus: G=E/(2(1+v)) =	79.23 [GPa]
Density of material: ρ =	7.8 [kg/dm3]

Bending moment and shear force distribution factors

Position	1	2	3	Select...
f <sub>bdg</sub>	12.00	24.00	12.00	
f <sub>shr</sub>	0.50	-	0.50	

**DESIGN LOAD SET:** L51 AC-II

Distributed pressure: [kN/m<sup>2</sup>] Load intensity: At point (x-distance from A)

At Left end: P <sub>A</sub> = 77.59	q <sub>A</sub> = 217.252	X <sub>A</sub> = 0 [m]
Intern. Point: P <sub>1</sub> =	q <sub>1</sub> = 0	X <sub>q1</sub> = [m]
At Right end: P <sub>B</sub> = 77.59	q <sub>B</sub> = 217.252	X <sub>A</sub> = 6.0 [m]

Concentrated loads:

Load no.	Force: [kN]	Moment: [kNm]	Location: [m]
Load no. 1	F <sub>1</sub>	M <sub>1</sub>	X <sub>1</sub>
Load no. 2	F <sub>2</sub>	M <sub>2</sub>	X <sub>2</sub>
Load no. 3	F <sub>3</sub>	M <sub>3</sub>	X <sub>3</sub>
Load no. 4	F <sub>4</sub>	M <sub>4</sub>	X <sub>4</sub>
Load no. 5	F <sub>5</sub>	M <sub>5</sub>	X <sub>5</sub>
Load no. 6	F <sub>6</sub>	M <sub>6</sub>	X <sub>6</sub>

**Axial load and end moments:**

Hull girder stress, Axial Load: σ<sub>hg</sub> = [Mpa] F<sub>x</sub> = 0.0 [kN]

Left end moment: (when f<sub>bdg1</sub>=0) M<sub>A</sub> = [kNm]

Right end moment: (when f<sub>bdg3</sub>=0) M<sub>B</sub> = [kNm]

Figure 50 – PSM Fore – Main Deck Transverse and Girders Check

- Lower Deck Transverse and Girders T400x8/200x10



NAUTICUS<sup>®</sup>  
HULL

Program: **Primary Supporting Members**

Rule ref: **DNV rules Pt.3. Ch.6 Sec.6 July 2015**

Rev: 2015-05-29

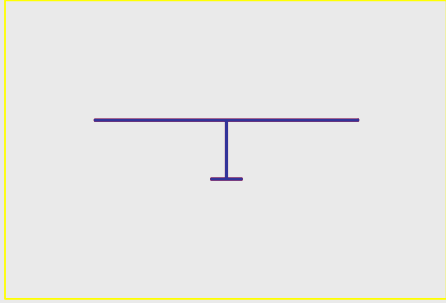
<input type="button" value="Select/ edit profile"/> <input type="button" value="Dim. Help..."/> <input type="button" value="Copy to Profile stack"/> <input type="button" value="Print"/> <input type="button" value="Results&gt;&gt;"/> <input type="button" value="Stack&gt;&gt;"/>	
Position: <b>Deck Transverse</b> Name / Id # <b>BuiltUpTbar 400 x 200 x 10 x 12</b> Total plate Width: 1746.2 [mm] Plate Thickness, pT: 10.0 [mm] Web Height, hw: 400.0 [mm] Web Thickness, t: 8.0 [mm] Flange width (incl. web), bf: 200.0 [mm] Flange thickness, tf: 10.0 [mm] Angle Between Profile & Plate: 90.0 [Degrees]	
Corrosion addition, plate $t_c$ 0.0 [mm] Corrosion addition, girder 0.0 [mm]	
<b>PROFILE PROPERTIES:</b>	
Total Area: $A_{tot\_n50} = 226.62$ [cm2] Effective Area: $A_{x\_n50} = 226.62$ [cm2] Shear Area in Y-dir.: $A_{yshr\_n50} = 192.63$ [cm2] Shear Area in Z-dir.: $A_{zshr\_n50} = 28.99$ [cm2] Torsional resistance: $Z_{x\_n50} = 71.1$ [cm3] Section modulus: $Z_{yTop\_n50} = 5951.4$ [cm3] Section modulus: $Z_{yBot\_n50} = 1192.9$ [cm3] Section modulus, z-axis: $Z_{z\_n50} = 5089.7$ [cm3]	Distance to Neutral axis: $Yna = 0.00$ [mm] Distance to Neutral axis: $Zna = 349.87$ [mm] Shear center offset: $eY = 0.00$ [mm] Shear center offset: $eZ = 64.52$ [mm] Torsional mom. of inertia: $I_x = 71.1$ [cm4] Moment of inertia: $I_y = 41737.5$ [cm4] Moment of inertia: $I_z = 444379.9$ [cm4] Centrifugal mom. of in.: $I_{yz} = 0.0$ [cm4] Web and Flange min thick.: $t >= 6.0$ [mm] Web pl. slenderness req.: $tw >= 3.5$ [mm] Flange slenderness req.: $tf >= 8.5$ [mm] Max unsupp. flange length: $S_b <= 3.6$ [m]
Req. net section mod. $Z_{n50} >= 484.2$ [cm3] Req. net shear area: $A_{shr\_n50} >= 10.1$ [cm2] Web stiff. inertia req.: $I_{st} >= -6.4$ [cm4]	<input type="button" value="Copy to Profile stack"/>
<input type="button" value="OK"/>	
<b>BEAMDATA:</b>	<b>DESIGN LOAD SET:</b> L51 AC-II
Effective bending span: $l_{bdg} = 5.0$ [m] Effective shear span: $l_{shr} = 5.0$ [m] Load breadth / PSM Spacing: $S = 2.8$ [m] Yield stress: $R_{eH} = 235.0$ [MPa] Perm. bending stress coeff.: $C_s = 0.85$ [-] Perm. combined str. coeff.: $C_{s1} = 0.95$ [-] Perm. bending stress coeff.: $C_{s2} = 0.85$ [-] Perm. shear stress coeff.: $C_t = 0.85$ [-] Young's modulus: $E = 206.0$ [GPa] Cross contraction: $v = 0.3$ [-] Shear Modulus: $G = E / (2(1+v)) = 79.23$ [GPa] Density of material: $\rho = 7.8$ [kg/dm3]	Load intensity: At point (x-distance from A) Distributed pressure: [kN/m2] $q_A = 46.424$ [kN/m] At Left end: $P_A = 16.58$ [kN/m] Intern. Point: $P_1 = 0$ [kN/m] At Right end: $P_B = 16.58$ [kN/m] $q_B = 46.424$ [kN/m] $X_A = 0$ [m] $X_{q1} = 0$ [m] $X_A = 5.0$ [m]
Bending moment and shear force distribution factors Position 1 2 3 Select.... $f_{bdg} = 12.00$ 24.00 12.00 $f_{shr} = 0.50$ - 0.50	Concentrated loads: Load no. 1 $F_1 =$ [kN] $M_1 =$ [kNm] $X_1 =$ [m] Load no. 2 $F_2 =$ [kN] $M_2 =$ [kNm] $X_2 =$ [m] Load no. 3 $F_3 =$ [kN] $M_3 =$ [kNm] $X_3 =$ [m] Load no. 4 $F_4 =$ [kN] $M_4 =$ [kNm] $X_4 =$ [m] Load no. 5 $F_5 =$ [kN] $M_5 =$ [kNm] $X_5 =$ [m] Load no. 6 $F_6 =$ [kN] $M_6 =$ [kNm] $X_6 =$ [m]
	Axial load and end moments: Hull girder stress, Axial Load: $\sigma_{hg} =$ [Mpa] $F_x = 0.0$ [kN] Left end moment: (when $f_{bdg1}=0$ ) $M_A =$ [kNm] Right end moment: (when $f_{bdg3}=0$ ) $M_B =$ [kNm]

Figure 51 – PSM Fore – Lower Deck Transverse and Girders Check

## 5 Conclusion

---

This report covers the scantling evaluation of a common chemical tanker midship section, fore area section, transverse bulkhead in midship area, transverse bulkhead in fore area and primary supporting members. Considering the assumptions presented in Ch.1 and Ch.3, the structure satisfies the BV Rules.

Based on the design calculations it can be concluded that the presented scantling design is representative for a common chemical tanker.



Waarderweg 40  
2031 BP Haarlem  
The Netherlands

Pettelaarpark 10-15  
5216 PD 's-Hertogenbosch  
The Netherlands

Nevelgaarde 10  
3436 ZZ Nieuwegein  
The Netherlands

**iv-Infra b.v.**  
Trapezium 322  
3364 DL Sliedrecht  
The Netherlands

Trompstraat 36a  
9190 Stekene  
Belgium

Westervoortsedijk 73  
Gebouw CB  
6827 AV Arnhem  
The Netherlands

[www.iv-infra.nl](http://www.iv-infra.nl)  
Telephone +31 88 943 3200  
P.O. Box 135  
3360 AC Sliedrecht  
[officemanagement.infra@iv.nl](mailto:officemanagement.infra@iv.nl)



**B.** R102-DP1 Container ship – Scantling calculation report



# 3D FEM gevolgschade schip-turbine

Container Ship – Scantling Calculations Report

Client: Rijkswaterstaat  
Document nr: 001  
Revision: 2  
Date: 24 February 2025

**Iv-Infra b.v.**

Engineering Company with a Passion for Technology



Client: Rijkswaterstaat  
Document title: 3D-FEM gevolgschade schip-turbine  
Document subtitle: Container Ship – Scantling Calculations Report  
Revision: 2  
Date: 24 February 2025

Revision	Status	Date	Author(s)	Checked	Approved	Description
0	TI	24-09-2024	IZ	GV, MMI	WL	Ter informatie
1	VC	26-11-2024	IZ	GV, MMI	WL	Voor commentaar
2	TI	24-02-2025	IZ	GV,MMI	WL	Ter informatie

The only difference between revision 2 and revision 1 is the removal of the ship names that the ship model is based on.

## Summary

In this report is presented the scantling evaluation of the midship and fore area of a container ship with the following main dimensions and characteristics:

<b>Vessel Characteristics</b>		<b>Unit</b>
<b>GT</b>	200000	t
<b>Lpp</b>	397.4	m
<b>B</b>	59	m
<b>D</b>	31.35	m
<b>T</b>	16	m
<b>Displacement</b>	223000	t
<b>Speed</b>	20	kn

This section was designed with Mars 2000 and checked according to the following rules:

- BV NR467 Rules for the Classifications of steel ships, January 2023 edition.

DNV Nauticus Hull - Primary Supporting Members spreadsheets were used for the design of PSM in midship cargo area and fore area.

The profiles used in the scantling definition are according to DIN Standard.

The following updates have been performed in revision 1:

- Update the hatch coaming material from HT390 to HT355 steel, see Figure 13;
- Update the hatch coaming scantling sizes due to material change, see Figure 11;
- Update result plots for midship section, see Figure 32 and Figure 33.

## TABLE OF CONTENTS

---

<b>1</b>	<b>Assumptions</b>	<b>5</b>
<b>2</b>	<b>Abbreviations</b>	<b>6</b>
<b>3</b>	<b>Scantling Design</b>	<b>7</b>
3.1.	Basic Ship Data	7
3.2.	Midship Section	10
3.3.	Transverse Bulkhead Midship	17
3.4.	Primary Supporting Members Midship	20
3.5.	Fore Section	21
3.6.	Transverse Bulkhead Fore	29
3.7.	Primary Supporting Members Fore	32
<b>4</b>	<b>Scantling Results</b>	<b>33</b>
4.1.	Transverse Section	33
4.2.	Transverse Bulkhead Midship	37
4.3.	Primary Supporting Members Midship	39
4.4.	Fore Section	41
4.5.	Transverse Bulkhead Fore	45
4.6.	Primary Supporting Members Fore	47
<b>5</b>	<b>Conclusion</b>	<b>50</b>

# 1 Assumptions

In this memo, a scantling design of a container ship is provided, which will be used during the ship impact simulations for project INF240746 RWS WV.L.

Considering similar vessels and the input “INFR240476 - Plan van Aanpak rev.0 – definitief”, the following technical particulars were assumed for the scantling calculation:

- Scantling Length: 397.4 m
- Depth: 31.5 m
- Breadth: 59 m
- Scantling Draught: 16 m
- Minimum Draught at ballast: 6 m
- Service Speed: 20 kn
- Block coefficient: 0.58
- Double bottom: 2.6 m
- Double Hull: 2.8 m
- Frame spacing: 3.15 m (mid)
- Webframe spacing: 3.15 m (mid)

The ship model is based on similar existing ships.

The following frame spacing was considered:

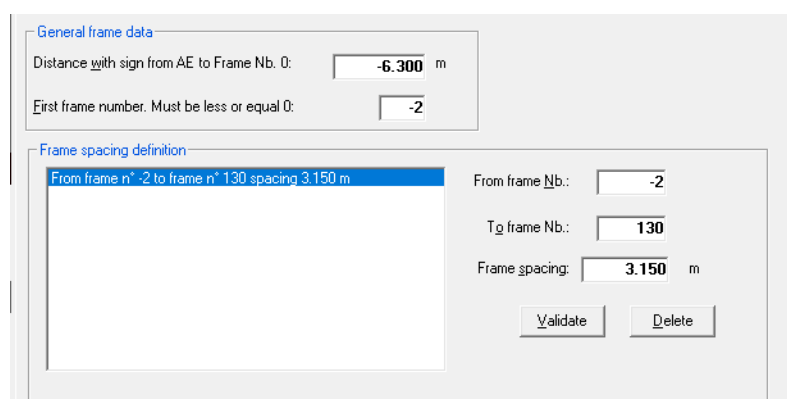


Figure 1 – Frame Spacing

The materials have been assumed to be Grade A steel with a yield stress of 235 MPa and high tensile strength steel (Grade HT36) with a specific minimum yield strength of 355 MPa. The Youngs modulus for all materials has been considered as 206000 N/mm<sup>2</sup>.



## 2 Abbreviations

---

BL	Base Line	
CL	Center Line	
FR	Frame	
PSM	Primary Supporting Member	



# 3 Scantling Design

## 3.1. Basic Ship Data

The following input has been used for the Basic ship data module (BSD).

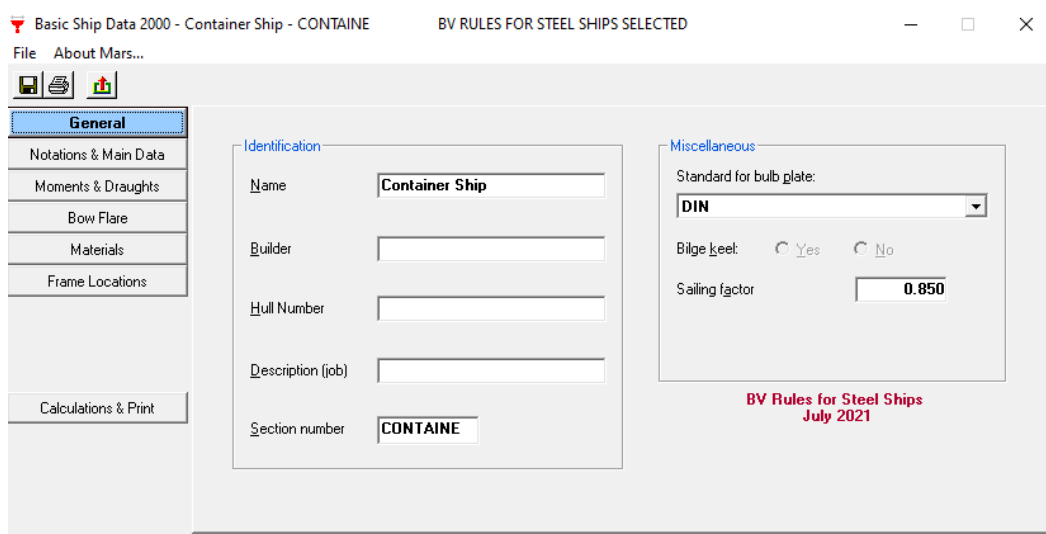


Figure 2 – Basic Ship Data – General

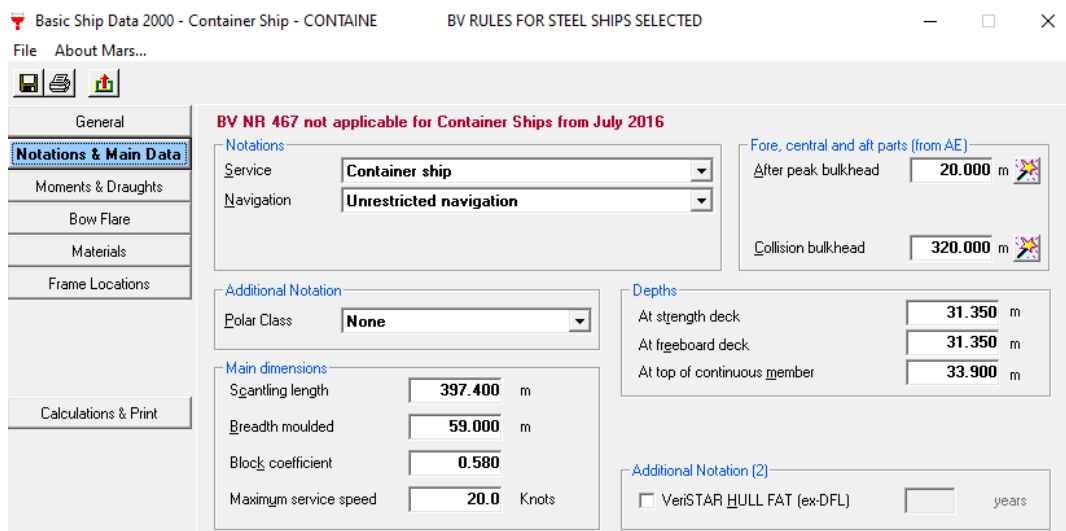


Figure 3 – Basic Ship Data – Class Notation and Main Data

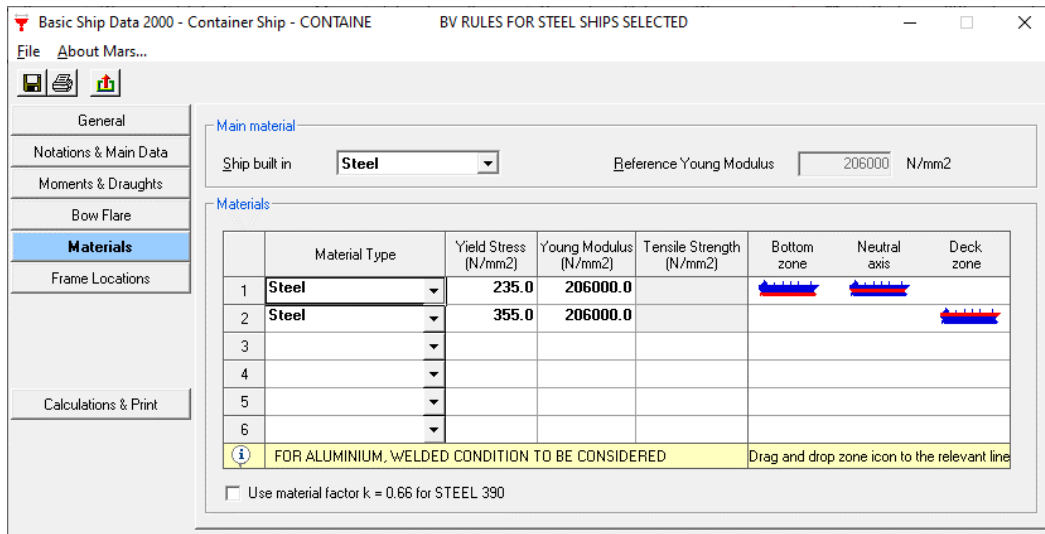


Figure 4 – Basic Ship Data - Materials

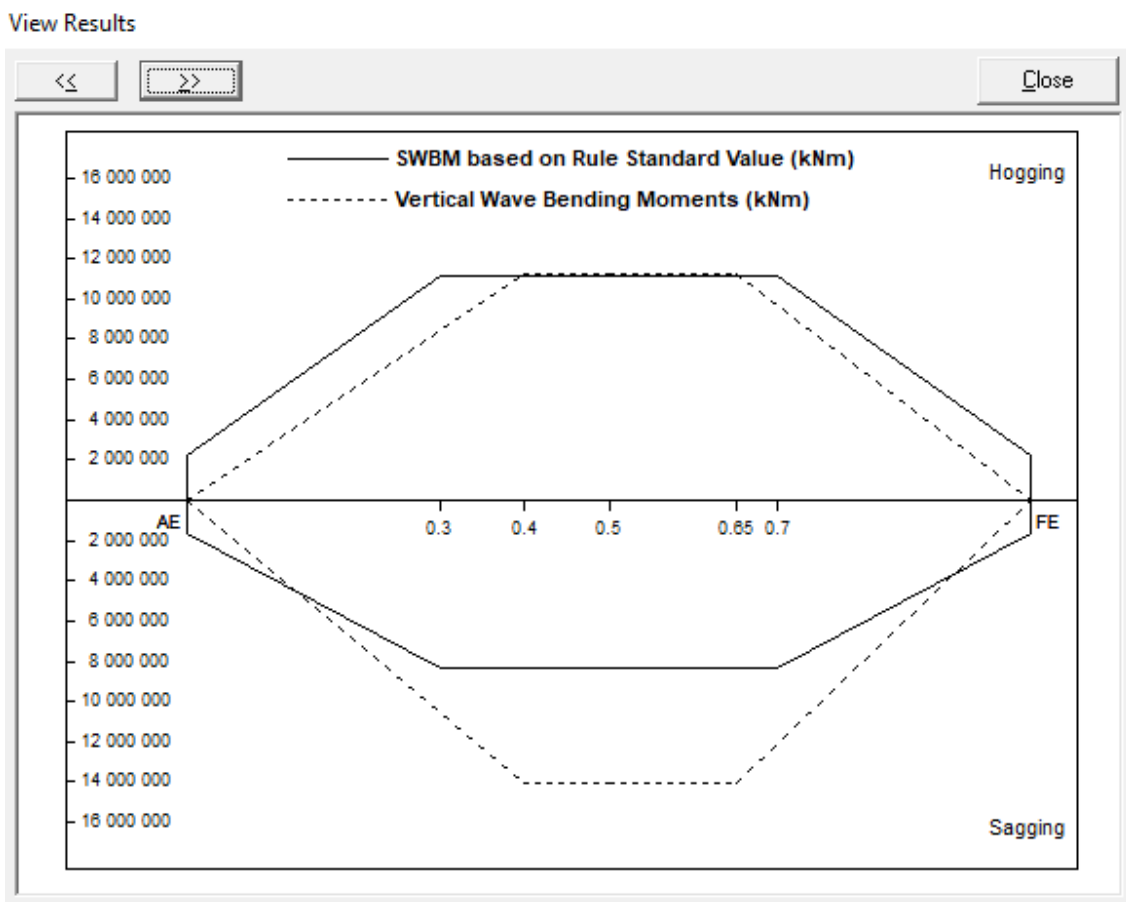


Figure 5 – SWBM and VWBM

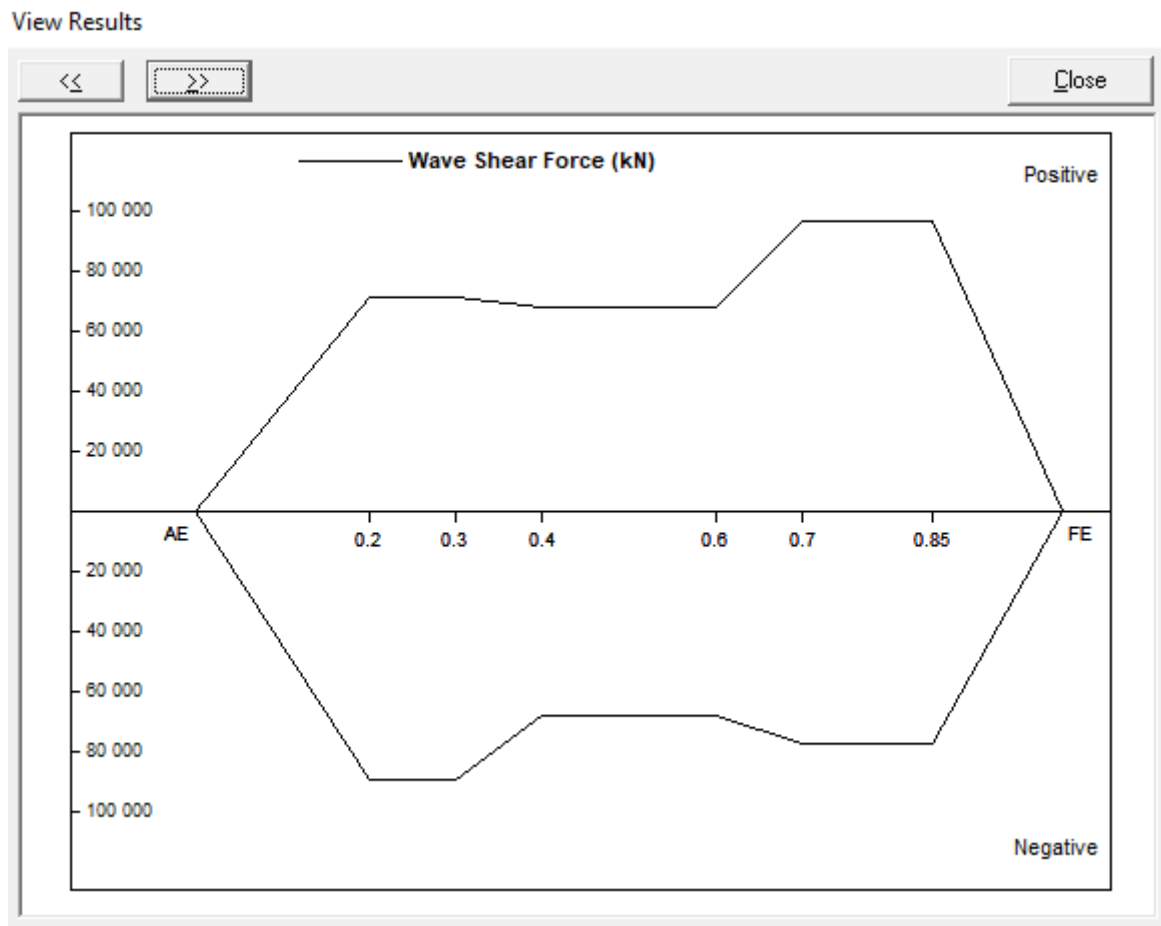


Figure 6 – Wave Shear Force

### 3.2. Midship Section

The location of the assessed cross section is FR 65+155mm, at 200 m from the aft end. The frame spacing for this area is 3.15 m, the webframe spacing is 3.15 m.

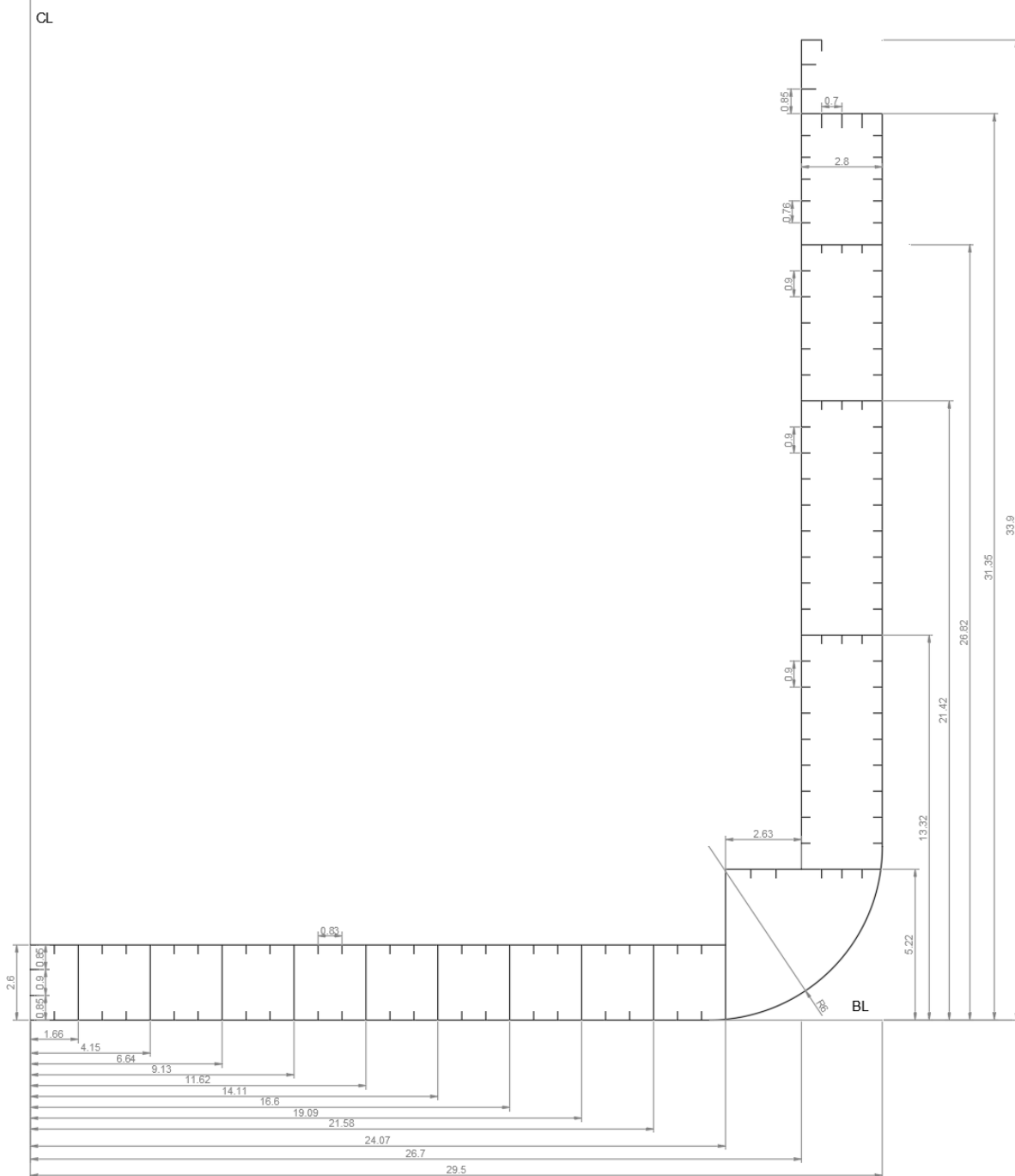


Figure 7 – Midship Section – Spacing (meters)




**Main Section Data**

Main | SW | Fatigue | Ship State | Wave | Flooding

**Name Location Dimensions**

Name:

Longitudinal Location (from AE):  m 

Breadth moulded:  m

Depth moulded:  m

Depth at top of continuous member:  m

**Materials**

in neutral axis      Extension heights:

in deck       m

in bottom       m

Input of:

Section just forward of the engine room bulkhead

Figure 8 – Midship Section – Main Section Data

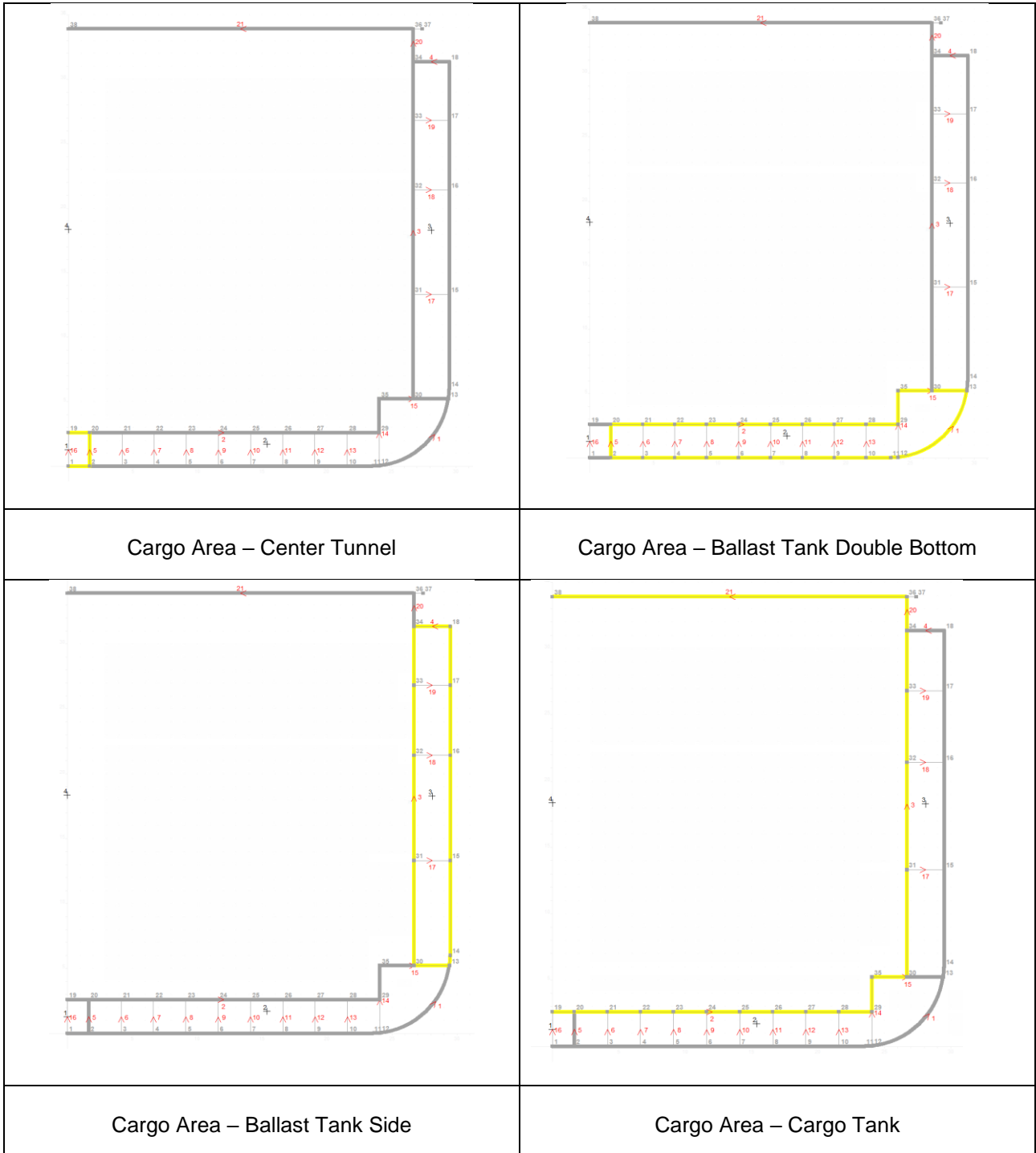


Figure 9 – Midship Section – Compartments

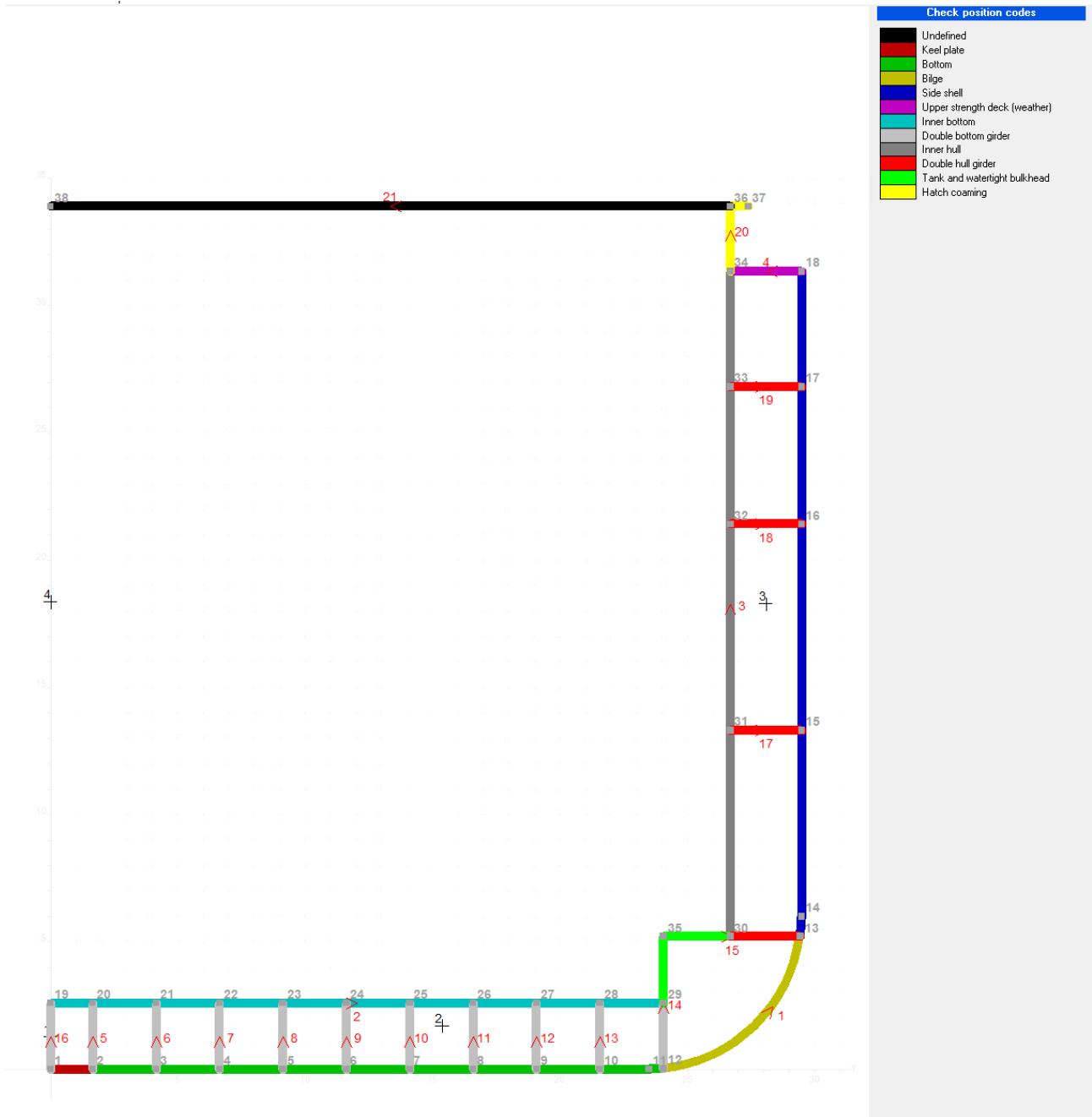


Figure 10 – Midship Section – Position Codes

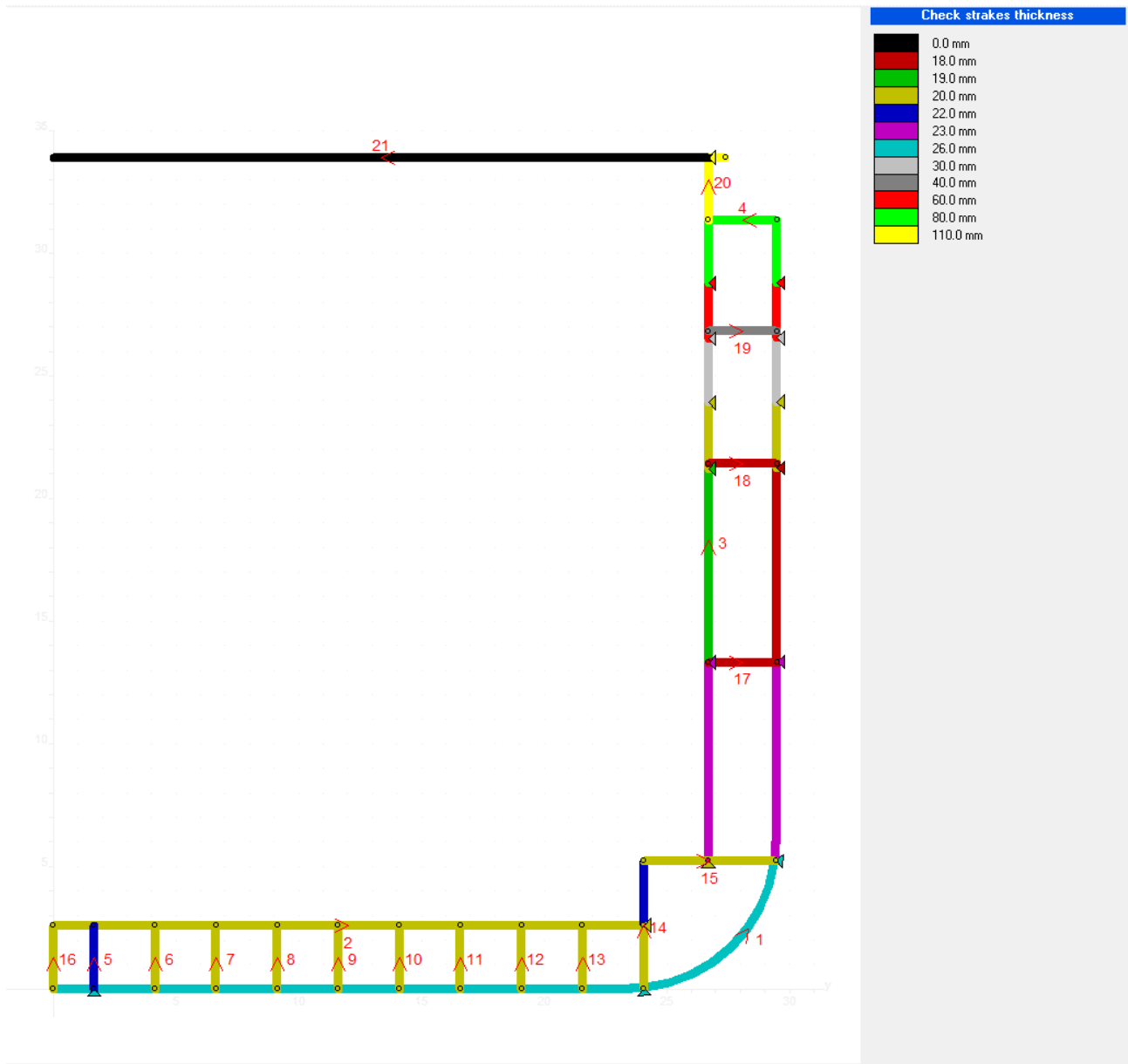


Figure 11 – Midship Section – Plate thickness



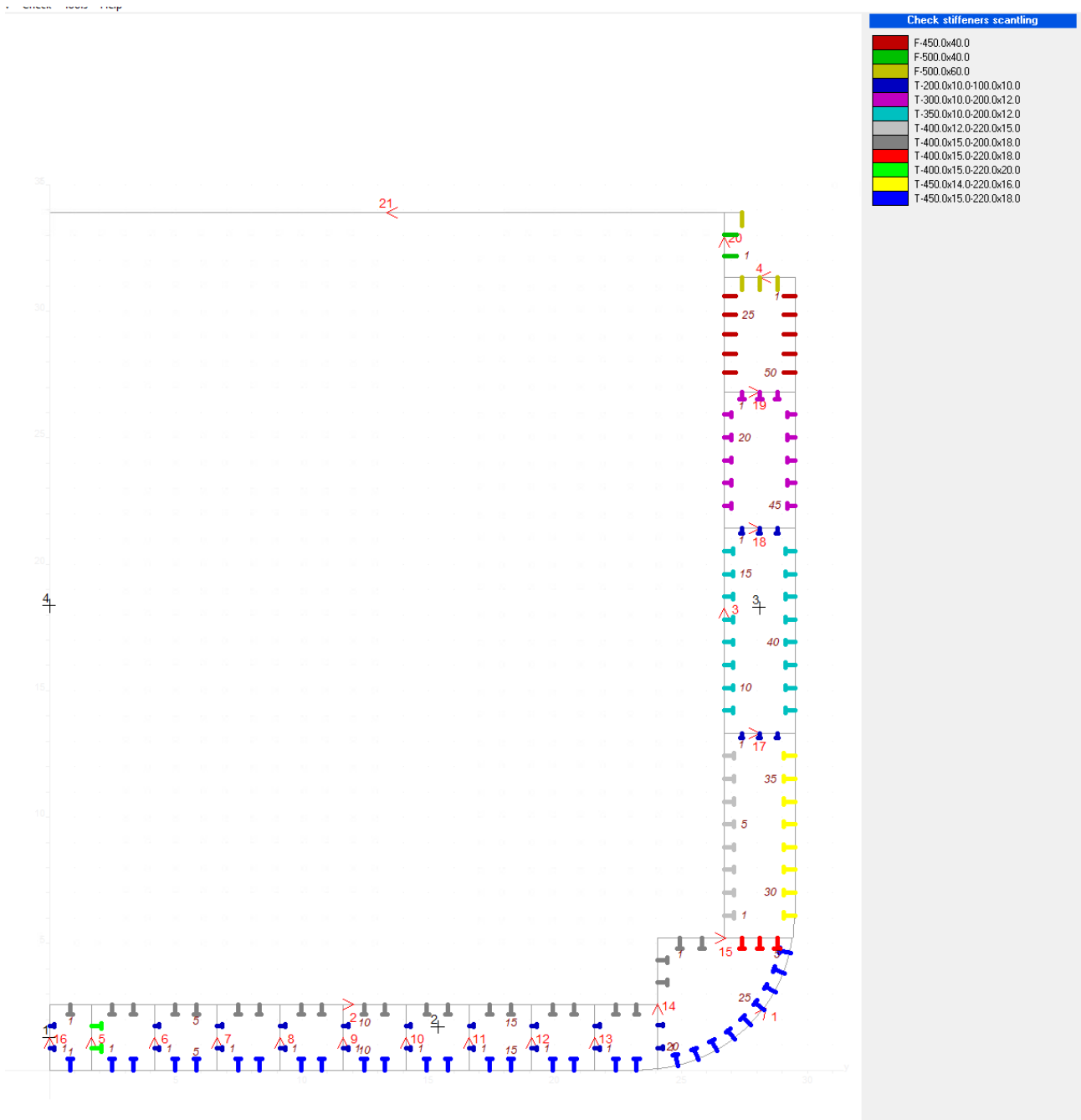


Figure 12 – Midship Section – Stiffeners Scantling

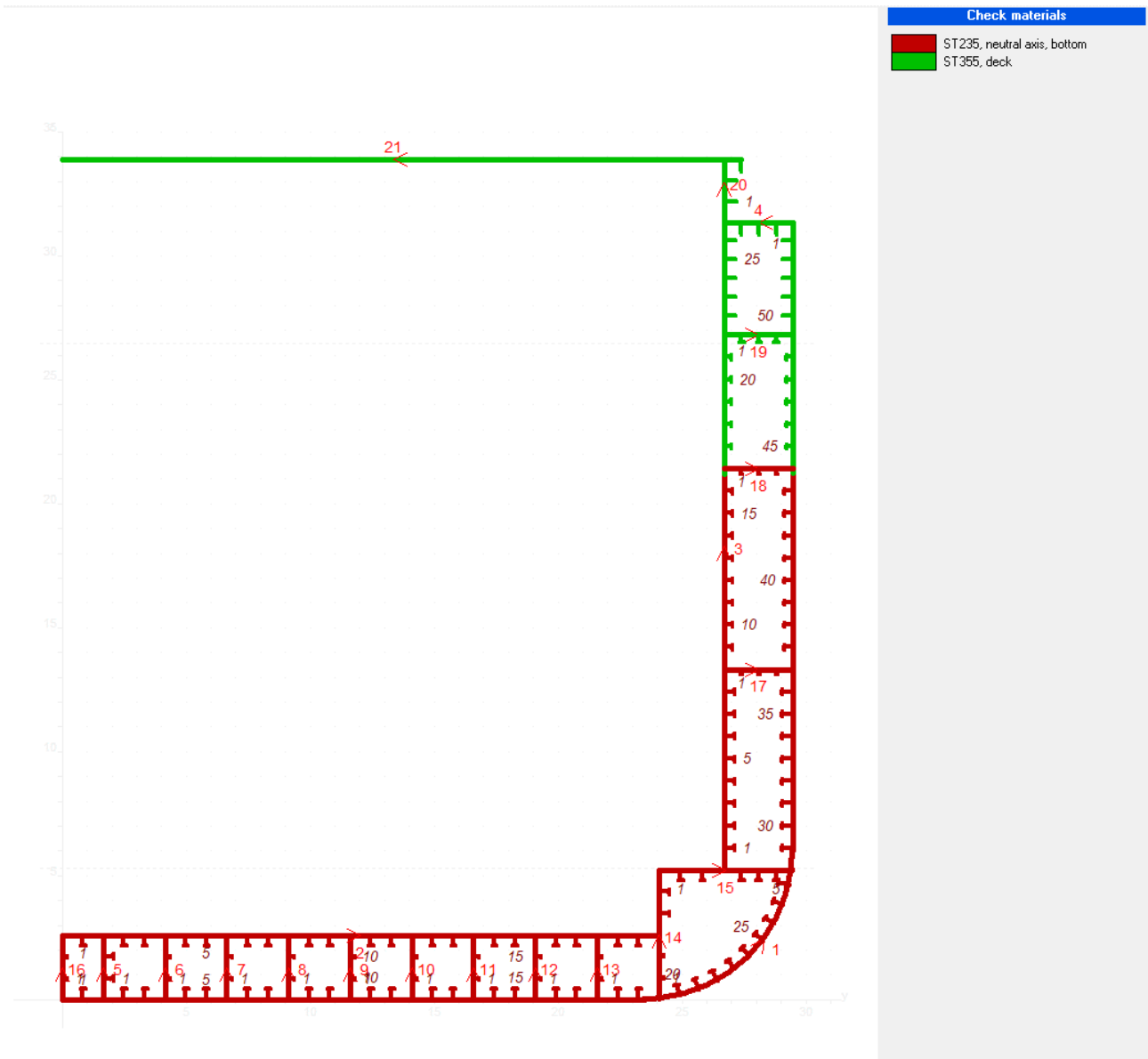


Figure 13 – Midship Section – Materials

### 3.3. Transverse Bulkhead Midship

The location of the assessed transverse bulkhead is at Fr.57, at 173.25m from the aft end.

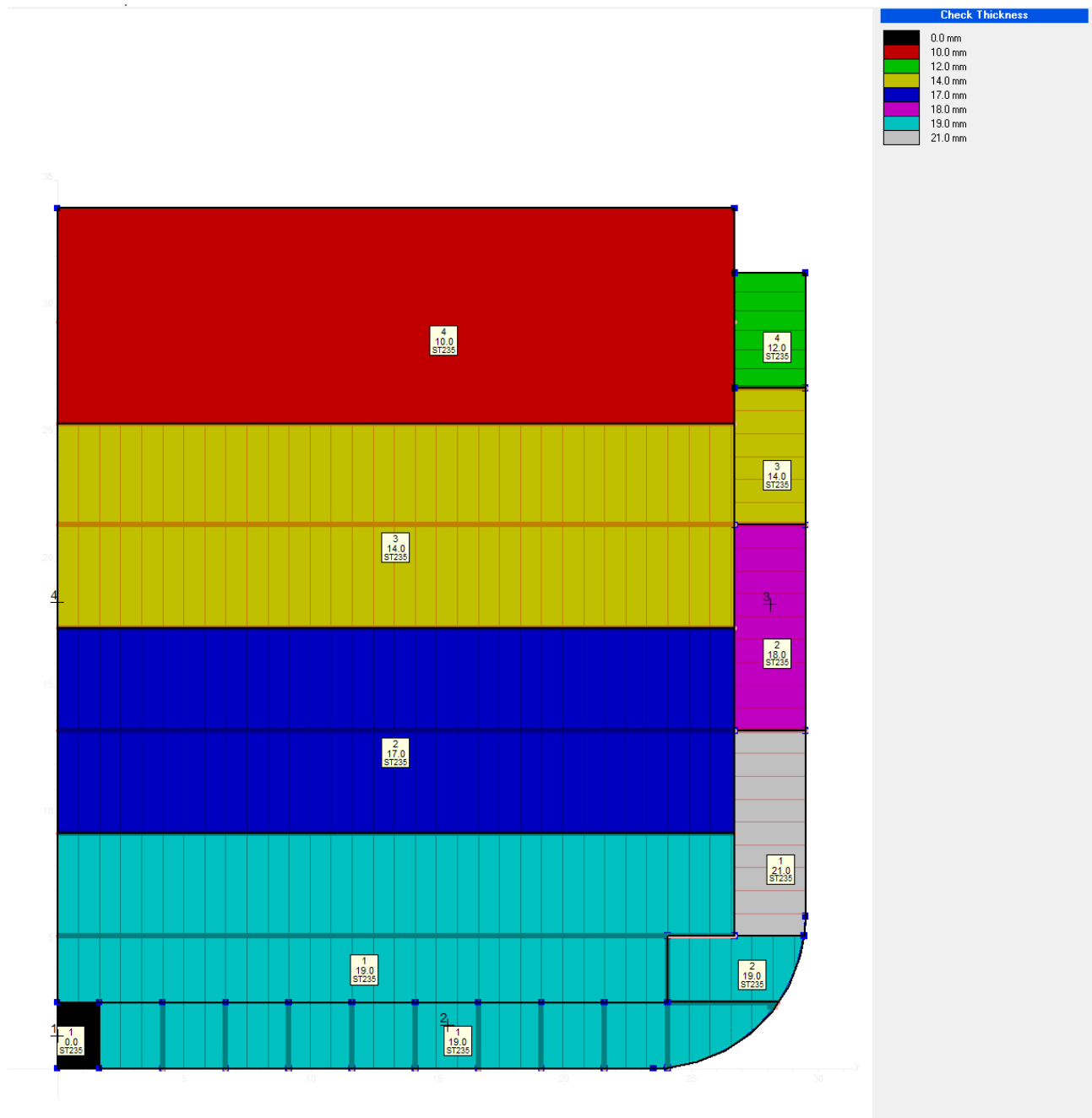


Figure 14 – Transverse Bulkhead – Plate thickness

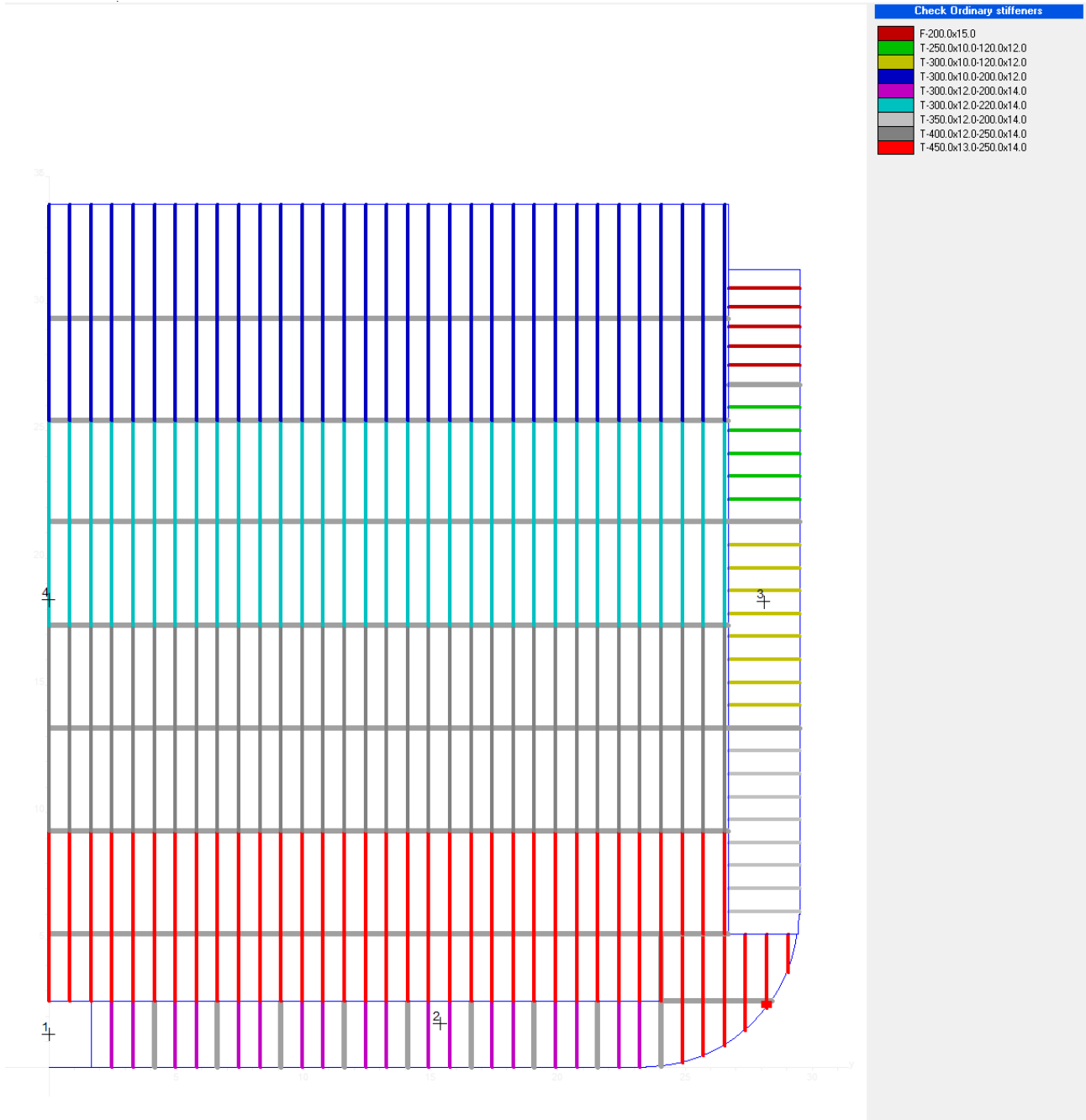


Figure 15 – Transverse Bulkhead – Stiffeners Scantling

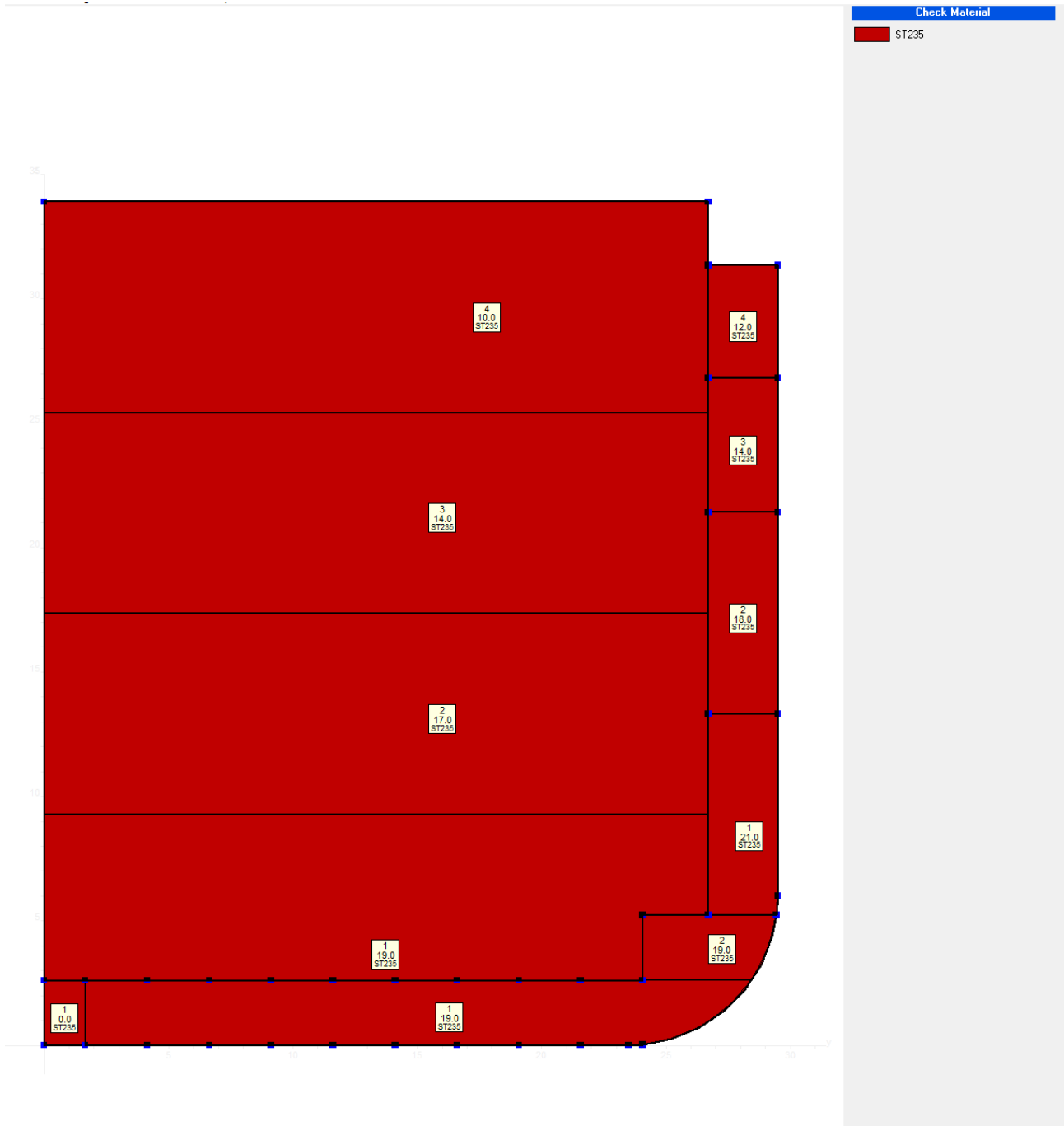


Figure 16 – Transverse Bulkhead – Materials

### 3.4. Primary Supporting Members Midship

The web frame spacing for the midship area is 3.15 m.

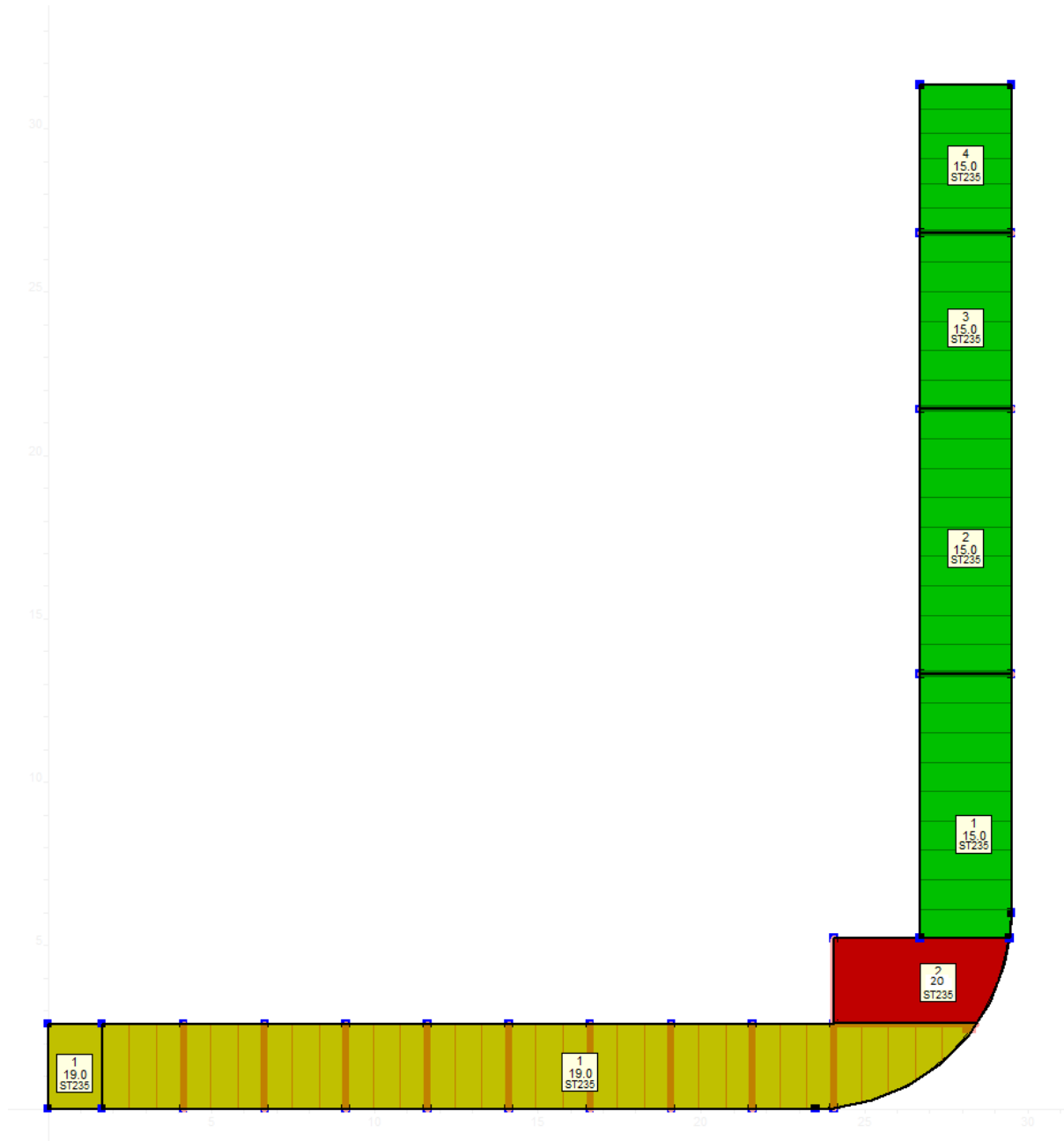


Figure 17 – Primary Supporting Members Sketch

### 3.5. Fore Section

The location of the assessed cross section is FR 170, at 129.6 m from the aft end.  
 The frame spacing for this area is 0.7m, the webframe spacing is 2.8 m.

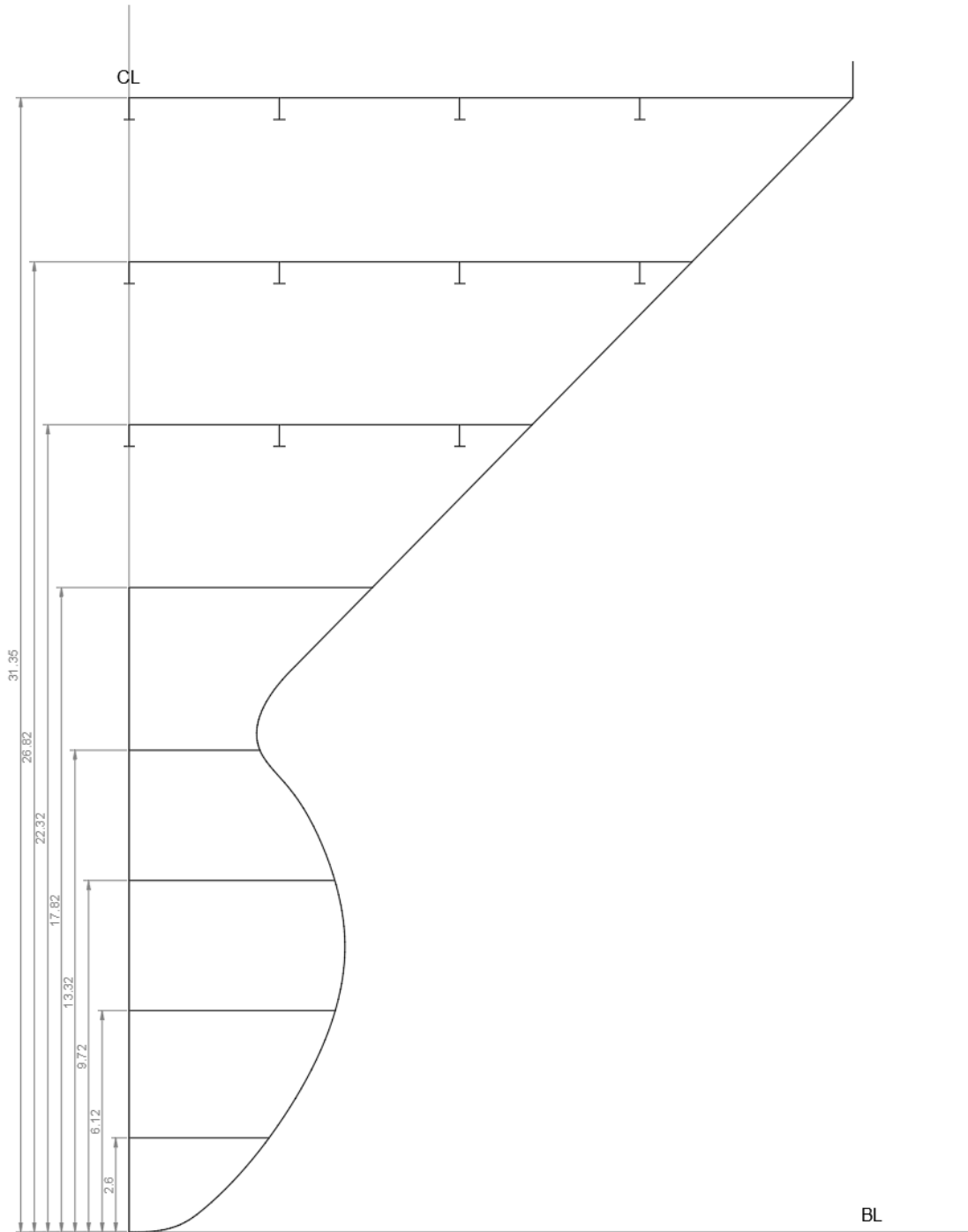


Figure 18 – Fore Section – Spacing (meters)



Main Section Data

Main | SW | Fatigue | Ship State | Wave | Flooding

Name Location Dimensions

Name: Fore Section

Longitudinal Location (from AE): 380.000 m

Breadth moulded: 40.000 m

Depth moulded: 31.350 m

Depth at top of continuous member: 31.350 m

Materials

ST235 in neutral axis Extension heights:

ST235 in deck 0.000 m

ST235 in bottom 0.000 m

Input of: Half section Default (BSD)

Section just forward of the engine room bulkhead

Ok Cancel

Figure 19 – Fore Section – Main Section Data



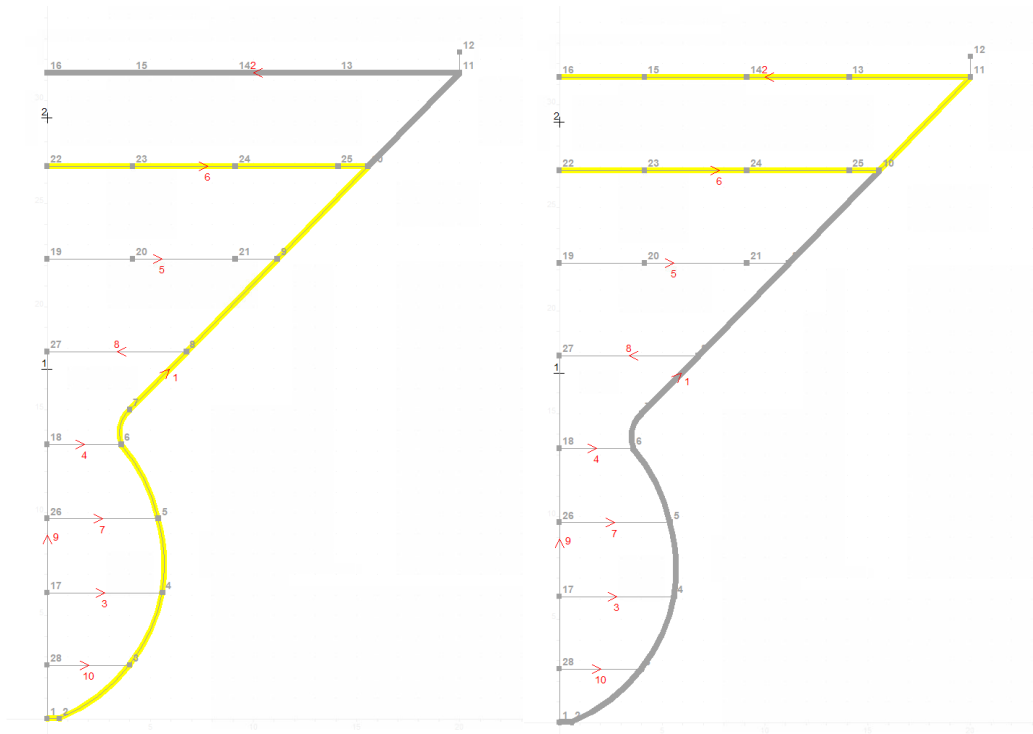


Figure 20 – Fore Section – Compartments

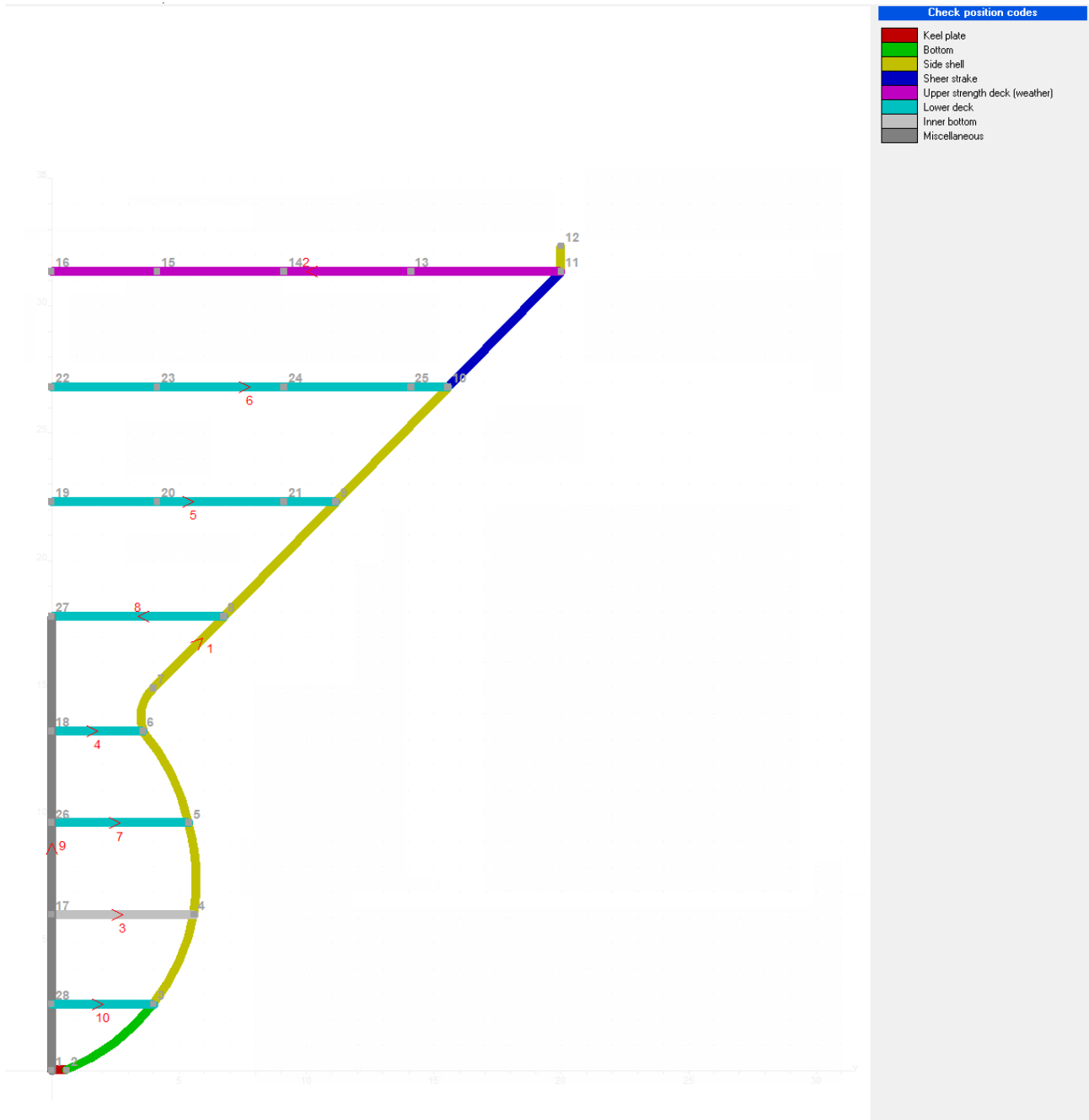


Figure 21 – Fore Section – Position Codes

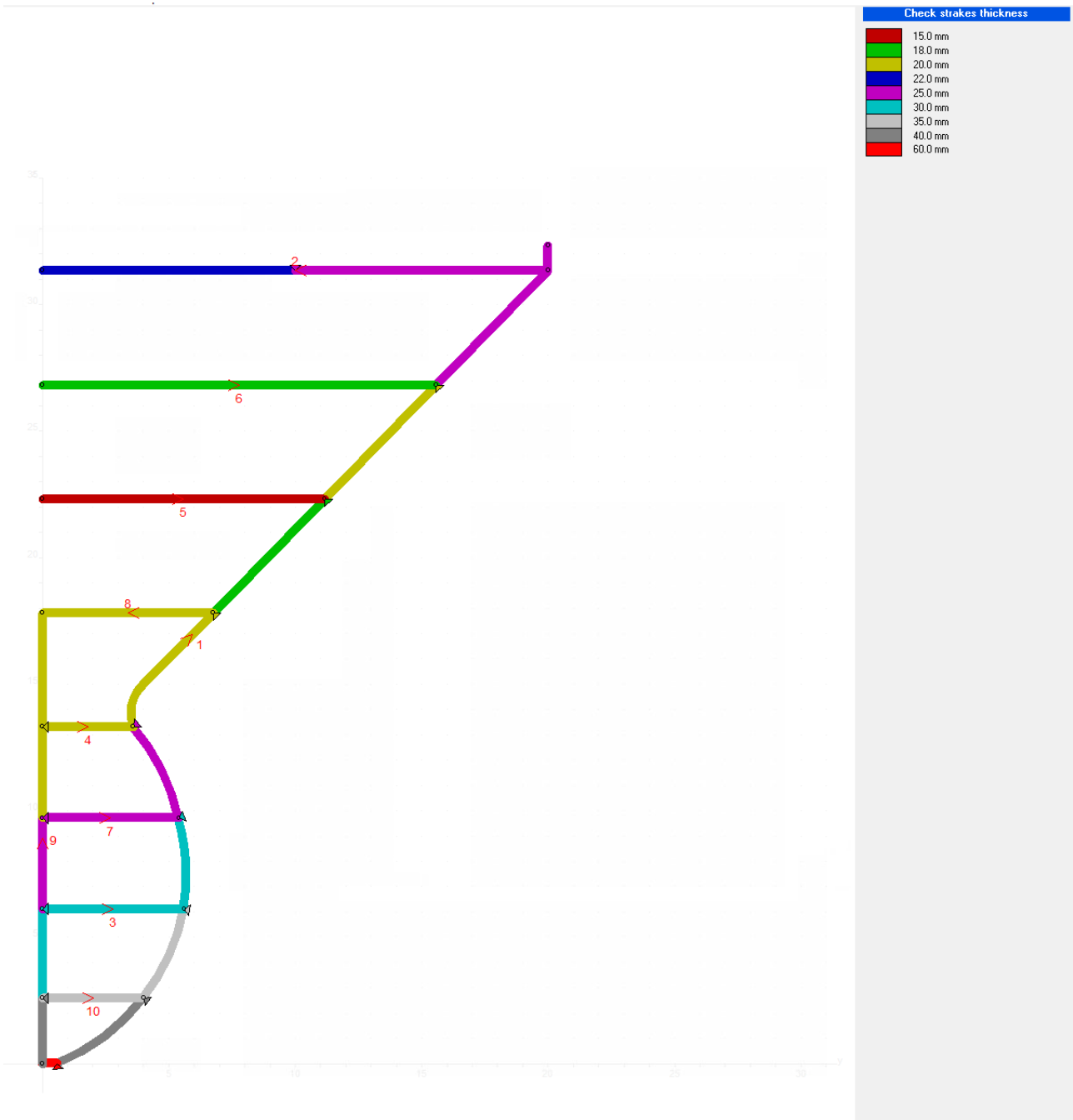


Figure 22 – Fore Section – Plate thickness

it section check tabs help

Check stiffeners scantling

T-600.0x15.0-300.0x20.0

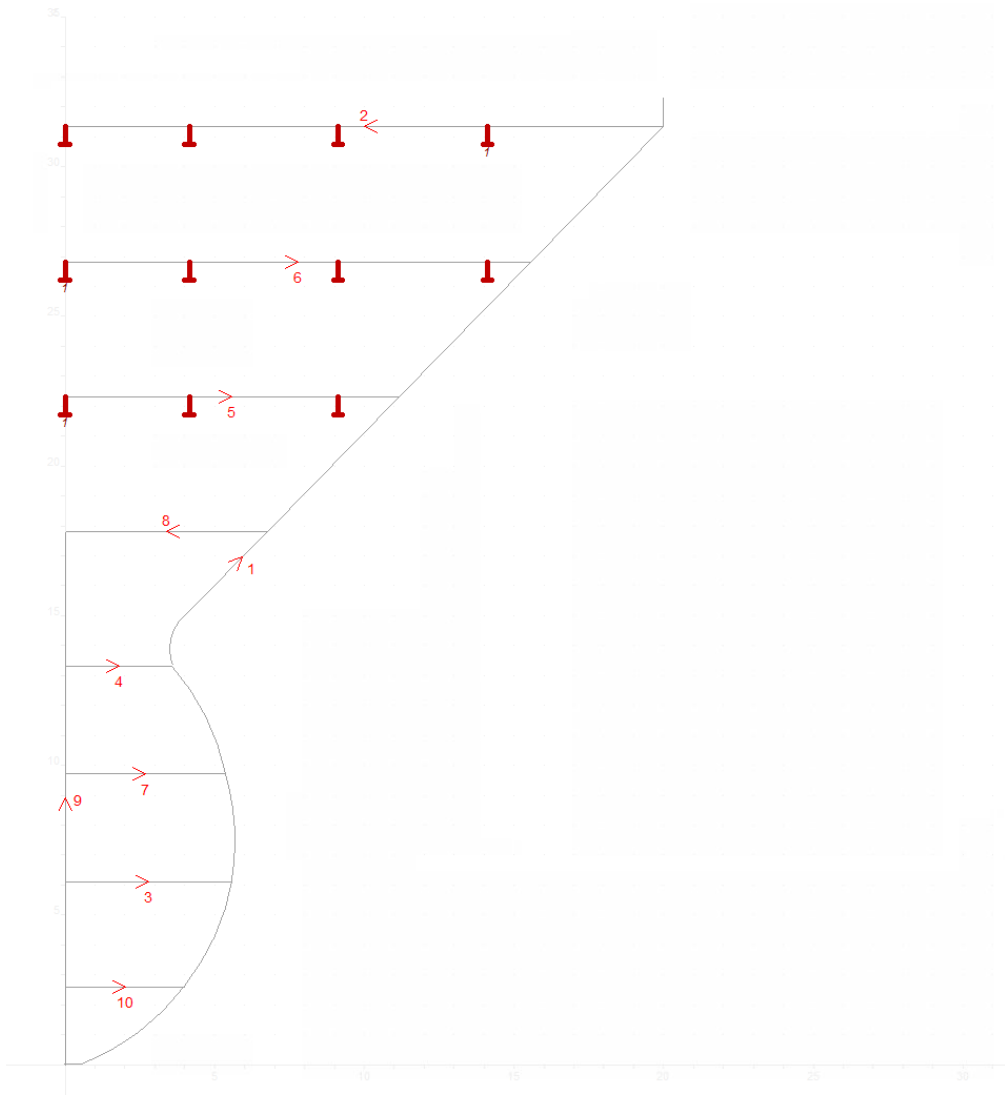


Figure 23 – Fore Section – Stiffeners Scantling



FILE CHECK RUNS HELP

Check transverse stiffeners scantling

- Primary supporting member
- A-300.0x14.0-100.0x16.0
- A-350.0x14.0-120.0x18.0
- A-350.0x314.0-120.0x18.0
- A-400.0x16.0-150.0x18.0
- A-450.0x16.0-150.0x18.0
- A-450.0x16.0-160.0x18.0

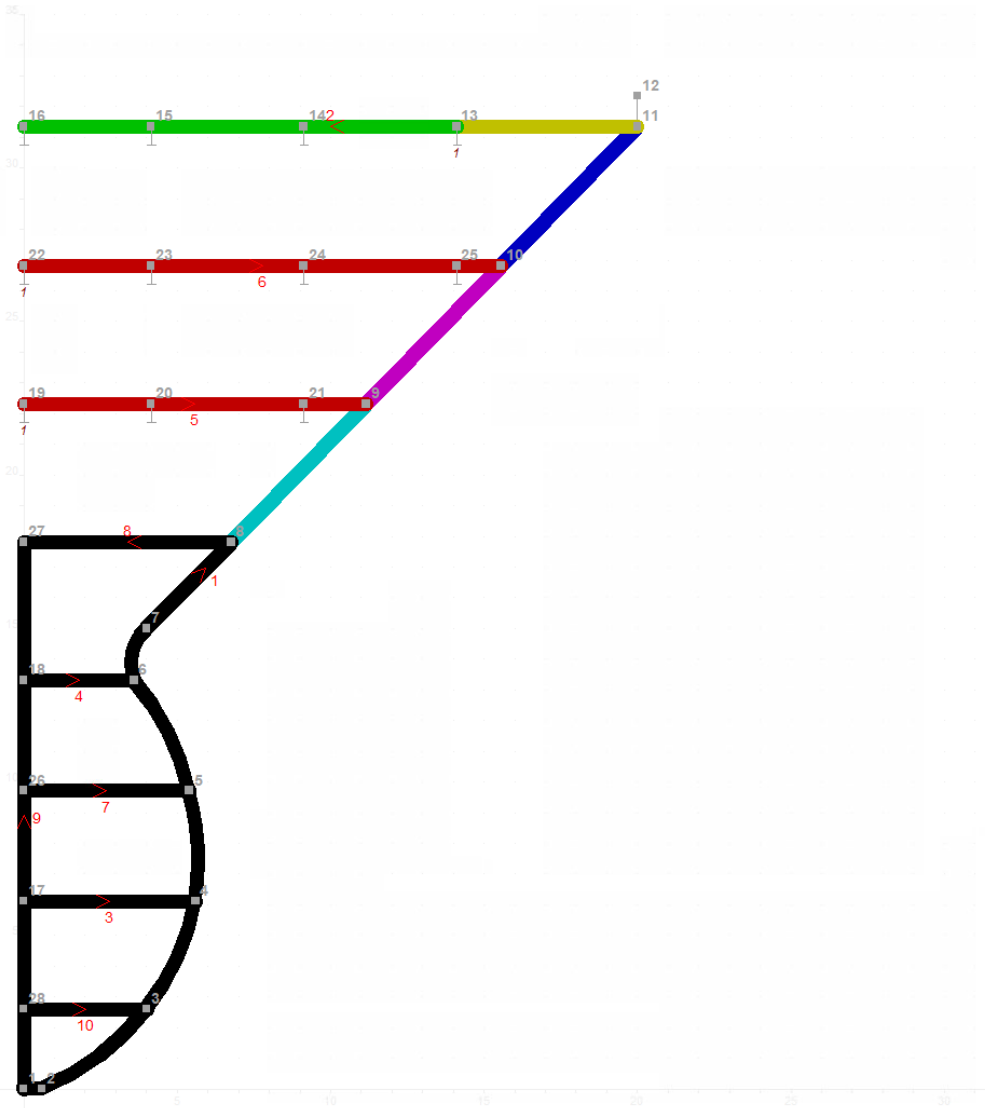


Figure 24 – Fore Section – Transverse Stiffeners Scantling

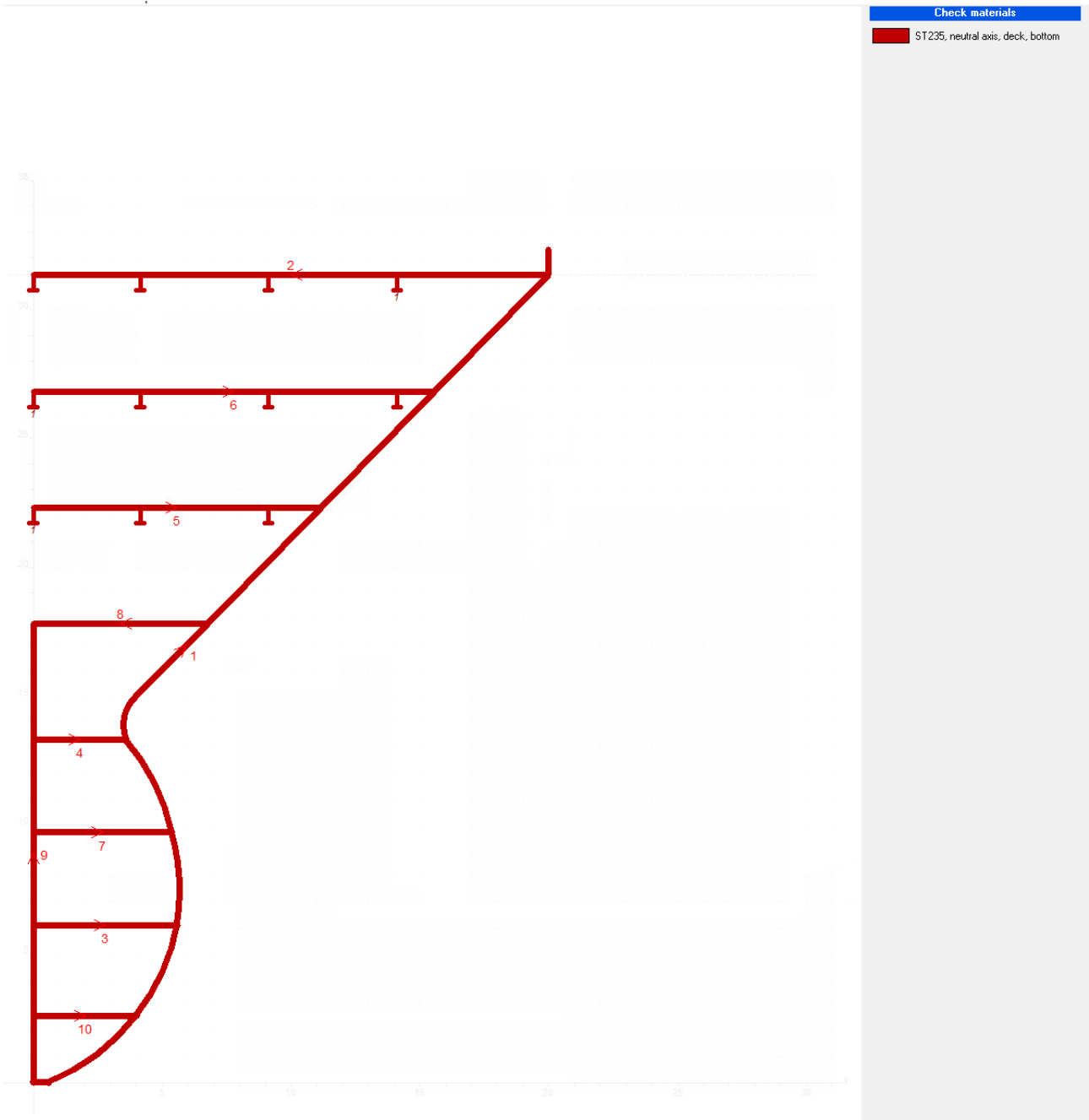


Figure 25 – Fore Section – Materials

### 3.6. Transverse Bulkhead Fore

The location of the assessed transverse bulkhead is FR 167, at 127.5 m from the aft end.

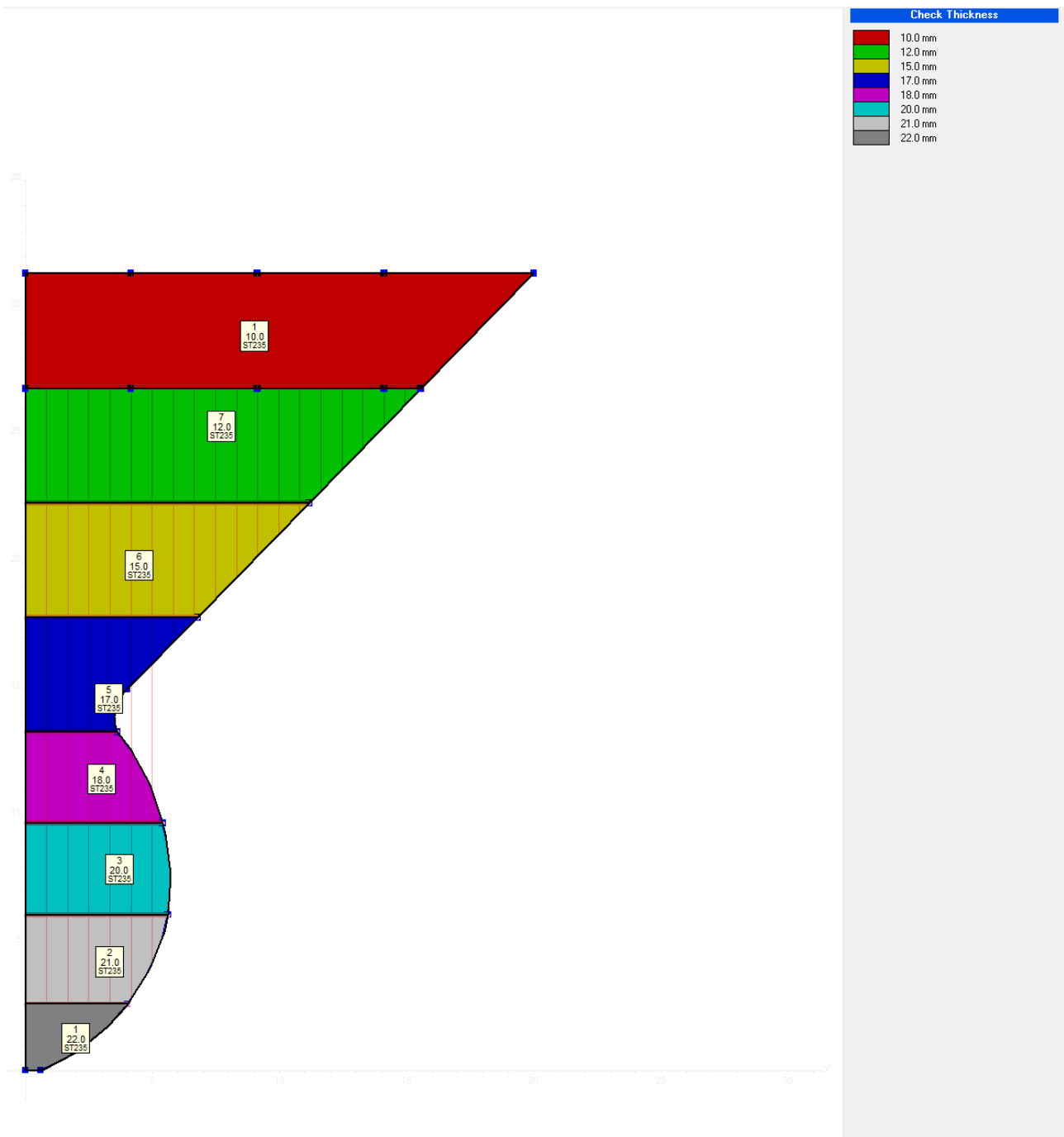


Figure 26 – Transverse Bulkhead Fore – Plate thickness

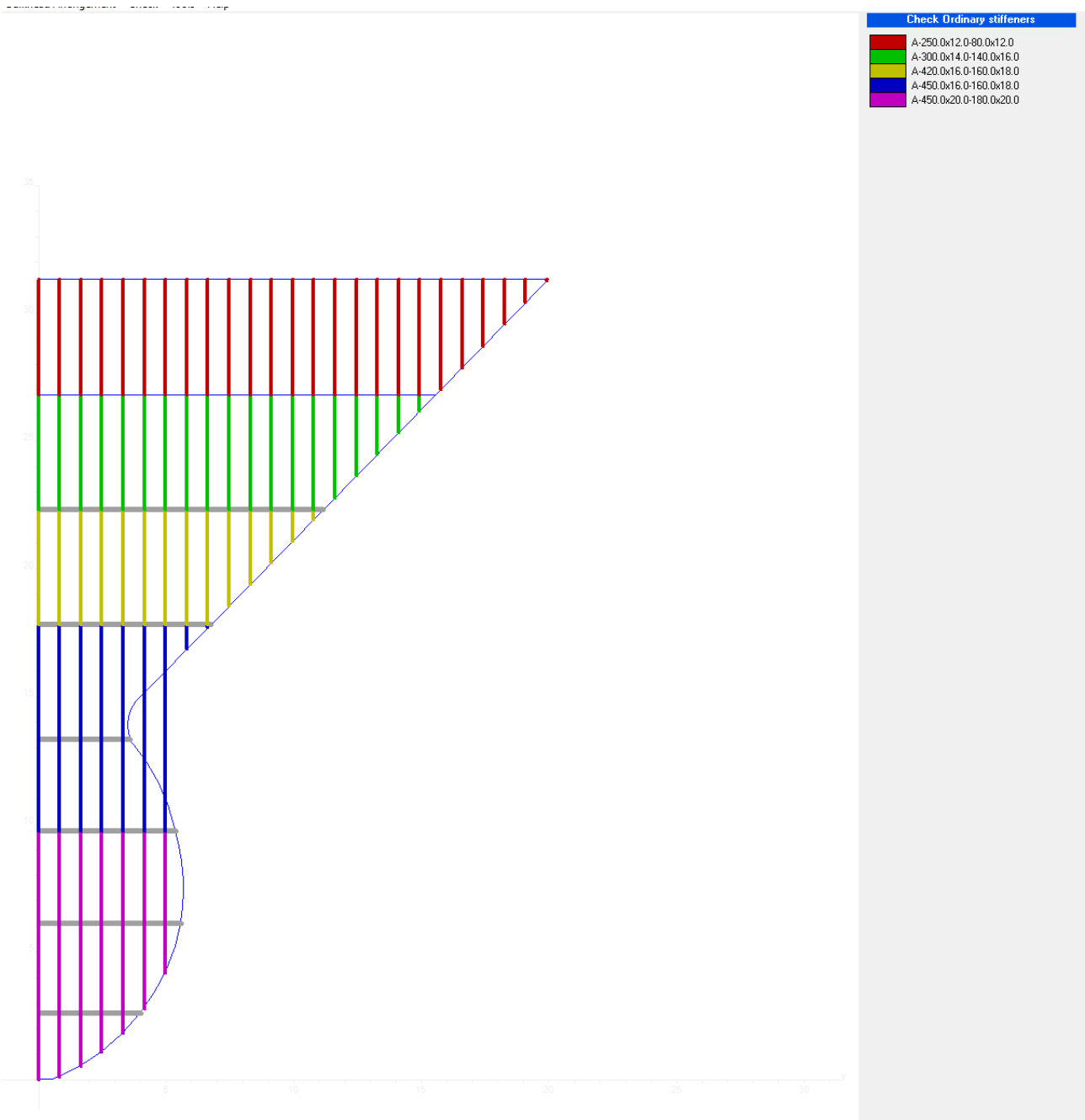


Figure 27 – Transverse Bulkhead Fore – Stiffeners Scantling



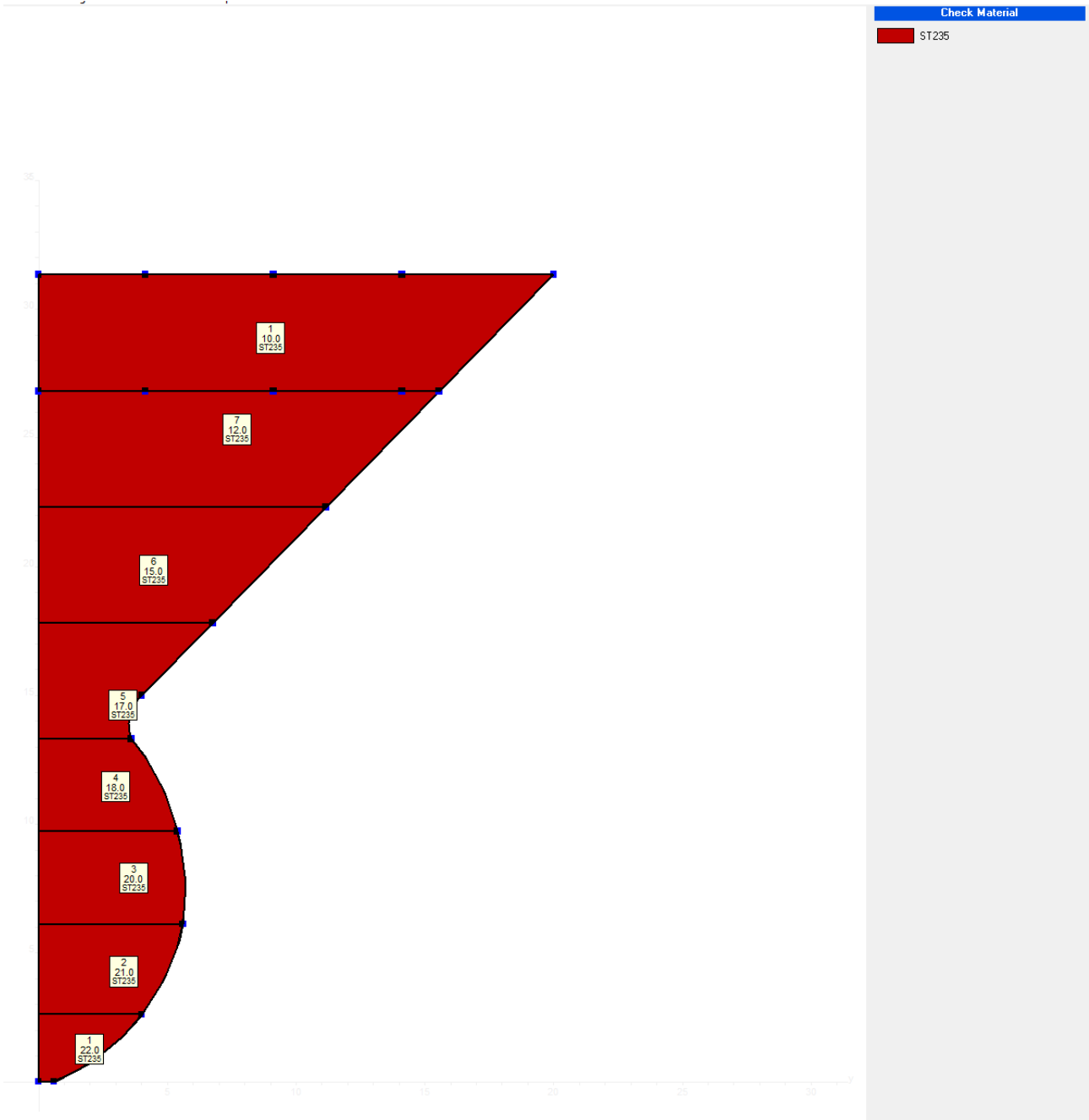


Figure 28 – Transverse Bulkhead Fore – Materials

### 3.7. Primary Supporting Members Fore

The web frame spacing for the fore area is 2.8m.

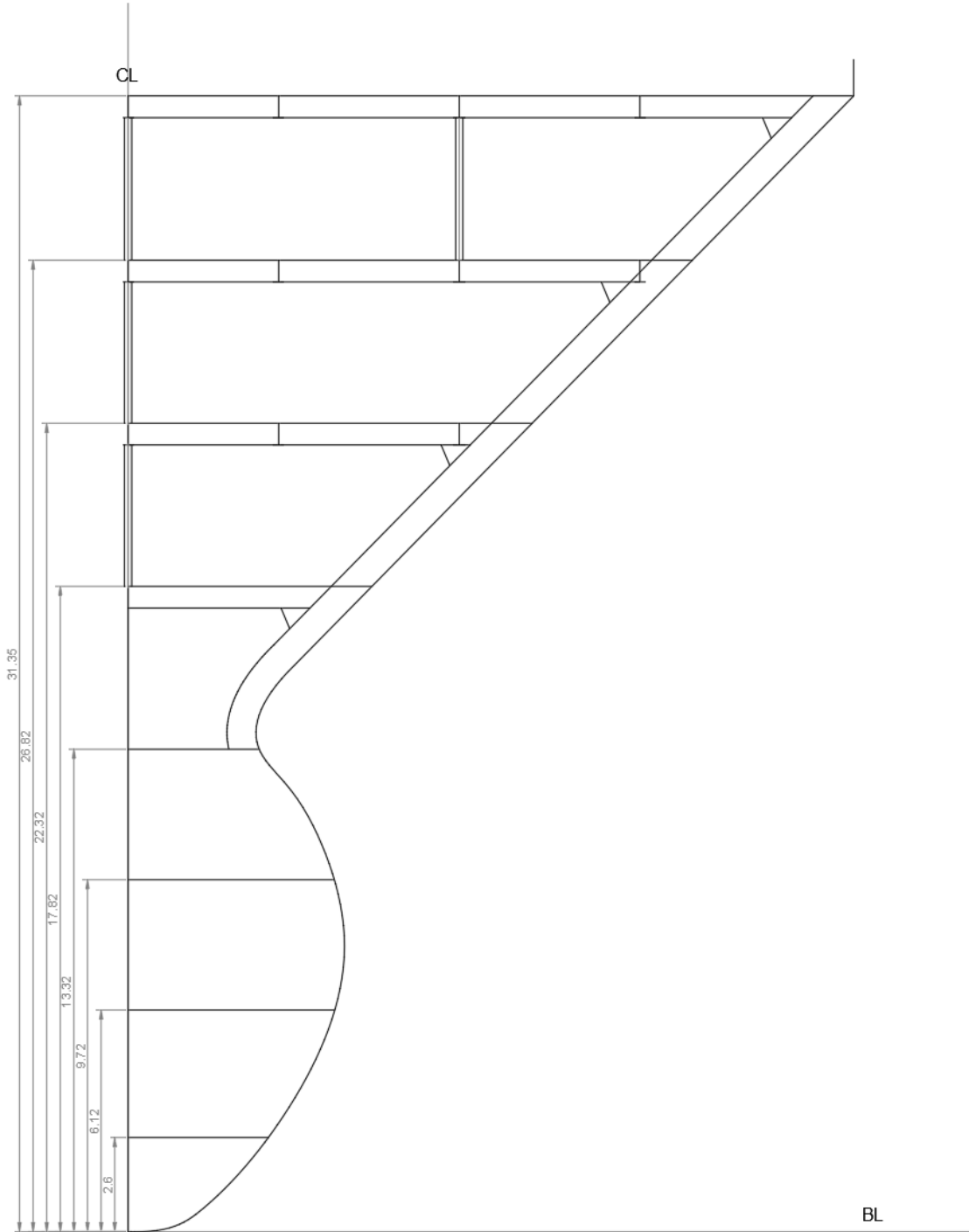


Figure 29 – Primary Supporting Members Fore Sketch

## 4 Scantling Results

### 4.1. Transverse Section

According to the calculation performed in BV Mars 2000, the designed cross section meets the BV Rules requirements.

Hull girder strength criteria			
	Hull Girder Loads	Section Moduli	Net/Gross Moduli
		Hogging	Sagging
Design S.W.B.M. (still water bending moment)	11 180 870.	- 8 324 084.	(kNm)
Design vertical wave bending moment (Rule)	11 230 130.	- 14 086 920.	(kNm)
Design horizontal wave bending moment (Rule)	5 176 865.		(kNm)
		Positive	Negative
Design vertical shear force	1.		(kN)
Rule vertical wave shear force	67 673.	- 67 673.	(kN)

Close

Figure 30 – Midship Section – Hull Girder Loads

Hull girder strength criteria				
	Hull Girder Loads	Section Moduli	Net/Gross Moduli	
	Rule	Actual	at z / BL	k
Modulus at deck	96.81553	99.41785 (m3)	31.350 (m)	0.72
Modulus at bottom	128.06290	135.69970 (m3)	0.000 (m)	1.00
Modulus at Zvt	87.08276	87.76217 (m3)	33.753 (m)	0.68
Inertia	1526.76600	1798.85300 (m4)	(0.4L admiship)	

Close

Figure 31 – Midship Section – Section Modulus and Inertia Check

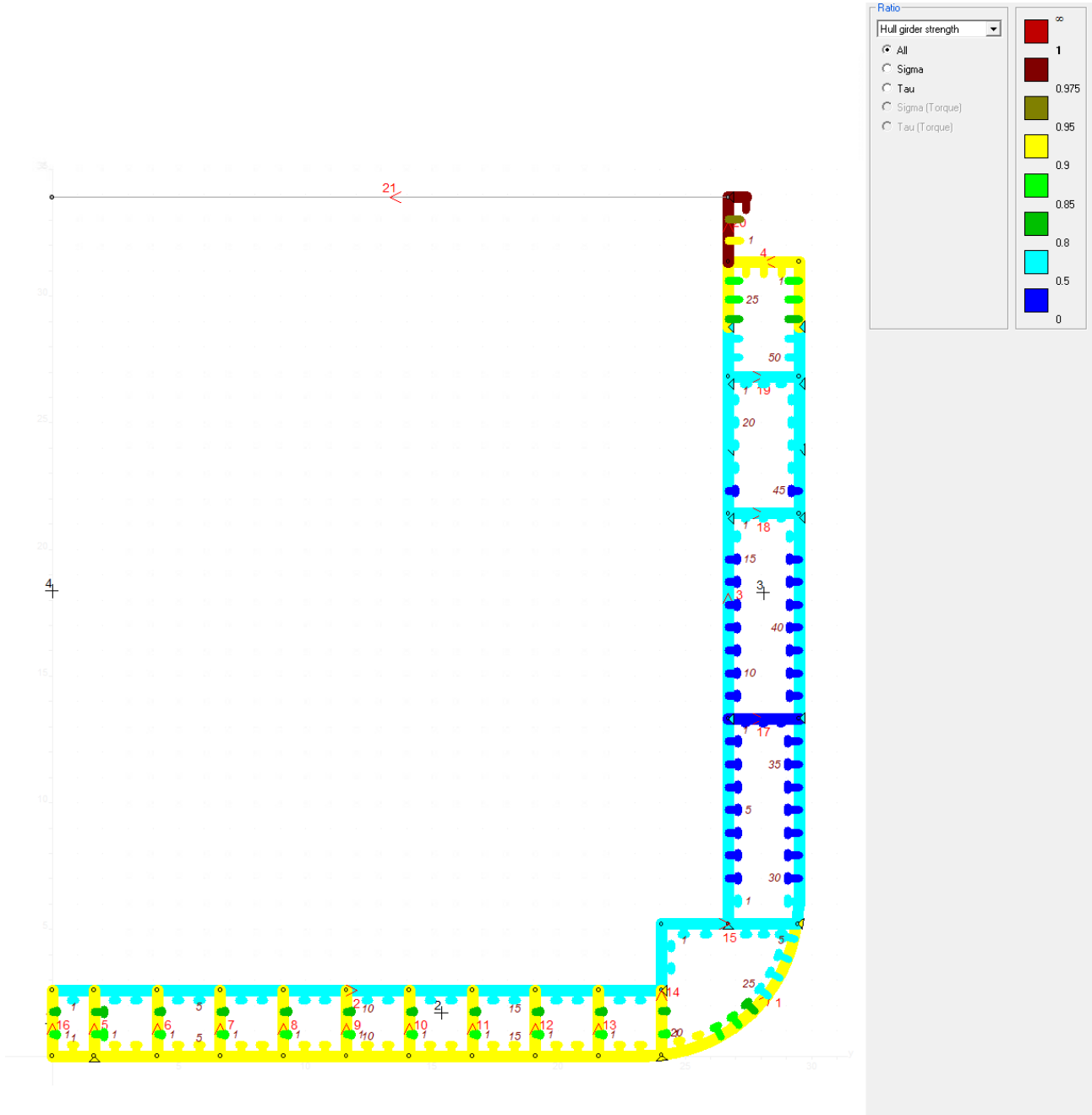


Figure 32 – Midship Section – Hull Girder Strength Check

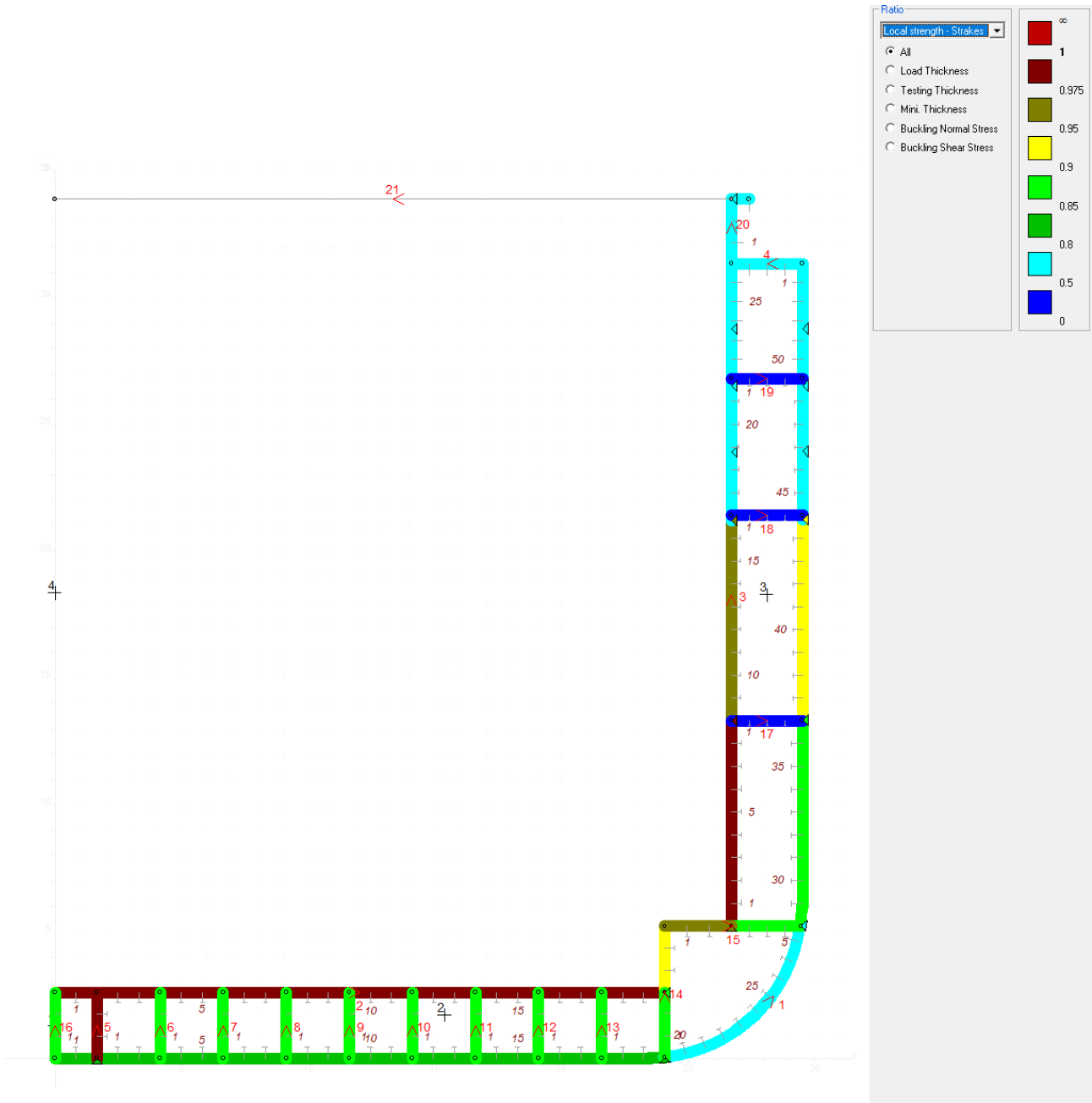


Figure 33 – Midship Section – Local Strength Check – Plates

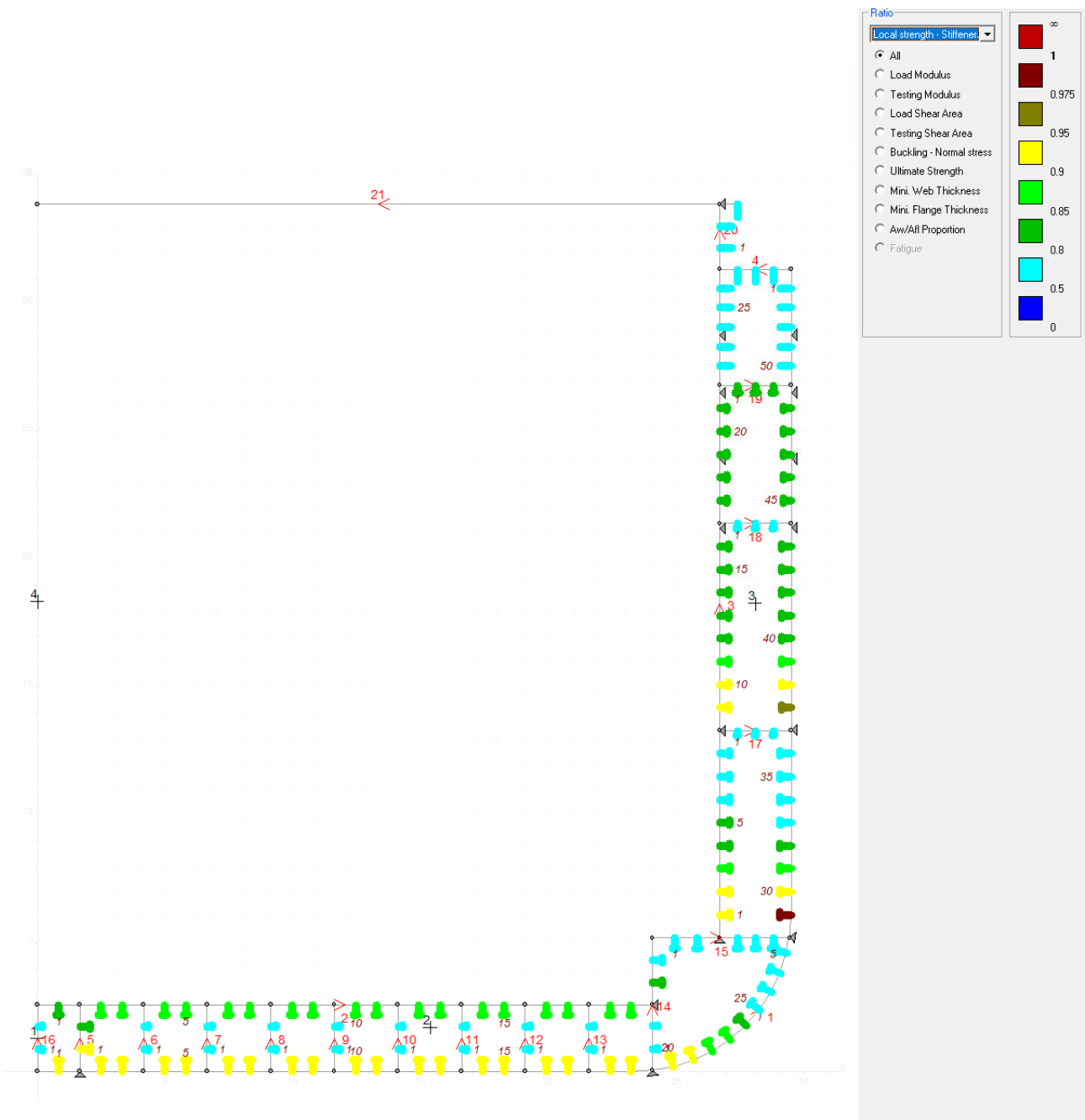
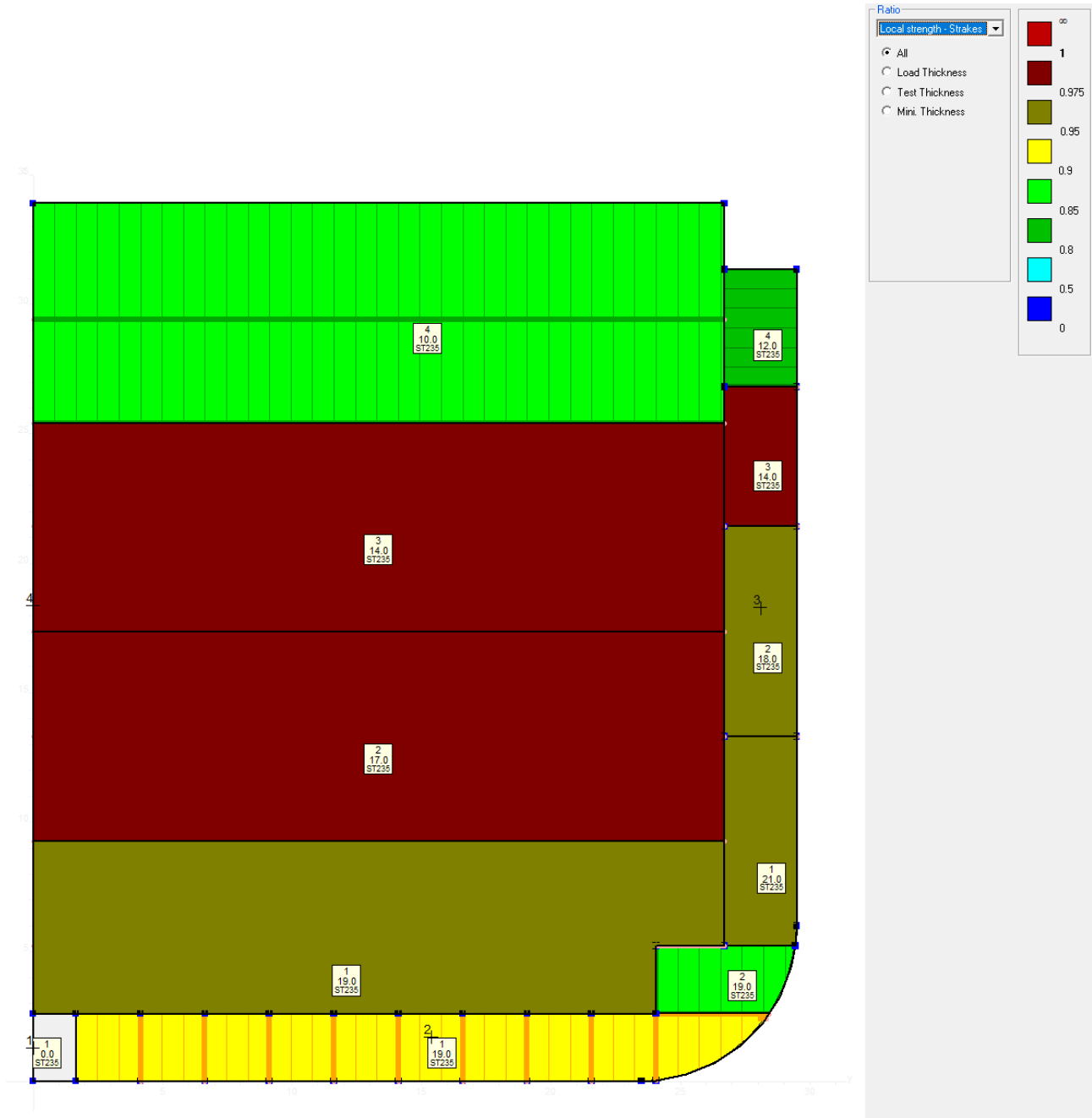


Figure 34 – Midship Section – Local Strength Check – Longitudinal Stiffeners

## 4.2. Transverse Bulkhead Midship

According to the calculation performed in BV Mars 2000, the designed transverse bulkhead meets the BV Rules requirements.



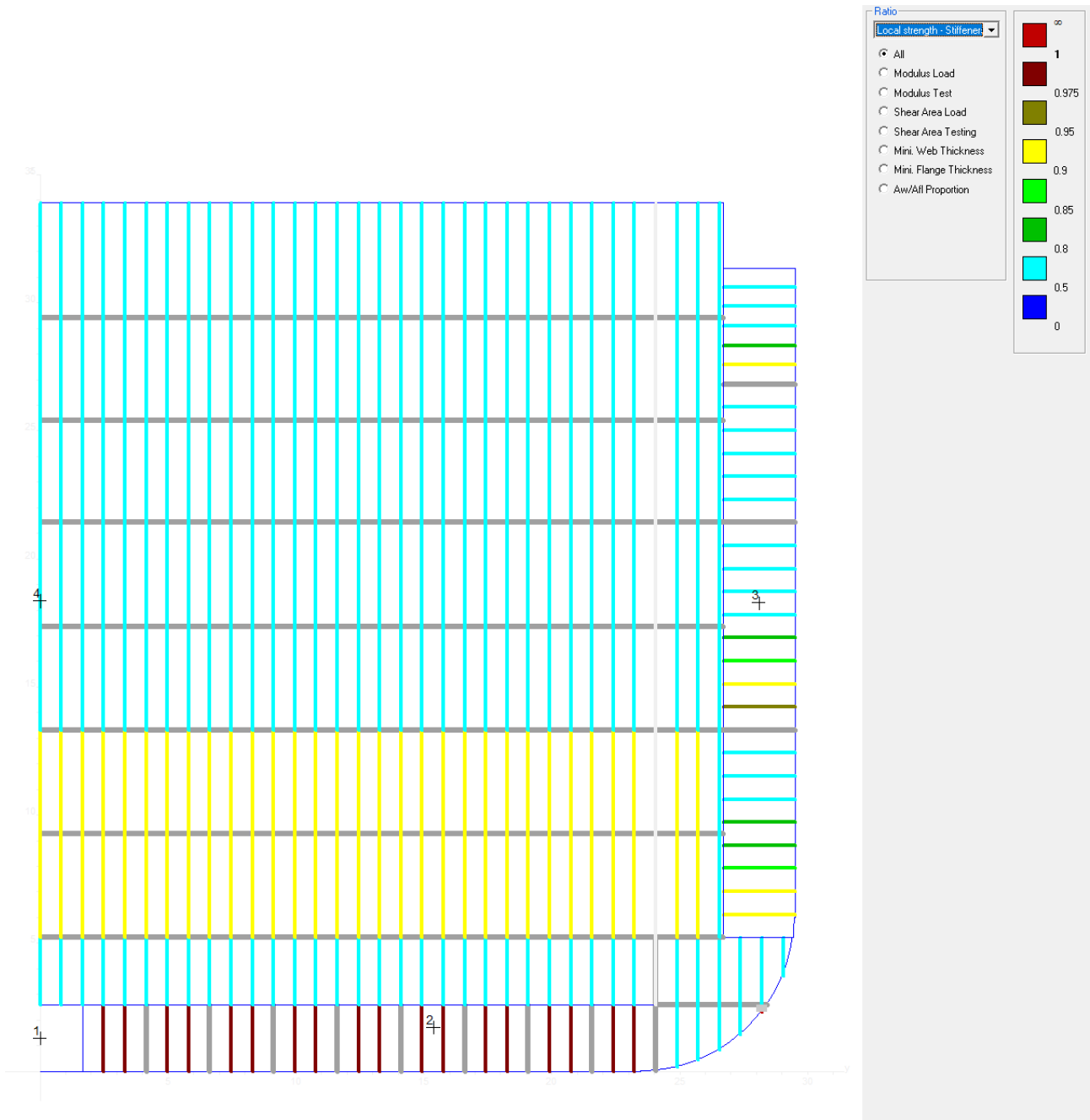



Figure 36 – Transverse Bulkhead – Local Strength Check – Stiffeners



### 4.3. Primary Supporting Members Midship

According to the calculation performed with DNV Nauticus Hull-Primary Supporting Members, the designed PSM meets the Rules requirements.

- Floor plate 19 mm.



Program: **Primary Supporting Members**  
 Rule ref: **DNV rules Pt.3. Ch.6 Sec.6 July 2015**  
 Rev: 2015-05-29

NAUTICUS™  
HULL

Select/ edit profile
Dim. Help...
Copy to Profile stack
Print
Results>>
Stack>>

Position:

Name / Id # DoubleSkin 2600 x20

PSM spacing, S: 3150.0 [mm]

Web Height between plates: 2600.0 [mm]

Thickness of top/inner plate: 20.0 [mm]

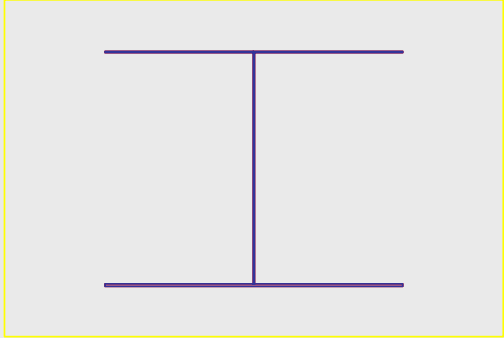
PSM Web plate Thickness: 19.0 [mm]

Thickness of bottom/outer plate: 26.0 [mm]

Corrosion addition, plate 0.0 [mm]

Corrosion addition, girder 0.0 [mm]



**PROFILE PROPERTIES:**

Total Area: A <sub>tot_n50</sub> =	1943.00	[cm2]	Distance to Neutral axis: Yna =	0.00	[mm]
Effective Area: A <sub>e_n50</sub> =	1943.00	[cm2]	Distance to Neutral axis: Zna =	1197.31	[mm]
Shear Area in Y-dir.: A <sub>yshr_n50</sub> =	966.01	[cm2]	Shear center offset: eY =	0.00	[mm]
Shear Area in Z-dir.: A <sub>zshr_n50</sub> =	473.02	[cm2]	Shear center offset: eZ =	-43.87	[mm]
Torsional resistance: Z <sub>x_n50</sub> =	9590398.8	[cm3]	Torsional mom. of inertia: Ix =	24935037.0	[cm4]
Section modulus: Z <sub>yTop_n50</sub> =	189084.4	[cm3]	Moment of inertia: Iy =	27392485.7	[cm4]
Section modulus: Z <sub>yBot_n50</sub> =	228783.8	[cm3]	Moment of inertia: Iz =	11981567.4	[cm4]
Section modulus, z-axis: Z <sub>z_n50</sub> =	76073.4	[cm3]	Centrifugal mom. of in.: Iyz =		[cm4]
Req. net section mod. Z <sub>n50</sub> >=	139656.6	[cm3]	Web and Flange min thick.: t >=	9.5	[mm]
Req. net shear area: A <sub>shr_n50</sub> >=	403.2	[cm2]	! Web pl. slenderness req.: tw >=	26.0	[mm]
Web stiff. inertia req.: I <sub>st</sub> >=	0.0	[cm4]	! Flange slenderness req.: tf >=	131.5	[mm]
	OK		Max unSUP. flange length: S <sub>b</sub> <=	63.5	[m]

**BEAM DATA:**

Effective bending span: l <sub>bdg</sub> =	24.0	[m]
Effective shear span: l <sub>shr</sub> =	24.0	[m]
Load breadth / PSM Spacing: S =	3.15	[m]
Yield stress: R <sub>elH</sub> =	235.0	[MPa]
Perm. bending stress coeff.: C <sub>s</sub> =	0.85	[-]
Perm. combined str. coeff.: C <sub>s1</sub> =	0.95	[-]
Perm. bending stress coeff.: C <sub>s2</sub> =	0.85	[-]
Perm. shear stress coeff.: C <sub>t</sub> =	0.85	[-]
Young's modulus: E =	206.0	[GPa]
Cross contraction: v =	0.3	[-]
Shear Modulus: G=E/(2(1+v)) =	79.23	[GPa]
Density of material: ρ =	7.8	[kg/dm3]

Bending moment and shear force distribution factors			
Position	1	2	3
f <sub>bdg</sub>	-	8.00	-
f <sub>shr</sub>	0.50	-	0.50

**DESIGN LOAD SET:** L51 AC-II

**Distributed pressure:** [kN/m2] Load intensity: At point (x-distance from A)

At Left end: P <sub>A</sub> =	123.0	q <sub>A</sub> =	387.45	X <sub>A</sub> =	0	[m]
Intern. Point: P <sub>1</sub> =		q <sub>1</sub> =	0	X <sub>q1</sub> =		[m]
At Right end: P <sub>B</sub> =	123.0	q <sub>B</sub> =	387.45	X <sub>A</sub> =	24.0	[m]

**Concentrated loads:** Force: [kN] Moment: [kNm] Location: [m]

Load no. 1	F <sub>1</sub> =		M <sub>1</sub> =		X <sub>1</sub> =	
Load no. 2	F <sub>2</sub> =		M <sub>2</sub> =		X <sub>2</sub> =	
Load no. 3	F <sub>3</sub> =		M <sub>3</sub> =		X <sub>3</sub> =	
Load no. 4	F <sub>4</sub> =		M <sub>4</sub> =		X <sub>4</sub> =	
Load no. 5	F <sub>5</sub> =		M <sub>5</sub> =		X <sub>5</sub> =	
Load no. 6	F <sub>6</sub> =		M <sub>6</sub> =		X <sub>6</sub> =	

**Axial load and end moments:**

Hull girder stress, Axial Load: σ<sub>hg</sub> = [Mpa] F<sub>x</sub> = 0.0 [kN]

Left end moment: (when f<sub>bdg1</sub>=0) M<sub>A</sub> = [kNm]

Right end moment: (when f<sub>bdg3</sub>=0) M<sub>B</sub> = [kNm]

Figure 37 – PSM – Floor Check

- Side webframe plate 15mm.



NAUTICUS<sup>®</sup>  
HULL

Program: **Primary Supporting Members**  
 Rule ref: **DNV rules Pt.3, Ch.6 Sec.6 July 2015**  
 Rev: 2015-05-29

Select/ edit profile		Dim. Help...	Copy to Profile stack	Print	Results>>	Stack>>
Position:						
Name / Id #	Double Skin 2800 x 20					
PSM spacing, S:	3150.0	[mm]				
Web Height between plates:	2800.0	[mm]				
Thickness of top/inner plate:	18.0	[mm]				
PSM Web plate Thickness:	15.0	[mm]				
Thickness of bottom/outer plate:	19.0	[mm]				
Corrosion addition, plate $t_c$ 0.0 [mm]						
Corrosion addition, girder 0.0 [mm]						
<b>PROFILE PROPERTIES:</b>						
Total Area: $A_{tot,n50}$	1585.50	[cm <sup>2</sup> ]	Distance to Neutral axis: $Y_{na}$	0.00	[mm]	Copy to Profile stack
Effective Area: $A_{s,n50}$	1585.50	[cm <sup>2</sup> ]	Distance to Neutral axis: $Z_{na}$	1390.82	[mm]	
Shear Area in Y-dir.: $A_{yshr,n50}$	777.01	[cm <sup>2</sup> ]	Shear center offset: $e_Y$	0.00	[mm]	
Shear Area in Z-dir.: $A_{zshr,n50}$	401.07	[cm <sup>2</sup> ]	Shear center offset: $e_Z$	-10.16	[mm]	
Torsional resistance: $Z_{t,n50}$	12335015.4	[cm <sup>3</sup> ]	Torsional mom. of inertia: $I_x$	23436529.3	[cm <sup>4</sup> ]	
Section modulus: $Z_{ytop,n50}$	178944.4	[cm <sup>3</sup> ]	Moment of inertia: $I_y$	25878625.0	[cm <sup>4</sup> ]	
Section modulus: $Z_{ybot,n50}$	186067.7	[cm <sup>3</sup> ]	Moment of inertia: $I_z$	9637306.9	[cm <sup>4</sup> ]	
Section modulus, z-axis: $Z_{z,n50}$	61189.3	[cm <sup>3</sup> ]	Centrifugal mom. of in.: $I_{yz}$		[cm <sup>4</sup> ]	
Req. net section mod. $Z_{s0} \geq$	113728.5	[cm <sup>3</sup> ]	Web and Flange min thick.: $t \geq$	9.5	[mm]	Floors
Req. net shear area: $A_{s0} \geq$	301.5	[cm <sup>2</sup> ]	! Web pl. slenderness req.: $tw \geq$	28.0	[mm]	
Web stiff. inertia req.: $I_{st} \geq$	0.0	[cm <sup>4</sup> ]	! Flange slenderness req.: $tf \geq$	131.5	[mm]	
			Max unupp. flange length: $S_b \leq$	62.7	[m]	Other area
OK			Not OK!			
<b>BEAM DATA:</b>						
Effective bending span: $l_{bdg}$	26.13	[m]	DESIGN LOAD SET: LS1 AC-II			
Effective shear span: $l_{bs}$	26.13	[m]	Distributed pressure: [kN/m <sup>2</sup> ]			
Load breadth / PSM Spacing: $S$	3.15	[m]	At Left end: $P_A = 84.5$ $q_A = 266.175$ $X_A = 0$ [m]			
Yield stress: $R_{eH}$	235.0	[MPa]	Interm. Point: $P_t = 0$ $q_t = 0$ $X_{qt} = 0$ [m]			
Penn. bending stress coeff.: $C_b$	0.85	[-]	At Right end: $P_B = 84.5$ $q_B = 266.175$ $X_B = 26.13$ [m]			
Penn. combined str. coeff.: $C_{s1}$	0.95	[-]	Conc. loads: Force: [kN] Moment: [kNm] Location: [m]			
Penn. bending stress coeff.: $C_{s2}$	0.85	[-]	Load no. 1 $F_1 =$ $M_1 =$ $X_1 =$			
Penn. shear stress coeff.: $C_s$	0.85	[-]	Load no. 2 $F_2 =$ $M_2 =$ $X_2 =$			
Young's modulus: $E$	206.0	[GPa]	Load no. 3 $F_3 =$ $M_3 =$ $X_3 =$			
Cross contraction: $\nu$	0.3	[-]	Load no. 4 $F_4 =$ $M_4 =$ $X_4 =$			
Shear Modulus: $G = E / (2(1+\nu))$	79.23	[GPa]	Load no. 5 $F_5 =$ $M_5 =$ $X_5 =$			
Density of material: $\rho$	0.0	[kg/dm <sup>3</sup> ]	Load no. 6 $F_6 =$ $M_6 =$ $X_6 =$			
<b>Bending moment and shear force distribution factors</b>						
Position	1	2	3	Select...		
$f_{bdg}$	-	8.00	-			
$f_{shr}$	0.50	-	0.50			
<b>Axial load and end moments:</b>						
Hull girder stress, Axial Load:	$\sigma_{hg}$	[Mpa]	$F_A$	0.0 [kN]		
Left end moment (when $f_{bdg1}=0$ )	$M_V$	[kNm]				
Right end moment (when $f_{bdg3}=0$ )	$M_B$	[kNm]				

Figure 38 – PSM – Side Webframe Check

#### 4.4. Fore Section

According to the calculation performed in BV Mars 2000, the designed cross section meets the BV Rules requirements.

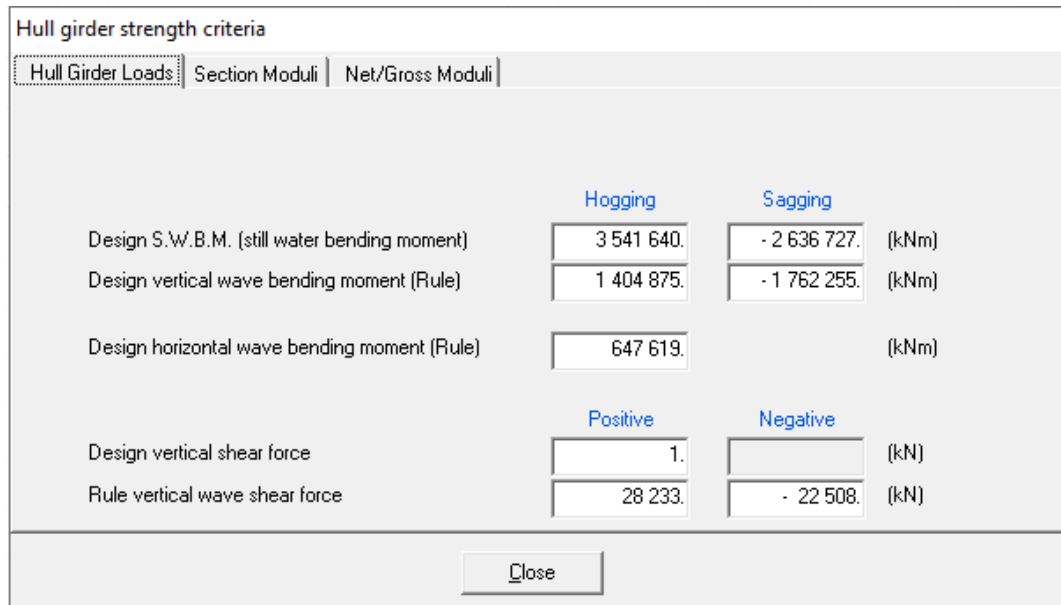


Figure 39 – Fore Section – Hull Girder Loads

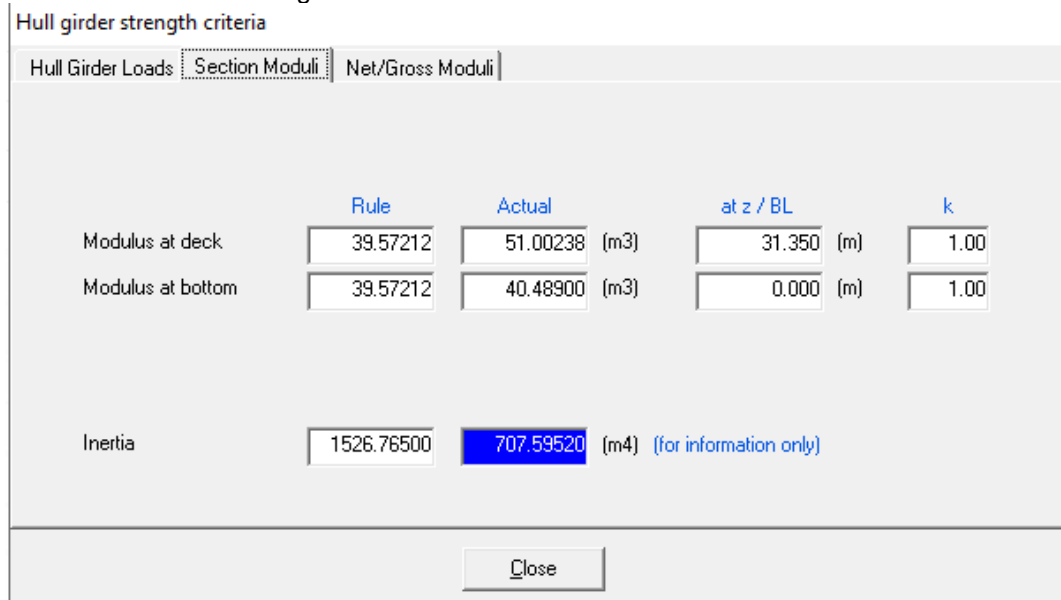


Figure 40 – Fore Section – Section Modulus and Inertia Check

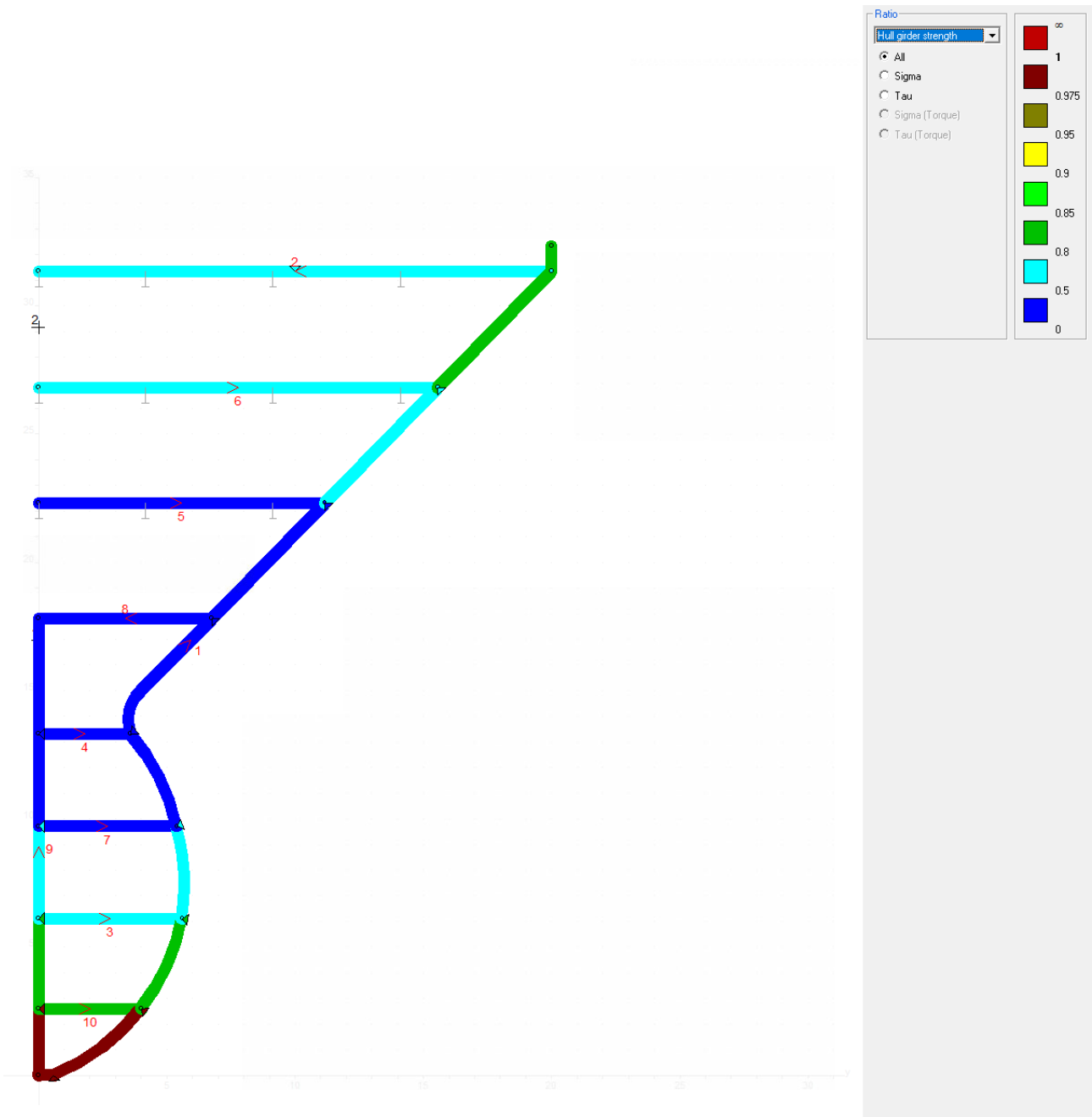


Figure 41 – Fore Section – Hull Girder Strength Check

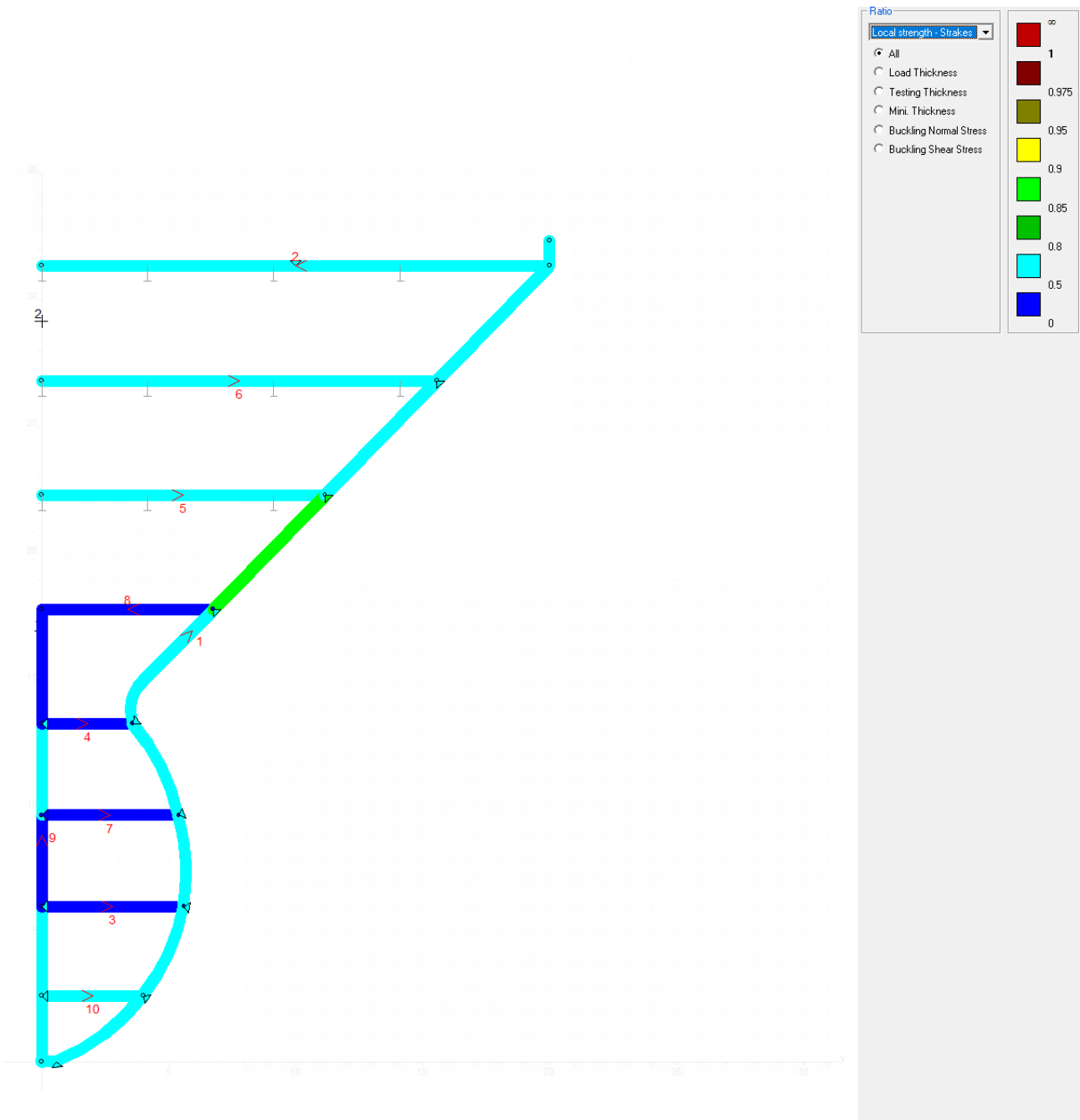


Figure 42 – Fore Section – Local Strength Check – Plates

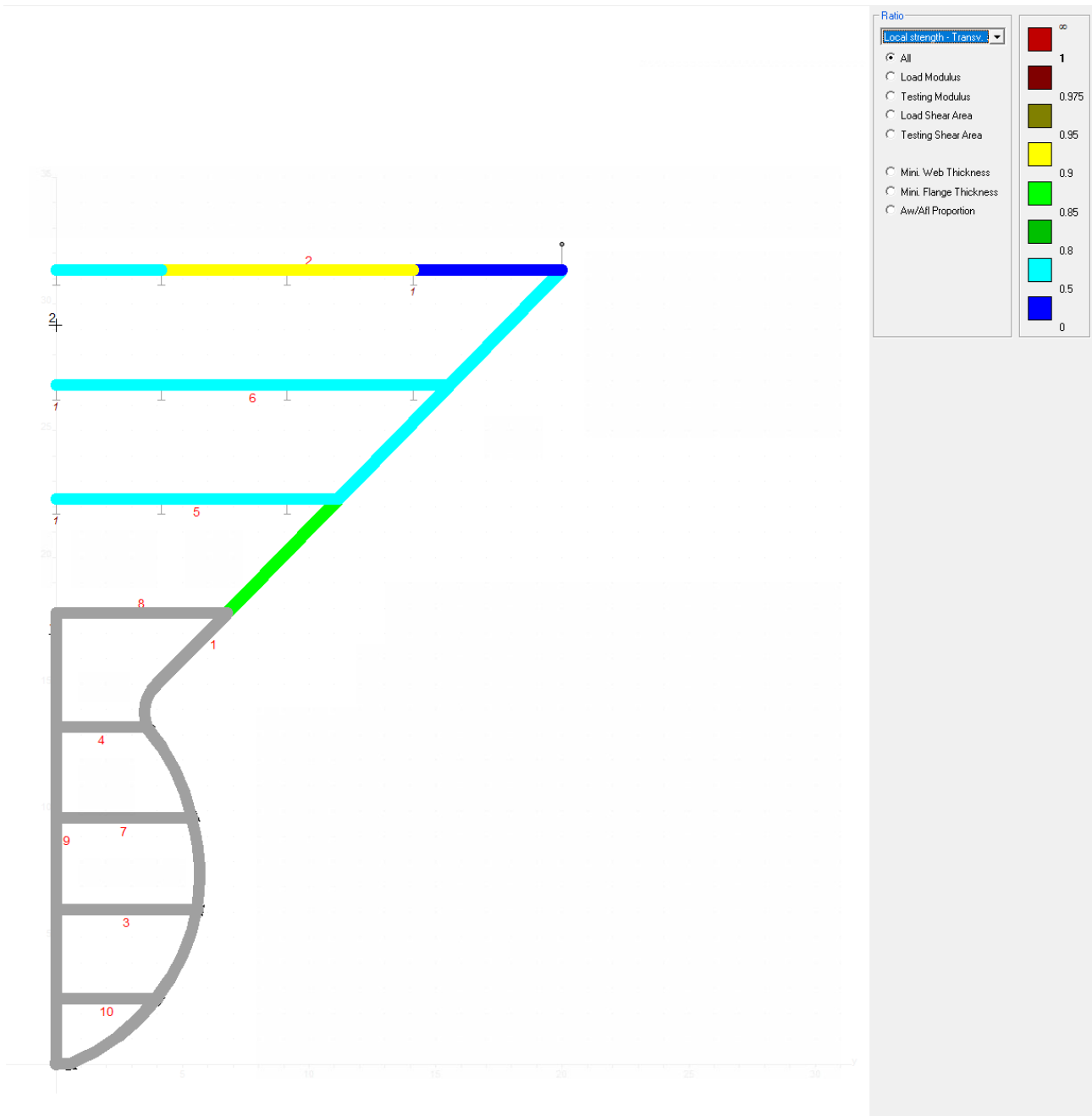


Figure 43 – Fore Section – Local Strength Check – Transverse Stiffeners

### 4.5. Transverse Bulkhead Fore

According to the calculation performed in BV Mars 2000, the designed transverse bulkhead meets the BV Rules requirements.

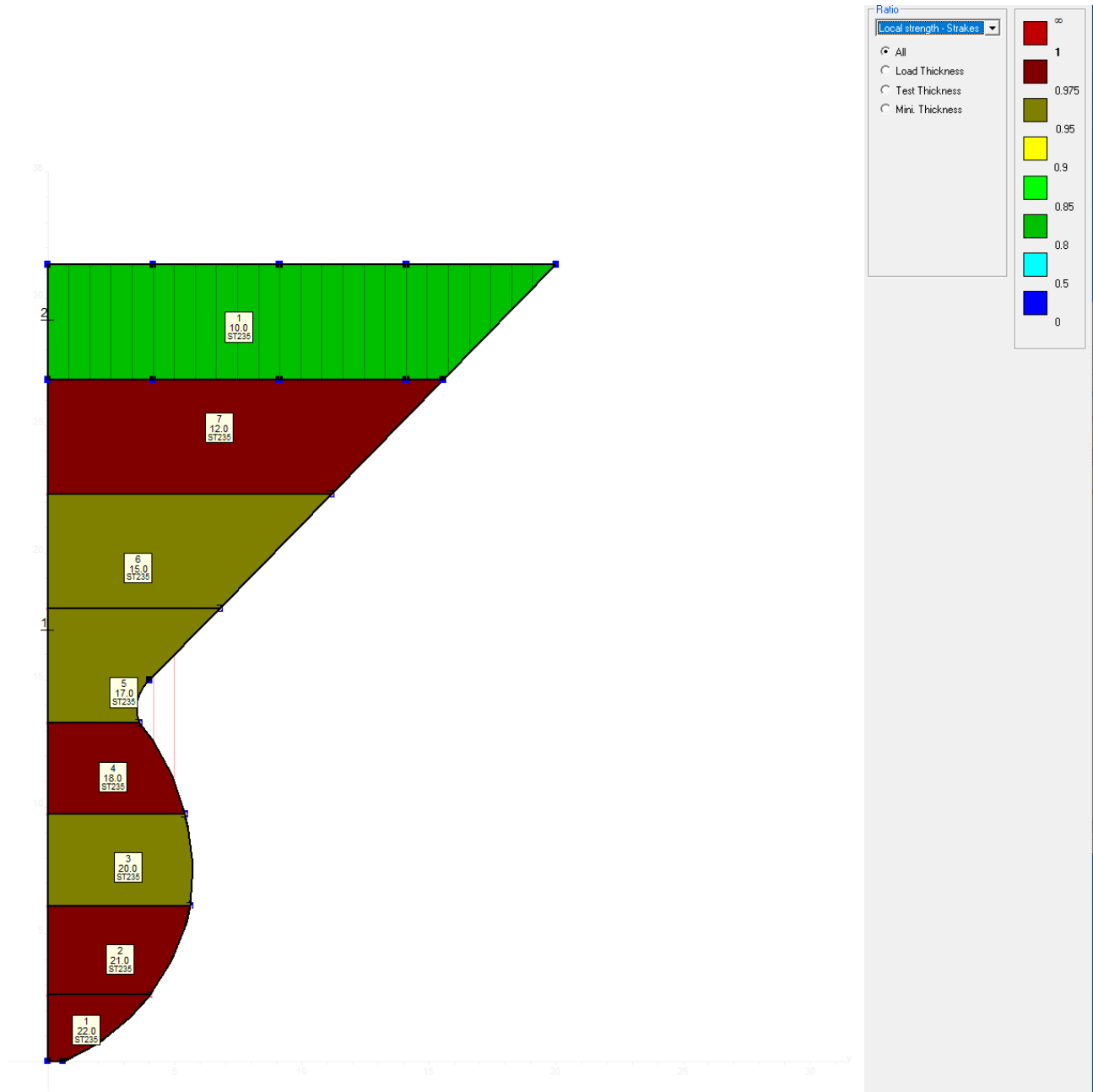


Figure 44 – Transverse Bulkhead Fore – Local Strength Check – Plates

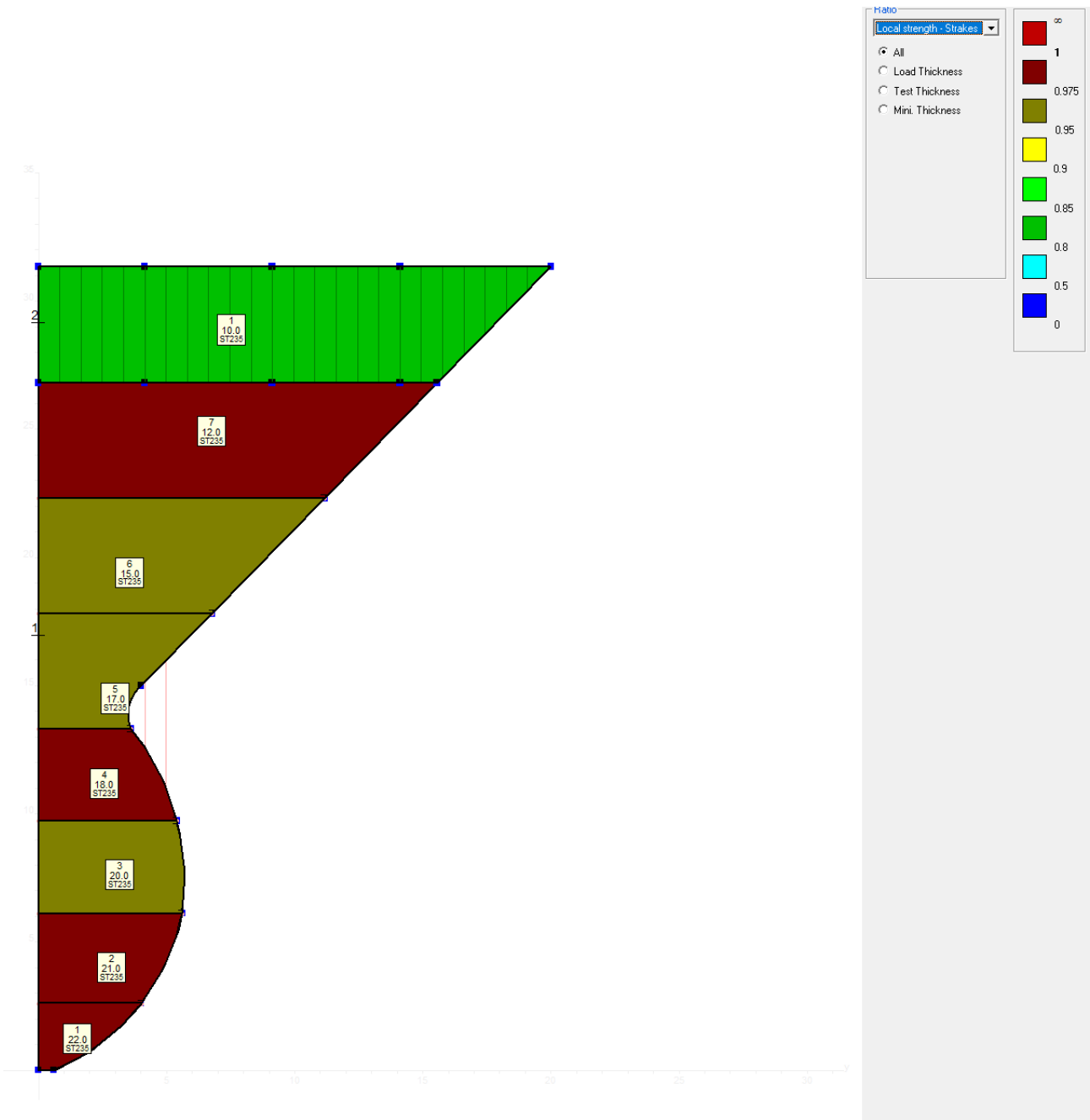



Figure 45 – Transverse Bulkhead Fore – Local Strength Check – Stiffeners



### 4.6. Primary Supporting Members Fore

According to the calculation performed with DNV Nauticus Hull-Primary Supporting Members, the designed PSM meets the Rules requirements.

- Main Deck Transverse and Girders T800x22/350x25



**DNV**

NAUTICUS™  
HULL

Program: **Primary Supporting Members**  
 Rule ref: **DNV rules Pt.3. Ch.6 Sec.6 July 2015**  
 Rev: 2015-05-29

Select/ edit profile
Dim. Help...
Copy to Profile stack
Print
Results>>
Stack>>

Position:

Name / Id # **BuiltUpTbar 800 x 350 x 22 x 20**

Total plate Width: 1916.9 [mm]

Plate Thickness, pT: 22.0 [mm]

Web Height, hw: 800.0 [mm]

Web Thickness, t: 22.0 [mm]

Flange width (incl. web), bf: 350.0 [mm]

Flange thickness, tf: 25.0 [mm]

Angle Between Profile & Plate: 90.0 [Degrees]

Corrosion addition, plate  $t_c$  0.0 [mm]

Corrosion addition, girder 0.0 [mm]

**PROFILE PROPERTIES:**

Total Area:  $A_{tot\_n50} = 685.22$  [cm2]

Effective Area:  $A_{e\_n50} = 685.22$  [cm2]

Shear Area in Y-dir.:  $A_{yshr\_n50} = 582.44$  [cm2]

Shear Area in Z-dir.:  $A_{zshr\_n50} = 160.54$  [cm2]

Torsional resistance:  $Z_{x\_n50} = 510.3$  [cm3]

Section modulus:  $Z_{yTop\_n50} = 30691.1$  [cm3]

Section modulus:  $Z_{yBot\_n50} = 10883.1$  [cm3]

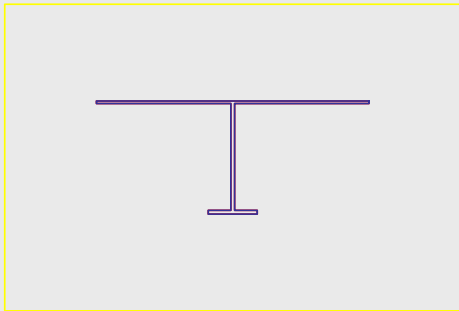
Section modulus, z-axis:  $Z_{z\_n50} = 13567.1$  [cm3]

Req. net section mod.  $Z_{n50} \geq 9815.0$  [cm3]

Req. net shear area:  $A_{shr\_n50} \geq 111.7$  [cm2]

Web stiff. inertia req.:  $I_{st} \geq 0.0$  [cm4]

OK



Distance to Neutral axis:  $Y_{na} = 0.00$  [mm]

Distance to Neutral axis:  $Z_{na} = 625.28$  [mm]

Shear center offset:  $eY = 0.00$  [mm]

Shear center offset:  $eZ = 205.07$  [mm]

Torsional mom. of inertia:  $I_x = 1122.7$  [cm4]

Moment of inertia:  $I_y = 680496.6$  [cm4]

Moment of inertia:  $I_z = 1300340.9$  [cm4]

Centrifugal mom. of in.:  $I_{yz} =$  [cm4]

Web and Flange min thick.:  $t \geq 0.0$  [mm]

Web pl. slenderness req.:  $tw \geq 8.0$  [mm]

Flange slenderness req.:  $tf \geq 14.5$  [mm]

! Max unSUP. flange length:  $S_b \leq 6.1$  [m]

Not OK!

BEAMDATA:
Copy to Beam

Effective bending span:  $l_{bdg} = 9.13$  [m]

Effective shear span:  $l_{shr} = 9.13$  [m]

Load breadth / PSM Spacing:  $S = 2.8$  [m]

Yield stress:  $R_{eH} = 235.0$  [MPa]

Perm. bending stress coeff.:  $C_s = 0.85$  [-]

Perm. combined str. coeff.:  $C_{s1} = 0.95$  [-]

Perm. bending stress coeff.:  $C_{s2} = 0.85$  [-]

Perm. shear stress coeff.:  $C_t = 0.85$  [-]

Young's modulus:  $E = 206.0$  [GPa]

Cross contraction:  $\nu = 0.3$  [-]

Shear Modulus:  $G=E/(2(1+\nu)) = 79.23$  [GPa]

Density of material:  $\rho = 7.8$  [kg/dm3]

Bending moment and shear force distribution factors

Position	1	2	3	Select...
$f_{bdg}$	12.00	24.00	12.00	
$f_{shr}$	0.50	-	0.50	

DESIGN LOAD SET: **L51** | **AC-II**

Distributed pressure: [kN/m2] | Load intensity: [kN/m] | At point (x-distance from A)

At Left end:  $P_A = 100.8$  |  $q_A = 282.24$  |  $X_A = 0$  [m]

Intern. Point:  $P_1 =$  |  $q_1 = 0$  |  $X_{q1} =$  [m]

At Right end:  $P_B = 100.8$  |  $q_B = 282.24$  |  $X_A = 9.13$  [m]

Concentrated loads: Force: [kN] | Moment: [kNm] | Location: [m]

Load no.	Force	Moment	Location
1	$F_1$	$M_1$	$X_1$
2	$F_2$	$M_2$	$X_2$
3	$F_3$	$M_3$	$X_3$
4	$F_4$	$M_4$	$X_4$
5	$F_5$	$M_5$	$X_5$
6	$F_6$	$M_6$	$X_6$

Axial load and end moments:

Hull girder stress, Axial Load:  $\sigma_{hg} =$  [Mpa] |  $F_x = 0.0$  [kN]

Left end moment: (when  $f_{bdg1}=0$ ) |  $M_A =$  [kNm]

Right end moment: (when  $f_{bdg3}=0$ ) |  $M_B =$  [kNm]

Figure 46 – PSM Fore – Main Deck Transverse Check

- Lower Deck Transverse and Girders T400x8/200x10



NAUTICUS™  
HULL

Program: **Primary Supporting Members**  
 Rule ref: **DNV rules Pt.3. Ch.6 Sec.6 July 2015**  
 Rev: 2015-05-29

Select/ edit profile		Dim. Help...	Copy to Profile stack	Print	Results>>	Stack>>
----------------------	--	--------------	-----------------------	-------	-----------	---------

Position:

Name / Id # **BuiltUpTbar 600 x 300 x 16 x 20**

Upper Flange Width:	1916.9	[mm]
Upper Flange Thickness:	18.0	[mm]
Web Height between flanges:	600.0	[mm]
Web Thickness:	16.0	[mm]
Lower Flange Width:	350.0	[mm]
Lower Flange Thickness:	20.0	[mm]
Radius, web & Upper Flange:	90.0	[mm]
Radius, web & Lower Flange:		[mm]
Corrosion addition, plate	0.0	[mm]
Corrosion addition, girder	0.0	[mm]

**PROFILE PROPERTIES:**

Total Area: Atot_n50 =	511.04	[cm2]
Effective Area: Ax_n50 =	511.04	[cm2]
Shear Area in Y-dir.: Ayshr_n50 =	434.39	[cm2]
Shear Area in Z-dir.: Azshr_n50 =	89.76	[cm2]
Torsional resistance: Zx_n50 =	299.0	[cm3]
Section modulus: ZyTop_n50 =	18739.6	[cm3]
Section modulus: ZyBot_n50 =	5852.5	[cm3]
Section modulus, z-axis: Zzn50 =	11098.3	[cm3]
Req. net section mod. Zn50 >=	5751.7	[cm3]
Req. net shear area: Ashr_n50 >=	65.5	[cm2]
Web stiff. inertia req.: Ist >=	0.0	[cm4]

Distance to Neutral axis: Yna =	0.00	[mm]
Distance to Neutral axis: Zna =	486.17	[mm]
Shear center offset: eY =	0.00	[mm]
Shear center offset: eZ =	138.68	[mm]
Torsional mom. of inertia: Ix =	538.3	[cm4]
Moment of inertia: Iy =	284531.0	[cm4]
Moment of inertia: Iz =	1063715.3	[cm4]
Centrifugal mom. of in.: Iyz =	0.0	[cm4]
Web and Flange min thick.: t >=	0.0	[mm]
Web pl. slenderness req.: tw >=	6.0	[mm]
Flange slenderness req.: tf >=	14.5	[mm]
! Max unsupp. flange length: Sb <=	6.4	[m]

**BEAM DATA:**

Effective bending span: l_bdg =	9.13	[m]
Effective shear span: l_shr =	9.13	[m]
Load breadth / PSM Spacing: S =	2.8	[m]
Yield stress: ReH =	235.0	[MPa]
Perm. bending stress coeff.: Cs =	0.85	[-]
Perm. combined str. coeff.: Cs1 =	0.95	[-]
Perm. bending stress coeff.: Cs2 =	0.85	[-]
Perm. shear stress coeff.: Ct =	0.85	[-]
Young's modulus: E =	206.0	[GPa]
Cross contraction: v =	0.3	[-]
Shear Modulus: G=E/(2(1+v)) =	79.23	[GPa]
Density of material: rho =	7.8	[kg/dm3]

Bending moment and shear force distribution factors

Position	1	2	3	Select....
f_bdg	12.00	24.00	12.00	
f_shr	0.50	-	0.50	

**DESIGN LOAD SET:** L51 AC-II

Load intensity: At point (x-distance from A)

Distributed pressure: [kN/m2]	?	[kN/m]	
At Left end: PA =	59.07	qA = 165.396	XA = 0 [m]
Interm. Point: P1 =		q1 = 0	Xq1 = [m]
At Right end: PB =	59.07	qB = 165.396	XA = 9.13 [m]

Concentrated loads: Force: [kN] Moment: [kNm] Location: [m]

Load no. 1	F1 =	M1 =	X1 =
Load no. 2	F2 =	M2 =	X2 =
Load no. 3	F3 =	M3 =	X3 =
Load no. 4	F4 =	M4 =	X4 =
Load no. 5	F5 =	M5 =	X5 =
Load no. 6	F6 =	M6 =	X6 =

**Axial load and end moments:**

Hull girder stress, Axial Load: sigma\_hg = [Mpa] Fx = 0.0 [kN]

Left end moment: (when f\_bdg1=0) MA = [kNm]

Right end moment: (when f\_bdg3=0) MB = [kNm]

Figure 47 – PSM Fore – Lower Deck Transverse and Girders Check

- Side Shell Webframe T600x16/300x20



NAUTICUS™  
HULL

Program: **Primary Supporting Members**  
 Rule ref: **DNV rules Pt.3. Ch.6 Sec.6 July 2015**  
 Rev: 2015-05-29

Select/ edit profile		Dim. Help...	Copy to Profile stack	Print	Results>>	Stack>>			
Position:									
Name / Id #	BuiltUpTbar 800 x 360 x 20 x 25								
Total plate Width:	1457.6	[mm]							
Plate Thickness, pT:	18.0	[mm]							
Web Height, hw:	800.0	[mm]							
Web Thickness, t:	20.0	[mm]							
Flange width (incl. web), bf:	350.0	[mm]							
Flange thickness, tf:	25.0	[mm]							
Angle Between Profile & Plate:	90.0	[Degrees]							
Corrosion addition, plate $t_c$ 0.0 [mm]									
Corrosion addition, girder 0.0 [mm]									
<b>PROFILE PROPERTIES:</b>									
Total Area: $A_{tot\_n50}$	509.87	[cm2]	Distance to Neutral axis: $Y_{na}$	0.00	[mm]	Copy to Profile stack			
Effective Area: $A_{x\_n50}$	509.87	[cm2]	Distance to Neutral axis: $Z_{na}$	564.67	[mm]				
Shear Area in Y-dir.: $A_{yshr\_n50}$	394.35	[cm2]	Shear center offset: $eY$	0.00	[mm]				
Shear Area in Z-dir.: $A_{zshr\_n50}$	148.18	[cm2]	Shear center offset: $eZ$	253.83	[mm]				
Torsional resistance: $Z_{x\_n50}$	327.7	[cm3]	Torsional mom. of inertia: $I_x$	655.5	[cm4]				
Section modulus: $Z_{yTop\_n50}$	20614.6	[cm3]	Moment of inertia: $I_y$	573760.5	[cm4]				
Section modulus: $Z_{yBot\_n50}$	10160.9	[cm3]	Moment of inertia: $I_z$	473507.7	[cm4]				
Section modulus, z-axis: $Z_{z\_n50}$	6497.1	[cm3]	Centrifugal mom. of in.: $I_{yz}$	0.0	[cm4]				
Req. net section mod. $Z_{n50} >=$	8669.9	[cm3]	Web and Flange min thick.: $t >=$	0.0	[mm]	Select location of PSM			
Req. net shear area: $A_{shr\_n50} >=$	143.0	[cm2]	Web pl. slenderness req.: $tw >=$	8.0	[mm]				
Web stiff. inertia req.: $I_{st} >=$	0.0	[cm4]	Flange slenderness req.: $tf >=$	14.5	[mm]				
			! Max unupp. flange length: $S_b <=$	6.2	[m]	0 Flange tripping supports			
OK Not OK!									
<b>BEAMDATA:</b>									
Effective bending span: $l_{bdg}$	6.3	[m]	<b>DESIGN LOAD SET:</b> L51 AC-II						
Effective shear span: $l_{shr}$	6.3	[m]	Distributed pressure: [kN/m2]	?	Load intensity: [kN/m]	At point (x-distance from A)			
Load breadth / PSM Spacing: $S$	2.8	[m]	At Left end: $P_A$	187.0	$q_A$	523.6	$X_A$	0	[m]
Yield stress: $R_{RH}$	235.0	[MPa]	Interm. Point: $P_1$		$q_1$	0	$X_{q1}$		[m]
Perm. bending stress coeff.: $C_s$	0.85	[-]	At Right end: $P_B$	187.0	$q_B$	523.6	$X_A$	6.3	[m]
Perm. combined str. coeff.: $C_{s1}$	0.95	[-]	<b>Concentrated loads:</b>						
Perm. bending stress coeff.: $C_{s2}$	0.85	[-]	Force: [kN]	?	Moment: [kNm]	Location: [m]			
Perm. shear stress coeff.: $C_t$	0.85	[-]	Load no. 1	$F_1$	$M_1$	$X_1$			
Young's modulus: $E$	206.0	[GPa]	Load no. 2	$F_2$	$M_2$	$X_2$			
Cross contraction: $\nu$	0.3	[-]	Load no. 3	$F_3$	$M_3$	$X_3$			
Shear Modulus: $G=E/(2(1+\nu))$	79.23	[GPa]	Load no. 4	$F_4$	$M_4$	$X_4$			
Density of material: $\rho$	7.8	[kg/dm3]	Load no. 5	$F_5$	$M_5$	$X_5$			
Load no. 6	$F_6$	$M_6$	$X_6$						
<b>Bending moment and shear force distribution factors</b>							<b>Axial load and end moments:</b>		
Position	1	2	3	Select...	Hull girder stress, Axial Load: $\sigma_{hg}$	[Mpa]	$F_x$	0.0	[kN]
$f_{bdg}$	12.00	24.00	12.00		Left end moment: (when $f_{bdg1}=0$ )	$M_A$			[kNm]
$f_{shr}$	0.50	-	0.50		Right end moment: (when $f_{bdg3}=0$ )	$M_B$			[kNm]

Figure 48 – PSM Fore – Side Shell Webframe Check

## 5 Conclusion

---

This report covers the scantling evaluation of a common container ship midship section, fore area section, transverse bulkhead in midship area, transverse bulkhead in fore area and primary supporting members. Considering the assumptions presented in Ch.1 and Ch.3, the structure satisfies the BV Rules.

Based on the design calculations it can be concluded that the presented scantling design is representative for a common container ship.

Waarderweg 40  
2031 BP Haarlem  
The Netherlands

Pettelaarpark 10-15  
5216 PD 's-Hertogenbosch  
The Netherlands

Nevelgaarde 10  
3436 ZZ Nieuwegein  
The Netherlands

**Iv-Infra b.v.**  
Trapezium 322  
3364 DL Sliedrecht  
The Netherlands

Trompstraat 36a  
9190 Stekene  
Belgium

Westervoortsedijk 73  
Gebouw CB  
6827 AV Arnhem  
The Netherlands

[www.iv-infra.nl](http://www.iv-infra.nl)  
Telephone +31 88 943 3200  
P.O. Box 135  
3360 AC Sliedrecht  
[officemanagement.infra@iv.nl](mailto:officemanagement.infra@iv.nl)



**C.** R103-DP1 Cruise ship – Scantling calculation report



# 3D FEM gevolgschade schip-turbine

Passenger Ship – Scantling Calculations Report

Client: Rijkswaterstaat  
Document nr: 001  
Revision: 2  
Date: 24 February 2024

**Iv-Infra b.v.**

Engineering Company with a Passion for Technology



Client: Rijkswaterstaat

Document title: 3D-FEM gevolgschade schip-turbine

Document subtitle: Passenger Ship – Scantling Calculations Report

Revision: 2

Date: 24 February 2024

Revision	Status	Date	Author(s)	Checked	Approved	Description
0	TI	24-08-2024	IZ	GV, MMI	WL	Ter informatie
1	TI	25-10-2024	IZ	GV, MMI	WL	Ter informatie
2	TI	24-02-2025	IZ	GV, MMI	WL	Ter informatie

The only difference between revision 2 and revision 1 is the removal of the ship names that the ship model is based on.



## Summary

In this report is presented the scantling evaluation of the midship and fore area of a passenger ship with the following main dimensions and characteristics:

<b>Vessel Characteristics</b>		<b>Unit</b>
<b>GT</b>	100000	t
<b>Lpp</b>	242	m
<b>B</b>	36	m
<b>D</b>	19.7	m
<b>T</b>	8.3	m
<b>Displacement</b>	45000	t
<b>Speed</b>	29	kn

This section was designed with Mars 2000 and checked according to the following rules:

- BV NR467 Rules for the Classifications of steel ships, January 2023 edition.

DNV Nauticus Hull - Primary Supporting Members spreadsheets were used for the design of PSM in midship cargo area and fore area.

The profiles used in the scantling definition are according to DIN Standard.

## TABLE OF CONTENTS

---

<b>1</b>	<b>Assumptions</b>	<b>5</b>
<b>2</b>	<b>Abbreviations</b>	<b>6</b>
<b>3</b>	<b>Scantling Design</b>	<b>7</b>
3.1.	Basic Ship Data	7
3.2.	Midship Section	10
3.3.	Transverse Bulkhead Midship	18
3.4.	Primary Supporting Members Midship	21
3.5.	Fore Section	23
3.6.	Transverse Bulkhead Fore	32
3.7.	Primary Supporting Members Fore	35
<b>4</b>	<b>Scantling Results</b>	<b>36</b>
4.1.	Transverse Section	36
4.2.	Transverse Bulkhead Midship	41
4.3.	Primary Supporting Members Midship	43
4.4.	Fore Section	49
4.5.	Transverse Bulkhead Fore	53
4.6.	Primary Supporting Members Fore	55
<b>5</b>	<b>Conclusion</b>	<b>58</b>

# 1 Assumptions

In this memo, a scantling design of a passenger ship is provided, which will be used during the ship impact simulations for project INF240746 RWS WVL.

Considering similar vessels and the input “INFR240476 - Plan van Aanpak rev.0 – definitief”, the following technical particulars were assumed for the scantling calculation:

- Scantling Length: 242 m
- Depth: 19.7 m
- Breadth: 36 m
- Scantling Draught: 8.3 m
- Minimum Draught at ballast: 6.5 m
- Service Speed: 29 kn
- Block coefficient: 0.607
- Double bottom: 1.5 m
- Frame spacing: 0.7 m (mid)
- Webframe spacing: 2.8 m (mid)

The ship model is based on similar existing ships.

The following frame spacing was considered:

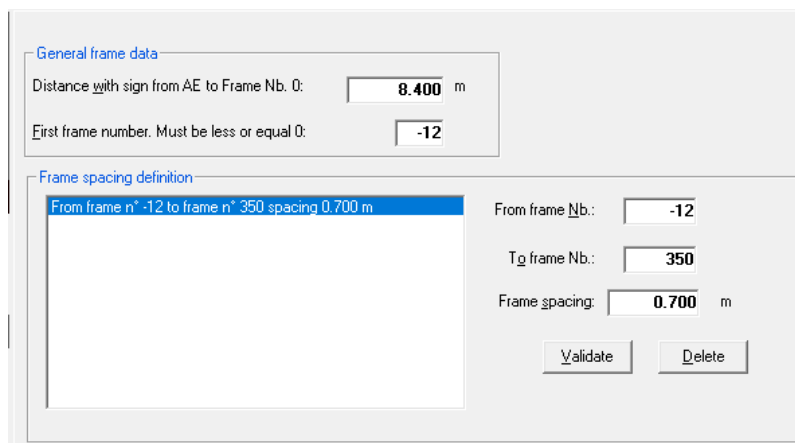


Figure 1 – Frame Spacing

The materials have been assumed to be Grade A steel with a yield stress of 235 MPa and high tensile strength steel (Grade HT36) with a specific minimum yield strength of 355 MPa. The Youngs modulus for all materials has been considered as 206000 N/mm<sup>2</sup>.



## 2 Abbreviations

---

BL	Base Line	
CL	Center Line	
FR	Frame	
PSM	Primary Supporting Member	

# 3 Scantling Design

## 3.1. Basic Ship Data

The following input has been used for the Basic ship data module (BSD).

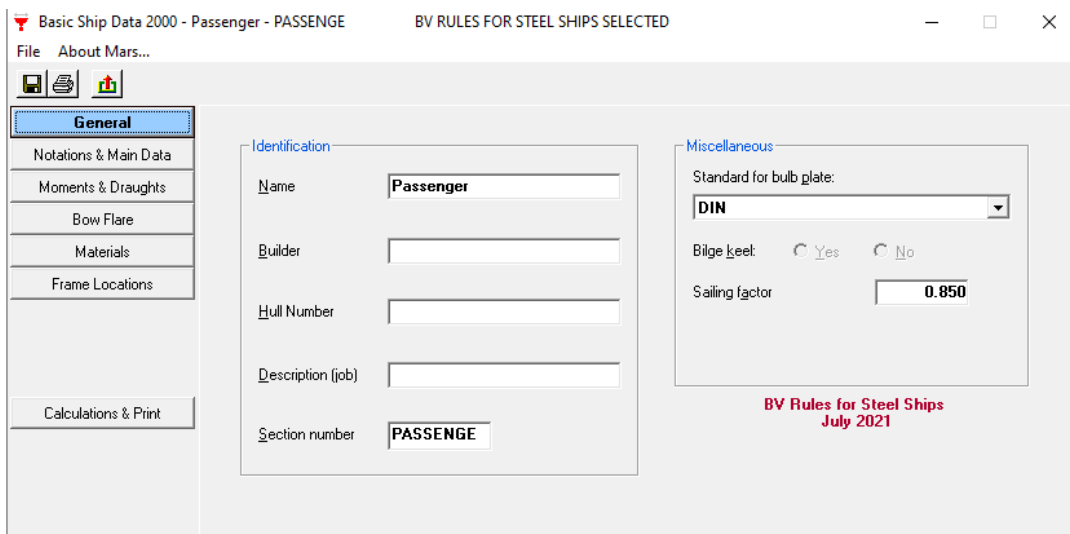


Figure 2 – Basic Ship Data – General

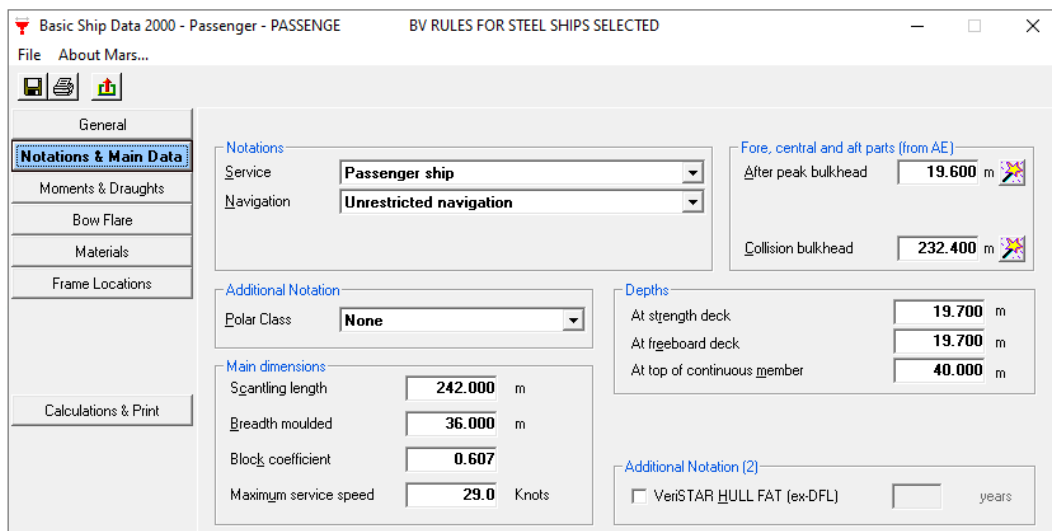


Figure 3 – Basic Ship Data – Class Notation and Main Data

Figure 4 – Basic Ship Data - Materials

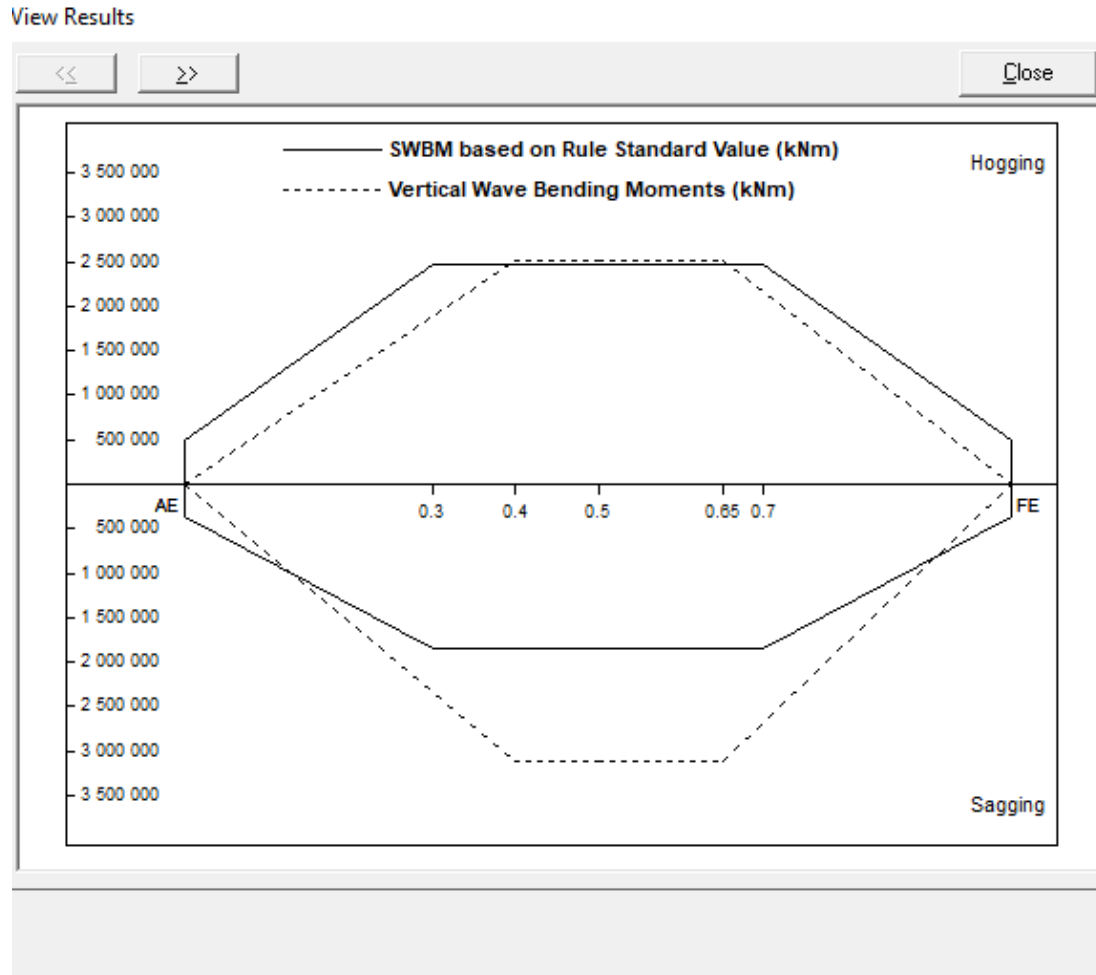


Figure 5 – SWBM and VWBM



View Results

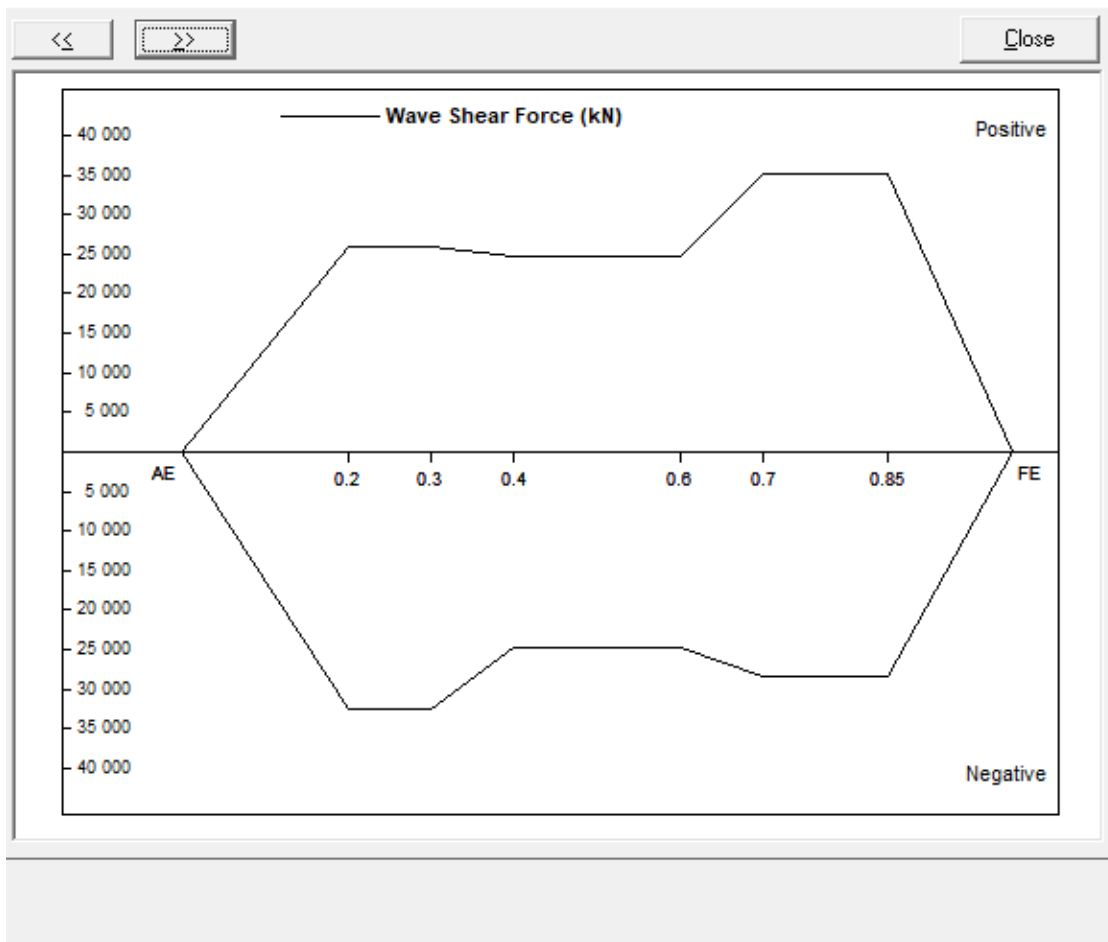


Figure 6 – Wave Shear Force

### 3.2. Midship Section

The location of the assessed cross section is FR 172+0.6m, at 129.4 m from the aft end. The frame spacing for this area is 0.7 m, the webframe spacing is 2.8 m.

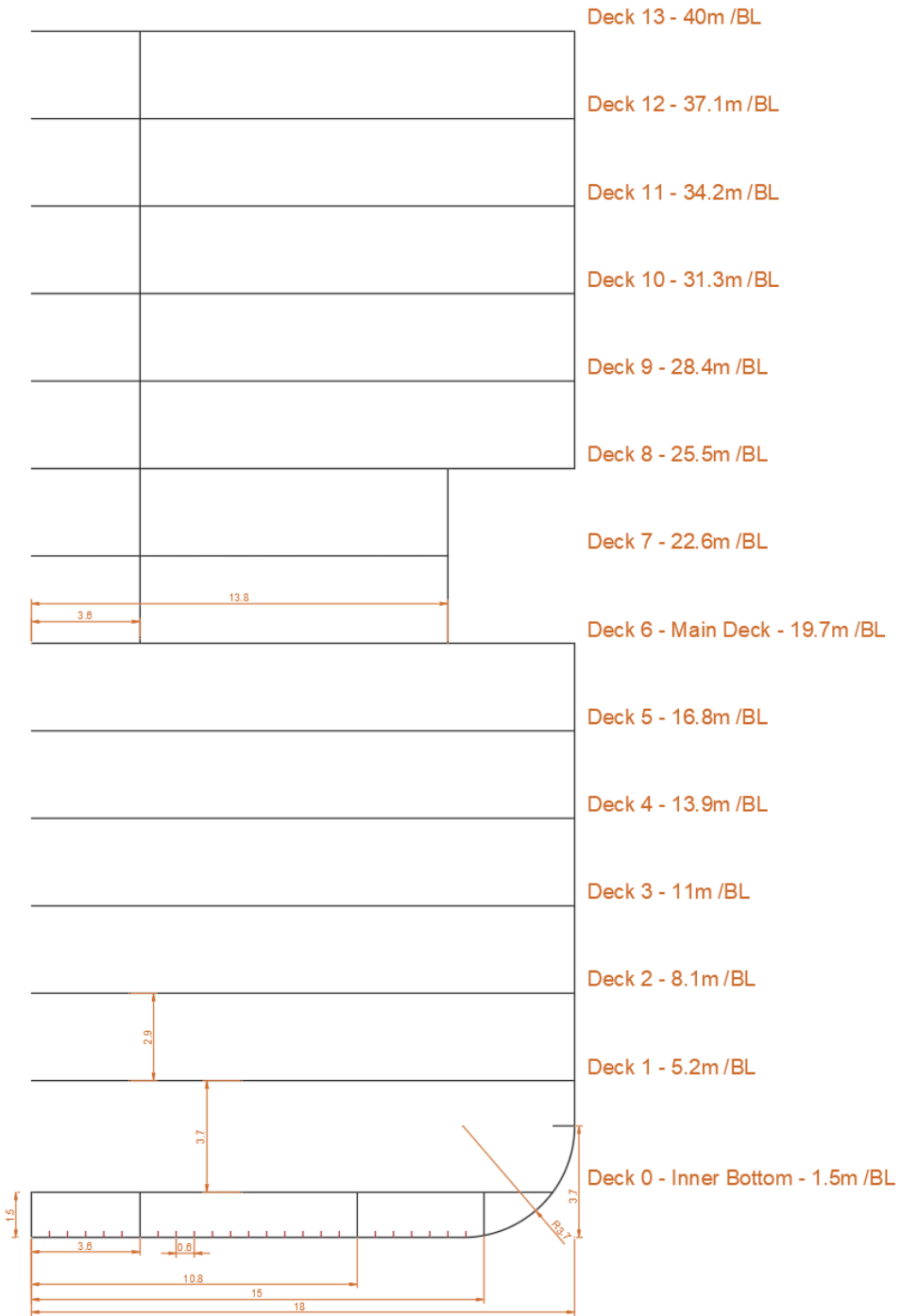


Figure 7 – Midship Section – Sketch (meters)






**Main Section Data**

Main | SW | Fatigue | Ship State | Wave | Flooding

**Name Location Dimensions**

Name:

Longitudinal Location (from AE):  m 

Breadth moulded:  m

Depth moulded:  m

Depth at top of continuous member:  m

**Materials**

in neutral axis      Extension heights:

in deck       m

in bottom       m

Input of:

Figure 8 – Midship Section – Main Section Data

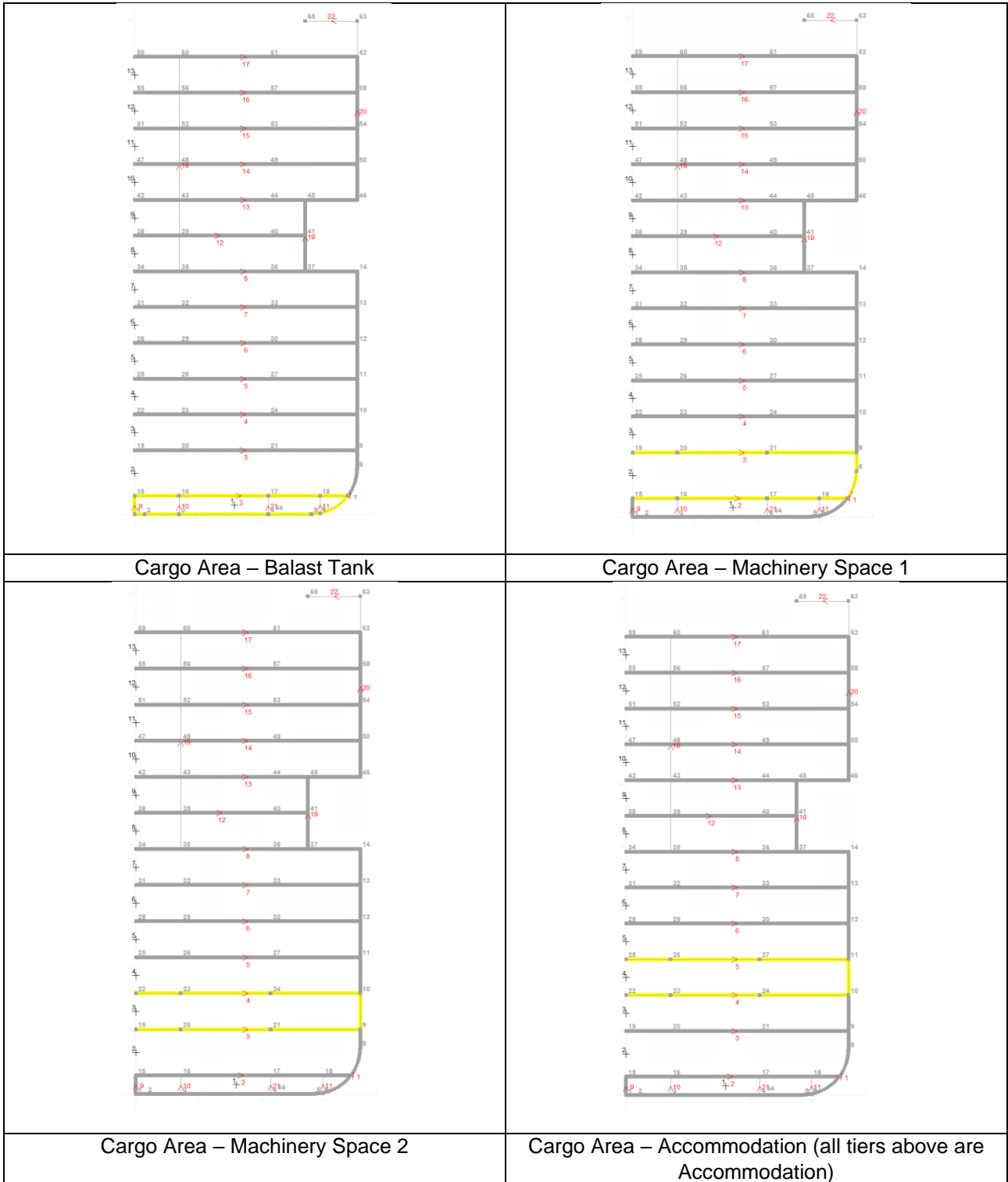


Figure 9 – Midship Section – Compartments

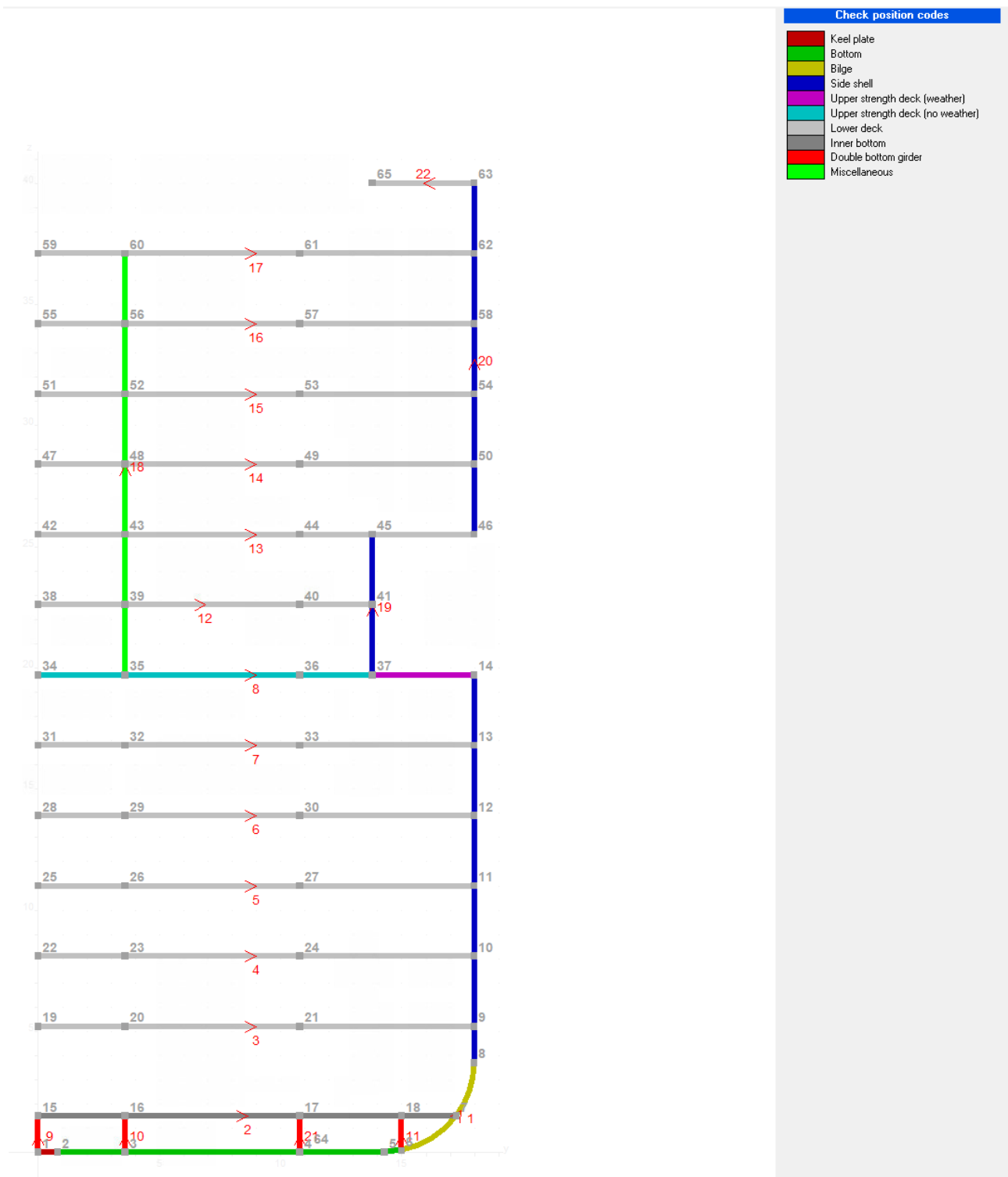


Figure 10 – Midship Section – Position Codes

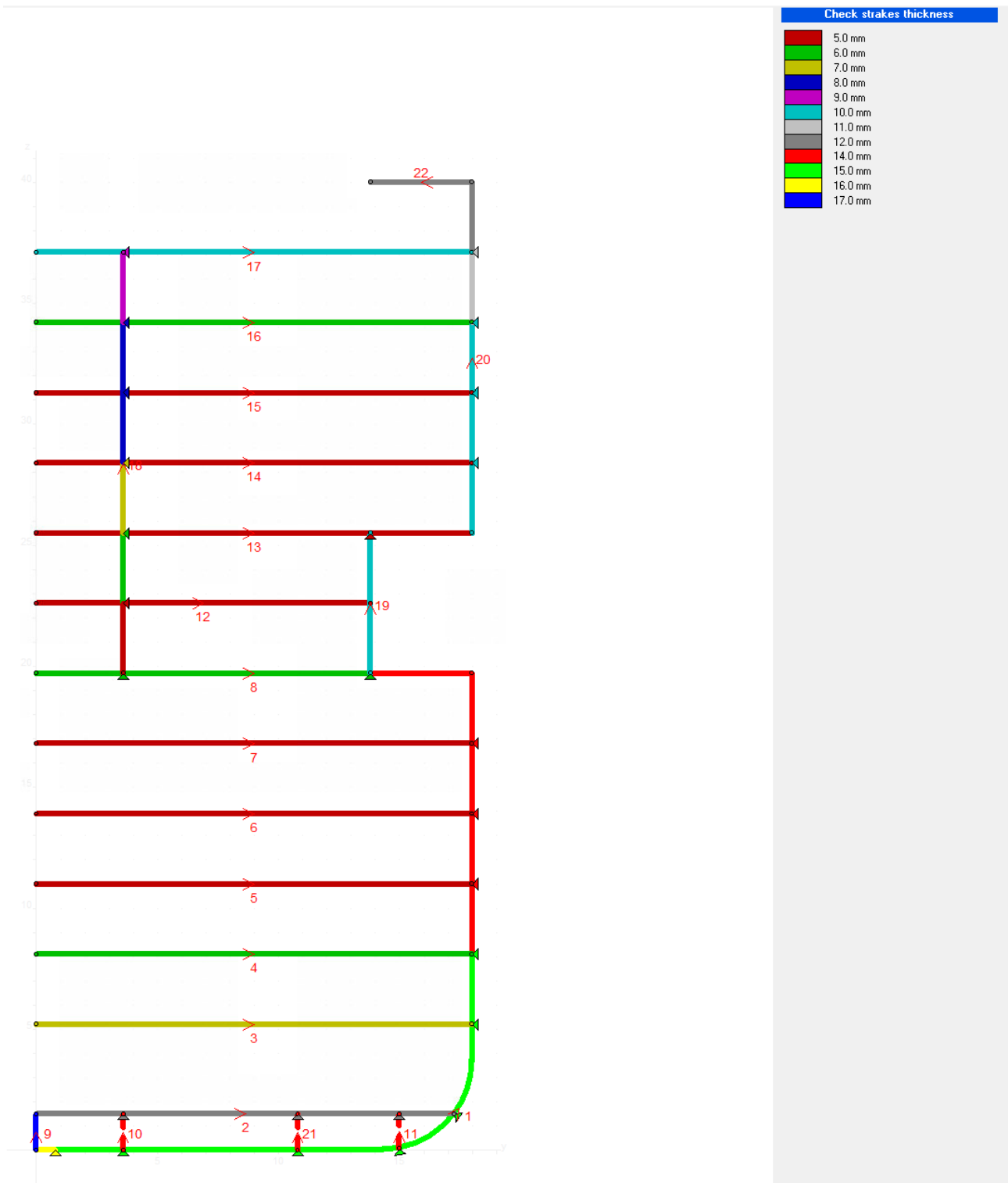


Figure 11 – Midship Section – Plate thickness

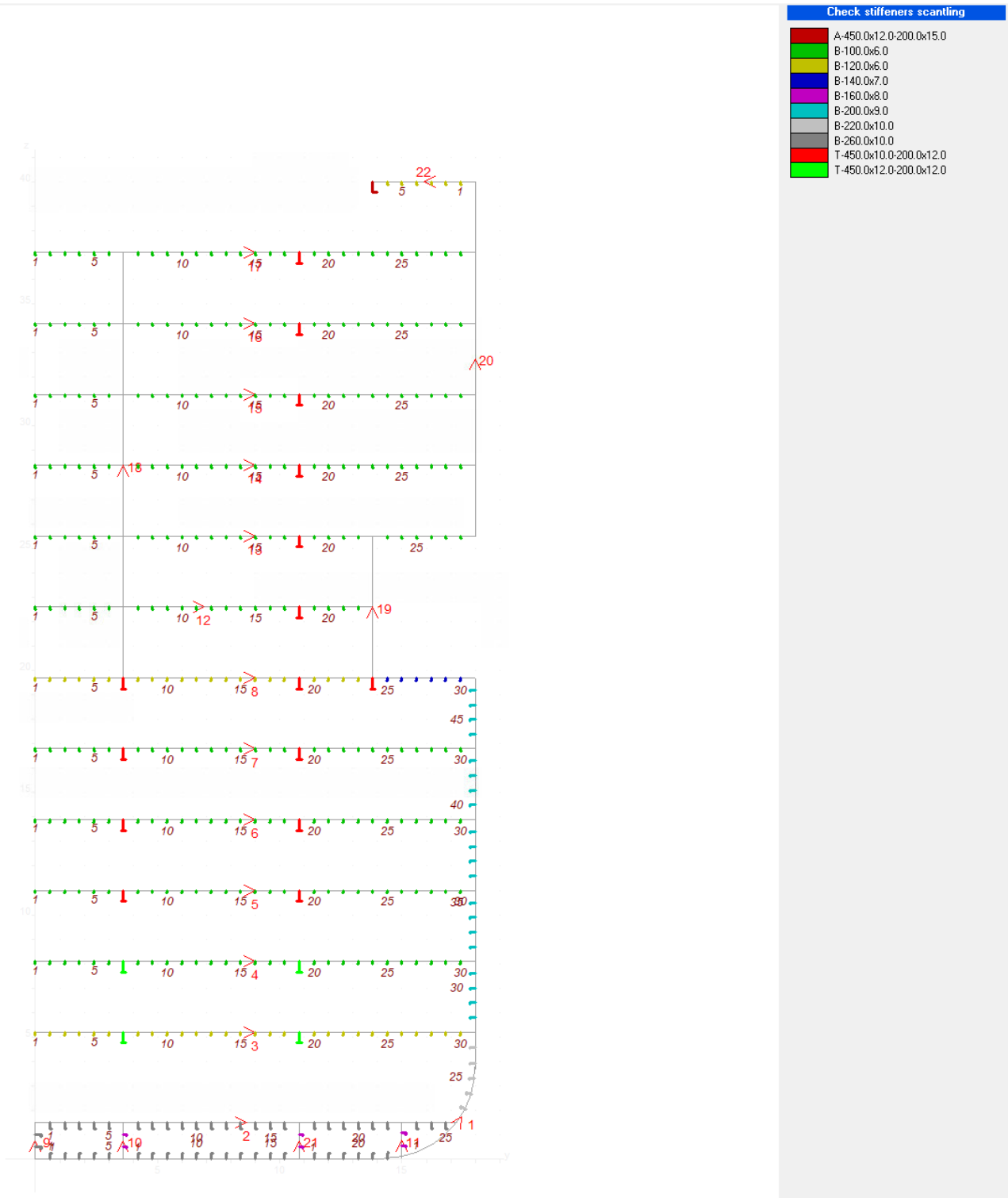


Figure 12 – Midship Section – Stiffeners Scantling

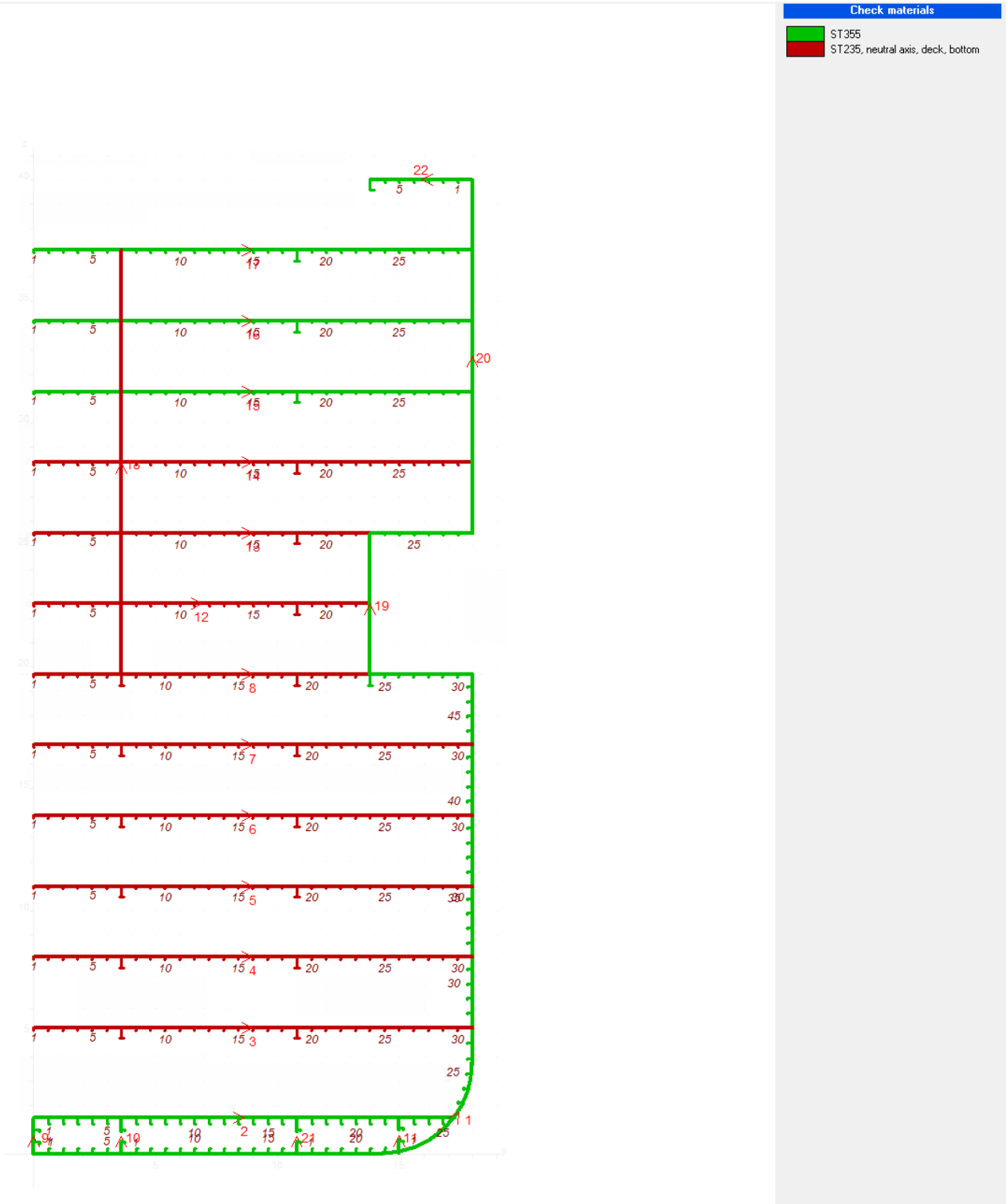


Figure 13 – Midship Section – Materials

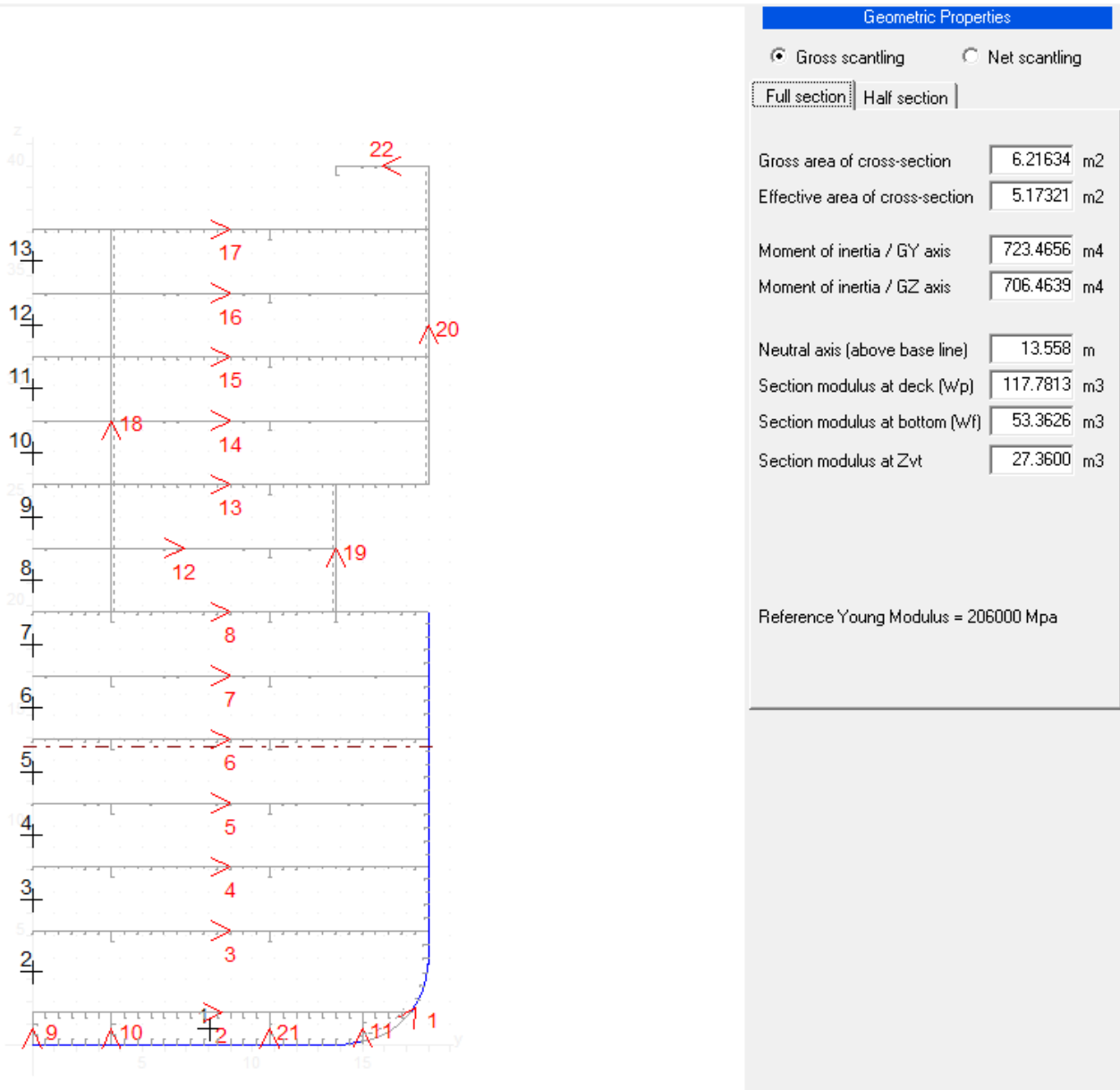


Figure 14 – Midship Section – Geometric Properties

### 3.3. Transverse Bulkhead Midship

The location of the assessed transverse bulkhead is FR 216, at 160 m from the aft end.

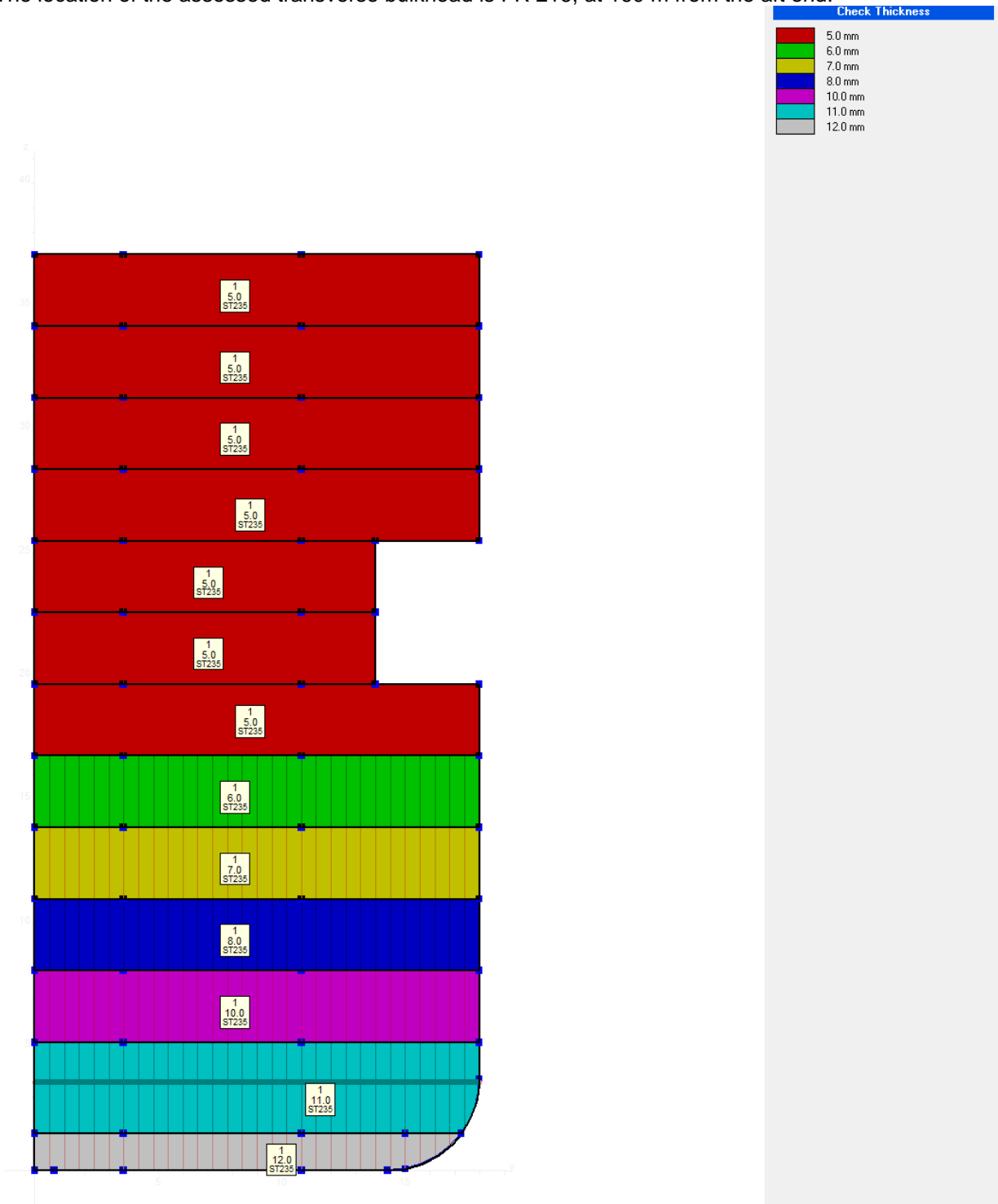


Figure 15 – Transverse Bulkhead – Plate thickness



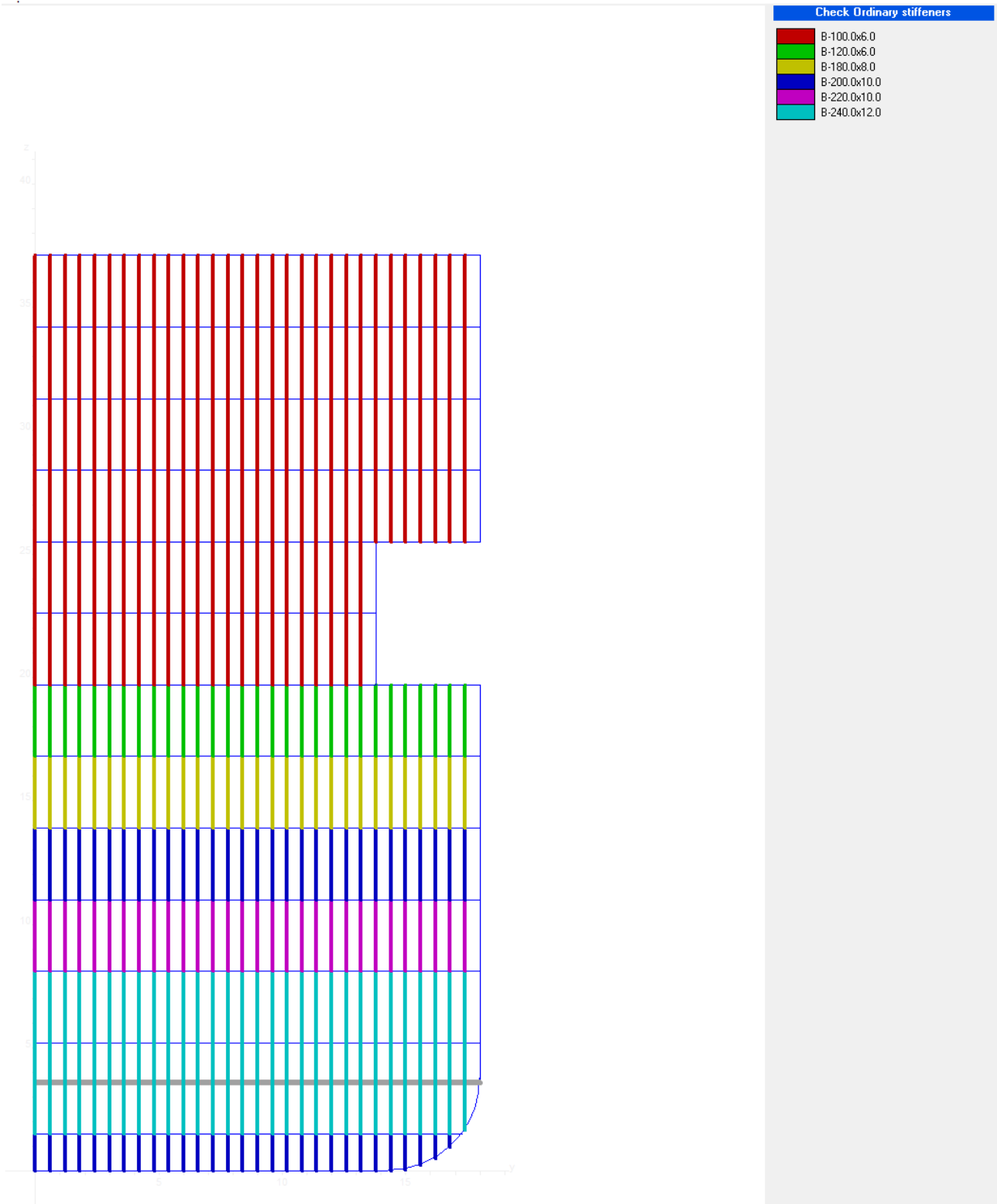


Figure 16 – Transverse Bulkhead – Stiffeners Scantling

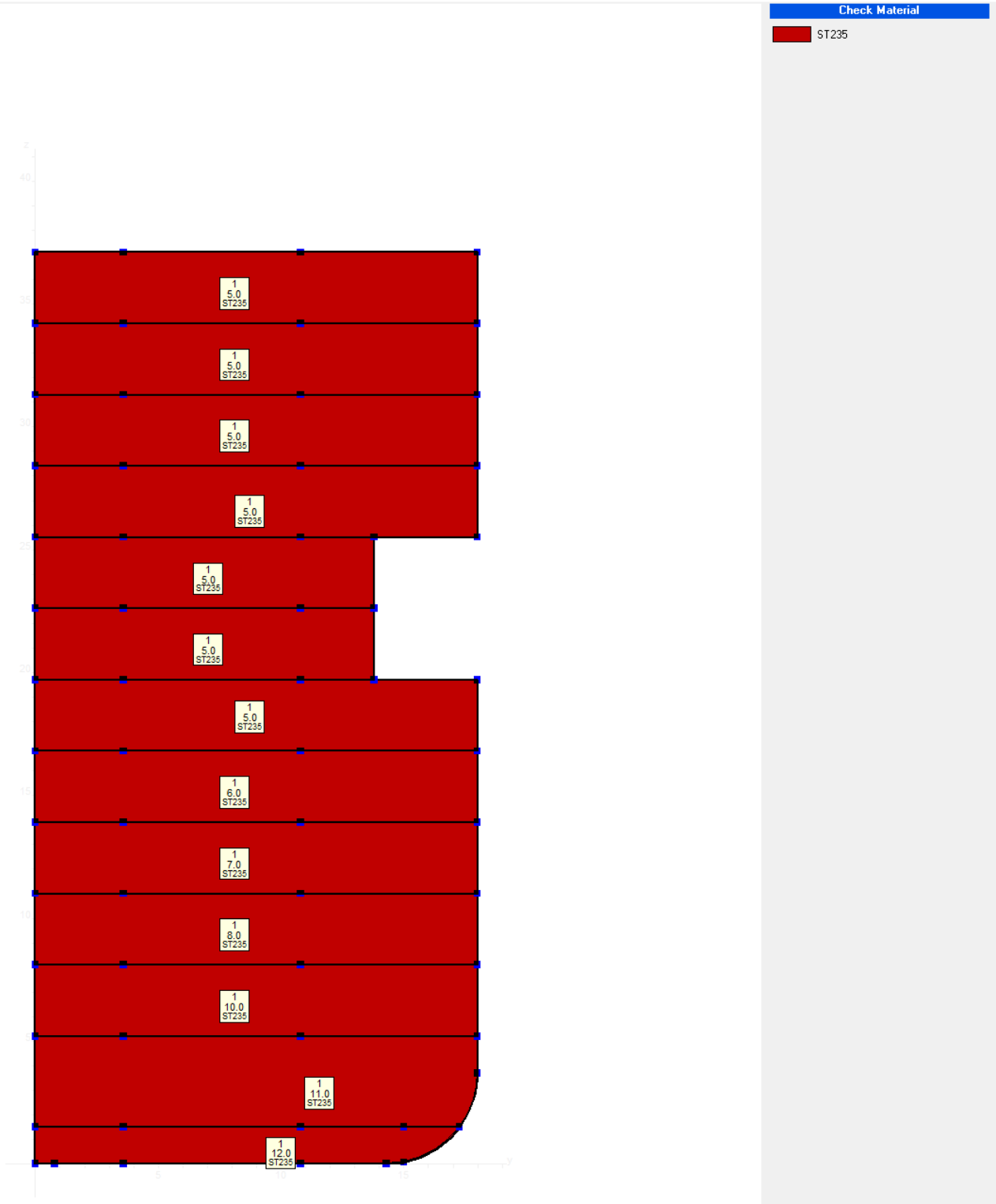


Figure 17 – Transverse Bulkhead – Materials

### 3.4. Primary Supporting Members Midship

The web frame spacing for the midship area is 2.8 m.

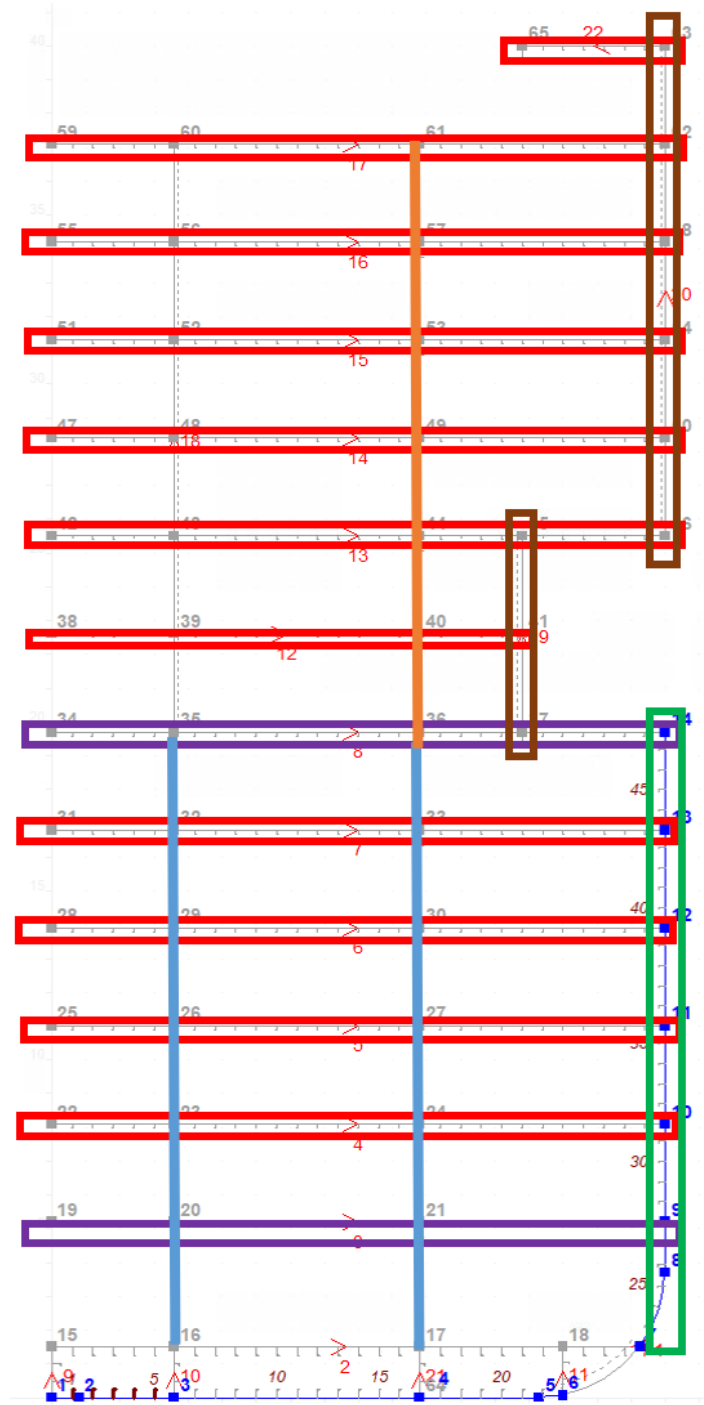


Figure 18 – Primary Supporting Members Sketch



<b>PSM Scantling</b>	<b>Profile</b>
Deck Transverse	T450x8/200x14
Deck Longitudinal Girder	T450x12/200x12
Deck Transverse	T450x7/150x10
Deck Longitudinal Girder	T450x10/200x12
Side Web Hull	T650x12/200x15
Side Web Superstructure	T300x7/150x10
Pillar Hull	Φ 219.1x16
Pillar Superstructure	Φ 139.7x10

### 3.5. Fore Section

The location of the assessed cross section is FR 315, at 228.9 m from the aft end. The frame spacing for this area is 0.7m, the webframe spacing is 2.8 m.

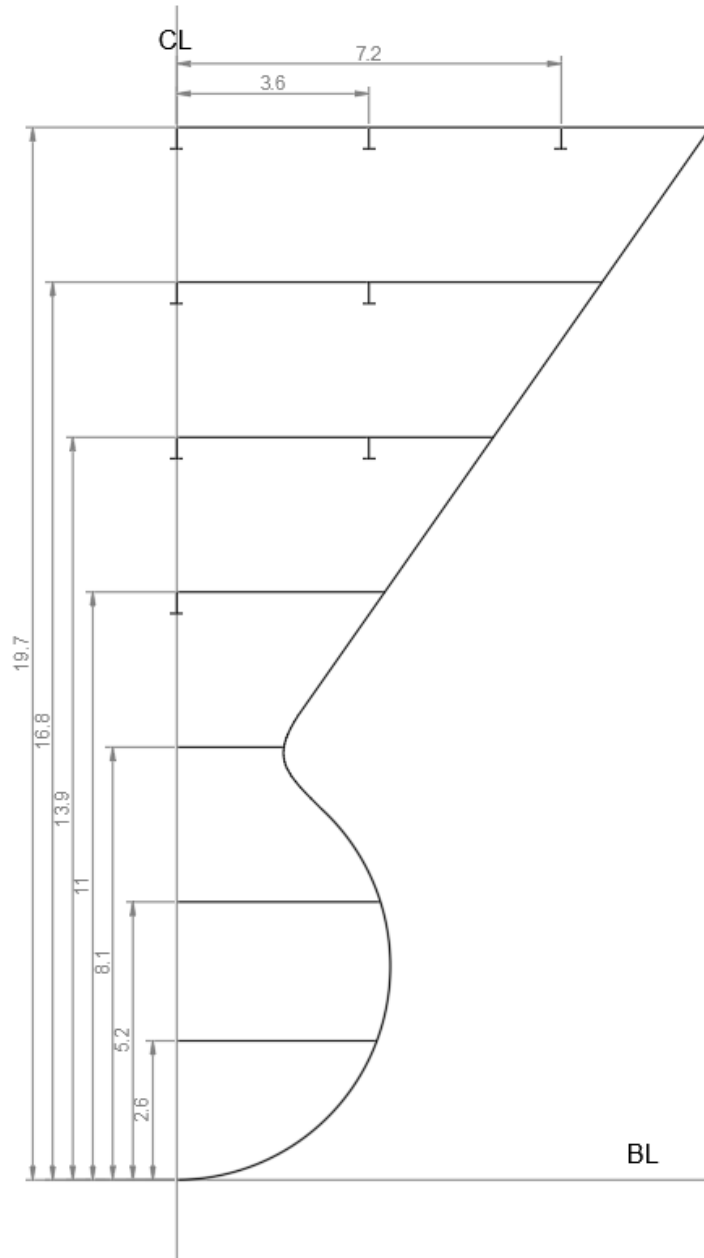


Figure 19 – Fore Section – Spacing (meters)




**Main Section Data**

Main | SW | Fatigue | Ship State | Wave | Flooding

**Name Location Dimensions**

Name:

Longitudinal Location (from AE):  m 

Breadth moulded:  m

Depth moulded:  m

Depth at top of continuous member:  m

**Materials**

in neutral axis      Extension heights:

in deck       m

in bottom       m

Input of:

Figure 20 – Fore Section – Main Section Data

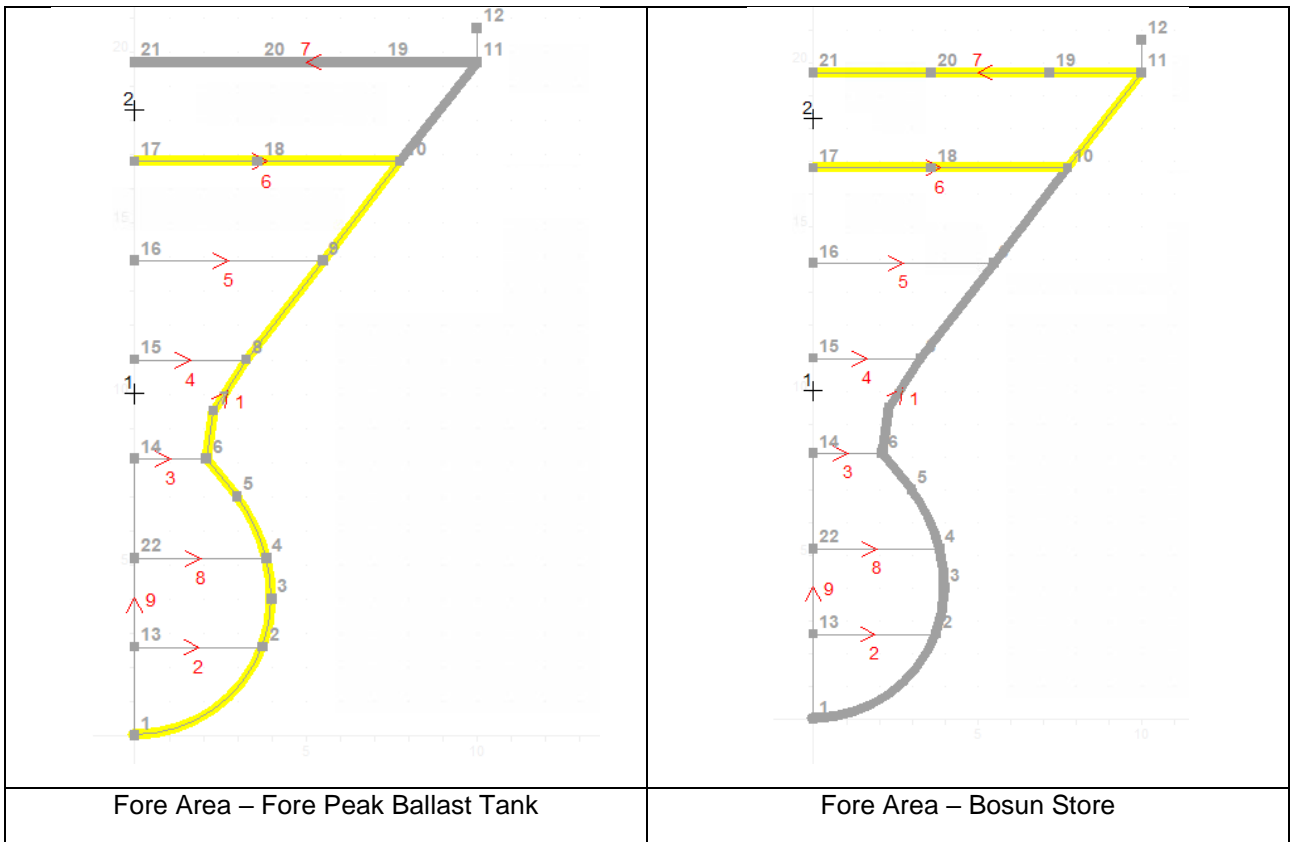


Figure 21 – Fore Section – Compartments

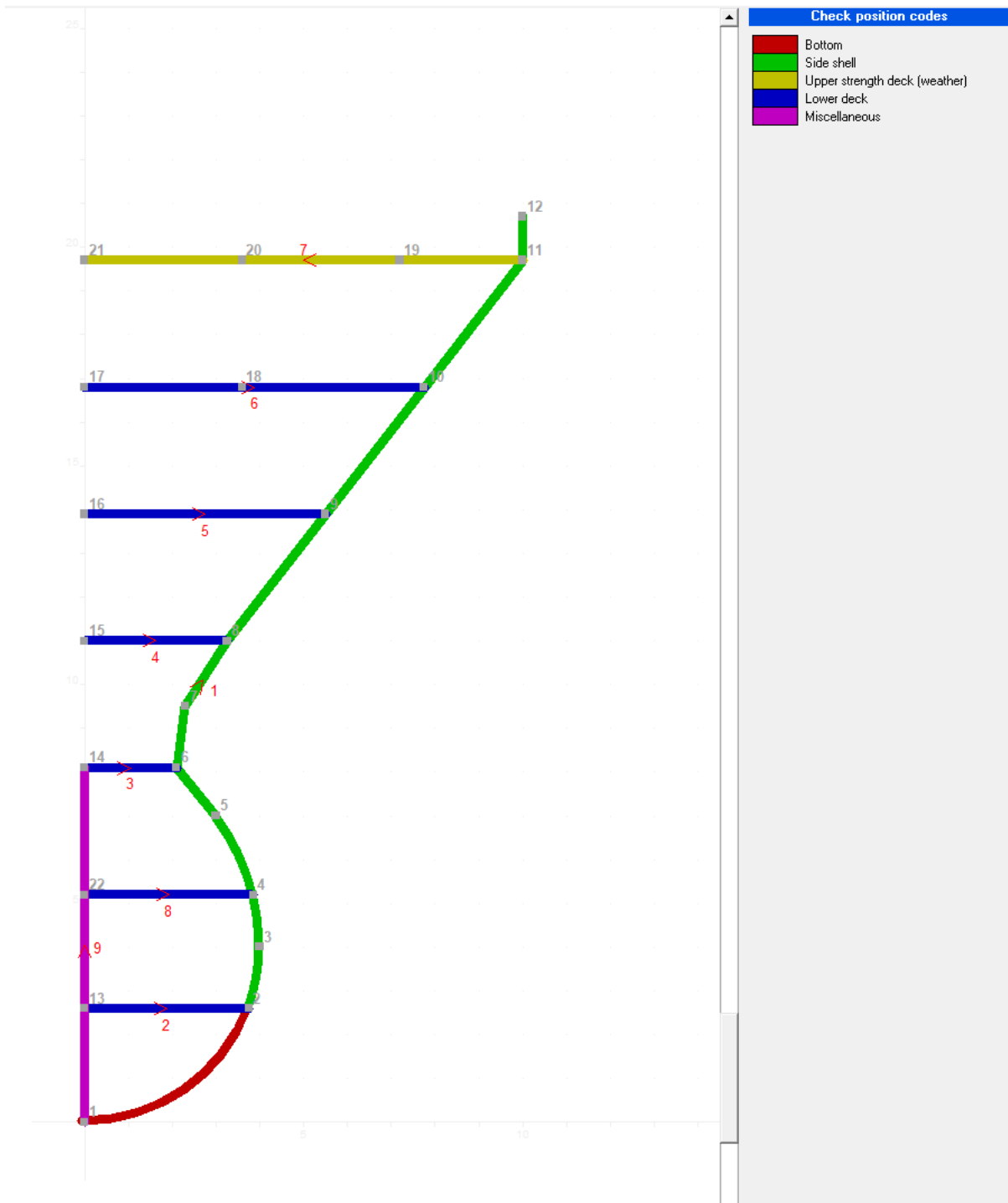


Figure 22 – Fore Section – Position Codes





Figure 23 – Fore Section – Plate thickness

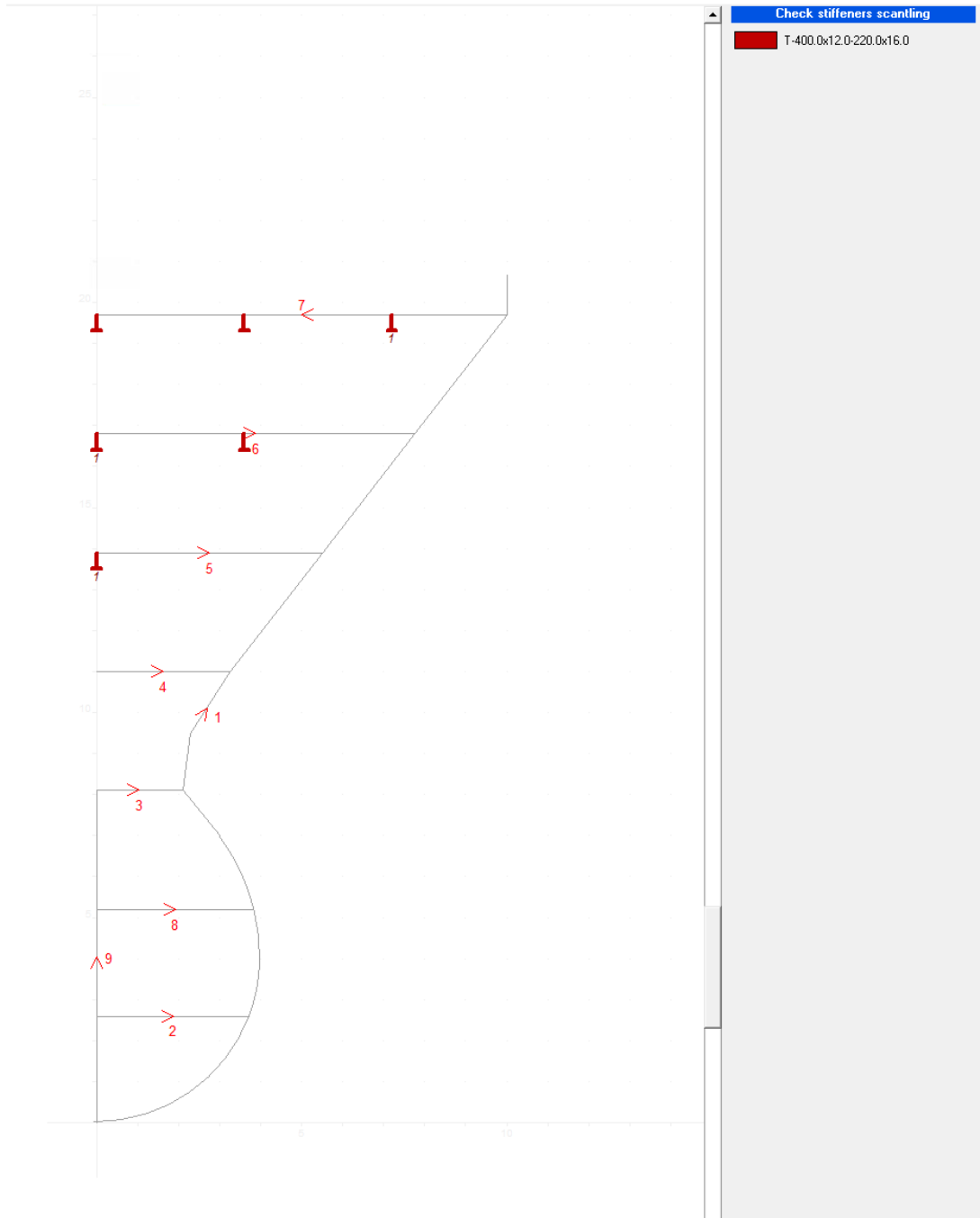


Figure 24 – Fore Section – Stiffeners Scantling

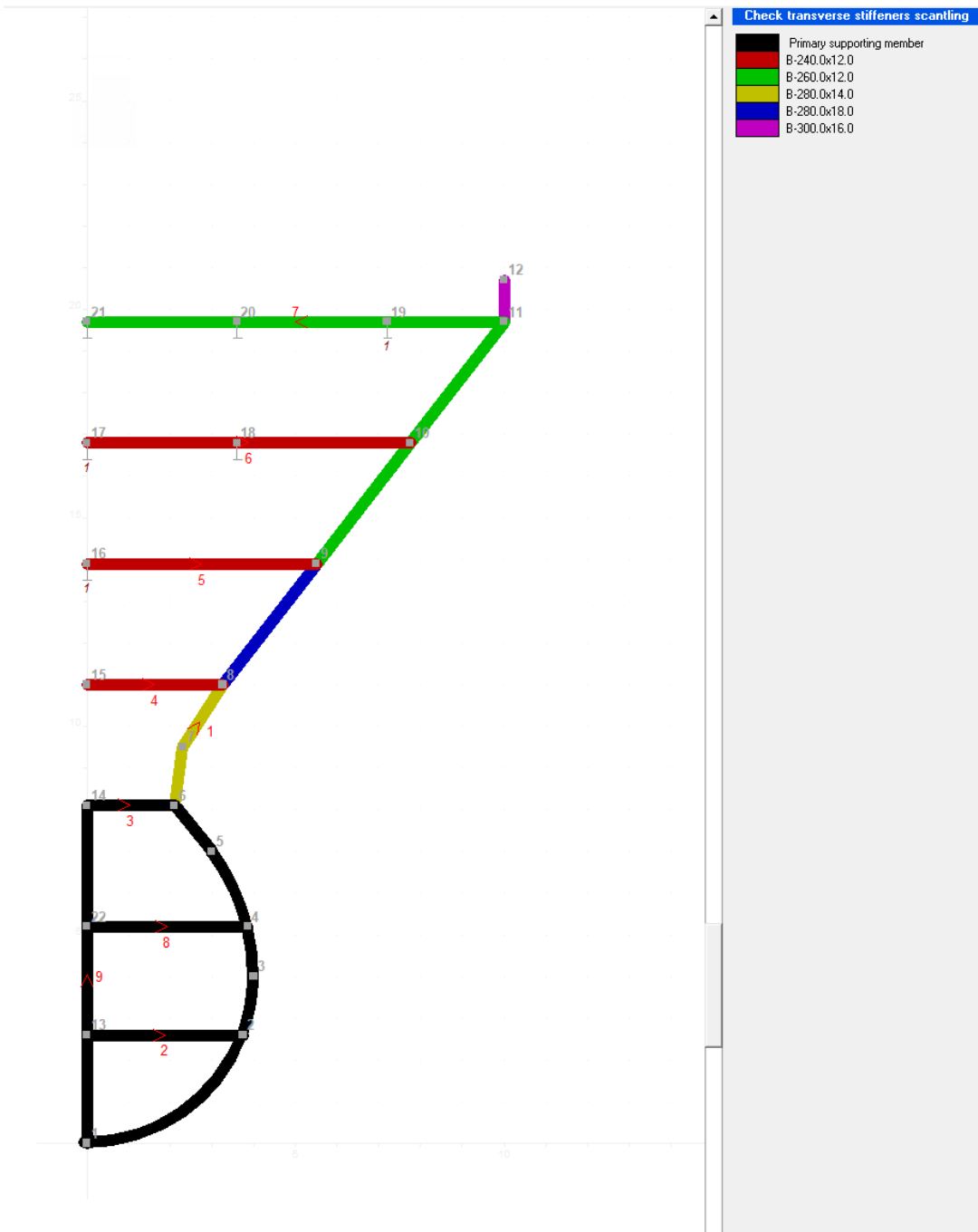


Figure 25 – Fore Section – Transverse Stiffeners Scantling

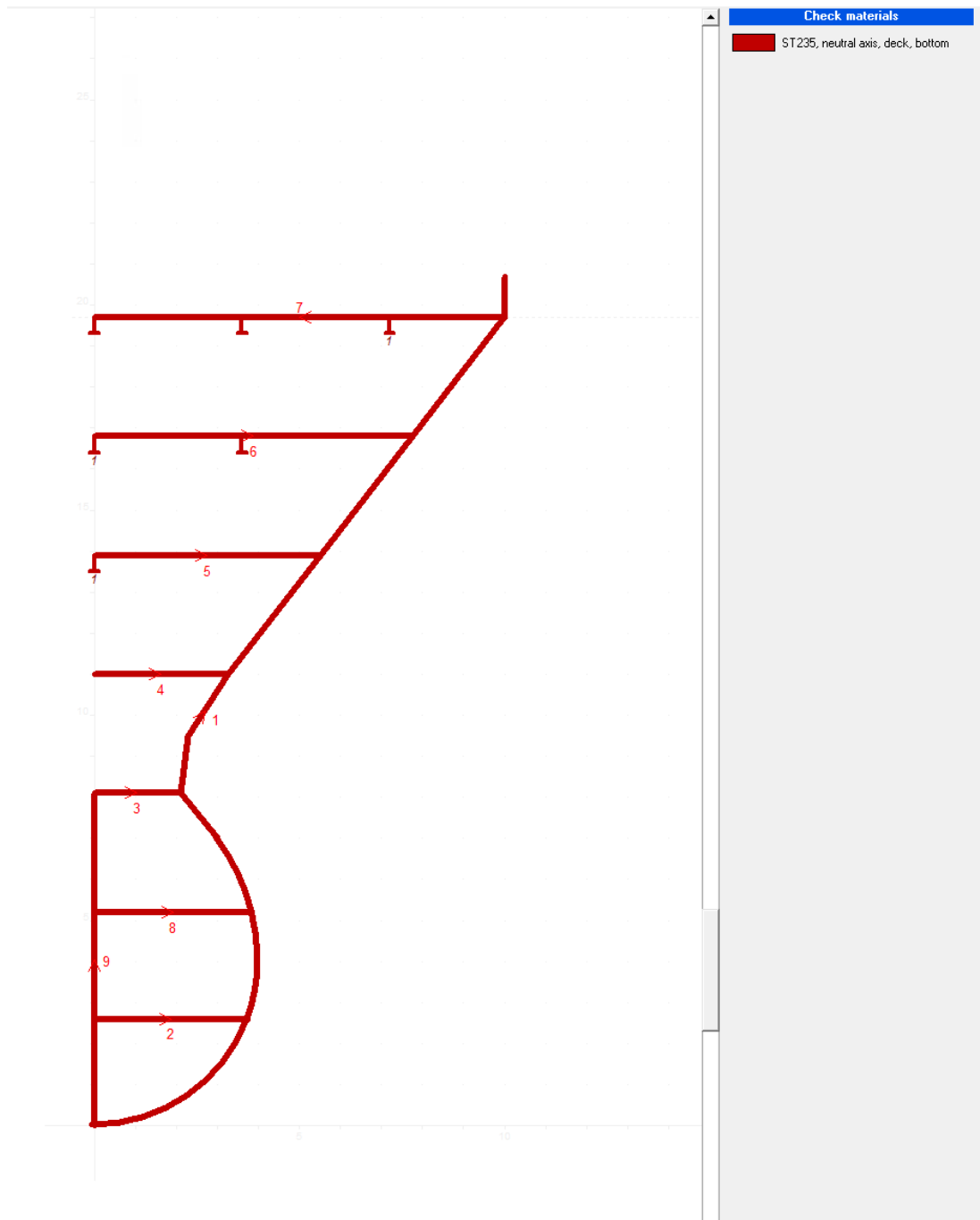


Figure 26 – Fore Section – Materials

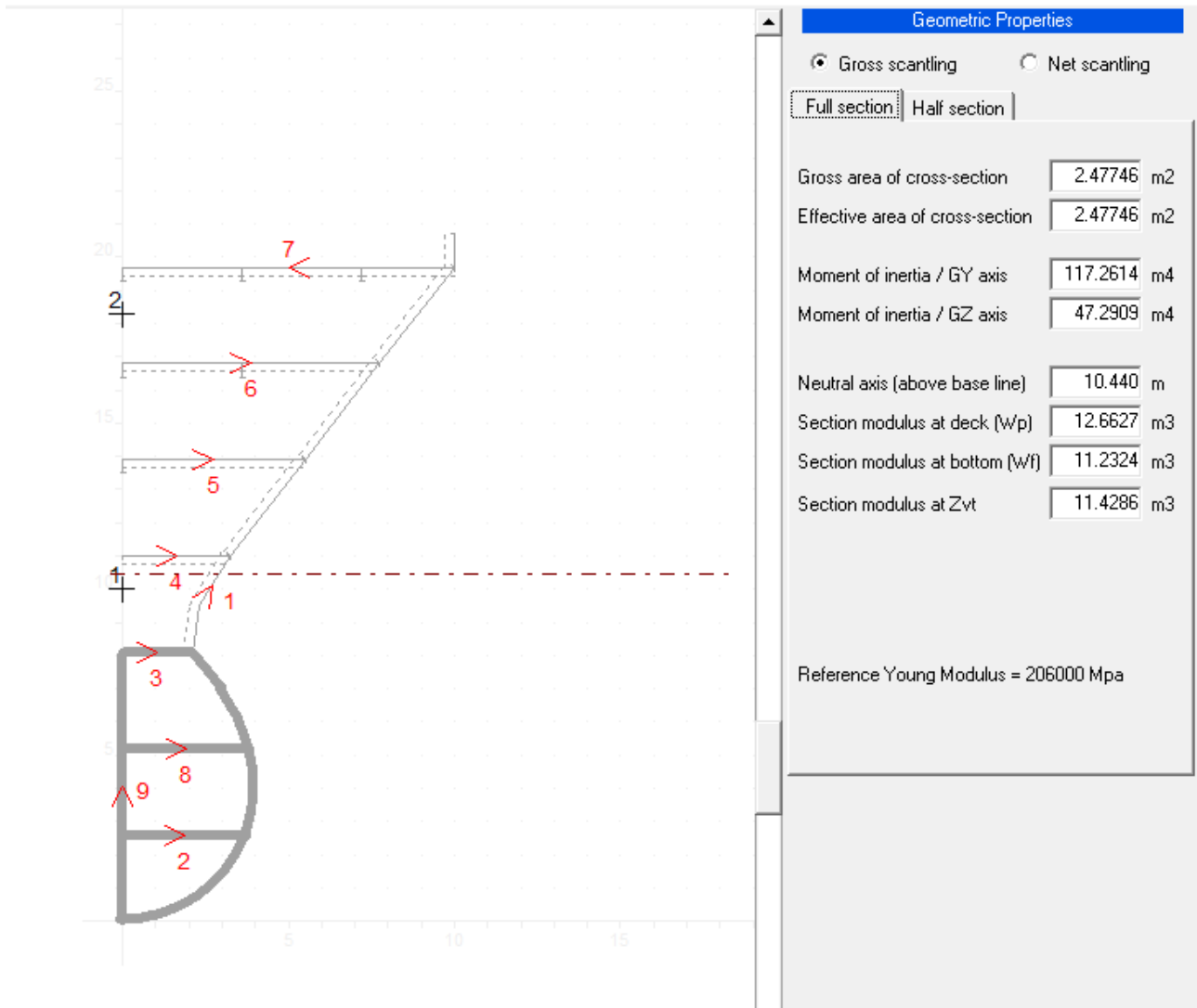


Figure 27 – Midship Section – Geometric Properties

### 3.6. Transverse Bulkhead Fore

The location of the assessed transverse bulkhead is FR 324, at 235.2 m from the aft end.

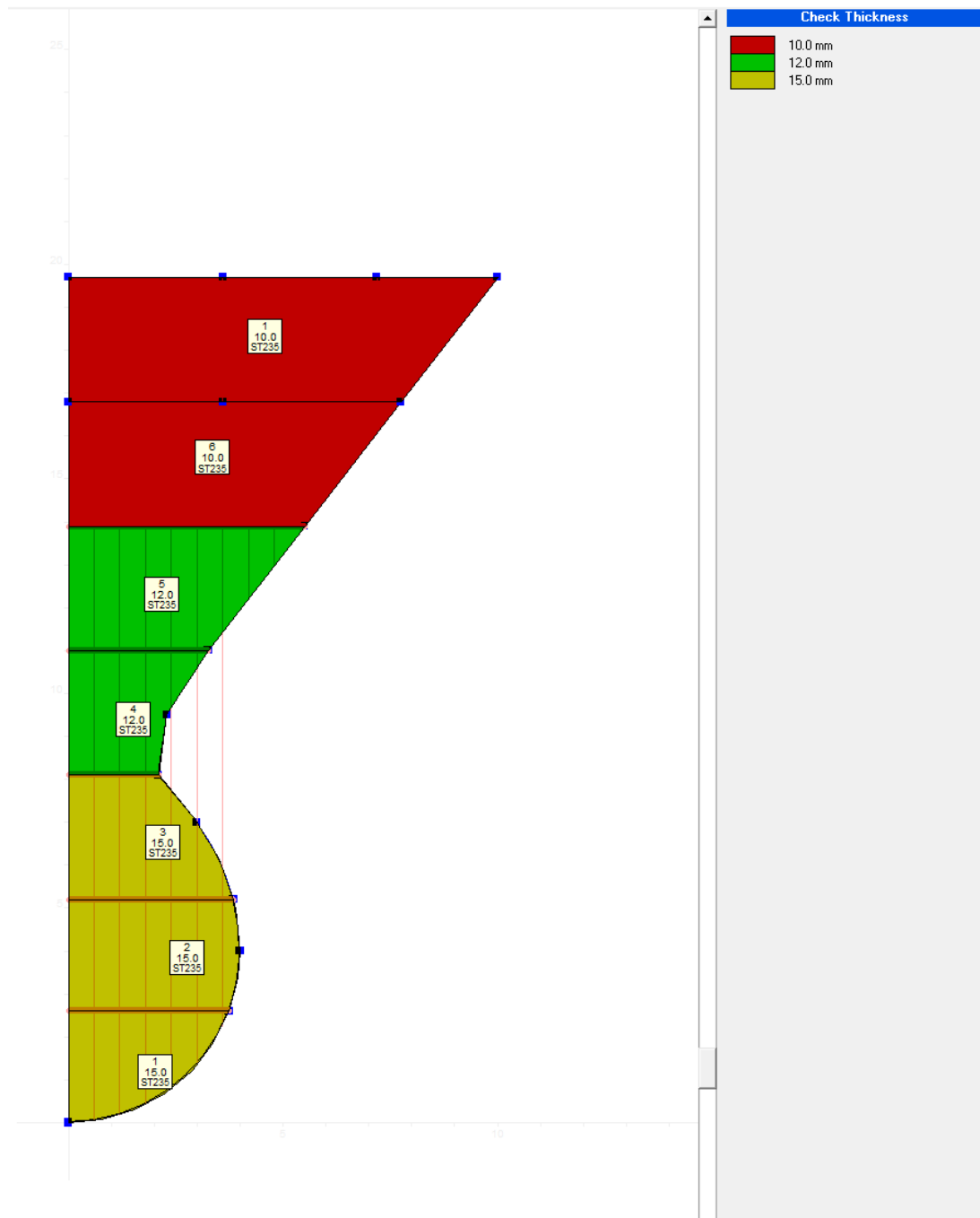


Figure 28 – Transverse Bulkhead Fore – Plate thickness

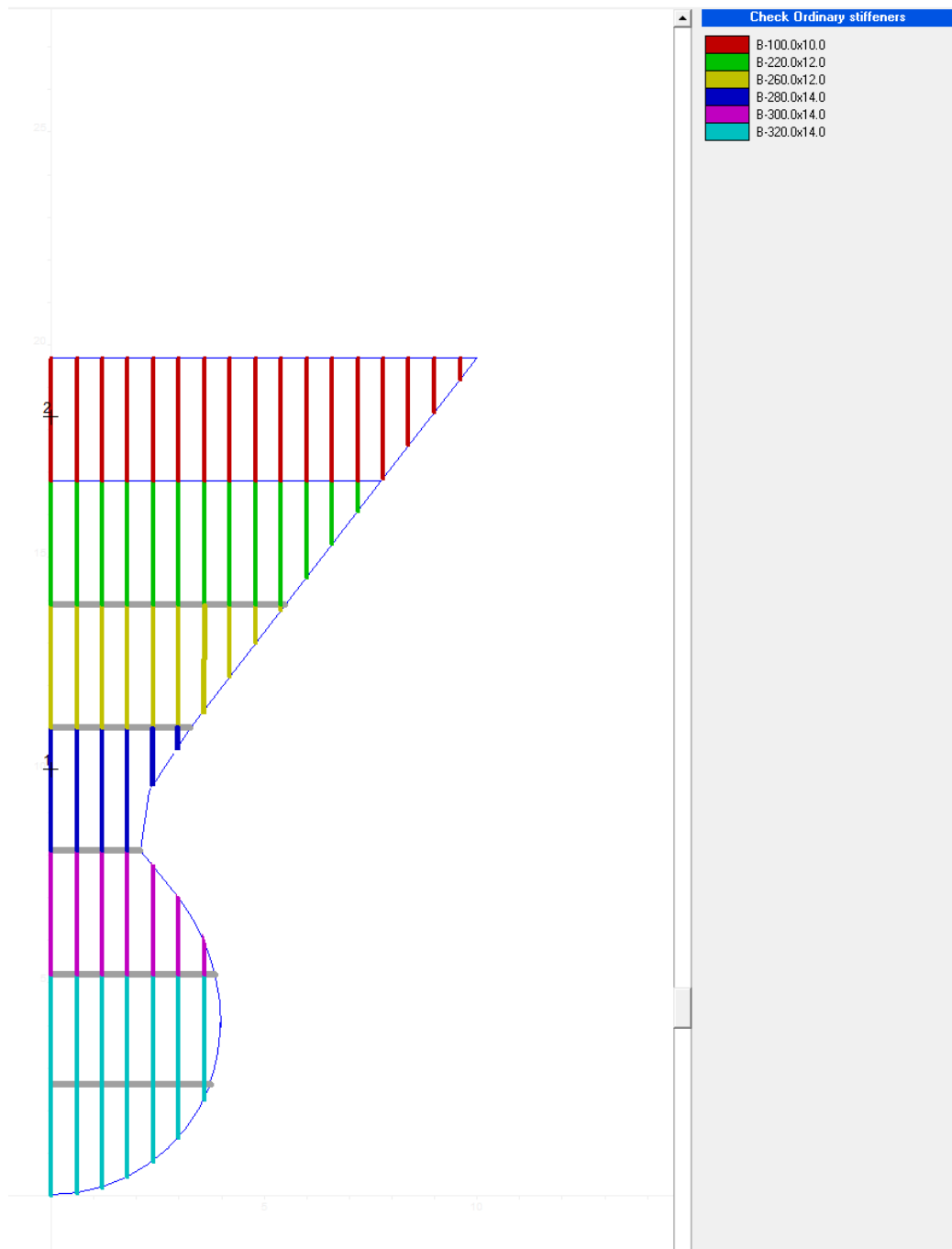


Figure 29 – Transverse Bulkhead Fore – Stiffeners Scantling

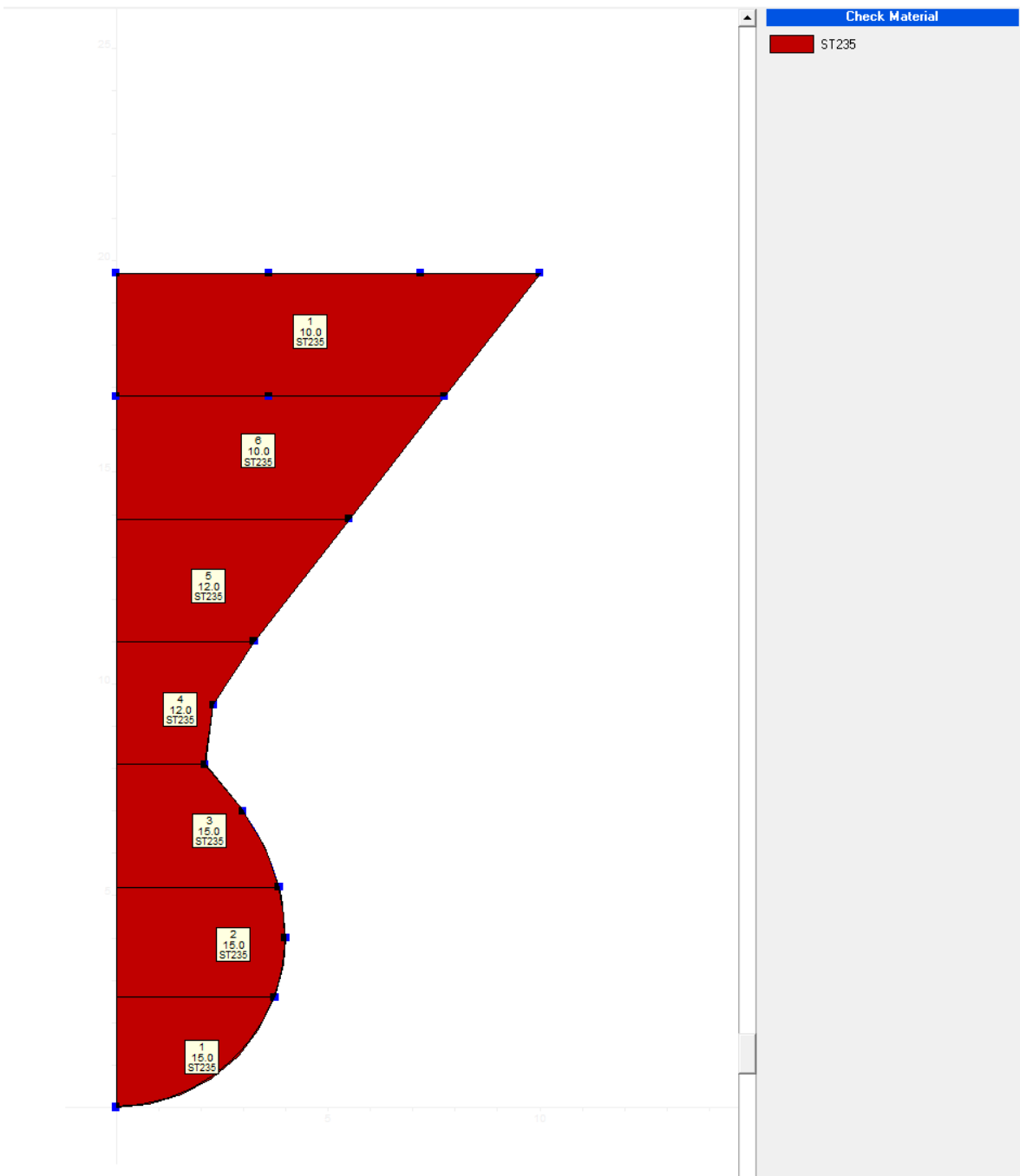


Figure 30 – Transverse Bulkhead Fore – Materials



### 3.7. Primary Supporting Members Fore

The web frame spacing for the fore area is 2.8m.

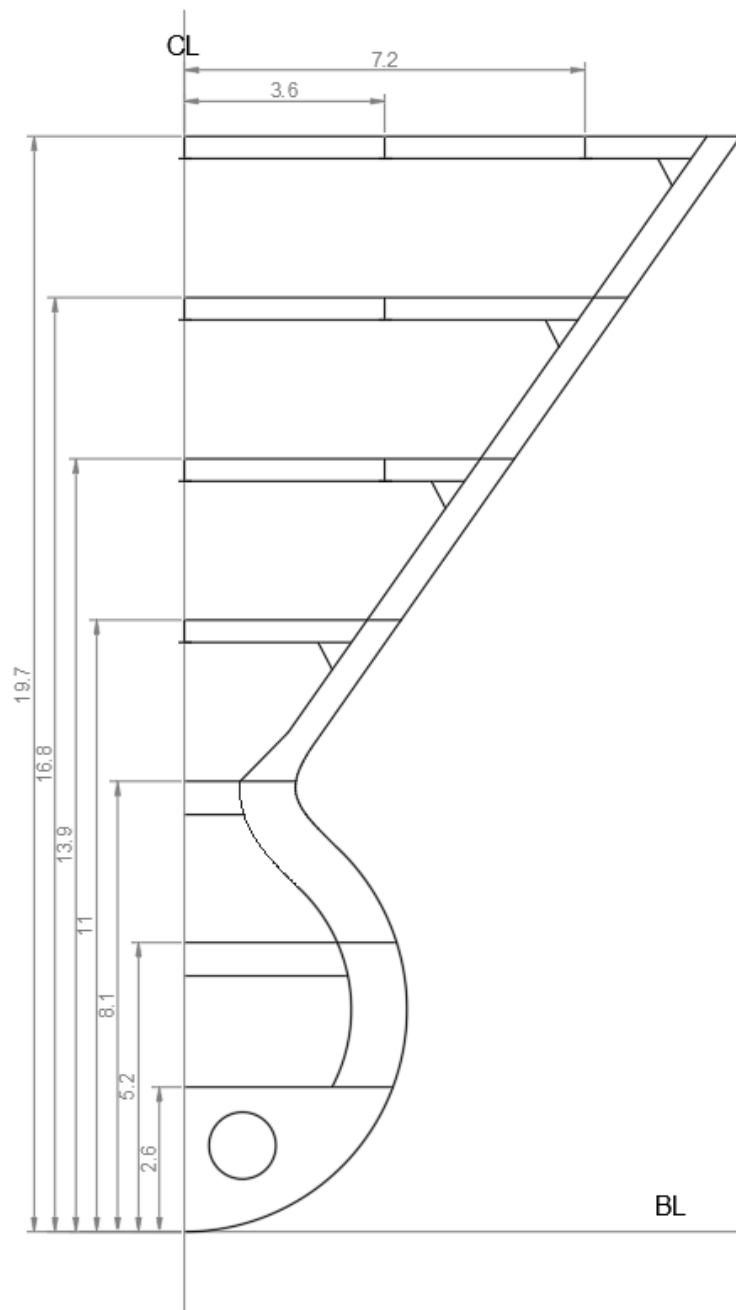


Figure 31 – Primary Supporting Members Fore Sketch

# 4 Scantling Results

## 4.1. Transverse Section

According to the calculation performed in BV Mars 2000, the designed cross section meets the BV Rules requirements.

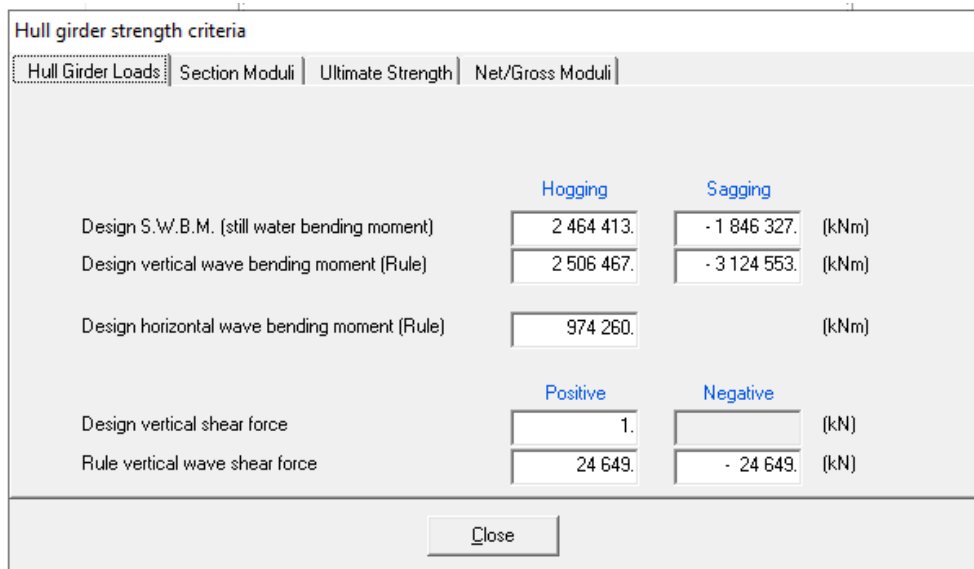


Figure 32 – Midship Section – Hull Girder Loads

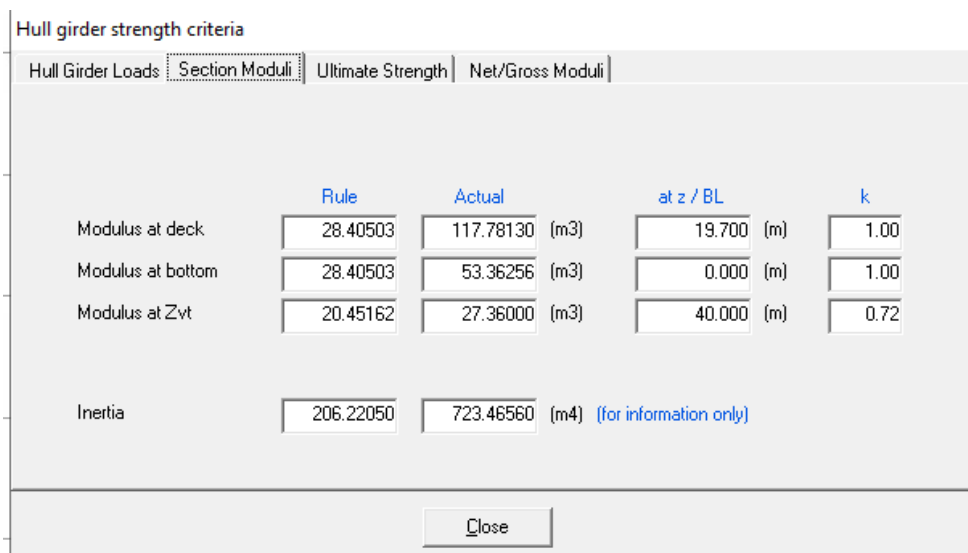


Figure 33 – Midship Section – Section Modulus and Inertia Check

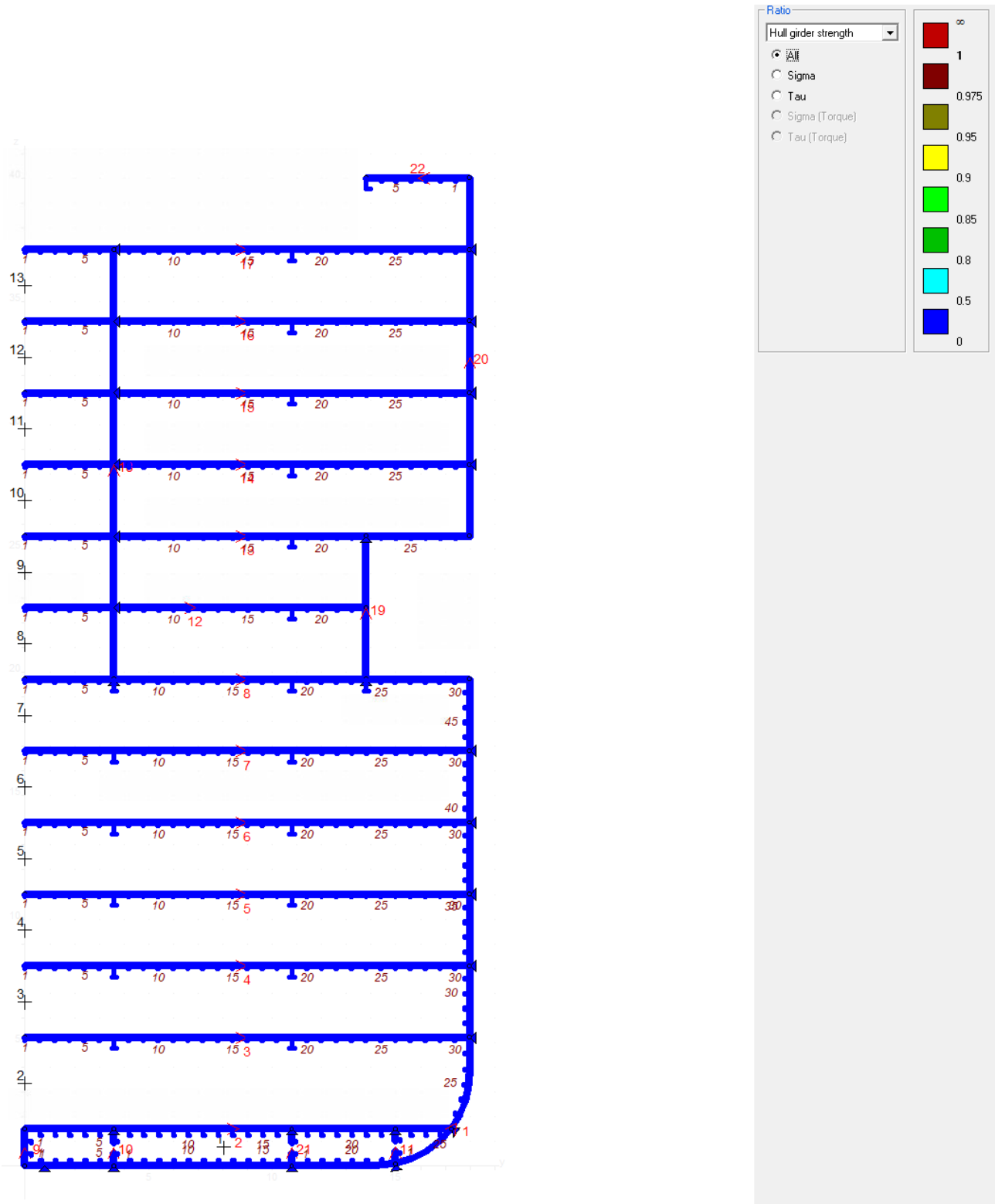


Figure 34 – Midship Section – Hull Grdner Strength Check

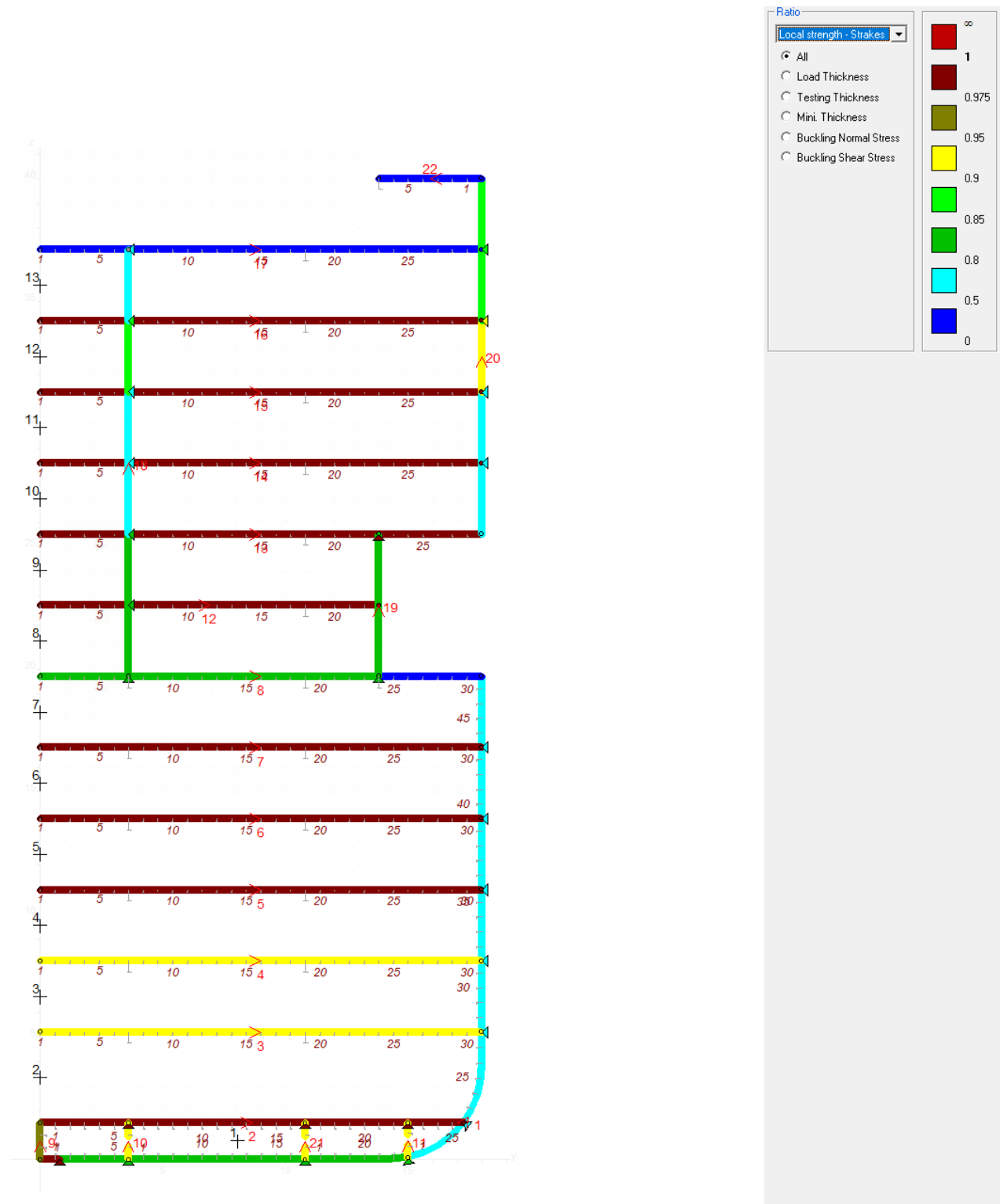


Figure 35 – Midship Section – Local Strength Check – Plates

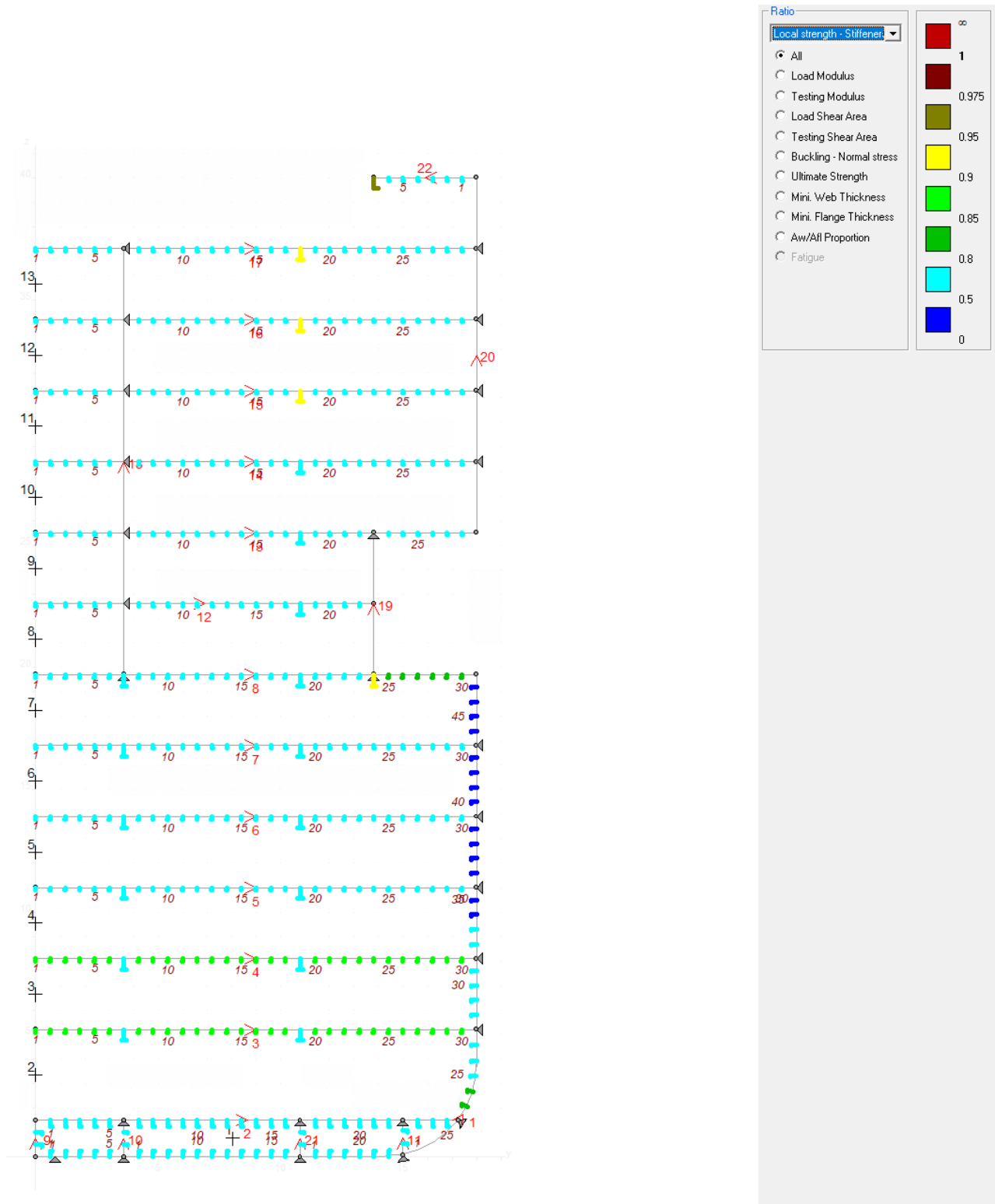


Figure 36 – Midship Section – Local Strength Check – Longitudinal Stiffeners

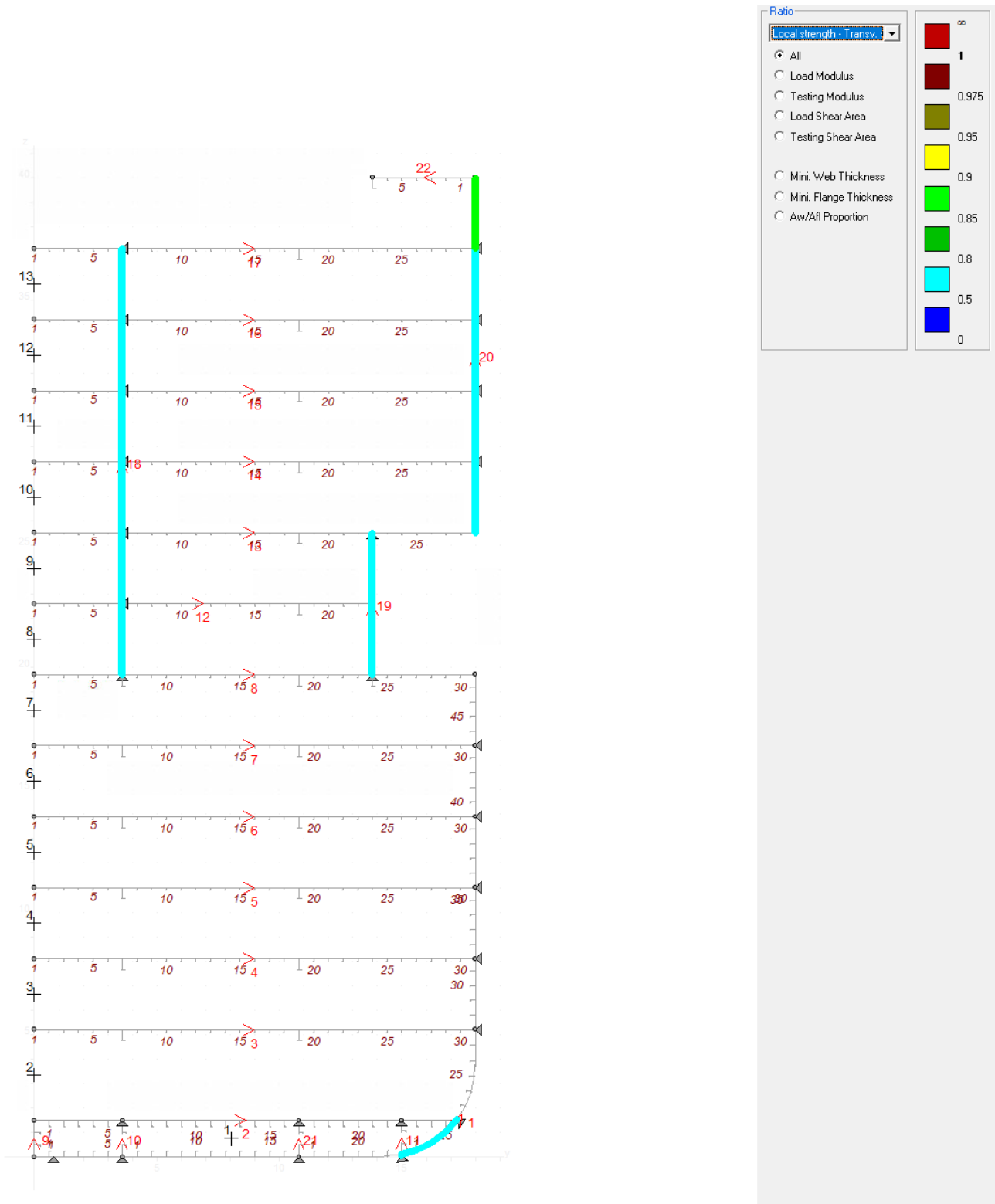


Figure 37 – Midship Section – Local Strength Check – Transverse Stiffeners

### 4.2. Transverse Bulkhead Midship

According to the calculation performed in BV Mars 2000, the designed transverse bulkhead meets the BV Rules requirements.

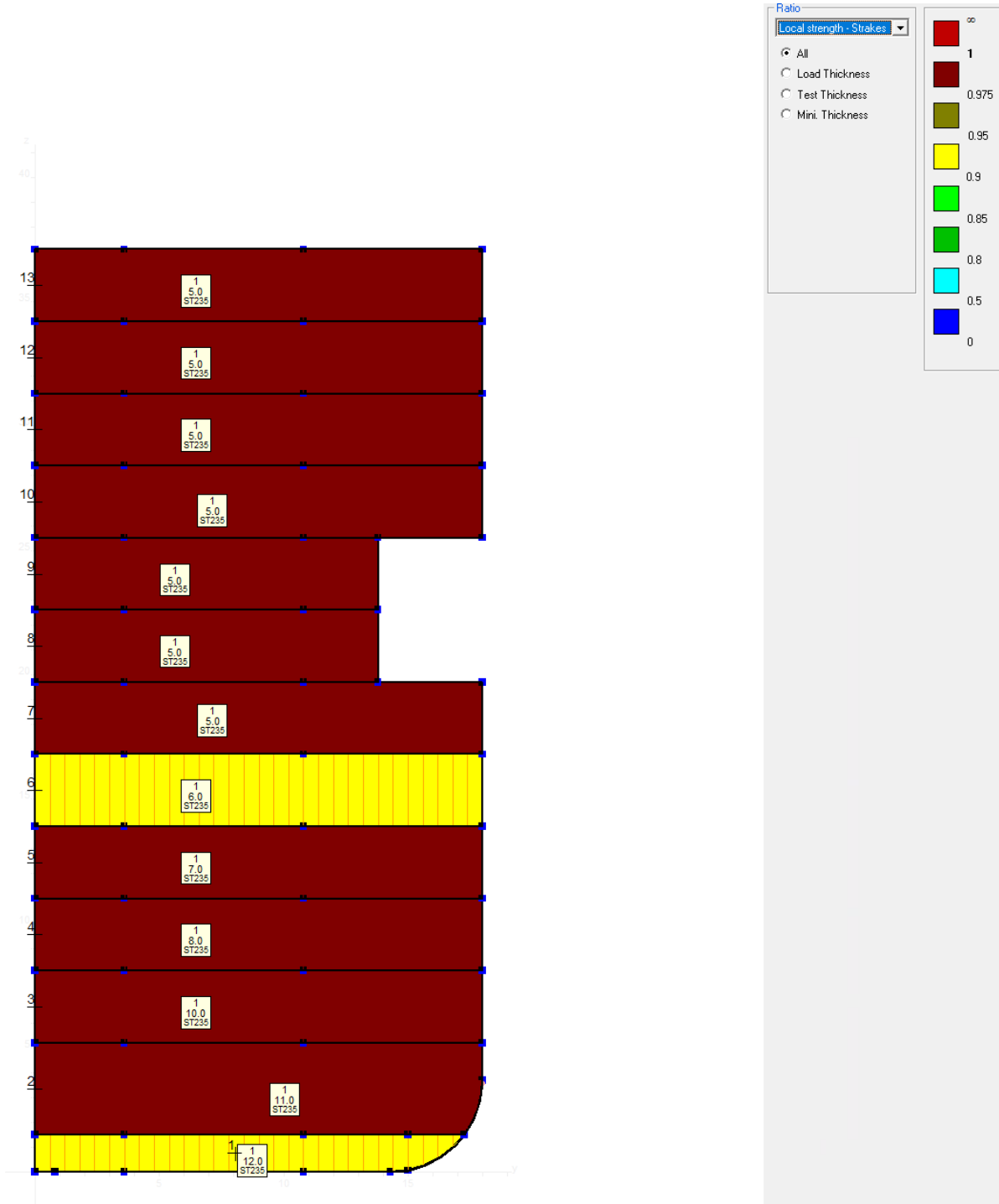


Figure 38 – Transverse Bulkhead – Local Strength Check – Plates

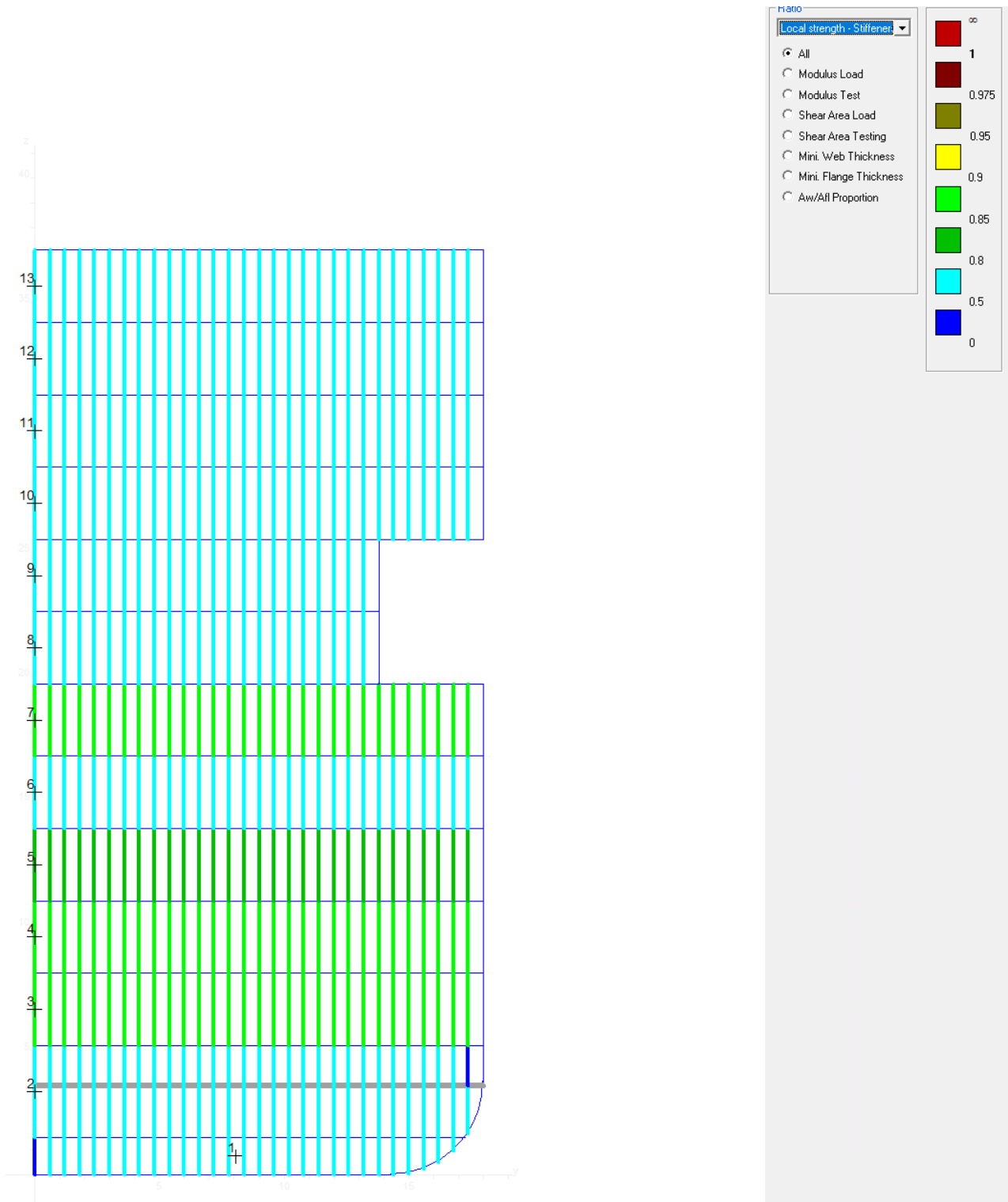



Figure 39 – Transverse Bulkhead – Local Strength Check – Stiffeners



### 4.3. Primary Supporting Members Midship

According to the calculation performed with DNV Nauticus Hull-Primary Supporting Members, the designed PSM meets the Rules requirements.

- Deck Transverse T450x8/200x14


NAUTICUS™  
HULL

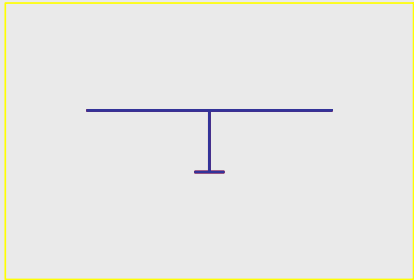
Program: **Primary Supporting Members**  
 Rule ref: **DNV rules Pt.3. Ch.6 Sec.6 July 2015**  
 Rev: 2015-05-29

Select/ edit profile
Dim. Help...
Copy to Profile stack
Print
Results>>
Stack->>

Position: **Deck Transverse**

Name / Id # **BuiltUpTbar 450 x 200 x 8 x 14**

Upper Flange Width:	1724.8	[mm]
Upper Flange Thickness:	7.0	[mm]
Web Height between flanges:	450.0	[mm]
Web Thickness:	8.0	[mm]
Lower Flange Width:	200.0	[mm]
Lower Flange Thickness:	14.0	[mm]
Radius, web & Upper Flange:	90.0	[mm]
Radius, web & Lower Flange:		[mm]
Corrosion addition, plate	0.0	[mm]
Corrosion addition, girder	0.0	[mm]



**PROFILE PROPERTIES:**

Total Area:	Atot_n50 =	184.74	[cm2]	Distance to Neutral axis: Yna =	0.00	[mm]
Effective Area:	Ax_n50 =	184.74	[cm2]	Distance to Neutral axis: Zna =	353.17	[mm]
Shear Area in Y-dir.:	Ayshr_n50 =	157.03	[cm2]	Shear center offset: eY =	0.00	[mm]
Shear Area in Z-dir.:	Azshr_n50 =	33.64	[cm2]	Shear center offset: eZ =	112.89	[mm]
Torsional resistance:	Zx_n50 =	54.4	[cm3]	Torsional mom. of inertia: Ix =	43.5	[cm4]
Section modulus:	ZyTop_n50 =	5101.8	[cm3]	Moment of inertia: Iy =	60112.3	[cm4]
Section modulus:	ZyBot_n50 =	1702.1	[cm3]	Moment of inertia: Iz =	300253.4	[cm4]
Section modulus, z-axis:	Zz_n50 =	3481.6	[cm3]	Centrifugal mom. of in.: Iyz =	0.0	[cm4]
Req. net section mod.	Zn50 >=	1478.6	[cm3]	Web and Flange min thick: t >=	6.0	[mm]
Req. net shear area:	Ashr_n50 >=	13.1	[cm2]	Web pl. slenderness req.: tw >=	7.0	[mm]
Web stiff. inertia req.:	Ist >=	-64.1	[cm4]	Flange slenderness req.: tf >=	8.5	[mm]
				Max unupp. flange length: Sb <=	3.7	[m]

**BEAMDATA:**

Effective bending span:	lbdg =	7.8	[m]
Effective shear span:	lshr =	7.8	[m]
Load breadth / PSM Spacing:	S =	2.8	[m]
Yield stress:	RcH =	235.0	[MPa]
Perm. bending stress coeff.:	Cs =	0.85	[-]
Perm. combined str. coeff.:	Cc1 =	0.95	[-]
Perm. bending stress coeff.:	Cc2 =	0.85	[-]
Perm. shear stress coeff.:	Ct =	0.85	[-]
Young's modulus:	E =	206.0	[GPa]
Cross contraction:	v =	0.3	[-]
Shear Modulus: G=E/(2(1+v)) =		79.23	[GPa]
Density of material:	ρ =	7.8	[kg/dm3]

Bending moment and shear force distribution factors

Position	1	2	3	Select....
fbdg	-	8.00	-	
fshr	0.50	-	0.50	

**DESIGN LOAD SET:** LS1 AC-II

Distributed pressure: [kN/m2] Load intensity: [kN/m] At point (x-distance from A)

At Left end: PA =	13.87	qA =	38.836	XA =	0	[m]
Interm. Point: P1 =		q1 =	0	Xq1 =		[m]
At Right end: PB =	13.87	qB =	38.836	XA =	7.8	[m]

Concentrated loads:

Force:	Moment:	Location:
[kN]	[kNm]	[m]
Load no. 1: F1 =	M1 =	X1 =
Load no. 2: F2 =	M2 =	X2 =
Load no. 3: F3 =	M3 =	X3 =
Load no. 4: F4 =	M4 =	X4 =
Load no. 5: F5 =	M5 =	X5 =
Load no. 6: F6 =	M6 =	X6 =

**Axial load and end moments:**

Hull girder stress, Axial Load: cng = [ ] [Mpa] Fx = 0.0 [kN]

Left end moment: (when fbdg1=0) MA = [ ] [kNm]

Right end moment: (when fbdg3=0) MB = [ ] [kNm]

Figure 40 – PSM – Deck Transverse Check

- Deck Longitudinal Girder T450x12/200x12



NAUTICUS™  
HULL

Program: **Primary Supporting Members**

Rule ref: **DNV rules Pt.3. Ch.6 Sec.6 July 2015**

Rev: 2015-05-29

Select/ edit profile	Dim. Help...	Copy to Profile stack	Print	Results>>	Stack->>																																																																								
<p>Position: <b>Deck Transverse</b></p> <p>Name / Id #: <b>BuiltUpTbar 450 x 200 x 12 x 12</b></p> <p>Total plate Width: 657.9 [mm]</p> <p>Plate Thickness, pT: 7.0 [mm]</p> <p>Web Height, hw: 450.0 [mm]</p> <p>Web Thickness, t: 12.0 [mm]</p> <p>Flange width (incl. web), bf: 200.0 [mm]</p> <p>Flange thickness, tf: 12.0 [mm]</p> <p>Angle Between Profile &amp; Plate: 90.0 [Degrees]</p>																																																																													
<p>Corrosion addition, plate: 0.0 [mm]</p> <p>Corrosion addition, girder: <math>t_c</math> 0.0 [mm]</p>																																																																													
<p><b>PROFILE PROPERTIES:</b></p> <table border="1"> <tr><td>Total Area: <math>A_{tot\_n50} =</math></td><td>124.05</td><td>[cm2]</td><td>Distance to Neutral axis: <math>Y_{na} =</math></td><td>0.00</td><td>[mm]</td></tr> <tr><td>Effective Area: <math>A_{x\_n50} =</math></td><td>124.05</td><td>[cm2]</td><td>Distance to Neutral axis: <math>Z_{na} =</math></td><td>277.14</td><td>[mm]</td></tr> <tr><td>Shear Area in Y-dir.: <math>A_{yshr\_n50} =</math></td><td>75.43</td><td>[cm2]</td><td>Shear center offset: <math>eY =</math></td><td>0.00</td><td>[mm]</td></tr> <tr><td>Shear Area in Z-dir.: <math>A_{zshr\_n50} =</math></td><td>49.20</td><td>[cm2]</td><td>Shear center offset: <math>eZ =</math></td><td>167.25</td><td>[mm]</td></tr> <tr><td>Torsional resistance: <math>Z_{x\_n50} =</math></td><td>36.4</td><td>[cm3]</td><td>Torsional mom. of inertia: <math>I_x =</math></td><td>43.7</td><td>[cm4]</td></tr> <tr><td>Section modulus: <math>Z_{yTop\_n50} =</math></td><td>2291.8</td><td>[cm3]</td><td>Moment of inertia: <math>I_y =</math></td><td>43970.7</td><td>[cm4]</td></tr> <tr><td>Section modulus: <math>Z_{yBot\_n50} =</math></td><td>1586.6</td><td>[cm3]</td><td>Moment of inertia: <math>I_z =</math></td><td>17417.5</td><td>[cm4]</td></tr> <tr><td>Section modulus, z-axis: <math>Z_{z\_n50} =</math></td><td>529.5</td><td>[cm3]</td><td>Centrifugal mom. of in.: <math>I_{yz} =</math></td><td>0.0</td><td>[cm4]</td></tr> <tr><td>Req. net section mod. <math>Z_{n50} &gt;=</math></td><td>530.8</td><td>[cm3]</td><td>Web and Flange min thick.: <math>t &gt;=</math></td><td>6.0</td><td>[mm]</td></tr> <tr><td>Req. net shear area: <math>A_{shr\_n50} &gt;=</math></td><td>13.1</td><td>[cm2]</td><td>Web pl. slenderness req.: <math>tw &gt;=</math></td><td>2.5</td><td>[mm]</td></tr> <tr><td>Web stiff. inertia req.: <math>I_{st} &gt;=</math></td><td>-4.0</td><td>[cm4]</td><td>Flange slenderness req.: <math>tf &gt;=</math></td><td>8.5</td><td>[mm]</td></tr> <tr><td></td><td></td><td></td><td>Max unsupp. flange length: <math>S_b &lt;=</math></td><td>3.4</td><td>[m]</td></tr> </table>						Total Area: $A_{tot\_n50} =$	124.05	[cm2]	Distance to Neutral axis: $Y_{na} =$	0.00	[mm]	Effective Area: $A_{x\_n50} =$	124.05	[cm2]	Distance to Neutral axis: $Z_{na} =$	277.14	[mm]	Shear Area in Y-dir.: $A_{yshr\_n50} =$	75.43	[cm2]	Shear center offset: $eY =$	0.00	[mm]	Shear Area in Z-dir.: $A_{zshr\_n50} =$	49.20	[cm2]	Shear center offset: $eZ =$	167.25	[mm]	Torsional resistance: $Z_{x\_n50} =$	36.4	[cm3]	Torsional mom. of inertia: $I_x =$	43.7	[cm4]	Section modulus: $Z_{yTop\_n50} =$	2291.8	[cm3]	Moment of inertia: $I_y =$	43970.7	[cm4]	Section modulus: $Z_{yBot\_n50} =$	1586.6	[cm3]	Moment of inertia: $I_z =$	17417.5	[cm4]	Section modulus, z-axis: $Z_{z\_n50} =$	529.5	[cm3]	Centrifugal mom. of in.: $I_{yz} =$	0.0	[cm4]	Req. net section mod. $Z_{n50} >=$	530.8	[cm3]	Web and Flange min thick.: $t >=$	6.0	[mm]	Req. net shear area: $A_{shr\_n50} >=$	13.1	[cm2]	Web pl. slenderness req.: $tw >=$	2.5	[mm]	Web stiff. inertia req.: $I_{st} >=$	-4.0	[cm4]	Flange slenderness req.: $tf >=$	8.5	[mm]				Max unsupp. flange length: $S_b <=$	3.4	[m]
Total Area: $A_{tot\_n50} =$	124.05	[cm2]	Distance to Neutral axis: $Y_{na} =$	0.00	[mm]																																																																								
Effective Area: $A_{x\_n50} =$	124.05	[cm2]	Distance to Neutral axis: $Z_{na} =$	277.14	[mm]																																																																								
Shear Area in Y-dir.: $A_{yshr\_n50} =$	75.43	[cm2]	Shear center offset: $eY =$	0.00	[mm]																																																																								
Shear Area in Z-dir.: $A_{zshr\_n50} =$	49.20	[cm2]	Shear center offset: $eZ =$	167.25	[mm]																																																																								
Torsional resistance: $Z_{x\_n50} =$	36.4	[cm3]	Torsional mom. of inertia: $I_x =$	43.7	[cm4]																																																																								
Section modulus: $Z_{yTop\_n50} =$	2291.8	[cm3]	Moment of inertia: $I_y =$	43970.7	[cm4]																																																																								
Section modulus: $Z_{yBot\_n50} =$	1586.6	[cm3]	Moment of inertia: $I_z =$	17417.5	[cm4]																																																																								
Section modulus, z-axis: $Z_{z\_n50} =$	529.5	[cm3]	Centrifugal mom. of in.: $I_{yz} =$	0.0	[cm4]																																																																								
Req. net section mod. $Z_{n50} >=$	530.8	[cm3]	Web and Flange min thick.: $t >=$	6.0	[mm]																																																																								
Req. net shear area: $A_{shr\_n50} >=$	13.1	[cm2]	Web pl. slenderness req.: $tw >=$	2.5	[mm]																																																																								
Web stiff. inertia req.: $I_{st} >=$	-4.0	[cm4]	Flange slenderness req.: $tf >=$	8.5	[mm]																																																																								
			Max unsupp. flange length: $S_b <=$	3.4	[m]																																																																								
<p><b>BEAM DATA:</b></p> <table border="1"> <tr><td>Effective bending span: <math>l_{bdg} =</math></td><td>2.8</td><td>[m]</td></tr> <tr><td>Effective shear span: <math>l_{shr} =</math></td><td>2.8</td><td>[m]</td></tr> <tr><td>Load breadth / PSM Spacing: <math>S =</math></td><td>7.8</td><td>[m]</td></tr> <tr><td>Yield stress: <math>R_{eH} =</math></td><td>235.0</td><td>[MPa]</td></tr> <tr><td>Perm. bending stress coeff.: <math>C_s =</math></td><td>0.85</td><td>[-]</td></tr> <tr><td>Perm. combined str. coeff.: <math>C_{s1} =</math></td><td>0.95</td><td>[-]</td></tr> <tr><td>Perm. bending stress coeff.: <math>C_{s2} =</math></td><td>0.85</td><td>[-]</td></tr> <tr><td>Perm. shear stress coeff.: <math>C_t =</math></td><td>0.85</td><td>[-]</td></tr> <tr><td>Young's modulus: <math>E =</math></td><td>206.0</td><td>[GPa]</td></tr> <tr><td>Cross contraction: <math>v =</math></td><td>0.3</td><td>[-]</td></tr> <tr><td>Shear Modulus: <math>G=E/(2(1+v)) =</math></td><td>79.23</td><td>[GPa]</td></tr> <tr><td>Density of material: <math>\rho =</math></td><td>7.8</td><td>[kg/dm3]</td></tr> </table> <p>Bending moment and shear force distribution factors</p> <table border="1"> <thead> <tr><th>Position</th><th>1</th><th>2</th><th>3</th><th>Select....</th></tr> </thead> <tbody> <tr><td><math>f_{bdg}</math></td><td>-</td><td>8.00</td><td>-</td><td></td></tr> <tr><td><math>f_{shr}</math></td><td>0.50</td><td>-</td><td>0.50</td><td></td></tr> </tbody> </table>						Effective bending span: $l_{bdg} =$	2.8	[m]	Effective shear span: $l_{shr} =$	2.8	[m]	Load breadth / PSM Spacing: $S =$	7.8	[m]	Yield stress: $R_{eH} =$	235.0	[MPa]	Perm. bending stress coeff.: $C_s =$	0.85	[-]	Perm. combined str. coeff.: $C_{s1} =$	0.95	[-]	Perm. bending stress coeff.: $C_{s2} =$	0.85	[-]	Perm. shear stress coeff.: $C_t =$	0.85	[-]	Young's modulus: $E =$	206.0	[GPa]	Cross contraction: $v =$	0.3	[-]	Shear Modulus: $G=E/(2(1+v)) =$	79.23	[GPa]	Density of material: $\rho =$	7.8	[kg/dm3]	Position	1	2	3	Select....	$f_{bdg}$	-	8.00	-		$f_{shr}$	0.50	-	0.50																						
Effective bending span: $l_{bdg} =$	2.8	[m]																																																																											
Effective shear span: $l_{shr} =$	2.8	[m]																																																																											
Load breadth / PSM Spacing: $S =$	7.8	[m]																																																																											
Yield stress: $R_{eH} =$	235.0	[MPa]																																																																											
Perm. bending stress coeff.: $C_s =$	0.85	[-]																																																																											
Perm. combined str. coeff.: $C_{s1} =$	0.95	[-]																																																																											
Perm. bending stress coeff.: $C_{s2} =$	0.85	[-]																																																																											
Perm. shear stress coeff.: $C_t =$	0.85	[-]																																																																											
Young's modulus: $E =$	206.0	[GPa]																																																																											
Cross contraction: $v =$	0.3	[-]																																																																											
Shear Modulus: $G=E/(2(1+v)) =$	79.23	[GPa]																																																																											
Density of material: $\rho =$	7.8	[kg/dm3]																																																																											
Position	1	2	3	Select....																																																																									
$f_{bdg}$	-	8.00	-																																																																										
$f_{shr}$	0.50	-	0.50																																																																										
<p><b>DESIGN LOAD SET:</b> LS1 AC-II</p> <p><b>Distributed pressure:</b> [kN/m2]</p> <p>At Left end: <math>P_A = 13.87</math> [kN/m] <math>q_A = 108.186</math> [kN/m] <math>X_A = 0</math> [m]</p> <p>Interm. Point: <math>P_1 = 0</math> [kN/m] <math>q_1 = 0</math> [kN/m] <math>X_{q1} = 0</math> [m]</p> <p>At Right end: <math>P_B = 13.87</math> [kN/m] <math>q_B = 108.186</math> [kN/m] <math>X_A = 2.8</math> [m]</p> <p><b>Concentrated loads:</b></p> <table border="1"> <thead> <tr><th>Force: [kN]</th><th>Moment: [kNm]</th><th>Location: [m]</th></tr> </thead> <tbody> <tr><td>Load no. 1: <math>F_1 =</math></td><td><math>M_1 =</math></td><td><math>X_1 =</math></td></tr> <tr><td>Load no. 2: <math>F_2 =</math></td><td><math>M_2 =</math></td><td><math>X_2 =</math></td></tr> <tr><td>Load no. 3: <math>F_3 =</math></td><td><math>M_3 =</math></td><td><math>X_3 =</math></td></tr> <tr><td>Load no. 4: <math>F_4 =</math></td><td><math>M_4 =</math></td><td><math>X_4 =</math></td></tr> <tr><td>Load no. 5: <math>F_5 =</math></td><td><math>M_5 =</math></td><td><math>X_5 =</math></td></tr> <tr><td>Load no. 6: <math>F_6 =</math></td><td><math>M_6 =</math></td><td><math>X_6 =</math></td></tr> </tbody> </table> <p><b>Axial load and end moments:</b></p> <p>Hull girder stress, Axial Load: <math>\sigma_{hg} = 55.74</math> [Mpa] <math>F_x = 691.5</math> [kN]</p> <p>Left end moment: (when <math>f_{bdg1}=0</math>) <math>M_A =</math> [kNm]</p> <p>Right end moment: (when <math>f_{bdg3}=0</math>) <math>M_B =</math> [kNm]</p>						Force: [kN]	Moment: [kNm]	Location: [m]	Load no. 1: $F_1 =$	$M_1 =$	$X_1 =$	Load no. 2: $F_2 =$	$M_2 =$	$X_2 =$	Load no. 3: $F_3 =$	$M_3 =$	$X_3 =$	Load no. 4: $F_4 =$	$M_4 =$	$X_4 =$	Load no. 5: $F_5 =$	$M_5 =$	$X_5 =$	Load no. 6: $F_6 =$	$M_6 =$	$X_6 =$																																																			
Force: [kN]	Moment: [kNm]	Location: [m]																																																																											
Load no. 1: $F_1 =$	$M_1 =$	$X_1 =$																																																																											
Load no. 2: $F_2 =$	$M_2 =$	$X_2 =$																																																																											
Load no. 3: $F_3 =$	$M_3 =$	$X_3 =$																																																																											
Load no. 4: $F_4 =$	$M_4 =$	$X_4 =$																																																																											
Load no. 5: $F_5 =$	$M_5 =$	$X_5 =$																																																																											
Load no. 6: $F_6 =$	$M_6 =$	$X_6 =$																																																																											

Figure 41 – PSM – Deck Longitudinal Girder Check

- Deck Transverse T450x7/150x10



NAUTICUS™  
HULL

Program: **Primary Supporting Members**

Rule ref: **DNV rules Pt.3. Ch.6 Sec.6 July 2015**

Rev: 2015-05-29

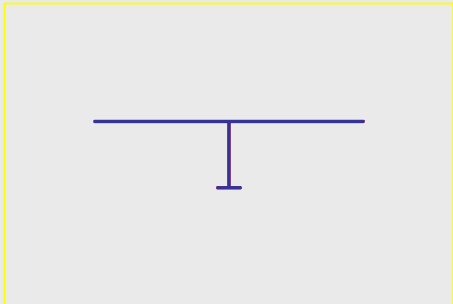
Select/ edit profile		Dim. Help...	Copy to Profile stack	Print	Results>>	Stack->>
Position: Deck Transverse Name / Id #: BuiltUpTbar 450 x 150 x 7 x 12						
Total plate Width:	1724.8 [mm]					
Plate Thickness, pT:	5.0 [mm]					
Web Height, hw:	450.0 [mm]					
Web Thickness, t:	7.0 [mm]					
Flange width (incl. web), bf:	150.0 [mm]					
Flange thickness, tf:	10.0 [mm]					
Angle Between Profile & Plate:	90.0 [Degrees]					
Corrosion addition, plate	0.0 [mm]					
Corrosion addition, girder	0.0 [mm]					
<b>PROFILE PROPERTIES:</b>						
Total Area: Atot_n50 =	132.74 [cm2]	Distance to Neutral axis: Yna =	0.00 [mm]	Copy to Profile stack		
Effective Area: Ax_n50 =	132.74 [cm2]	Distance to Neutral axis: Zna =	356.81 [mm]			
Shear Area in Y-dir.: Ayshr_n50 =	112.83 [cm2]	Shear center offset: eY =	0.00 [mm]			
Shear Area in Z-dir.: Azshr_n50 =	28.18 [cm2]	Shear center offset: eZ =	105.08 [mm]			
Torsional resistance: Zx_n50 =	23.9 [cm3]	Torsional mom. of inertia: Ix =	16.7 [cm4]			
Section modulus: ZyTop_n50 =	3530.2 [cm3]	Moment of inertia: Iy =	38191.4 [cm4]			
Section modulus: ZyBot_n50 =	1070.3 [cm3]	Moment of inertia: Iz =	214081.2 [cm4]			
Section modulus, z-axis: Zz_n50 =	2482.4 [cm3]	Centrifugal mom. of in.: Iyz =	0.0 [cm4]			
Req. net section mod. Zn50 >=	739.8 [cm3]	Web and Flange min thick.: t >=	6.0 [mm]	Other PSM		
Req. net shear area: Ashr_n50 >=	6.6 [cm2]	Web pl. slenderness req.: tw >=	7.0 [mm]			
Web stiff. inertia req.: Ist >=	-56.1 [cm4]	Flange slenderness req.: tf >=	6.5 [mm]			
	OK	Max unsupp. flange length: Sb <=	3.0 [m]	3 Flange tripping supports		
			OK			
<b>BEAM DATA:</b>		<b>DESIGN LOAD SET:</b> LS1 AC-II				
Effective bending span: lbdg =	7.8 [m]	Distributed pressure: [kN/m2]		Load intensity: At point		
Effective shear span: lshr =	7.8 [m]	At Left end: PA = 6.94		qA = 19.432 [kN/m] XA = 0 [m]		
Load breadth / PSM Spacing: S =	2.8 [m]	Interm. Point: P1 =		q1 = 0 [kN/m] Xq1 = [m]		
Yield stress: ReH =	235.0 [MPa]	At Right end: PB = 6.94		qB = 19.432 [kN/m] XA = 7.8 [m]		
Perm. bending stress coeff.: Cs =	0.85 [-]	Concentrated loads:		Force: Moment: Location:		
Perm. combined str. coeff.: Cs1 =	0.95 [-]	Load no. 1 F1 =		M1 = X1 =		
Perm. bending stress coeff.: Cs2 =	0.85 [-]	Load no. 2 F2 =		M2 = X2 =		
Perm. shear stress coeff.: Ct =	0.85 [-]	Load no. 3 F3 =		M3 = X3 =		
Young's modulus: E =	206.0 [GPa]	Load no. 4 F4 =		M4 = X4 =		
Cross contraction: v =	0.3 [-]	Load no. 5 F5 =		M5 = X5 =		
Shear Modulus: G=E/(2(1+v)) =	79.23 [GPa]	Load no. 6 F6 =		M6 = X6 =		
Density of material: rho =	7.8 [kg/dm3]	Axial load and end moments:				
Bending moment and shear force distribution factors		Hull girder stress, Axial Load: sigma_hg = [Mpa] Fx = 0.0 [kN]				
Position	1	2	3	Select....		
f_bdg	-	8.00	-			
f_shr	0.50	-	0.50	Left end moment: (when f_bdg1=0) MA = [kNm]		
				Right end moment: (when f_bdg3=0) MB = [kNm]		

Figure 42 – PSM – Deck Transverse Check

- Deck Longitudinal Girder T450x10/200x12



NAUTICUS™  
HULL

Program: **Primary Supporting Members**  
 Rule ref: **DNV rules Pt.3. Ch.6 Sec.6 July 2015**  
 Rev: 2015-05-29

Select/ edit profile		Dim. Help...	Copy to Profile stack	Print	Results>>	Stack>>
----------------------	--	--------------	-----------------------	-------	-----------	---------

Position: **Deck Transverse**

Name / Id #: **BuiltUpTbar 450 x 200 x 12 x 12**

Upper Flange Width:	657.9	[mm]
Upper Flange Thickness:	5.0	[mm]
Web Height between flanges:	450.0	[mm]
Web Thickness:	10.0	[mm]
Lower Flange Width:	200.0	[mm]
Lower Flange Thickness:	12.0	[mm]
Radius, web & Upper Flange:	90.0	[mm]
Radius, web & Lower Flange:		[mm]
Corrosion addition, plate:	0.0	[mm]
Corrosion addition, girder:	0.0	[mm]

**PROFILE PROPERTIES:**

Total Area: Atot_n50 =	101.90	[cm2]
Effective Area: Ax_n50 =	101.90	[cm2]
Shear Area in Y-dir.: Ayshr_n50 =	65.16	[cm2]
Shear Area in Z-dir.: Azshr_n50 =	41.28	[cm2]
Torsional resistance: Zx_n50 =	28.0	[cm3]
Section modulus: ZyTop_n50 =	1756.7	[cm3]
Section modulus: ZyBot_n50 =	1447.5	[cm3]
Section modulus, z-axis: Zzn50 =	385.1	[cm3]
Req. net section mod. Zn50 >=	265.6	[cm3]
Req. net shear area: Ashr_n50 >=	6.6	[cm2]
Web stiff. inertia req.: Ist >=	-3.4	[cm4]

Distance to Neutral axis: Yna =	0.00	[mm]
Distance to Neutral axis: Zna =	256.04	[mm]
Shear center offset: eY =	0.00	[mm]
Shear center offset: eZ =	179.50	[mm]
Torsional mom. of inertia: Ix =	28.0	[cm4]
Moment of inertia: Iy =	37060.0	[cm4]
Moment of inertia: Iz =	12668.8	[cm4]
Centrifugal mom. of in.: Iyz =	0.0	[cm4]
Web and Flange min thick.: t >=	6.0	[mm]
Web pl. slenderness req.: tw >=	2.5	[mm]
Flange slenderness req.: tf >=	8.5	[mm]
Max unsupp. flange length: Sb <=	3.5	[m]

**BEAM DATA:**

Effective bending span: lbdg =	2.8	[m]
Effective shear span: lshr =	2.8	[m]
Load breadth / PSM Spacing: S =	7.8	[m]
Yield stress: ReH =	235.0	[MPa]
Perm. bending stress coeff.: Cs =	0.85	[-]
Perm. combined str. coeff.: Cs1 =	0.95	[-]
Perm. bending stress coeff.: Cs2 =	0.85	[-]
Perm. shear stress coeff.: Cc =	0.85	[-]
Young's modulus: E =	206.0	[GPa]
Cross contraction: v =	0.3	[-]
Shear Modulus: G=E/(2(1+v)) =	79.23	[GPa]
Density of material: rho =	7.8	[kg/dm3]

Bending moment and shear force distribution factors

Position	1	2	3	Select...
fbdg	-	8.00	-	
fshr	0.50	-	0.50	

**DESIGN LOAD SET:** L51 AC-II

Load intensity: At point (x-distance from A)

Distributed pressure: [kN/m2]	qA = 54.132	XA = 0
At Left end: PA = 6.94	q1 = 0	Xq1 = 0
Interm. Point: P1 =	qB = 54.132	XA = 2.8
At Right end: PB = 6.94		

Concentrated loads: Force [kN] Moment [kNm] Location [m]

Load no. 1	F1 =	M1 =	X1 =
Load no. 2	F2 =	M2 =	X2 =
Load no. 3	F3 =	M3 =	X3 =
Load no. 4	F4 =	M4 =	X4 =
Load no. 5	F5 =	M5 =	X5 =
Load no. 6	F6 =	M6 =	X6 =

**Axial load and end moments:**

Hull girder stress, Axial Load: sigma_hg =	72.51	[Mpa]	Fx = 738.8	[kN]
Left end moment: (when fbdg1=0)	MA =	[kNm]		
Right end moment: (when fbdg3=0)	MB =	[kNm]		

Figure 43 – PSM – Deck Longitudinal Girder Check

- Side Webframe T600x12/200x15



NAUTICUS™  
HULL

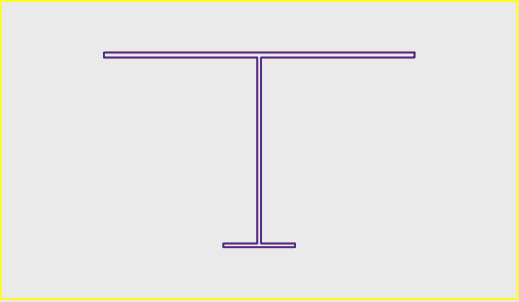
Program: **Primary Supporting Members**

Rule ref: **DNV rules Pt.3. Ch.6 Sec.6 July 2015**  
Rev: 2015-05-29

Select/ edit profile		Dim. Help...	Copy to Profile stack	Print	Results>>	Stack>>
----------------------	--	--------------	-----------------------	-------	-----------	---------

Position: <b>Side Web Hull</b>	
Name / Id #	<b>BuiltUpTbar 650 x 200 x 12 x 15</b>
Total plate Width:	869.4 [mm]
Plate Thickness, pT:	15.0 [mm]
Web Height, hw:	650.0 [mm]
Web Thickness, t:	12.0 [mm]
Flange width (incl. web), bf:	200.0 [mm]
Flange thickness, tf:	15.0 [mm]
Angle Between Profile & Plate:	90.0 [Degrees]
Corrosion addition, plate	0.0 [mm]
Corrosion addition, girder	0.0 [mm]



<b>PROFILE PROPERTIES:</b>			
Total Area: Atot_n50 =	238.41 [cm2]	Distance to Neutral axis: Yna =	0.00 [mm]
Effective Area: Ax_n50 =	238.41 [cm2]	Distance to Neutral axis: Zna =	480.04 [mm]
Shear Area in Y-dir.: Aysht_n50 =	167.17 [cm2]	Shear center offset: eY =	0.00 [mm]
Shear Area in Z-dir.: Azsht_n50 =	69.87 [cm2]	Shear center offset: eZ =	184.46 [mm]
Torsional resistance: Zx_n50 =	103.1 [cm3]	Torsional mom. of inertia: Ix =	154.7 [cm4]
Section modulus: ZyTop_n50 =	7905.6 [cm3]	Moment of inertia: Iy =	158082.5 [cm4]
Section modulus: ZyBot_n50 =	3293.1 [cm3]	Moment of inertia: Iz =	83152.0 [cm4]
Section modulus, z-axis: Zz_n50 =	1912.9 [cm3]	Centrifugal mom. of in.: Iyz =	[cm4]
Req. net section mod. Zn50 >=	3042.3 [cm3]	Web and Flange min thick.: t >=	6.0 [mm]
Req. net shear area: Ashr_n50 >=	57.0 [cm2]	Web pl. slenderness req.: tw >=	3.5 [mm]
Web stiff. inertia req.: It >=	-9.1 [cm4]	Flange slenderness req.: tf >=	8.5 [mm]
	OK	Maxunsupp. flange length: Sb <=	3.3 [m]

<b>BEAMDATA:</b>		<b>DESIGN LOAD SET:</b> L51 AC-II	
Effective bending span: lbdg =	3.7 [m]	Distributed pressure: [kN/m2]	?
Effective shear span: lshr =	3.7 [m]	At Left end: PA =	126.83
Load breadth / PSM Spacing: S =	2.8 [m]	Interm. Point: P1 =	0
Yield stress: RHH =	235.0 [MPa]	At Right end: PB =	126.83
Perm. bending stress coeff.: Cs =	0.85 [-]	Load intensity: [kN/m]	?
Perm. combined str. coeff.: Cs1 =	0.95 [-]	At point (x-distance from A)	
Perm. bending stress coeff.: Cs2 =	0.85 [-]	qA =	355.124
Perm. shear stress coeff.: Ct =	0.85 [-]	q1 =	0
Young's modulus: E =	206.0 [GPa]	qB =	355.124
Cross contraction: v =	0.3 [-]	XA =	0 [m]
Shear Modulus: G=E/(2(1+v)) =	79.23 [GPa]	Xq1 =	[m]
Density of material: rho =	7.8 [kg/dm3]	XA =	3.7 [m]
<b>Bending moment and shear force distribution factors</b>		<b>Concentrated loads:</b>	
Position	1	2	3
fbdg	-	8.00	-
fshr	0.50	-	0.50
		Force: [kN]	Moment: [kNm]
		Location: [m]	
		Load no. 1 F1 =	M1 =
		Load no. 2 F2 =	M2 =
		Load no. 3 F3 =	M3 =
		Load no. 4 F4 =	M4 =
		Load no. 5 F5 =	M5 =
		Load no. 6 F6 =	M6 =
		<b>Axial load and end moments:</b>	
		Hull girder stress, Axial Load: sigmahg =	[Mpa] Fx = 0.0 [kN]
		Left end moment: (when fbdg1=0) MA =	[kNm]
		Right end moment: (when fbdg3=0) MB =	[kNm]

Figure 44 – PSM – Side Webframe Hull Check

- Side Webframe Superstructure T300x7/150x10



NAUTICUS™  
HULL

Program: **Primary Supporting Members**

Rule ref: **DNV rules Pt.3. Ch.6 Sec.6 July 2015**  
Rev: 2015-05-29

Select/ edit profile		Dim. Help...	Copy to Profile stack	Print	Results>>	Stack>>
----------------------	--	--------------	-----------------------	-------	-----------	---------

Position: **Side Web Superstructure**  
Name / Id #: **BuiltUpTbar 300 x 150 x 7 x 10**

Total plate Width: 681.4 [mm]  
Plate Thickness, pT: 5.0 [mm]  
Web Height, hw: 300.0 [mm]  
Web Thickness, t: 7.0 [mm]  
Flange width (incl. web), bf: 150.0 [mm]  
Flange thickness, tf: 10.0 [mm]  
Angle Between Profile & Plate: 90.0 [Degrees]

Corrosion addition, plate: 0.0 [mm]  
Corrosion addition, girder: 0.0 [mm]

**PROFILE PROPERTIES:**

Total Area: Atot_n50 =	70.07	[cm2]
Effective Area: Ax_n50 =	70.07	[cm2]
Shear Area in Y-dir.: Aysht_n50 =	59.56	[cm2]
Shear Area in Z-dir.: Azsht_n50 =	19.80	[cm2]
Torsional resistance: Zx_n50 =	15.3	[cm3]
Section modulus: ZyTop_n50 =	1046.0	[cm3]
Section modulus: ZyBot_n50 =	593.5	[cm3]
Section modulus, z-axis: Zz_n50 =	395.2	[cm3]
Req. net section mod. Zn50 >=	534.9	[cm3]
Req. net shear area: Ashr_n50 >=	12.8	[cm2]
Web stiff. inertia req.: It >=	-2.8	[cm4]

Distance to Neutral axis: Yna = 0.00 [mm]  
Distance to Neutral axis: Zna = 200.97 [mm]  
Shear center offset: eY = 0.00 [mm]  
Shear center offset: eZ = 105.11 [mm]  
Torsional mom. of inertia: Ix = 10.7 [cm4]  
Moment of inertia: Iy = 11928.0 [cm4]  
Moment of inertia: Iz = 13464.5 [cm4]  
Centrifugal mom. of in.: Iyz = 0.0 [cm4]  
Web and Flange min thick.: t >= 6.0 [mm]  
Web pl. slenderness req.: tw >= 2.5 [mm]  
Flange slenderness req.: tf >= 6.5 [mm]  
Maxunsupp. flange length: Sb <= 3.0 [m]

**BEAMDATA:**

Effective bending span: lbdg = 2.9 [m]  
Effective shear span: lshr = 2.9 [m]  
Load breadth / PSM Spacing: S = 2.8 [m]  
Yield stress: RHH = 235.0 [MPa]  
Perm. bending stress coeff.: Cs = 0.85 [-]  
Perm. combined str. coeff.: Cs1 = 0.95 [-]  
Perm. bending stress coeff.: Cs2 = 0.85 [-]  
Perm. shear stress coeff.: Ct = 0.85 [-]  
Young's modulus: E = 206.0 [GPa]  
Cross contraction: v = 0.3 [-]  
Shear Modulus: G=E/(2(1+v)) = 79.23 [GPa]  
Density of material: rho = 7.8 [kg/dm3]

Bending moment and shear force distribution factors

Position	1	2	3	Select...
fbdg	-	8.00	-	
fshr	0.50	-	0.50	

**DESIGN LOAD SET:** L51 AC-II

Distributed pressure: [kN/m2] ? Load intensity: [kN/m] At point (x-distance from A)

At Left end: PA = 36.3 qA = 101.64 XA = 0 [m]  
Interm. Point: P1 = 0 q1 = 0 Xq1 = 0 [m]  
At Right end: PB = 36.3 qB = 101.64 XA = 2.9 [m]

Concentrated loads: Force: [kN] ? Moment: [kNm] Location: [m]

Load no. 1 F1 = M1 = X1 =  
Load no. 2 F2 = M2 = X2 =  
Load no. 3 F3 = M3 = X3 =  
Load no. 4 F4 = M4 = X4 =  
Load no. 5 F5 = M5 = X5 =  
Load no. 6 F6 = M6 = X6 =

**Axial load and end moments:**  
Hull girder stress, Axial Load: sigmaNg = [Mpa] Fx = 0.0 [kN]  
Left end moment: (when fbdg1=0) MA = [kNm]  
Right end moment: (when fbdg3=0) MB = [kNm]

Figure 45 – PSM – Side Webframe Superstructure Check

#### 4.4. Fore Section

According to the calculation performed in BV Mars 2000, the designed cross section meets the BV Rules requirements.

Hull girder strength criteria			
Hull Girder Loads	Section Moduli	Net/Gross Moduli	
		Hogging	Sagging
Design S.W.B.M. (still water bending moment)	848 627.	- 635 788.	(kNm)
Design vertical wave bending moment (Rule)	387 659.	- 483 255.	(kNm)
Design horizontal wave bending moment (Rule)	150 683.		(kNm)
		Positive	Negative
Design vertical shear force	1.		(kN)
Rule vertical wave shear force	12 714.	- 10 199.	(kN)

Close

Figure 46 – Fore Section – Hull Girder Loads

Hull girder strength criteria				
Hull Girder Loads	Section Moduli	Net/Gross Moduli		
	Rule	Actual	at z / BL	k
Modulus at deck	9.89030	12.66268 (m3)	19.700 (m)	1.00
Modulus at bottom	9.89030	11.23236 (m3)	0.000 (m)	1.00
Inertia	206.22050	117.26140 (m4)	(for information only)	

Close

Figure 47 – Fore Section – Section Modulus and Inertia Check

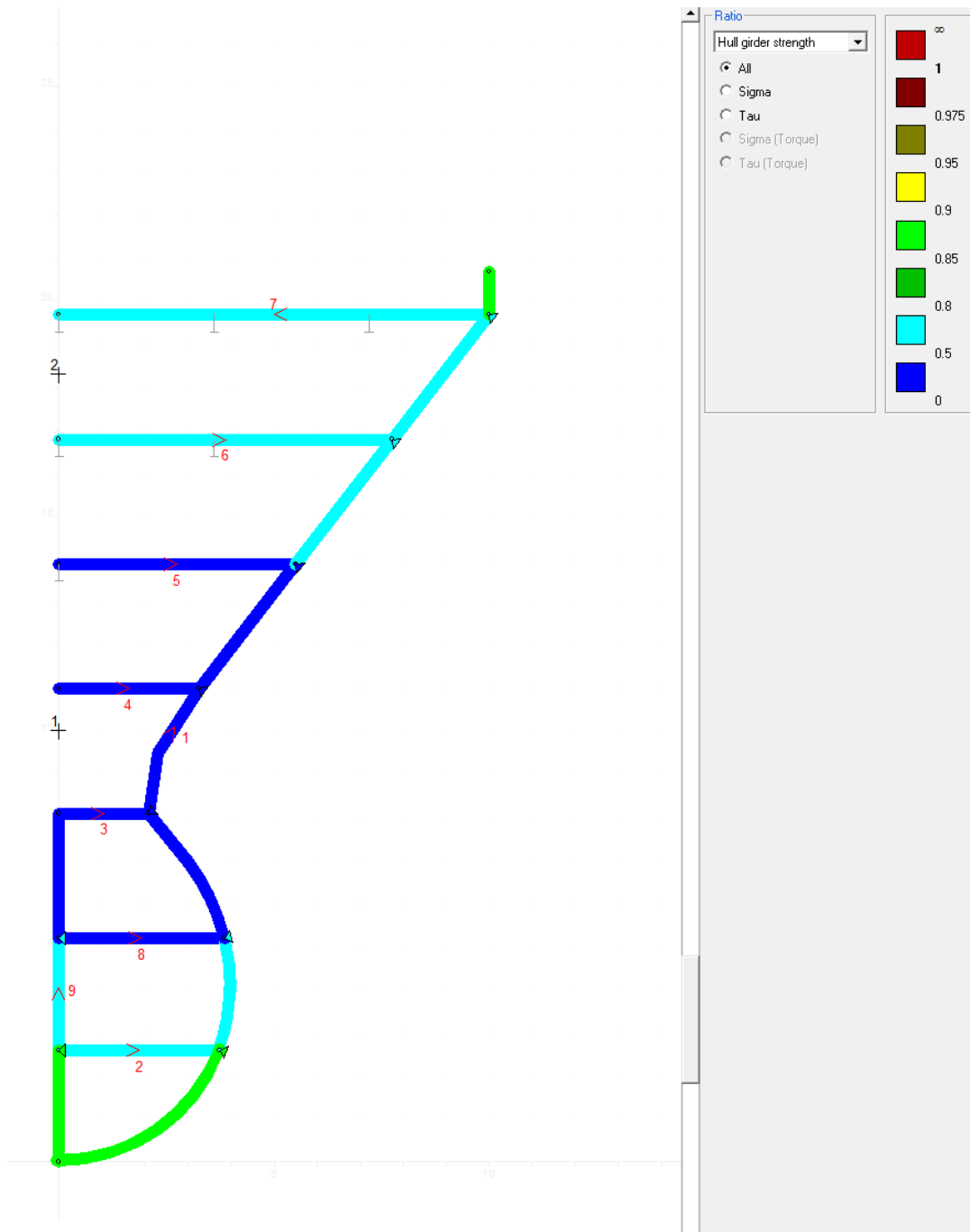


Figure 48 – Fore Section – Hull Girder Strength Check



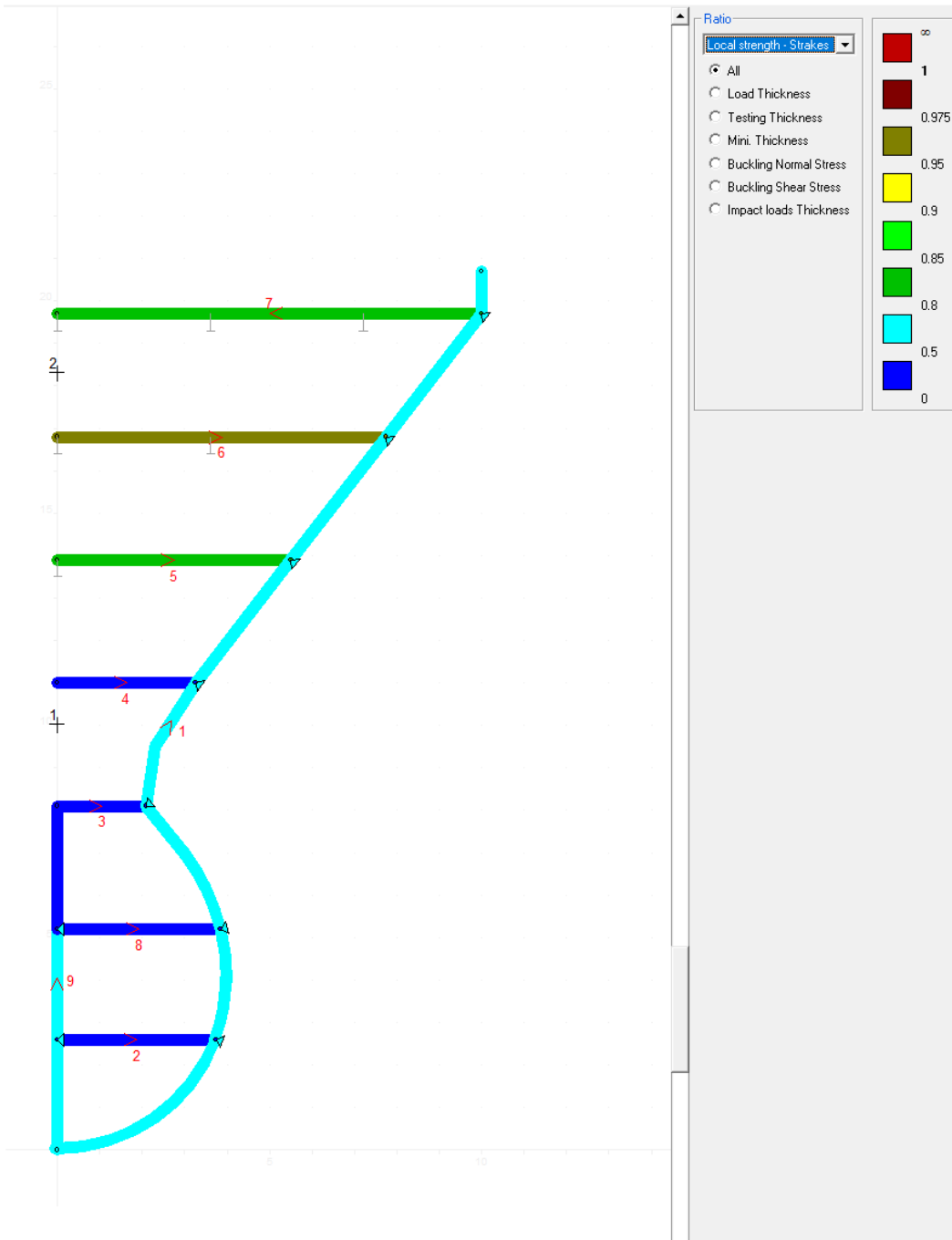


Figure 49 – Fore Section – Local Strength Check – Plates

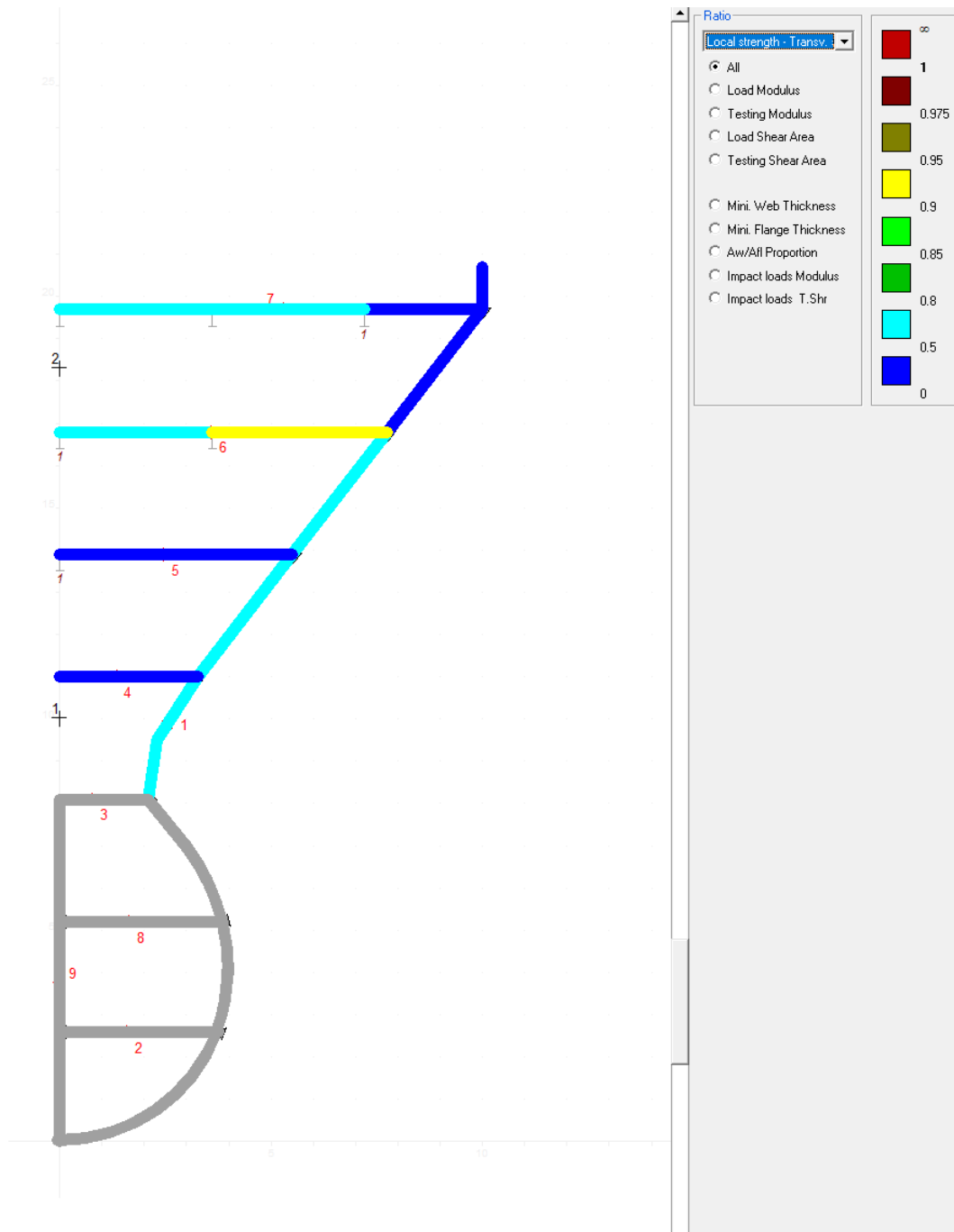


Figure 50 – Fore Section – Local Strength Check – Transverse Stiffeners

#### 4.5. Transverse Bulkhead Fore

According to the calculation performed in BV Mars 2000, the designed transverse bulkhead meets the BV Rules requirements.

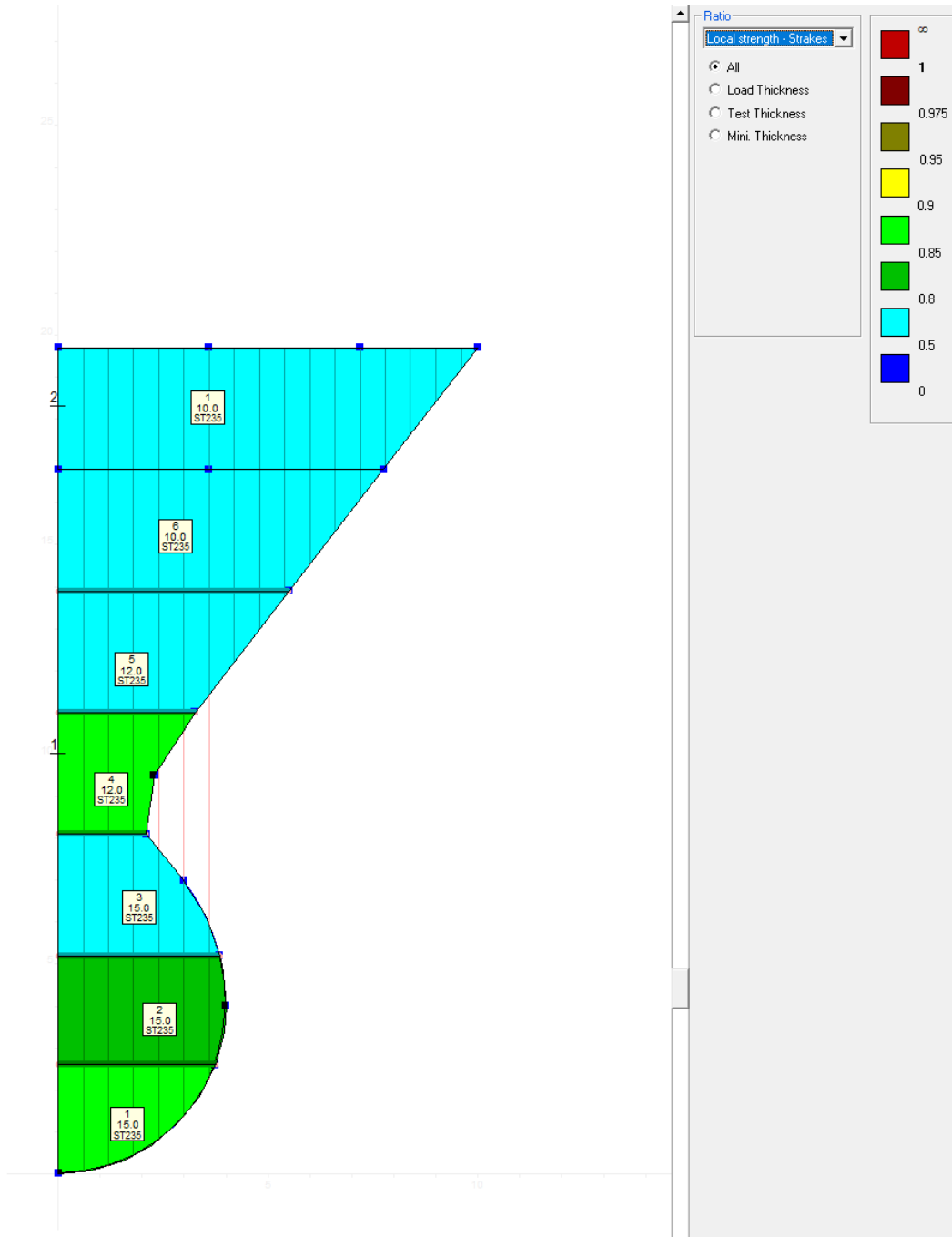


Figure 51 – Transverse Bulkhead Fore – Local Strength Check – Plates




Figure 52 – Transverse Bulkhead Fore – Local Strength Check – Stiffeners

### 4.6. Primary Supporting Members Fore

According to the calculation performed with DNV Nauticus Hull-Primary Supporting Members, the designed PSM meets the Rules requirements.

- Main Deck Transverse T600x14/300x16


NAUTICUS™  
HULL

Program: **Primary Supporting Members**  
 Rule ref: **DNV rules Pt.3. Ch.6 Sec.6 July 2015**  
 Rev: 2015-05-29

Select/ edit profile		Dim. Help...	Copy to Profile stack	Print	Results>>	Stack>>
----------------------	--	--------------	-----------------------	-------	-----------	---------

Position:

Name / Id # **BuiltUpTbar 600 x 300 x 14 x 18**

Total plate Width: 1899.8 [mm]

Plate Thickness, pT: 17.0 [mm]

Web Height, hw: 600.0 [mm]

Web Thickness, t: 14.0 [mm]

Flange width (incl. web), bf: 300.0 [mm]

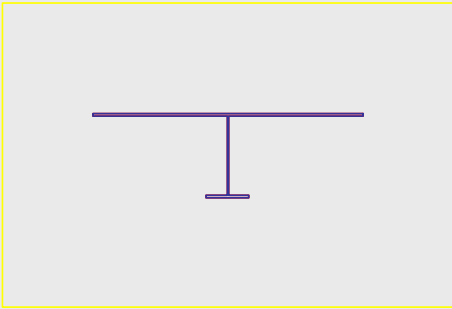
Flange thickness, tf: 16.0 [mm]

Angle Between Profile & Plate: 90.0 [Degrees]

Corrosion addition, plate  $t_c$  0.0 [mm]

Corrosion addition, girder 0.0 [mm]



**PROFILE PROPERTIES:**

Total Area: $A_{tot\_n50}$	=	454.97	[cm2]	Distance to Neutral axis: $Y_{na}$	=	0.00	[mm]
Effective Area: $A_{e\_n50}$	=	454.97	[cm2]	Distance to Neutral axis: $Z_{na}$	=	502.50	[mm]
Shear Area in Y-dir.: $A_{yshr\_n50}$	=	386.72	[cm2]	Shear center offset: $eY$	=	0.00	[mm]
Shear Area in Z-dir.: $A_{zshr\_n50}$	=	76.40	[cm2]	Shear center offset: $eZ$	=	119.72	[mm]
Torsional resistance: $Z_{x\_n50}$	=	237.0	[cm3]	Torsional mom. of inertia: $I_x$	=	403.0	[cm4]
Section modulus: $Z_{yTop\_n50}$	=	16854.4	[cm3]	Moment of inertia: $I_y$	=	219949.9	[cm4]
Section modulus: $Z_{yBot\_n50}$	=	4377.1	[cm3]	Moment of inertia: $I_z$	=	974998.6	[cm4]
Section modulus, z-axis: $Z_{z\_n50}$	=	10264.2	[cm3]	Centrifugal mom. of in.: $I_{yz}$	=	0.0	[cm4]
Req. net section mod. $Z_{n50} \geq$		3783.9	[cm3]	Web and Flange min thick.: $t \geq$		0.0	[mm]
Req. net shear area: $A_{shr\_n50} \geq$		69.0	[cm2]	Web pl. slenderness req.: $tw \geq$		6.0	[mm]
Web stiff. inertia req.: $I_{st} \geq$		0.0	[cm4]	Flange slenderness req.: $tf \geq$		12.5	[mm]
				! Max un_supp. flange length: $S_b <$		5.3	[m]

Copy to Profile stack

**BEAM DATA:**

Effective bending span:  $l_{bdg}$  = 5.7 [m]

Effective shear span:  $l_{shr}$  = 5.7 [m]

Load breadth / PSM Spacing:  $S$  = 2.8 [m]

Yield stress:  $R_{eH}$  = 235.0 [MPa]

Perm. bending stress coeff.:  $C_s$  = 0.85 [-]

Perm. combined str. coeff.:  $C_{s1}$  = 0.95 [-]

Perm. bending stress coeff.:  $C_{s2}$  = 0.85 [-]

Perm. shear stress coeff.:  $C_t$  = 0.85 [-]

Young's modulus:  $E$  = 206.0 [GPa]

Cross contraction:  $\nu$  = 0.3 [-]

Shear Modulus:  $G=E/(2(1+\nu))$  = 79.23 [GPa]

Density of material:  $\rho$  = 7.8 [kg/dm3]

Bending moment and shear force distribution factors

Position	1	2	3	Select...
$f_{bdg}$	12.00	24.00	12.00	
$f_{shr}$	0.50	-	0.50	

**DESIGN LOAD SET:** L51 AC-II

Distributed pressure: [kN/m2] Load intensity: At point (x-distance from A)

At Left end: $P_A$ = 99.7	$q_A$ = 279.16	$X_A$ = 0 [m]
Intern. Point: $P_1$ =	$q_1$ = 0	$X_{q1}$ = [m]
At Right end: $P_B$ = 99.7	$q_B$ = 279.16	$X_A$ = 5.7 [m]

Concentrated loads: Force: [kN] Moment: [kNm] Location: [m]

Load no. 1	$F_1$	$M_1$	$X_1$
Load no. 2	$F_2$	$M_2$	$X_2$
Load no. 3	$F_3$	$M_3$	$X_3$
Load no. 4	$F_4$	$M_4$	$X_4$
Load no. 5	$F_5$	$M_5$	$X_5$
Load no. 6	$F_6$	$M_6$	$X_6$

**Axial load and end moments:**

Hull girder stress, Axial Load:  $\sigma_{hg}$  = [Mpa]  $F_x$  = 0.0 [kN]

Left end moment: (when  $f_{bdg1}=0$ )  $M_A$  = [kNm]

Right end moment: (when  $f_{bdg3}=0$ )  $M_B$  = [kNm]

Figure 53 – PSM Fore – Main Deck Transverse Check

- Lower Deck Transverse T600x12/300x14



NAUTICUS™  
HULL

Program: **Primary Supporting Members**  
 Rule ref: **DNV rules Pt.3. Ch.6 Sec.6 July 2015**  
 Rev: 2015-05-29

Select/ edit profile		Dim. Help...	Copy to Profile stack	Print	Results>>	Stack>>
Position:						
Name / Id #	BuiltUpTbar 600 x 220 x 12 x 14					
Total plate Width:	1899.8	[mm]				
Plate Thickness, pT:	17.0	[mm]				
Web Height, hw:	600.0	[mm]				
Web Thickness, t:	12.0	[mm]				
Flange width (incl. web), bf:	300.0	[mm]				
Flange thickness, tf:	14.0	[mm]				
Angle Between Profile & Plate:	90.0	[Degrees]				
Corrosion addition, plate <input type="checkbox"/>						
Corrosion addition, girder	0.0	[mm]				
<b>PROFILE PROPERTIES:</b>						
Total Area: Atot_n50 =	436.97	[cm2]	Distance to Neutral axis: Yna =	0.00	[mm]	Copy to Profile stack
Effective Area: Ax_n50 =	436.97	[cm2]	Distance to Neutral axis: Zna =	512.51	[mm]	
Shear Area in Y-dir.: Aysbr_n50 =	371.42	[cm2]	Shear center offset: eY =	0.00	[mm]	
Shear Area in Z-dir.: Azsbr_n50 =	65.23	[cm2]	Shear center offset: eZ =	108.00	[mm]	
Torsional resistance: Zx_n50 =	218.1	[cm3]	Torsional mom. of inertia: Ix =	370.8	[cm4]	
Section modulus: ZyTop_n50 =	16579.6	[cm3]	Moment of inertia: Iy =	196455.9	[cm4]	
Section modulus: ZyBot_n50 =	3833.2	[cm3]	Moment of inertia: Iz =	974543.5	[cm4]	
Section modulus, z-axis: Zz_n50 =	10259.4	[cm3]	Centrifugal mom. of in.: Iyz =	0.0	[cm4]	
Req. net section mod. Zn50 >=	3545.3	[cm3]	Web and Flange min thick.: t >=	0.0	[mm]	Select location of PSM
Req. net shear area: Ashr_n50 >=	52.6	[cm2]	Web pl. slenderness req.: tw >=	6.0	[mm]	
Web stiff. inertia req.: It >=	0.0	[cm4]	Flange slenderness req.: tf >=	12.5	[mm]	
			! Max unSUPP. flange length: Sb <=	5.4	[m]	0 Flange tripping supports
OK						
<b>Not OK!</b>						
<b>BEAMDATA:</b>						
Effective bending span: lbdg = 7.0 [m]						
Effective shear span: lshr = 7.0 [m]						
Load breadth / PSM Spacing: S = 2.8 [m]						
Yield stress: Rch = 235.0 [MPa]						
Perm. bending stress coeff.: Cb = 0.85 [-]						
Perm. combined str. coeff.: Cs1 = 0.95 [-]						
Perm. bending stress coeff.: Cc2 = 0.85 [-]						
Perm. shear stress coeff.: Cc1 = 0.85 [-]						
Young's modulus: E = 206.0 [GPa]						
Cross contraction: v = 0.3 [-]						
Shear Modulus: G=E/(2(1+v)) = 79.23 [GPa]						
Density of material: ρ = 7.8 [kg/dm3]						
Bending moment and shear force distribution factors						
Position	1	2	3	Select....		
fbdg	12.00	24.00	12.00			
fshr	0.50	-	0.50			
<b>DESIGN LOAD SET:</b> LS1 AC-II						
<b>Distributed pressure:</b> [kN/m2] ? Load intensity: [kN/m] At point (x-distance from A)						
At Left end: PA =	61.94	qA =	173.432	XA =	0	[m]
Intern. Point: P1 =		q1 =	0	Xq1 =		[m]
At Right end: PB =	61.94	qB =	173.432	XA =	7.0	[m]
<b>Concentrated loads:</b> Force: [kN] ? Moment: [kNm] Location: [m]						
Load no. 1	F1 =	M1 =		X1 =		
Load no. 2	F2 =	M2 =		X2 =		
Load no. 3	F3 =	M3 =		X3 =		
Load no. 4	F4 =	M4 =		X4 =		
Load no. 5	F5 =	M5 =		X5 =		
Load no. 6	F6 =	M6 =		X6 =		
<b>Axial load and end moments:</b>						
Hull girder stress, Axial Load:	σng =		[Mpa]	Fx =	0.0	[kN]
Left end moment: (when fbdg1=0)	MA =		[kNm]			
Right end moment: (when fbdg3=0)	MB =		[kNm]			

Figure 54 – PSM Fore – Lower Deck Transverse Check

- Side Shell Webframe T600x16/300x20



NAUTICUS™  
HULL

Program: **Primary Supporting Members**  
 Rule ref: **DNV rules Pt.3. Ch.6 Sec.6 July 2015**  
 Rev: 2015-05-29

Select/ edit profile		Dim. Help...	Copy to Profile stack	Print	Results>>	Stack>>
----------------------	--	--------------	-----------------------	-------	-----------	---------

Position:  
 Name / Id #: **BuiltUpTbar 600 x 300 x 12 x 14**

Total plate Width: 869.4 [mm]  
 Plate Thickness, pT: 17.0 [mm]  
 Web Height, hw: 600.0 [mm]  
 Web Thickness, t: 16.0 [mm]  
 Flange width (incl. web), bf: 300.0 [mm]  
 Flange thickness, tf: 20.0 [mm]  
 Angle Between Profile & Plate: 90.0 [Degrees]

Corrosion addition, plate:  $t_c$  0.0 [mm]  
 Corrosion addition, girder: 0.0 [mm]

**PROFILE PROPERTIES:**

Total Area: $A_{tot\_n50}$	=	303.80	[cm2]
Effective Area: $A_{x\_n50}$	=	303.80	[cm2]
Shear Area in Y-dir.: $A_{yshr\_n50}$	=	197.24	[cm2]
Shear Area in Z-dir.: $A_{zshr\_n50}$	=	90.23	[cm2]
Torsional resistance: $Z_{x\_n50}$	=	173.3	[cm3]
Section modulus: $Z_{yTop\_n50}$	=	8906.4	[cm3]
Section modulus: $Z_{yBot\_n50}$	=	4969.7	[cm3]
Section modulus, z-axis: $Z_{z\_n50}$	=	2245.6	[cm3]
Req. net section mod. $Z_{n50} >=$		2398.7	[cm3]
Req. net shear area: $A_{shr\_n50} >=$		67.4	[cm2]
Web stiff. inertia req.: $I_{st} >=$		0.0	[cm4]

Distance to Neutral axis:  $Y_{na}$  = 0.00 [mm]  
 Distance to Neutral axis:  $Z_{na}$  = 408.86 [mm]  
 Shear center offset:  $eY$  = 0.00 [mm]  
 Shear center offset:  $eZ$  = 191.12 [mm]  
 Torsional mom. of inertia:  $I_x$  = 294.7 [cm4]  
 Moment of inertia:  $I_y$  = 203189.7 [cm4]  
 Moment of inertia:  $I_z$  = 97615.5 [cm4]  
 Centrifugal mom. of in.:  $I_{yz}$  = 0.0 [cm4]  
 Web and Flange min thick.:  $t >=$  0.0 [mm]  
 Web pl. slenderness req.:  $tw >=$  6.0 [mm]  
 Flange slenderness req.:  $tf >=$  12.5 [mm]  
 Maxunsupp. flange length:  $S_b <=$  5.4 [m]

Req. net section mod.  $Z_{n50} >=$  2398.7 [cm3] OK  
 Req. net shear area:  $A_{shr\_n50} >=$  67.4 [cm2] OK  
 Web stiff. inertia req.:  $I_{st} >=$  0.0 [cm4] OK

**BEAMDATA:**

Effective bending span:  $l_{bdg}$  = 3.7 [m]  
 Effective shear span:  $l_{shr}$  = 3.7 [m]  
 Load breadth / PSM Spacing:  $S$  = 2.8 [m]  
 Yield stress:  $R_{RH}$  = 235.0 [MPa]  
 Perm. bending stress coeff.:  $C_s$  = 0.85 [-]  
 Perm. combined str. coeff.:  $C_{s1}$  = 0.95 [-]  
 Perm. bending stress coeff.:  $C_{s2}$  = 0.85 [-]  
 Perm. shear stress coeff.:  $C_t$  = 0.85 [-]  
 Young's modulus:  $E$  = 206.0 [GPa]  
 Cross contraction:  $\nu$  = 0.3 [-]  
 Shear Modulus:  $G=E/(2(1+\nu))$  = 79.23 [GPa]  
 Density of material:  $\rho$  = 7.8 [kg/dm3]

Bending moment and shear force distribution factors

Position	1	2	3	Select...
$f_{bdg}$	12.00	24.00	12.00	
$f_{shr}$	0.50	-	0.50	

**DESIGN LOAD SET:** L51 AC-II

Distributed pressure: [kN/m2] ? Load intensity: [kN/m] At point (x-distance from A)

At Left end:  $P_A$  = 150.0  $q_A$  = 420  $X_A$  = 0 [m]  
 Interm. Point:  $P_1$  =  $q_1$  = 0  $X_{q1}$  = [m]  
 At Right end:  $P_B$  = 150.0  $q_B$  = 420  $X_A$  = 3.7 [m]

Concentrated loads: Force: [kN] ? Moment: [kNm] Location: [m]

Load no. 1	$F_1$	$M_1$	$X_1$
Load no. 2	$F_2$	$M_2$	$X_2$
Load no. 3	$F_3$	$M_3$	$X_3$
Load no. 4	$F_4$	$M_4$	$X_4$
Load no. 5	$F_5$	$M_5$	$X_5$
Load no. 6	$F_6$	$M_6$	$X_6$

**Axial load and end moments:**  
 Hull girder stress, Axial Load:  $\sigma_{hg}$  = [Mpa]  $F_x$  = 0.0 [kN]  
 Left end moment: (when  $f_{bdg1}=0$ )  $M_A$  = [kNm]  
 Right end moment: (when  $f_{bdg3}=0$ )  $M_B$  = [kNm]

Figure 55 – PSM Fore – Side Shell Webframe Check



## 5 Conclusion

---

This report covers the scantling evaluation of a common passenger ship midship section, fore area section, transverse bulkhead in midship area, transverse bulkhead in fore area and primary supporting members. Considering the assumptions presented in Ch.1 and Ch.3, the structure satisfies the BV Rules.

Based on the design calculations it can be concluded that the presented scantling design is representative for a common passenger ship.



Waarderweg 40  
2031 BP Haarlem  
The Netherlands

Pettelaarpark 10-15  
5216 PD 's-Hertogenbosch  
The Netherlands

Nevelgaarde 10  
3436 ZZ Nieuwegein  
The Netherlands

**iv-Infra b.v.**  
Trapezium 322  
3364 DL Sliedrecht  
The Netherlands

Trompstraat 36a  
9190 Stekene  
Belgium

Westervoortsedijk 73  
Gebouw CB  
6827 AV Arnhem  
The Netherlands

[www.iv-infra.nl](http://www.iv-infra.nl)  
Telephone +31 88 943 3200  
P.O. Box 135  
3360 AC Sliedrecht  
[officemanagement.infra@iv.nl](mailto:officemanagement.infra@iv.nl)



**D.** R104-DP2.3 Memo Steel material model



## Memo

To: RWS WVL  
From: Iv  
Author: GVA; MNA  
Checked by: YYA  
Approved by: WLA  
Date: 30 December 2024  
Reference: INFR240476-RWS WVL  
Document no.: INFR240476-R104-DP2/3  
Subject: Memo Steel Material Model  
Revision: 2

---



# 1 Introduction

---

This memo provides an overview of the material modelling approach utilized for impact simulations within the scope of the project INF240746 RWS WV. The focus is on defining the material properties relevant to structural simulations, particularly in scenarios involving high-stress impacts.

The document outlines the methods used to characterize the behavior of structural materials under various loading conditions, with an emphasis on their performance during extreme events. By applying established modelling techniques, this report ensures that the simulations accurately reflect the real-world response of materials, thereby supporting the integrity and safety of the structures being studied.

The material models described in this report are based on standard engineering practices and guidelines, offering a detailed examination of the stress-strain relationships essential for accurate impact predictions. This includes a discussion on the methods for defining material behavior in both elastic and plastic regions, as well as the criteria for simulating different stress conditions.

In this project, the designed ship and the wind turbine are made by two steel material grades, as following:

Table 1. Steel material grades Used in the design of the ship and wind turbine

Steel material grade	Ship	Wind turbine
S235	x	
S355	x	x

The standards and the references that have been used in this memo are provided in Table 2.



Table 2. Used standards and references

Ref.	Document	Title	Date
1.	DNV-OS-A101	Safety principles and arrangements	March 2023
2.	DNV-RP-C204	Structural design against accidental loads.	September 2019
3.	DNV-RP-C208	Determination of structural capacity by non-linear finite element analysis methods.	October 2022
5.	NEN-EN 10025-2	Hot-rolled products of structural steels – Part 2	Augustus 2019
6.	NEN-EN 10025-3	Hot-rolled products of structural steels – Part 3	Augustus 2019
7.	INFR240476-R101-DP1-v0a;	3D FEM gevolgschade schip-turbine (Chemical Tanker – Scantling Calculations Report)	September 2024
8.	INFR240476-R102-DP1-v0a;	3D FEM gevolgschade schip-turbine (Container Ship – Scantling Calculations Report)	September 2024
9.	INFR240476-R103-DP1-v0a	3D FEM gevolgschade schip-turbine (Passenger Ship – Scantling Calculations Report)	September 2024
10.	Bijlage K Annex 01-05 081R030M010-App-A - Properties Windfarm 2 - Foundation 'WD 34.6m PD 28.75m'	Excel file containing information and data about Wind Farm 2	-

The turbine foundation monopile for Windfarm 2 is made entirely of S355 steel. The monopile wall thicknesses vary from 16 mm up to 88 mm. Additionally, certain components of the monopile feature a wall thickness of 245 mm, which is specifically used for the flange section to enhance structural integrity and load-bearing capacity.

Table 3. Material thickness range

Steel material grade	Thickness range	Reference N. in Table 2
S235	9 mm to 60 mm	7, 8, 9
S355	16 mm to 245 mm	10



## 2 Material model steel

---

The LS-DYNA material model \*MAT\_024 (\*MAT\_PIECEWISE\_LINEAR\_PLASTICITY) is commonly used for simulating impacts, particularly in scenarios where plastic deformation and structural integrity are critical (for more details see ref. [1]<sup>1</sup>). This model has been widely applied in various engineering projects, including ship collision simulations and wind turbine foundation assessments (Abedini, M., Zhang, C. [2]<sup>2</sup>, Peixinho, N., and Pinho, A. [3]<sup>3</sup> and Yongli Ren et al. [4]<sup>4</sup>).

This material model describes the non-linear, elastic-plastic behavior. It uses a piecewise linear approach to define the stress-strain curve. Additionally, the strain at fracture or maximum strain can also be specified.

Key features of this material model:

- **FAIL (Failure Strain):** Effective plastic strain to failure. When the plastic strain reaches this value, the element is deleted from the calculation.
- **N (Piecewise Points):** An array of stress and strain values that defines the piecewise linear approximation of the stress-strain curve.

---

<sup>1</sup> LS-DYNA, KEYWORD USER'S MANUAL, VOLUME II, Material Models

<sup>2</sup> Abedini, M., Zhang, C. Performance Assessment of Concrete and Steel Material Models in LS-DYNA for Enhanced Numerical Simulation, A State of the Art Review. Arch Computat Methods Eng 28, 2921–2942 (2021). <https://doi.org/10.1007/s11831-020-09483-5>

<sup>3</sup> Peixinho, N., and Pinho, A. (November 17, 2006). "Study of Viscoplasticity Models for the Impact Behavior of High-Strength Steels." ASME. J. Comput. Nonlinear Dynam. April 2007; 2(2): 114–123. <https://doi.org/10.1115/1.2447129>

<sup>4</sup> Yongli Ren, Zhaolong Yu, Xugang Hua, Jørgen Amdahl, Zili Zhang, Zhengqing Chen, Experimental and numerical investigation on the deformation behaviors of large diameter steel tubes under concentrated lateral impact loads, International Journal of Impact Engineering, <https://doi.org/10.1016/j.ijimpeng.2023.104696>.



### 3 Material data

The material data for the steel grades S235 and S355 are determined from the DNV material curves (reference: DNV RP-C208, page 26), which are according to EN 10025. These material curves are built up in three parts, as is shown in Figure 1. All Parts (Part 1, 2 and 3) represent the plastic regions. The data for defining these regions per steel grade are described in paragraph 3.1.

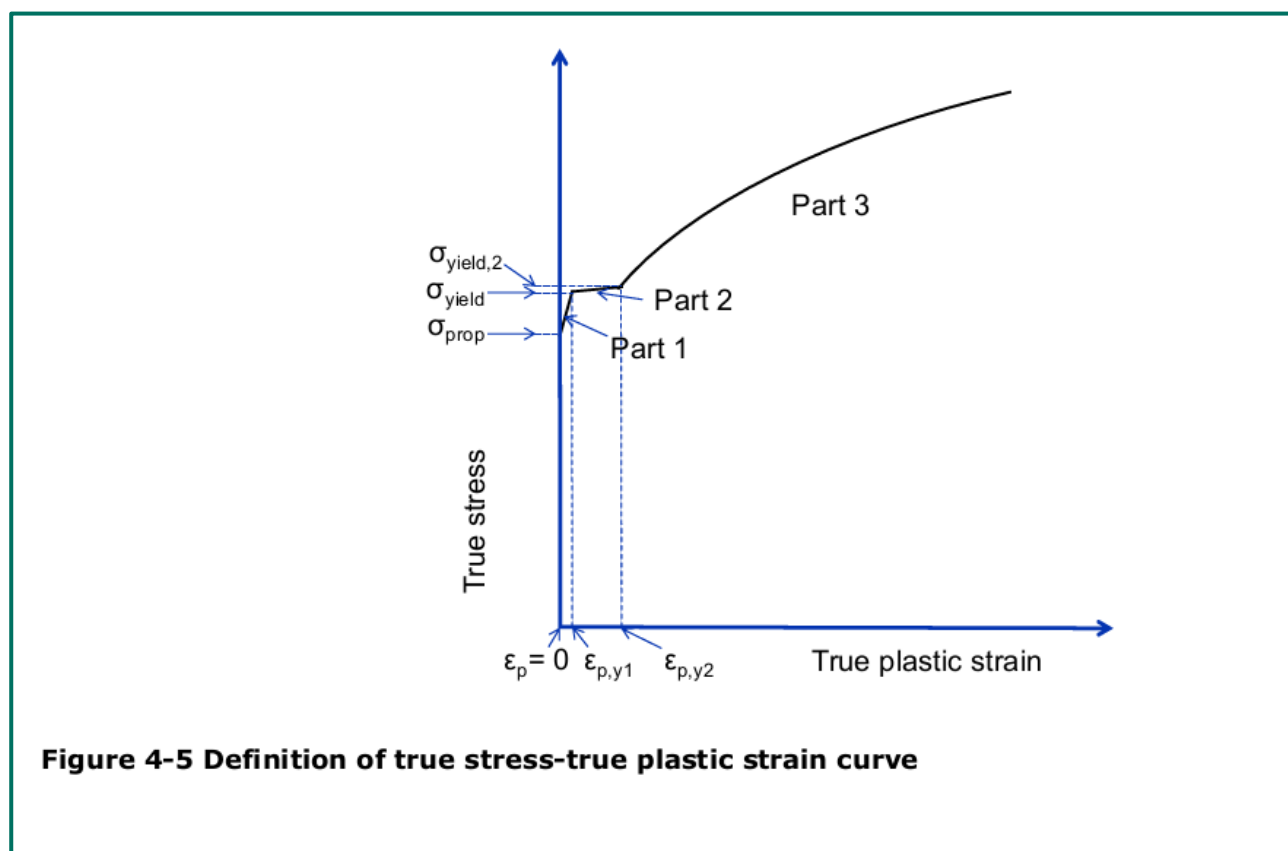


Figure 1. True stress vs true Strain - DNV RP-C208, page 26



### 3.1. Material properties for part 1 to 4

The material properties for S235 and S355 with different thicknesses are given in Figure 2 to Figure 3. All stress-strain values are true stress-strain values, not engineering stress-strain values.

**Table 4-2 Proposed properties for S235 steels (true stress strain)**

Thickness [mm]	S235			
	$t \leq 16$	$16 < t \leq 40$	$40 < t \leq 63$	$63 < t \leq 100$
<b>E [MPa]</b>	210000	210000	210000	210000
$\sigma_{prop}$ [MPa]	211.7	202.7	193.7	193.7
$\sigma_{yield}$ [MPa]	236.2	226.1	216.1	216.1
$\sigma_{yield,2}$ [MPa]	243.4	233.2	223.0	223.0
$\epsilon_{p,y1}$	0.004	0.004	0.004	0.004
$\epsilon_{p,y2}$	0.02	0.02	0.02	0.02
<b>K [MPa]</b>	520	520	520	520
<b>n</b>	0.166	0.166	0.166	0.166

Figure 2. Table 4-2 Properties S235, DNV RP-C208, page 27

Figure 3 shows that DNV RP-C208 does not provide material properties for S355 with a thickness exceeding 100 mm. Further details regarding this material and thickness ranges are discussed in Chapter 5, Section 5.2.

**Table 4-4 Proposed properties for S355 steels (true stress strain)**

Thickness [mm]	S355			
	$t \leq 16$	$16 < t \leq 40$	$40 < t \leq 63$	$63 < t \leq 100$
<b>E [MPa]</b>	210000	210000	210000	210000
$\sigma_{prop}$ [MPa]	320.0	311.0	301.9	283.9
$\sigma_{yield}$ [MPa]	357.0	346.9	336.9	316.7
$\sigma_{yield,2}$ [MPa]	363.3	353.1	342.9	322.5
$\epsilon_{p,y1}$	0.004	0.004	0.004	0.004
$\epsilon_{p,y2}$	0.015	0.015	0.015	0.015
<b>K [MPa]</b>	740	740	725	725
<b>n</b>	0.166	0.166	0.166	0.166

Figure 3. Table 4-4 DNV Properties S355, RP-C208, page 28





The relation between stress and strain for part 3 in Figure 1 is illustrated in Figure 4.

For Part 3 as shown in Figure 4-5, the relation between stress and strain is given as shown in Equation (8).

$$\sigma = K \left( \varepsilon_p + \left( \frac{\sigma_{yield, 2}}{K} \right)^{\frac{1}{n}} - \varepsilon_{p,y2} \right)^n \quad \text{for } \varepsilon_p > \varepsilon_{p,y2} \quad (8)$$

Figure 4. Stress vs strain relationship Part 3 - DNV RP-C204, page 27

### 3.2. Plastic strain limit DNV/Eurocode

The stress-strain curve from DNV in Figure 1 does not have an end point where the failure strain is defined. The only fracture strain values in DNV RP-C204 are shown in Figure 5. However these critical strain ( $\varepsilon_{cr}$ ) should be applied to an idealized bi-linear stress-strain relation, but not to be adopted for non-linear finite element analysis, as stated in DNV RP-C204, A.12.

**Table 3-3 Proposed values for  $\varepsilon_{cr}$  and  $H$  for different steel grades**

Steel grade	$\varepsilon_{cr}$	$H$
S 235	20 %	0.0022
S 355	15 %	0.0034
S 460	10 %	0.0034

Figure 5. Table 3-3 Tensile fracture in yield hinges, DNV RP-C204, page 38

In order to define the ultimate tensile strength and the fracture strain for the material models, EN 10025-2 is used for different steel grades. Tensile strength  $R_m$  (Figure 7) will be used as the end point of part 3 in the material curve, and minimum percentage elongation after fracture  $\varepsilon_{fr}$  (Figure 6) will be used as the failure strain after the tensile strength is reached and the material starts to neck. To define this, we will add part 4 in the material curve, see further Chapter 4. Note: the minimum yield strength  $R_{eH}$  in Figure 7 will not be used, they match with  $\sigma_{yield}$  in Figure 2 to Figure 3.



Designation		Orientation of test pieces <sup>a</sup>	Minimum percentage elongation after fracture <sup>a</sup>										
Steel name	Steel number		$L_0 = 80$ mm					$L_0 = 5,65 \sqrt{S_0}$					
			Nominal thickness mm					Nominal thickness mm					
		$\leq 1$	$> 1$ $\leq 1,5$	$> 1,5$ $\leq 2$	$> 2$ $\leq 2,5$	$> 2,5$ $< 3$	$\geq 3$ $\leq 40$	$> 40$ $\leq 63$	$> 63$ $\leq 100$	$> 100$ $\leq 150$	$> 150$ $\leq 250$	$> 250$ $\leq 400$	
S235JR	1.0038	l t	17	18	19	20	21	26	25	24	22	21	21
S235J0	1.0114		15	16	17	18	19	24	23	22	22	21	21
S235J2	1.0117												
S275JR	1.0044	l t	15	16	17	18	19	23	22	21	19	18	18
S275J0	1.0143		13	14	15	16	17	21	20	19	19	18	18
S275J2	1.0145												
S355JR	1.0045	l t	14	15	16	17	18	22	21	20	18	17	17
S355J0	1.0553		12	13	14	15	16	20	19	18	18	17	17
S355J2	1.0577												
S355K2	1.0596												

Figure 6. Mechanical properties steel grades S235 to S355 - EN10025-2:2019, Table 6, page 28

Designation		Minimum yield strength $R_{eH}$ <sup>a</sup>									Tensile strength $R_m$ <sup>a</sup>				
Steel name	Steel number	MPa									MPa				
		Nominal thickness mm									Nominal thickness mm				
		$\leq 16$	$> 16$ $\leq 40$	$> 40$ $\leq 63$	$> 63$ $\leq 80$	$> 80$ $\leq 100$	$> 100$ $\leq 150$	$> 150$ $\leq 200$	$> 200$ $\leq 250$	$> 250$ $\leq 400$	$< 3$	$\geq 3$ $\leq 100$	$> 100$ $\leq 150$	$> 150$ $\leq 250$	$> 250$ $\leq 400$
S235JR	1.0038	235	225	215	215	215	195	185	175	165	360 to 510	360 to 510	350 to 500	340 to 490	330 to 480
S235J0	1.0114														
S235J2	1.0117														
S275JR	1.0044	275	265	255	245	235	225	215	205	195	430 to 580	410 to 560	400 to 540	380 to 540	380 to 540
S275J0	1.0143														
S275J2	1.0145														
S355JR	1.0045	355	345	335	325	315	295	285	275	265	510 to 680	470 to 630	450 to 600	450 to 600	450 to 600
S355J0	1.0553														
S355J2	1.0577														
S355K2	1.0596														

Figure 7. Mechanical properties - Tensile properties – NEN-EN10025-2:2019, Table 6, page 27



### 3.3. Tensile strength and plastic strain limit

The tensile strength and the plastic strain limit at fracture are chosen according to EN-10025-2. Minimum values of ultimate tensile strength and failure strain per steel grade, taking into account the nominal thickness, are applied to ensure conservative approach.

Table 4. Applied ultimate tensile stress and strain at failure values

Steel Grade	Ultimate tensile strength range $\sigma_{ult,t}$ [MPa]	Strain at failure $\epsilon_{fr}$ [%]	Figure(s)
S235	358 - 360	23	Figure 6, Figure 7
S355	446 - 470	19	Figure 6, Figure 7

### 3.4. Strain rates effect

Strain rate effects are not considered in these analyses, as their impact is minimal. Paragraph 4.6.8 of DNV RP-C208 (page 29) states that it is safe to exclude this effect from the simulations. Additionally, not cyclic loading is expected from the impact simulations.



## 4 Applied stress-strain curve in material model

As mentioned in previous chapter, the true stress-strain curve in DNV does not have an end point representing the failure of the material. To do so, we will model the steel material as a combination of a stepwise linear function (Parts 1 to 2) and a power law with a yield plateau (Parts 3 and 4) as shown in Figure 8, of which Part 4 is added by us to take into account the failure of the material.

Part 1 to 2 will follow the true stress-strain curve as provided in Figure 4-5 of DNVGL-RP-C208.

Part 3 of the true stress-strain curve will be limited to the tensile strength of the material,  $\sigma_{ult,t}$ , in accordance with EN-10025-2.

Part 4 covers the region after the material reaches the tensile strength until the failure strain ( $\epsilon_{fr}$ ). To ensure the model convergence, a small slope of  $\tan^{-1}(E/10000)$  will be applied. The effective plastic strain (FAIL) in the material card is determined by  $\epsilon_{fail} = \epsilon_{fr} - \epsilon_{prop}$ .

The applied stress-strain curves and material data of the two steel grades are reported in Chapter 5.

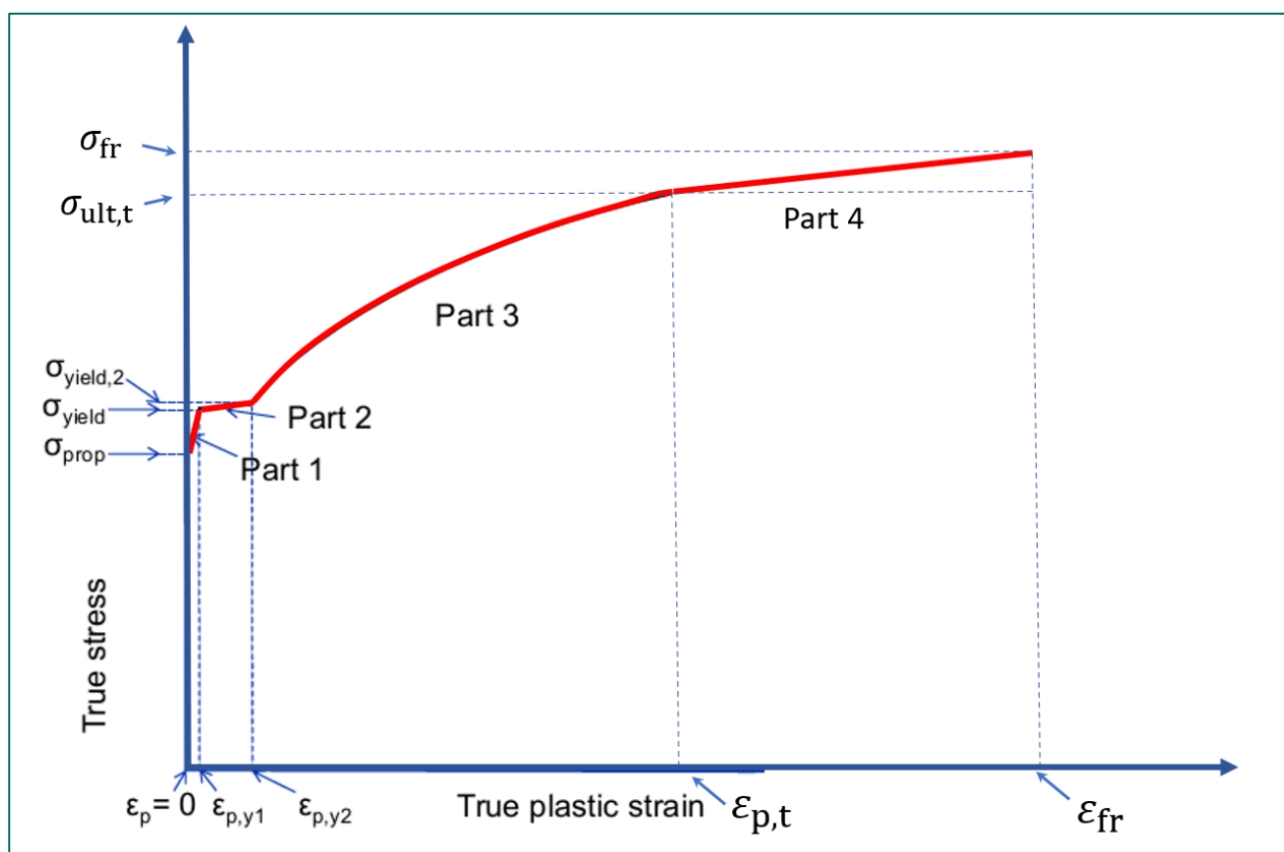


Figure 8. Proposed material stress – strain curve (red) based on DNVGL-RP-C208 and EN10025-2



## 5 Used material data

This chapter presents the stress-strain curves for the two steel grades: S235 and S355.

All curves follow a similar trend, showing an initial steep increase in stress with relatively small strain, indicating the elastic region where the material deforms but can return to its original shape. After reaching the yield point, the curves plateau, showing the plastic region, where the material undergoes permanent deformation. This is where the curves become flatter, indicating strain hardening. The stress levels for different thicknesses tend to converge and stabilize, beyond which the material shows minimal further strain increase, indicating that the material has reached a stable plastic deformation.

### 5.1. Stress-strain curve S235

Figure 9 shows a stress-strain curve for the steel grade S235, with different curves representing the material behavior for various material thickness ranges. Because the material properties for the thickness ranges  $40 < t \leq 63$  and  $63 < t \leq 100$  are identical, they share the same stress-strain curve.

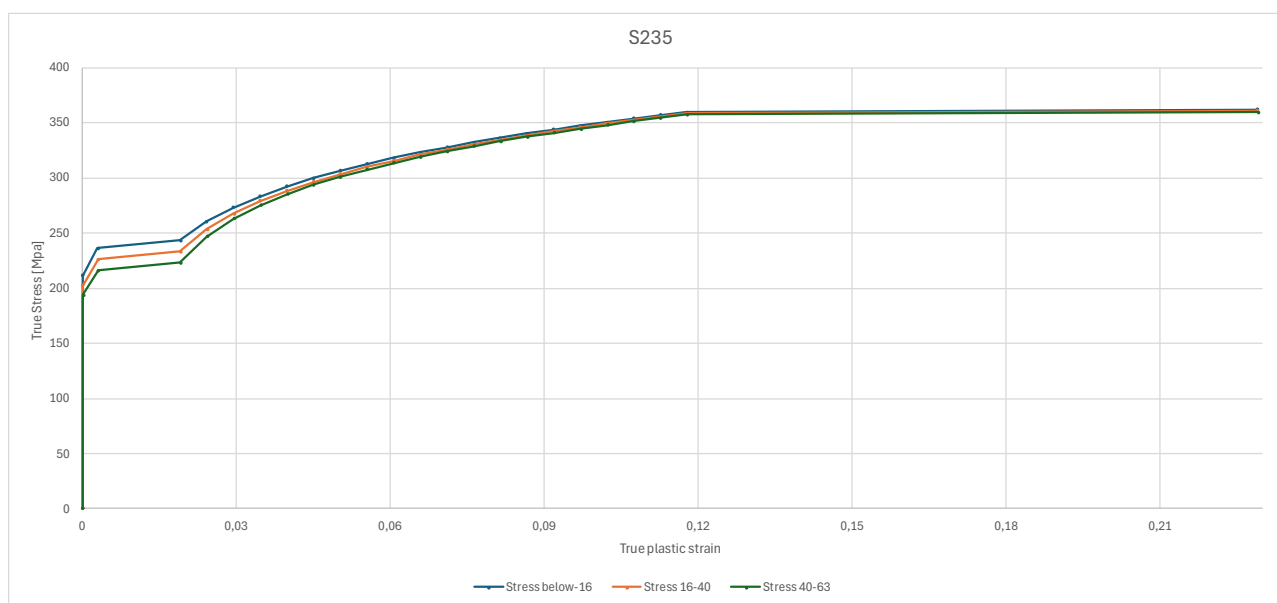


Figure 9. Stress-strain curve for steel grade S235



Table 5. Material properties of S235 steel for various thickness ranges

Parameter	Thickness t≤16 mm	Thickness 16<t≤40 mm	Thickness 40<t≤63 mm	Thickness 63<t≤100 mm
E [MPa]	210,000	210,000	210,000	210,000
$\sigma_{prop}$ [MPa]	211.7	202.7	193.7	193.7
$\epsilon_{prop}$ [-]	0.00101	0.00097	0.00092	0.00092
$\sigma_{yield}$ [MPa]	236.2	226.1	216.1	216.1
$\epsilon_{p,y1}$ [-]	0.004	0.004	0.004	0.004
$\sigma_{yield,2}$ [MPa]	243.4	233.2	223.0	223.0
$\epsilon_{p,y2}$ [-]	0.020	0.020	0.020	0.020
$\sigma_{ult,t}$ [MPa]	360	359	358	358
$\epsilon_{p,t}$ [-]	0.11779	0.11783	0.11788	0.11788
$\sigma_{fr}$ [MPa]	362.3	361.0	360.0	360.0
$\epsilon_{fr}$ [-]	0.23	0.23	0.23	0.23
$\epsilon_{fail}$ [-]	0.22899	0.22903	0.22908	0.22908
K [MPa]	520	520	520	520
n [-]	0.166	0.166	0.166	0.166
Tang. modules [MPa]	21	21	21	21

Figure 10 shows the values for S235 (for thicknesses below 16 mm) used in LS-DYNA<sup>5</sup>.

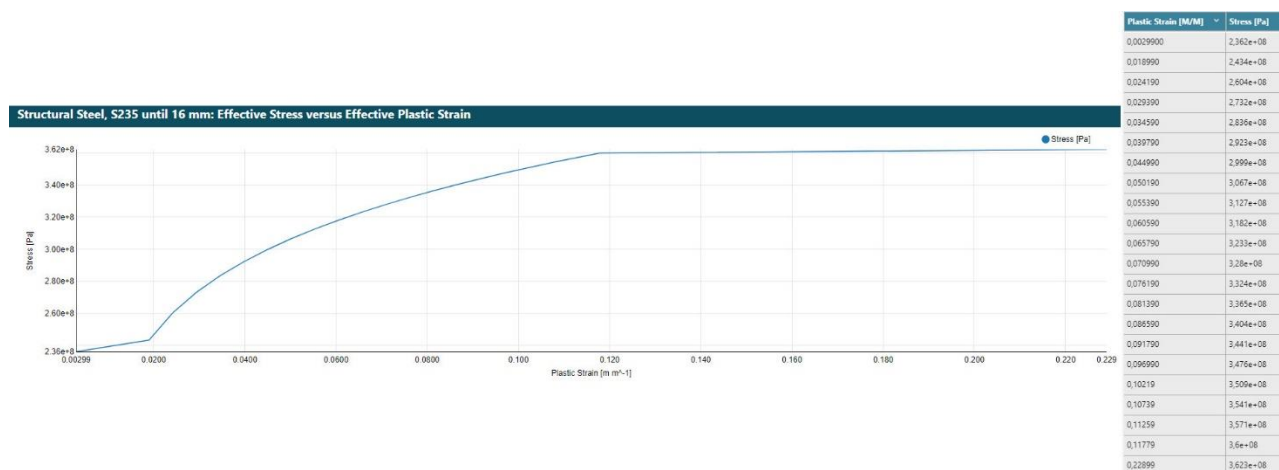


Figure 10. Material card from LS-DYNA for S235 (t ≤ 16 mm)

<sup>5</sup> For the sake of brevity, LS-DYNA details for other materials with different thicknesses are not shown in this report. However, it should be noted that the same graphs as in Figure 9 and Figure 11 are used in LS-DYNA for these materials with different thicknesses.



## 5.2. Stress-strain curve S355

Figure 11 shows a stress-strain curve for the steel grade S355, with different curves representing the material behavior for various material thickness ranges.

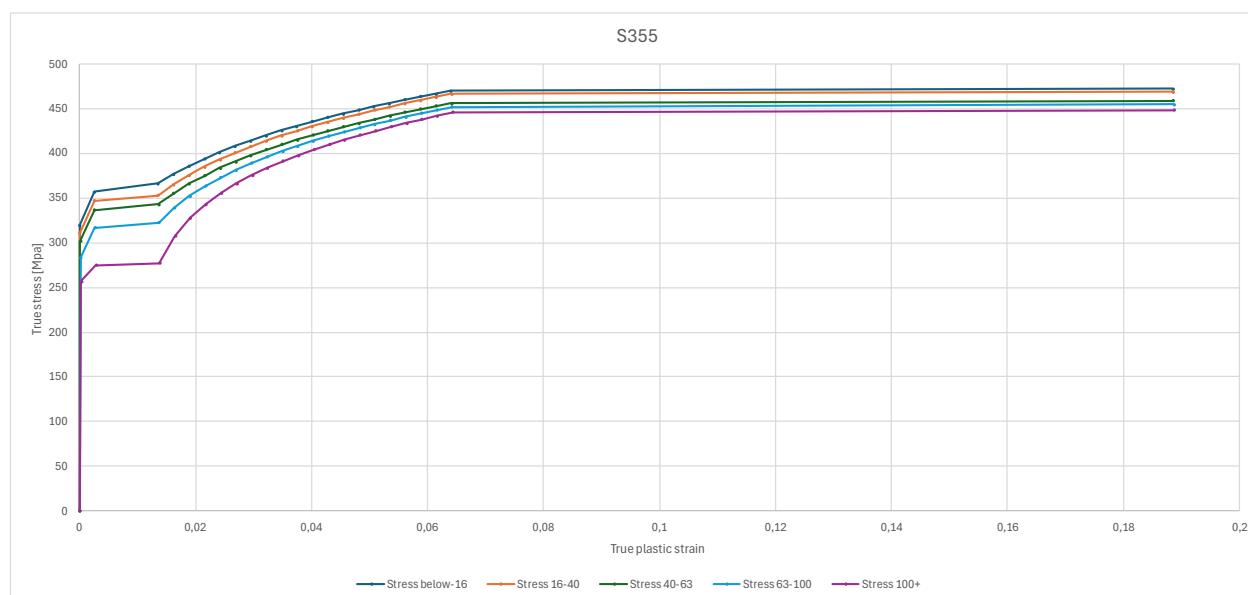


Figure 11. Stress-strain curve for steel grade S355

As mentioned in section 3.1, DNV RP-C208 does not provide material properties for S355 with a thickness above 100 mm. For S355, the elasticity modulus  $E$ ,  $\epsilon_{p,y1}$ , and  $\epsilon_{p,y2}$ , are constant values. According to EN 10025-2, table 6 (Figure 7), different yield stresses are specified for thicknesses above 100 mm. Since the thickness range extends up to 245 mm, the relevant thickness range is selected as 200–250 mm, with a yield stress of 275 MPa for this range.

The differences in  $\epsilon_{prop}$  between thicknesses below 16 mm and 16-40 mm is  $4.2857 \times 10^{-5}$ , between thicknesses below 16-40 mm and 40-63 mm is  $4.3333 \times 10^{-5}$ , between thicknesses 40-63 mm and 63-100 mm is  $8.571 \times 10^{-5}$ . For the reason that the difference in  $\epsilon_{prop}$  between the last two thickness be in the neighbour of the other thickness ranges, the calculated range for the last two thicknesses is divided by 2, which is  $4.2857 \times 10^{-5}$ . Therefore,  $\epsilon_{prop}$  for the thicknesses above 100 mm range can be calculated as  $\epsilon_{p,prop} - 3 \times \Delta \epsilon_{p,prop}$  ( $0.00135 - 3 \times 4.2857 \times 10^{-5} = 0.00122$ ).

Using  $E \times \epsilon_{prop}$  ( $210000 \times 0.00122$ ), then  $\sigma_{prop}$  is 256.2 MPa. Finally,  $\sigma_{yield,2}$  can be determined as  $\sigma_{yield} + (\epsilon_{p,y2} - \epsilon_{p,y1}) \times E/10000$ , resulting in 277.3 MPa.



Table 6. Material properties of S355 steel for various thickness ranges

Parameter	Thickness $t \leq 16$ mm	Thickness $16 < t \leq 40$ mm	Thickness $40 < t \leq 63$ mm	Thickness $63 < t \leq 100$ mm	Thickness $t > 100$ mm
E [MPa]	210,000	210,000	210,000	210,000	<b>210,000</b>
$\sigma_{prop}$ [MPa]	320.0	311.0	301.9	283.9	<b>256.2</b>
$\epsilon_{prop}$ [-]	0.00152	0.00148	0.00144	0.00135	<b>0.00122</b>
$\sigma_{yield}$ [MPa]	357.0	346.9	336.9	316.7	<b>275</b>
$\epsilon_{p,y1}$ [-]	0.004	0.004	0,004	0.004	<b>0.004</b>
$\sigma_{yield,2}$ [MPa]	366.3	353.1	342.9	322.5	<b>277.3</b>
$\epsilon_{p,y2}$ [-]	0.015	0.015	0.015	0.015	<b>0.015</b>
$\sigma_{ult,t}$ [MPa]	470	467	456	452	<b>446</b>
$\epsilon_{p,t}$ [-]	0.064	0.06406	0.06410	0.06419	<b>0.06432</b>
$\sigma_{fr}$ [MPa]	472.7	469.2	459.0	454.7	<b>448.7</b>
$\epsilon_{fr}$ [-]	0.19	0.19	0.19	0.19	<b>0.19</b>
$\epsilon_{fail}$ [-]	0.188	0.18852	0.18856	0.18865	<b>0.18878</b>
K [MPa]	740	740	725	725	<b>725</b>
n	0.166	0.166	0.166	0.166	<b>0.166</b>
Tang modules [MPa]	21	21	21	21	<b>21</b>





## E. R105-DP2.3 Memo Soil Material Model



## Memo

To: RWS WVL  
From: Iv  
Author: GVA; MNA; YYA  
Checked by: YYA  
Approved by: WLA  
Date: 30 December 2024  
Document no.: INFR240476-R105-DP2.3  
Reference: INFR240476 RWS WVL  
Subject: Memo Soil Material Model  
Revision: 4

---



## TABLE OF CONTENTS

---

<b>1</b>	<b>Introduction</b>	<b>3</b>
<b>2</b>	<b>Unidirectional (2D) to Multi-directional (3D) P-y curves</b>	<b>5</b>
2.1.	Unidirectional (2D) vs. Multi-directional (3D)	5
2.2.	Derivation of Multi-directional P-y Curves	6
<b>3</b>	<b>Validation multi-directional P-y curves</b>	<b>10</b>
3.1.	Unidirectional beam model and Multidirectional shell model	10
3.2.	General boundary conditions of validation models	12
3.3.	Results model validation	13
3.3.1.	Lateral displacement $u_y$ and lateral reaction force P	13
3.3.2.	Modal Analysis	14
<b>4</b>	<b>Dynamic effect of P-y curves</b>	<b>16</b>
<b>5</b>	<b>Summary and conclusion</b>	<b>18</b>
<b>6</b>	<b>Approach of generating multi-directional P-y curves</b>	<b>19</b>
6.1.	Provided unidirectional P-y curves	19
6.2.	Applied multi-directional model of P-y curves	20



# 1 Introduction

---

This memo describes the modelling approach for the soil-structure interaction between the wind turbine monopile and the soil, based on the provided P-y curves (ref. [4]) by the client of this project (RWS - Rijkswaterstaat). This will be used as one of the boundary conditions of the monopile in the 3D FEM ship impact simulations for this project.

P-y curves represent the relationship between lateral soil resistance (P) and lateral deflection (y) and are commonly used to model the nonlinear behaviour of soil in response to lateral loading. These curves are crucial for capturing the soil's response to lateral forces acting on the monopile, ensuring realistic boundary conditions in the simulation. In principle, there are static and dynamic P-y curves. Depending on the loading conditions, the soil will behave differently. This behaviour is also reflected in the P-y curves, resulting in either a static or a dynamic P-y curve. This will be further explained in Chapter 4.

The provided P-y curves have the following characteristics:

- Unidirectional;
- Static;
- Data specific from the provided monopile.

These P-y curves provide basic information of the soil-monopile interaction, but for 3D FEM ship impact analyses, more aspects need to be taken into account.

First of all, the unidirectional P-y curves are not suitable for event like ship impact and/or accompanying wind/wave loads, since these loads are far from unidirectional. In this case, it is necessary to convert the provided unidirectional P-y curves to multi-directional P-y curves, the approach, based on ref. [5], and resultant multi-directional P-y curves are elaborated in Chapter 2. The generated multi-directional model with regards to the unidirectional model is validated in Chapter 3.

Secondly, since the 3D FEM ship impact is a dynamic analysis, the soil reacts differently than in a static analysis. In Chapter 4, the approach for incorporating the dynamic effects into the model is explained.

The conclusion based on above mentioned investigations is given in Chapter 5. Chapter 6 is the detailed information of the applied approach to generate multi-directional P-y curves and the results of the validation models. This chapter is provided as appendix to the memo.

Because soil-structure interaction is a complex behaviour and the focus of this study is on the ship rather than the monopile, some aspects that do not influence the impact simulations are assumed to be included in the provided P-y curves and will thus not be taken into account. This approach simplifies the simulations by using limited parameters, avoids misinterpretation of the provided P-y curves, and aligns with the previous study.



Standards and reference used in this memo are provided in Table 1.

Table 1. Used standards and references

Ref.	Document no.	Title	Date
1.	DNV-OS-A101	Safety principles and arrangements	March 2023
2.	DNV-RP-C204	Structural design against accidental loads.	September 2019
3.	DNV-RP-C208	Determination of structural capacity by non-linear finite element analysis methods.	October 2020
4.	Bijlage K Annex 01-05 081R030M010-App-A	Properties Windfarm 2 - Foundation 'WD 34.6m PD 28.75m' P-y curves WindFarm 2	2024
5.	<a href="https://doi/10.1680/jgeot.18.P.297">https://doi/10.1680/jgeot.18.P.297</a>	Pile response to multi-directional lateral loading using P-y curves approach, Géotechnique 71, No. 4, 288–298, Lovera, A. et al. (2021).	2021



## 2 Unidirectional (2D) to Multi-directional (3D) P-y curves

The literature (ref. [5]) addresses the challenge of modelling the behaviour of piles subjected to multi-directional lateral loads, which is particularly relevant for offshore structures like wind turbines. Traditionally, pile design under lateral loads is based on unidirectional loading, which doesn't fully capture the complexities of real-world conditions where loads vary in directions. The authors of ref. [5] propose an extension of the widely used P-y curve method to account for multi-directional loading, maintaining the simplicity of the original approach while improving its accuracy for more complex scenarios.

### 2.1. Unidirectional (2D) vs. Multi-directional (3D)

**Unidirectional Model:** The P-y curve method models soil resistance to lateral pile movement as a series of springs along the pile's length, with each spring representing the lateral soil reaction at a specific depth. This method typically assumes that loads are only allowed to act in the spring direction (Figure 1 [a]).

**Multi-directional Model:** The proposed model extends this concept by introducing multiple springs arranged around the pile's perimeter at each depth, allowing it to capture the effects of lateral loads from different directions. These non-linear compression only springs in this model are activated based on the direction of the load, and their responses are combined to predict the overall pile behaviour (Figure 1 [b]).

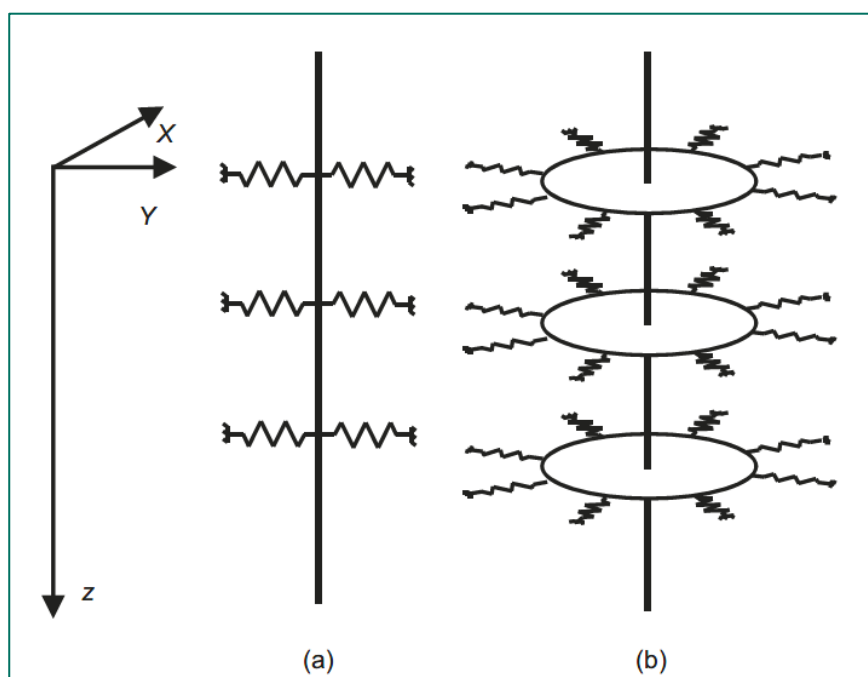


Figure 1. Unidirectional vs multi-directional models (ref. [5])



## 2.2. Derivation of Multi-directional P-y Curves

In ref. [5], methods to convert a unidirectional P-y curve into a multi-directional one are provided. This involves adjusting the spring stiffness to account for the distribution of load among the multiple springs around the pile. Several types of P-y curves (linear, elasto-plastic, power law, hyperbolic tangent and hyperbolic) are provided with explicit formulas for adapting these curves to a multi-directional context.

The provided P-y data for Windfarm 2 contain 59 different soil layers with penetration depths ranging -34.6 to -63.35 m LAT , with one P-y curve per layer. Figure 2 illustrates P-y data for the first soil layer at a depth of -34.6 m LAT, extending up to 2 meter.

Note: the provided P-y curve continues to 15 meters displacement, of which the gradient after 2 meters is almost zero, which means the curve continues almost horizontally when the soil reaches its ultimate capacity  $P_u$ .

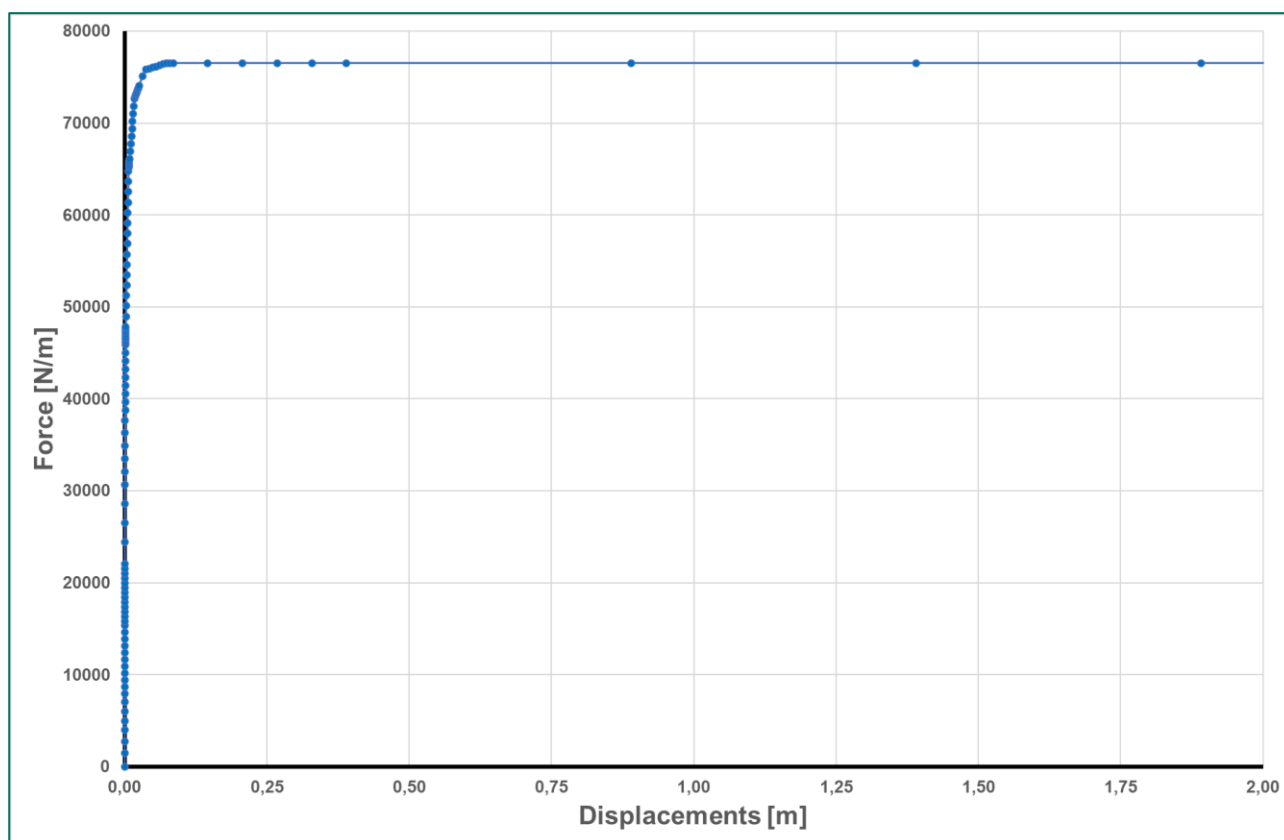


Figure 2. P-y curve of the first soil layer -34.6 m LAT up to y = 2 m



The data in Figure 2 show a steep increase in stiffness in the initial part until it reaches the ultimate limit. This happens even around a displacement of 0.1 m as shown in Figure 3.

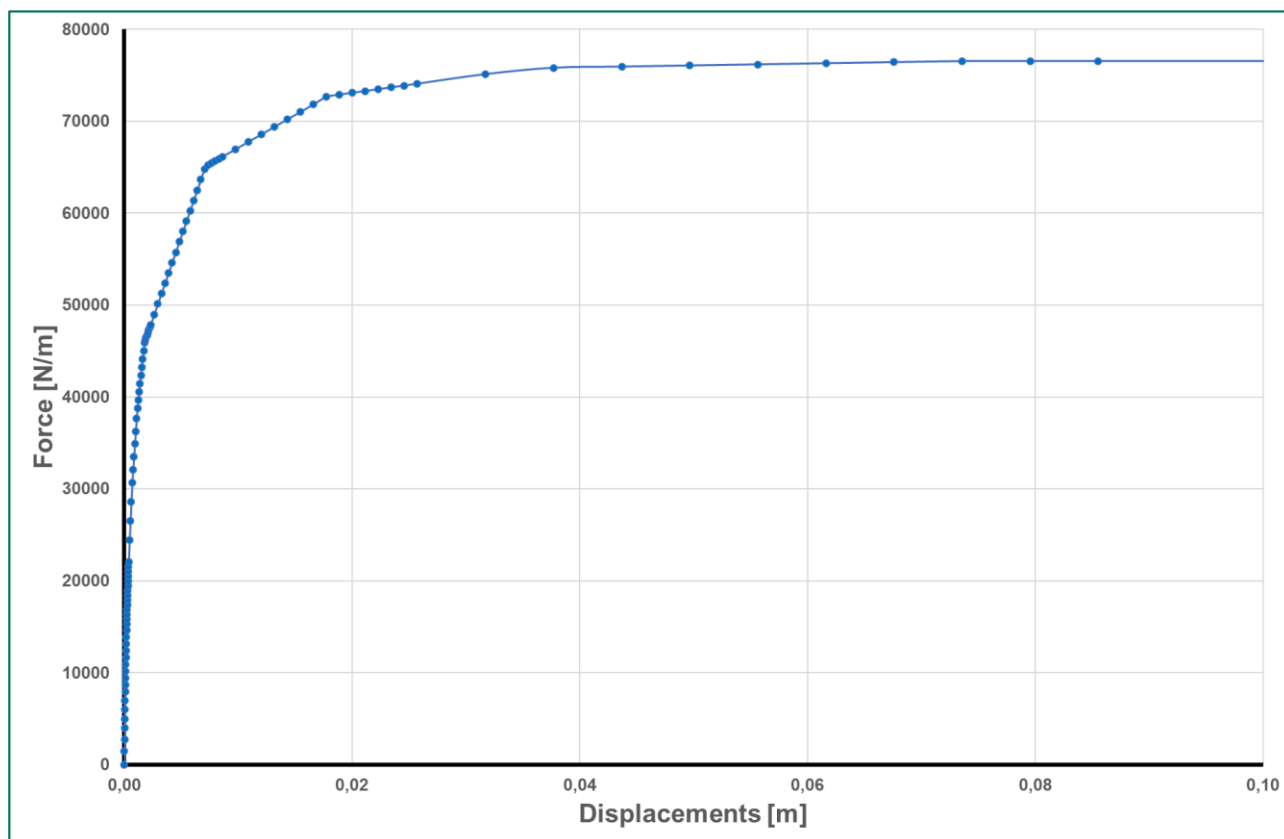


Figure 3. P-y curve of the first soil layer -34.6 [m] zoomed in to  $y = 0.1$  m





Depending on the P-y data (the relationship between the initial stiffness  $k$  and the ultimate reaction  $P_u$ ), several types of functions can be used to convert the unidirectional P-y curves to multi-directional P-y curves. By analysing the provided P-y curves, the hyperbolic function appears to be the best fit for our case. In Figure 4, a comparison is made between the original provided unidirectional curve (blue) and the curve fit (red) P-y curve with hyperbolic function for the first soil layer at -34.6 m LAT. The small difference shown in Figure 4 is due to the perfect hyperbolic curve compared to the point-data of the provided P-y data.

A detailed description of approach used for generating the multi-directional P-y curves using hyperbolic function is referred to chapter 6. The quality of the curve fit is checked using the RMSE (Root Mean Square Error), which is 0.0284 [-] for this soil layer. The RMSE is calculated over all the data points. As seen in the Figure 4, the difference is limited to a small part of the figure, which has no significant influence on the RMSE.

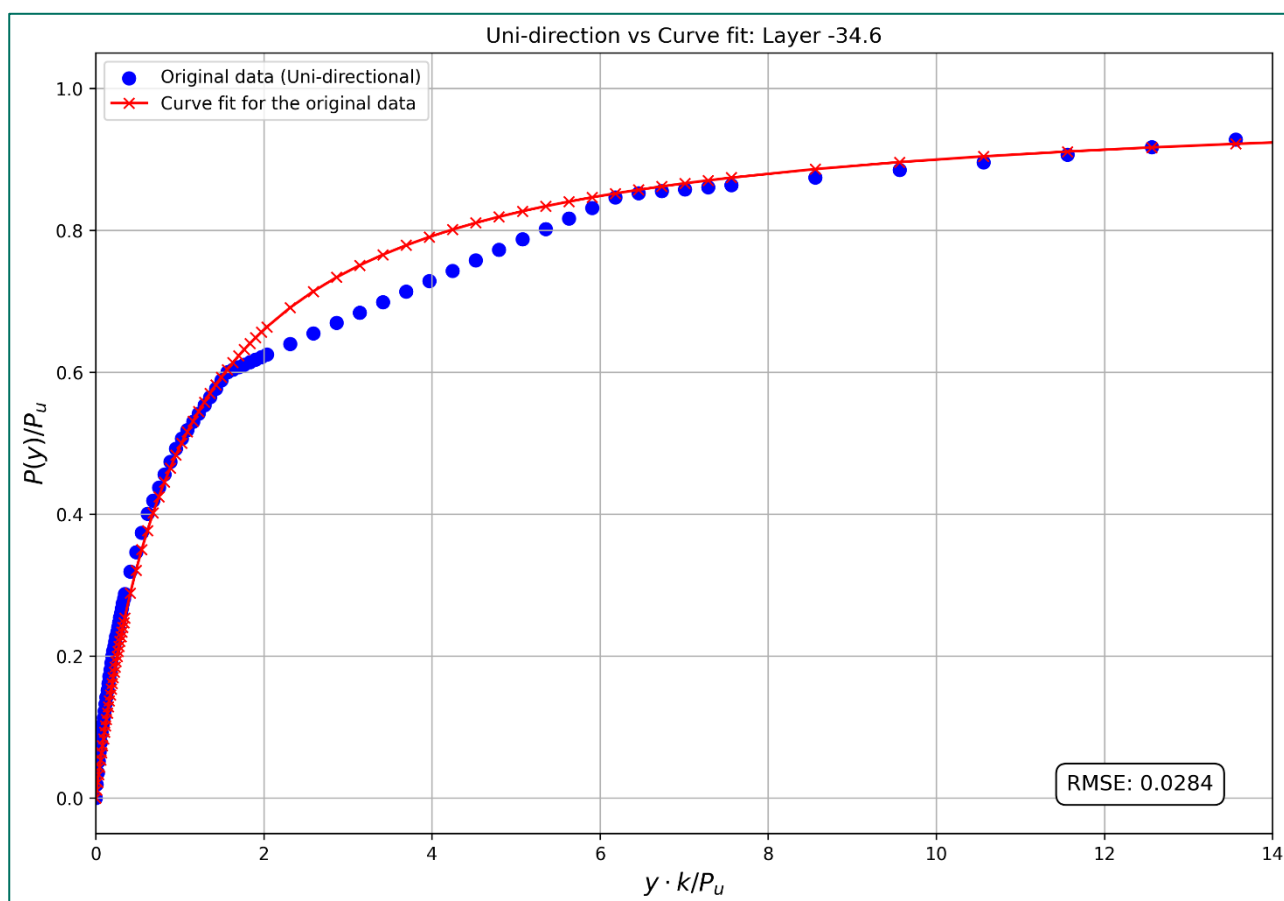


Figure 4. Unidirectional vs curve fit with hyperbolic function



Figure 5 shows the P-y curves for unidirectional curve fit and multi-directional cases for three different N (number of spring per layer) at -34.6 m LAT. It can be seen that it matches perfectly according to the hyperbolic P-y curves in ref. [5], as shown in Figure 6 below.

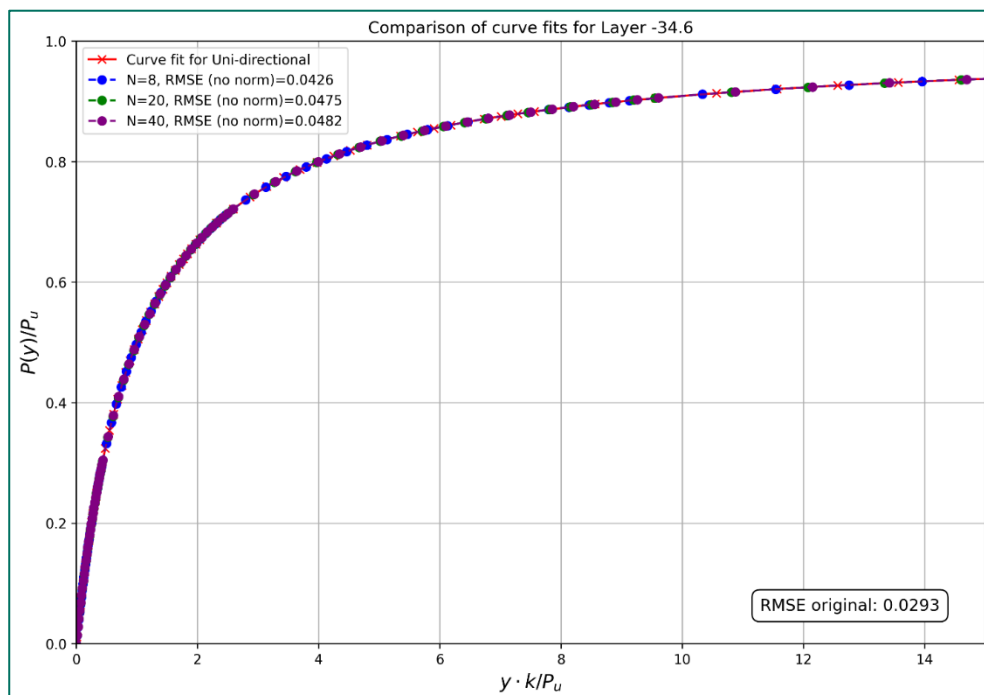


Figure 5. Unidirectional curve fit vs multi-directional with different numbers of springs

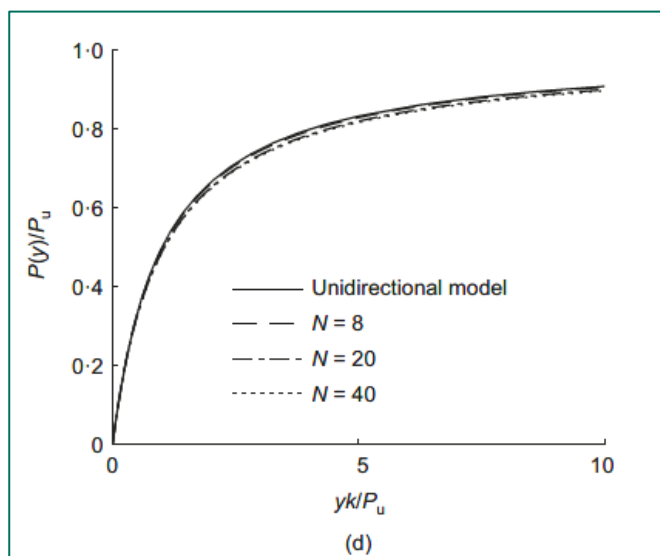


Figure 6. Hyperbolic P-y curves of unidirectional P-y curve with resultant reaction of the multi-directional model for various values of N: Fig. 4(d) of ref. [5]



## 3 Validation multi-directional P-y curves

---

### 3.1. Unidirectional beam model and Multidirectional shell model

To validate the multi-directional P-y curves, static analysis with a lateral load on top of the model and modal analysis is performed on both models with beam elements using unidirectional P-y curves and shell elements using multi-directional P-y curves. Modal analysis is a technique used in engineering to determine the natural frequencies, mode shapes, and damping characteristics of a structure or system. These natural frequencies are the specific frequencies at which the structure tends to vibrate when subjected to an external force or disturbance. By understanding these properties, engineers can identify potential resonance issues, improve structural performance, and design systems to avoid excessive vibrations under operating conditions.



A monopile model is set up for validation, see Figure 7. This model is simplified in dimensions compared to the specific monopile of this project. The cross-section of the beam is the same as the properties of the shell model. The p-y curves make the spring nonlinear because they are based on a hyperbolic function. Therefore, the soil is modelled as non-linear compression-only springs for both unidirectional and multi-directional P-y curves. 'Compression-only' means that the spring is only activated under compression and will follow the p-y curve in that region. To evenly distribute 40 non-linear springs (15 m in length) along the perimeter of the cross-section of the shell model, the mesh size is set to 0.5 m for the defined diameter of the pile. For the beam model, since the springs are non-linear compression only springs, 2 springs are modelled in the beam model at each soil layer. [Because the provide p-y curves are delivered in N/m and the soil layers are provided per 0.5m the soil force in the p-y curve data is divided by 2. Also the mesh nodes locations a defined in such a way that the soil spring are located in the centre of each layer.](#)

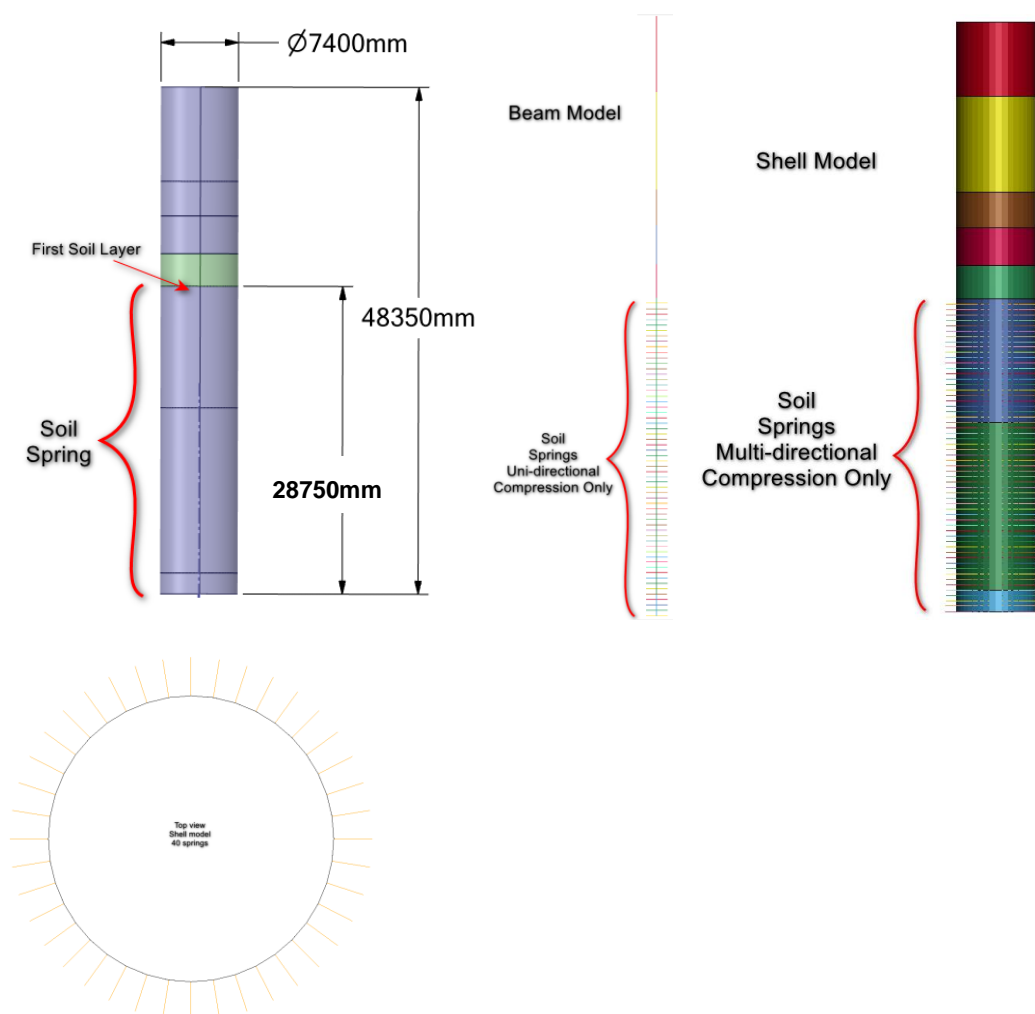


Figure 7. Overview model with beam elements and with shell elements

### 3.2. General boundary conditions of validation models

A displacement of 2000 mm is applied on top of the foundations, while the model is constrained at the bottom in axial direction, see Figure 8. For shell model, remote points are applied in the region where non-linear springs are applied, so that the effect of local deformation of the shell element due to the reaction force can be eliminated.

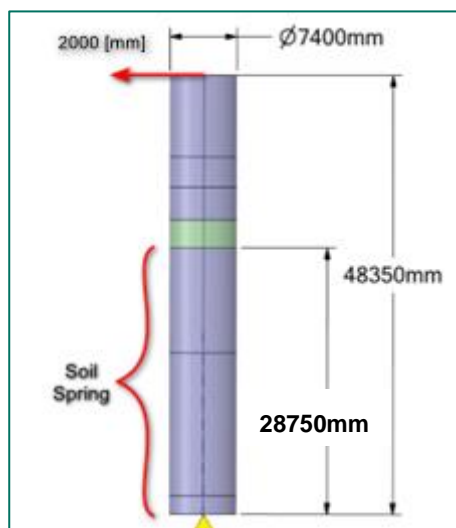


Figure 8. Applied displacement and general boundary conditions

The resultant lateral deformations  $U_y$  of both models are shown in Figure 9.

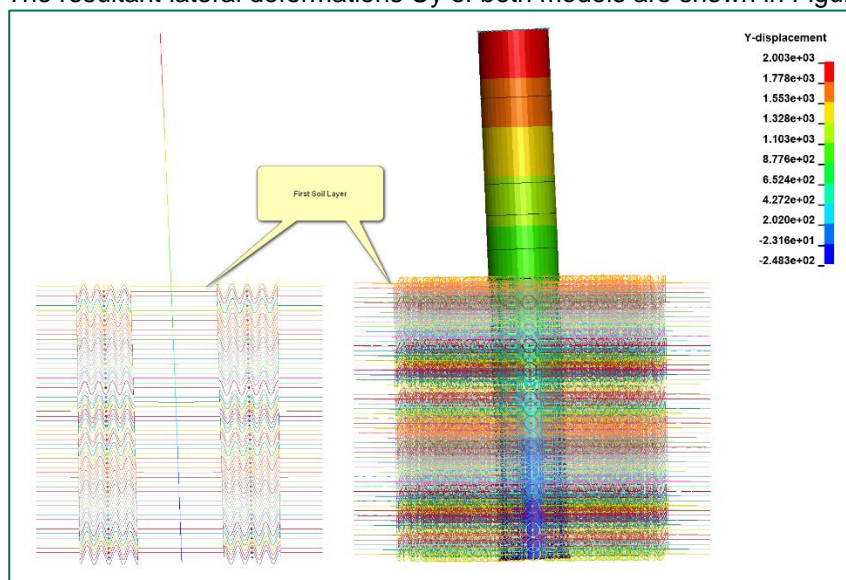


Figure 9. Horizontal deformation  $U_y$  [mm] - beam and shell model



### 3.3. Results model validation

The following sections provide the lateral displacement  $U_y$  and reaction force  $P$  of the springs for both the beam and shell models, of the first soil layer at -34.6 m LAT. Additionally, a modal analysis has been performed to validate the response of both models.

#### 3.3.1. Lateral displacement $u_y$ and lateral reaction force $P$

As can be seen in Figure 10, the difference is small enough that the multi-directional shell model is validated to exhibit the same force-displacement behaviour as the unidirectional beam model. In the first (left) part of Figure 10, the results are in good agreement with each other. However, towards the end, there is a small difference. This difference is due to the fact that, in the shell model, the forces tend to cause deformation in both horizontal directions (X and Y). In contrast, the beam cross-section only deforms in the Y direction.

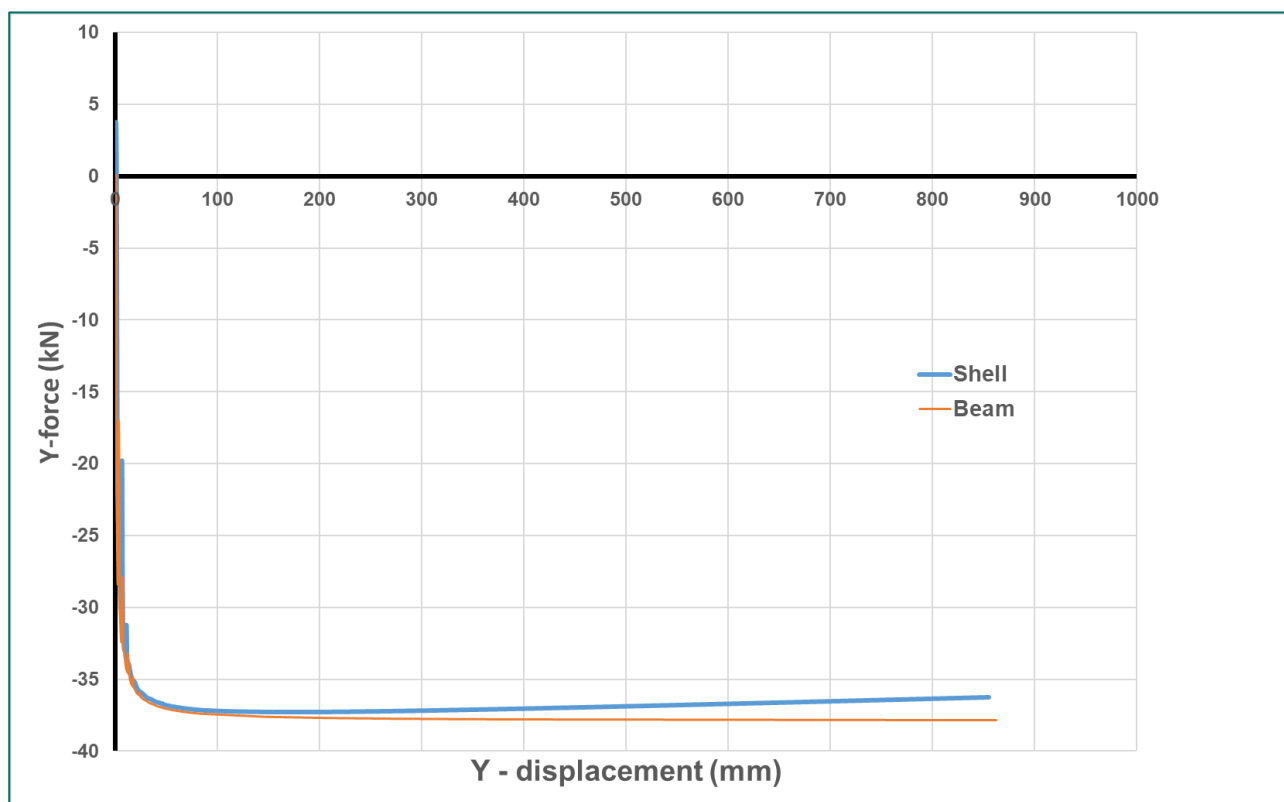


Figure 10. Reaction forces  $P_y$  over lateral displacement  $u_y$  in the first soil layer of beam and shell model



### 3.3.2. Modal Analysis

To validate the response of both models, modal analysis is performed with the same boundary conditions, expect for the lateral displacement on the top of the models.

The resultant natural frequency of first 3 modes of the unidirectional beam model and the multidirectional shell model are shown in Figure 11 to Figure 13, and the difference in Table 2.

The small difference in the frequency of the first mode likely occurs because the first mode typically corresponds to the overall structural deformation as bending. Both beam and shell models capture these behaviours similarly, as the first mode is often more dependent on global stiffness and mass distribution, which are comparable in both models. The shell model reflects more accurate behaviour of the structure in 3D which often results in a lower frequency. In the second mode, the frequencies are nearly identical, since it is hardly affected by the soil springs. The relative larger difference in the frequency of the third mode can be attributed to the fact that higher modes often involve more complex deformation patterns. Shell elements are better suited to capturing local deformation or higher-order stress states, such as torsion or local bending, which may not be as accurately represented by the simpler beam model. This results in the larger difference in frequency for the third mode, that the beam model's inability to fully capture the detailed local deformations and stresses that the shell model accounts for in higher modes.

Table 2. Natural frequency of the first 3 modes of beam and shell model

Frequency [Hz]	Unidirectional beam model	Multi-directional shell model	Difference [%]
1 <sup>st</sup> mode	15	14	-7
2 <sup>nd</sup> mode	23	23	0
3 <sup>rd</sup> mode	37	33	-11

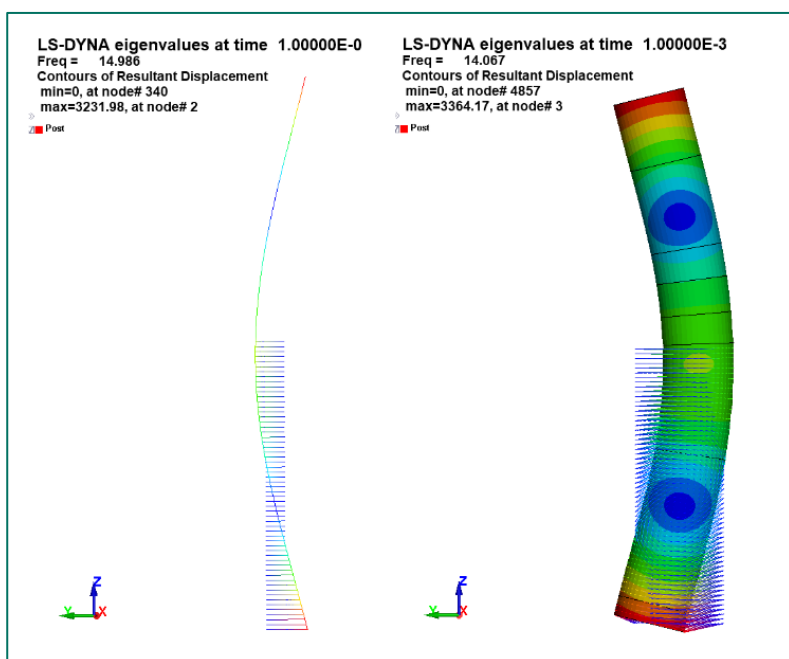


Figure 11. First mode frequency for the beam and shell model

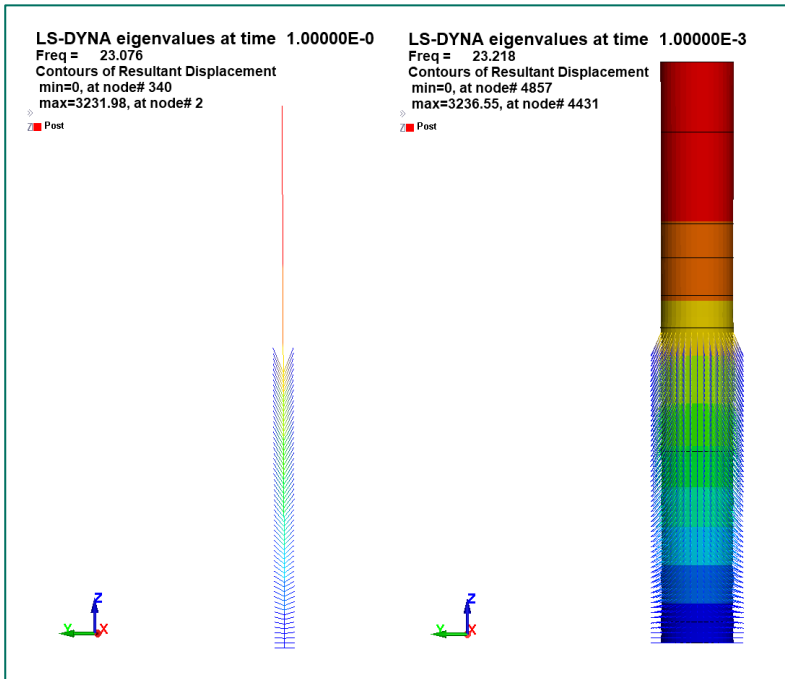


Figure 12. Second mode frequency for the beam and shell model

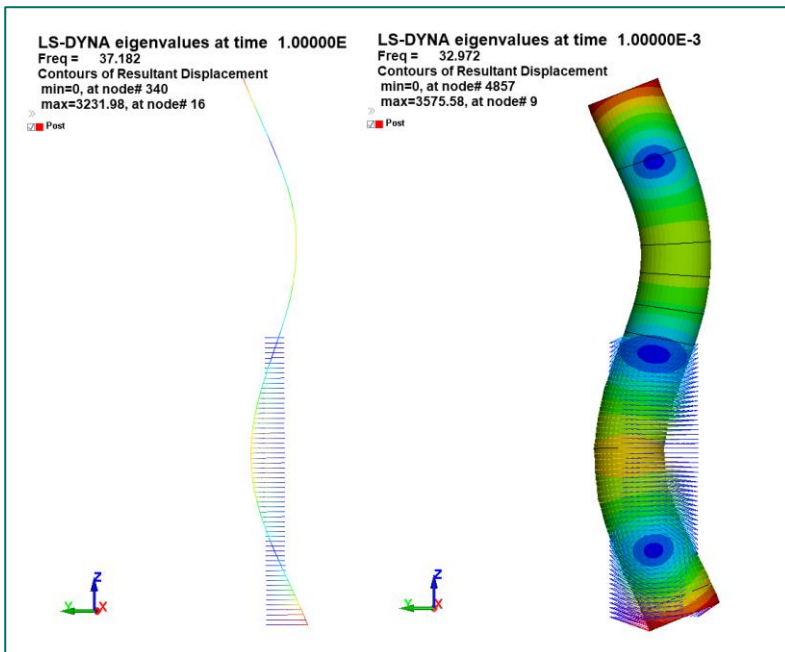


Figure 13. Third mode frequency for the beam and shell model





## 4 Dynamic effect of P-y curves

Since the provided P-y curves in ref. [4] are static ones, a dynamic amplification factor will be applied to include the dynamic effect. Various studies show different approaches to define the amplification factor, the most common ones are:

- 1) This dynamic amplification factor can be added on the static reaction force  $P_{\text{stat}}$  based on the velocity of the element by LS-DYNA (Figure 14), or
- 2) the factor can be added on the elastic modulus (i.e. initial stiffness  $K_{\text{ini}}$ ) and the ultimate soil reaction  $P_u$  of the static P-y curves. (Figure 15)

For the first approach, the method described in LS-DYNA (KEYWORD USER'S MANUAL - VOLUME I \*SECTION\_DISCRETE - Remark 2) allows to convert the static p-y curve to a dynamic p-y curve via a velocity dependent amplification factor. This method is more realistic but will not be used in this project because the parameter  $k_d$  is lacking of reference.

**Forces and Amplification Factors.** If  $k_d$  is nonzero, the forces computed from the spring elements are assumed to be the static values and are scaled by an amplification factor to obtain the dynamic value:

$$F_{\text{dynamic}} = \left(1 + k_d \frac{V}{V_0}\right) F_{\text{static}}$$

where

$V$  = absolute value of the relative velocity between the nodes.

$V_0$  = dynamic test velocity.

For example, if it is known that a component shows a dynamic crush force at 15 m/s equal to 2.5 times the static crush force, use  $k_d = 1.5$  and  $V_0 = 15$ .

Figure 14. Dynamic amplification factor on static reaction forces proposed by LS-DYNA

Other research has resulted in applying an amplification factor of 2.5 to convert the static p-y curve to a dynamic p-y curve. The amplification factor will be applied to the initial stiffness  $K_{\text{ini}}$  and the ultimate soil reaction  $P_u$  of the hyperbolic p-y curve. The factor 2.5 is chosen because standard amplifications factors for this conversion range from 2 until 3. See below reference from CROW HANDBOEK ZANDBOEK, page 443.

### 6.4.3.4 Globale correlatie van statische en dynamische elasticiteitsmodulus

De elasticiteitsmodulus ontleend aan statische beproevingsmethoden zoals de statische plaatbelastingsproef of de Benkelman-balk ligt veel lager dan de in de vorige paragraaf genoemde dynamische elasticiteitsmodulus. Janse [1982] noemt in dat verband:

$$E_{\text{dyn}} \approx (2 - 3) E_{\text{stat}}$$

Figure 15. Relation between dynamic and static elastic modulus of the soil (CROW handbook zandboek, page 443)



In below Figure 16 an overview of the static and the dynamic P-y curve with an amplification factor of 2.5 for the first soil layer per spring is shown. The increased stiffness of dynamic P-y curves ensure the realistic behaviour of the monopile during the collision simulation, so that the damage of the colliding ship will not be under estimated. Additionally, the amplification factor applied to the p-y curves will make the monopile behave stiffer, potentially leading to conservative results for the ship.

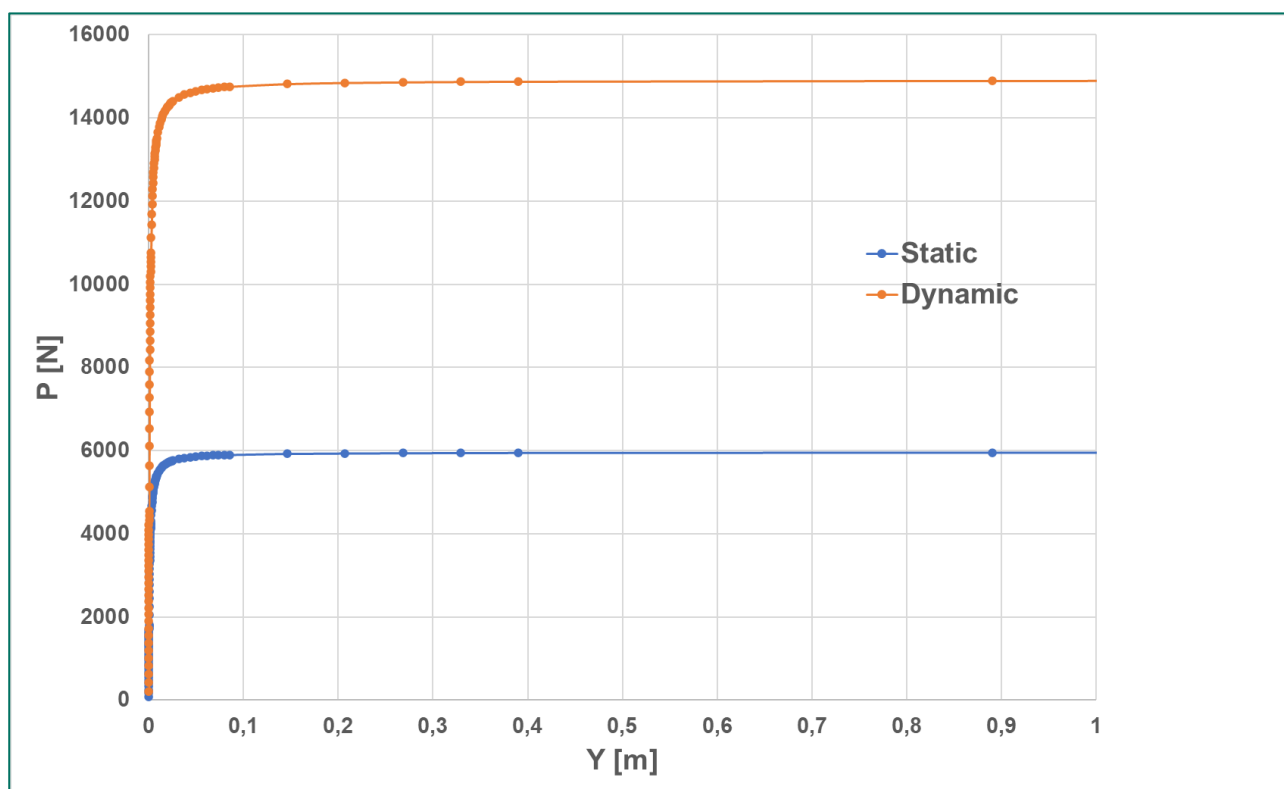


Figure 16. Static vs. dynamic P-y curve of the 1<sup>st</sup> soil layer (up to 1 m) -34.6 [m]



## 5 Summary and conclusion

---

This memo outlines the methodology for simulating soil-structure interaction during ship impacts on monopile foundations using non-linear spring models based on P-y curves from Windfarm 2 data. The original unidirectional P-y curves can only be used in a 2D collision simulation. Since the collision simulation that will be performed is in 3D, these p-y curves are not suitable. Therefore, they need to be converted into multi-directional curves to reflect the complex behaviour of ship impacts.

The approach, based on ref. [5], extends the traditional unidirectional P-y method by adding springs around the pile's perimeter. Therefore, the P-y functions of the multi-directional model have the same mathematical expressions as for the unidirectional case. In this way, impact and loads from different directions can be considered in one simple 3D shell model. The generated multi-directional P-y curves are validated through static lateral loading and modal analysis between a unidirectional beam model and a multi-directional shell model.

Results from simulations using the multi-directional P-y curves closely align with the traditional unidirectional approach. This conversion allows for a more accurate representation of reaction of the monopile during ship impacts. Furthermore, a dynamic amplification factor of 2.5 is applied to the provided static P-y curves so that the dynamic reaction of the soil-structure interaction can also be taken into account in the impact simulations.

Other aspects that have influence on the P-y curves, such as the influence of the pile diameter, are assumed to be included in the provided data. No further adjustment will be performed for this project to ensure compliance with the assumptions of the previous study.

By using a dynamic amplification factor for the soil (P-y curve), the support structure will behave stiffer, making the results more conservative for the ship. In this way, simulations can be simplified with limited parameters, while the damage of the colliding ship, focus of this project, will not be underestimated.



## 6 Approach of generating multi-directional P-y curves

### 6.1. Provided unidirectional P-y curves

The original unidirectional P-y data of all 59 layers are provided in an Excel spreadsheet (ref. [4]). In Figure 17, they are plotted in one chart as P-y curves.

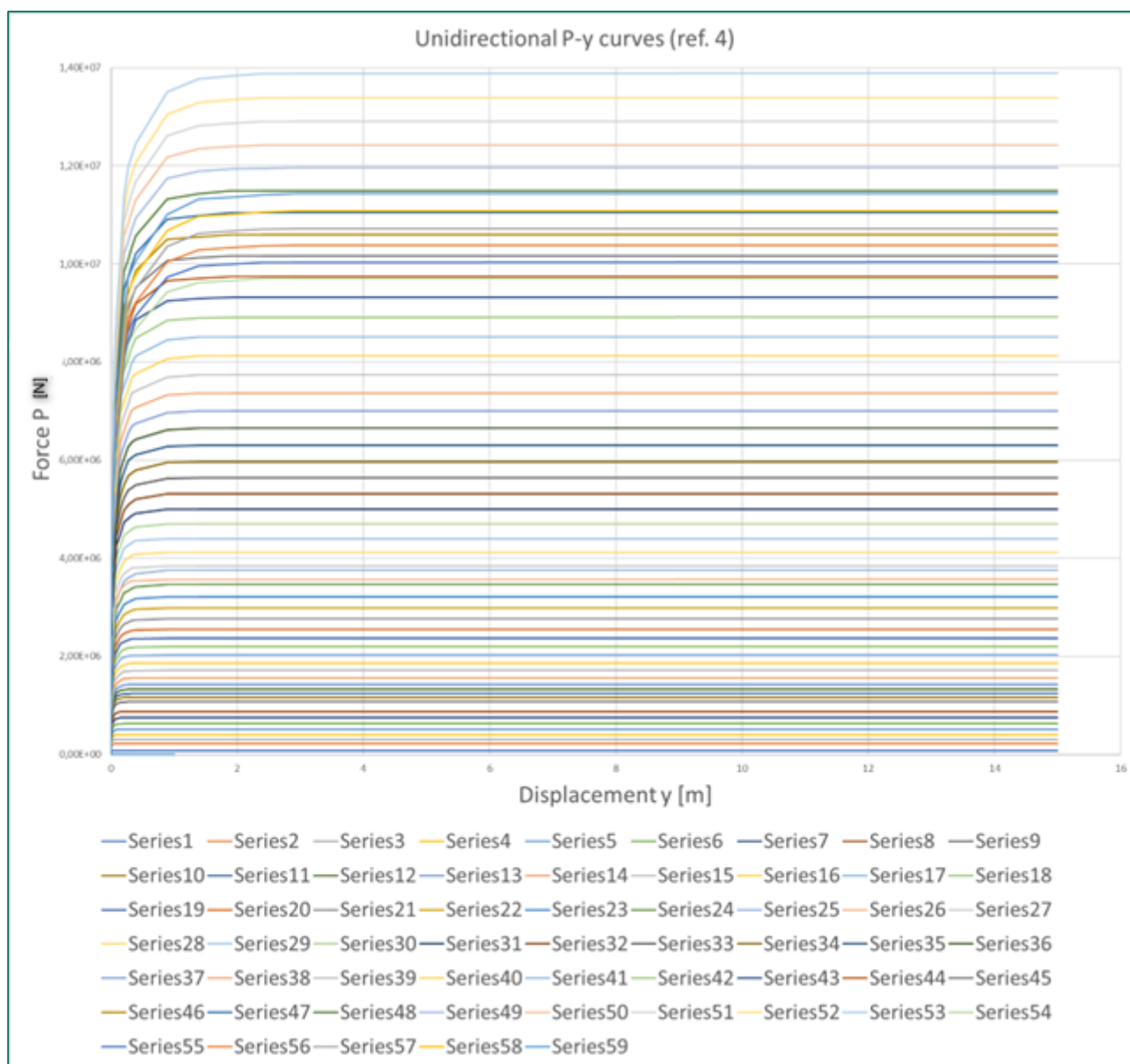


Figure 17 Chart of provided unidirectional P-y curves – in total 59 layers (ref. [4])



## 6.2. Applied multi-directional model of P-y curves

Based on the provided P-y data, the hyperbolic function (below (14a) from ref. [5]) appears to be the best fit among all provided different types in ref. [5], in which  $P_u$  is the ultimate reaction and  $k$  is the initial stiffness of the unidirectional P-y curve. The comparison between the curve fit and provided data of the first soil layer at -34.6 m LAT (series 1 in Figure 17) is shown below.

$$P(y) = \frac{y}{1/k + y/P_u} \quad (14a)$$

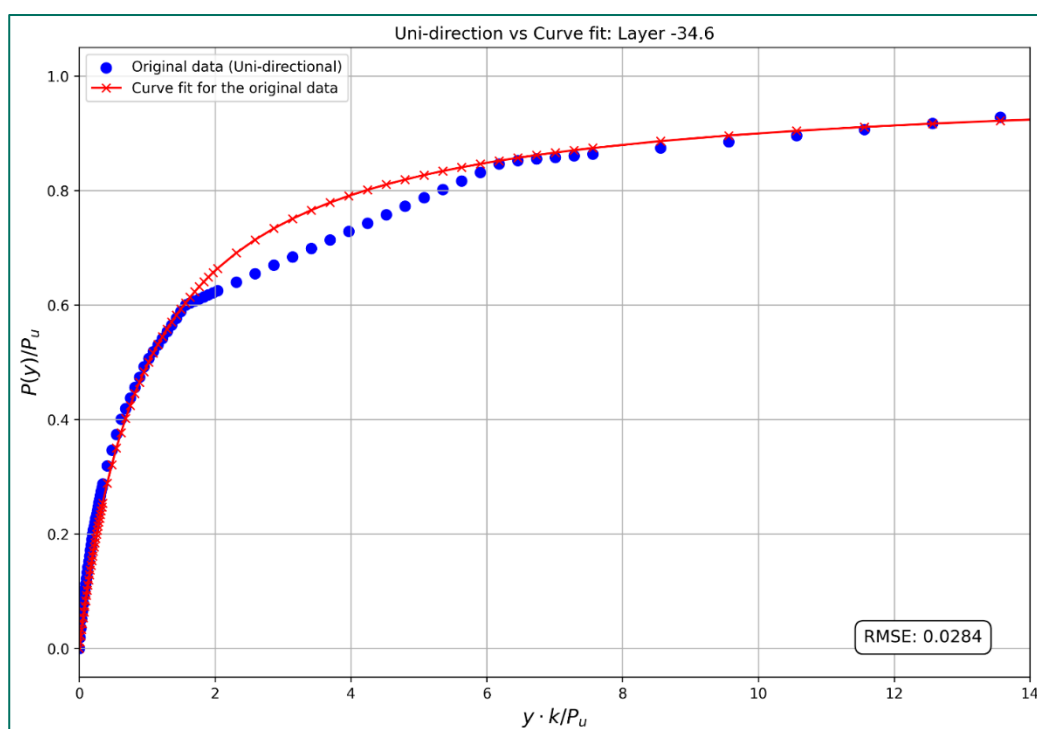


Figure 18. Unidirectional vs curve fit with hyperbolic function

The relation between the unidirectional and multi-directional models on the ultimate reaction and initial stiffness is as following (formula (7) and (9) from ref. 5),

$$\tilde{k} = \frac{4k}{N} \quad (7)$$

$$\tilde{P}_u = \tan\left(\frac{\pi}{N}\right) P_u \quad (9)$$

in which  $N$  = number of springs per layer in multi-directional model.

The multi-directional P-y curves can be determined as (formula (14b) from ref. 5):

$$\tilde{P}(y) = \frac{y}{1/\tilde{k} + y/\tilde{P}_u} \quad (14b)$$



Figure 19 shows the derived multi-directional P-y curve for the first layer at -34.6 m LAT, up to 1 meter, with different number of springs in the perimeter of the monopile.

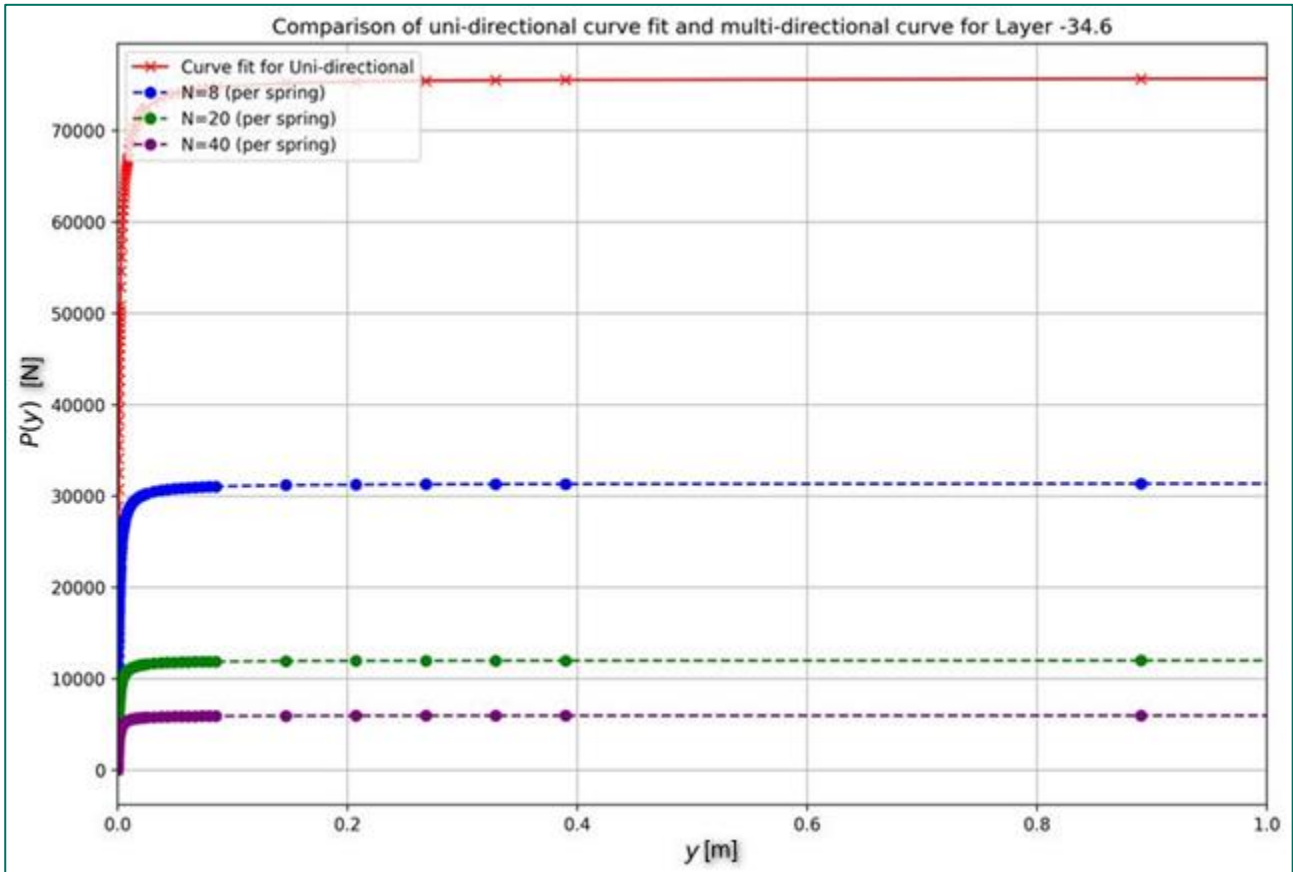


Figure 19. Multi-directional P-y curves (up to 1m) of different number of springs in the perimeter of the monopile at -34.6 m LAT



## F. R106-DP2.3 Memo FE Modelling Approach



## Memo

To: RWS WVL  
From: Iv  
Author: GVA; MNA  
Checked by: YYA  
Approved by: WLA  
Date: 10 February 2025  
Reference: INFR240476-RWS WVL  
Document no.: INFR240476-R106-DP2/3  
Subject: Memo FE Modelling Approach  
Revision: 3

---





# TABLE OF CONTENTS

---

<b>1</b>	<b>Introduction</b>	<b>3</b>
<b>2</b>	<b>Model Overview</b>	<b>5</b>
2.1.	Cross-section selection	5
2.2.	Modelling plate stiffeners	6
2.3.	Boundary and initial conditions	8
2.4.	Analysis settings	9
<b>3</b>	<b>Comparison of the results</b>	<b>11</b>
3.1.	Energy analysis	11
3.2.	Deformation analysis	13
3.3.	Inside collision zone	15
3.3.1.	Effective plastic strain	15
3.3.2.	Influence of mesh element size	18
3.4.	Out of collision zone	19
3.4.1.	Von-Mises stress	19
3.4.2.	Elastic deformation	21
3.5.	Influence of integration points	22
3.5.1.	Inside collision zone	22
3.5.2.	Out of collision zone	22
3.6.	Mesh size combination	23
<b>4</b>	<b>Conclusion</b>	<b>25</b>



# 1 Introduction

---

Offshore wind farms are rapidly expanding in the North Sea. This growth, combined with high maritime traffic in the region, has created increasingly crowded conditions. As the number of wind turbines and associated infrastructure increases, ensuring the safety of vessels navigating these busy waters and maintaining the structural integrity of the wind farms has become a critical concern.

To assess the damage to ships and wind turbines in the event of a collision, both the ships and the wind turbine must be modelled in Ansys. The background context of this project can be found in references [1]<sup>1</sup>, [2]<sup>2</sup> and [3]<sup>3</sup>. Achieving a balance between simulation accuracy and computational efficiency is a key challenge in FEM modelling, particularly for large structural models. The goal of this memo is to identify the method to achieve this balance. Calculation time is heavily influenced by factors such as mesh size element quantity, and the type of elements used (for instance shell, beam, or shell-beam combination). This balance is especially important when modelling components like plate stiffeners, where reducing calculation time without compromising accuracy is a priority due to the model's considerable size. The function of the plate stiffeners, regardless of how they are modelled, is to provide stiffness to the plate, which in turn enhances its stability.

The shell-only model gives the most accurate results but is rather expensive<sup>4</sup>. In practice, plate stiffeners are often modelled partly or fully as beam elements to reduce simulation time. Therefore, assessing the applicability of beam elements, particularly in regions subjected to collision, is crucial. If beam elements can achieve results comparable to shell elements, they could serve as a computationally efficient alternative without compromising accuracy in results. Based on the results, the most efficient modelling strategy that ensures reliable results will be selected for similar FEM ship models.

This memo presents the results of a collision test on a section of a chemical tanker to investigate the influence of different modelling approaches for plate stiffeners on structural response. This study specifically examines three stiffener modelling approaches: shell-only elements, beam-only elements, and shell-beam combination.

- Shell-only elements: The plate stiffeners (web and flange) are modelled solely as shell elements.
- Beam-only elements: The plate stiffeners (web and flange) are modelled solely as beam elements.
- Shell-beam combination: The plate stiffeners are modelled as shell (web) and beam (flange).

The research question for this study focuses on whether the results from beam-only or shell-beam combination stiffeners are comparable to those of the shell-only model. Additionally, it examines up to which

---

<sup>1</sup> Bijlage K Annex 01-03 081R030M010-Rev5 - 3D FEM analysis effects ship collision against wind turbine monopile.pdf.

<sup>2</sup> Bijlage K Annex 01-02 081R030M011-Rev2 - Investigation of ship impact against wind turbine foundation Dutch NS.pdf

<sup>3</sup> Bijlage K Annex 01-01 081R030M006-Rev4 - Investigation of ship impact against wind turbine foundation in Dutch NS.pdf

<sup>4</sup> S. Sreenath et al., Beam and shell element model for advanced analysis of steel structural members, Journal of Constructional Steel Research, <https://doi.org/10.1016/j.jcsr.2011.05.003>



mesh size and number of integration points the results remain in good agreement and evaluates the extent of differences between the approaches, considering calculation time as a critical factor.

This memo begins with a comprehensive overview of the three modelling approaches, detailing the structure and how the different plate stiffeners are modelled. Then, a detailed explanation is provided about the boundary and initial conditions, as well as the formulation used in Ansys LS-DYNA for shell and beam elements. A section also discusses the different mesh sizes and the reasoning behind their selection. Following this, a discussion highlights the collision test results for each modelling approach, including variations in accuracy and computational efficiency inside and outside the collision zone. Additionally, a mesh convergence analysis is conducted for all modelling approaches to ensure the accuracy and reliability of the results. For the shell-only model, an investigation is also conducted for two different integration points. Finally, the memo concludes with recommendations for selecting the most effective modelling approach for similar engineering applications, balancing reliability with computational demands.



## 2 Model Overview

### 2.1. Cross-section selection

Due to the complexity of the chemical tanker model (see Figure 1), only a section (red part) of the side of the chemical tanker has been selected for study, focusing on its structural integrity under collision loading.

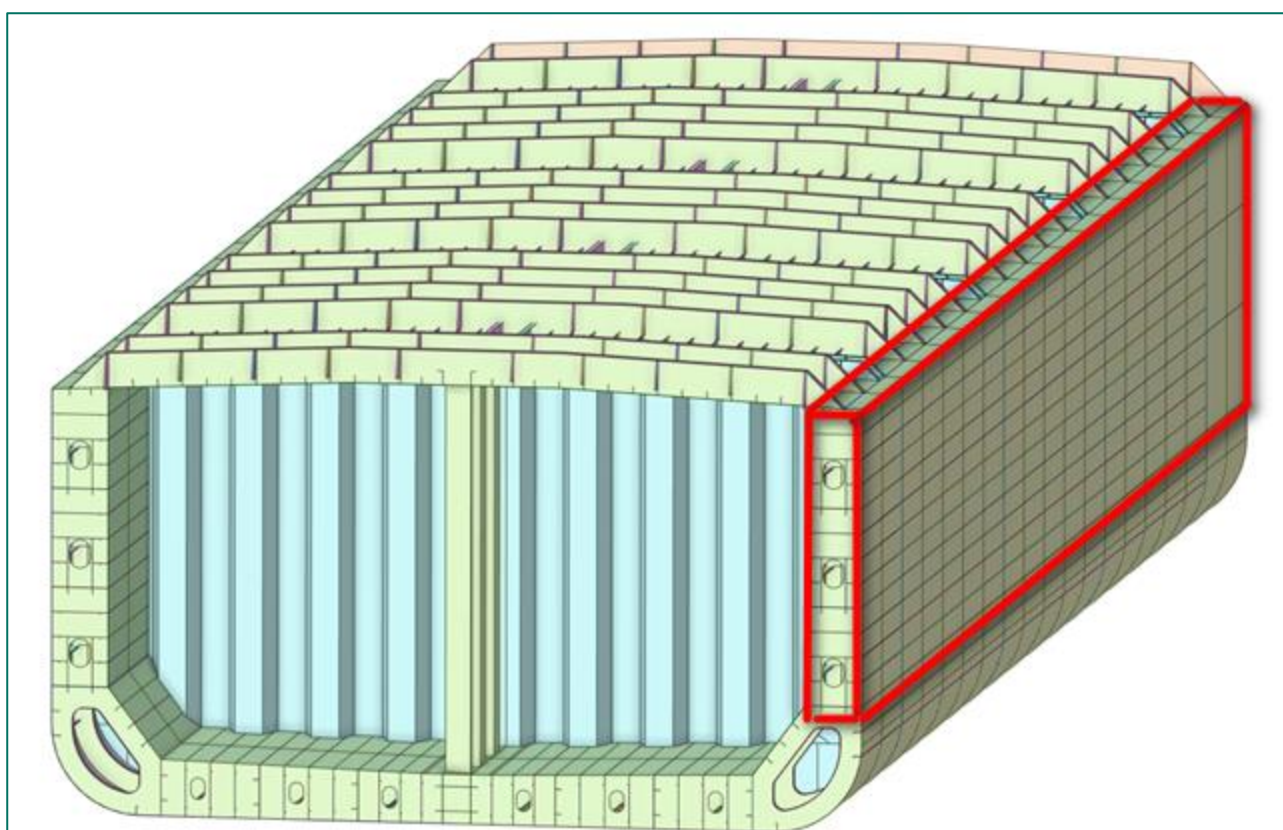


Figure 1. Chemical tanker model



As shown in Figure 2, the bulb flats (Holland profiles) serve as plate stiffeners, providing additional stiffness and rigidity to the steel plating of the ship's hull. The plate stiffeners consist of two parts: the web and the flange, as illustrated in Figure 2.

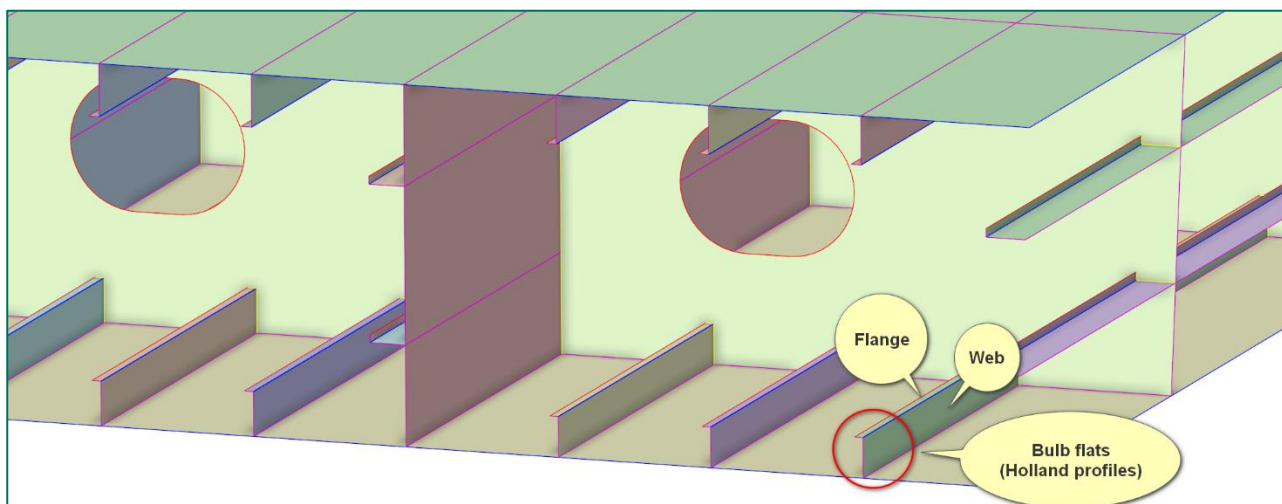


Figure 2. The bulb flats (Holland profiles) details

## 2.2. Modelling plate stiffeners

A picture of bulb flat (Holland profiles) and its cross-section can be seen in Figure 3. In this figure,  $b$  represents the width,  $e$  represents the thickness,  $c$  represents the bulb, and  $r$  represents the radius.

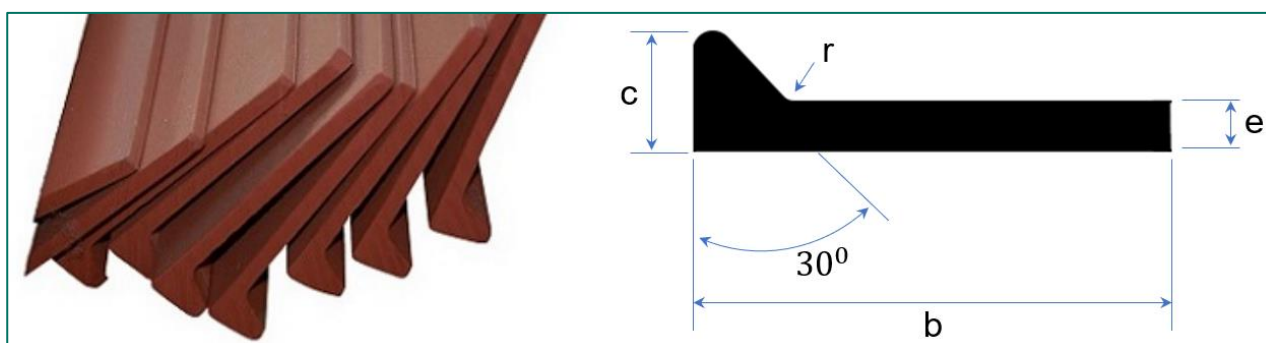


Figure 3. Bulb flats (Holland profiles)

The objective is to model these plate stiffeners using three different approaches, as mentioned in chapter 1. For simplicity, an L-shaped<sup>5</sup> profile is chosen, as illustrated Figure 4. Table 1 provides details on the modelling of the web and flange components for each approach.

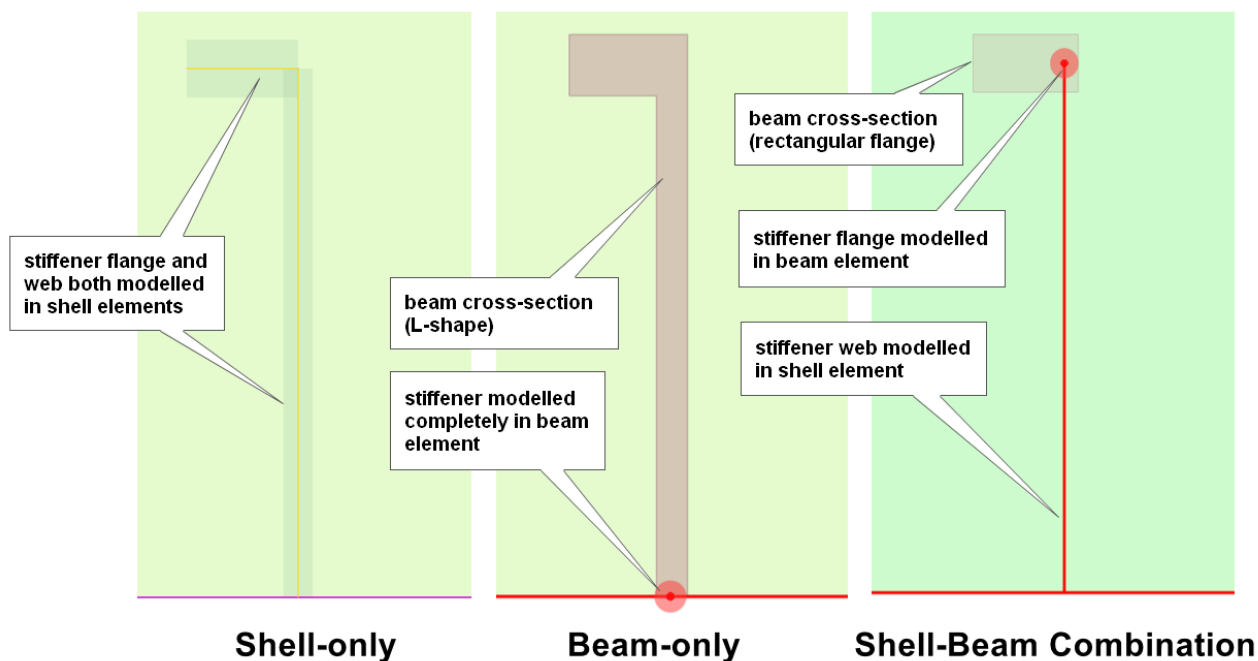


Figure 4. Three different approaches (modelling) in Ansys (LS-DYNA)

Table 1. Details on the modelling of the web and flange components for each approach

Steel material grade	Web	Flange
Shell-only	Shell	Shell
Beam-only	Beam	Beam
Shell-Beam combination	Shell	beam

The height of the web varies between 162 mm and 233 mm, while the width of the flange ranges between 35 mm and 48 mm.

<sup>5</sup> A L-shape profile (also known as equivalent angle) is usually used to model the bulb flat stiffeners in FE models (ref. DNVGL-RU-SHIP). Another alternative is to model it as an asymmetrical T-profile (ref. DNV-RP-C206). Both can be used in FE modelling. The L-shape is chosen in this memo and project to avoid too small mesh sizes resulting from the asymmetrical T-profile in shell.



### 2.3. Boundary and initial conditions

It is assumed that the edges of the upper surface are simply supported (blue lines on the upper surface in Figure 5); This boundary condition aligns with the primary focus of this study on the overall structural response rather than on specific shear force distributions. Since all the modelling approaches have the same boundary conditions, the results are comparable. A rigid body (ball) with a mass of 33,000 kg was selected to collide with the chosen chemical tanker's section at velocities of 8 m/s and 12 m/s in the -y direction. The selected velocities allow for an analysis of the differing behaviours of the modelling approaches and to examine various failure modes<sup>6</sup>. The ball is free to move without any boundary constraints applied (the ball move without constraints except for its initial velocity in the -y direction). There is a 10 mm distance between the ball and the top surface of the chemical tanker's. The mass of the chemical tanker's section is 67,000 kg. The masses for both the ball and the chemical tanker's section were chosen randomly. This setup allows for the examination of plastic deformation and the failure mechanisms of each approach.

After creating the related models, a collision simulation was performed in Ansys (LS-DYNA), as shown in Figure 5. For the sake of clarity the zone that the ball hit to the surface is called inside the collision zone and the surface out of that is named as out of collision zone (more details can be found in section 3.4.1).

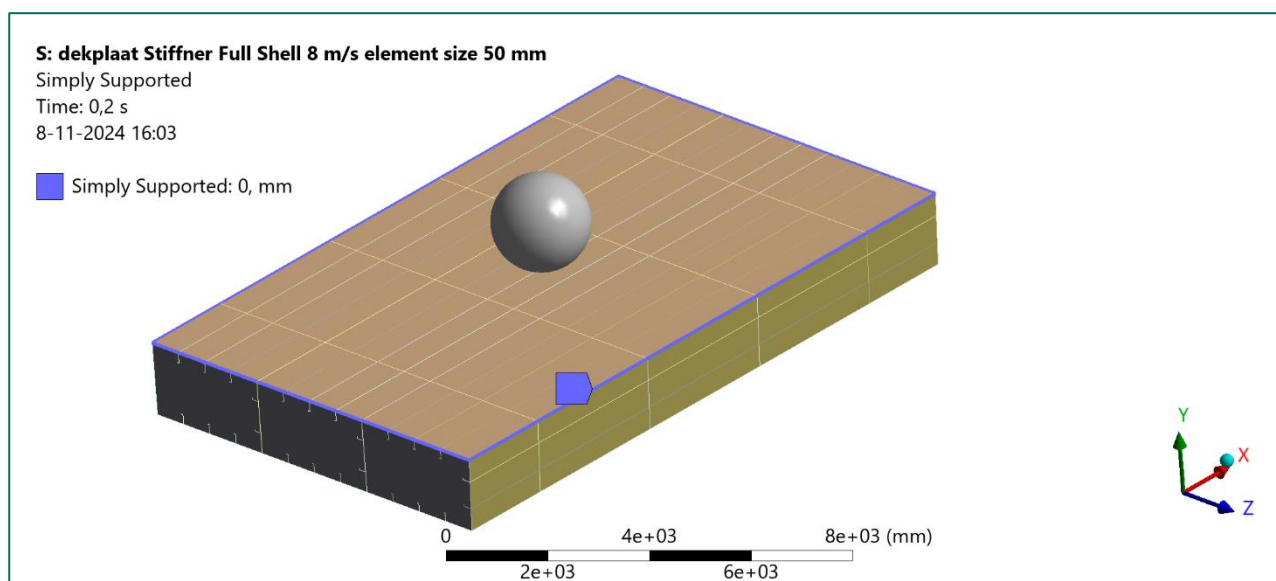


Figure 5. Model in Ansys LS-DYNA for collision simulation

<sup>6</sup> As mentioned earlier, the primary goal of this memo is to identify the most effective modelling approach for similar engineering applications, balancing reliability with the computational demands for shorter computation times. For the actual collision simulation of the chemical tanker or passenger ship (cruise), the real velocity and mass will be selected. Therefore, varying the velocity or other parameters as sensitivity variables is beyond the scope of this investigation.



## 2.4. Analysis settings

In Ansys, the explicit and implicit methods differ in how they solve equations and their suitability for different types of simulations. The implicit method solves equations globally and is well-suited for static or slow dynamic problems, where larger time steps can be used. However, for problems involving rapid changes, such as high-speed impacts or large deformations, the explicit method is preferred. Unlike the implicit method, which requires equilibrium at each time step and is more suited for quasi-static problems, the explicit solver works incrementally, allowing it to efficiently simulate the short-duration, transient events characteristic of collisions. The physics preference has been set to Explicit in this study (memo).

For all simulations, linear element order has been chosen, as LS-DYNA requires linear elements. In all modelling approaches for the rigid body (ball), an element size of 50 mm is used. To enable a meaningful comparison, element sizes of 50 mm, 100 mm, and 150 mm were selected across all models. This choice was made because, with a mesh element size of 150 mm, only two elements fit along the height (233 mm) of the web section (Figure 6). A 100 mm mesh size allows for three elements along the same height (Figure 7), and a 50 mm mesh size allows for five elements (Figure 8).

The width of the flange is much smaller than the height of the web of the stiffener. Using a finer mesh size for the flange would lead to prohibitively high computational costs.

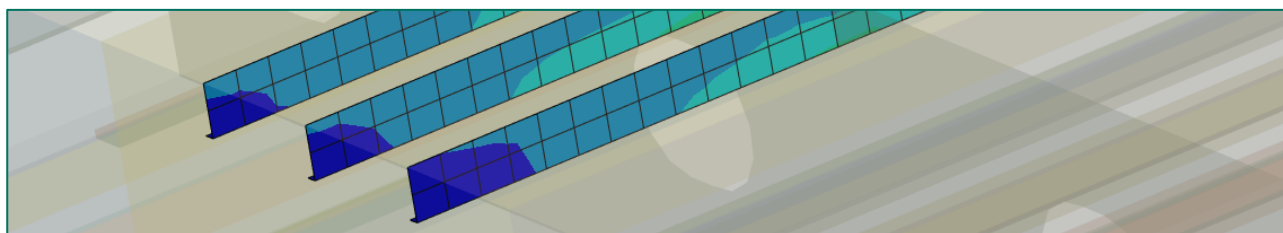


Figure 6. Mesh element size of 150 mm, with two elements along the height of the web section

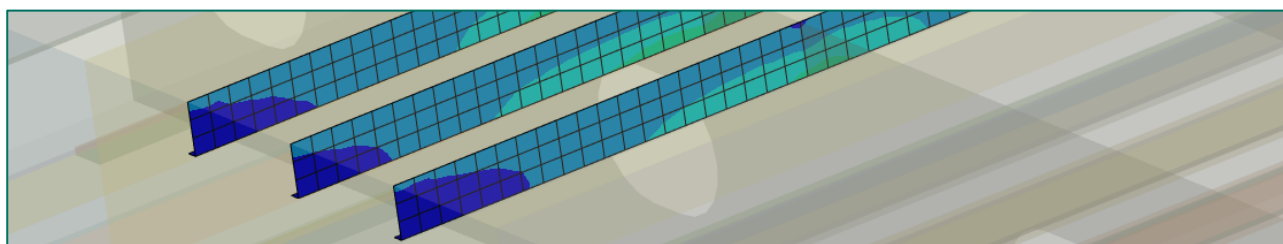


Figure 7. Mesh element size of 100 mm, with three elements along the height of the web section

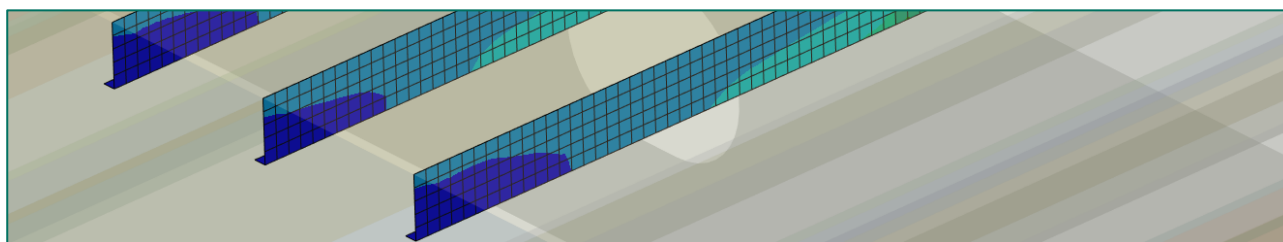


Figure 8. Mesh element size of 50 mm, with five elements along the height of the web section





S235 material has been used. The material properties is provided in Table 2<sup>7</sup>. The failure strain in this material is  $\epsilon_{fr} = 22.8\%$ .

Table 2. Material properties of S235 steel

Parameter	Value
E [MPa]	210,000
$\sigma_{prop}$ [MPa]	211.7
$\epsilon_{prop}$ [-]	0.00101
$\sigma_{yield1}$ [MPa]	236.2
$\epsilon_{p\_y1}$ [-]	0.004
$\sigma_{yield2}$ [MPa]	243.4
$\epsilon_{p\_y2}$ [-]	0.020
$\sigma_{ult,t.}$ [MPa]	360
$\epsilon_{fr}$ [-]	0.228
$\epsilon_{p\_y4}$ [-]	0.23

To ensure consistency, an end time of 0.2 seconds has been applied across simulations. This duration was chosen because the transfer of internal energy to kinetic energy occurs at around 0.06 seconds (further details are provided in chapter 3.1). The Hughes-Liu formulation with three integration points is used for the shell elements, while the Hughes-Liu formulation with cross-sectional integration is used for the beam elements. Through-thickness integration points using the Gaussian integration scheme were selected for the shell elements.

For the fully shell model, a comparison is made between the Hughes-Liu formulation with three integration points and six integration points. Using the three integration points, which provide acceptable results within an acceptable range, can be more efficient in terms of calculation time.

During the collision, the rigid body's (ball's) kinetic energy decreases as the structure absorbs and stores it as internal energy, representing deformation within the material. This energy exchange highlights how kinetic energy converts to internal energy in response to collision. Other energy forms, such as thermal energy, are not considered in this memo, as they are either assumed to be negligible or fall outside the scope of this analysis. The time step size remained constant, mass scaling was not applied, and hourglass control was not activated.

<sup>7</sup> Further details about the material properties can be found in the memo 'INFR240476 RWS WVL Memo Steel Material Model, rev.1.



## 3 Comparison of the results

This chapter provides a comprehensive comparison of energy, deformation, effective plastic strain in the collision zone, von-Mises stress, and elastic deformation outside the collision zone for different modelling approaches and various mesh element sizes. Additionally, the influence of integration points for the shell-only model is evaluated. Results for the shell-only model with 3 and 6 integration points are presented for effective plastic strain within the collision zone and for von-Mises stress outside the collision zone. In all sections of this chapter (excluding section 3.5), three integration points are used. Furthermore, in all sections of this chapter (excluding section 3.3), the results are provided for the velocity of 8 m/s.

### 3.1. Energy analysis

Figure 9 shows an energy comparison among the three different modelling approaches at a rigid body (ball) velocity of 8 m/s for the mesh element size of 50 mm. This velocity represents the speed of the rigid body at the moment of collision with the top surface (For the sake of brevity, the results for a velocity of 12 m/s are not shown). As illustrated in Figure 9, the total energy for all approaches follows a similar trend and is in good agreement. This similarity in energy behaviour indicates that, despite the different element types used to model the plate stiffeners, the overall energy absorption capacity of the structure remains consistent across the three modelling approaches. The moment of complete transformation from kinetic energy to internal energy occurs at 0.06 s for all approaches.

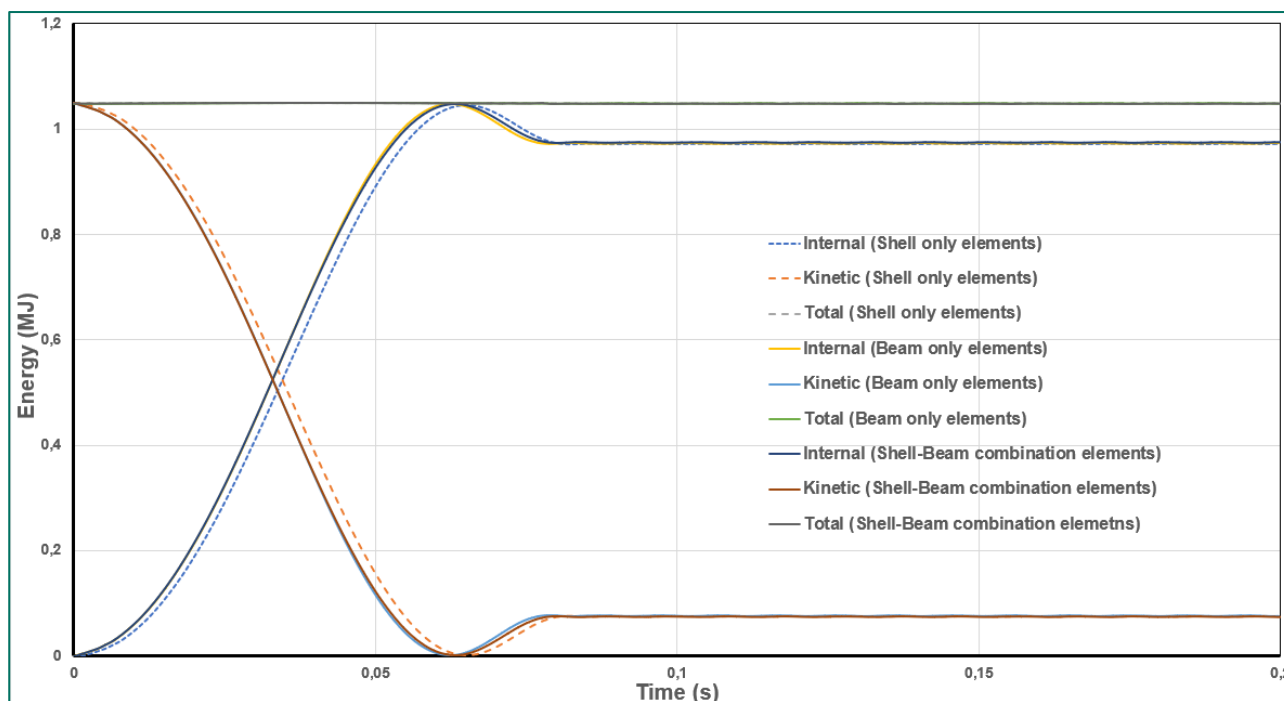


Figure 9. The energy comparison for velocity of 8 m/s and element mesh size of 50 mm



The kinetic energy (theory) is calculated using the formula  $E = \frac{1}{2}mV^2$ , where  $m$  is the mass and  $V$  is the velocity of the rigid body. Therefore, the kinetic energy is 1.05 MJ for the velocity of 8 m/s and 2.37 MJ for the velocity of 12 m/s. These values for the kinetic energy are consistent across all modelling approaches for mesh element size of 50 mm.

In all modelling approaches with different mesh sizes, the initial kinetic energy (as input for all models) at velocities of 8 m/s and 12 m/s is identical. In Table 3, a comparison is made between the initial kinetic energy (1.05 MJ) and internal energy at 0.06 s for different mesh sizes for the velocity of 8 m/s.

Table 3. Comparing initial kinetic energy (1.05 MJ) and internal energy for different mesh sizes for velocity of 8 m/s at 0.06 s

Modelling approach	Max. internal energy (MJ)	Deviation (%)
Shell-only		
50 mm	1.04	1.0
100 mm	1.04	1.0
150 mm	1.04	1.0
Beam-only	1.04	1.0
50 mm	1.04	1.0
100 mm	1.04	1.0
150 mm	1.04	1.0
Shell-Beam	1.04	1.0
50 mm	1.04	1.0
100 mm	1.04	1.0
150 mm	1.04	1.0

There is a 1% deviation between the initial and kinetic energy (1.05 MJ) for all mesh sizes. The consistent energy levels across the shell, beam, and shell-beam models indicate that, despite differing methods of representing the plate stiffeners, the energy remains unaffected.



### 3.2. Deformation analysis

To compare the top surface deformation results in the collision zone, the results are provided at 0.06 s. Figure 10 illustrates the total deformation of the top surface in the shell-only model approach, with a rigid body (ball) collision velocity of 8 m/s for the element size of 50 mm.

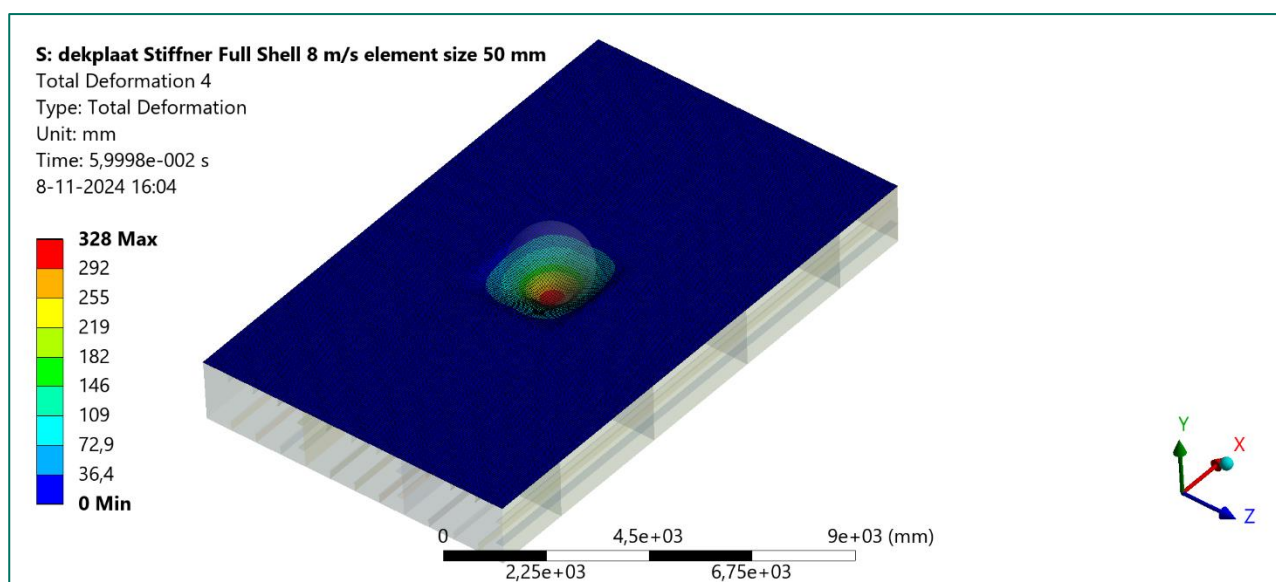


Figure 10. The total deformation of the top surface for the shell-only model for velocity of 8 m/s and element size of 50 mm at 0.06 s

Table 4 compares the total deformation of the top surface at 0.06 s, with regards to the deformation of fully shell model with the mesh size of 50 mm for the velocity of 8 m/s.

Table 4. Comparing total deformation of the top surface for the velocity of 8 m/s for different mesh element sizes at 0.06 s

Modelling approach	Max. total deformation (mm)	Deviation (%)
Shell-only		
50 mm	328	-
100 mm	328	0.0
150 mm	327	0.3
Beam-only		
50 mm	325	0.9
100 mm	325	0.9
150 mm	326	0.9
Shell-Beam		
50 mm	326	0.6
100 mm	326	0.6
150 mm	325	0.9



Based on the results, there is a deviation of less than 1% among the results of different models for different mesh size. These results are also consistent with the energy summary provided in section 3.1. Despite differences in how the bulb flats (Holland profiles) are modelled, the deformation of the top surface under the collision is nearly identical. The similarity in deformation across the shell, beam, and shell-beam models suggests that, although each approach represents the plate stiffeners differently, the deformation of the top surface remains consistent.



### 3.3. Inside collision zone

Studying the effective plastic strain in the collision zone is crucial. This section provides the results for effective plastic strain and compares the results for different mesh sizes. As mentioned in section 2.4, the failure threshold for the material's effective plastic strain is 0.228. This value is used to assess failure both on the top surface and in the plate stiffeners beneath it. All results in this section are shown at 0.06 s.

#### 3.3.1. Effective plastic strain

To visually illustrate the results, the outcomes for three cases are shown in Figure 11 to Figure 15 at 0.06 s. As seen in Figure 11, for the shell-only model and a velocity of 8 m/s, the effective plastic strain is less than 0.228, indicating no failure in the top surface or the stiffeners beneath it. This also applies to all other modelling approaches at a velocity of 8 m/s across different mesh sizes.

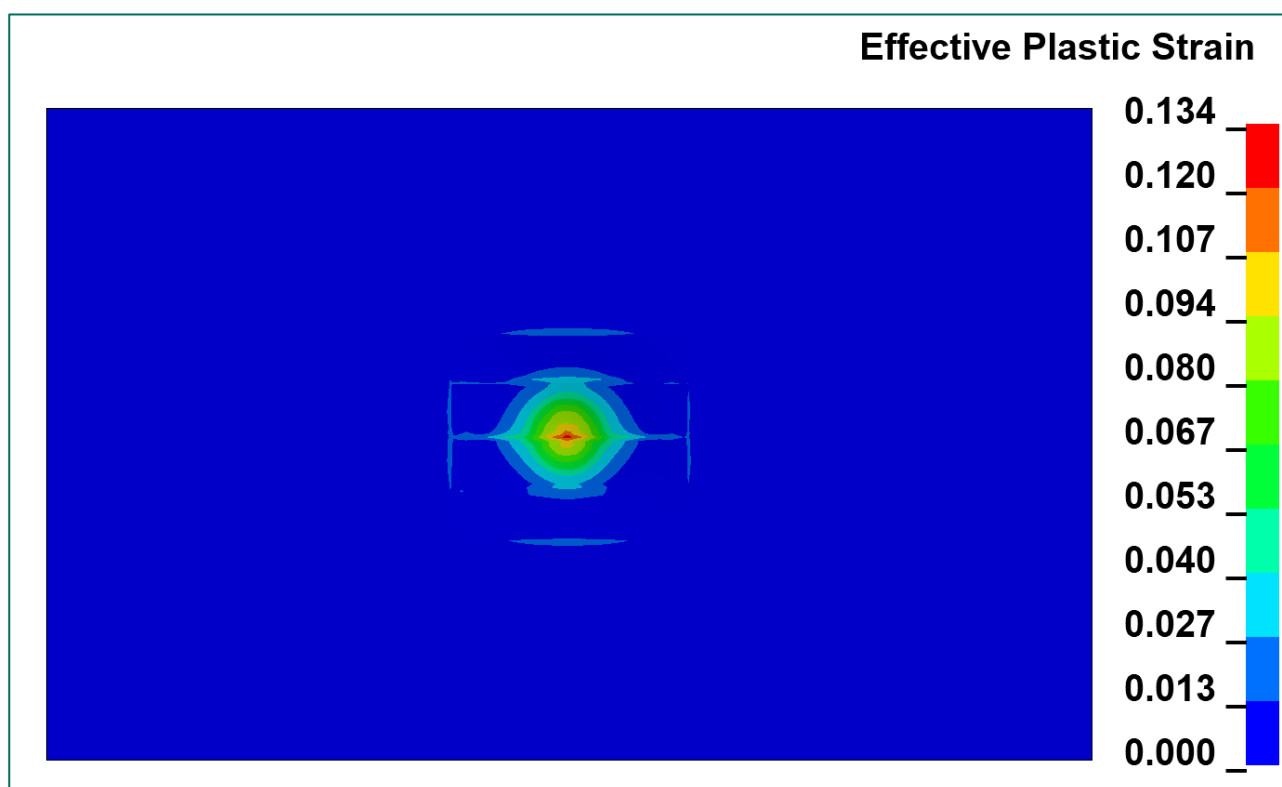


Figure 11. Effective plastic strain of the top surface for Shell-only model for the velocity of 8 m/s and the mesh element size of 50 mm at 0.06 s (top view)



For the shell-only model at a velocity of 12 m/s, failure occurs in the top surface (see Figure 12); however, there is no failure is observed in the stiffeners below the top surface (see Figure 13).

In contrast, for the beam-only model at the same velocity, failure occurs in the top surface (see Figure 14), and in the stiffeners<sup>8</sup> below it (see Figure 15).

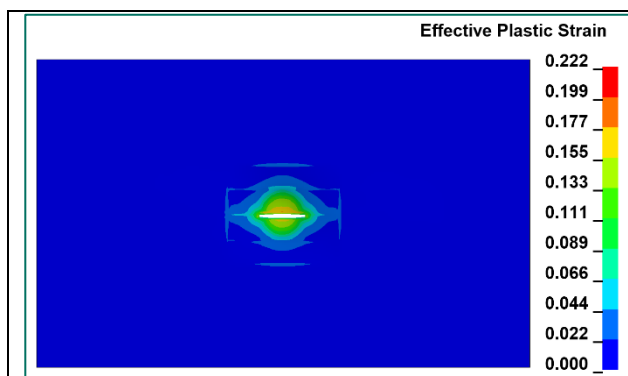


Figure 12. Effective plastic strain of the top surface for Shell-only model for the velocity of 12 m/s and the mesh element size of 50 mm at 0.06 s (top view)

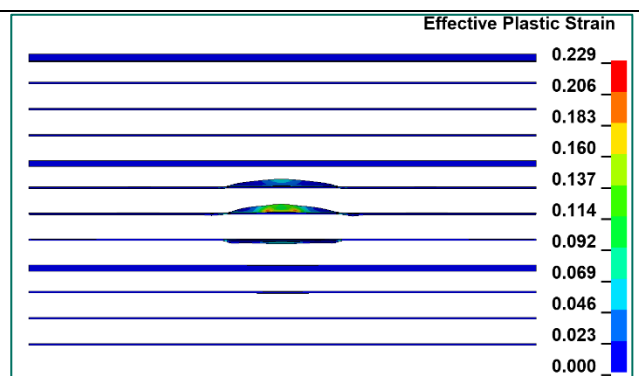


Figure 13. Effective plastic strain of the stiffeners for Shell-only model for the velocity of 12 m/s and the mesh element size of 50 mm at 0.06 s (top view)

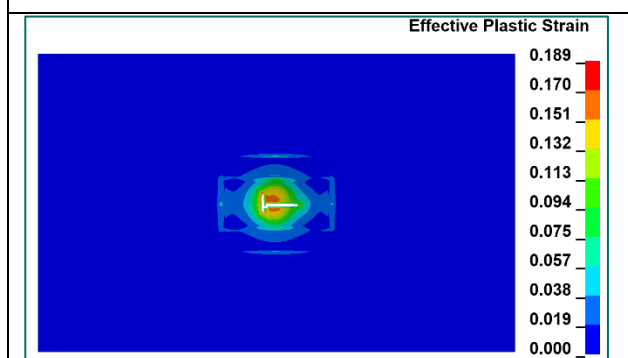


Figure 14. Effective plastic strain of the top surface for Beam-only model for the velocity of 12 m/s and the mesh element size of 50 mm at 0.06 s (top view)

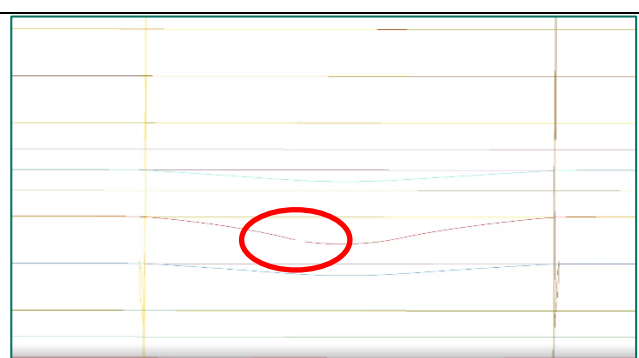


Figure 15. Failed stiffeners in Beam-only model for the velocity of 12 m/s and the mesh element size of 50 mm at 0.06 s

<sup>8</sup> The effective plastic strain results for the beam stiffeners are not visible in LS-PrePost.



Table 5. Failure of top surface and the plate stiffeners beneath the top surface at 0.06 s for the velocity of 12 m/s for different mesh sizes

Modelling approach	Top surface fails?	Plate stiffeners beneath the top surface fail?
Shell-only		
50 mm	✓	×
100 mm	✓	×
150 mm	✓	×
Beam-only		
50 mm	✓	✓
100 mm	✓	✓
150 mm	×	✓
Shell-Beam		
50 mm	✓	×
100 mm	✓	×
150 mm	×	×





### 3.3.2. Influence of mesh element size

Table 6 and Table 7 compare the deviation in effective plastic strain for the same approaches with different mesh sizes, using a 50 mm element size as the baseline, for 8 m/s and 12 m/s.

Table 6. Comparing effective plastic strain for the velocity of 8 m/s for different mesh element sizes at 0.06 s

Modelling approach	Effective plastic strain	Deviation (%)
Shell-only		
<b>50 mm</b>	<b>0.170</b>	-
100 mm	0.138	18.8
150 mm	0.120	29.4
Beam-only		
50 mm	0.108	36.5
100 mm	0.089	47.6
150 mm	0.087	48.8
Shell-Beam		
50 mm	0.162	4.7
100 mm	0.134	21.2
150 mm	0.123	27.6

Table 7. Comparing effective plastic strain for the velocity of 12 m/s for different mesh element sizes at 0.06 s

Modelling approach	Effective plastic strain	Deviation (%)
Shell-only		
<b>50 mm</b>	<b>0.229</b>	-
100 mm	0.204	10.9
150 mm	0.192	16.2
Beam-only		
50 mm	0.189	17.5
100 mm	0.204	10.9
150 mm	0.193	15.7
Shell-Beam		
50 mm	0.229	0.0
100 mm	0.205	10.5
150 mm	0.185	19.2

Based on the results, the effective plastic strain - a criterion for material failure - suggests that using shell-beam models is a promising approach in the collision zone. Additionally, as the flange width is a maximum of 48 mm, the mesh size should ideally be finer than 50 mm (e.g., 25 mm or 10 mm) to achieve accurate results. However, employing such a fine mesh for the flange would result in prohibitively high computational costs. Therefore, opting for a mesh element size of 100 mm offers a practical balance to reduce calculation time while maintaining reasonable accuracy.



### 3.4. Out of collision zone

This section provides the results for von-Mises stress and elastic deformation and compares the results for different mesh sizes out of the collision zone. As can be seen in the material properties in section 2.4, the values above the  $\sigma_{yield1} = 236.2$  MPa is related to the plastic regions.

#### 3.4.1. Von-Mises stress

To provide a clearer view of the area defined as 'outside the collision zone', the black rectangle in Figure 16 indicates the collision zone. Figure 16, also illustrates the von-Mises stress (Max. over time) of the top surface in the shell-only model approach, with a rigid body (ball) collision velocity of 8 m/s and element size of 50 mm out of the collision zone.

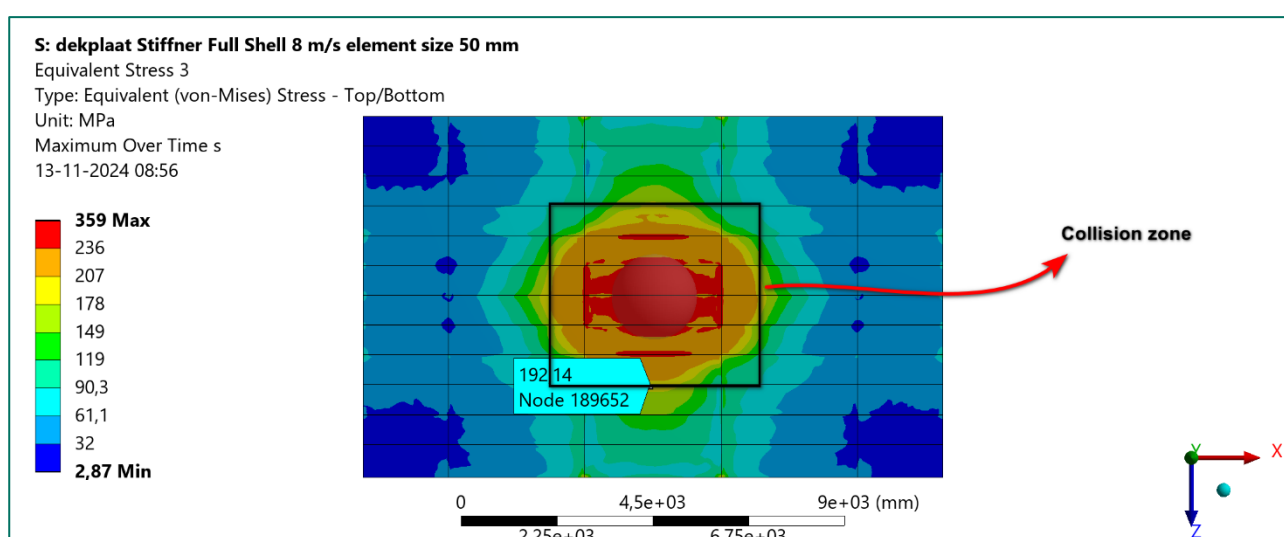


Figure 16. The stress (von-Mises) of the top surface for the shell-only model for a velocity of 8 m/s and element size of 50 mm out of the collision zone



Table 8 compare the stress of the top surface (Max. over time) out of the collision zone, using the fully shell model with the mesh size of 50 mm as the reference for comparison for a velocity of 8 m/s.

Table 8. The stress (von-Mises) of the top surface out of the collision zone for different mesh sizes for the velocity of 8 m/s

Modelling approach	Maximum von-Mises stress (MPa)	Deviation (%)
Shell-only		
<b>50 mm</b>	<b>192</b>	-
100 mm	191	0.5
150 mm	191	0.5
Beam-only		
50 mm	188	2.1
100 mm	185	3.6
150 mm	184	4.2
Shell-Beam		
50 mm	191	0.5
100 mm	190	1.0
150 mm	187	2.6

Based on the results, there is a maximum deviation of 4.2 percent among the values. Additionally, the stress values outside the collision zone are less than the yield stress,  $\sigma_{\text{yield}1} = 236.2$  MPa. Regardless of the specific method used to model the plate stiffeners, the stress response of the top surface under collision is remarkably consistent out of the collision zone. The similarity in stress across the shell, beam, and shell-beam models indicates that, despite varying representations of the plate stiffeners, the stress on the top surface remains largely unaffected out the collision zone.



### 3.4.2. Elastic deformation

Figure 17 illustrates the elastic (Max. over time) deformation of the top surface in the shell-only model approach, with a rigid body (ball) collision velocity of 8 m/s and element size of 50 mm out of the collision zone.

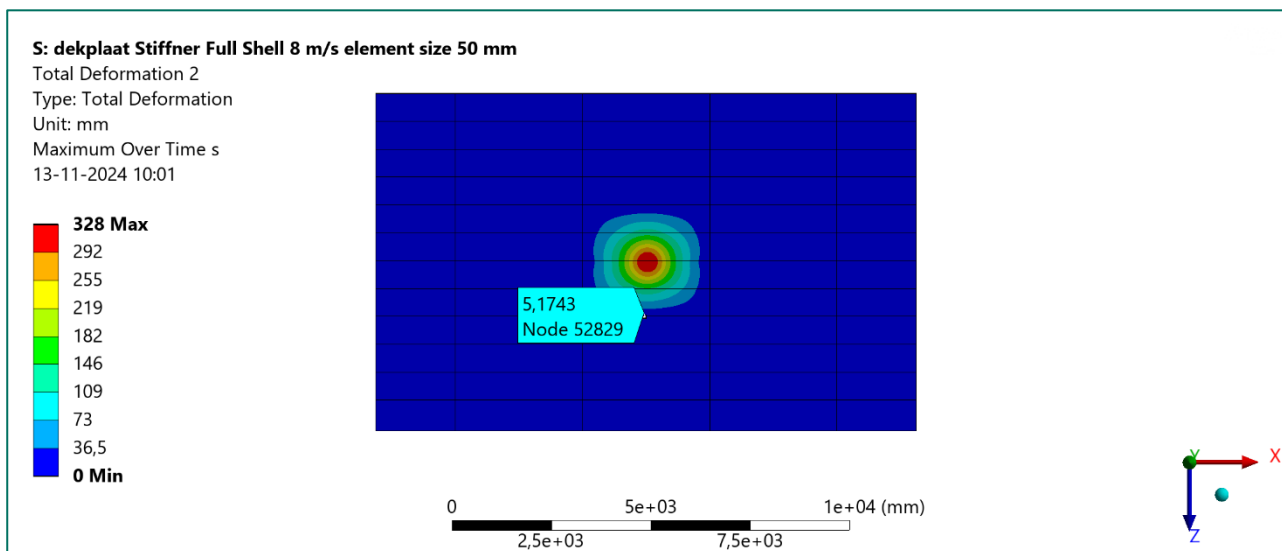


Figure 17. Elastic deformation of the top surface (Max. over time) out of the collision zone for the mesh size of 50 mm and the velocity of 8 m/s

Table 9 compare the elastic deformation of the top surface (Max. over time) out of the collision zone, using the fully shell model with the mesh size of 50 mm as the reference for comparison.

Table 9. The elastic deformation of the top surface (Max. over time) out of the collision zone for the velocity of 8 m/s

Modelling approach	Max. elastic deformation (mm)	Deviation (%)
Shell-only		
50 mm	5.1	-
100 mm	5.1	0.0
150 mm	5.0	2.0
Beam-only		
50 mm	5.4	-5.9
100 mm	5.4	-5.9
150 mm	5.2	-2.0
Shell-Beam		
50 mm	5.1	0.0
100 mm	5.1	0.0
150 mm	5.1	0.0

Based on the results, there is a maximum deviation of 6 percent among the values. Regardless of the specific method used to model the plate stiffeners, the stress response of the top surface under collision is remarkably consistent out of the collision zone.



### 3.5. Influence of integration points

For the shell-only model, a comparison was made using two different integration points - 3 and 6 - in the Hughes-Liu formulation in ANSYS. This comparison was conducted for varying mesh sizes within the collision zone and outside the collision zone.

#### 3.5.1. Inside collision zone

Inside the collision zone the results of effective plastic strain for shell-only model is provided to compare for different mesh sizes of 150 mm with different integration points for the velocity of 8 m/s at 0.06 s. The comparison in Table 10 is made between 3 and 6 integration points with the same element size.

Table 10. Comparison of effective plastic strain for the velocity of 8 m/s for different integration points at 0.06 s

Shell-only model	Element size (mm)	Max. effective plastic strain	Deviation (%)
<b>6 point</b>	<b>50</b>	<b>0.190</b>	-
3 point	50	0.170	10.5
<b>6 point</b>	<b>100</b>	<b>0.149</b>	-
3 point	100	0.138	7.4
<b>6 point</b>	<b>150</b>	<b>0.129</b>	-
3 point	150	0.120	7.0

Based on the results, models with 6 integration points and element size of 100 mm are promising for the collision zone.

#### 3.5.2. Out of collision zone

Out of the collision zone the results of von-Mises stress (Max. over time) for shell-only model for the top surface is provided to compare for different mesh sizes with different integration points for the velocity of 8 m/s.

Table 11. Comparison of von-Mises stress for the velocity of 8 m/s for different integration points

Shell-only model	Element size (mm)	Max. von-Mises stress (MPa)	Deviation (%)
<b>6 point</b>	<b>50</b>	<b>200</b>	-
6 point	100	199	0.5
6 point	150	199	0.5
3 point	50	192	4.0
3 point	100	191	4.5
3 point	150	191	4.5

Based on the results, for shell models out of the impact zone, the von-Mises stress is lower than  $\sigma_{\text{yield1}} = 236.2$  MPa. Additionally, there is no significant difference between the results for different mesh sizes or integration points (3 or 6). Regardless of the method used to model the plate stiffeners, the von-Mises stress on the top surface outside the impact zone remains remarkably consistent.



### 3.6. Mesh size combination

Figure 18 shows a shell-only model with a combination of two mesh element sizes. In this model, the ball and collision zone are modelled with a mesh size of 50 mm, while the rest is modelled with a mesh size of 150 mm. A comparison is made between the effective plastic strain results of this model in the collision zone and the results of the shell-only model with a mesh size of 50 mm for all parts of the model (for the velocity of 8 m/s).

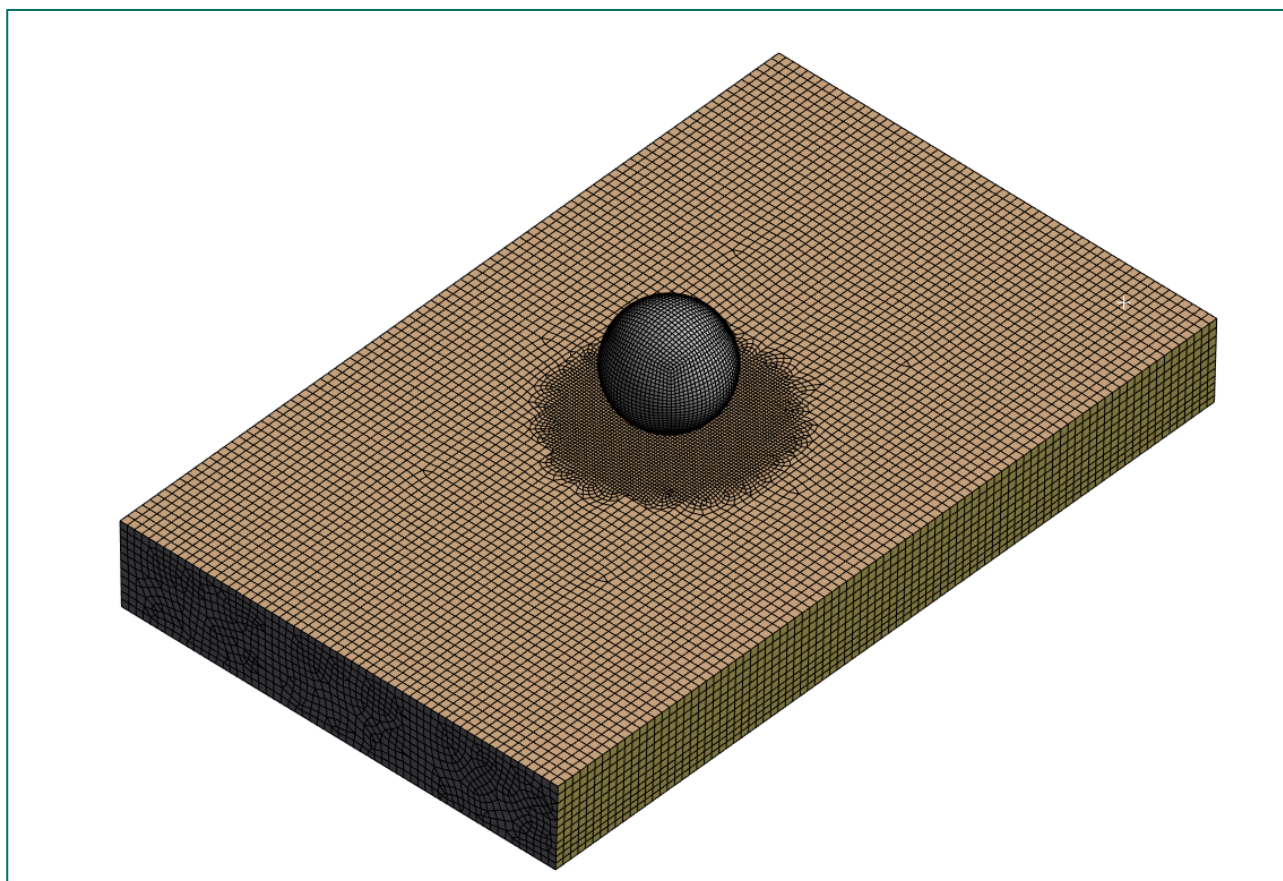


Figure 18. A shell-only model with a combination of two mesh element sizes of 50 mm and 150 mm for the velocity of 8 m/s with three integration points

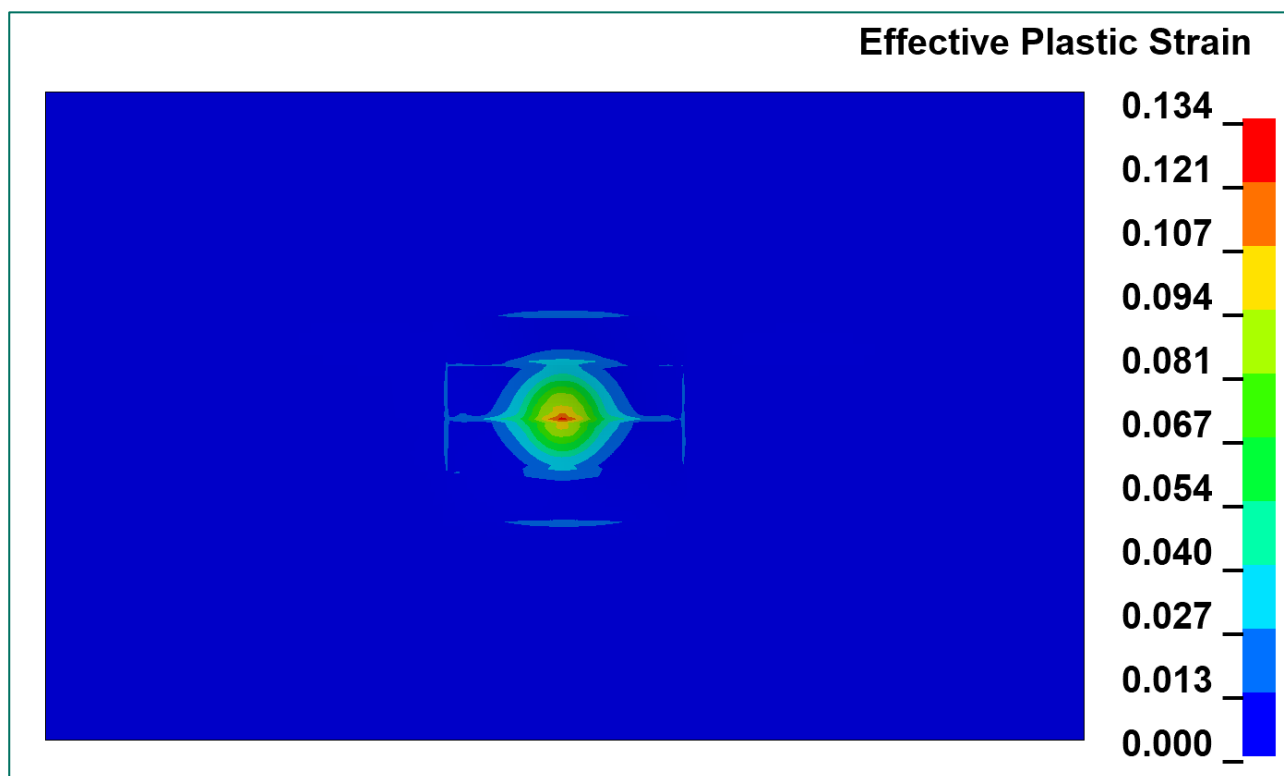


Figure 19. Effective plastic strain of the top surface for Shell-only model for the velocity of 8 m/s and the mesh element sizes of 50 mm and 150 mm for the velocity of 8 m/s at 0.06 s (top view)

As illustrated in Table 12, the effective plastic strain for the velocity of 8 m/s in the shell-only model with a combination of mesh sizes (50 mm and 150 mm) is in good agreement with the effective plastic strain of the shell-only model with a mesh size of 50 mm only.

Table 12. Comparing effective plastic strain of the top surface for the velocity of 8 m/s for different mesh element sizes inside the collision zone at 0.06 s with three integration points

Modelling approach	Effective plastic strain	Deviation (%)
Shell-only 50 mm	0.134	-
Shell-only Combination of 50 mm and 150 mm	0.134	0.0

For large structures such as chemical tankers or passenger vessels, it is crucial to strike a balance between computational efficiency and accuracy. When evaluating damage or failure, attention should be given to the inner layers rather than just the outermost layer. Focusing solely on plastic strain in the first layer of shell-only elements within the collision zone may result in overly conservative conclusions for these types of structures.



## 4 Conclusion

---

This memo explores the potential for reducing simulation time by applying beam elements to plate stiffeners, particularly within the collision zone and also outside the collision zone. This research compares various plate stiffener modelling approaches (shell-only, beam-only, and shell-beam combination) with different mesh sizes and integration points to evaluate their effects on energy, deformation, effective plastic strain, von-Mises stress, and elastic deformation. In the collision zone, the focus is on effective plastic strain to assess failure, while outside the collision zone, elastic behaviour is examined.

- The energy summary for all three plate stiffener models shows consistent energy transfer behaviour (section 3.1). The similarity in energy absorption across the shell, beam, and shell-beam models indicates that the overall energy behaviour is unaffected by the modelling approach. Additionally, the top surface deformation under collision is nearly identical across all models, aligning with the energy summary results.
- Based on the results (section 3.3), in the collision zone, the effective plastic strain - used as a criterion for material failure - indicates that shell-beam combination models are effective and show good agreement with the results of shell-only models, while require significantly less computation time.
- The results show that (section 3.4), regardless of the modelling method for the plate stiffeners, the top surface stress response outside the collision zone is consistently similar.
- Based on the results (sub-section 3.5.1), six integration points provide sufficient accuracy for the collision zone.
- Based on the results (sub-section 3.5.2), for shell models out of the impact zone, there is no significant difference between the results for different mesh sizes or integration points (3 or 6).

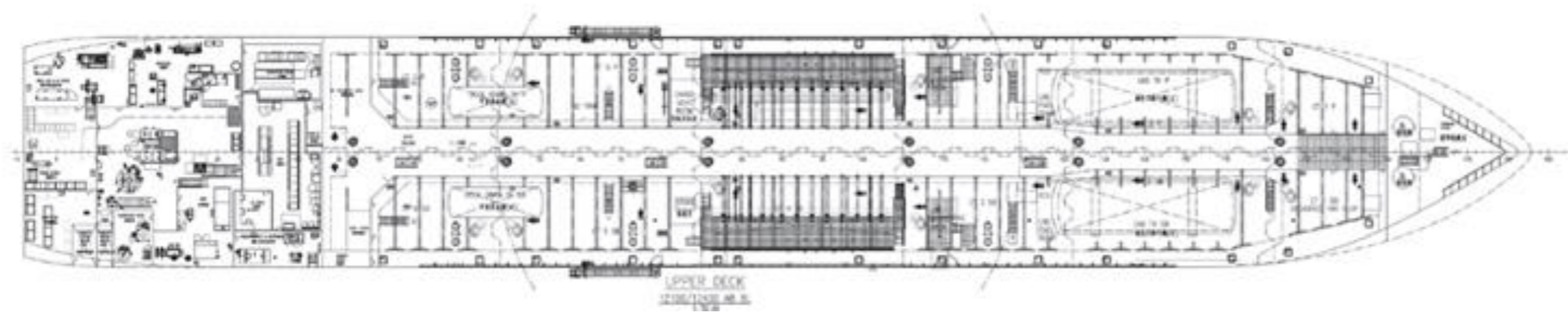
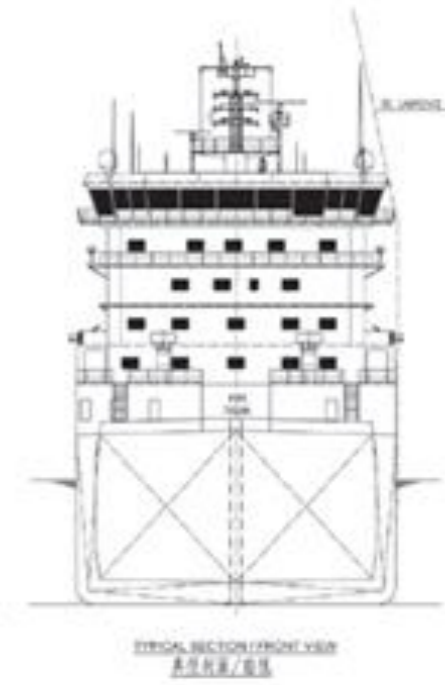
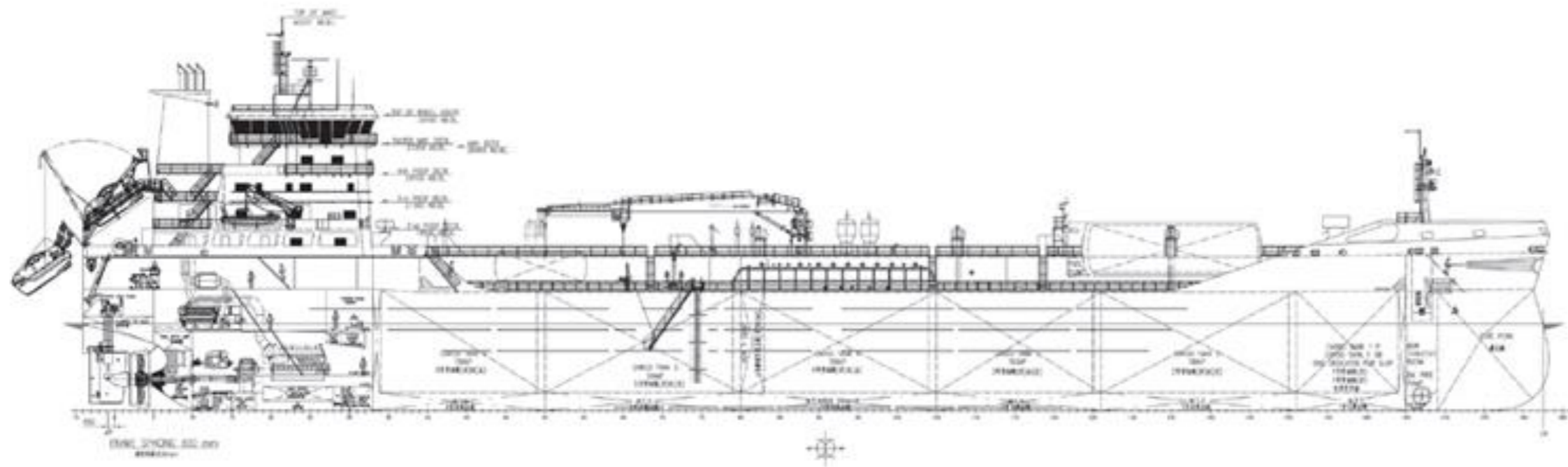
In summary, it can be concluded that for areas outside the collision zone, modelling the plate stiffeners as beam-only elements is an effective approach to reduce simulation computation time. Within the collision zone, using a shell-beam model with an element size of at most 100 mm and preferably six integration points is recommended for achieving accurate results. This is also consistent with the methods used in other similar simulations, as stated in the reference provided in the Introduction.





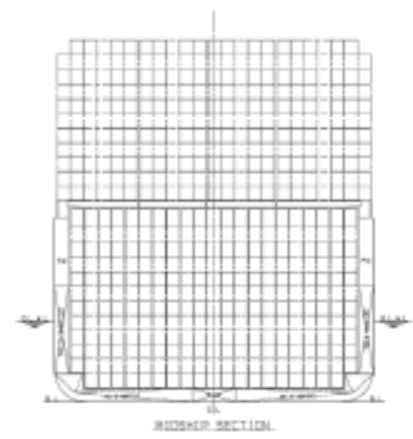
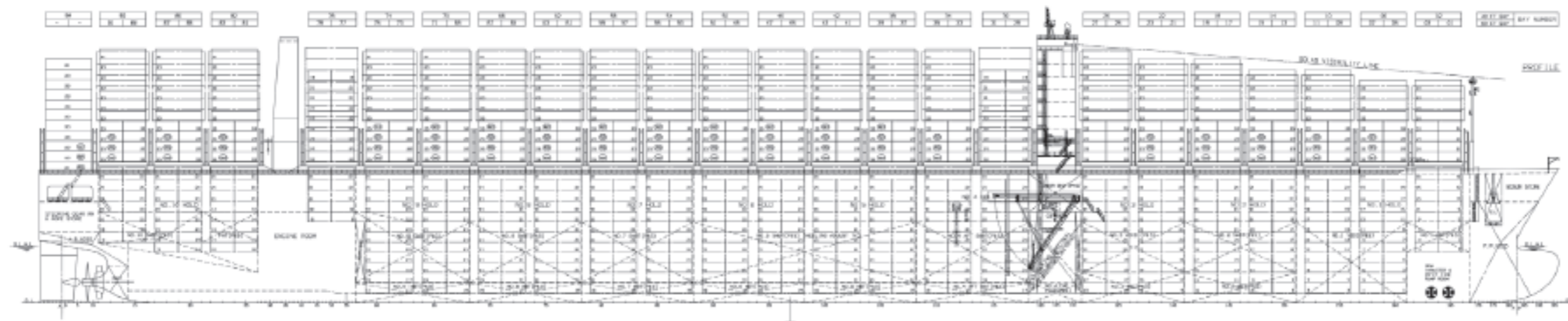
## G. Drawings Ship's types

### G.1. *Chemical tanker*



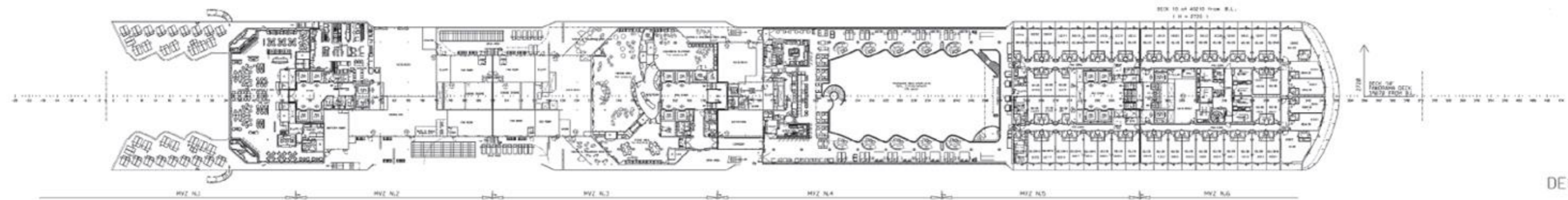
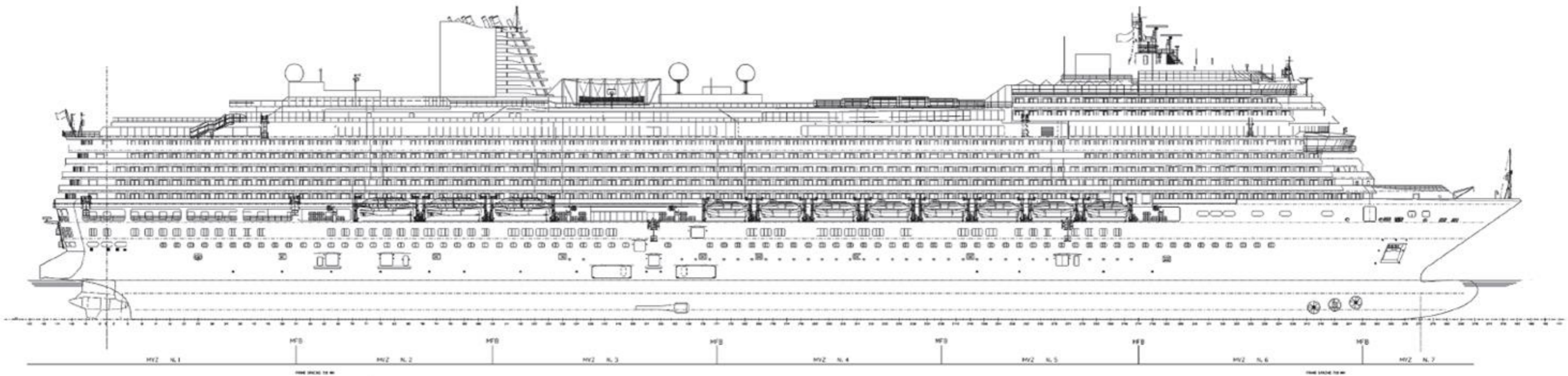


## G.2. *Container Ship*

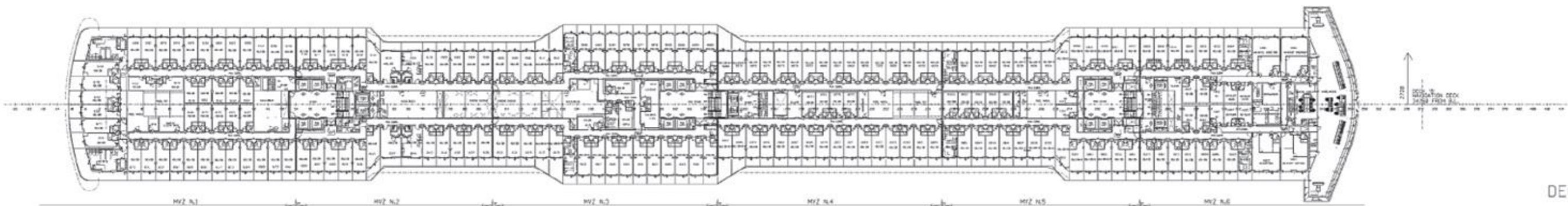




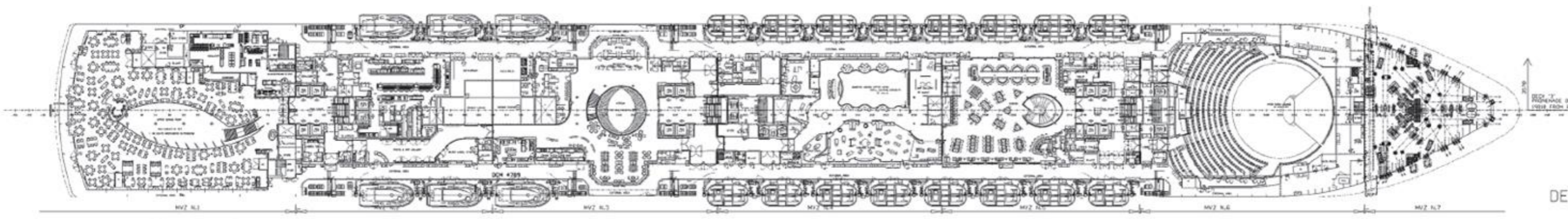
### **G.3. *Passenger Vessel***



DECK 10



DECK 8



DECK 3

## H. FEM support structure modal validation

A modal analysis of the turbine support structure is performed to compare three key modes with a previous analysis *ref. [4]*. The previous model, performed using Ansys, utilized beam elements, whereas this simulation employs shell elements in LS-DYNA for enhanced geometric detail and accuracy. The analysis is a prestressed modal analysis, incorporating the nacelle mass at the top, distributed masses along the height of the support structure, and the effects of wind and wave loading. Also the soils structure interactions, also described in this document, is included. This comparison ensures consistency in dynamic behavior despite differences in modeling approaches and software.

Two comparisons are conducted during the modal analysis of the turbine support structure:

1. With soil interaction using p-y curves and an amplification factor of 1.0 – Represents the baseline scenario without additional dynamic effects.
2. With soil interaction using p-y curves and an amplification factor of 2.5 – Captures the dynamic amplification effects due to soil-structure interaction under more extreme loading conditions.

### p-y curve magnification factor of 1.0

Table 41. Mode 1 with a factor 1.0

Mode shape	Ref. [4]	
Mode 1	0.205	0.217

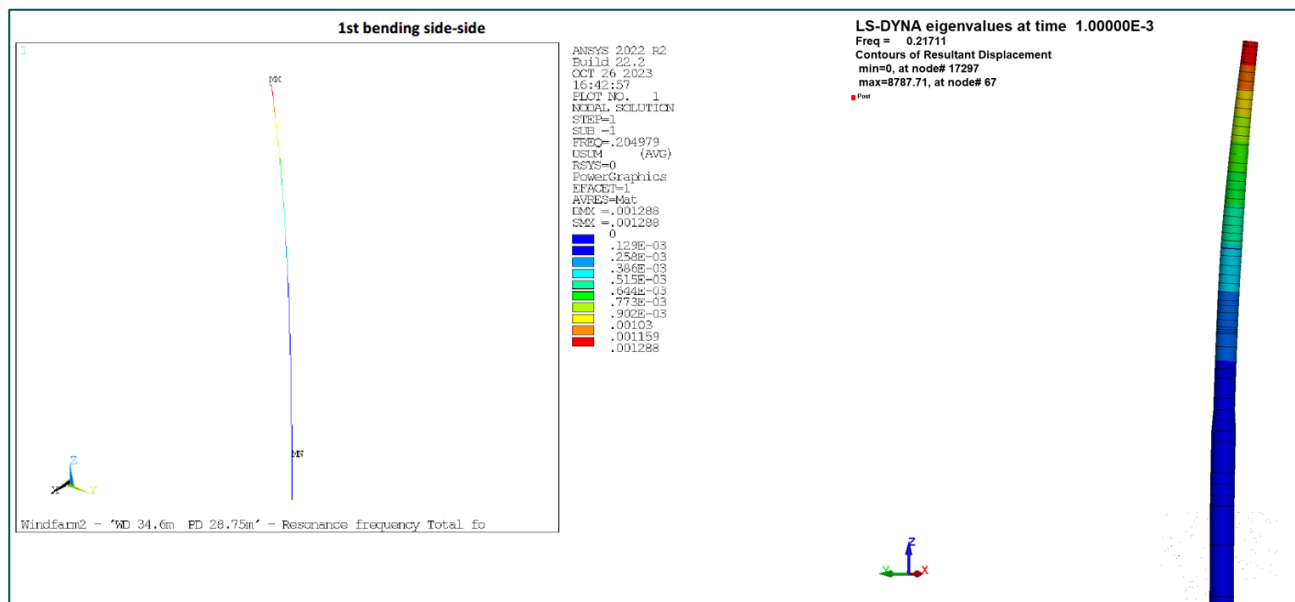


Figure 63. 1st mode – beam element (left) and shell elements (right)

Table 42. Mode 2 with a factor 1.0

Mode shape	Ref. [4]	Shell
Mode 2	0.841	0.7293

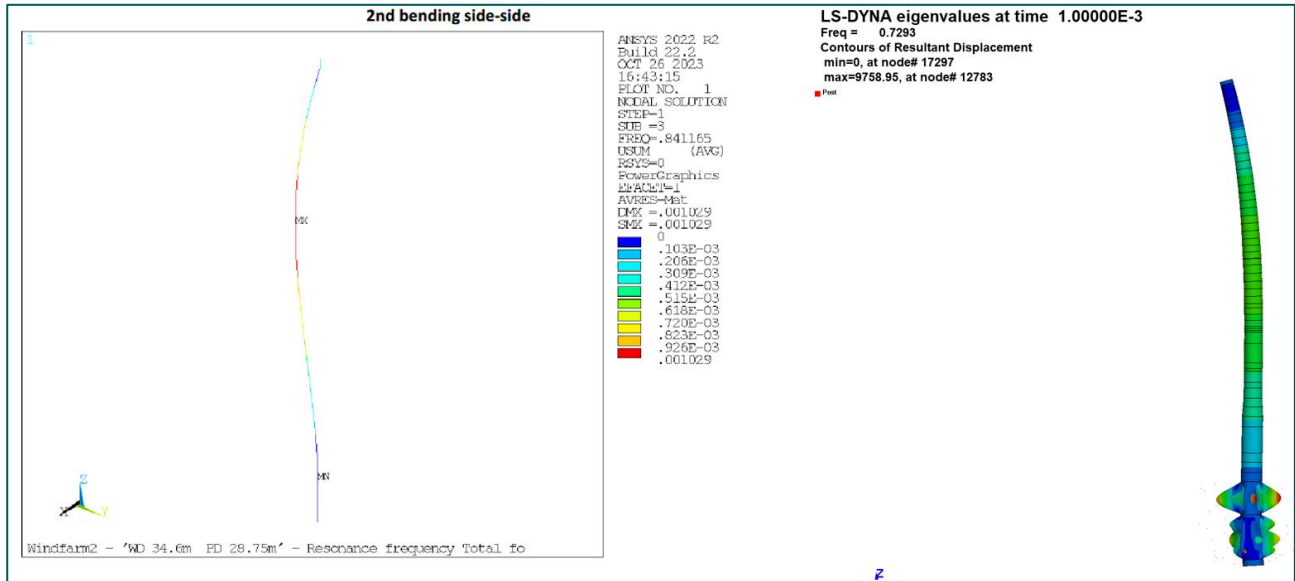


Figure 64. 2nd mode – beam element (left) and shell elements (right)



Table 43. Mode 3 with a factor 1.0

Mode shape	Ref. [4]	Shell
Mode 3	1.522	1.4973

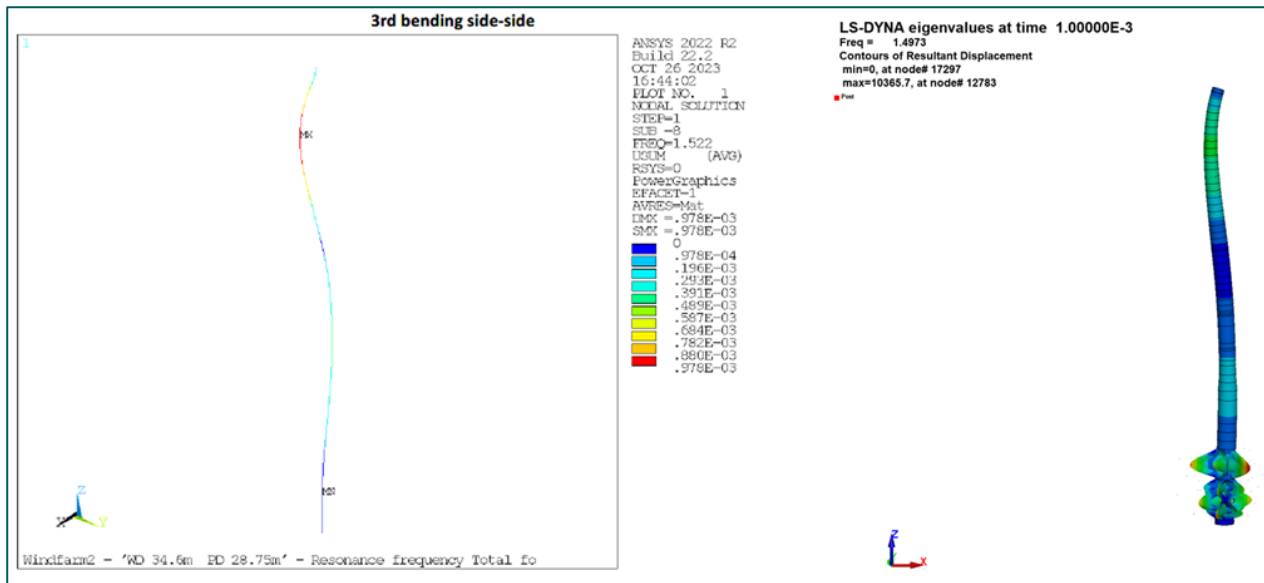


Figure 65. 3rd mode – beam element (left) and shell elements (right)

### p-y curve magnification factor of 2.5

Table 44. Mode 1 with a factor 2.5

Mode shape	Ref. [4]	
Mode 1	0.205	0.205

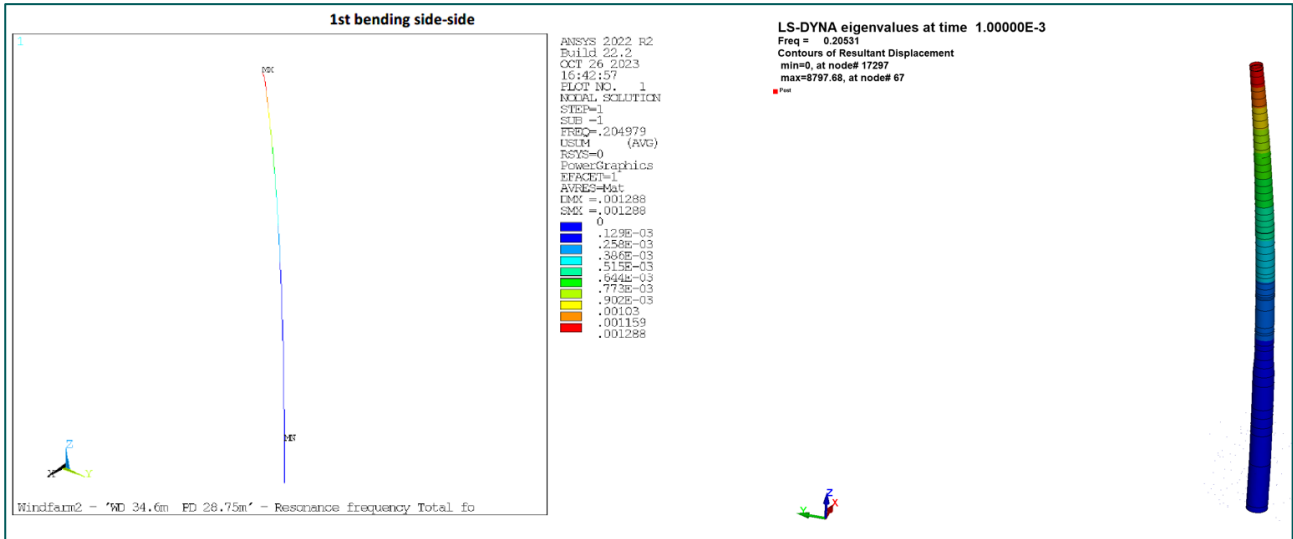


Figure 66. 1st mode – beam element (left) and shell elements (right)

Table 45. Mode 2 with a factor 2.5

Mode shape	Ref. [4]	Shell
Mode 2	0.841	1.066

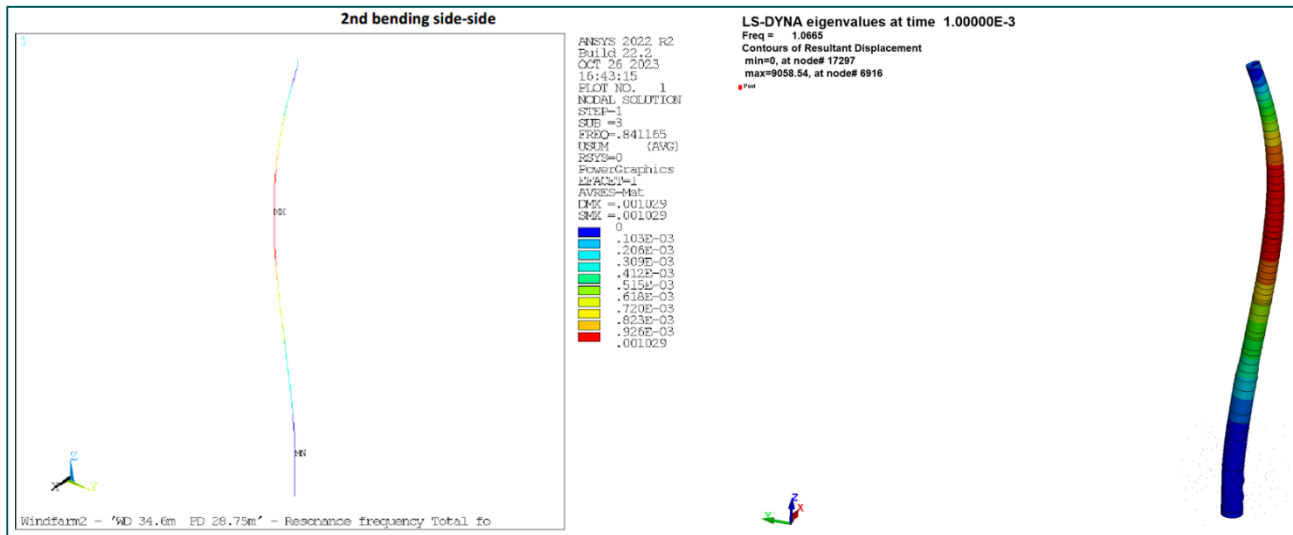


Figure 67. 2nd mode – beam element (left) and shell elements (right)

Table 46. Mode 3 with a factor 2.5

Mode shape	Ref. [4]	Shell
Mode 3	1.522	2.224

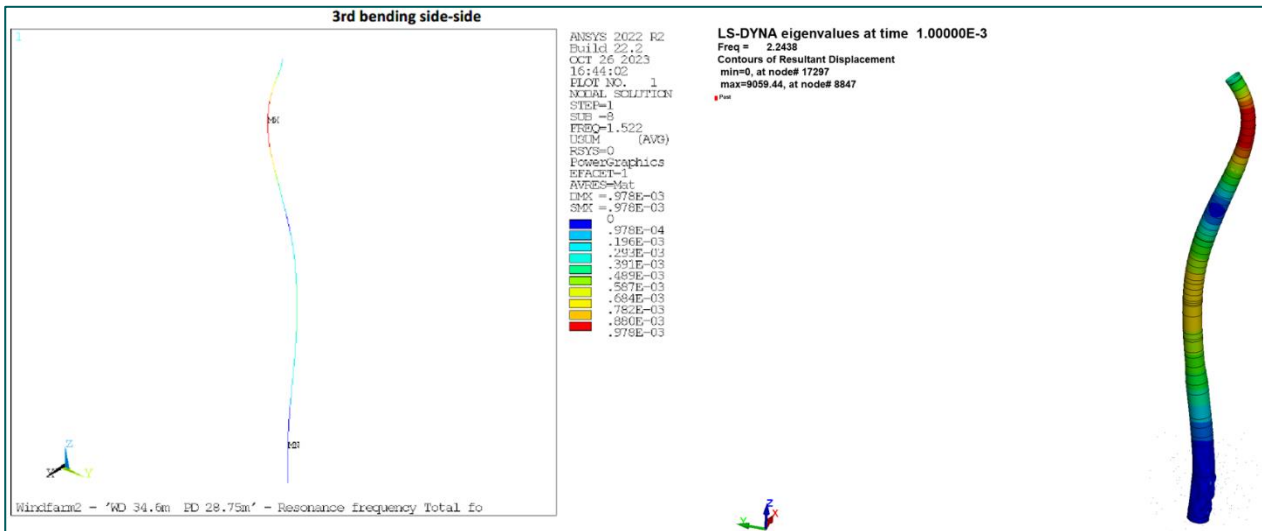


Figure 68. 3rd mode – beam element (left) and shell elements (right)



### Summary and conclusion

In the table below, a summary of the result comparison is provided between the results from *ref. [4]* and the current shell element analysis with two different p-y curve amplification factors: 1.0 and 2.5. This comparison highlights the influence of soil-structure interaction dynamics on the modal behavior of the turbine support structure.

Table 47. Modal results summary

Mode shape	Ref. [4]	Shells p-y curve factor 1.0	Shells p-y curve factor 2.5
Mode 1	0.205	0.217	0.205
Mode 2	0.841	0.729	1.066
Mode 3	1.522	1.497	2.224

Based on these results, it can be concluded that the outcomes are in agreement with each other. The model with a p-y curve amplification factor of 2.5 exhibits slightly stiffer behavior, which ensures a conservative approach for assessing the potential damage to the ship.

## I. FEM Model validation and verification

To validate and verify the calculation method, two separate models were developed to simulate the collision between a wind turbine foundation and a chemical tanker's starboard side and bow. For both the models one part remains rigid. This way we can validate the simulations without influence of flexible to flexible interactions.

- In the first model, the foundation tower is treated as a fully rigid structure, while the ship's starboard side is represented using shell elements.
  - Initial velocity: 4 knots (2.06 m/s)
  - Mass: 3.885e7 kg
  - Kinematic energy: 82.25 MJ
- In the second model, the foundation tower is modeled with shell elements, whereas the ship's bow is treated as a fully rigid component.
  - Initial velocity: 10 knots (5.14 m/s)
  - Mass: 2.205e7 kg
  - Kinematic energy: 291.78 MJ

This approach ensures the correct conversion of initial kinetic energy into internal energy, allowing for thorough verification of the simulation methodology.

### I.1. Verification model with rigid tower foundation

As shown in *Figure 69*, all the kinetic energy (82.25 MJ) from the ship is converted into internal energy upon impact. Over time, the ship rebounds, converting some of the internal energy back into kinetic energy. This rebound causes the ship to detach from the foundation tower.

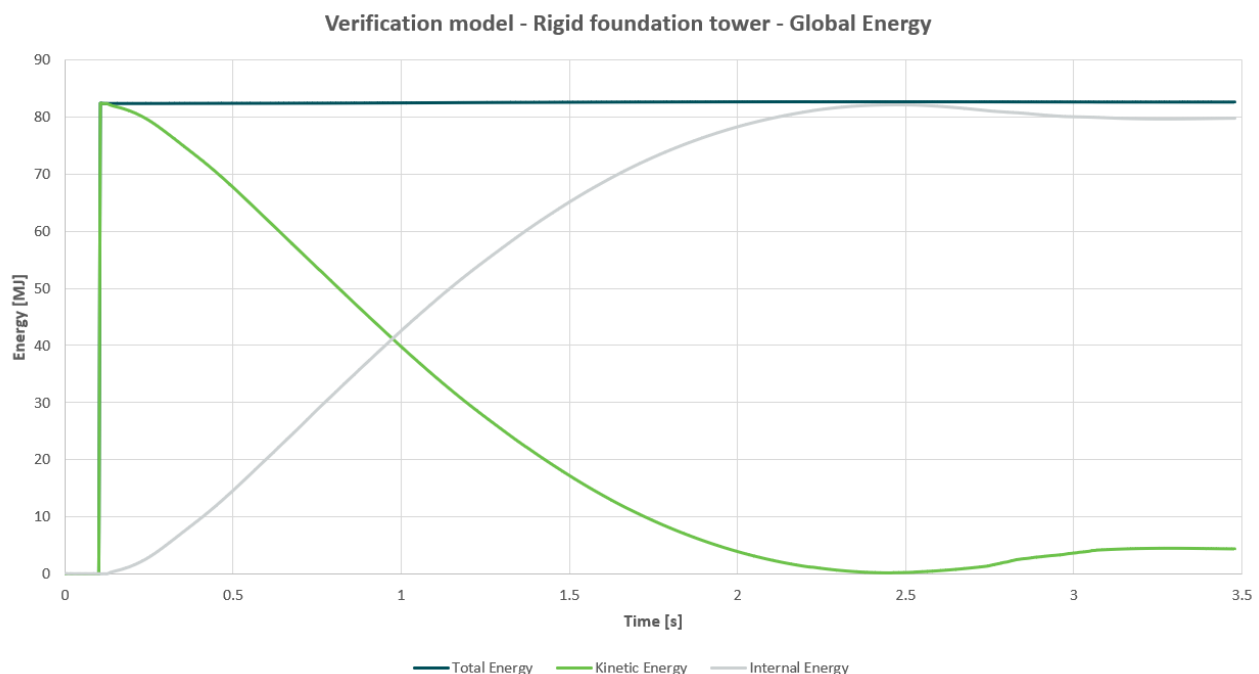


Figure 69. Global energy Distribution over time

The impact force, with a maximum of 39.8 MN, between the vessel and the foundation over the time is shown in *Figure 70*.

Verification model - Rigid foundation tower - Impact Force

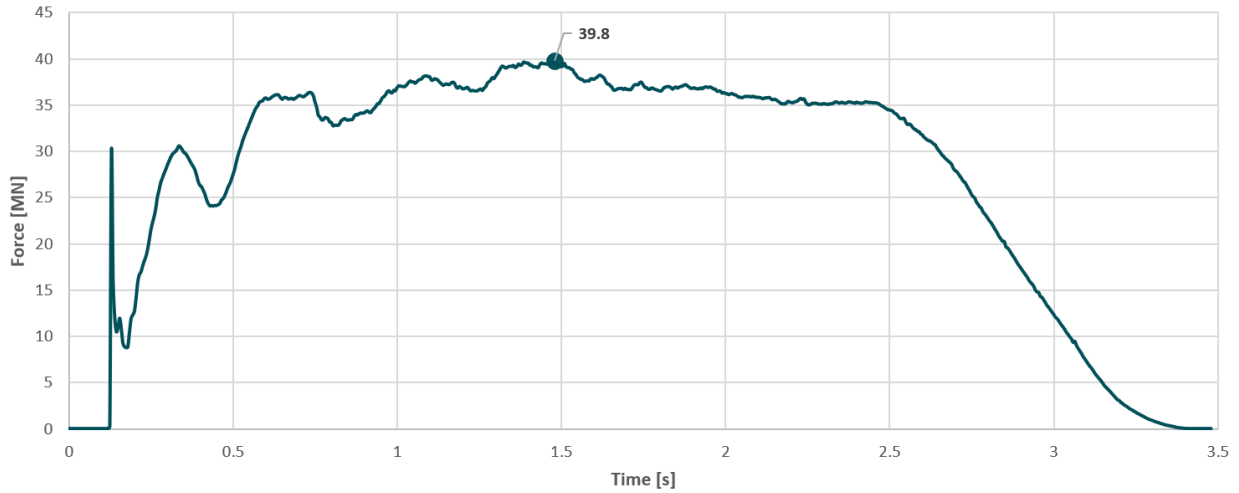


Figure 70. Impact Force over time

Figure 71 shows the deformation of the ship after the collision.

LS-DYNA keyword deck by LS-PrePost  
Time = 3.4848  
Contours of Relative Resultant Displacement  
min=0, at node# 104876  
max=2137.42, at node# 264835

Relative Resultant Displacement

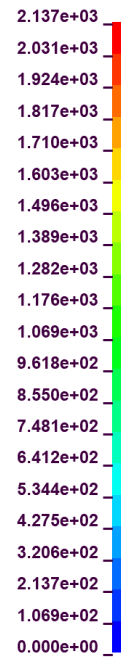
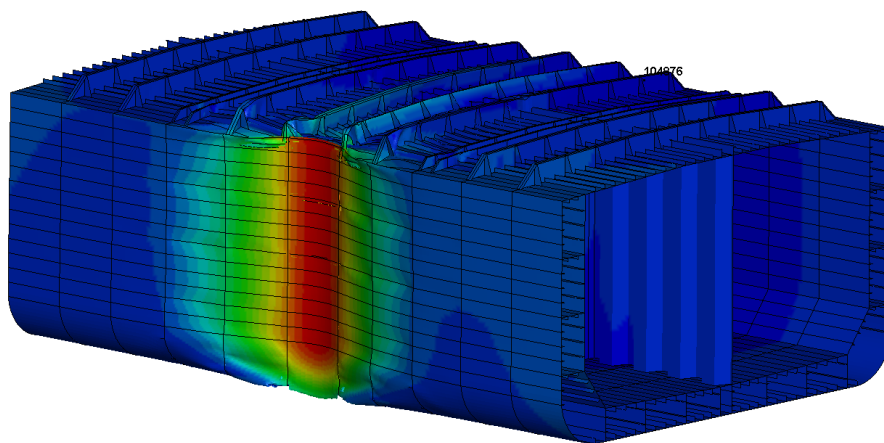
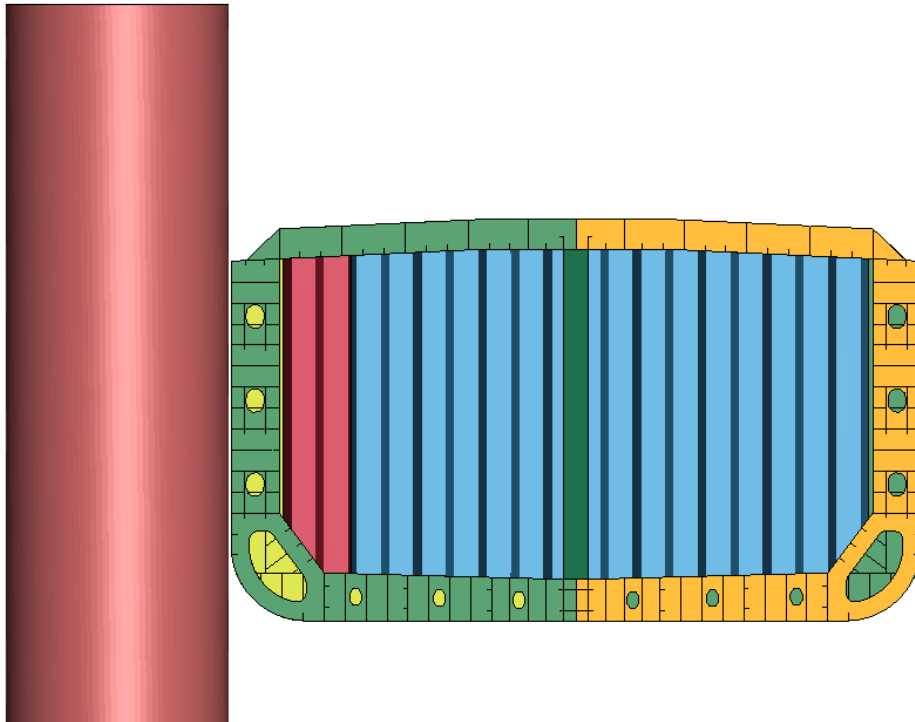


Figure 71. Resultant displacement SB side

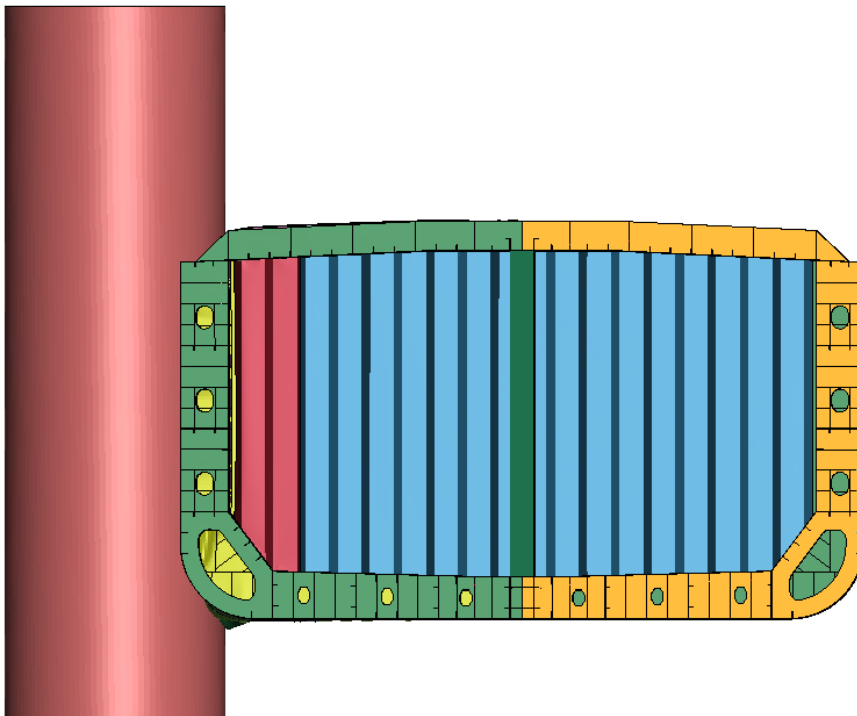
Table 48. Visual timelapse verification model with rigid tower foundation

**Verification model with rigid tower foundation**

t = 0 s



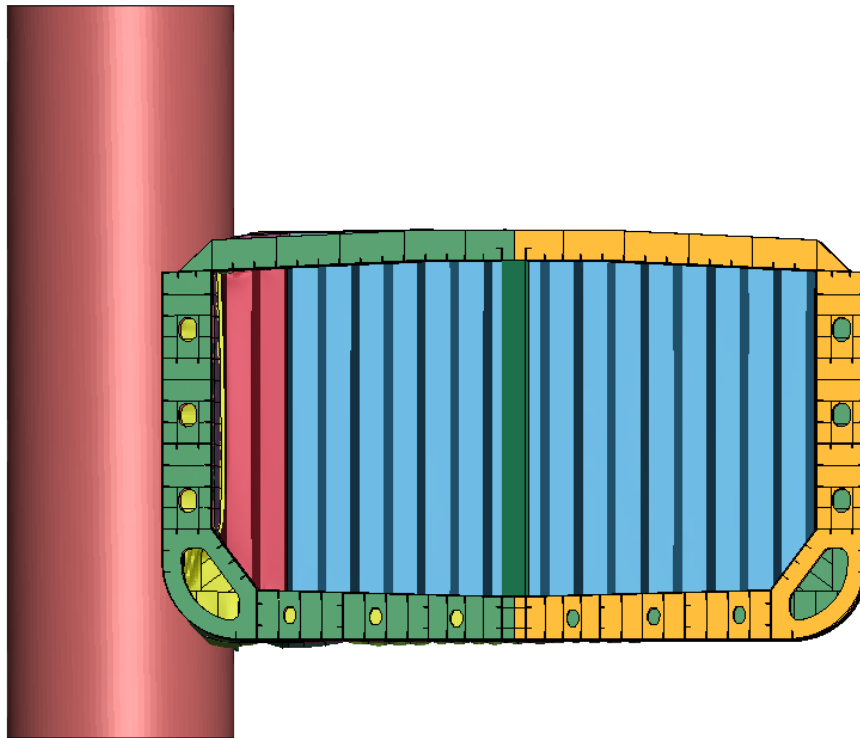
t = 1.0 s



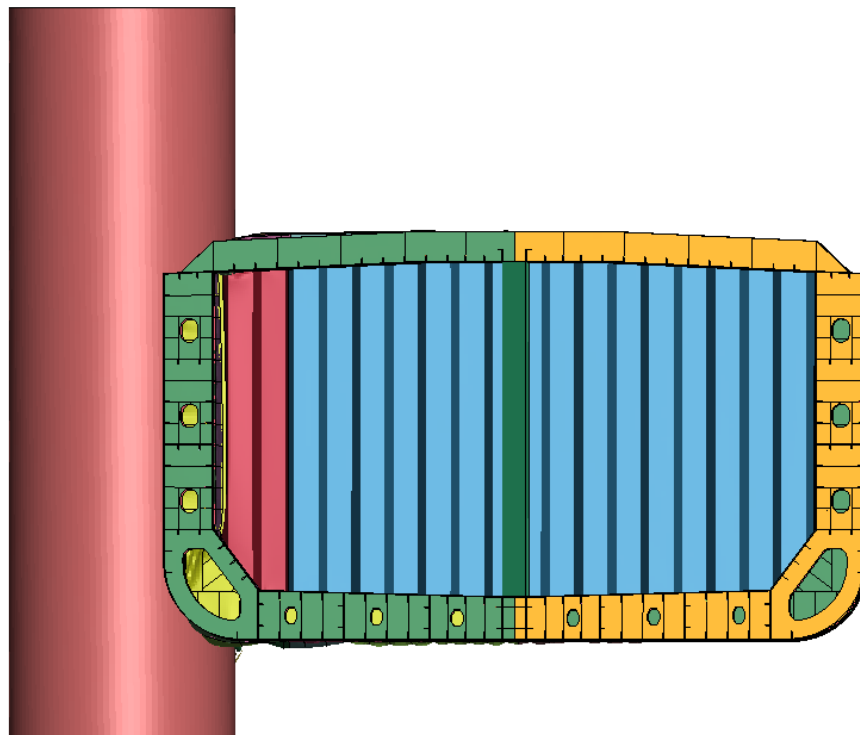


Verification model with rigid tower foundation

t = 2.0 s

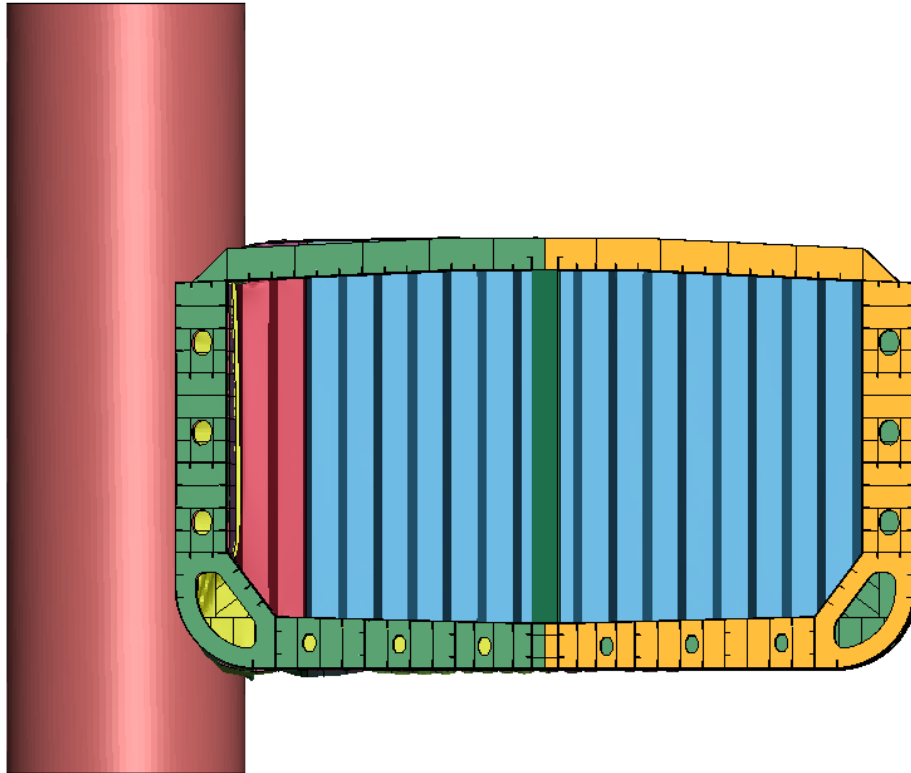


t = 3.0 s



Verification model with rigid tower foundation

t = 3.5 s



## 1.2. Verification model with rigid bow of chemical tanker

After the ship strikes the foundation tower, the kinetic energy (291.78 MJ) is partially converted into internal energy, as shown in *Figure 72*. The visual timelapse (*Table 49*) demonstrates that the impact causes the tower to collapse, generating kinetic energy from both the deformation and the mass set in motion. This kinetic energy is reflected as a progressive increase in internal energy over time, explaining the observed rise in both total and internal energy as time advances.

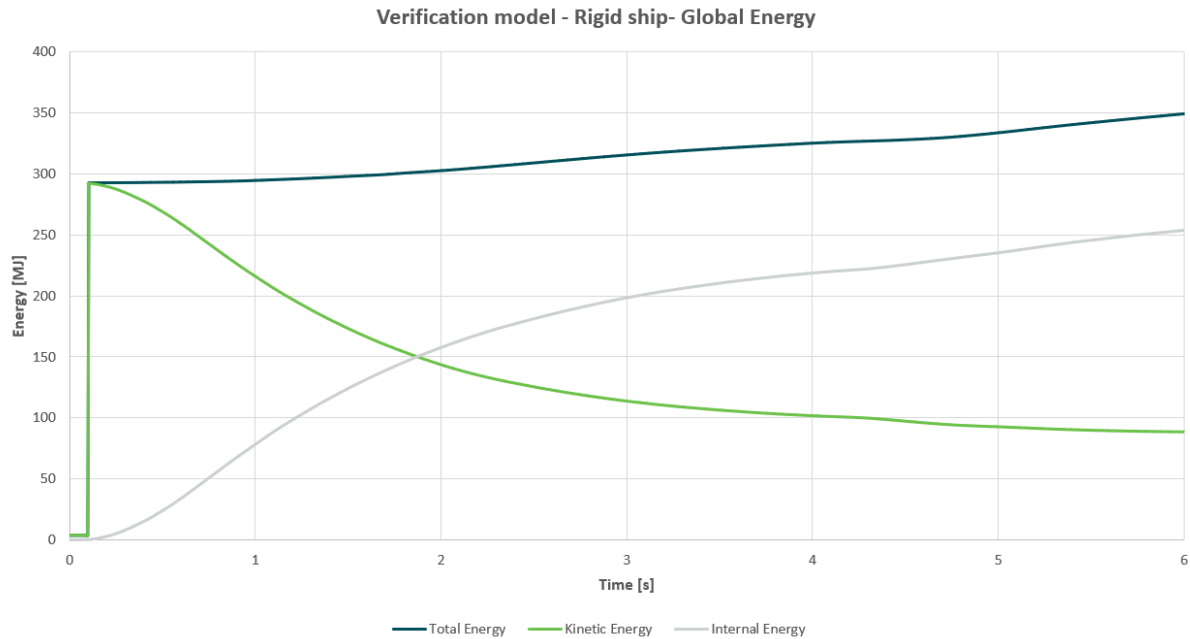


Figure 72. Global energy Distribution over time

The impact force with a maximum of 30.9 MN between the vessel and the foundation over the time is shown in *Figure 73*.

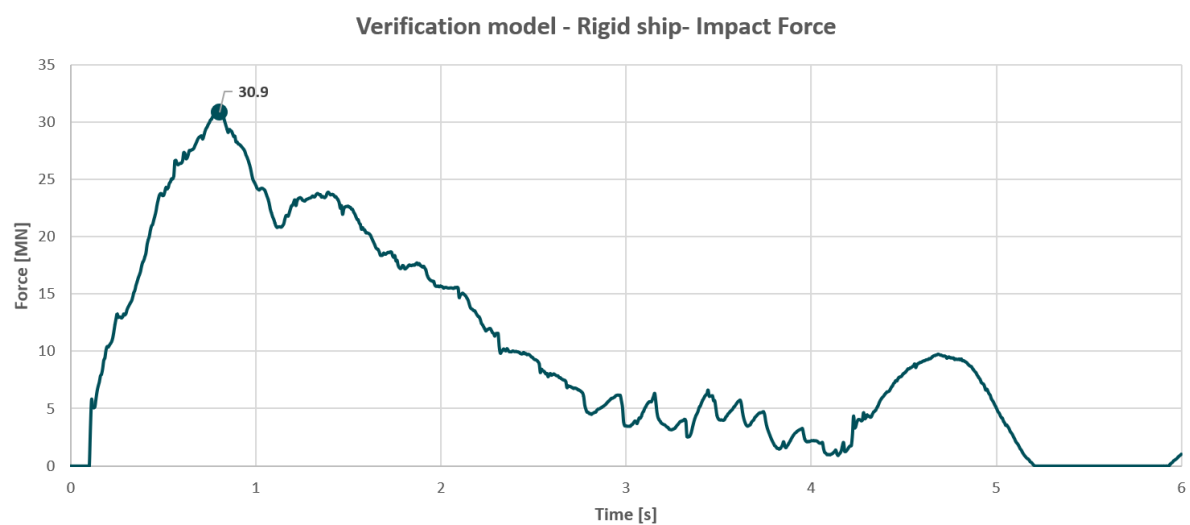


Figure 73. Impact Force over time

Table 49. Visual timeline simulation verification model with rigid bow

**Verification model with rigid bow**

**t = 0 s**





Verification model with rigid bow

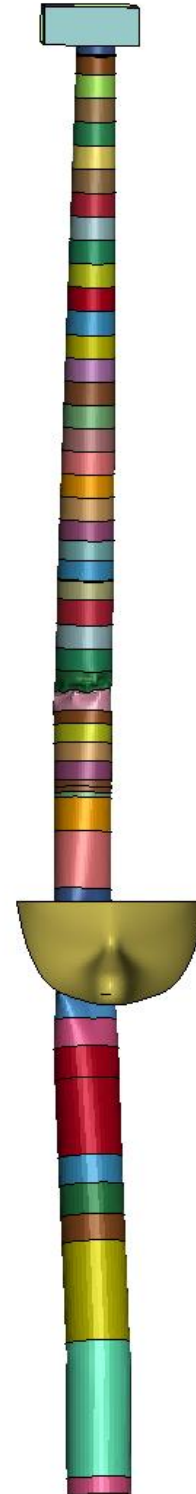
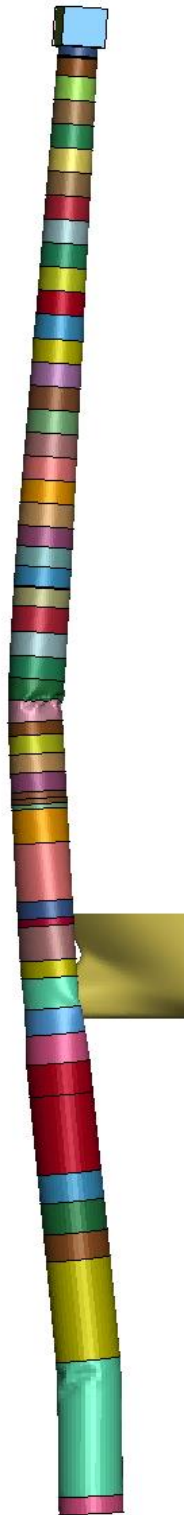
t = 1.02 s





Verification model with rigid bow

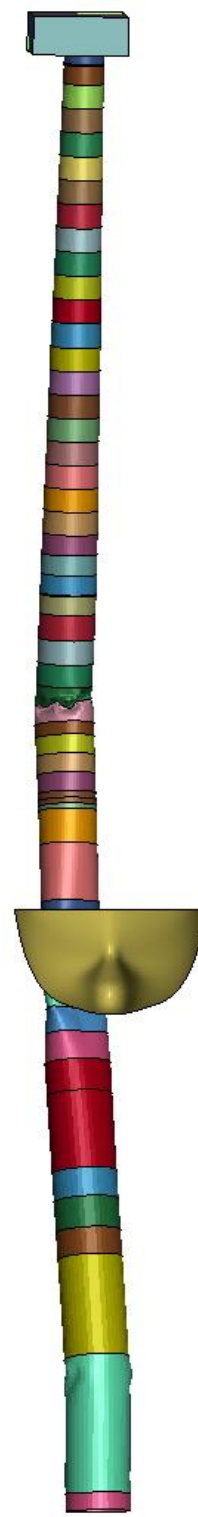
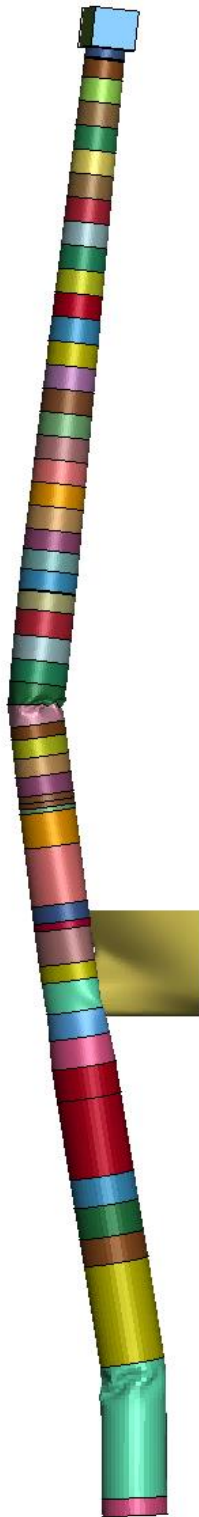
t = 1.98 s





Verification model with rigid bow

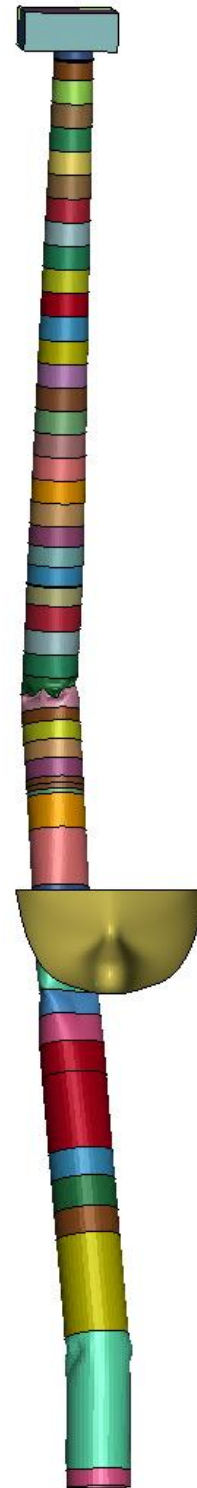
t = 3 s





Verification model with rigid bow

$t = 4.02$  s







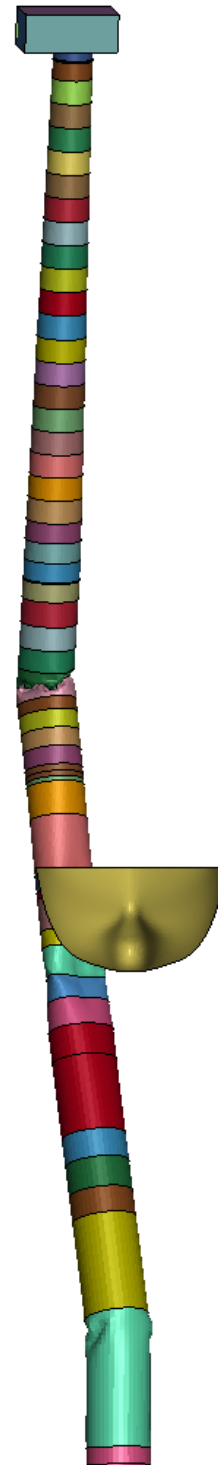
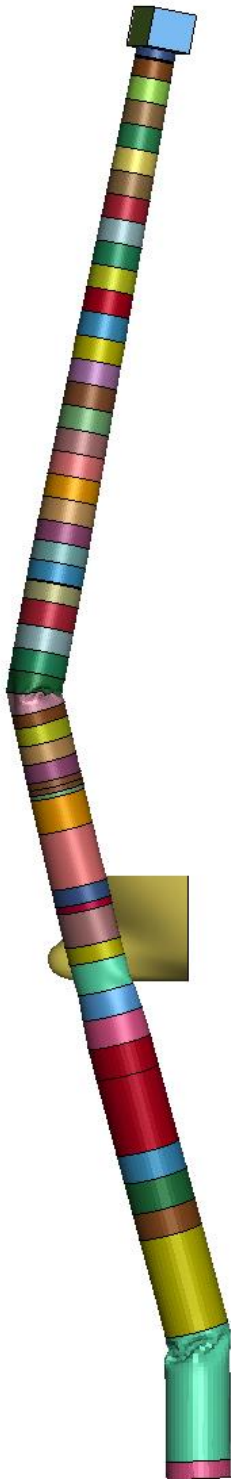
Verification model with rigid bow

t = 4.98 s



Verification model with rigid bow

t = 6 s





### **I.3. Full mid section vs half midsection validation**

The objective of this study is to compare various simulation methodologies for assessing the impact of bending moments during the collision between a ship section and a turbine support structure. For validation, the midsection of a passenger vessel was selected. The comparison encompasses three potential approaches:

- Utilizing a super element for half of the vessel
- Modeling the entire vessel
- Modeling half of the vessel

In ANSYS LS-Dyna, superelements are a computational strategy used to simplify and expedite finite element analyses for large or complex models. They represent a condensed or reduced representation of a portion of the model, allowing computational effort to focus on specific areas of interest while still considering the influence of the rest of the structure.

To ensure the reliability and validation of the results when using superelements, a simplified beam model was initially created. The results were in agreement, thus a superelement was created for the half sections of the passenger vessel. While the results appeared promising, further validation was needed. However, due to an approaching deadline, it was decided to stop additional research. Therefore, the results are excluded from this paragraph and the investigation focuses on the midsection of a passenger ship, modeled in two configurations: a half model and a full model. The comparison aims to evaluate how the structural configuration affects the bending moments experienced during the collision.

Understanding the role of bending moments is crucial for assessing the structural integrity and response of the turbine support structure under dynamic impact loads. By analyzing the results of these two modeling approaches, this study seeks to determine whether the half-model representation accurately captures the behavior of the full model during collision events. This insight will help optimize computational resources while ensuring the accuracy of simulation results.

### I.3.1. Geometry

In this section, the geometry of the modeling approach for the midsection of the passenger vessel is presented. We describe the process of modeling both the half-section and the full-section of the midsection of the vessel. The sections where the impact will take place are modeled in greater detail, incorporating all stiffeners with beam elements to accurately capture the structural response. All dimensions used in this modeling adhere to the specifications provided in paragraph 5.5.3.1, ensuring consistency and precision in the simulation results.

#### I.3.1.1. Half mid-section

In this approach, as shown in *Figure 74* half of the midsection of the passenger vessel is modeled in Ansys. This model represents half of the full midsection, with the excluded section being supported and a rigid constraint added to the purple-colored edges. This rigid connection is used to eventually add the missing mass of the excluded section.

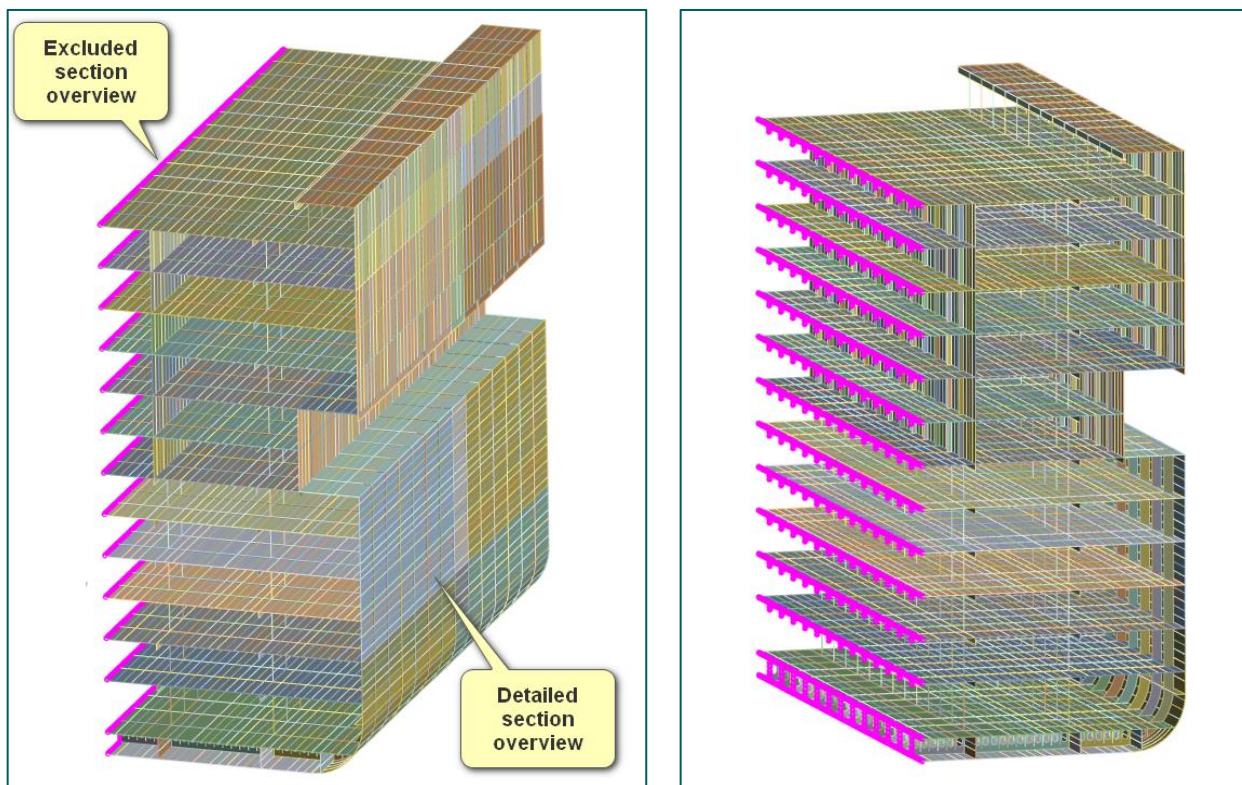


Figure 74 - Half mid section of the passenger vessel.

### I.3.1.2. Full section

In this approach, as shown in *Figure 75*, the full midsection of the passenger vessel is modeled in Ansys. The half closer to the collision side is represented with all stiffeners and structural details, ensuring an accurate depiction of local deformations. In contrast, the half section farther from the impact location is modeled with less detail to optimize computational efficiency while maintaining the overall structural response.

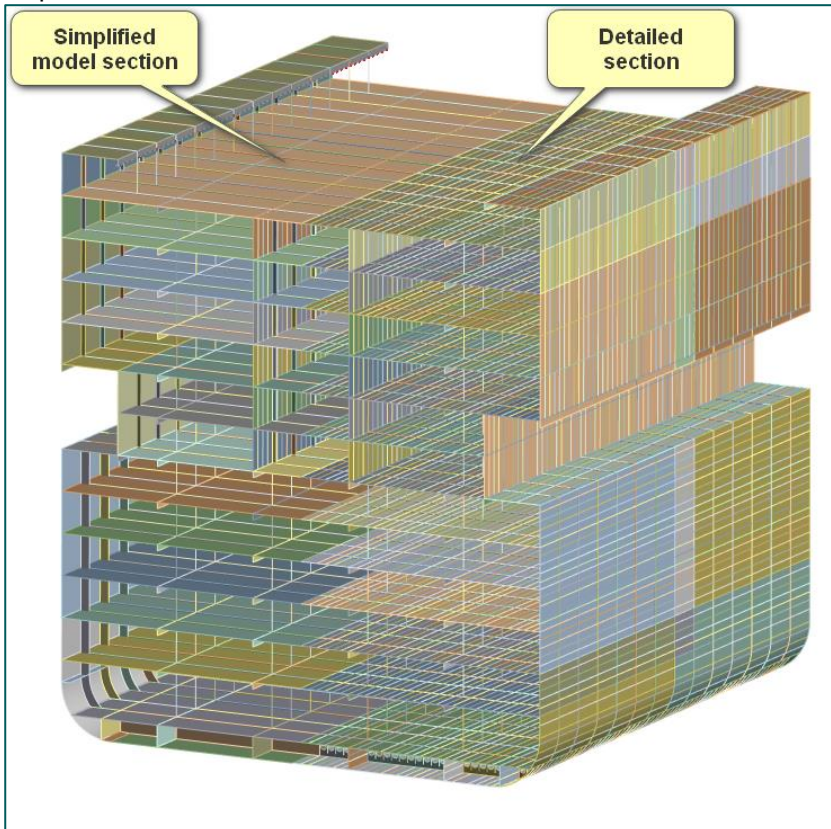


Figure 75 - Full mid section – Detailed and simplified

### 1.3.2. Boundary conditions

Two rigid remote points are established where the degrees of freedom are constrained (Rigid remote point left and right). An additional remote point is created at the center of the mid-section. The constraints on the left and right remote points are set to capture the bending moment accurately. However, the remote point in the middle has no constraints and is free to move. Due to the rigid nature of the remote point connection, this connection itself does not deform.

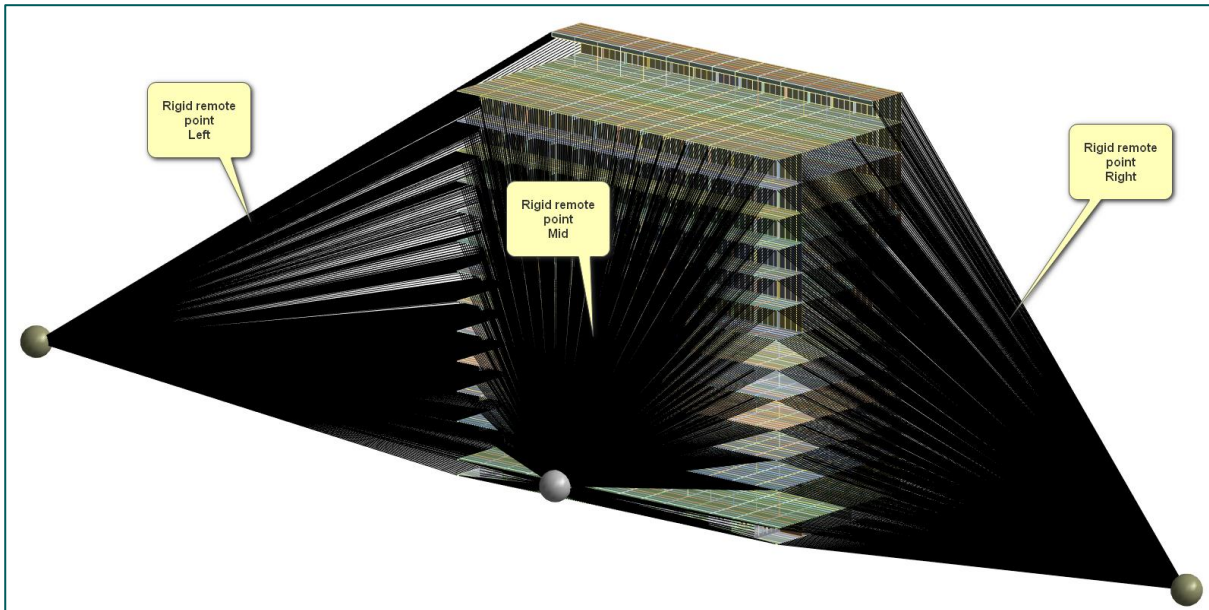


Figure 76 – Rigid Connection on the half mid section of the passenger vessel

For the full mid-section, the rigid remote points on the left and right are in the same locations compared to the half mid-section model. The degrees of freedom for these remote points are constrained in the same way as explained for the half mid-section.

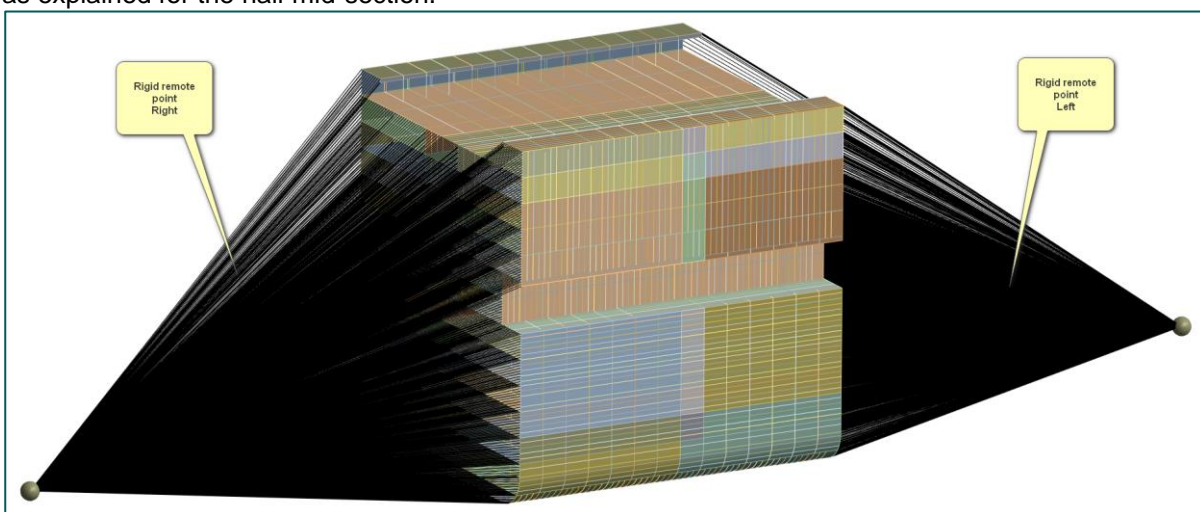


Figure 77 – Rigid connection on the full section of the passenger vessel

### I.3.3. Loading

A force of  $6 \times 10^7$  [N] is applied to account for the impact force. This force is based on the forces that are observed during the collision simulations.

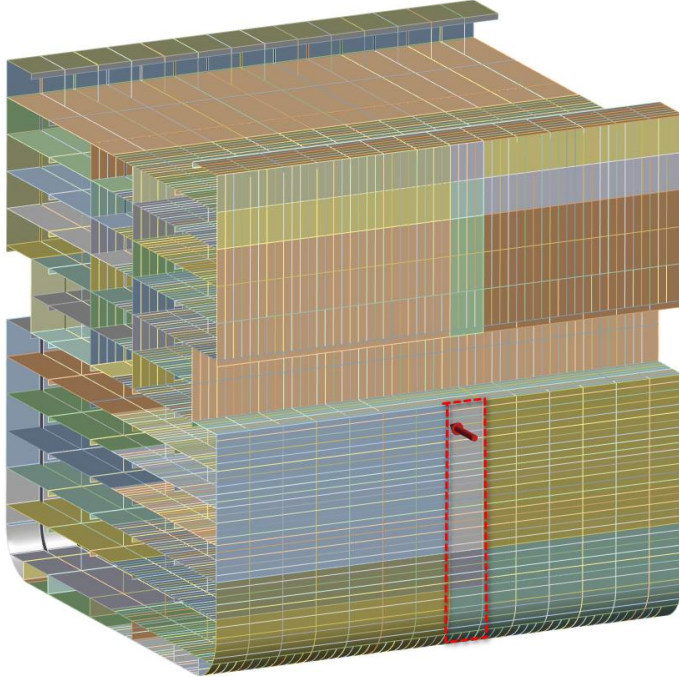


Figure 78 – Static loading

### I.3.4. Results comparison

The deformation results show a significant disparity due to the differences in global stiffness between the two models. Deformations of 1.749 meters for the half model and 1.587 meters for the full model. The half model, with its higher deformation, suggests a less stiff structure, potentially leading to inaccurate representations of the vessel's behavior during collisions. In contrast, the full model provides a more stable and reliable depiction, reflecting lower deformation and thus greater structural integrity. This consistency in the full model's performance is crucial for precise assessments of the vessel's response under various loading conditions, reinforcing the decision to use it for further analyses. By ensuring minimal discrepancies and enhanced accuracy, the full section model offers a more robust foundation for evaluating the structural impacts of collisions, contributing to more reliable and precise simulation results.

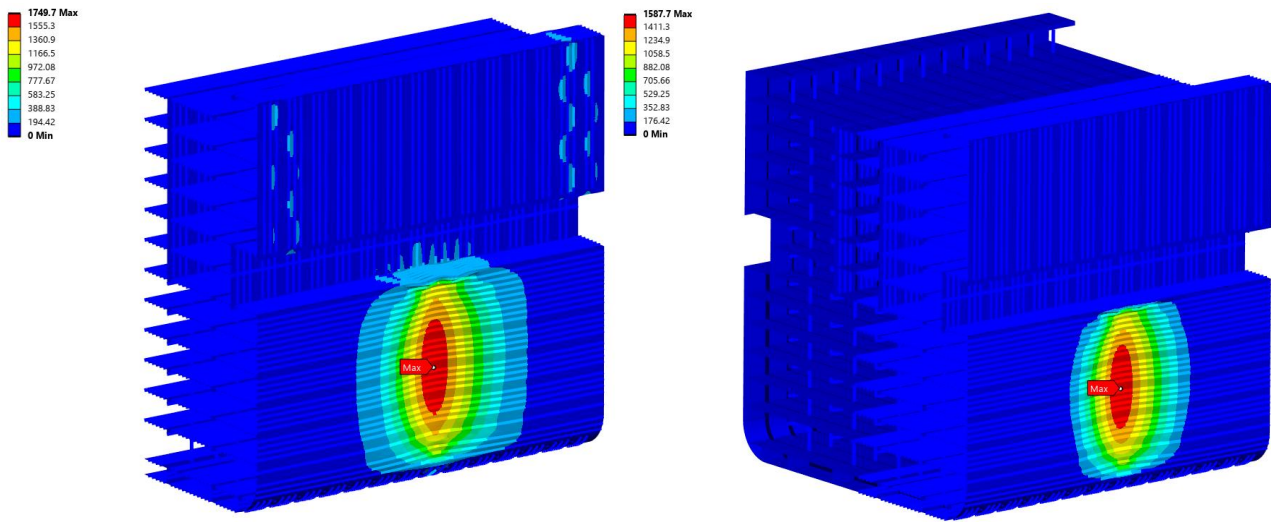


Figure 79 – Comparison of the deformations

Additionally, the Von-Mises stresses are compared, showing different global stress values. The maximum stress is 470 MPa for the half model and 450 MPa for the full model.

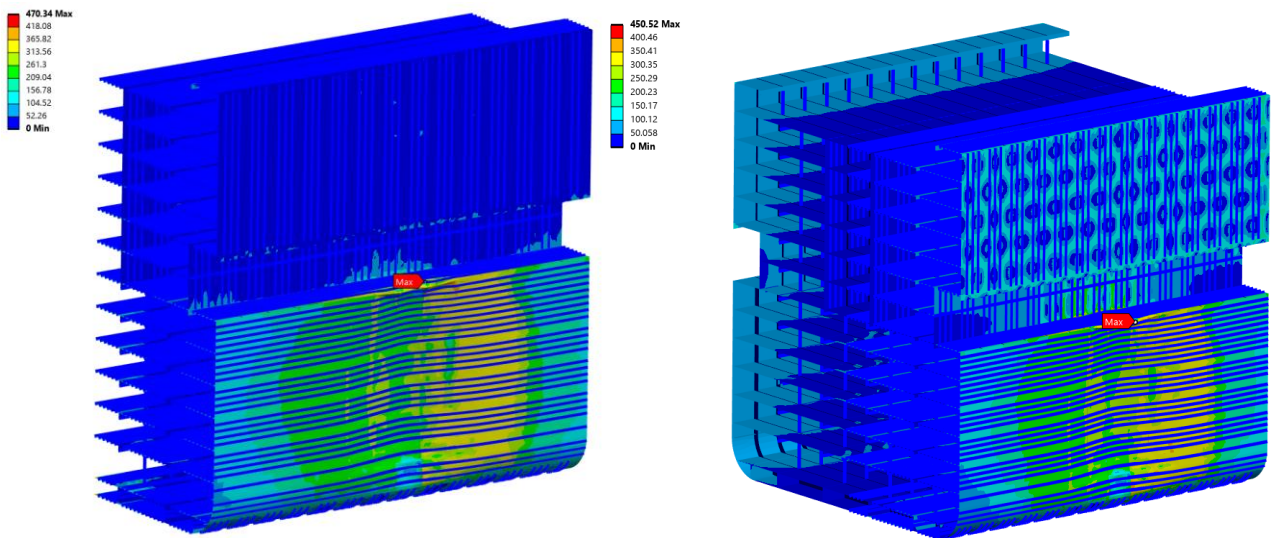


Figure 80 – Comparison of the Von-Mises stresses



The bending stresses of the section due to the impact are significant, and the stresses along the length of the vessel are also compared. It is observed that there are global differences. The maximum normal stress is 520 MPa for the half section and 470 MPa for the full section.

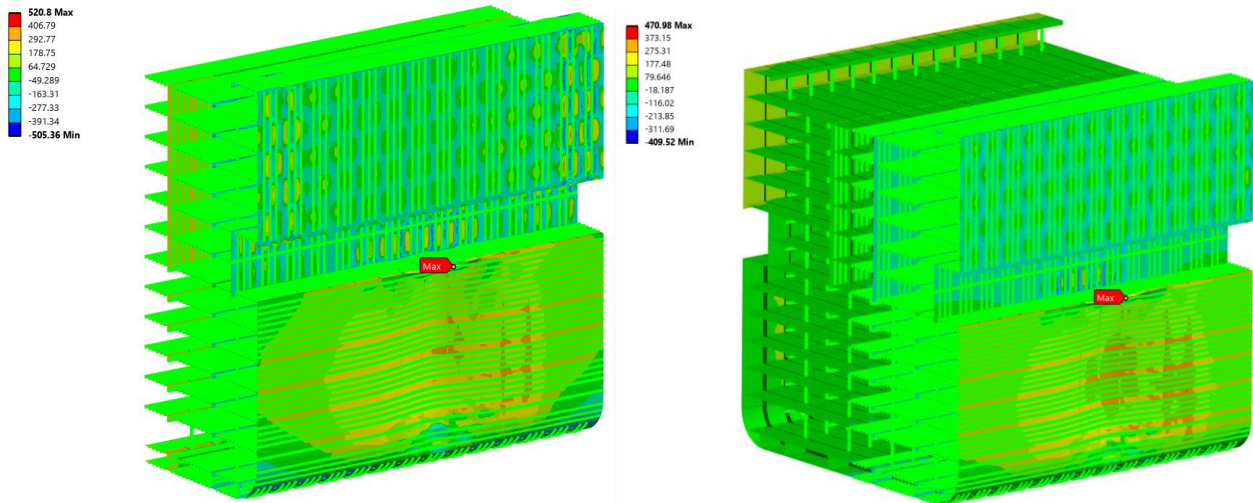


Figure 81 Normal stress along the vessels length



### **1.3.5. Conclusion**

The analysis of the half and full midsection models indicates that, although both models demonstrate consistent local stiffness and structural integrity, the observed differences in deformation and stress distribution are significant enough to impact the overall accuracy of the simulation results. The half model shows higher deformation and stress values compared to the full model. Consequently, we have decided to use the full section model for further analyses to ensure a more reliable and precise evaluation of the structural response under load conditions.

By choosing the full section model, we aim to minimize discrepancies and enhance the accuracy of our collision simulations, providing a more robust basis for our structural assessments.

The major distinction lies in the disparate global stiffness, which highlights the importance of maintaining detailed structural elements to achieve accurate simulation results. The detailed full section model demonstrates lower deformation and stress values, indicating greater structural integrity. In contrast, the simplified half section model exhibits higher deformation and stress values, revealing potential inaccuracies in depicting the vessel's behavior under load. This comparison underscores the necessity of using a detailed full section model to ensure the fidelity and precision of the structural assessments, thereby providing a more reliable foundation for further analyses.

### I.3.6. Full detailed mid-section comparison Half simplified mid-section

In this paragraph, we will describe the comparison between a detailed full section model and a model with a half section detailed and a half section without beam stiffeners. Additionally, small shell stiffeners and other minor details have been suppressed. Boundary conditions are the same compared to paragraph H.3.2. The loading condition is the same as paragraph H.3.3.

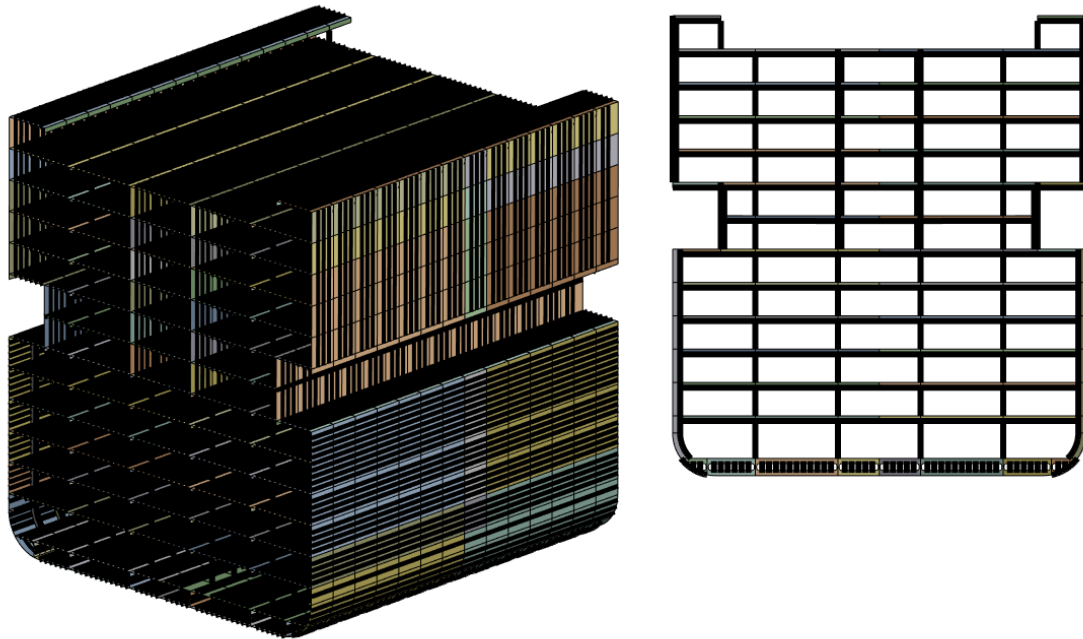


Figure 82 – Full detailed mid-section

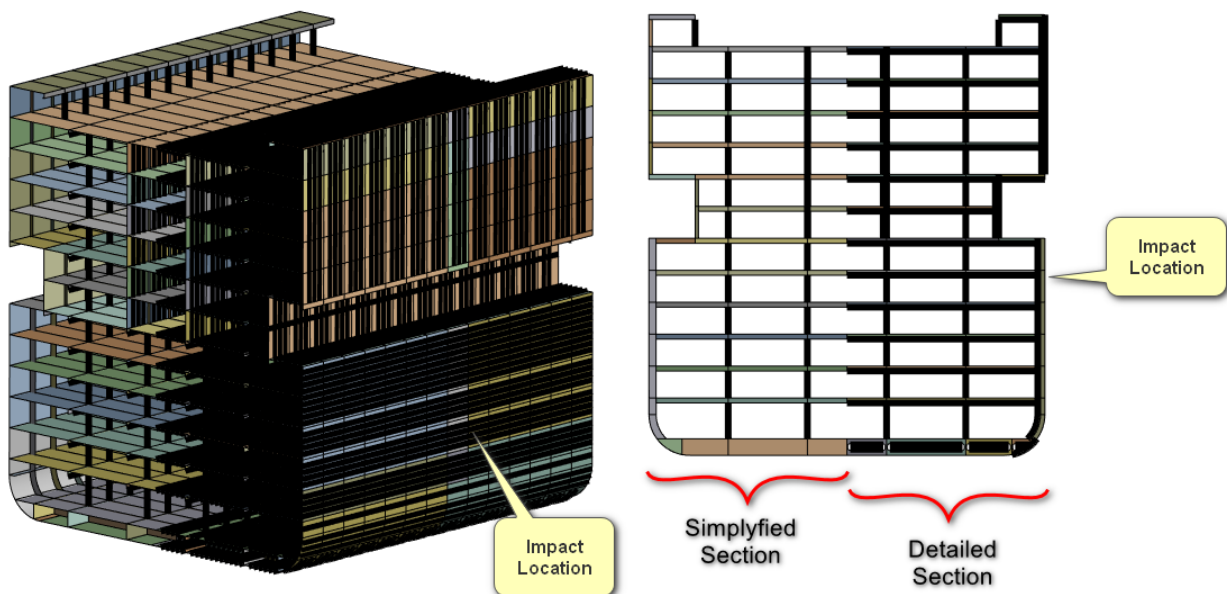


Figure 83 - Half simplified mid-section

### I.3.7. Results comparison

This paragraph shows the result comparison between the two simulations. The deformations are slightly different, showing bigger deformation for the simplified half mid-section.

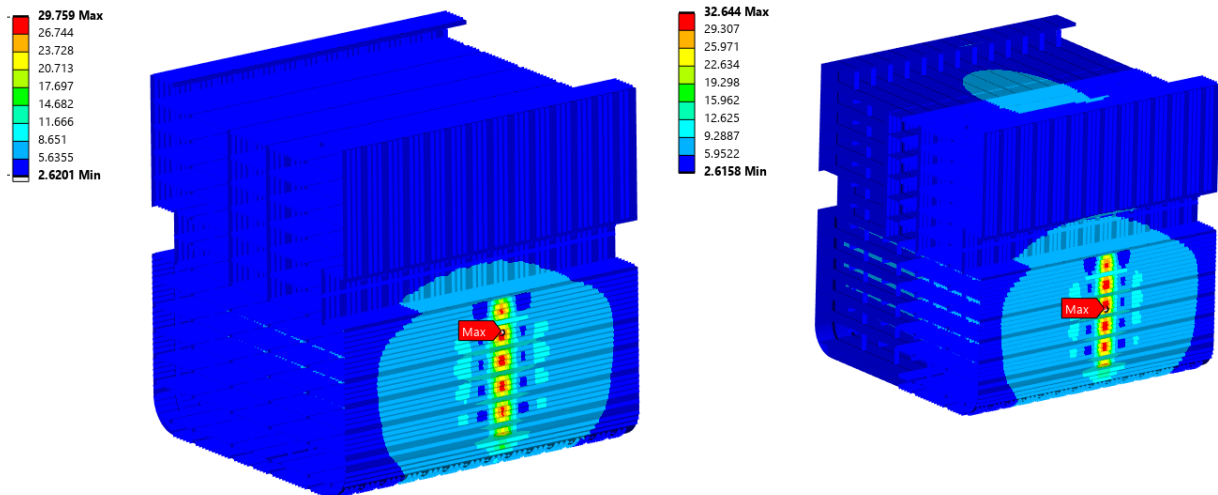


Figure 84 - Deformation comparison

The bending stiffness is an important parameter that will influence the results for the impact scenarios. Normal stress along the ship's length is therefore compared. The results show bigger stresses for the half simplified mid-sections.

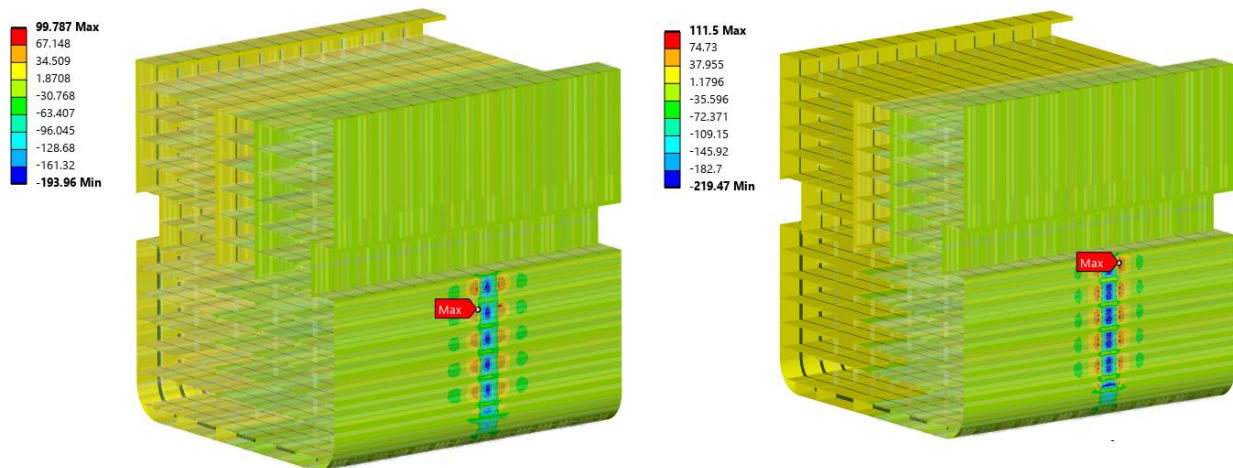


Figure 85 – Normal stress along the length of the ship



### **I.3.8. Conclusion**

Based on the results, the deformation and stress show a small increase for the simplified half mid-section. Because the simulation time is also an important factor, the simplified half mid-section approach was chosen for the collision scenarios. The results indicate that this is a conservative approach for assessing the ship damage, providing a reliable margin of safety in the impact scenarios.

## J. FEM Model Input and Output

### J.1. Results Ship Collision

#### J.1.1. Simulation 1

Figure 86 shows the global Kinetic and Internal Energy over time during the collision. Initially, the kinetic energy is 292 MJ, which is determined by the ship's speed and mass. As the collision progresses, the total energy increases due to the collapse of the turbine tower foundation, resulting in a rise in both kinetic and internal energy.

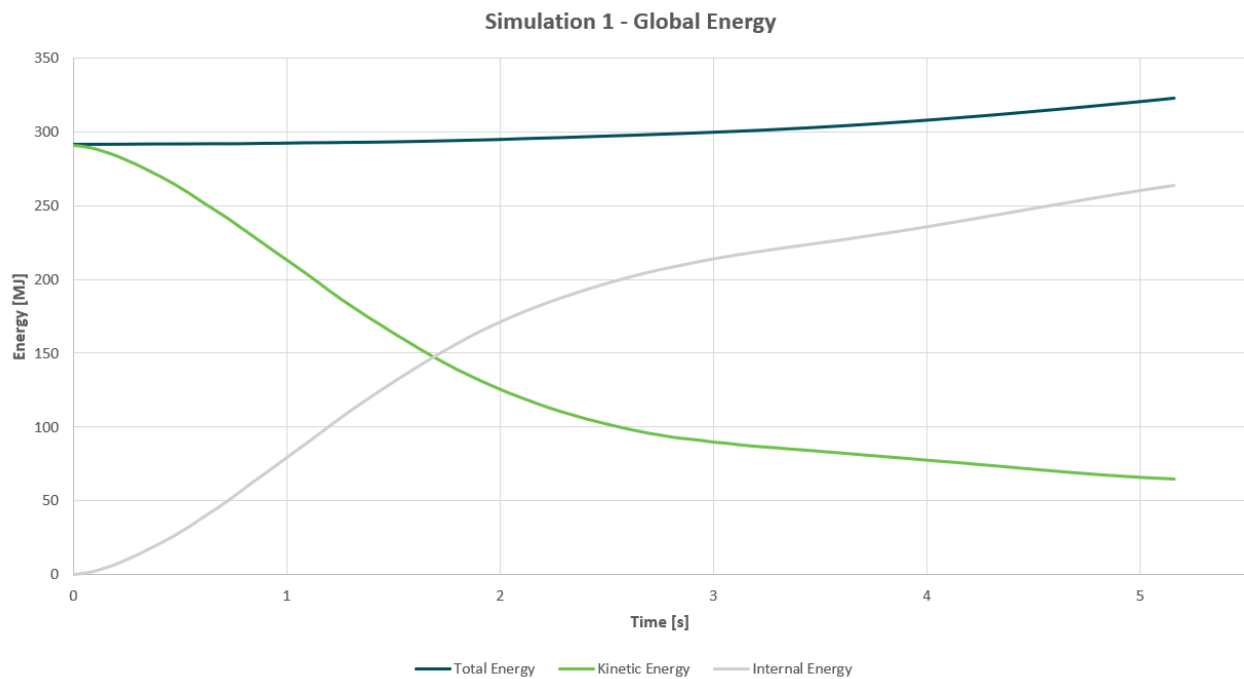


Figure 86. Global energy Distribution over time

Figure 87 displays the Kinetic and Internal Energy of the ship. The initial kinetic energy of the ship differs from the global results presented in Figure 86. This discrepancy arises because the energy associated with the additional mass and the added water mass cannot be separated. The missing portion of the initial kinetic energy corresponds to the ratio of the additional masses to the total mass, indicating that the results are accurate. In total, 232 MJ (= initial – end) kinetic energy is dissipated, of which 38 MJ is absorbed by the vessel as internal energy. The rest is absorbed by the wind turbine foundation.

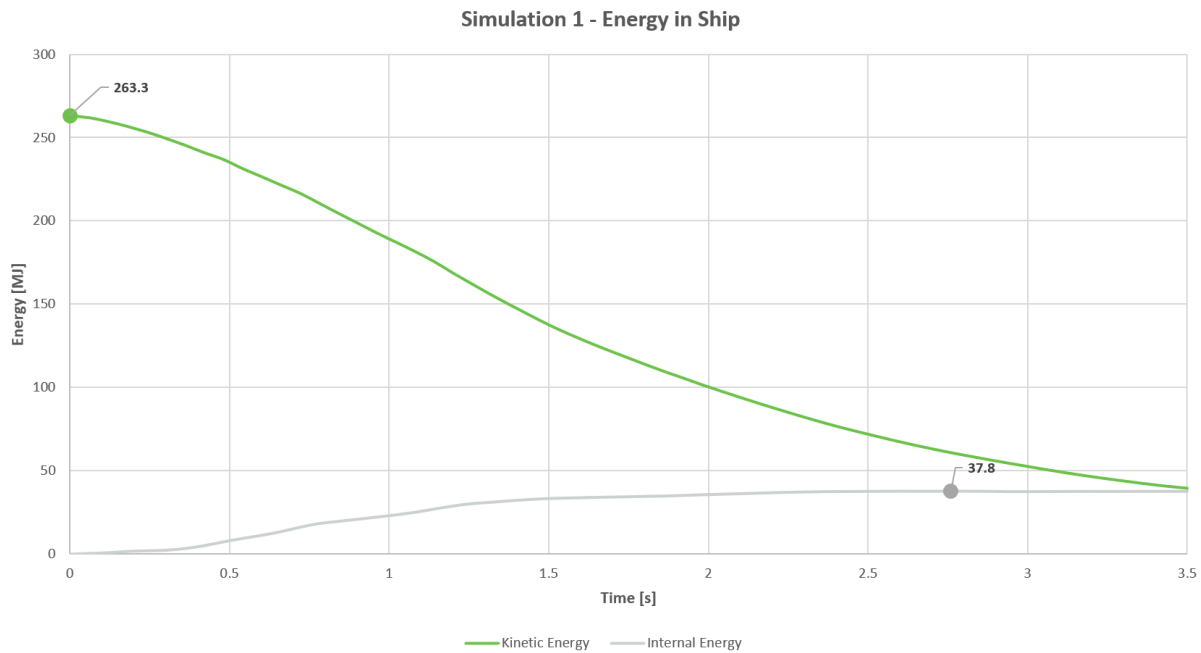


Figure 87. Kinetic and Internal Energy of ship over time

The impact force between the vessel and the foundation over the time is shown in Figure 88.

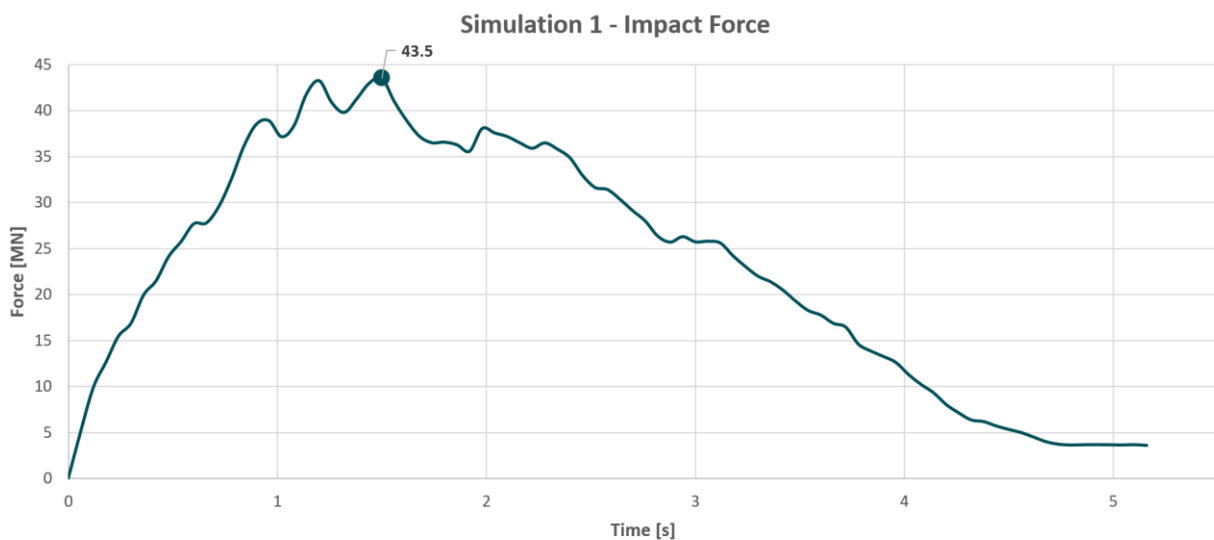


Figure 88. Impact Force over time

The failed elements and effective plastic strain of the bow are shown in *Figure 89* and *Figure 90*.

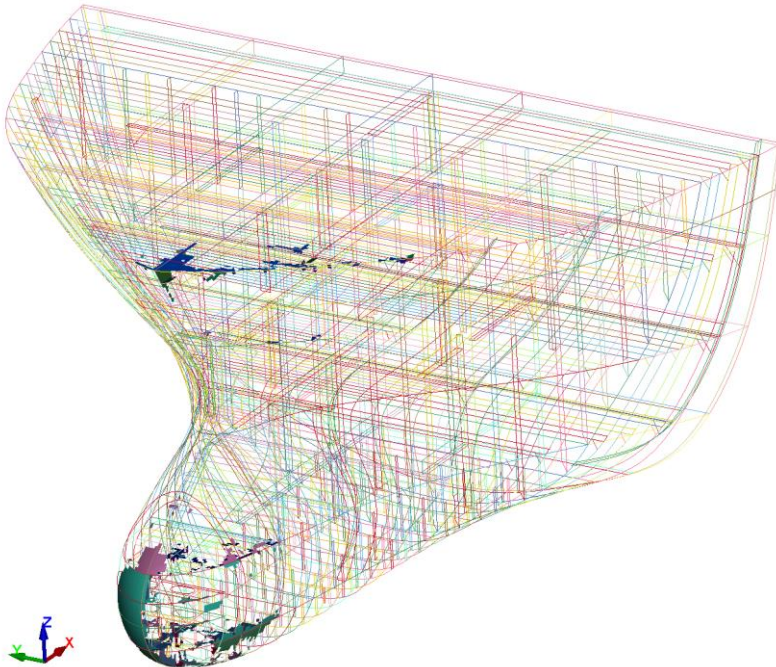


Figure 89. Failed elements simulation 1

LS-DYNA keyword deck by LS-PrePost  
Time = 5.2175  
Contours of Effective Plastic Strain  
reference shell surface  
min=0, at elem# 2258441  
max=0.229031, at elem# 2308878

Effective Plastic Strain

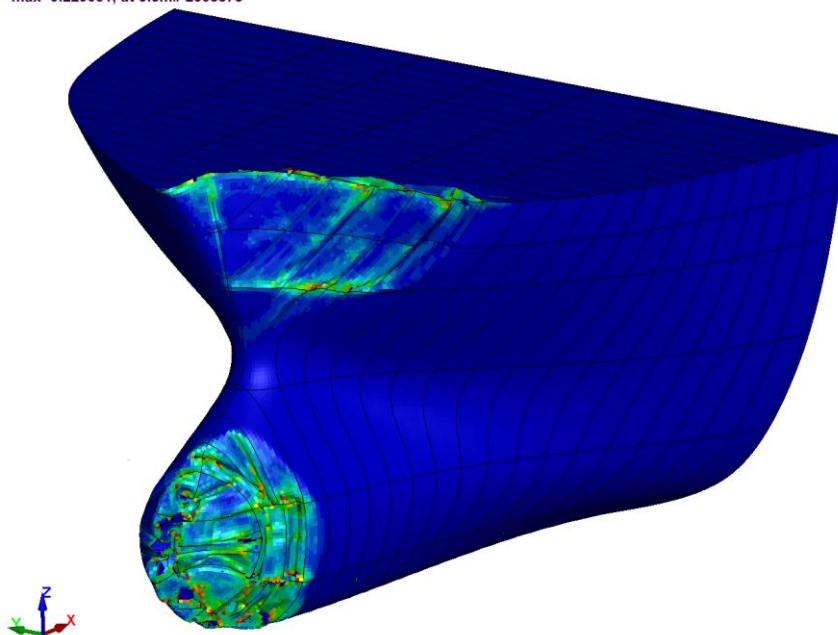
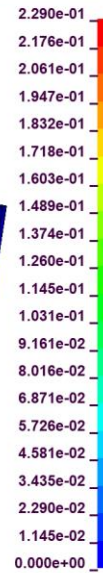


Figure 90. Effective Plastic Strain simulation 1



Figure 91 shows the deformation of the ship after the collision.

**LS-DYNA keyword deck by LS-PrePost**

Time = 5.2175

Contours of Relative Resultant Displacement

min=0, at node# 2209876

max=17156.8, at node# 2233629

**Relative Resultant Displacement**

2.246e+03

2.134e+03

2.021e+03

1.909e+03

1.797e+03

1.684e+03

1.572e+03

1.460e+03

1.348e+03

1.235e+03

1.123e+03

1.011e+03

8.984e+02

7.861e+02

6.738e+02

5.615e+02

4.492e+02

3.369e+02

2.246e+02

1.123e+02

0.000e+00

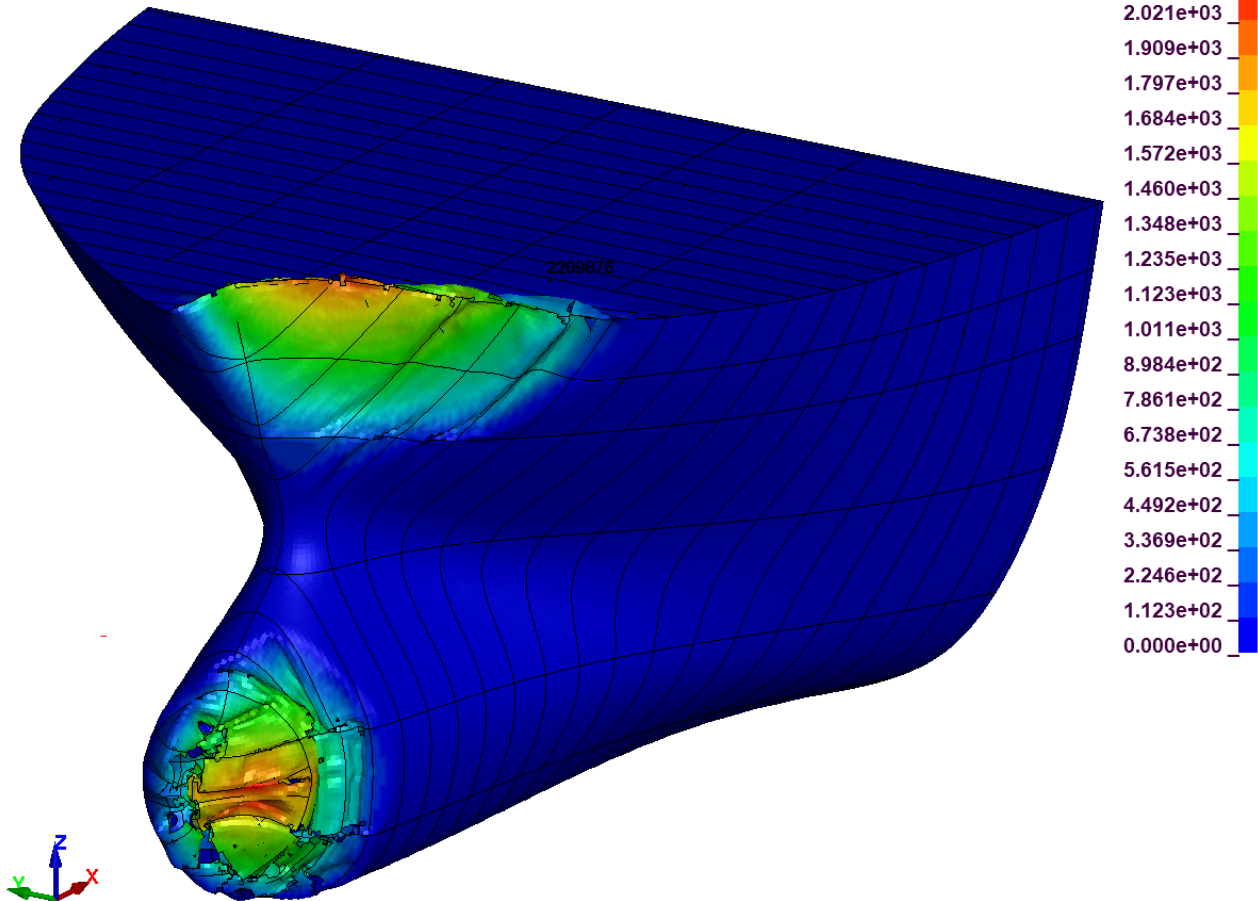


Figure 91. Resultant Displacement Bow [mm]

Figure 92 shows the deformation of the foundation, which indicates a clear buckling failure of the foundation.

## LS-DYNA keyword deck by LS-PrePost

Time = 5.2175

Contours of Resultant Displacement

min=1.90491, at node# 2320812

max=32231.7, at node# 2333568

Resultant Displacement

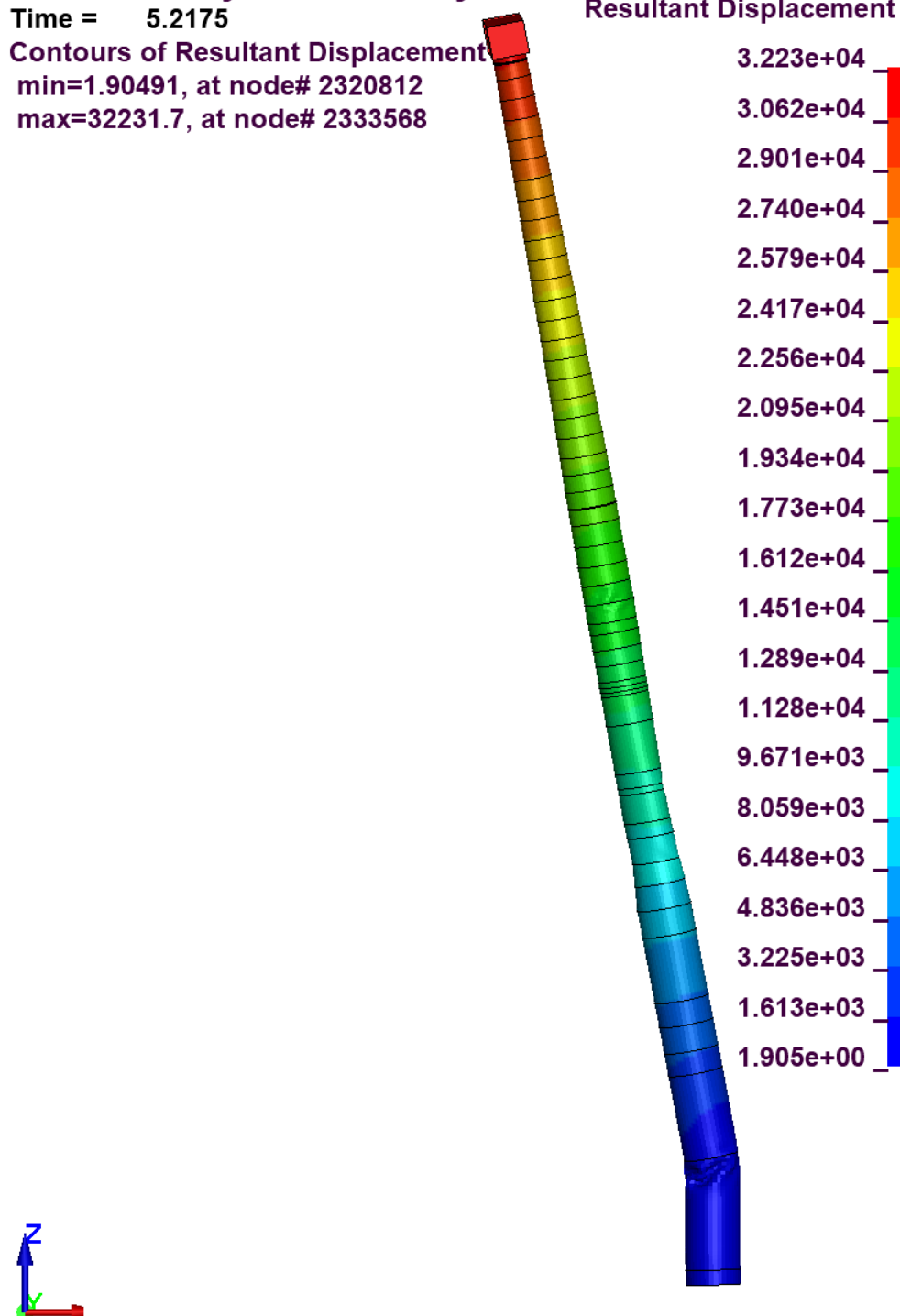


Figure 92. Resultant Displacement Foundation Tower [mm]

Table 50. Visual timeline simulation 1

**Simulation 1**

t = 0 s





Simulation 1

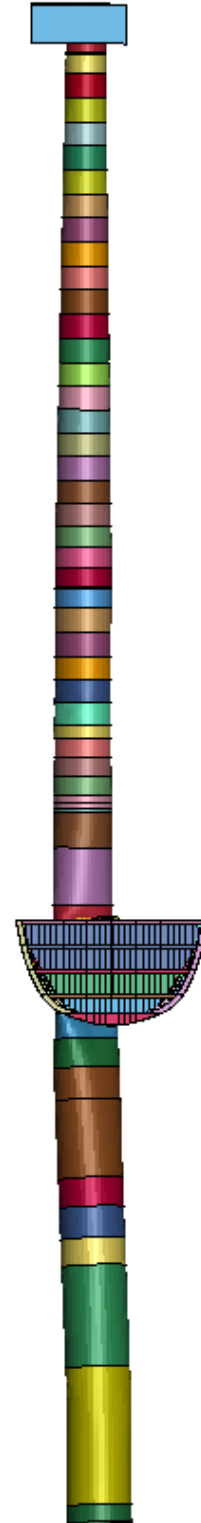
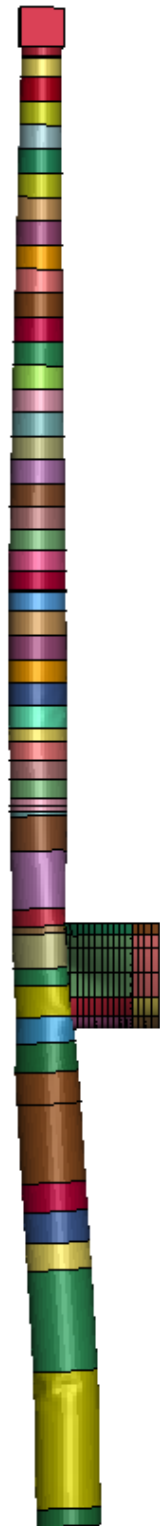
t = 1.02 s





Simulation 1

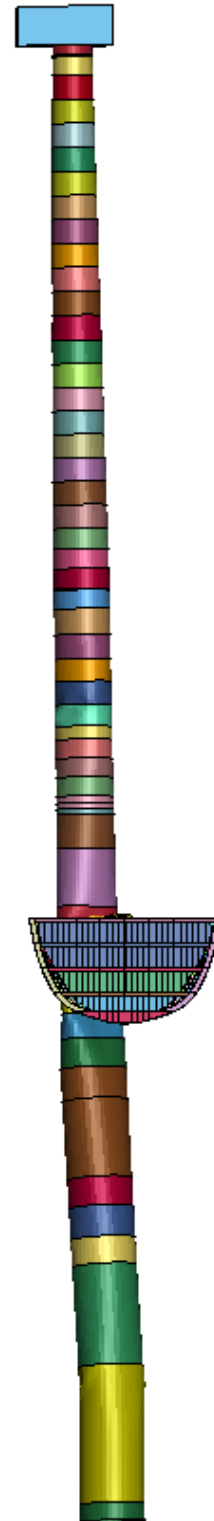
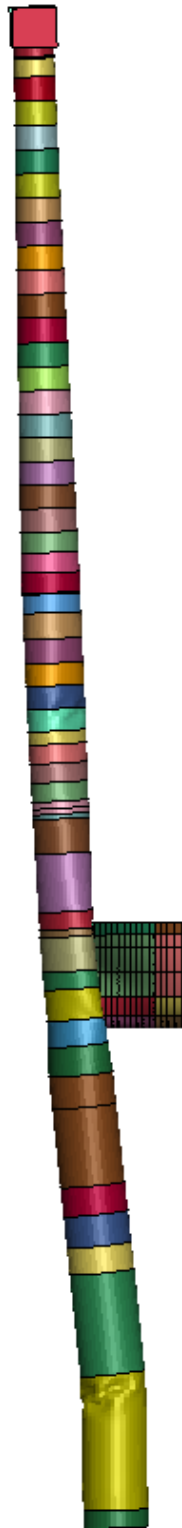
t = 1.98 s





Simulation 1

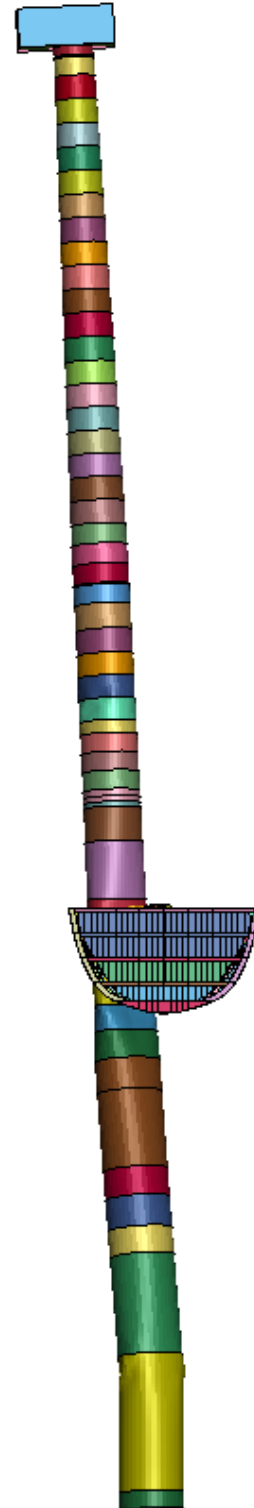
t = 3 s





Simulation 1

t = 4.02





Simulation 1

t = 4.98







Simulation 1

t = 5.22 s



### J.1.2. Simulation 2

Figure 93 shows the global Kinetic and Internal Energy over time during the collision. Initially, the kinetic energy is 1167 MJ, which is determined by the ship's speed and mass. As the collision progresses, the total energy increases due to the collapse of the turbine tower foundation, resulting in a rise in both kinetic and internal energy.

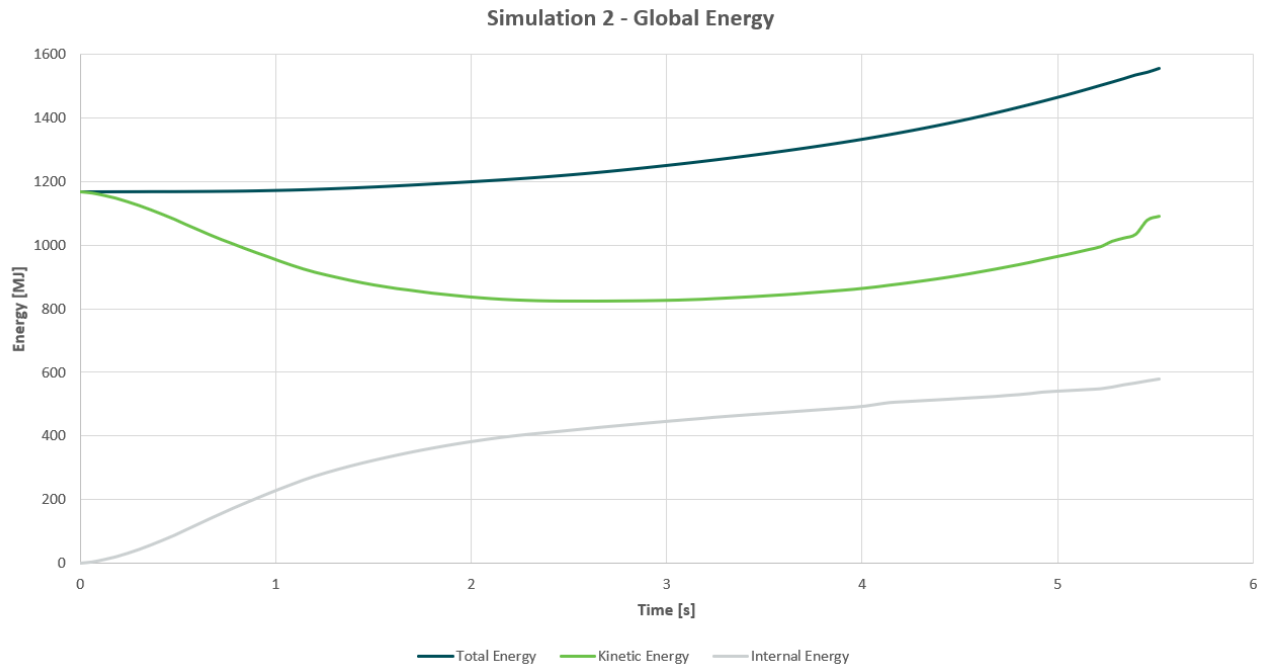


Figure 93. Global energy Distribution over time

Figure 94 displays the Kinetic and Internal Energy of the ship. The initial kinetic energy of the ship differs from the global results presented in Figure 93. This discrepancy arises because the energy associated with the additional mass and the added water mass cannot be separated. The missing portion of the initial kinetic energy corresponds to the ratio of the additional masses to the total mass, indicating that the results are accurate. In total, 398 MJ (= initial – end) kinetic energy is dissipated, of which 69 MJ is absorbed by the vessel as internal energy. The rest is absorbed by the wind turbine foundation.

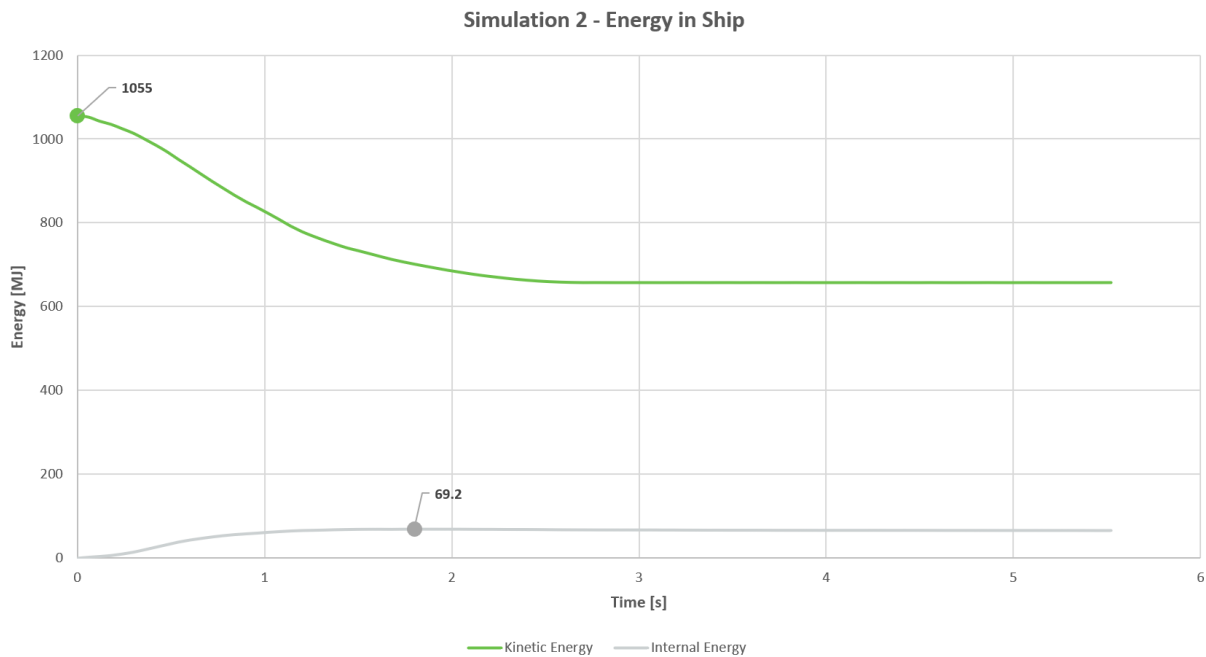


Figure 94. Kinetic and Internal Energy of ship over time

The impact force between the vessel and the foundation over the time is shown in *Figure 95*.

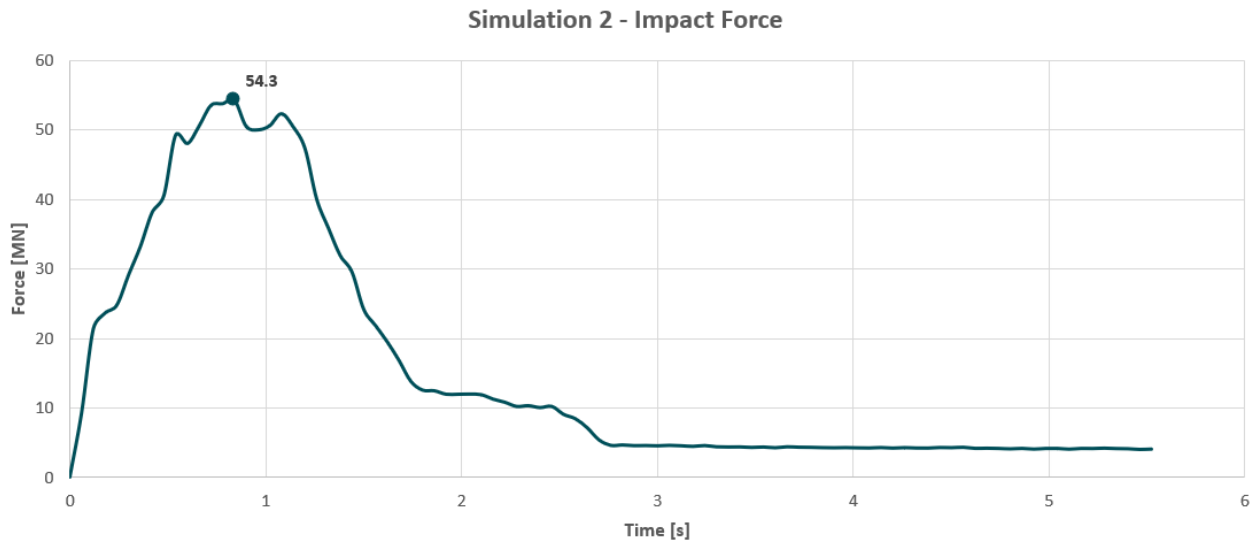


Figure 95. Impact Force over time

The failed elements and effective plastic strain of the bow are shown in *Figure 96* and *Figure 97*.

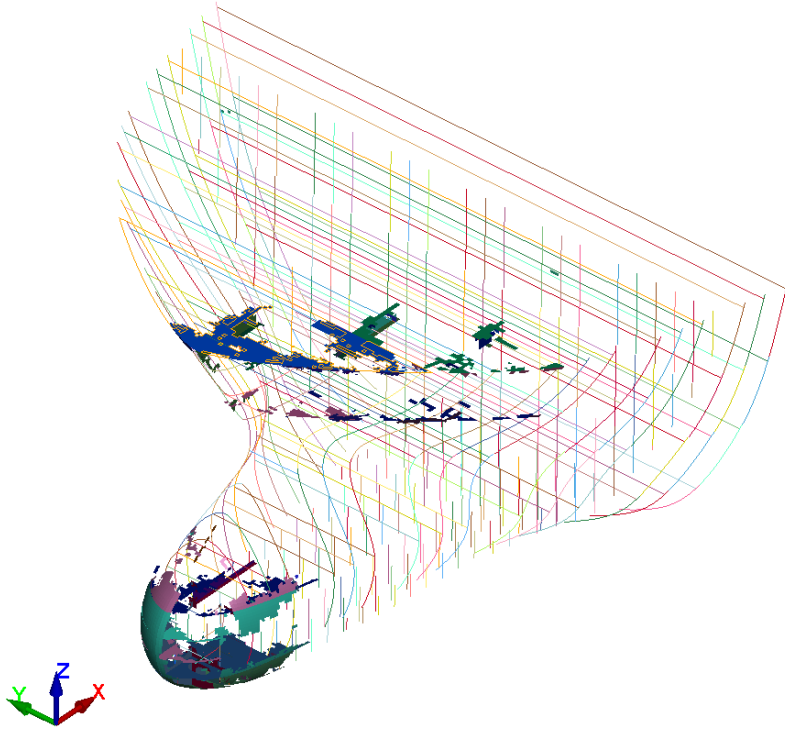


Figure 96. Failed elements simulation 2

LS-DYNA keyword deck by LS-PrePost  
Time = 5.5553  
Contours of Effective Plastic Strain  
reference shell surface  
min=0, at elem# 2258441  
max=0.228991, at elem# 2292705

Effective Plastic Strain

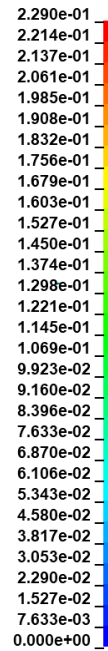


Figure 97. Effective Plastic Strain simulation 2

Figure 98 shows the deformation of the ship after the collision.

### LS-DYNA keyword deck by LS-PrePost

Time = 5.5553

Contours of Relative Resultant Displacement

min=0, at node# 2237596

max=37685.9, at node# 2228238

Relative Resultant Displacement

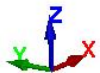
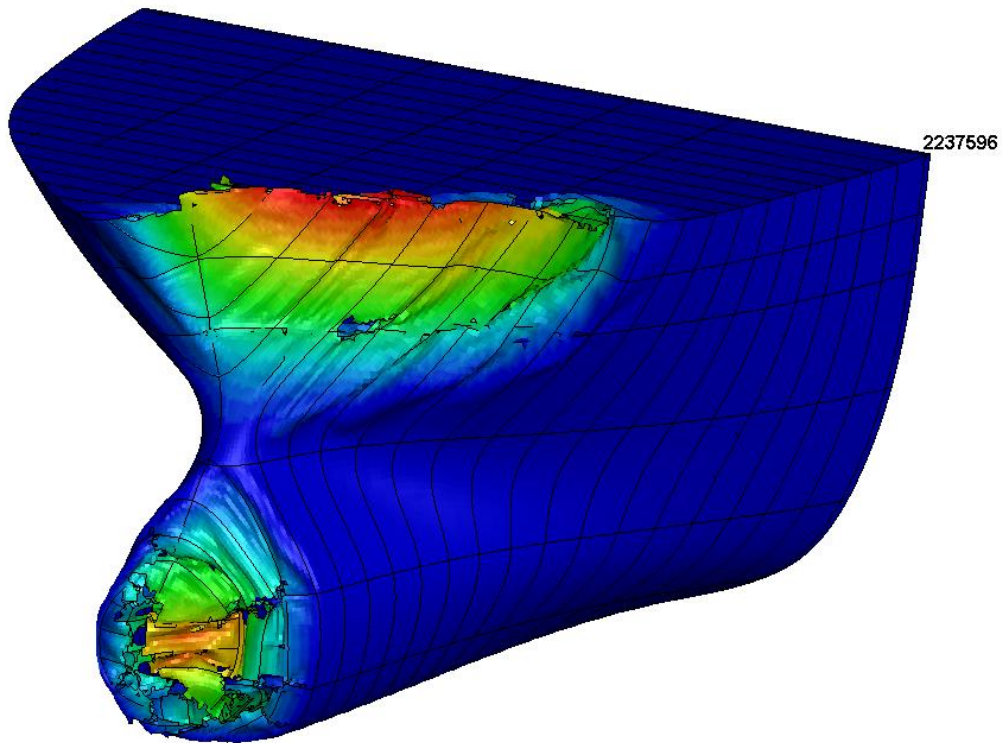
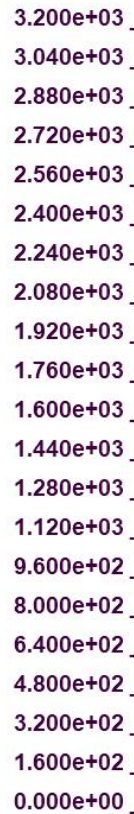


Figure 98. Resultant Displacement Bow [mm]

Figure 99 shows the deformation of the foundation, which indicates a clear buckling failure of the foundation.

**LS-DYNA keyword deck by LS-PrePost**

Time = 5.5553

Contours of Resultant Displacement

min=5.34355, at node# 2320793

max=63978.3, at node# 2323996

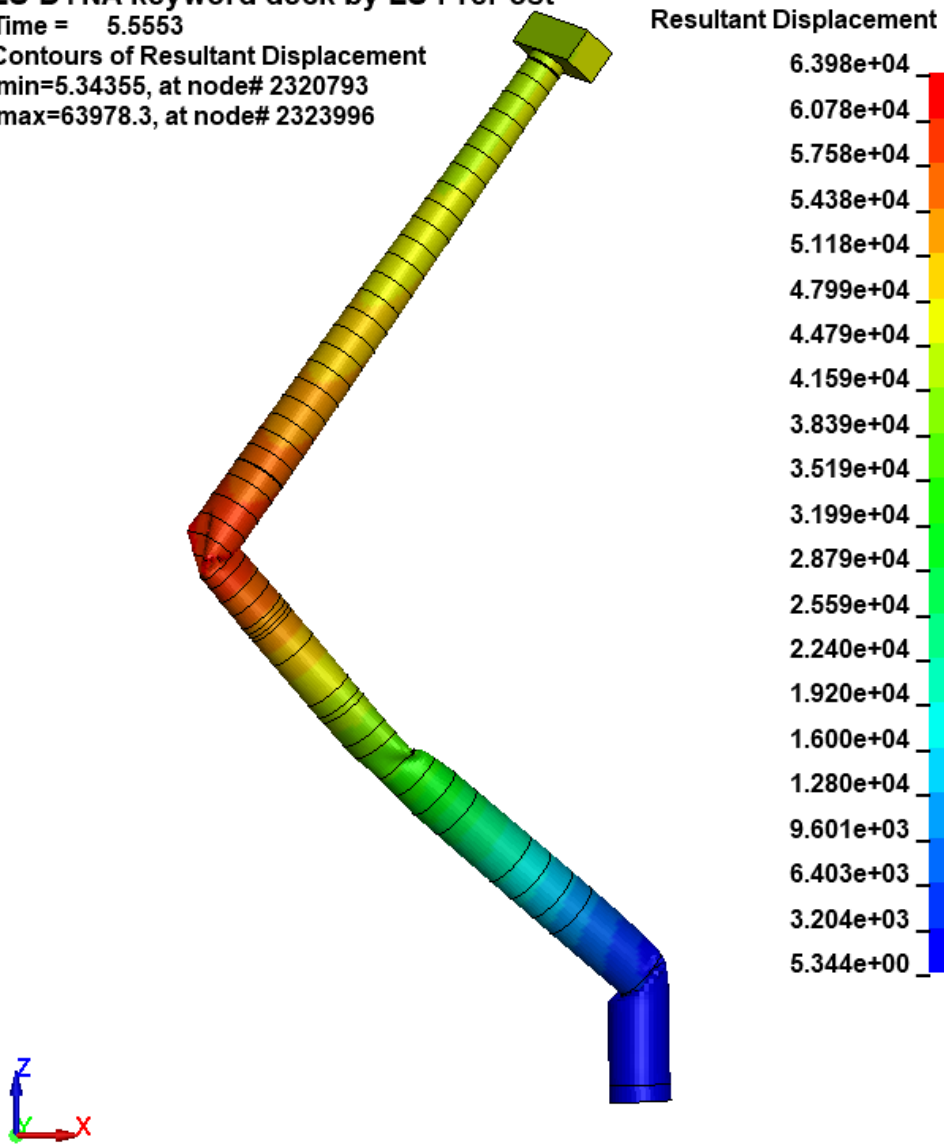


Figure 99. Resultant Displacement Foundation Tower [mm]

Table 51. Visual timeline simulation 2

**Simulation 2**







Simulation 2

t = 1.02 s





Simulation 2

t = 1.98 s





Simulation 2

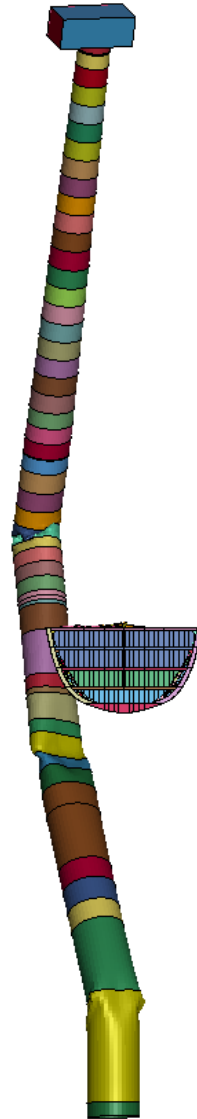
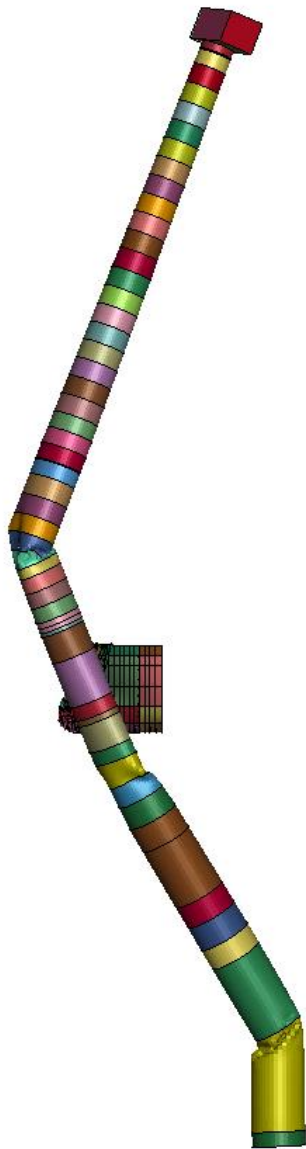
t = 3 s





Simulation 2

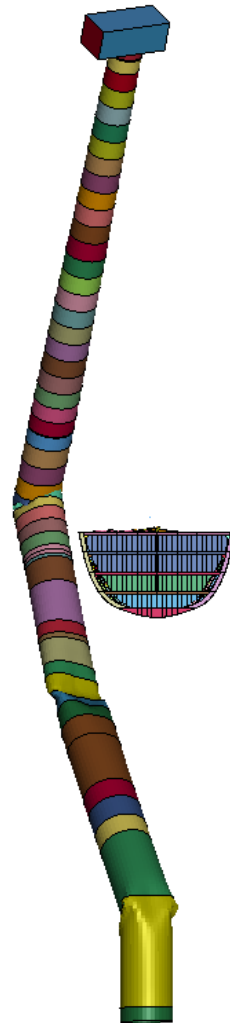
t = 4.02 s





Simulation 2

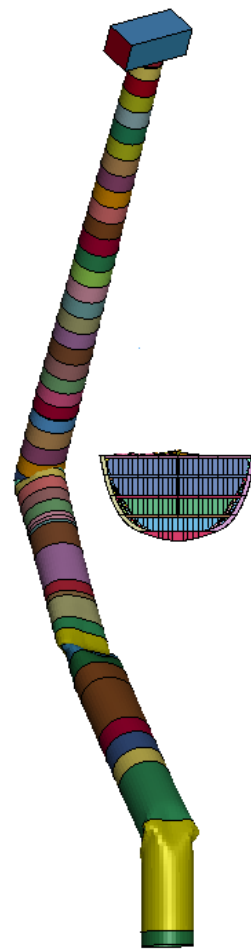
t = 4.98 s





Simulation 2

t = 5.55 s



### J.1.3. Simulation 3

Figure 100 shows the global kinetic and internal energy over time during the collision. Initially, the kinetic energy is 21 MJ, determined by the ship's speed and mass. Since the impact does not cause the tower to fall, the total energy remains constant.

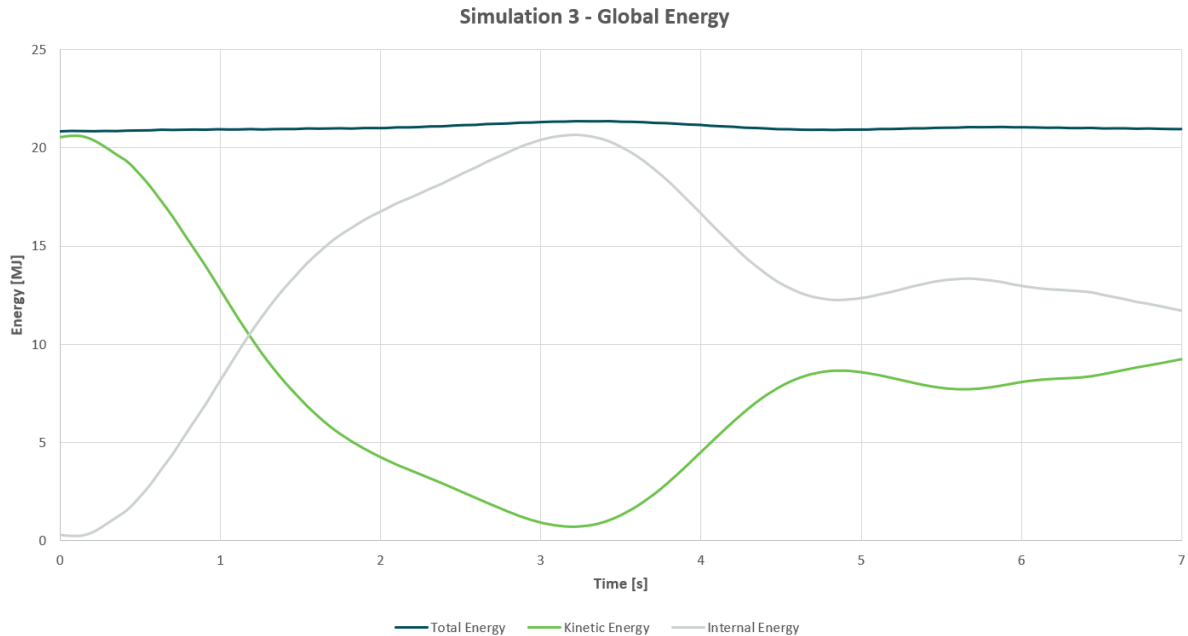


Figure 100. Global energy Distribution over time

Figure 101 displays the kinetic and internal energy of the ship. As shown, the maximum internal energy of the ship reaches 4.9 MJ.

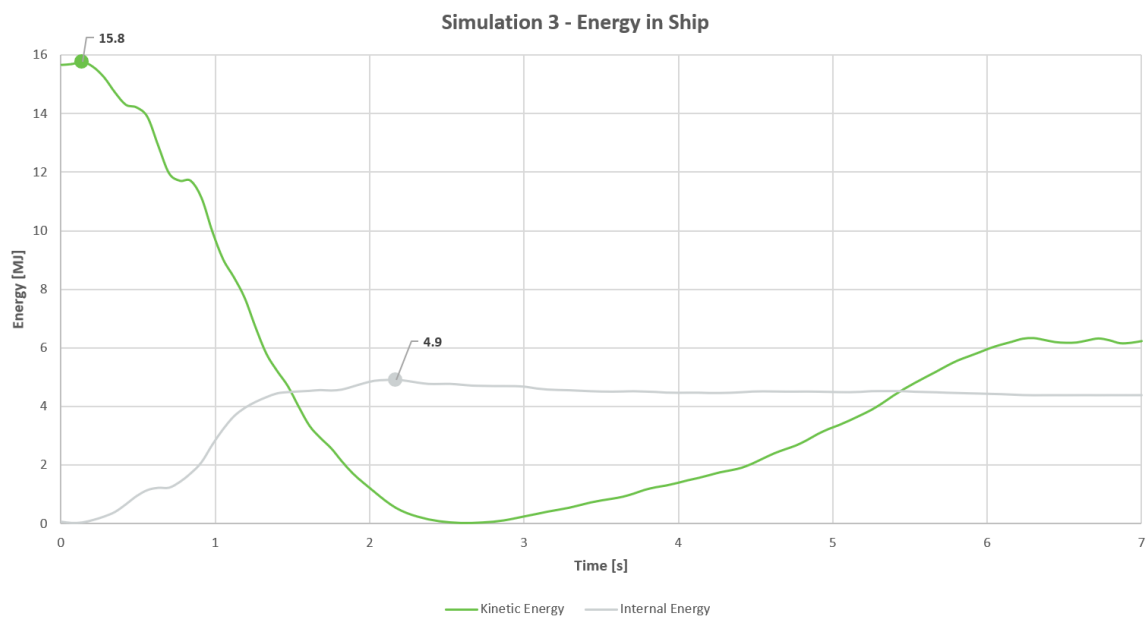


Figure 101. Kinetic and Internal Energy of ship over time

The impact force between the vessel and the foundation over the time is shown in *Figure 102*.

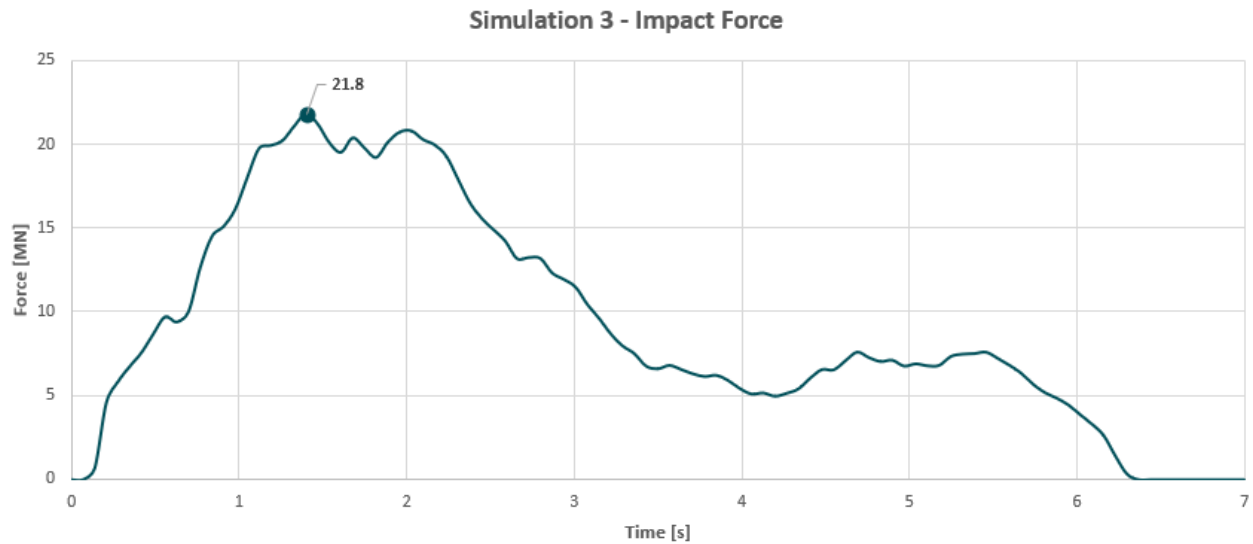


Figure 102. Impact Force over time



The effective plastic strain of the SB side is shown in *Figure 103*.

LS-DYNA keyword deck by LS-PrePost  
Time = 7  
Contours of Effective Plastic Strain  
reference shell surface  
min=0, at elem# 2307647  
max=0.103499, at elem# 2318878

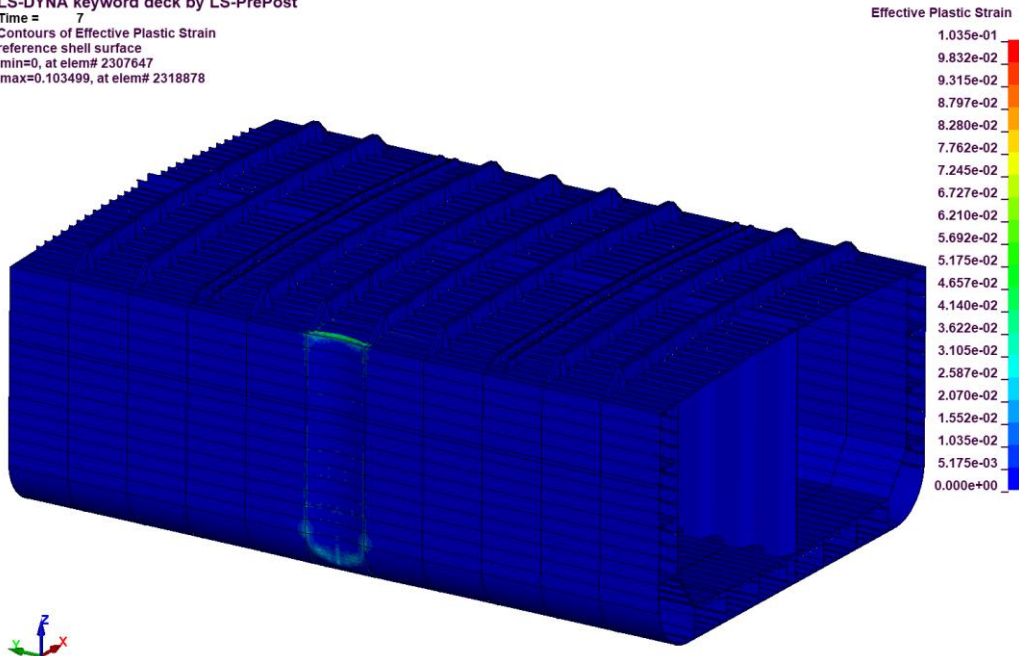


Figure 103. Effective Plastic Strain simulation 3

*Figure 104* shows the deformation of the ship after the collision.

LS-DYNA keyword deck by LS-PrePost  
Time = 7  
Contours of Relative Resultant Displacement  
min=0, at node# 2423017  
max=327.936, at node# 2413766

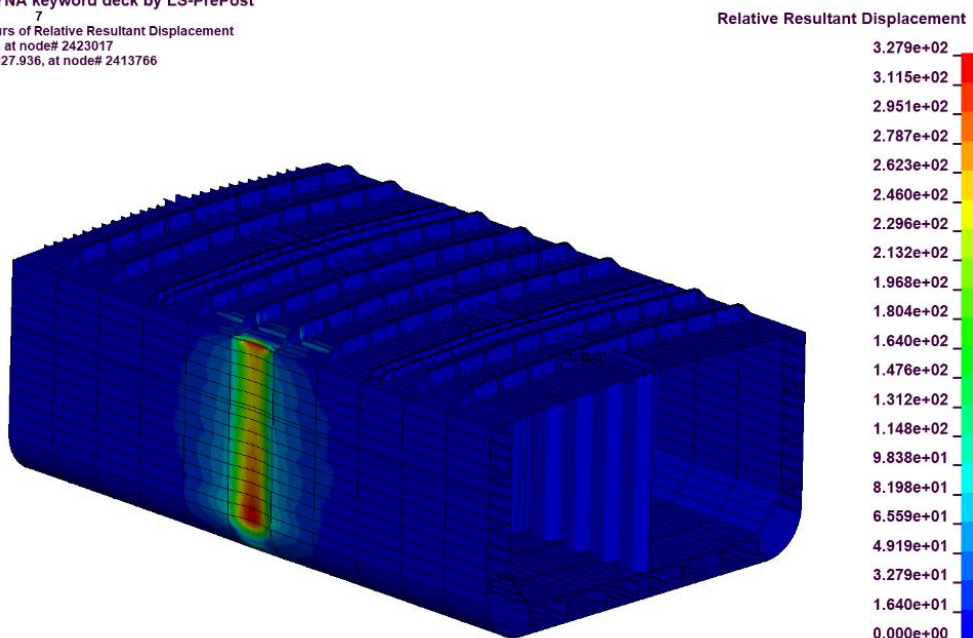


Figure 104. Resultant Displacement SB side [mm]

Figure 105 shows the deformation of the foundation, which indicates a clear buckling failure of the foundation.

### LS-DYNA keyword deck by LS-PrePost

Time = 7

Contours of Resultant Displacement  
min=0.108197, at node# 2103  
max=855.525, at node# 16281

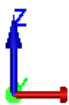
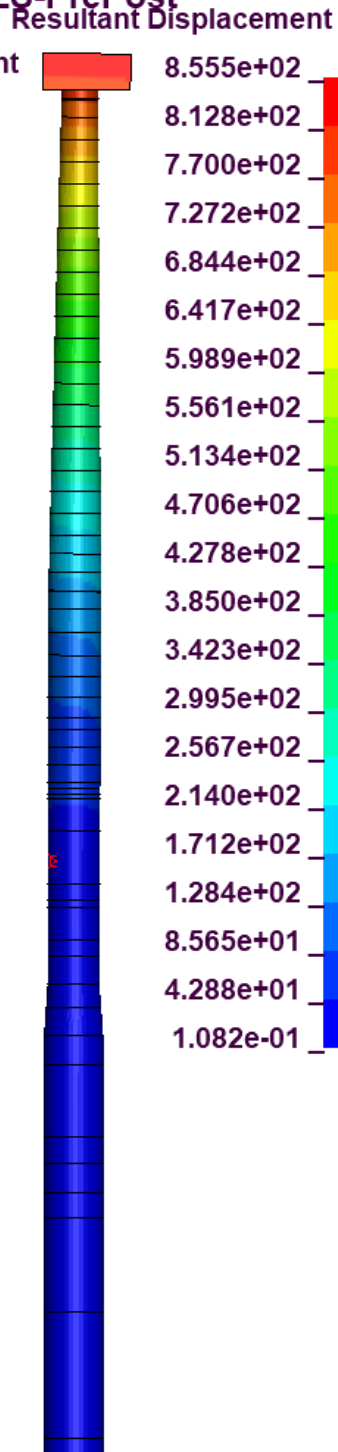


Figure 105. Resultant Displacement Foundation Tower [mm]

Table 52. Visual timeline simulation 3





#### J.1.4. Simulation 4

Figure 106 shows the global kinetic and internal energy over time during the collision. Initially, the kinetic energy is 82 MJ, determined by the ship's speed and mass. Since the impact does not cause the tower to fall, the total energy remains constant. Over time, the ship rebounds, converting some of the internal energy back into kinetic energy. This rebound causes the ship to detach from the foundation tower.

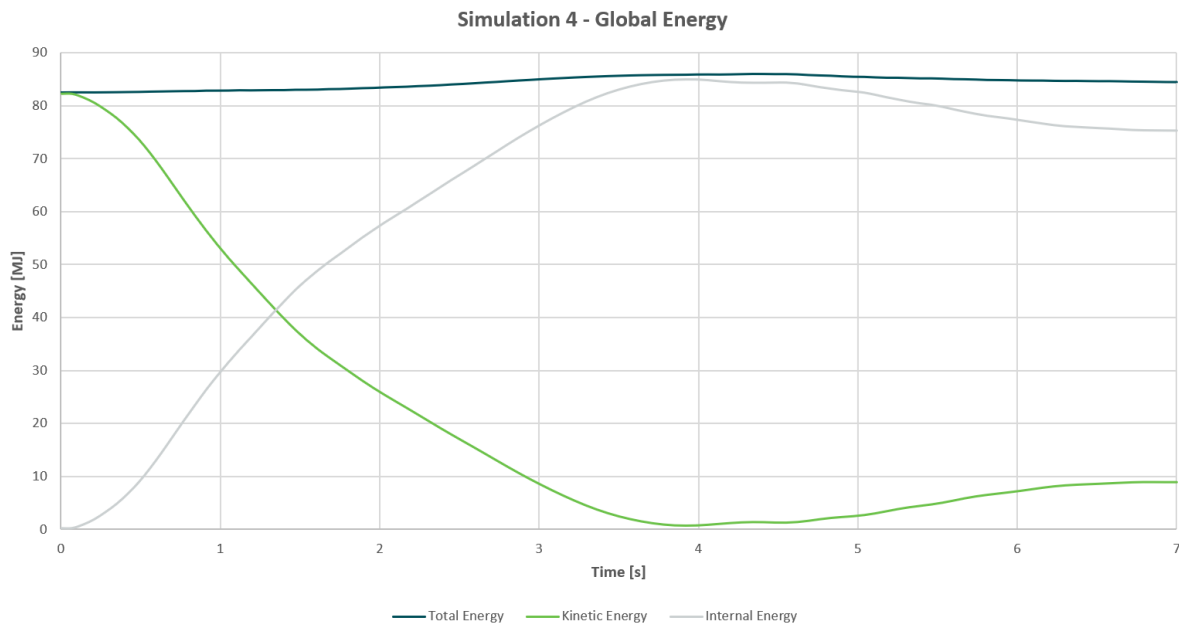


Figure 106. Global energy Distribution over time

Figure 107 displays the kinetic and internal energy of the ship. As shown, the maximum internal energy of the ship reaches 15.4 MJ.

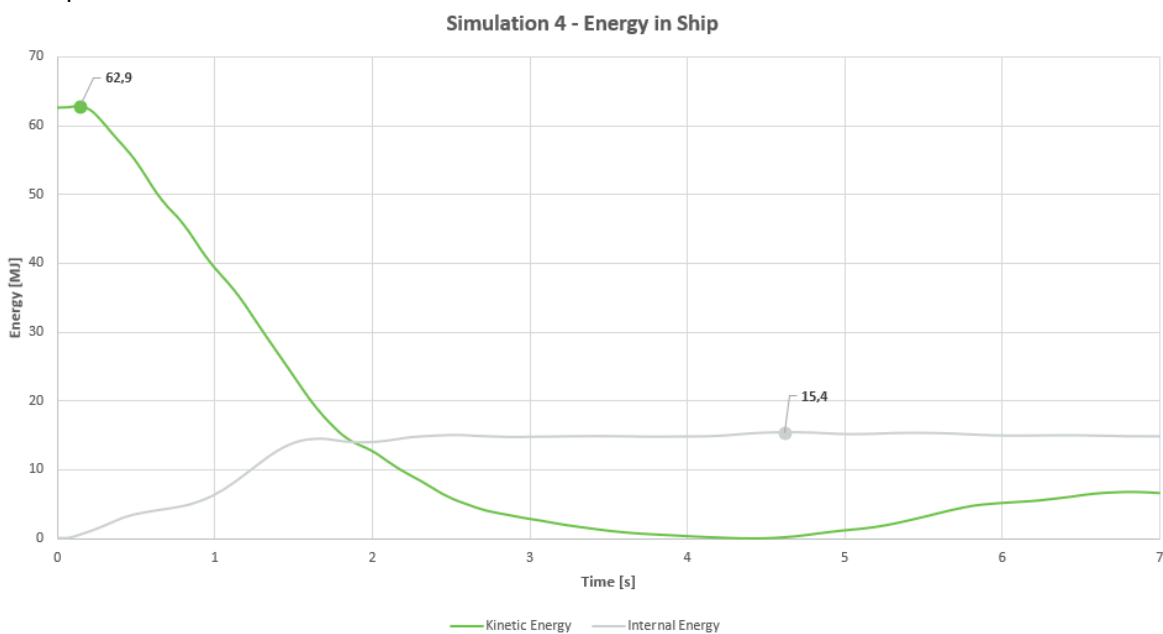


Figure 107. Kinetic and Internal Energy of ship over time

The impact force between the vessel and the foundation over the time is shown in *Figure 108*.

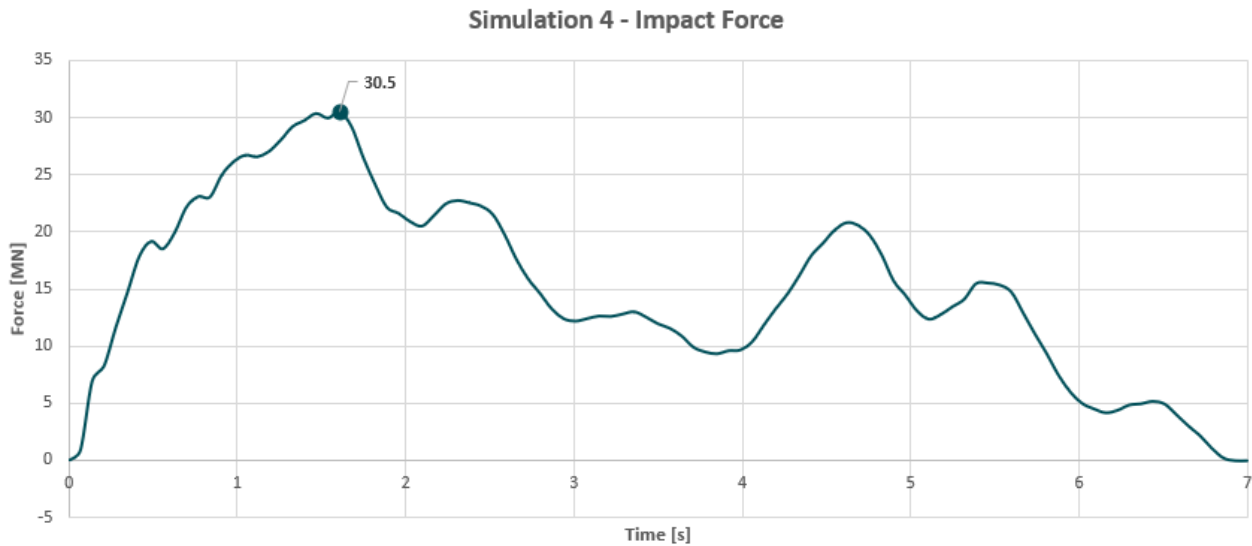


Figure 108. Impact Force over time

The effective plastic strain of the SB side is shown in *Figure 109*.

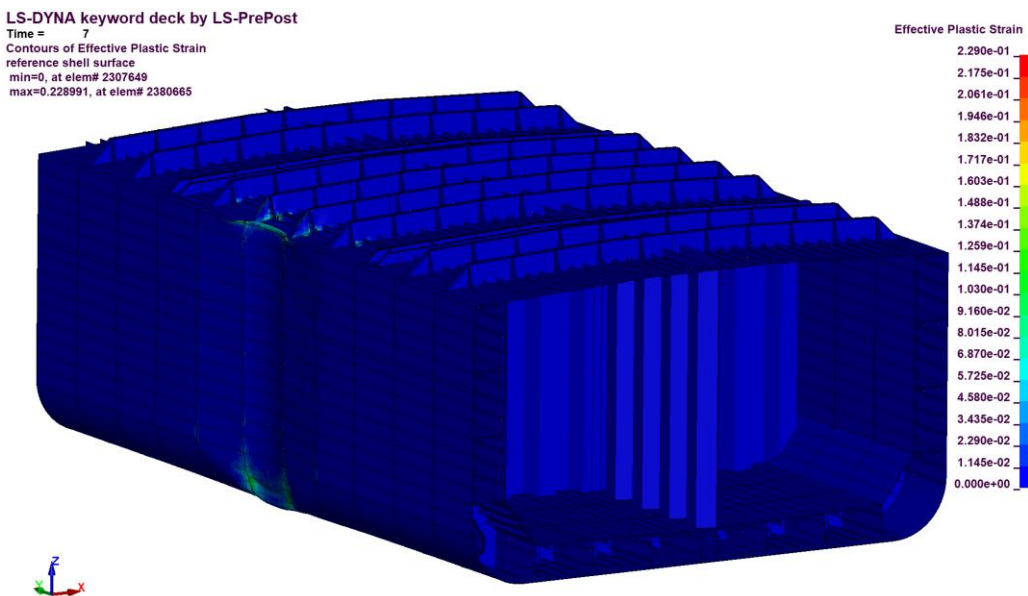


Figure 109. Effective Plastic Strain simulation 4



Figure 110 shows the deformation of the ship after the collision.

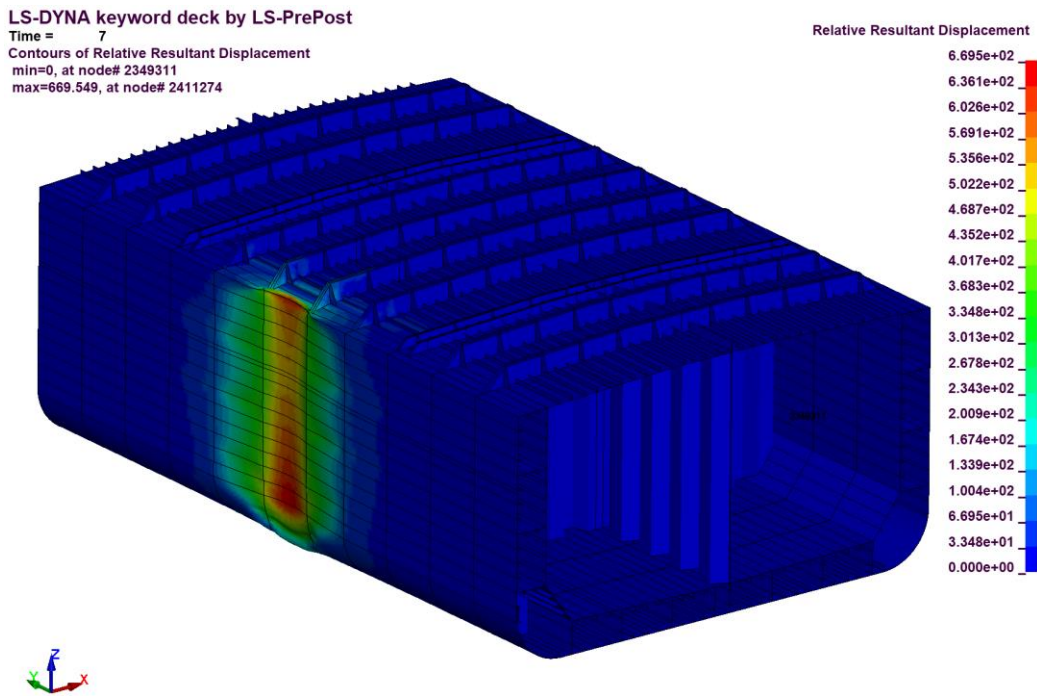


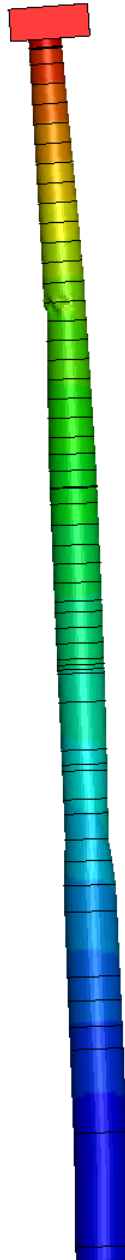
Figure 110. Resultant Displacement SB side

Figure 111 shows the deformation of the foundation, which indicates a clear buckling failure of the foundation.

**LS-DYNA keyword deck by LS-PrePost**

Time = 7

Contours of Resultant Displacement  
min=2.8743, at node# 2813  
max=8198.19, at node# 16257



**Resultant Displacement**

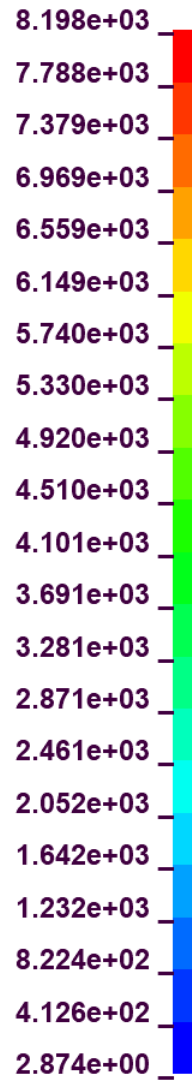
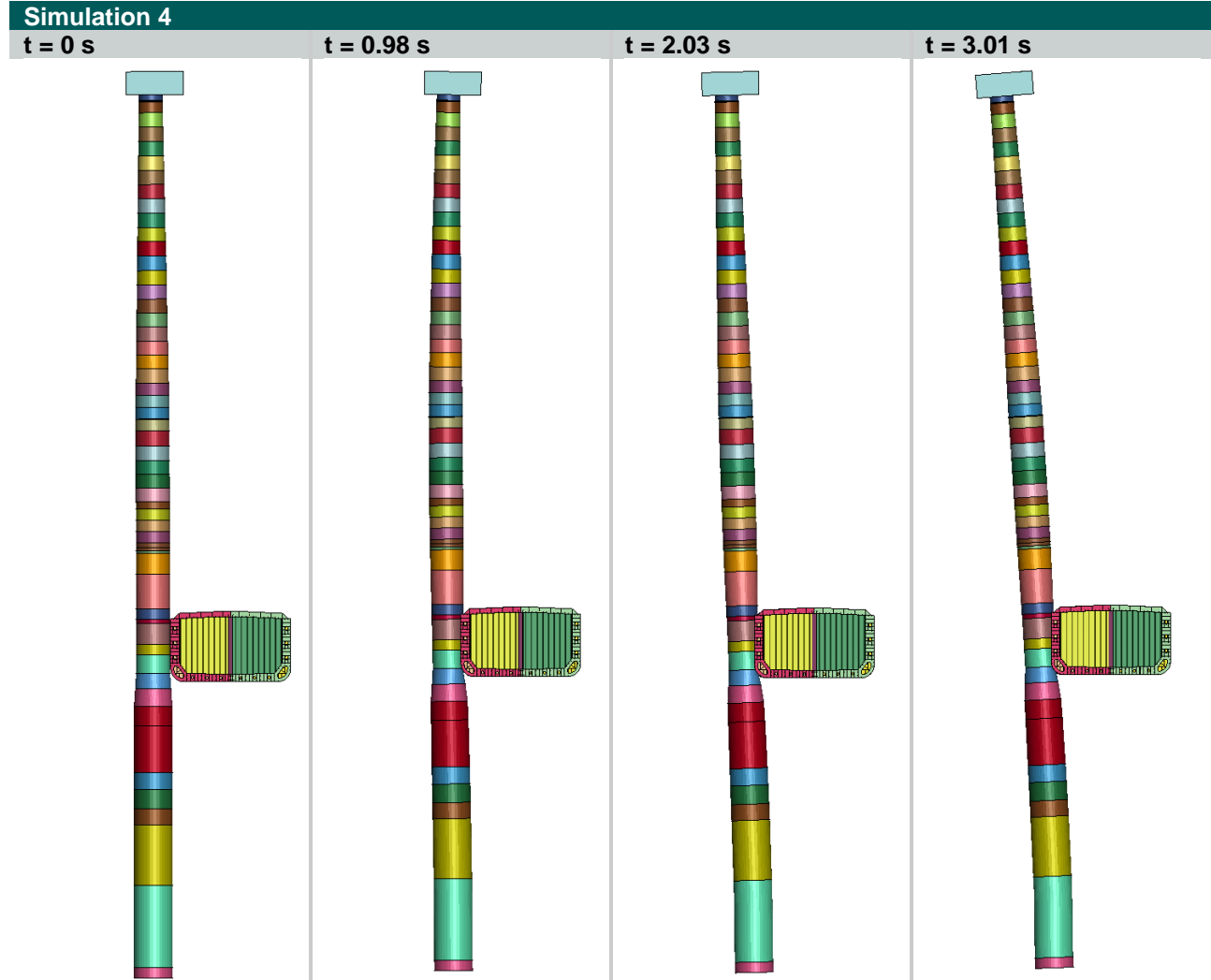
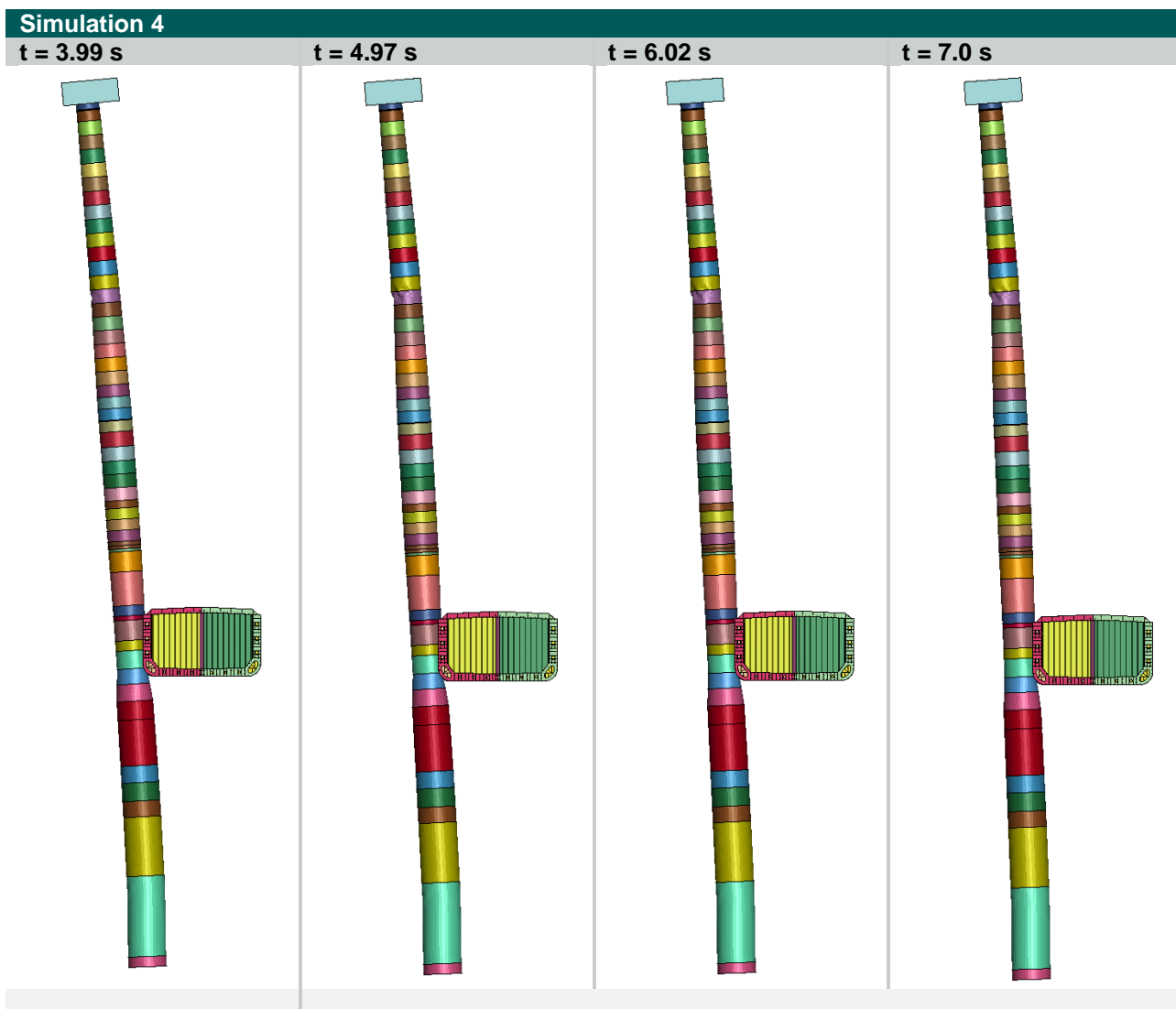


Figure 111. Resultant Displacement Foundation Tower



Table 53. Visual timeline simulation 4





### J.1.5. Simulation 5

Figure 112 shows the global kinetic and internal energy over time during the collision. Initially, the kinetic energy is 3098 MJ, determined by the ship's speed and mass. As the collision progresses, the total energy increases due to the collapse of the turbine tower foundation, leading to a rise in both kinetic and internal energy. However, the increase in kinetic energy resulting from the tower's collapse is negligible compared to the decrease in kinetic energy due to the reduction in the container ship's speed.

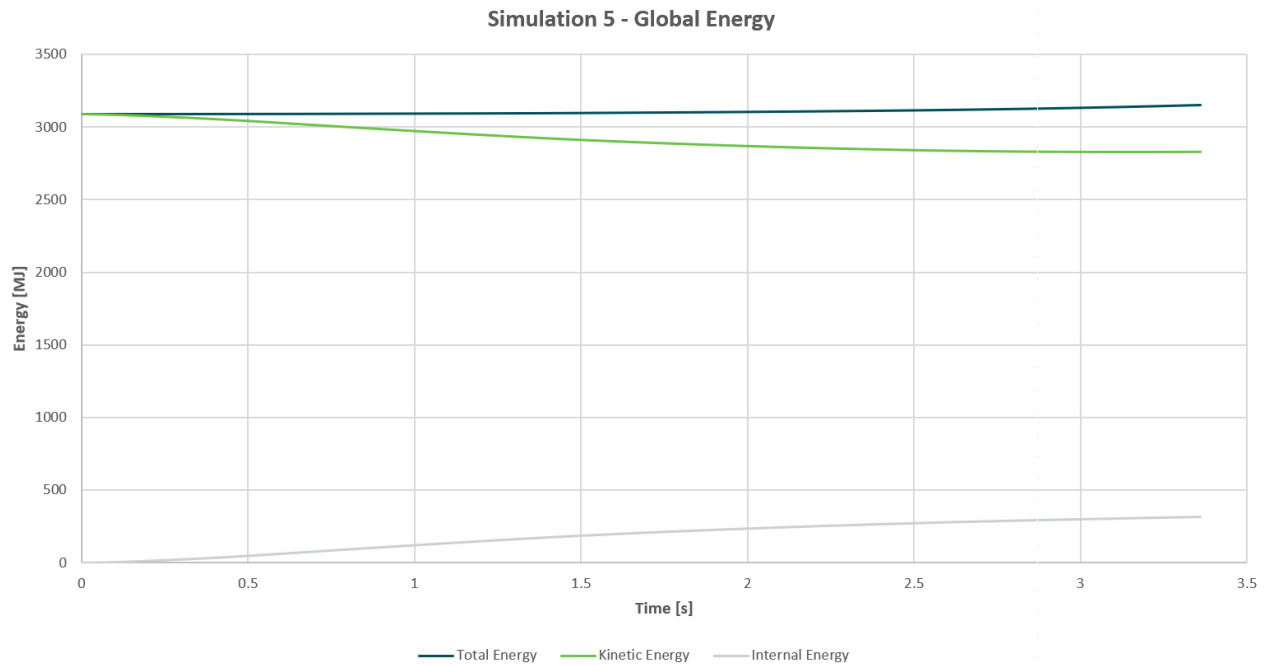


Figure 112. Global energy Distribution over time

Figure 113 displays the kinetic and internal energy of the ship. As shown, the maximum internal energy of the ship reaches 7.6 MJ which is negligible in comparison to the kinetic energy, primarily due to the ship's massive size.

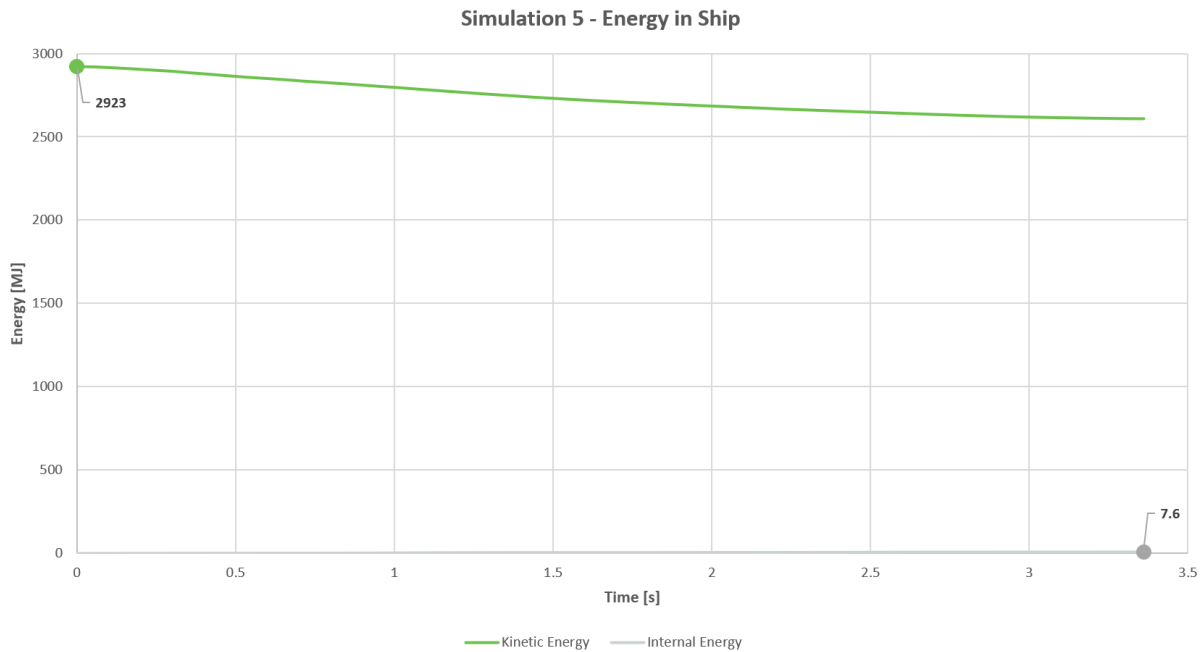


Figure 113. Kinetic and Internal Energy of ship over time

The impact force between the vessel and the foundation over the time is shown in Figure 114.

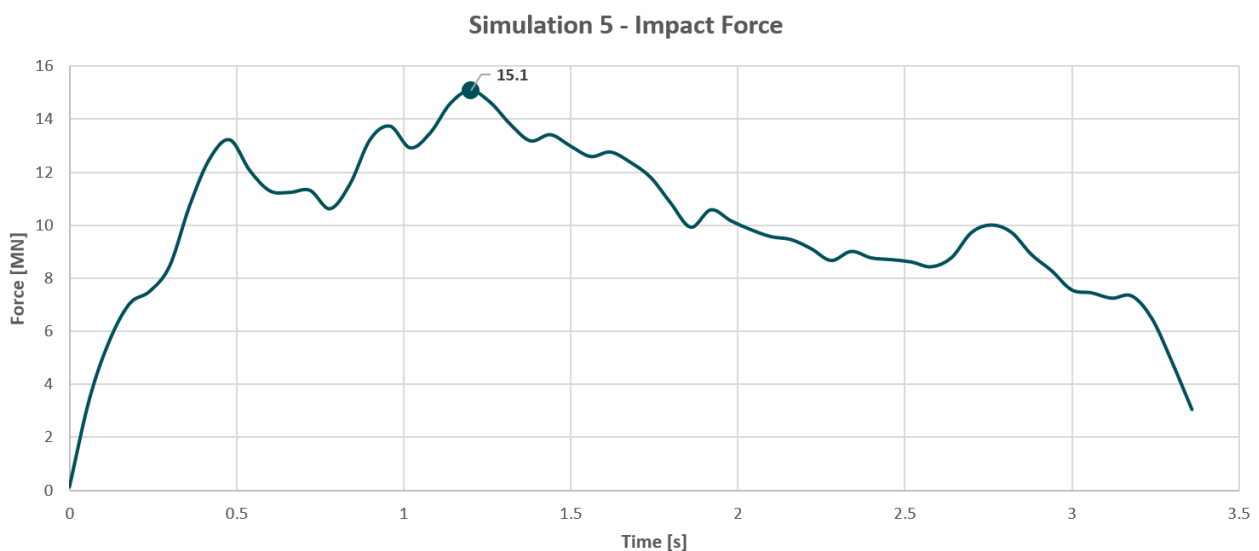


Figure 114. Impact Force over time



The effective plastic strain of the bow is shown in *Figure 115*.

LS-DYNA keyword deck by LS-PrePost

Time = 3.382

Contours of Effective Plastic Strain

reference shell surface

min=0, at elem# 628188

max=0.229031, at elem# 789390

Effective Plastic Strain

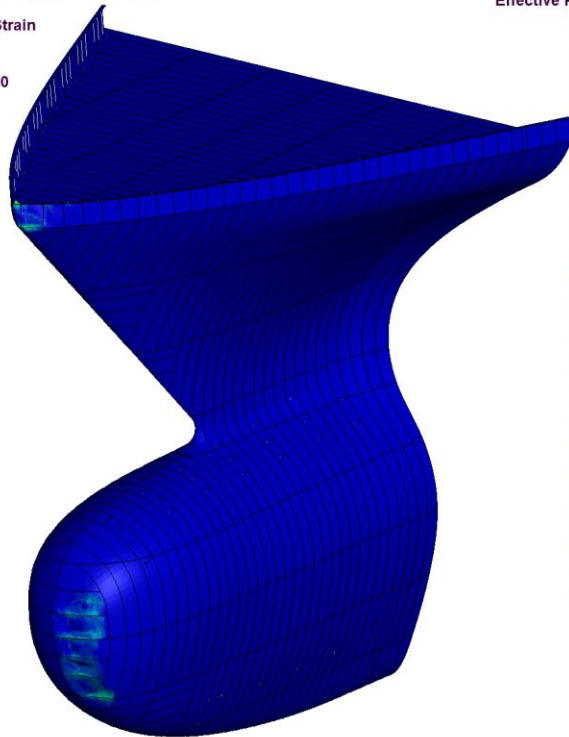


Figure 115. Effective Plastic Strain simulation 5

Figure 116 shows the deformation of the ship after the collision.

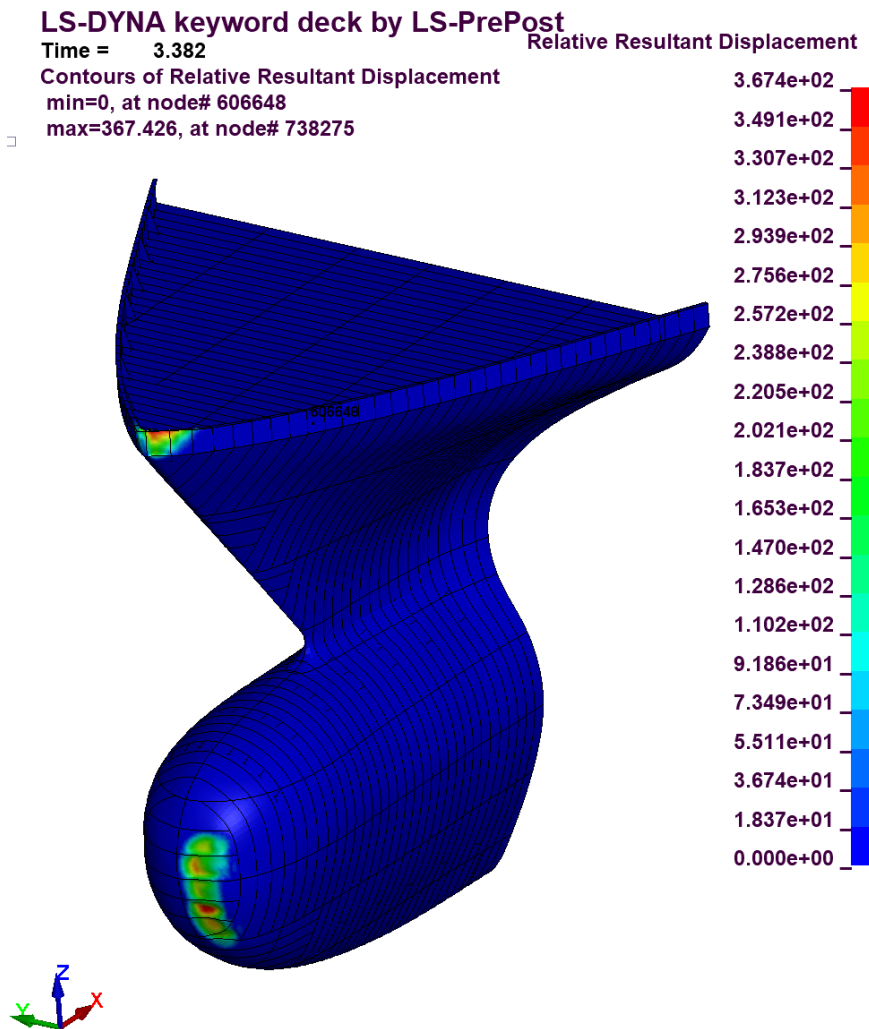


Figure 116. Resultant Displacement Bow [mm]

Figure 117 shows the deformation of the foundation, which indicates a clear buckling failure of the foundation.



Figure 117. Resultant Displacement Foundation Tower [mm]

Table 54. Visual timeline simulation 5

**Simulation 5**

t = 0 s







Simulation 5

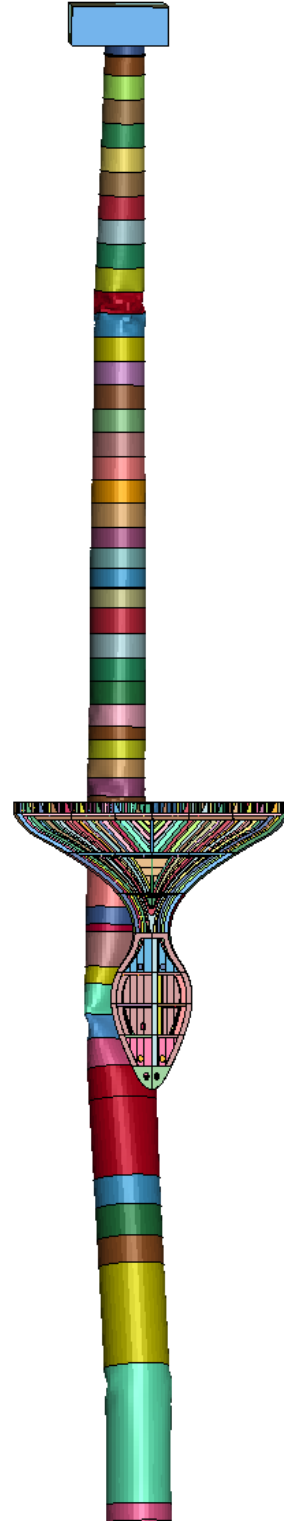
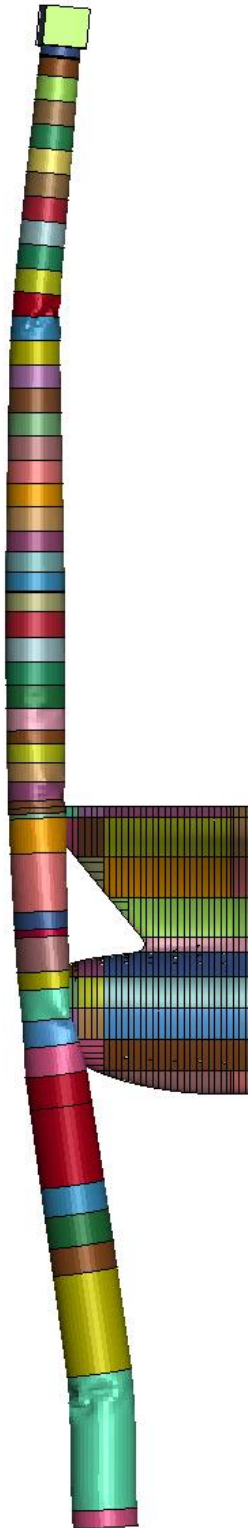
t = 1.02 s





Simulation 5

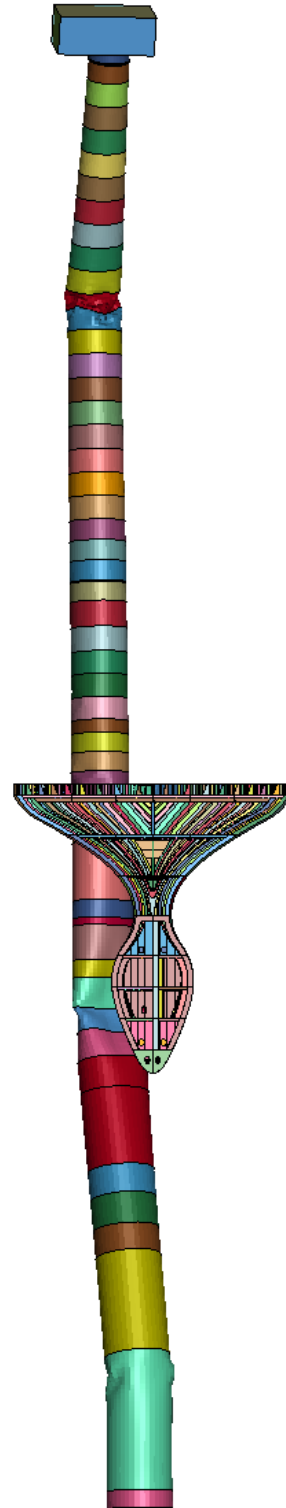
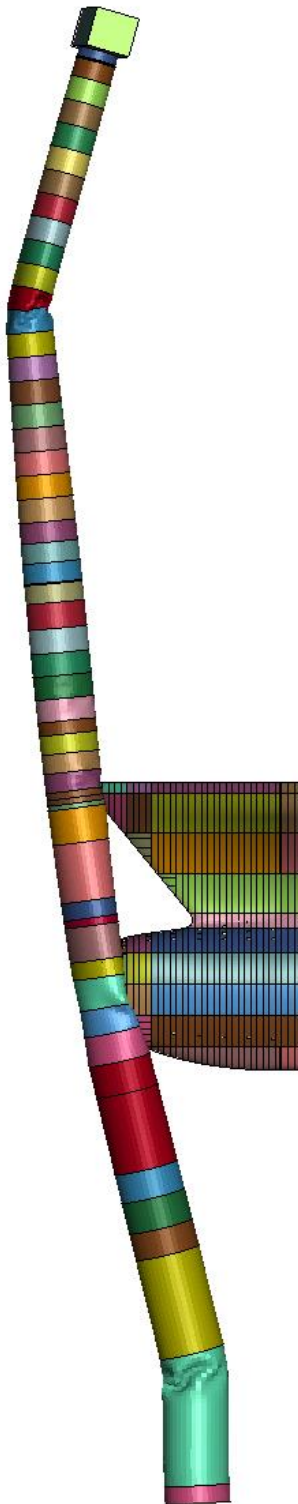
t = 1.98 s





### Simulation 5

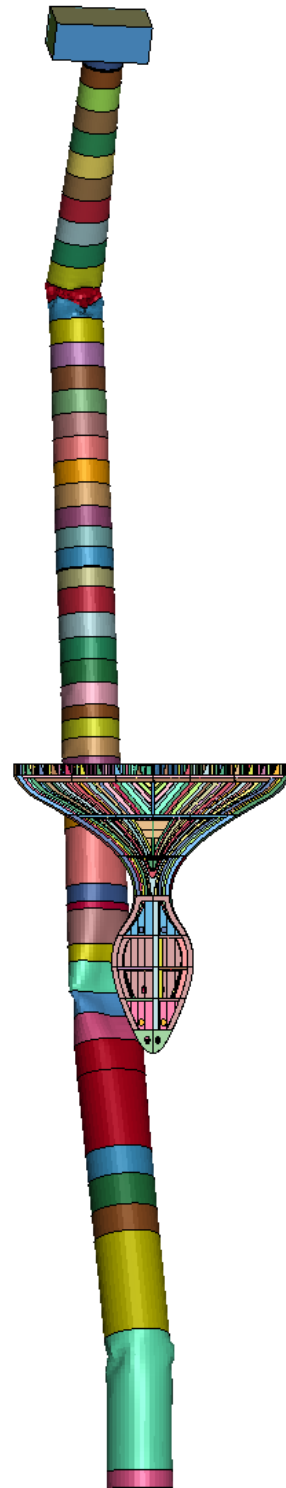
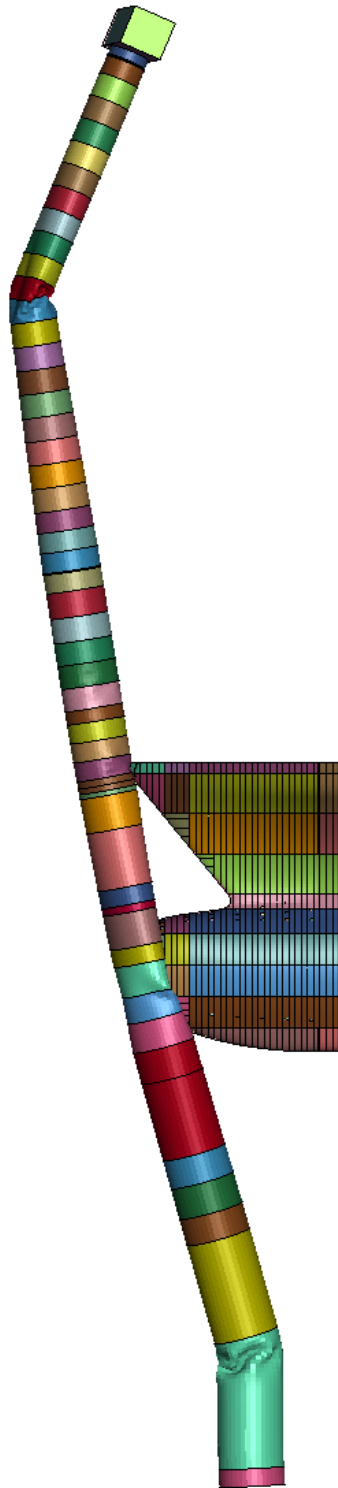
t = 3 s





Simulation 5

t = 3.38 s



### J.1.6. Simulation 6

Figure 118 shows the global kinetic and internal energy over time during the collision. Initially, the kinetic energy is 12396 MJ, determined by the ship's speed and mass. As the collision progresses, the total energy increases due to the collapse of the turbine tower foundation, leading to a rise in both kinetic and internal energy. However, the increase in kinetic energy resulting from the tower's collapse is negligible compared to the decrease in kinetic energy due to the reduction in the container ship's speed.

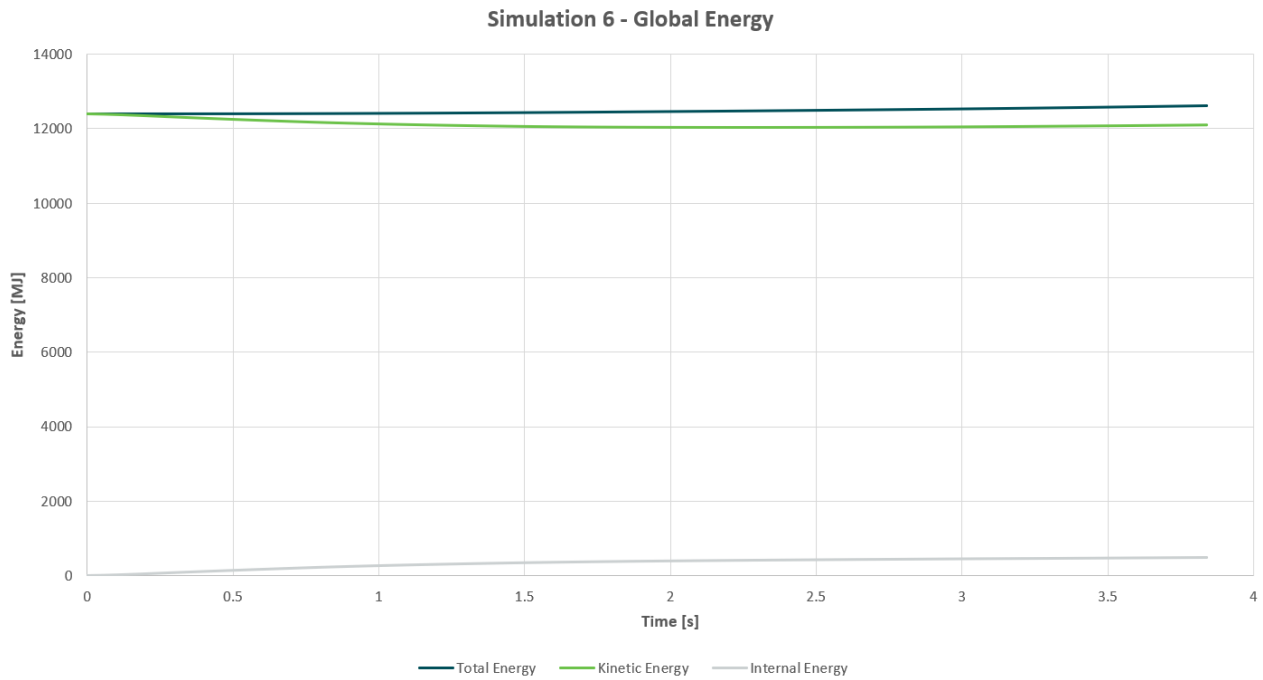


Figure 118. Global energy Distribution over time

Figure 119 displays the kinetic and internal energy of the ship. As shown, the maximum internal energy of the ship reaches 13.3 MJ which is negligible in comparison to the kinetic energy, primarily due to the ship's massive size.

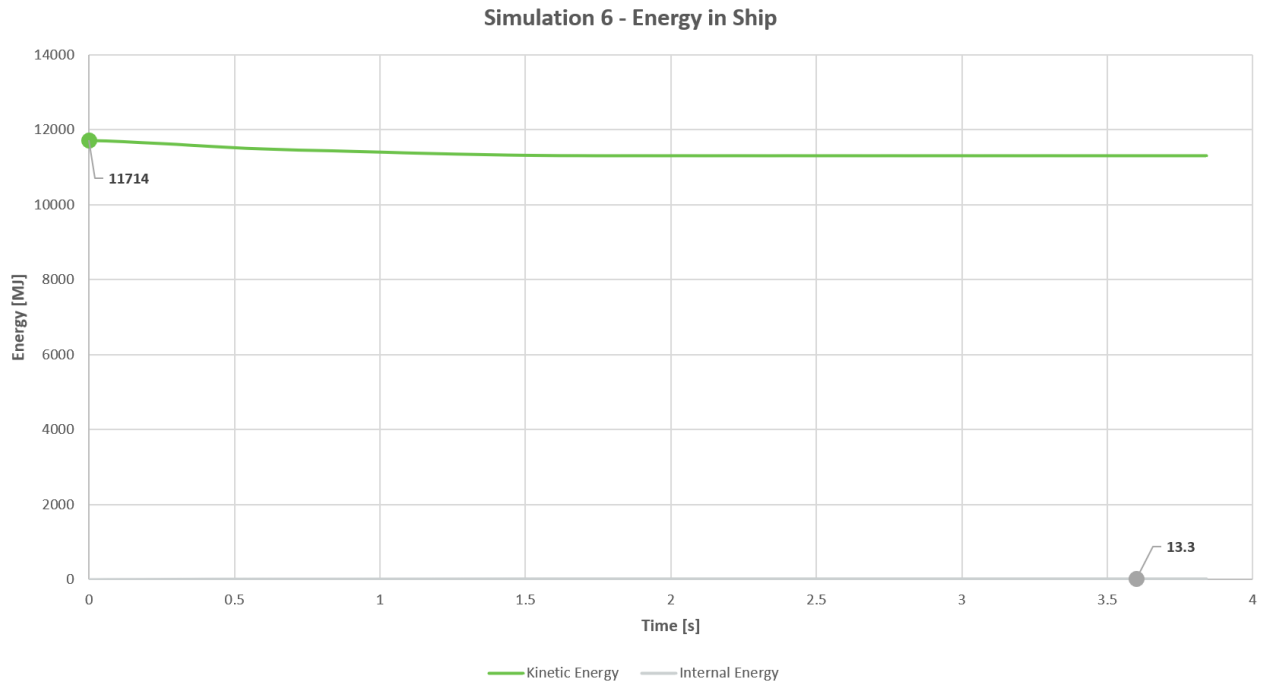


Figure 119. Kinetic and Internal Energy of ship over time

The impact force between the vessel and the foundation over the time is shown in Figure 120.

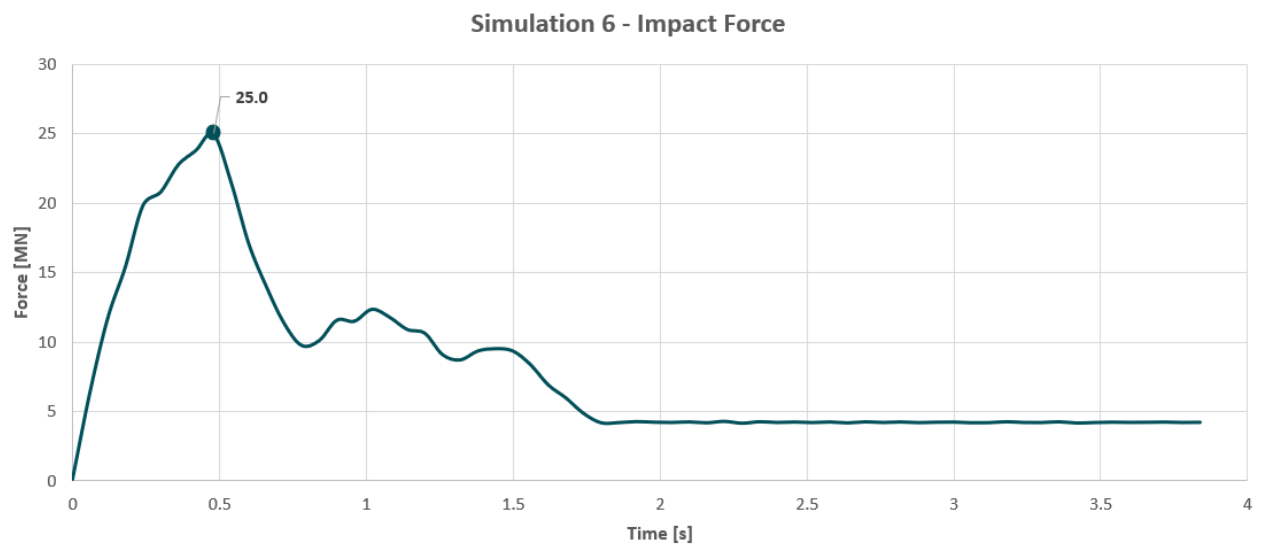


Figure 120. Impact Force over time

The failed elements and effective plastic strain of the bow are shown in *Figure 121* and *Figure 122*.

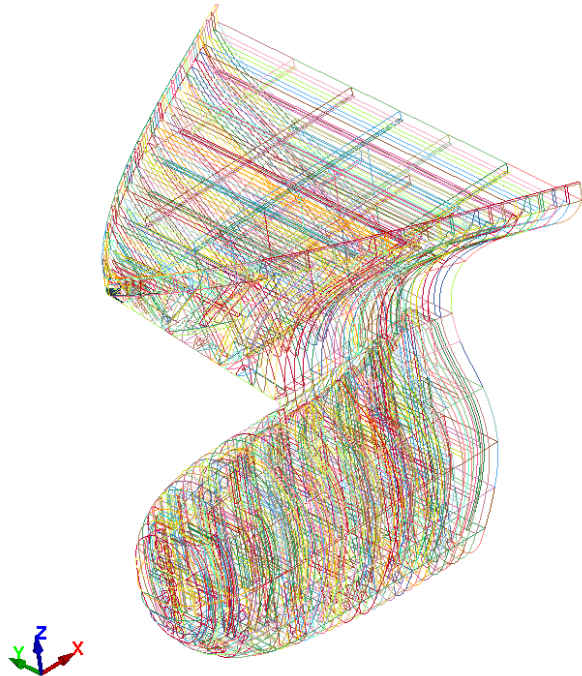


Figure 121. Failed elements simulation 6

LS-DYNA keyword deck by LS-PrePost

Time = 3.8704

Contours of Effective Plastic Strain

reference shell surface

min=0, at elem# 628212

max=0.229031, at elem# 680105

Effective Plastic Strain

2.290e-01

2.176e-01

2.061e-01

1.947e-01

1.832e-01

1.718e-01

1.603e-01

1.489e-01

1.374e-01

1.260e-01

1.145e-01

1.031e-01

9.161e-02

8.016e-02

6.871e-02

5.726e-02

4.581e-02

3.435e-02

2.290e-02

1.145e-02

0.000e+00

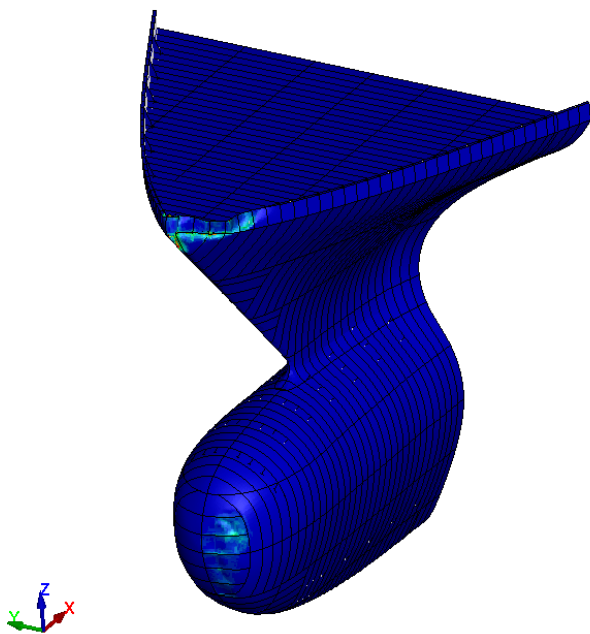


Figure 122. Effective Plastic Strain simulation 6

Figure 123 shows the deformation of the ship after the collision.

**LS-DYNA keyword deck by LS-PrePost**

Time = 3.8704

Contours of Relative Resultant Displacement

min=0, at node# 598808

max=2012.95, at node# 708876

**Relative Resultant Displacement**

2.013e+03

1.912e+03

1.812e+03

1.711e+03

1.610e+03

1.510e+03

1.409e+03

1.308e+03

1.208e+03

1.107e+03

1.006e+03

9.058e+02

8.052e+02

7.045e+02

6.039e+02

5.032e+02

4.026e+02

3.019e+02

2.013e+02

1.006e+02

0.000e+00

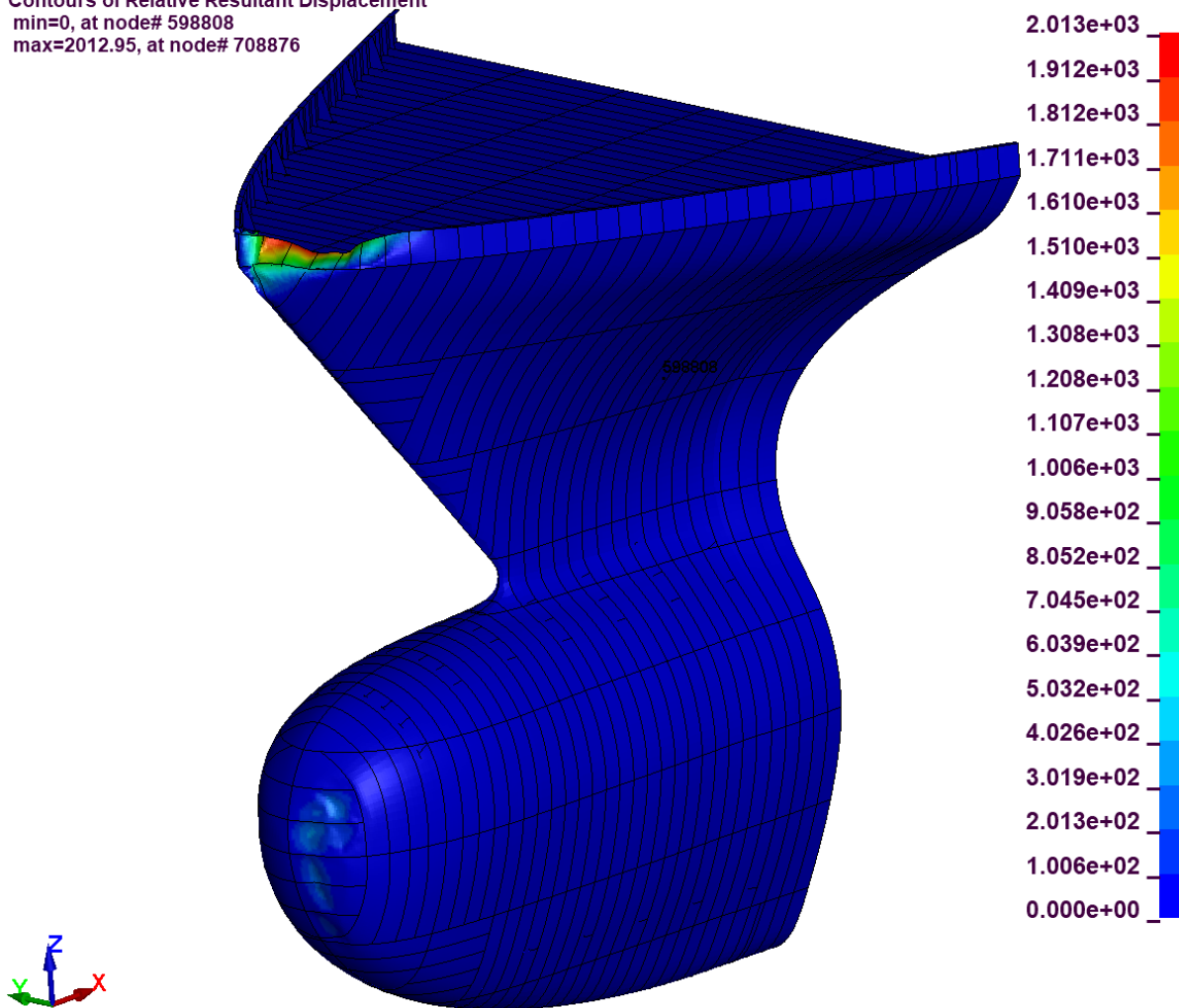


Figure 123. Resultant Displacement Bow



Figure 124 shows the deformation of the foundation, which indicates a clear buckling failure of the foundation.

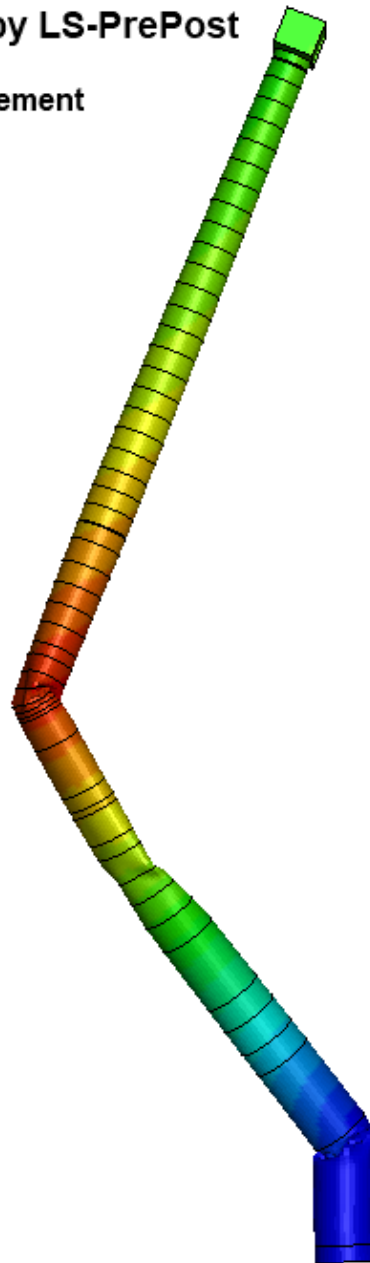
### LS-DYNA keyword deck by LS-PrePost

Time = 3.8704

Contours of Resultant Displacement

min=8.67225, at node# 3453

max=44621, at node# 4228



### Resultant Displacement

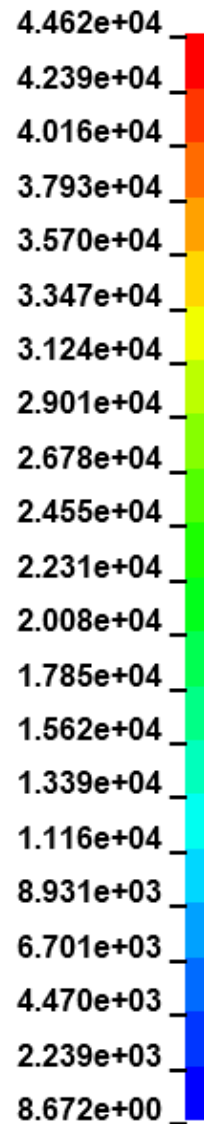


Figure 124. Resultant Displacement Foundation Tower

Table 55. Visual timeline simulation 6

**Simulation 6**

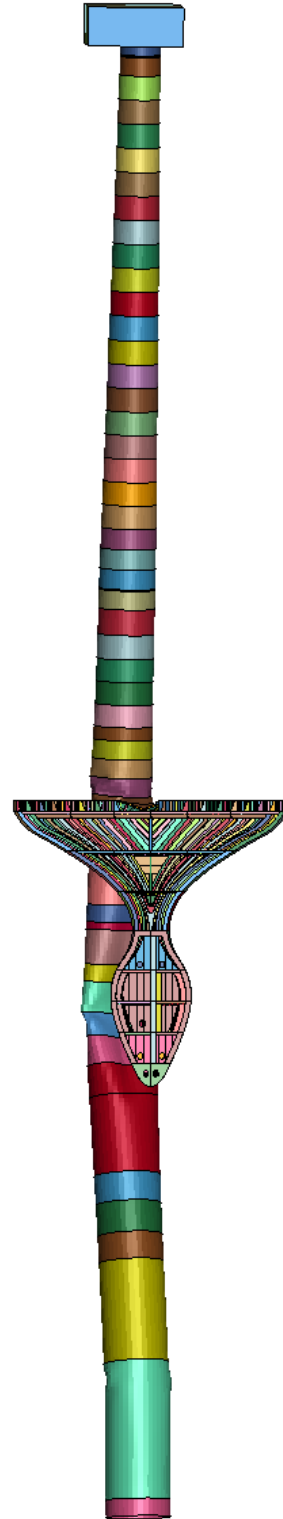
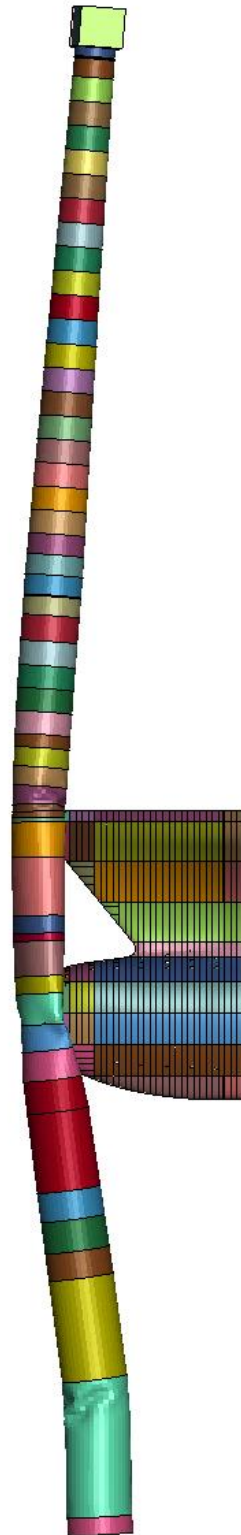
t = 0 s





Simulation 6

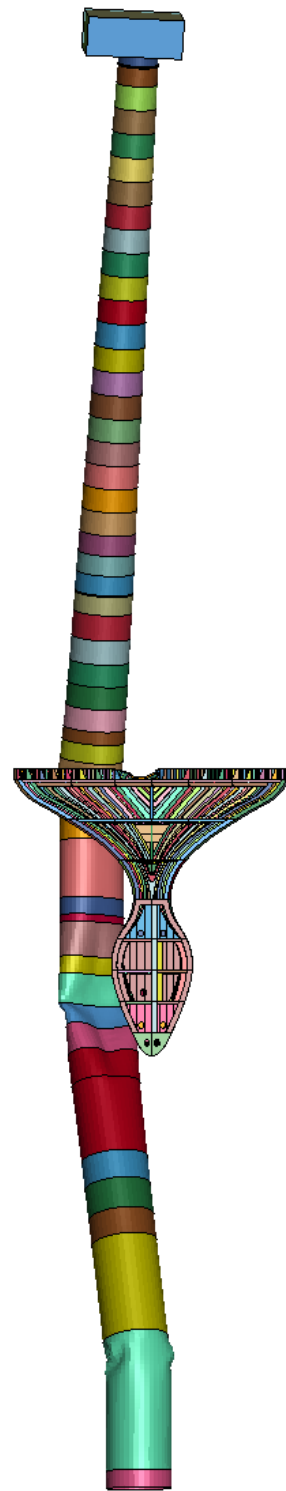
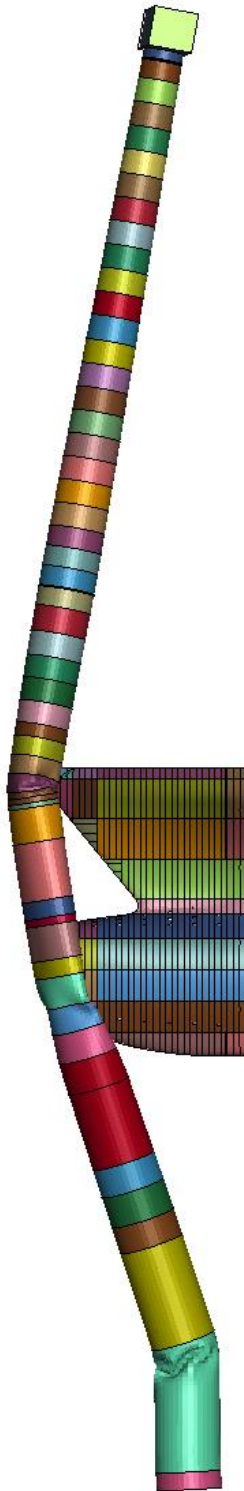
t = 1.02 s





Simulation 6

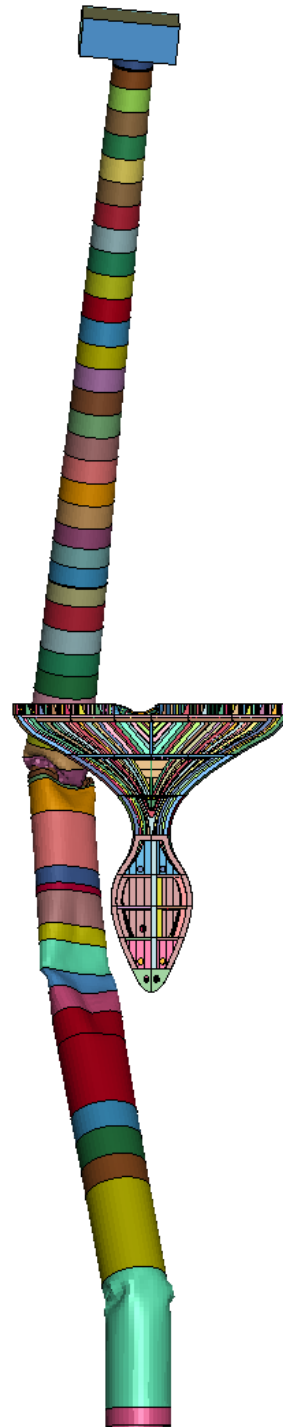
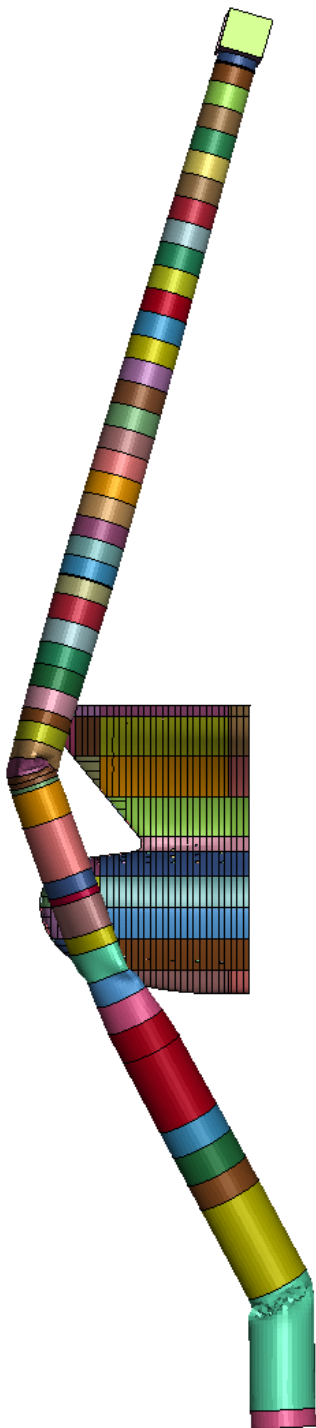
t = 1.98 s





Simulation 6

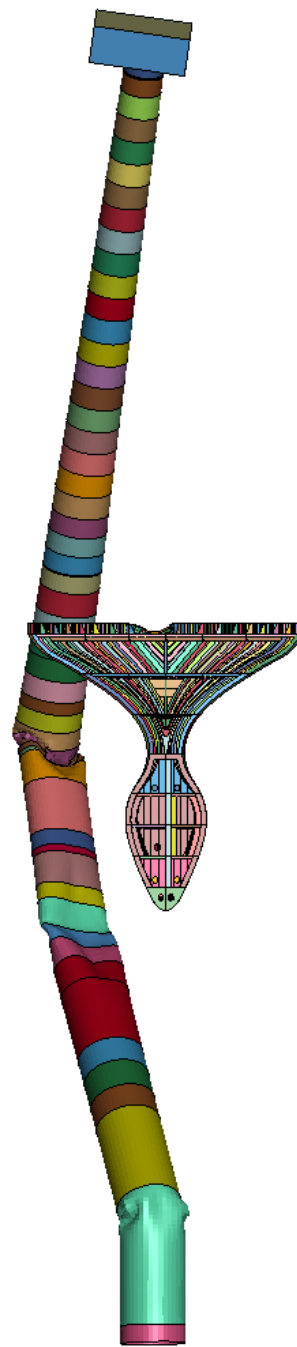
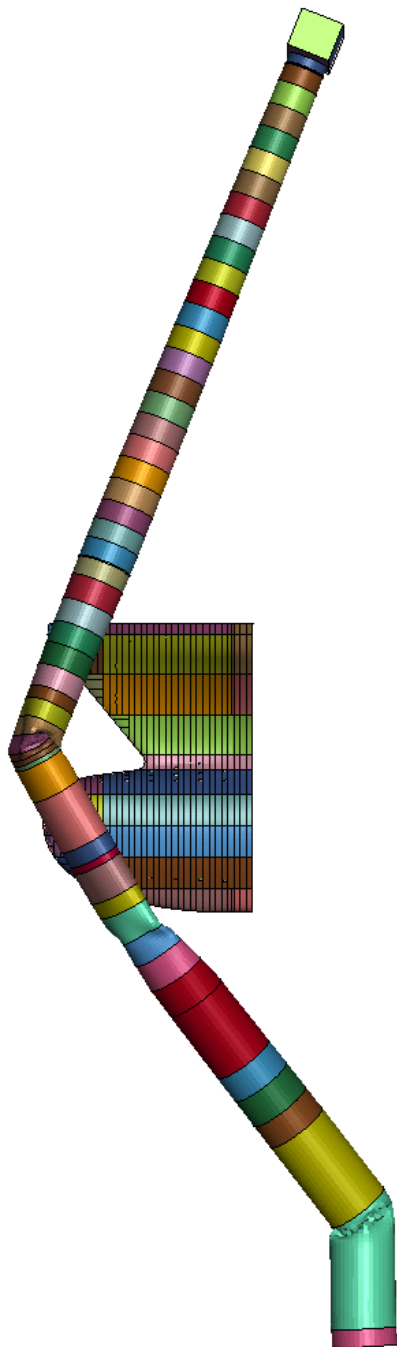
t = 3 s





Simulation 6

t = 3.87 s



### J.1.7. Simulation 7

Figure 125 shows the global Kinetic and Internal Energy over time during the collision. Initially, the kinetic energy is 218 MJ, which is determined by the ship's speed and mass. As the collision progresses, the total energy increases due to the collapse of the turbine tower foundation, resulting in a rise in internal energy.

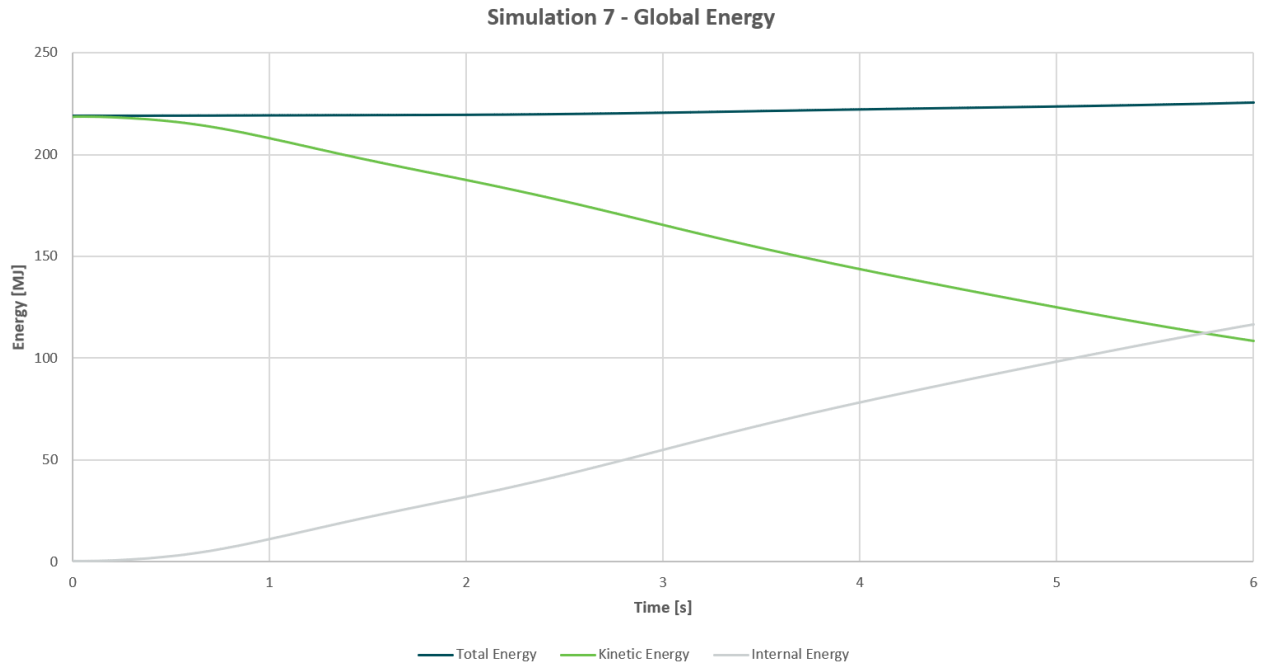


Figure 125. Global energy Distribution over time

The impact force between the vessel and the foundation over the time is shown in Figure 126.

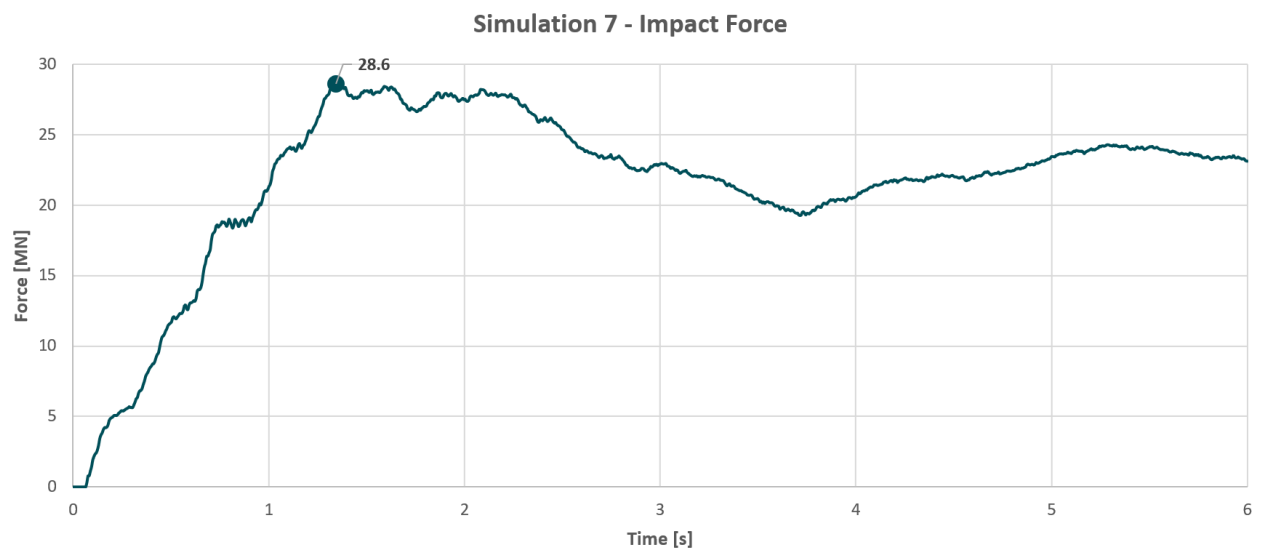


Figure 126. Impact Force over time

The effective plastic strain of the SB side is shown in *Figure 127*.

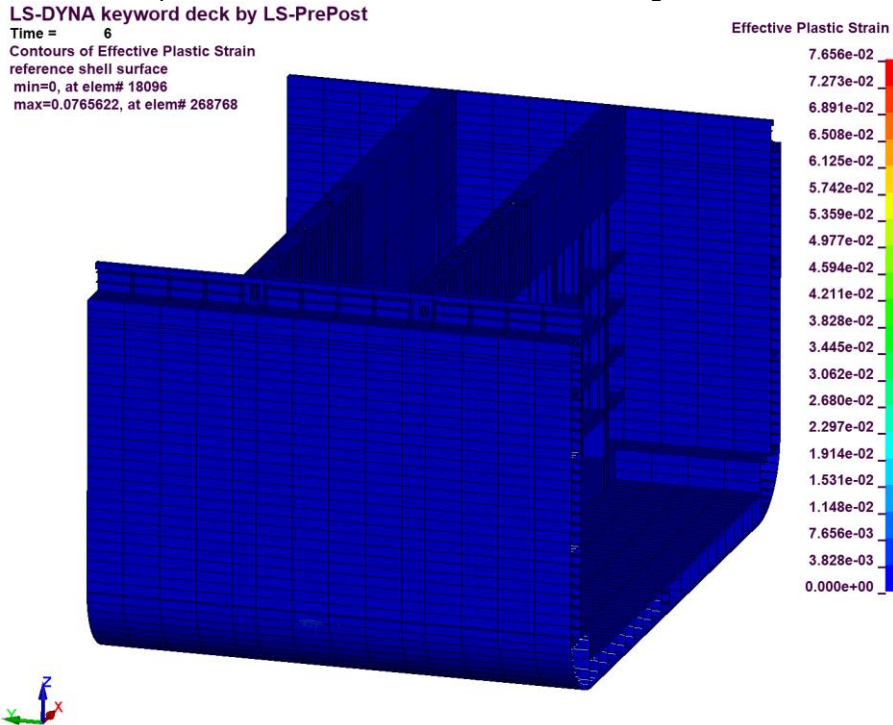


Figure 127. Effective Plastic Strain simulation 7

*Figure 128* shows the deformation of the ship after the collision.

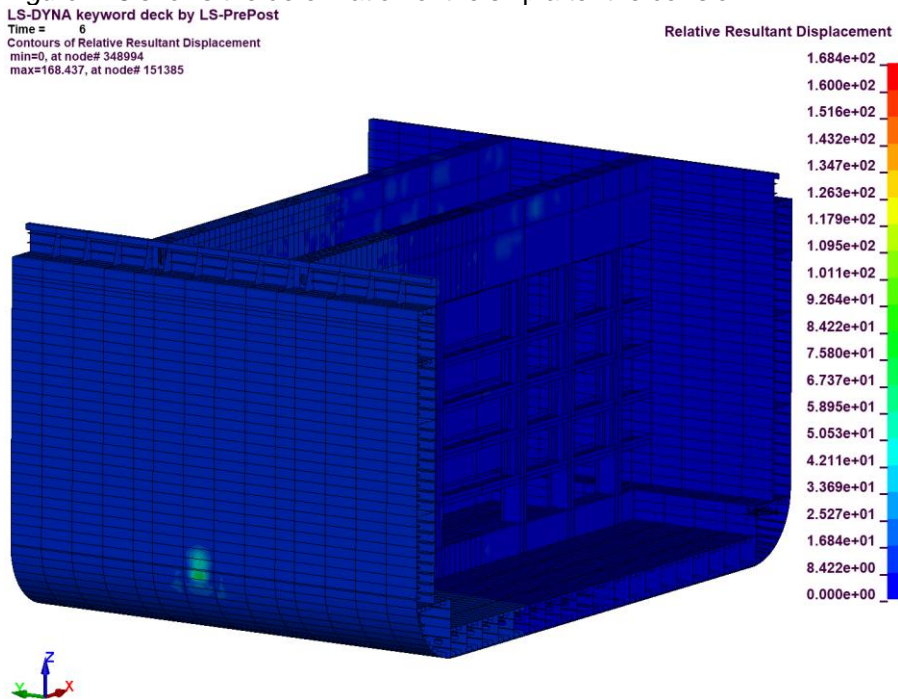


Figure 128. Resultant Displacement SB side [mm]



Figure 129 shows the deformation of the foundation, which indicates a clear buckling failure of the foundation.

### LS-DYNA keyword deck by LS-PrePost

Time = 6

Contours of Resultant Displacement

min=10.4031, at node# 2851

max=14848.5, at node# 16245

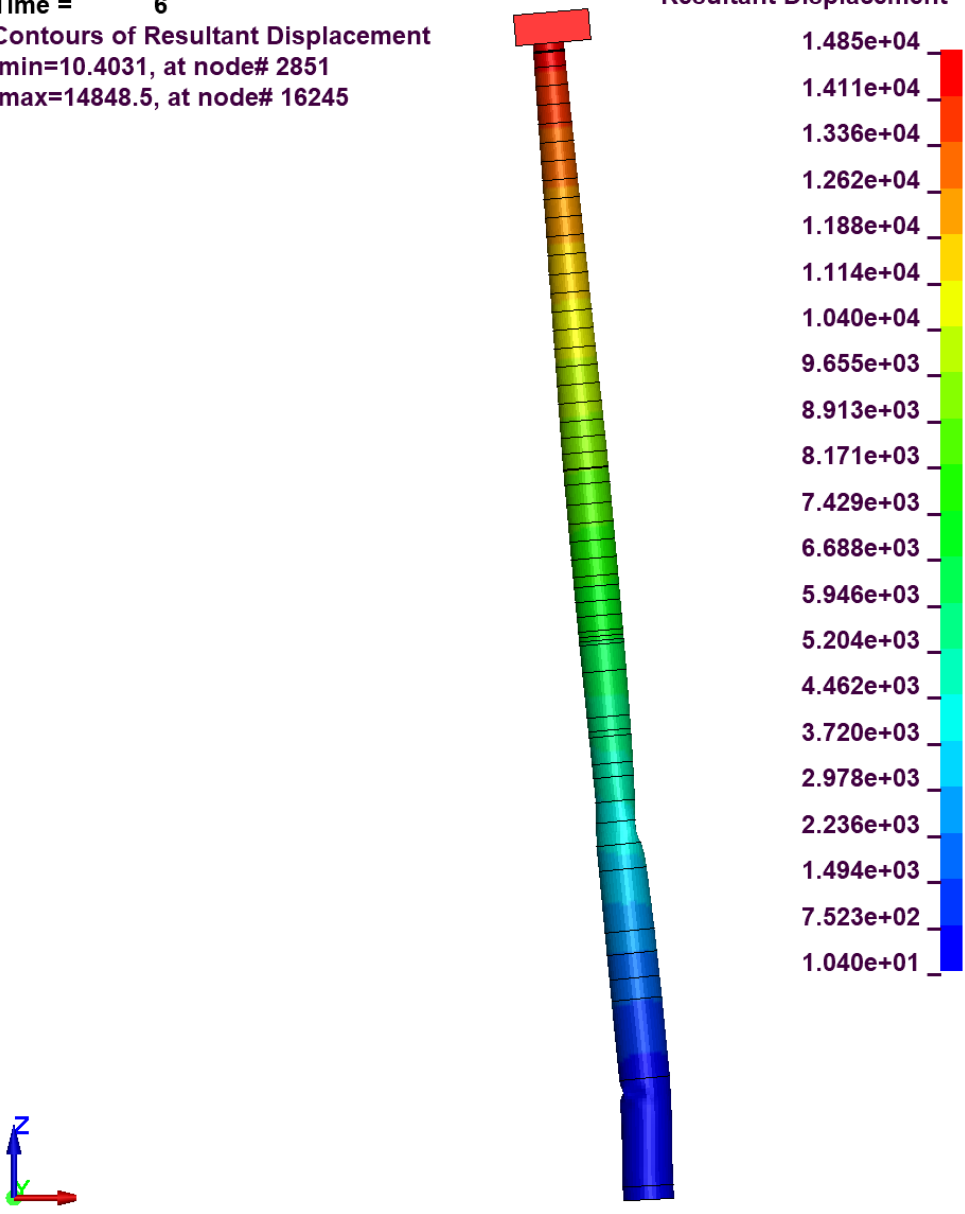
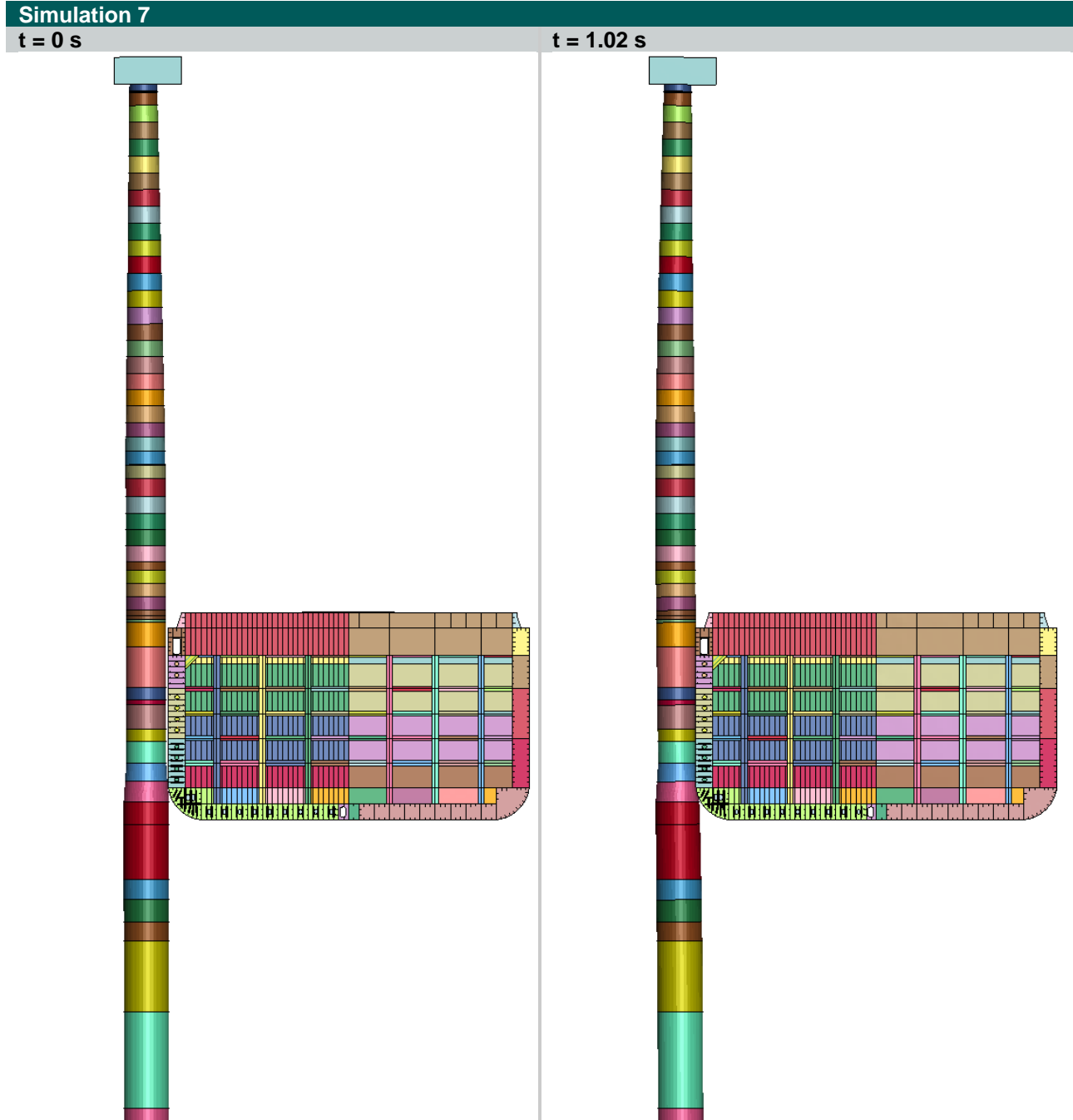


Figure 129. Resultant Displacement Foundation Tower [mm]

Table 56. Visual timeline simulation 7





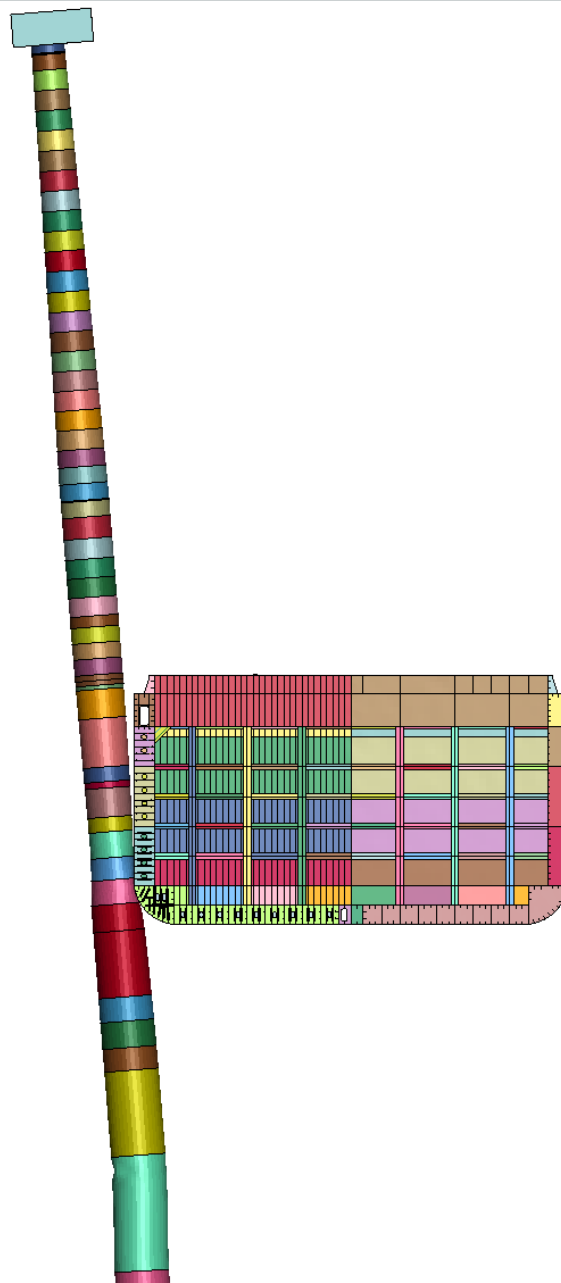
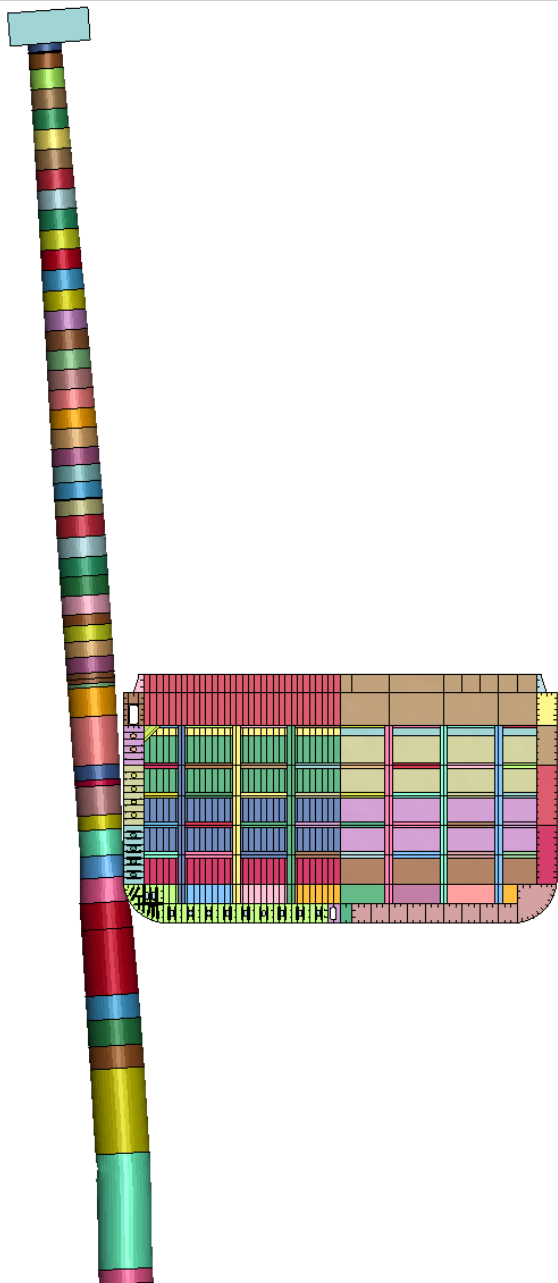
**Simulation 7**  
t = 1.98 s t = 3 s



### Simulation 7

t = 4.02 s

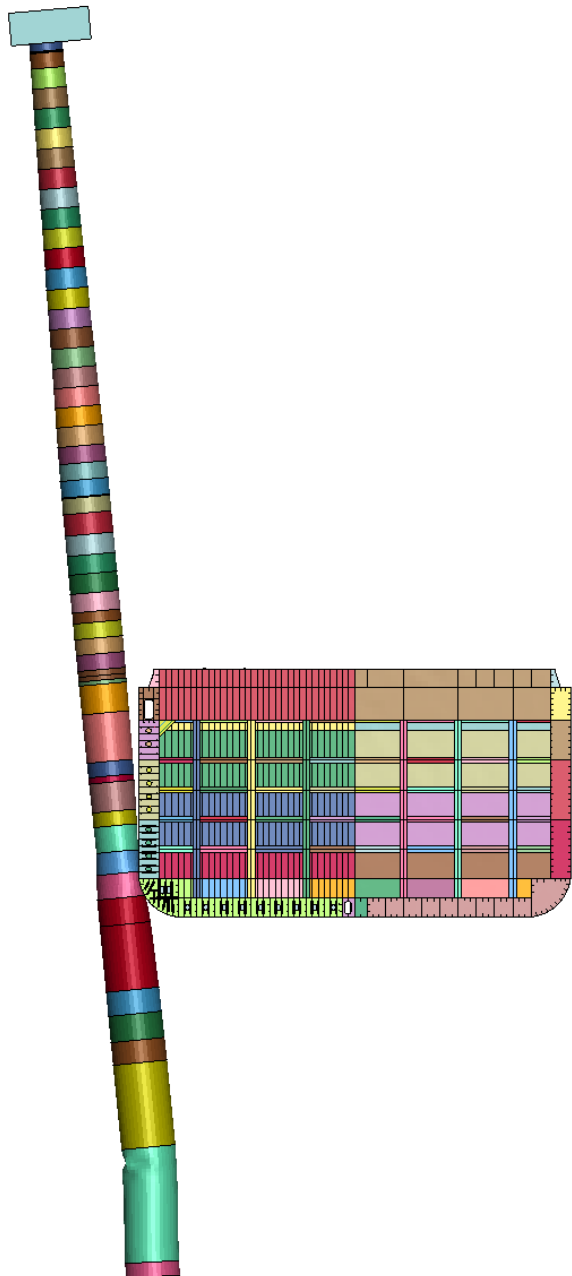
t = 4.98 s





## Simulation 7

6.0 s



### J.1.8. Simulation 8

Figure 130 shows the global kinetic and internal energy over time during the collision. Initially, the kinetic energy is 873 MJ, determined by the ship's speed and mass. As the collision progresses, the total energy increases due to the collapse of the turbine tower foundation, leading to a rise in internal energy and a leveling off in the decline of kinetic energy.

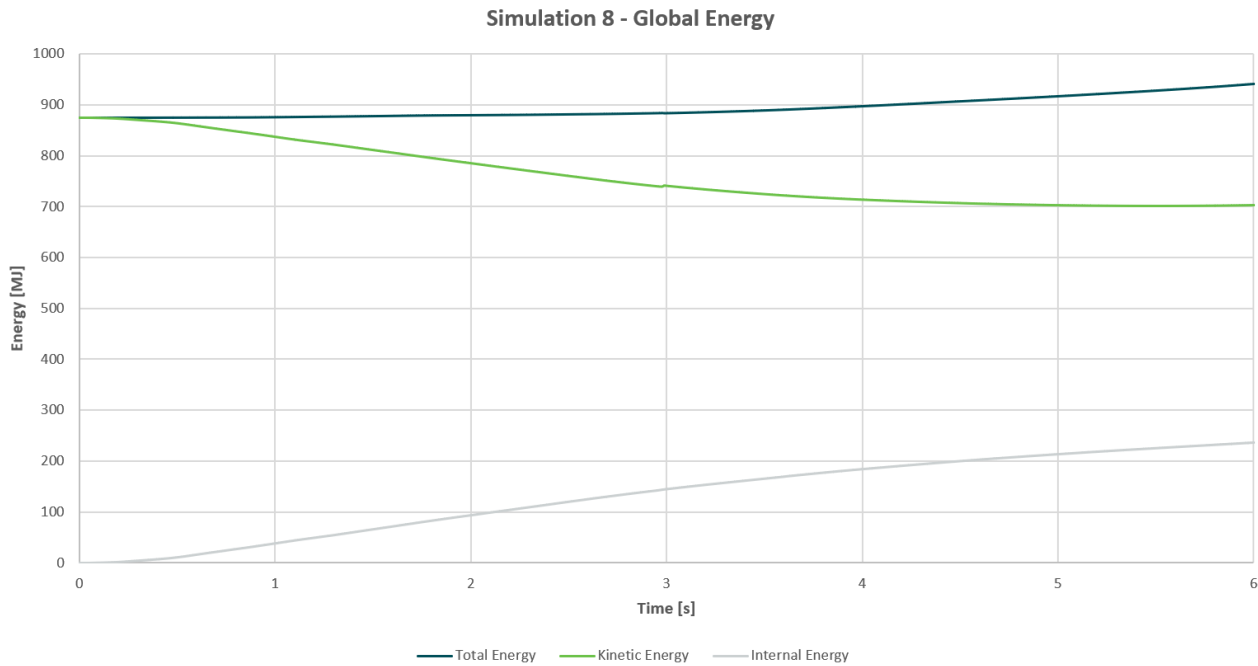


Figure 130. Global energy Distribution over time

The impact force between the vessel and the foundation over the time is shown in Figure 131.

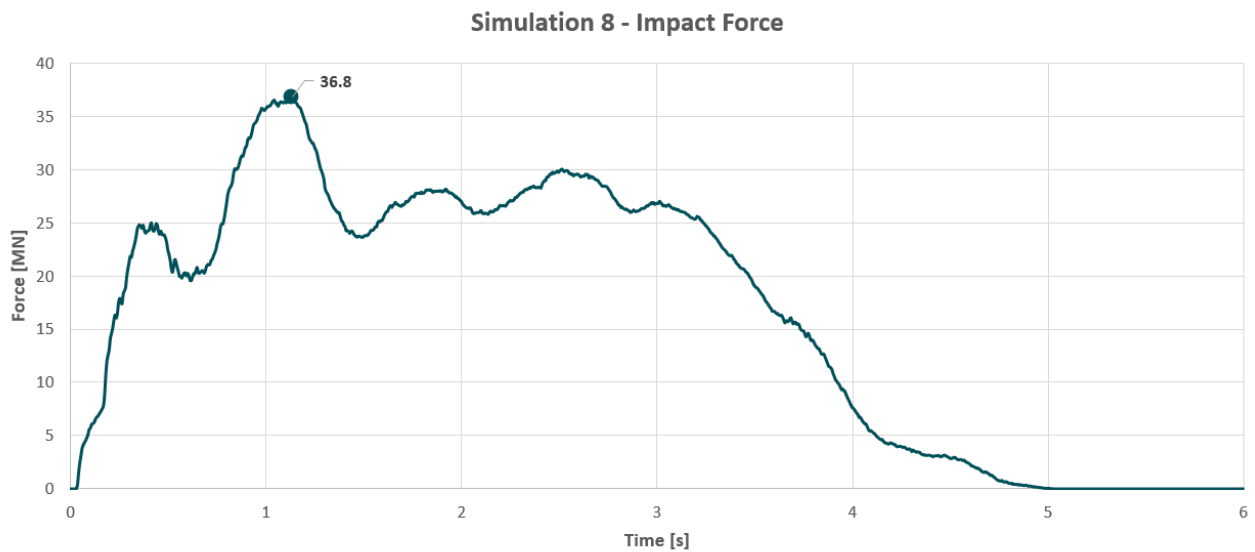


Figure 131. Impact Force over time

The effective plastic strain of the SB side is shown in *Figure 132*.

LS-DYNA keyword deck by LS-PrePost

Time = 6

Contours of Effective Plastic Strain

reference shell surface

min=0, at elem# 18096

max=0.0743344, at elem# 268770

Effective Plastic Strain

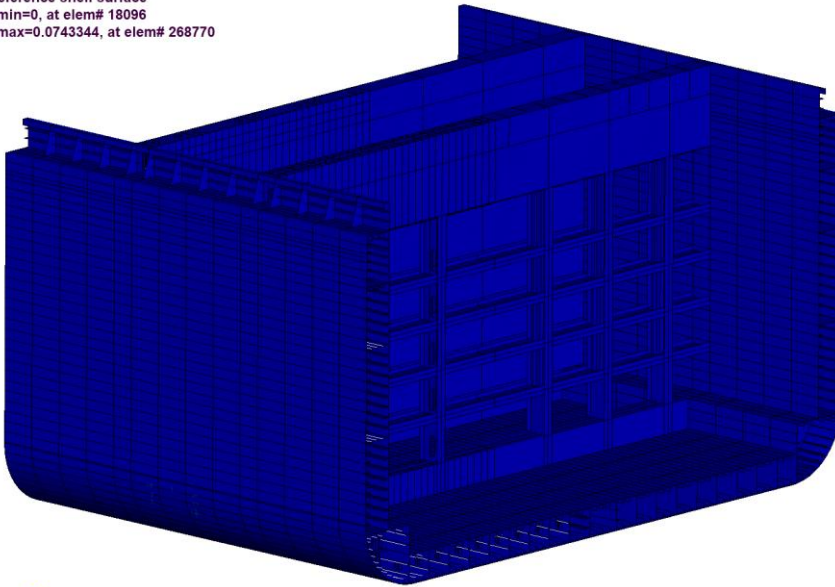


Figure 132. Effective Plastic Strain simulation 8

*Figure 133* shows the deformation of the ship after the collision.

LS-DYNA keyword deck by LS-PrePost

Time = 6

Contours of Relative Resultant Displacement

min=0, at node# 330885

max=106.825, at node# 151370

Relative Resultant Displacement

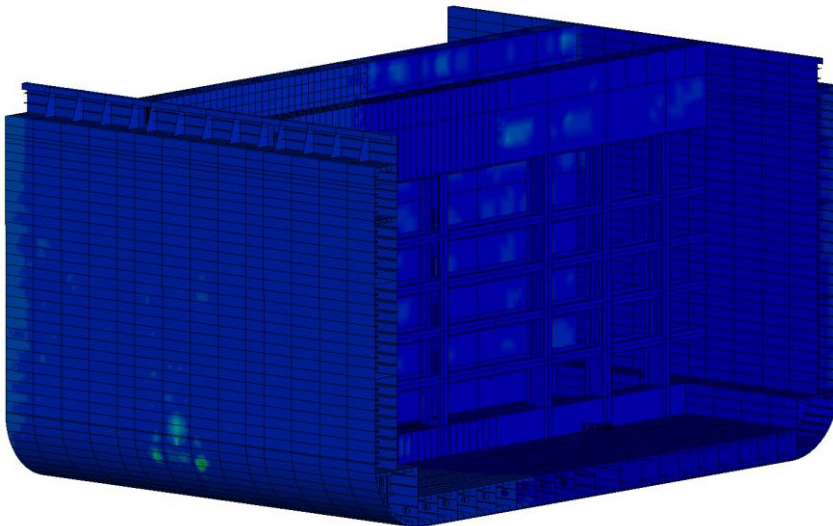


Figure 133. Resultant Displacement SB side [mm]

Figure 134 shows the deformation of the foundation, which indicates a clear buckling failure of the foundation.

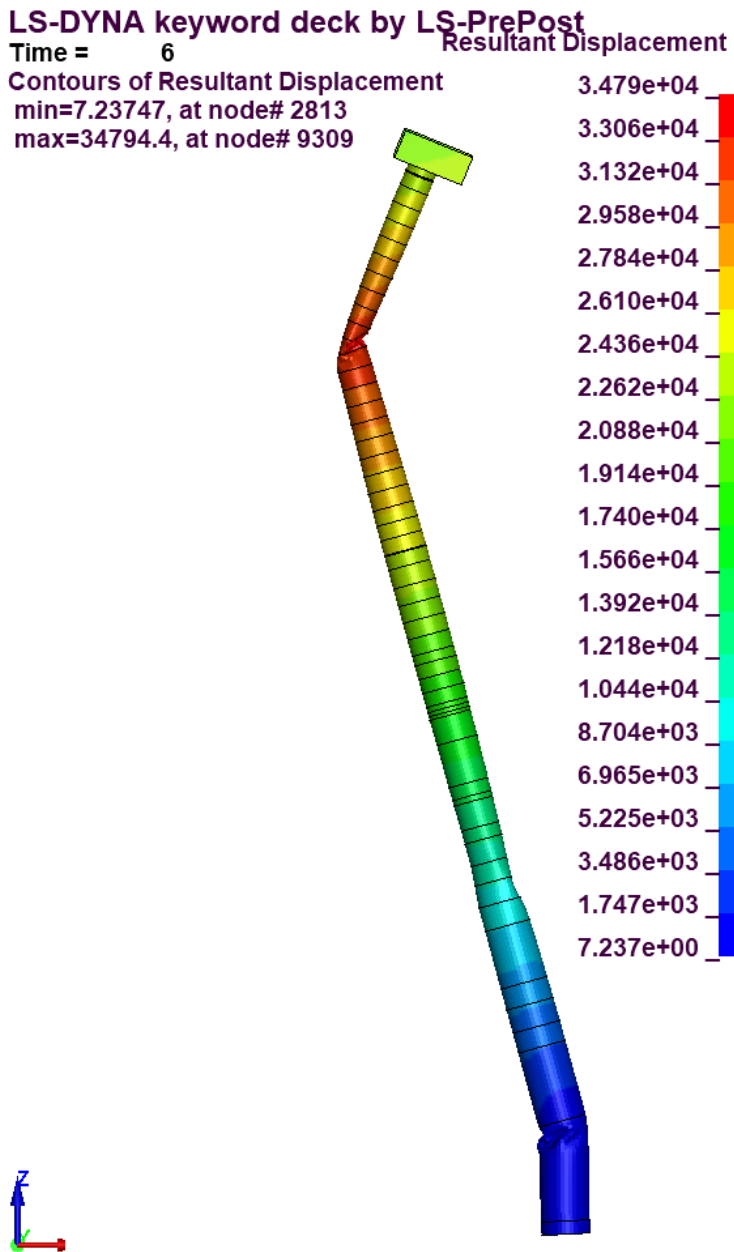
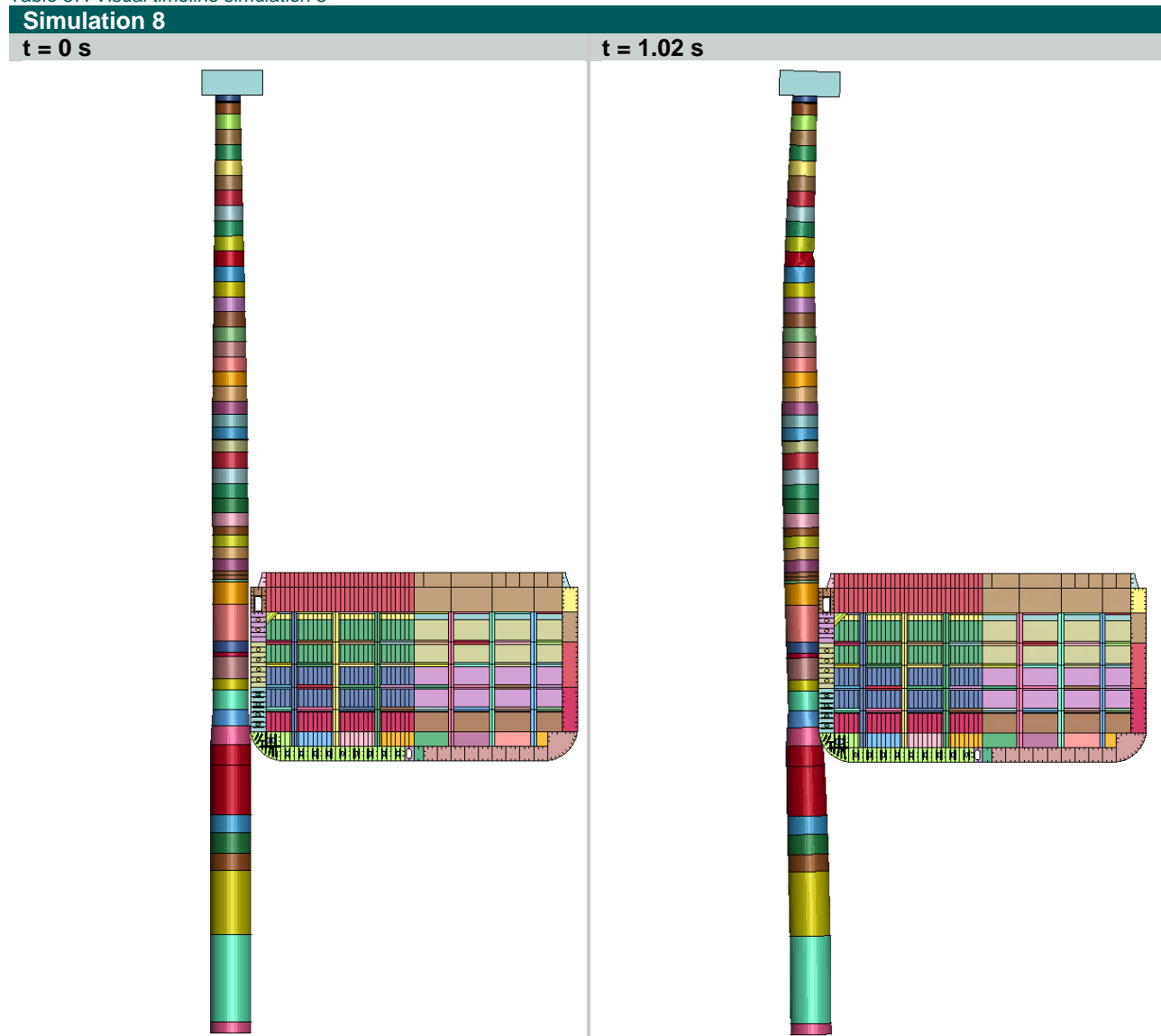


Figure 134. Resultant Displacement Foundation Tower [mm]



Table 57. Visual timeline simulation 8

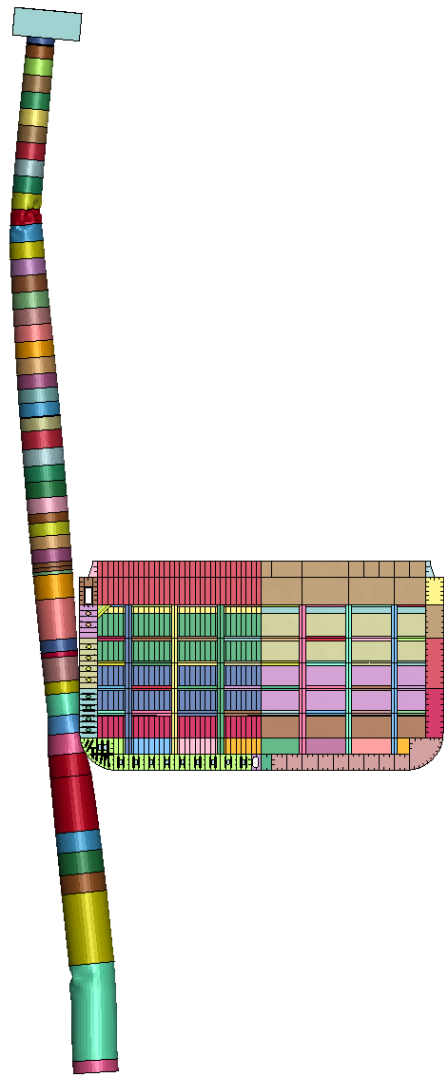
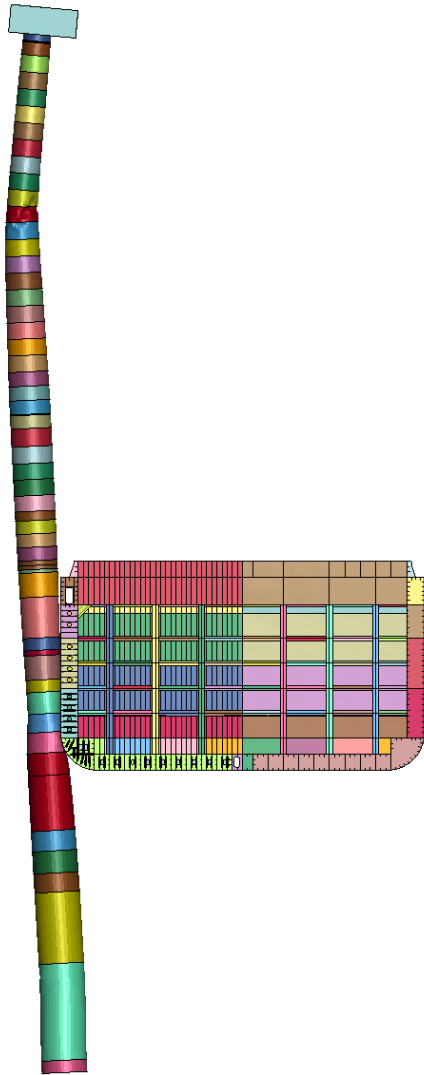




Simulation 8

t = 1.98 s

t = 3 s

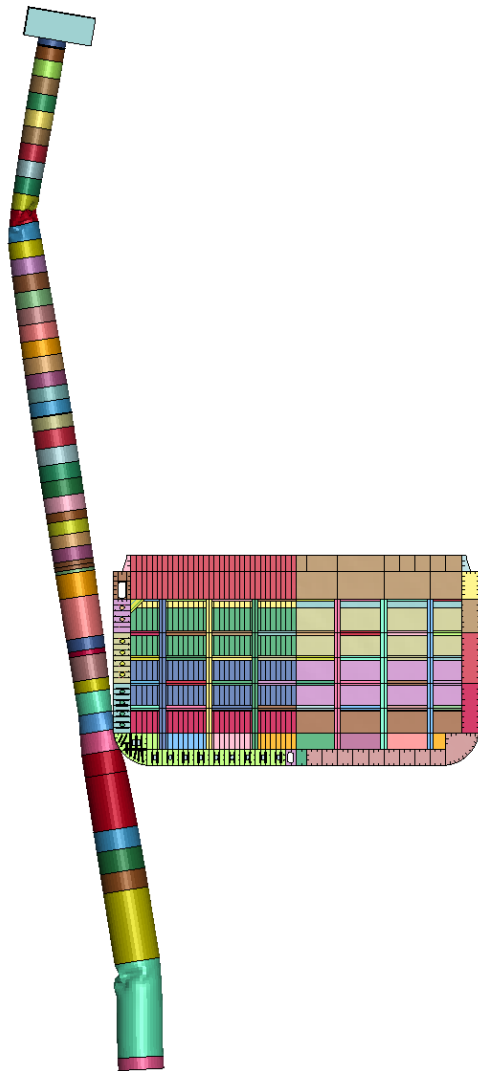




Simulation 8

t = 4.02 s

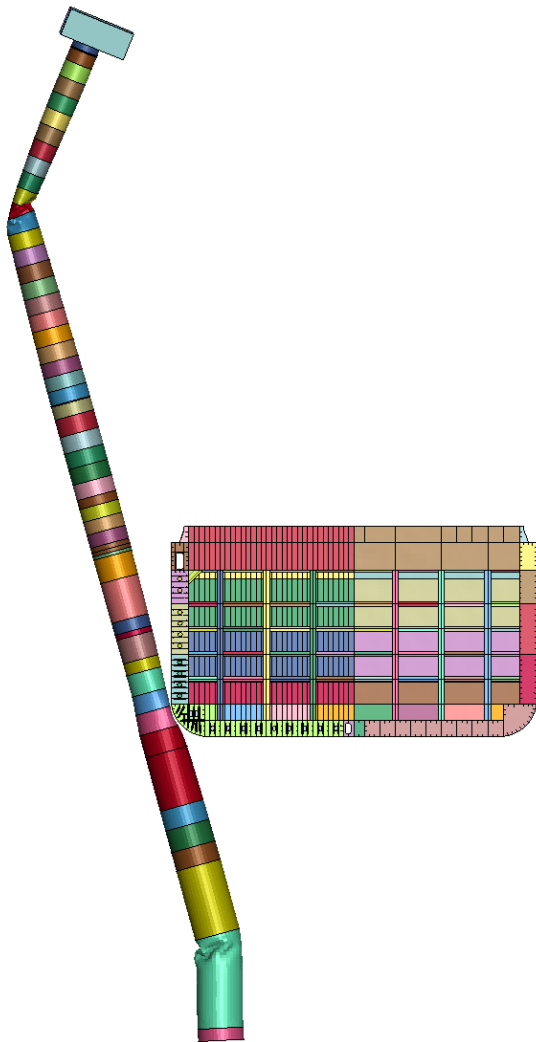
t = 4.98 s





Simulation 8

t = 5.55 s



### J.1.9. Simulation 9

Figure 135 shows the global Kinetic and Internal Energy over time during the collision. Initially, the kinetic energy is 2373 MJ, which is determined by the ship's speed and mass. As the collision progresses, the total energy increases due to the collapse of the turbine tower foundation, resulting in a rise in both kinetic and internal energy.

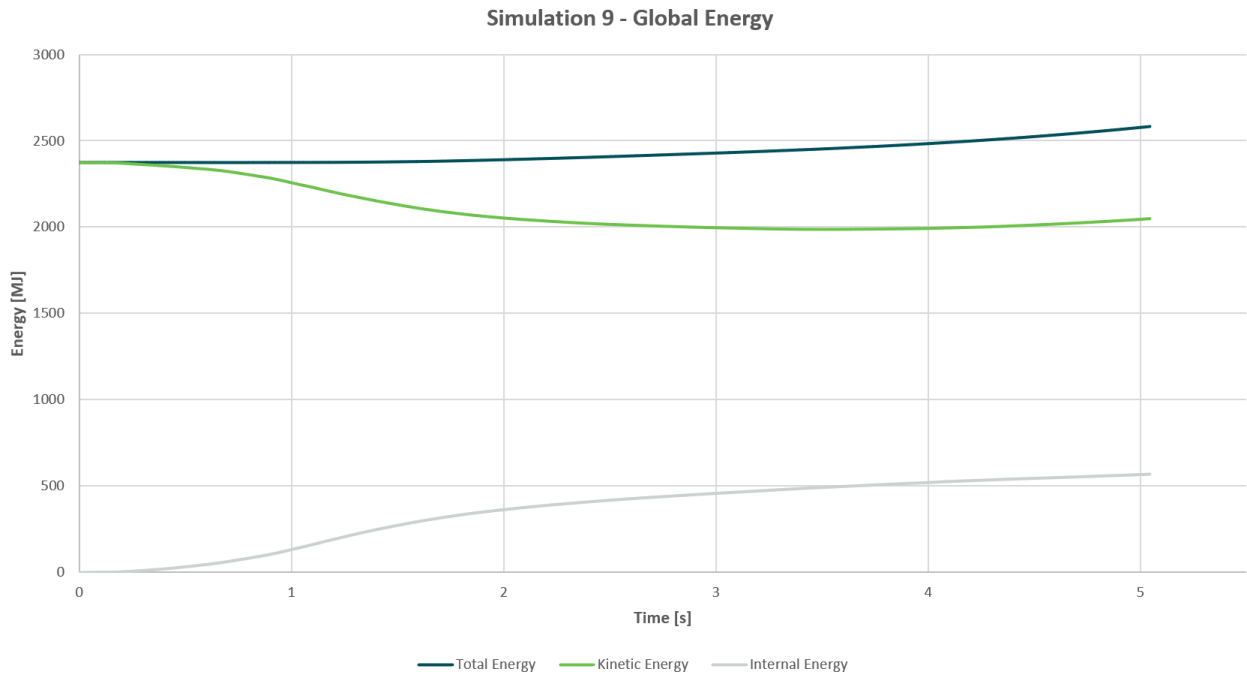


Figure 135. Global energy Distribution over time

The impact force between the vessel and the foundation over the time is shown in Figure 136.

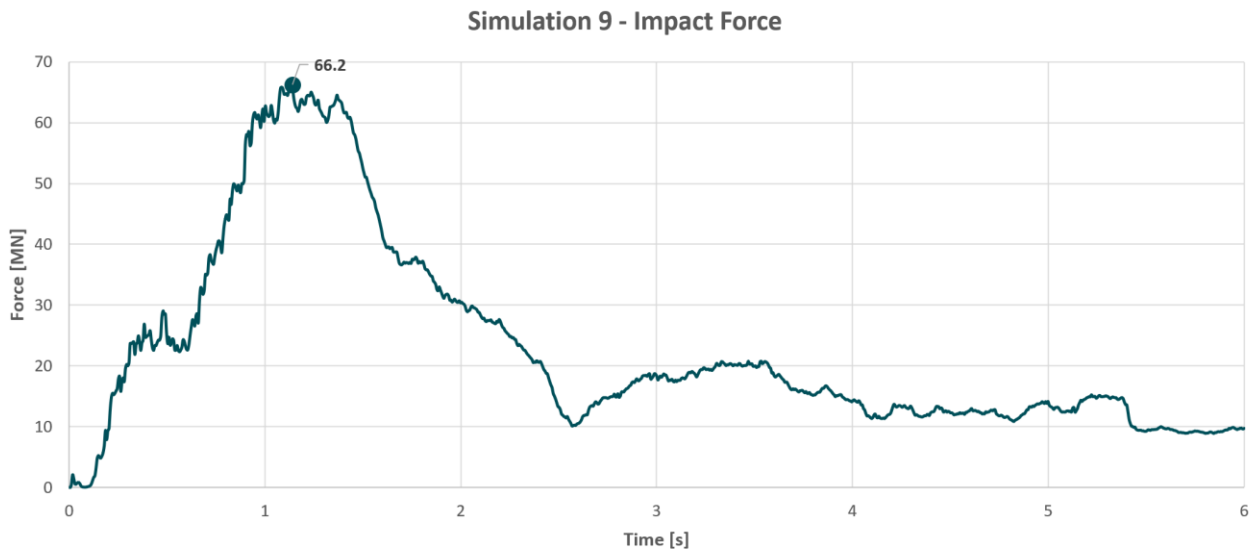


Figure 136. Impact Force over time

The failed elements and effective plastic strain of the bow are shown in *Figure 137* and *Figure 138*.

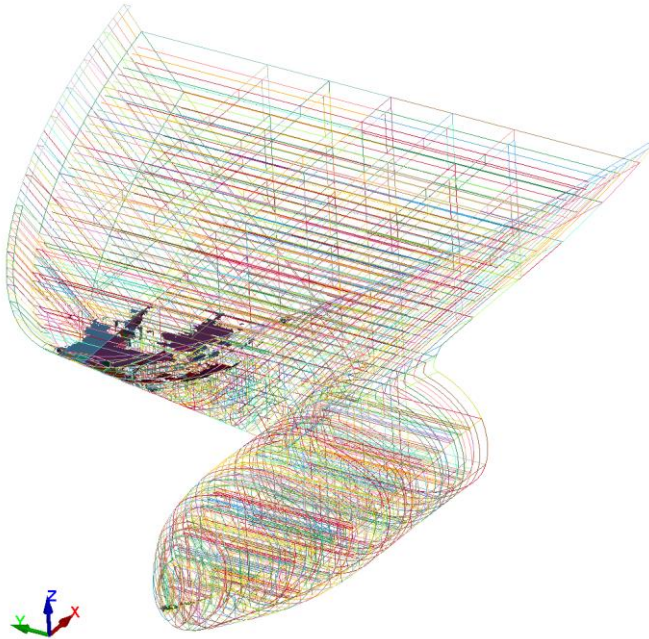


Figure 137. Failed elements simulation 9  
LS-DYNA keyword deck by LS-PrePost  
Time = 6  
Contours of Effective Plastic Strain  
reference shell surface  
min=0, at elem# 1  
max=0.229031, at elem# 6492

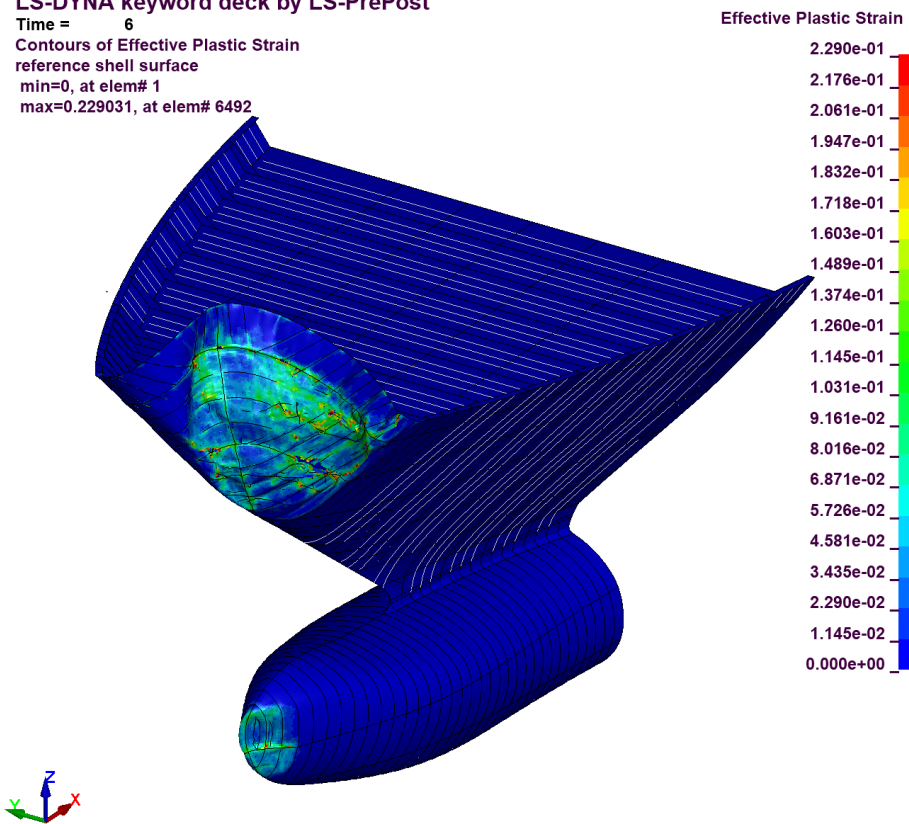


Figure 138. Effective Plastic Strain simulation 9

Figure 139 shows the deformation of the ship after the collision.

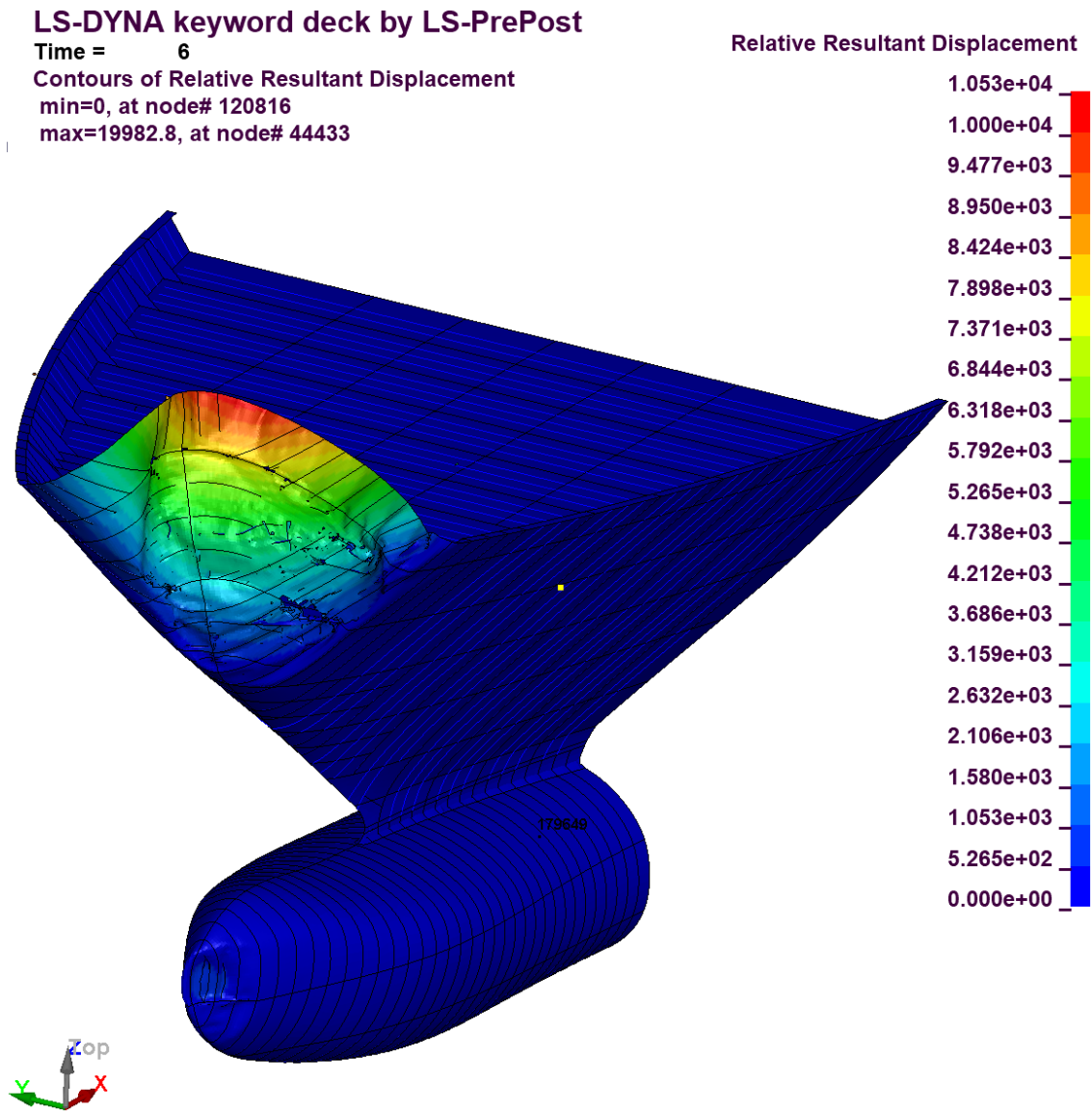


Figure 139. Resultant Displacement Bow [mm]

Figure 140 shows the deformation of the foundation, which indicates a clear buckling failure of the foundation.

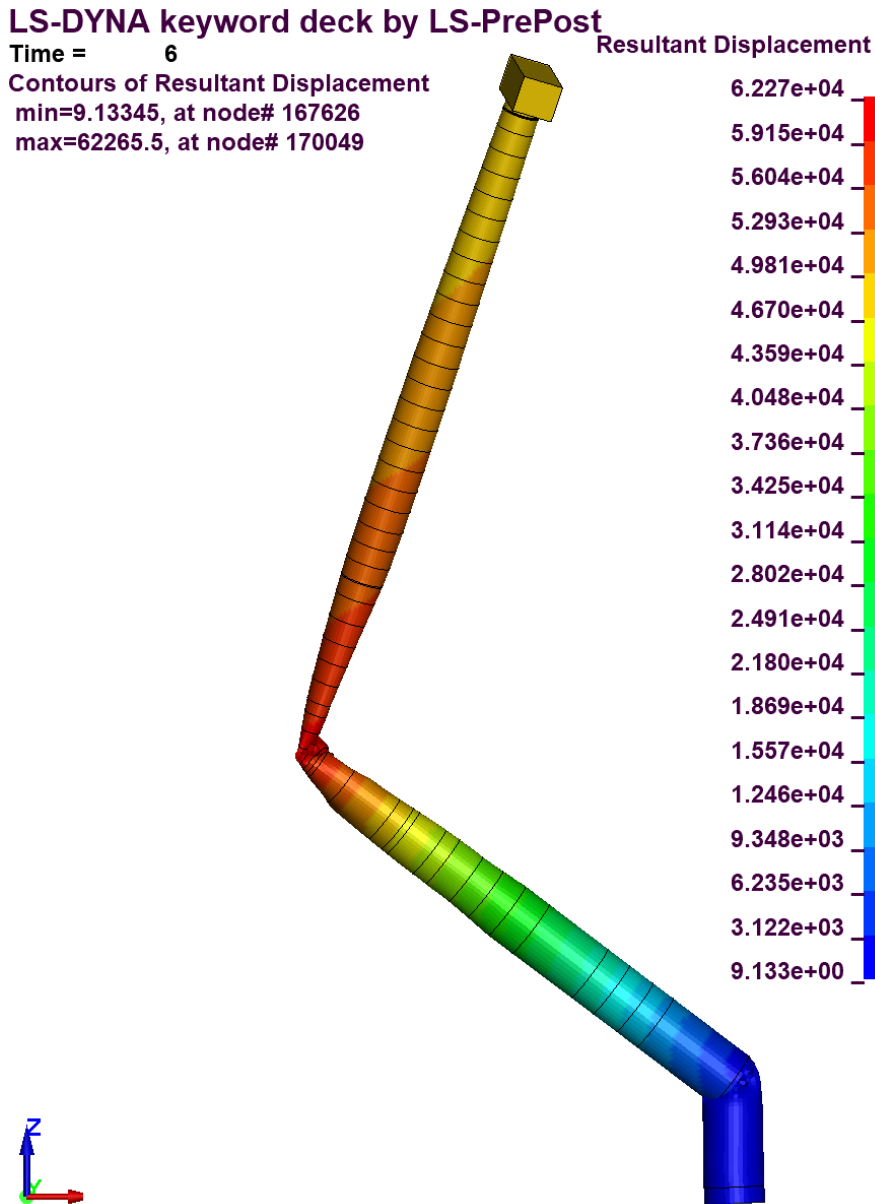
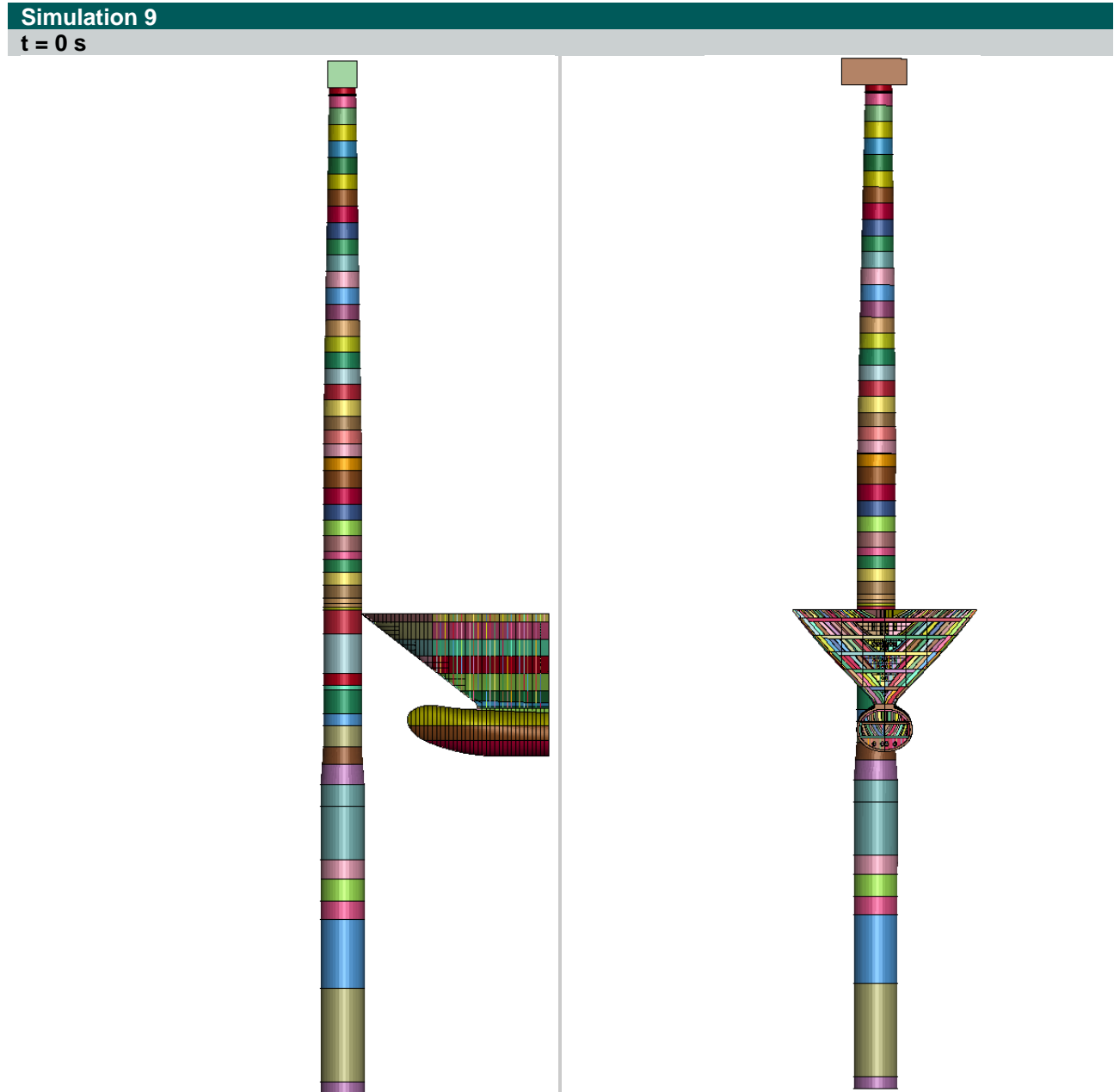


Figure 140. Resultant Displacement Foundation Tower [mm]



Table 58. Visual timeline simulation 9





Simulation 9

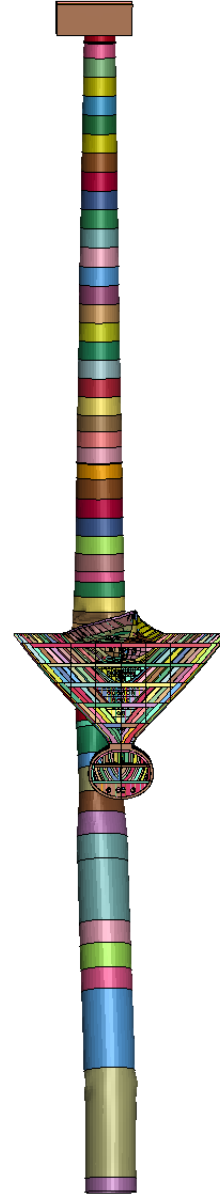
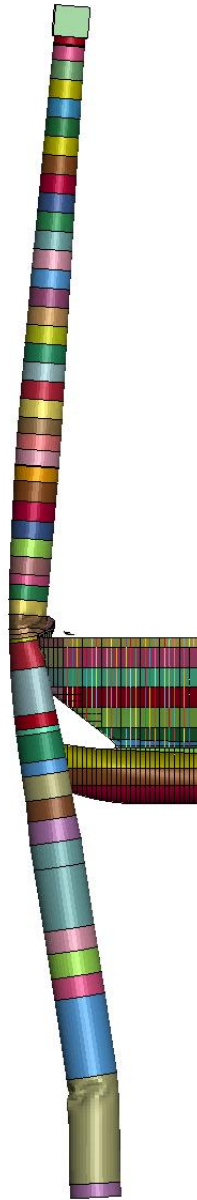
t = 1.02 s





Simulation 9

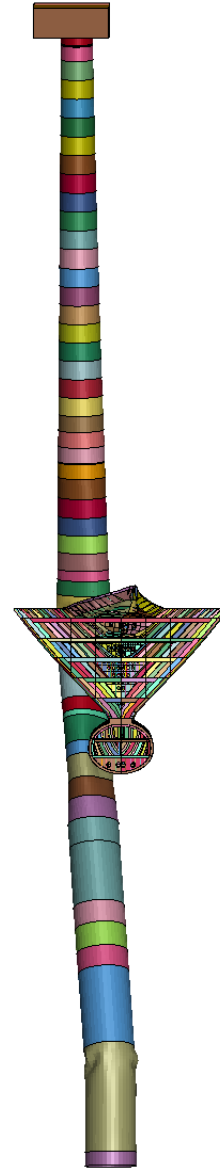
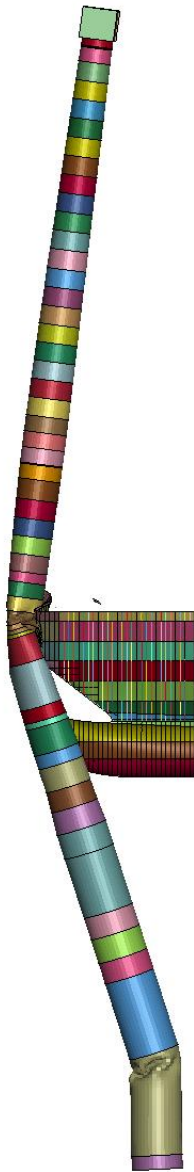
t = 1.98 s





Simulation 9

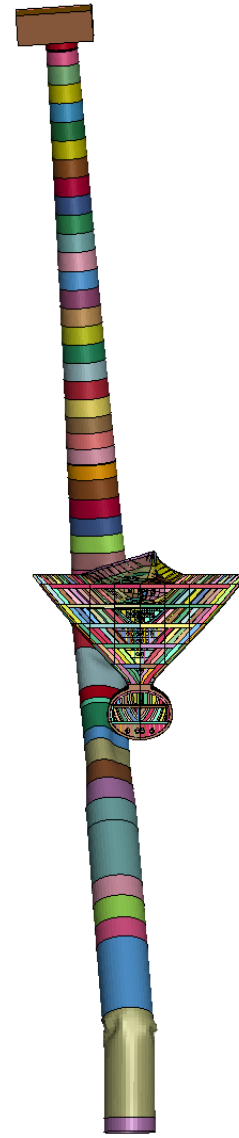
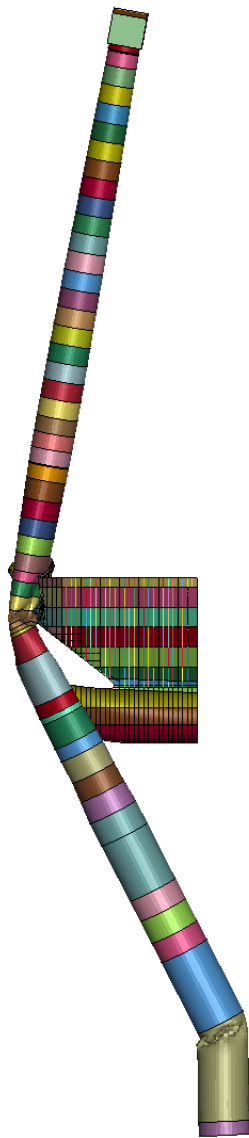
t = 3 s





Simulation 9

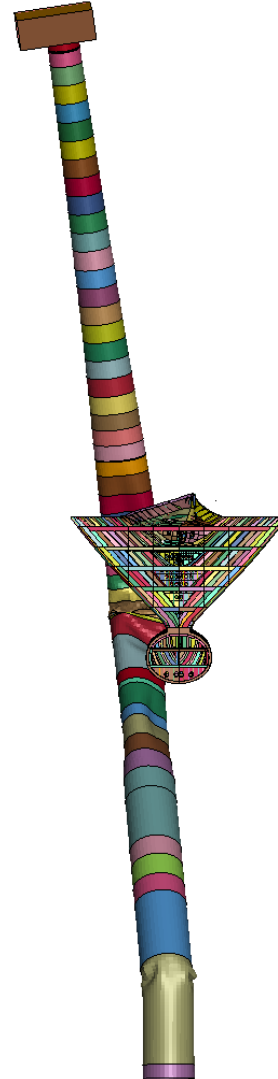
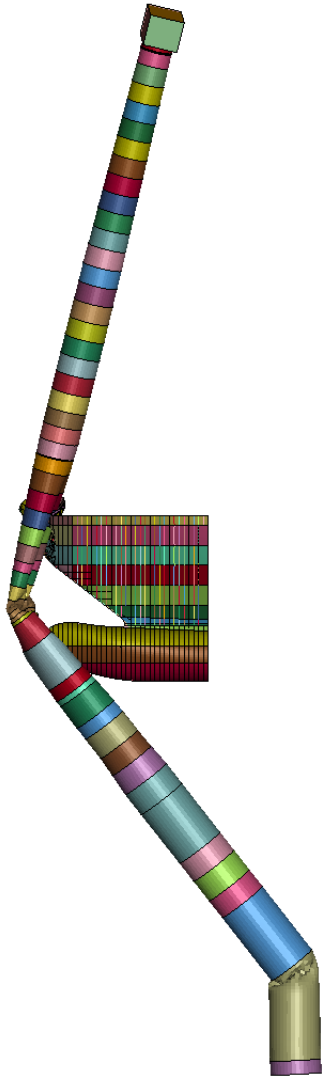
t = 4.02 s





Simulation 9

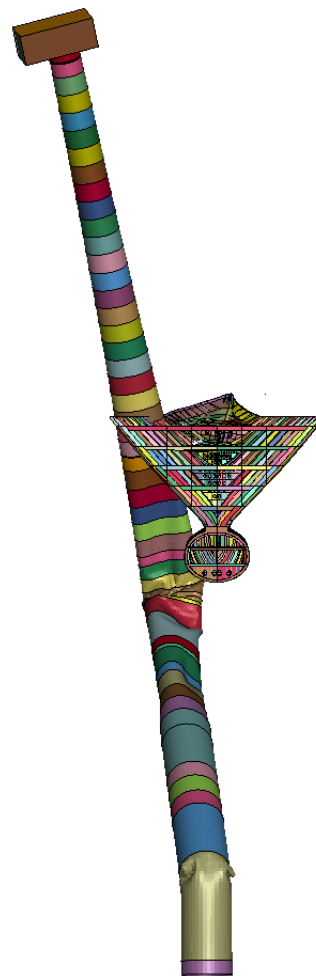
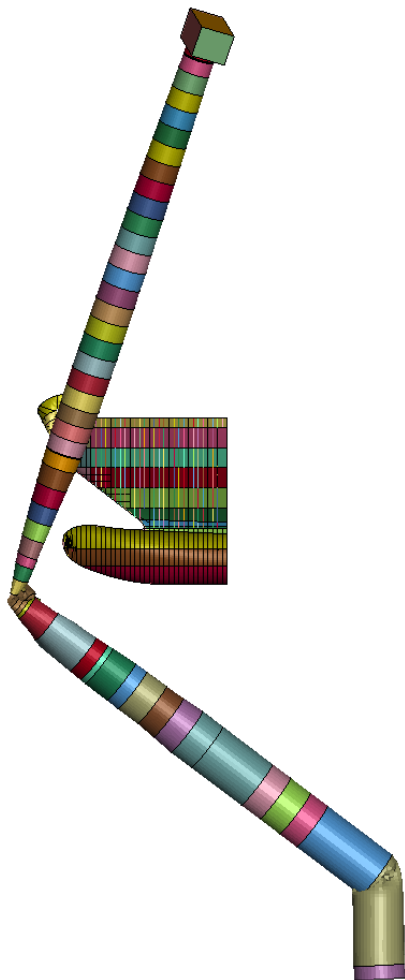
t = 4.98 s





Simulation 9

t = 5.55 s



### J.1.10. Simulation 10

Figure 141 shows the global Kinetic and Internal Energy over time during the collision. Initially, the kinetic energy is 5340 MJ, which is determined by the ship's speed and mass. As the collision progresses, the total energy increases due to the collapse of the turbine tower foundation, resulting in a rise in both kinetic and internal energy.

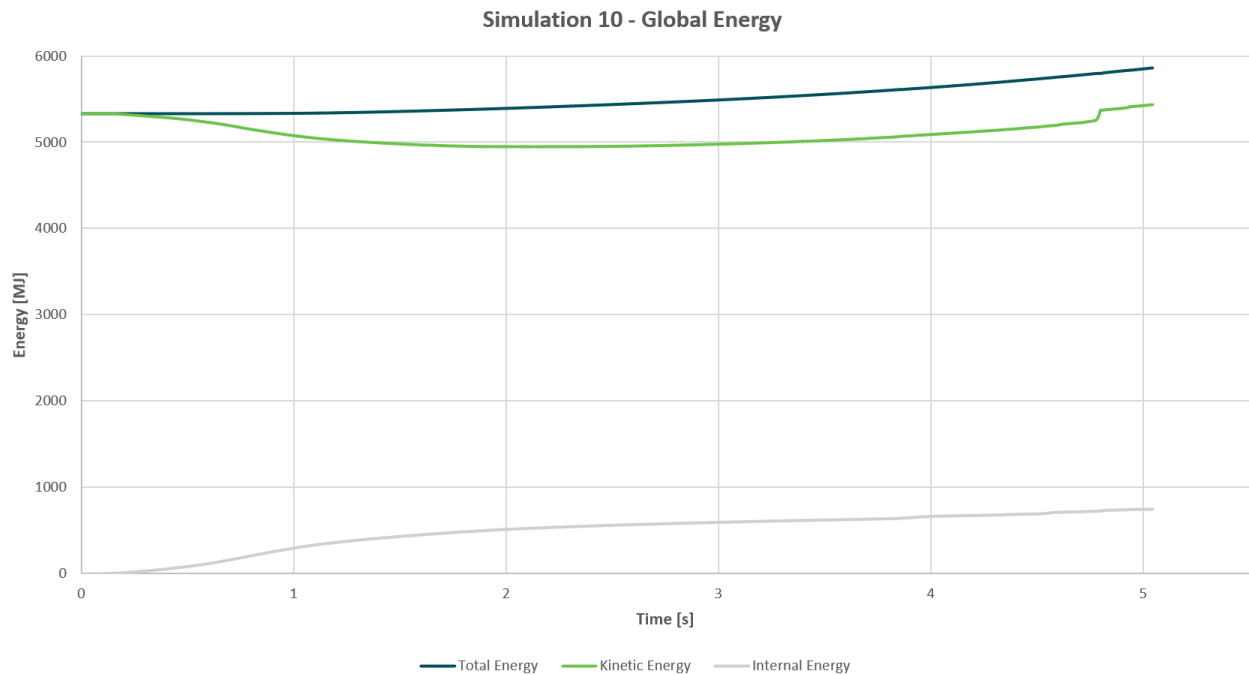


Figure 141. Global energy Distribution over time

The impact force between the vessel and the foundation over the time is shown in Figure 142.

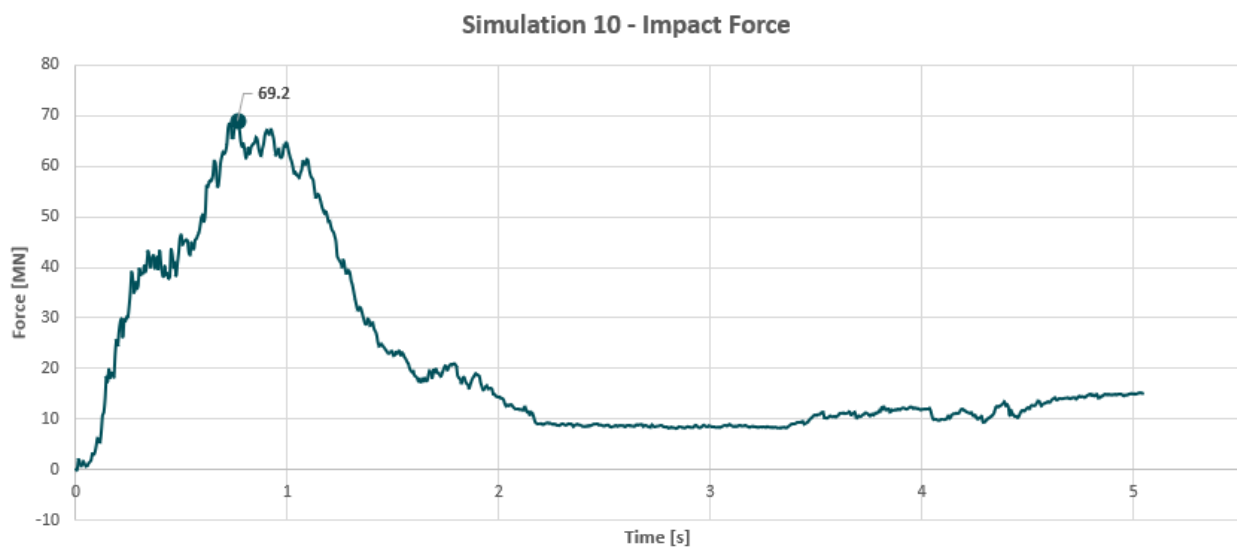


Figure 142. Impact Force over time



The failed elements and effective plastic strain of the bow are shown in *Figure 143* and *Figure 144*.

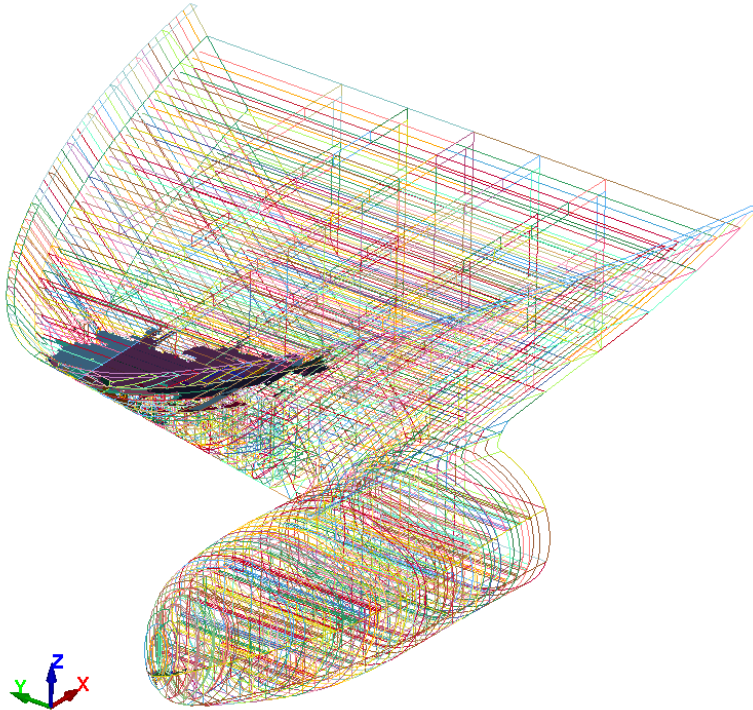


Figure 143. Failed elements simulation 10  
LS-DYNA keyword deck by LS-PrePost  
Time = 5.0464  
Contours of Effective Plastic Strain  
reference shell surface  
min=0, at elem# 1  
max=0.229031, at elem# 7070

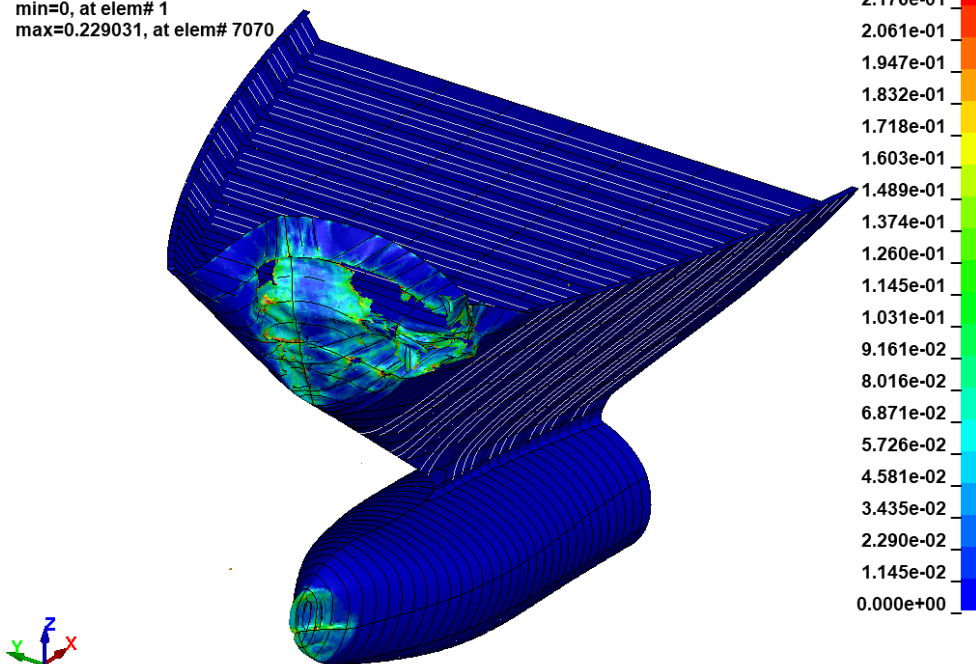


Figure 144. Effective Plastic Strain simulation 10

Figure 145 shows the deformation of the ship after the collision.

### LS-DYNA keyword deck by LS-PrePost

Time = 5.0464

Contours of Relative Resultant Displacement

min=0, at node# 67527

max=148287, at node# 45987

Relative Resultant Displacement

1.229e+04

1.167e+04

1.106e+04

1.044e+04

9.830e+03

9.215e+03

8.601e+03

7.987e+03

7.372e+03

6.758e+03

6.144e+03

5.529e+03

4.915e+03

4.300e+03

3.686e+03

3.072e+03

2.457e+03

1.843e+03

1.229e+03

6.144e+02

0.000e+00

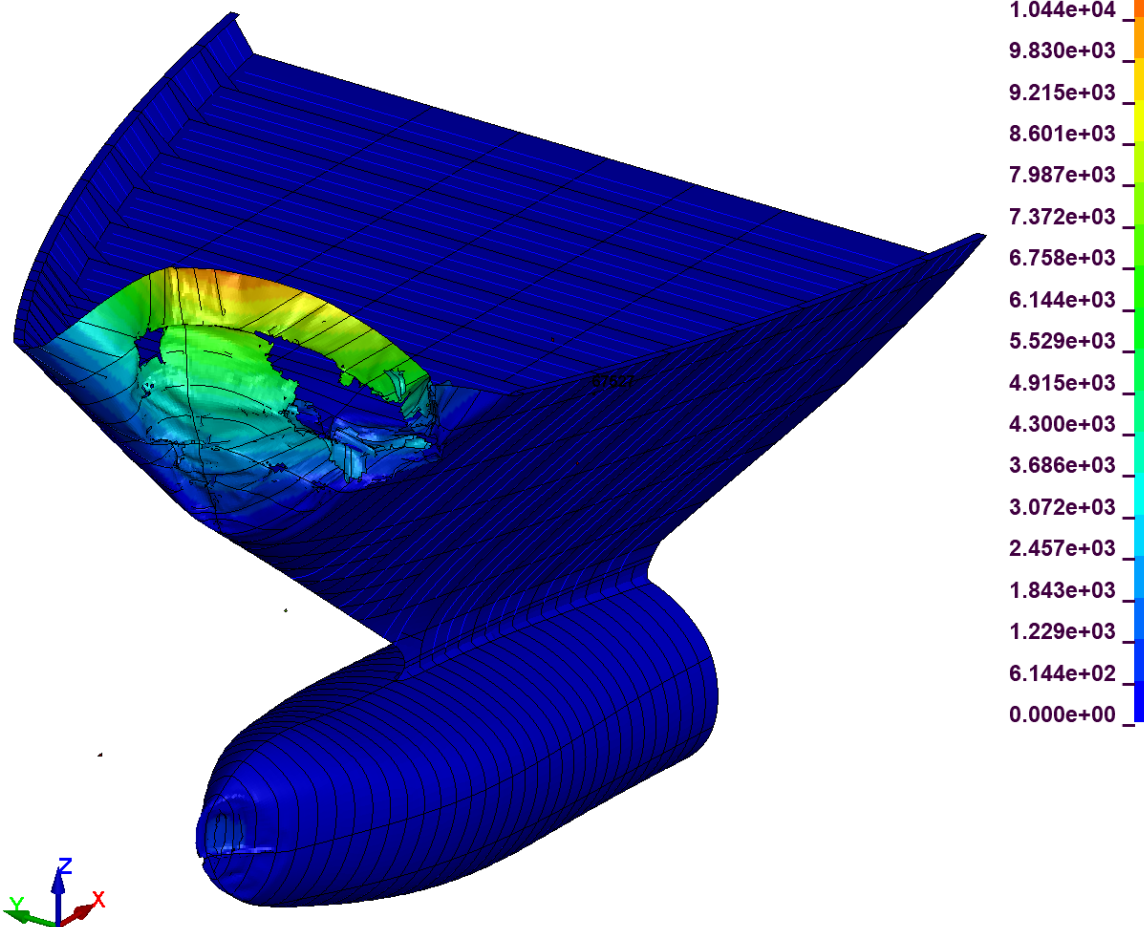


Figure 145. Resultant Displacement Bow [mm]

Figure 146 shows the deformation of the foundation, which indicates a clear buckling failure of the foundation.

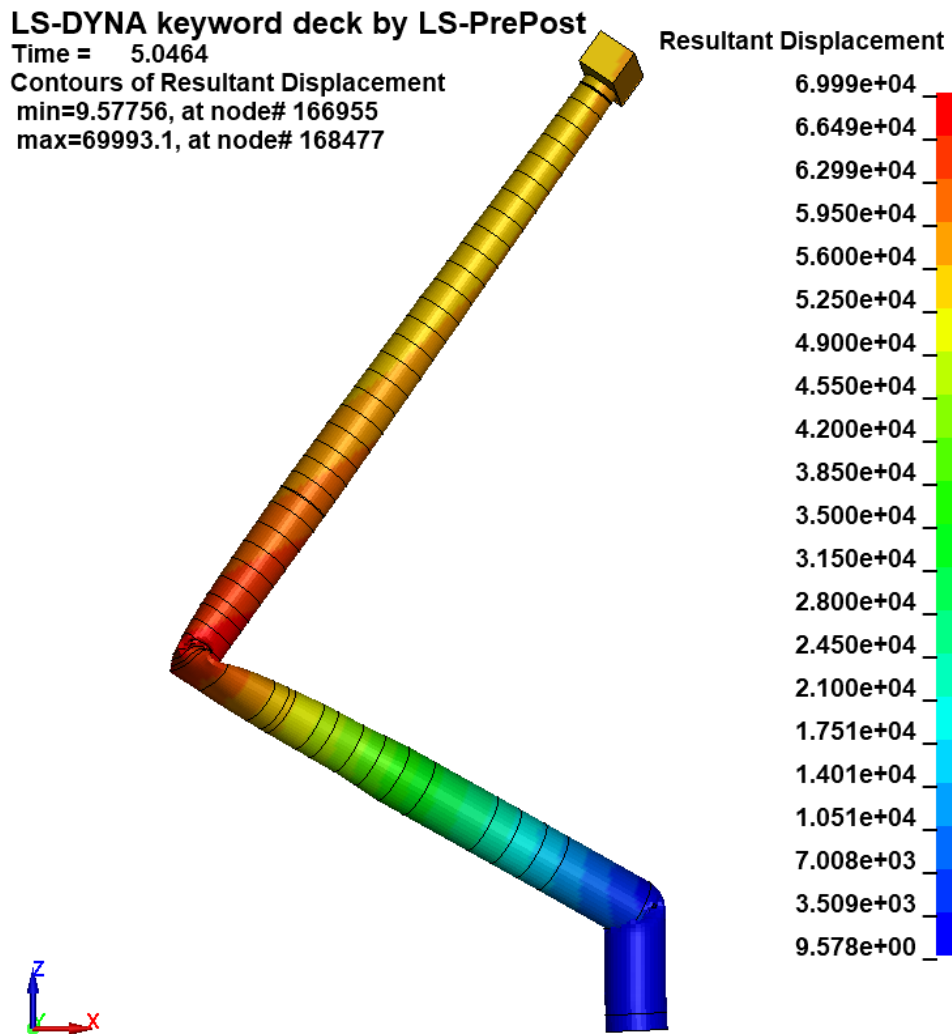


Figure 146. Resultant Displacement Foundation Tower [mm]



Table 59. Visual timeline simulation 10

**Simulation 10**

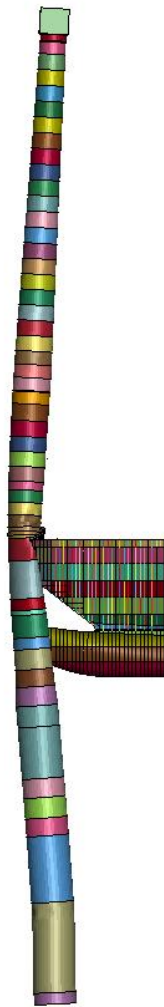
**t = 0 s**





Simulation 10

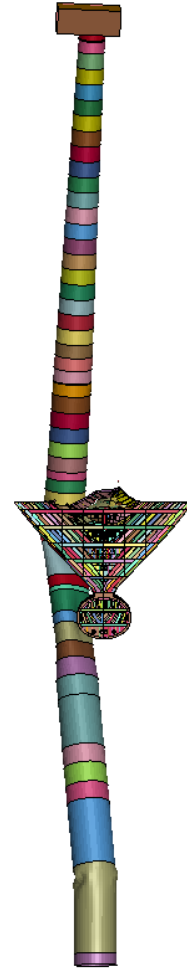
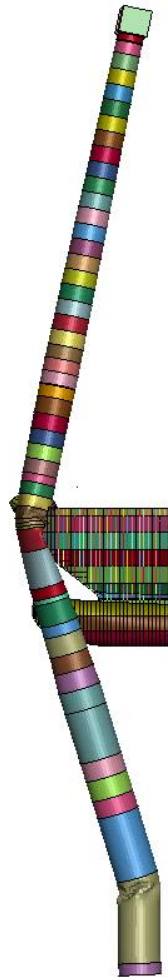
t = 1.02 s





Simulation 10

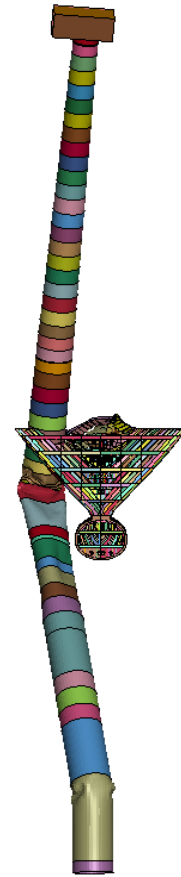
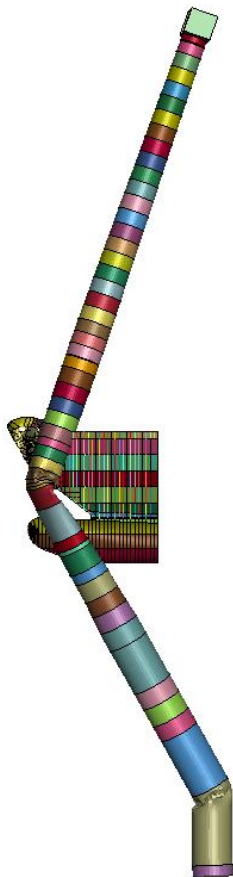
t = 1.98 s





Simulation 10

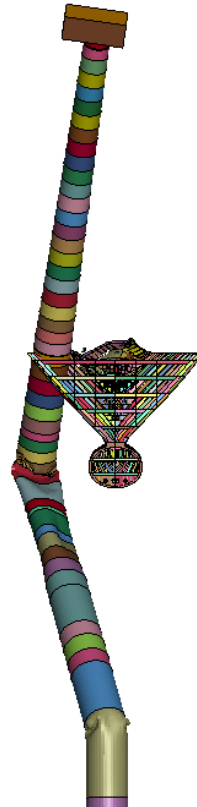
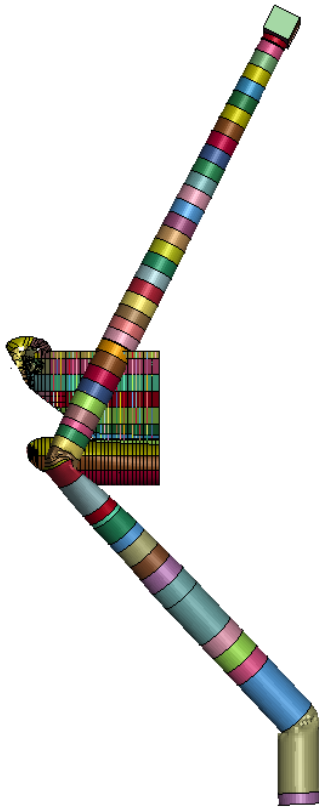
t = 3 s





Simulation 10

t = 4.02







Simulation 10

t = 5.05 s



### J.1.11. Simulation 11

Figure 147 shows the global kinetic and internal energy over time during the collision. Initially, the kinetic energy is 42 MJ, determined by the ship's speed and mass. Since the impact does not cause the tower to fall, the total energy remains constant.

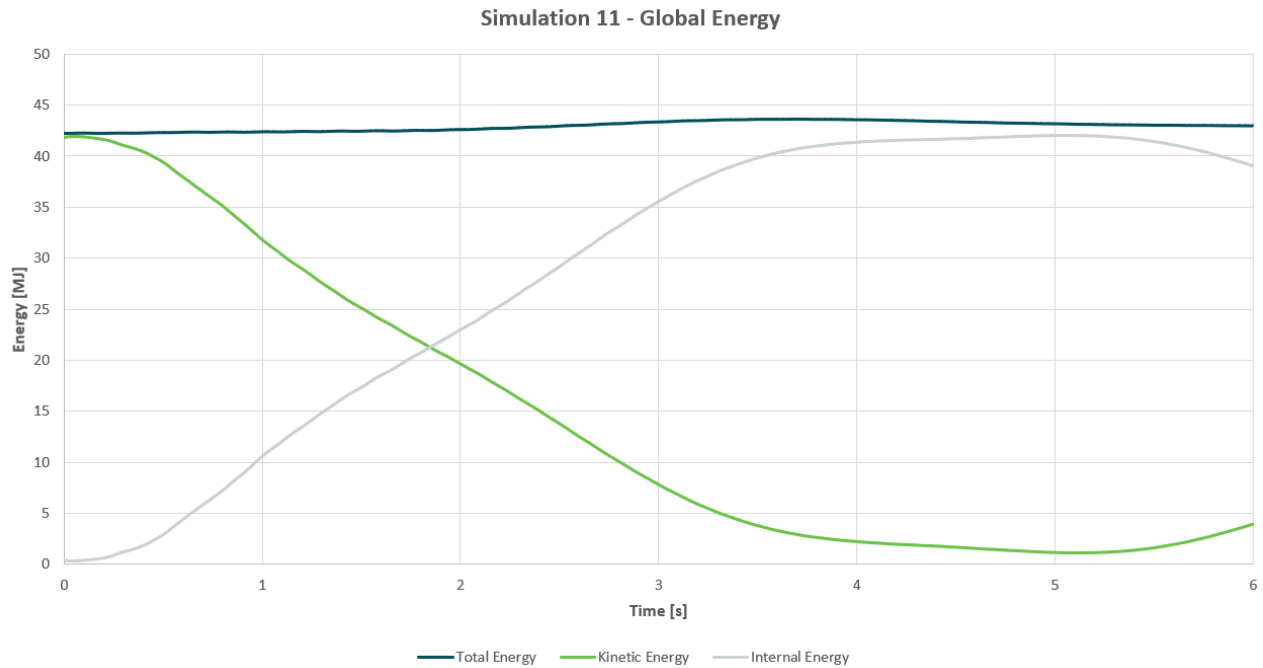


Figure 147. Global energy Distribution over time

The impact force between the vessel and the foundation over the time is shown in Figure 148.

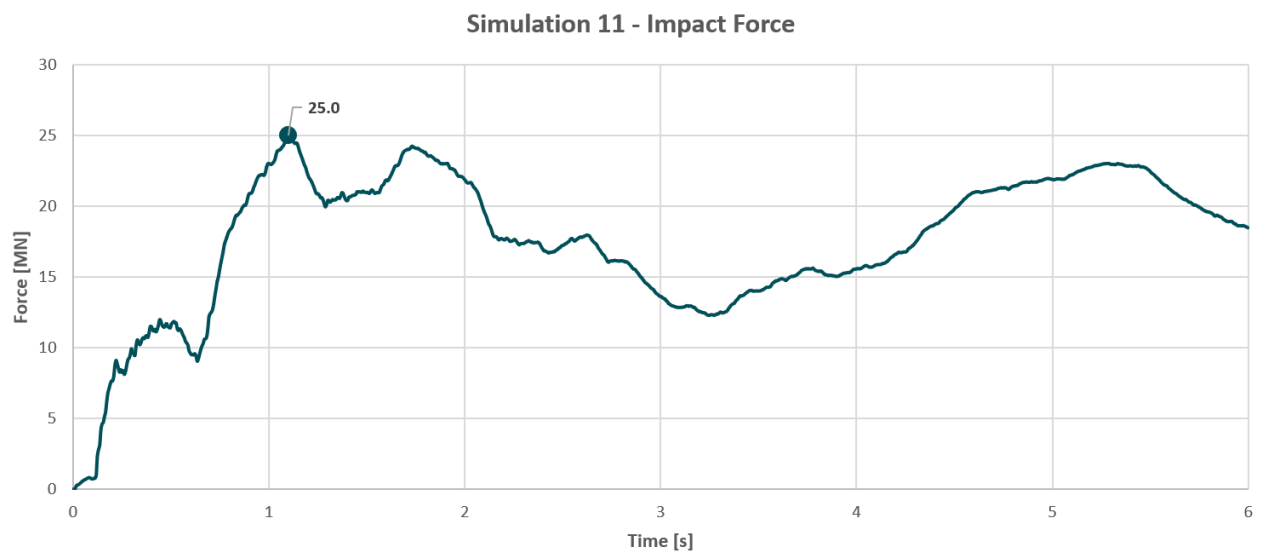


Figure 148. Impact Force over time

The effective plastic strain of the SB side is shown in *Figure 149*.

### LS-DYNA keyword deck by LS-PrePost

Time = 6  
Contours of Effective Plastic Strain  
reference shell surface  
min=0, at elem# 873832  
max=0.114349, at elem# 1098541

### Effective Plastic Strain

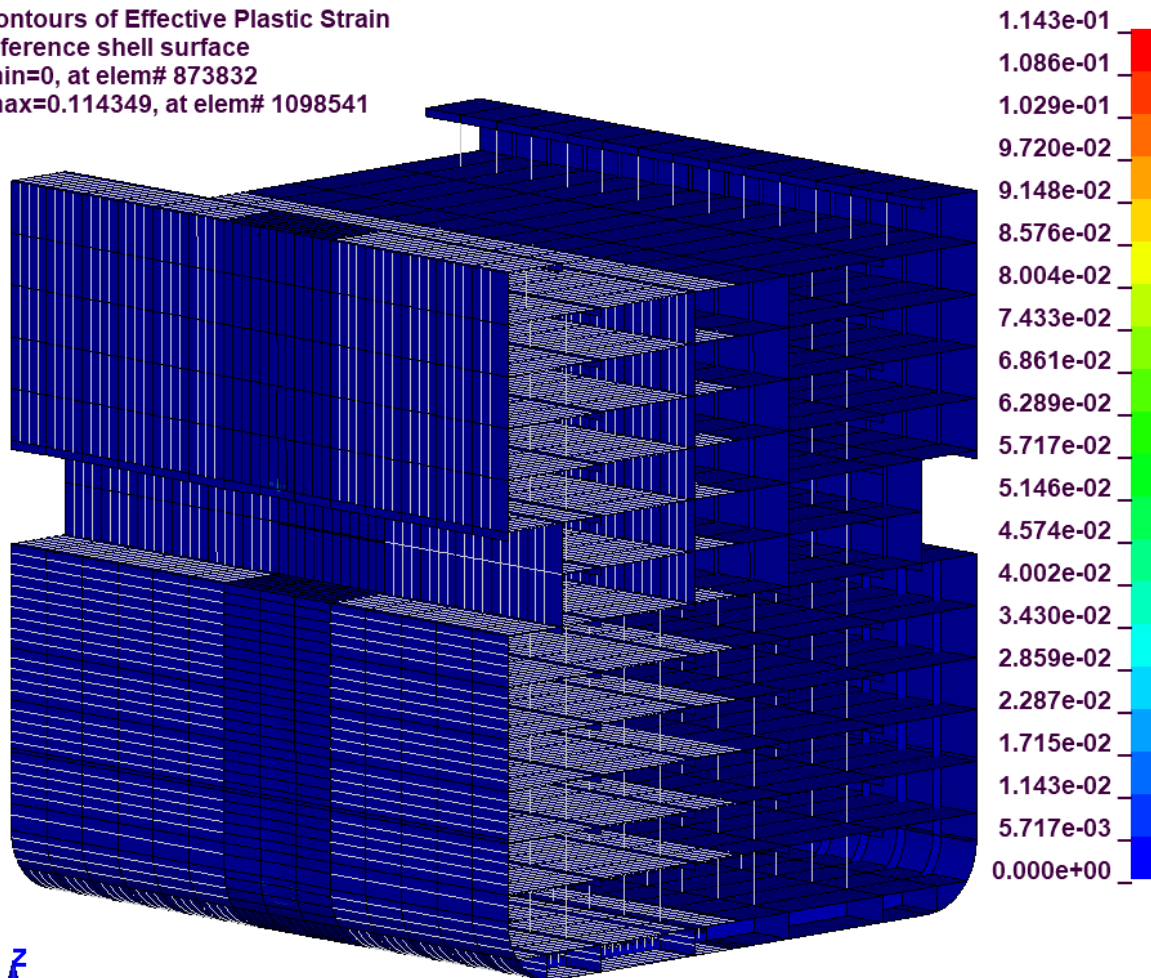


Figure 149. Effective Plastic Strain simulation 11

Figure 150 shows the deformation of the ship after the collision.

LS-DYNA keyword deck by LS-PrePost

Time = 3.18

Contours of Relative Resultant Displacement

min=0, at node# 1132140

max=153.901, at node# 1077368

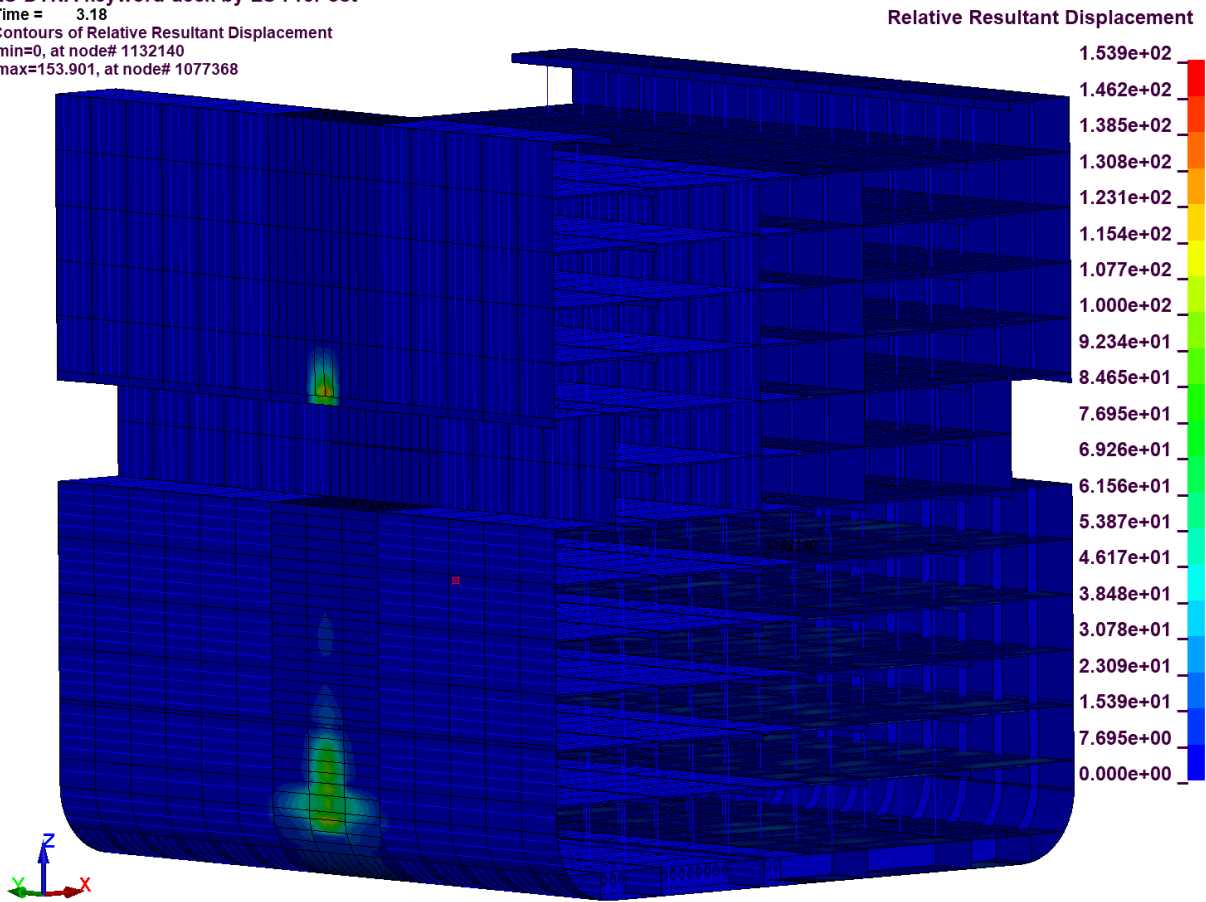


Figure 150. Resultant Displacement SB side [mm]

Figure 151 shows the deformation of the foundation, which indicates a clear buckling failure of the foundation.

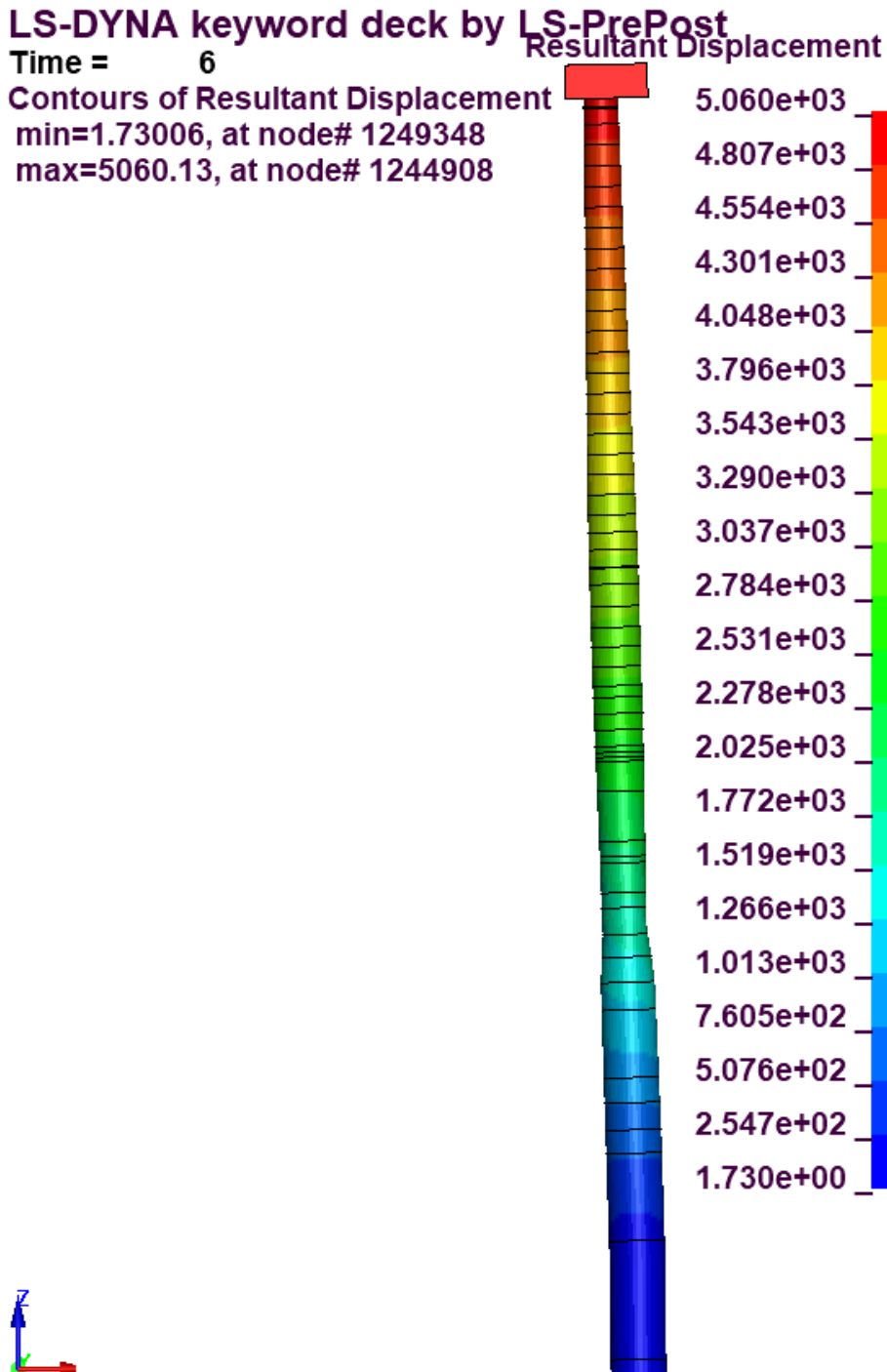
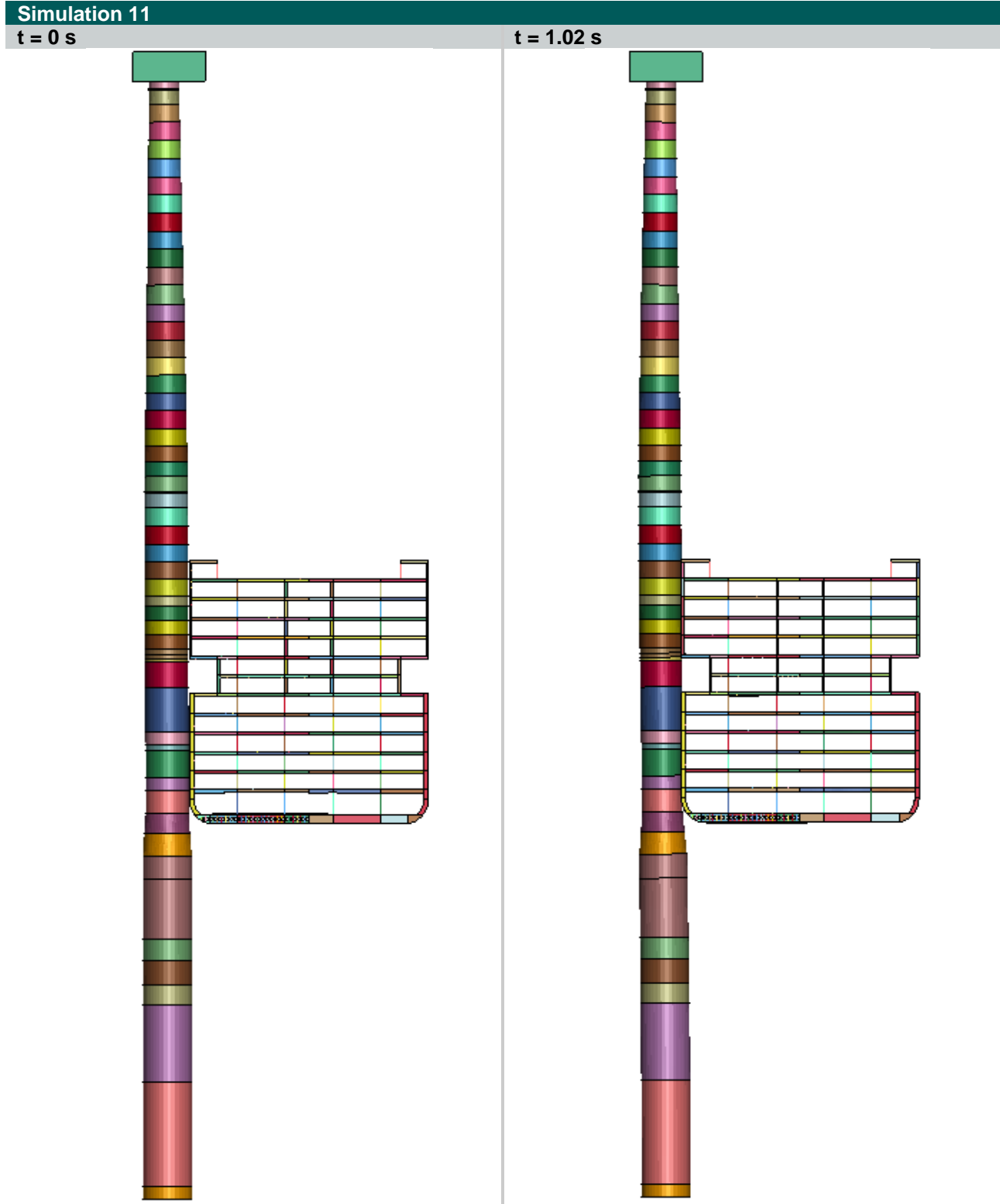


Figure 151. Resultant Displacement Foundation Tower [mm]



Table 60. Visual timeline simulation 11



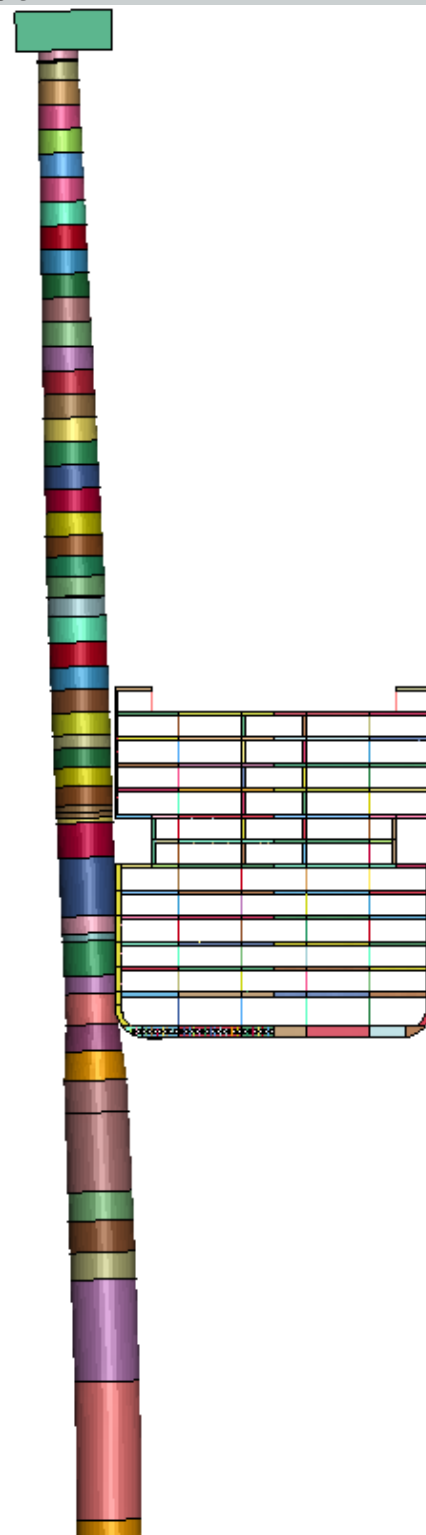
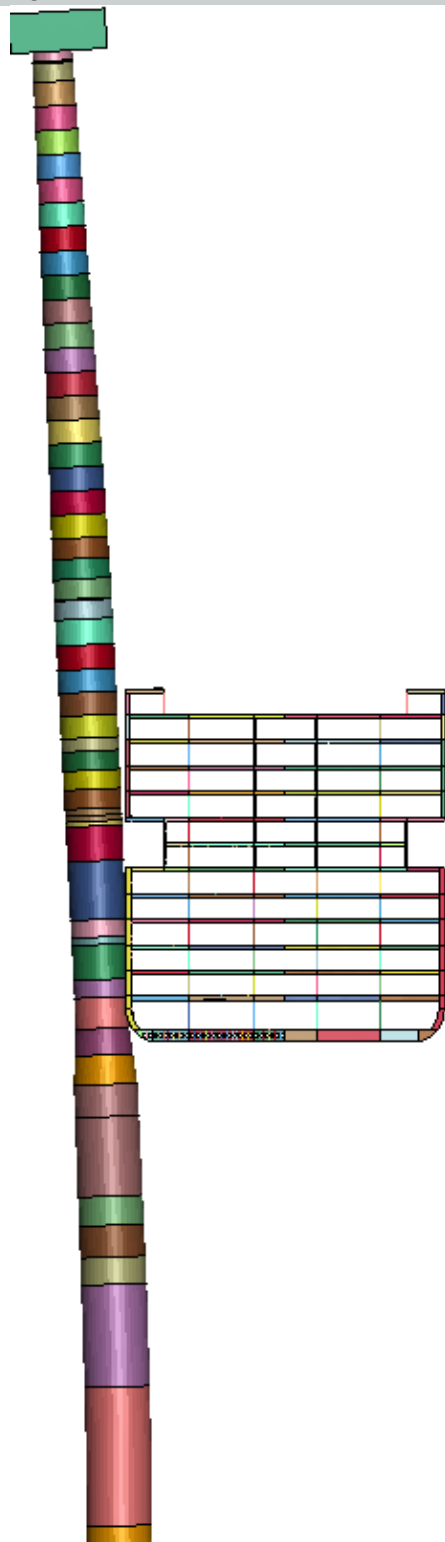




Simulation 11

t = 4.02 s

t = 4.98 s

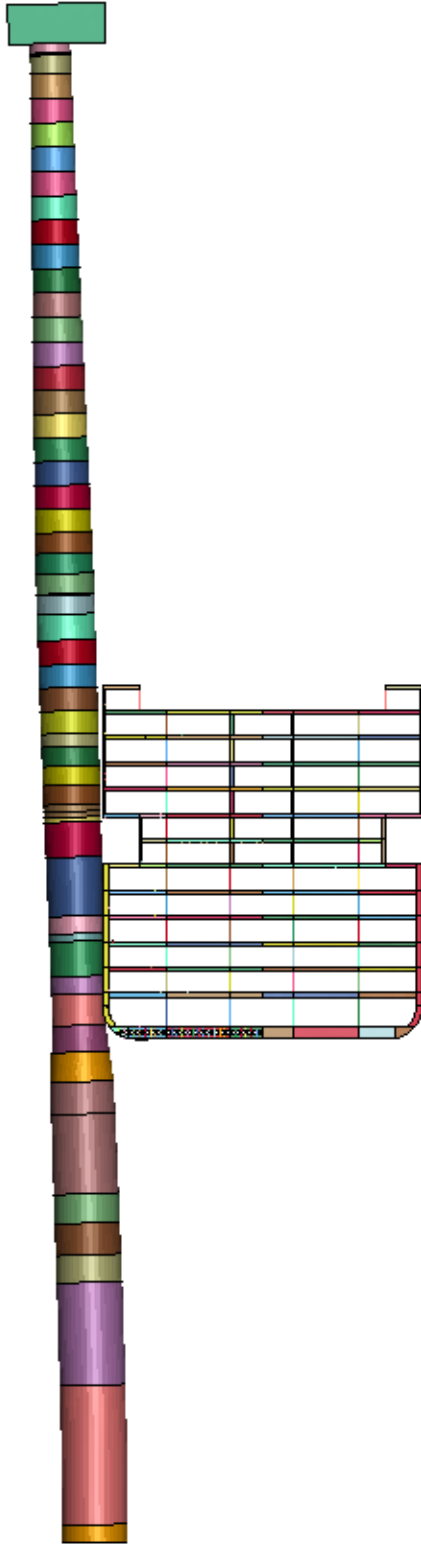






Simulation 11

t = 5.55 s



### J.1.12. Simulation 12

Figure 152 shows the global Kinetic and Internal Energy over time during the collision. Initially, the kinetic energy is 167 MJ, which is determined by the ship's speed and mass. As the collision progresses, the total energy increases due to the collapse of the turbine tower foundation, resulting in a rise in total energy.

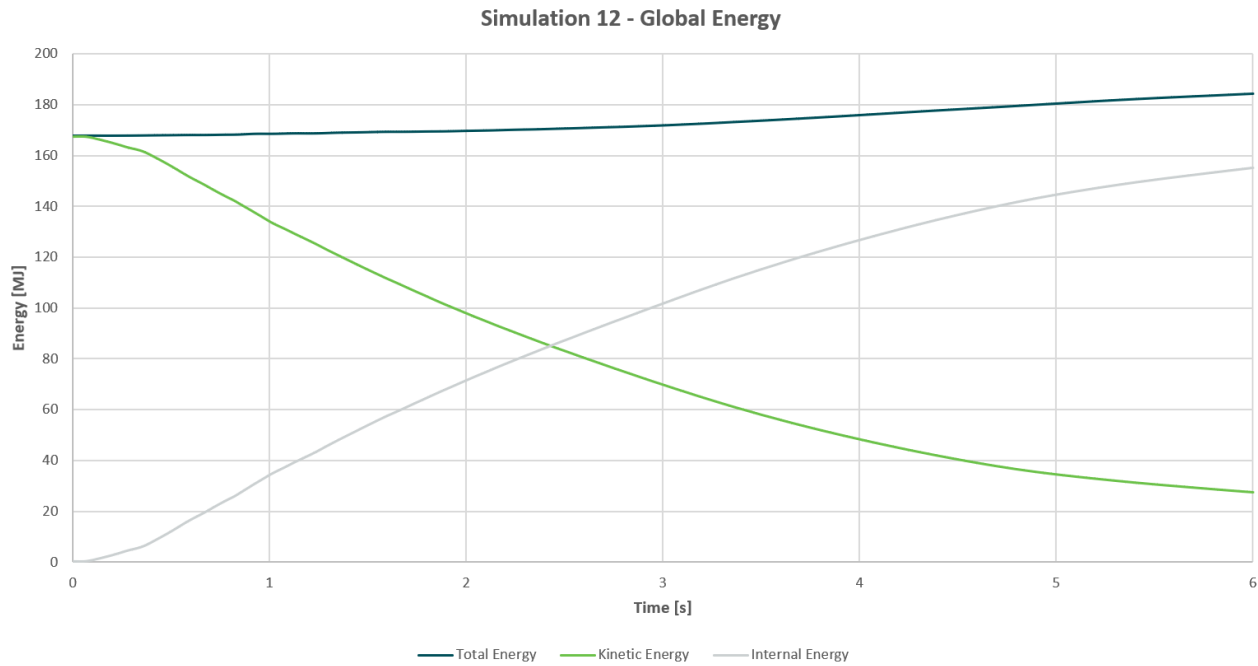


Figure 152. Global energy Distribution over time

The impact force between the vessel and the foundation over the time is shown in Figure 153.

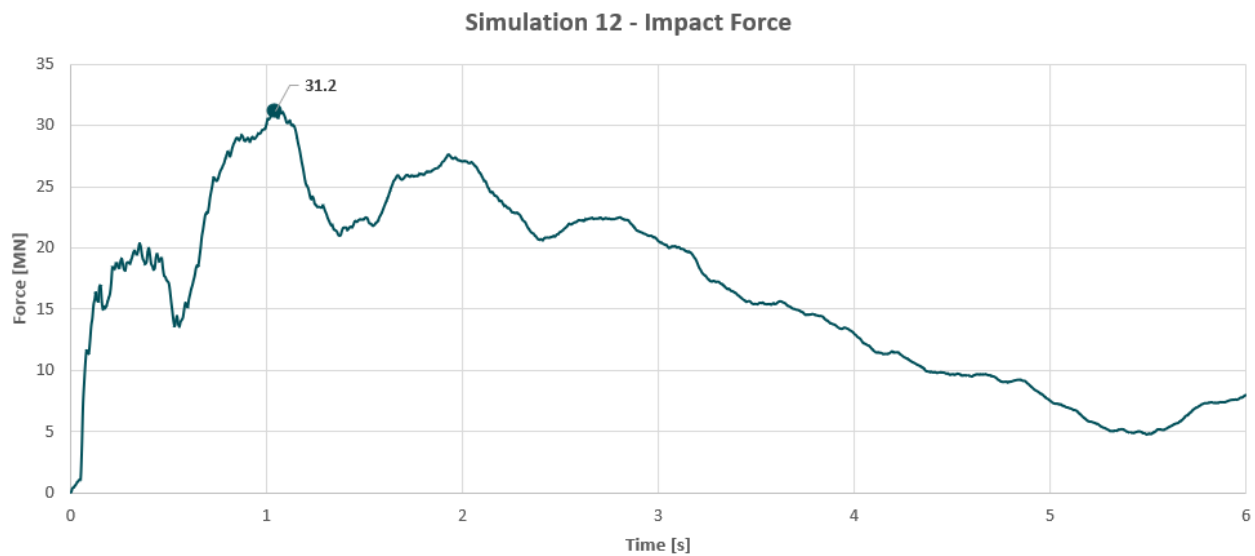


Figure 153. Impact Force over time

Figure 154 shows the deformation of the ship after the collision.

LS-DYNA keyword deck by LS-PrePost

Time = 6

Contours of Relative Resultant Displacement

min=0, at node# 1130465

max=349.254, at node# 1116879

Relative Resultant Displacement

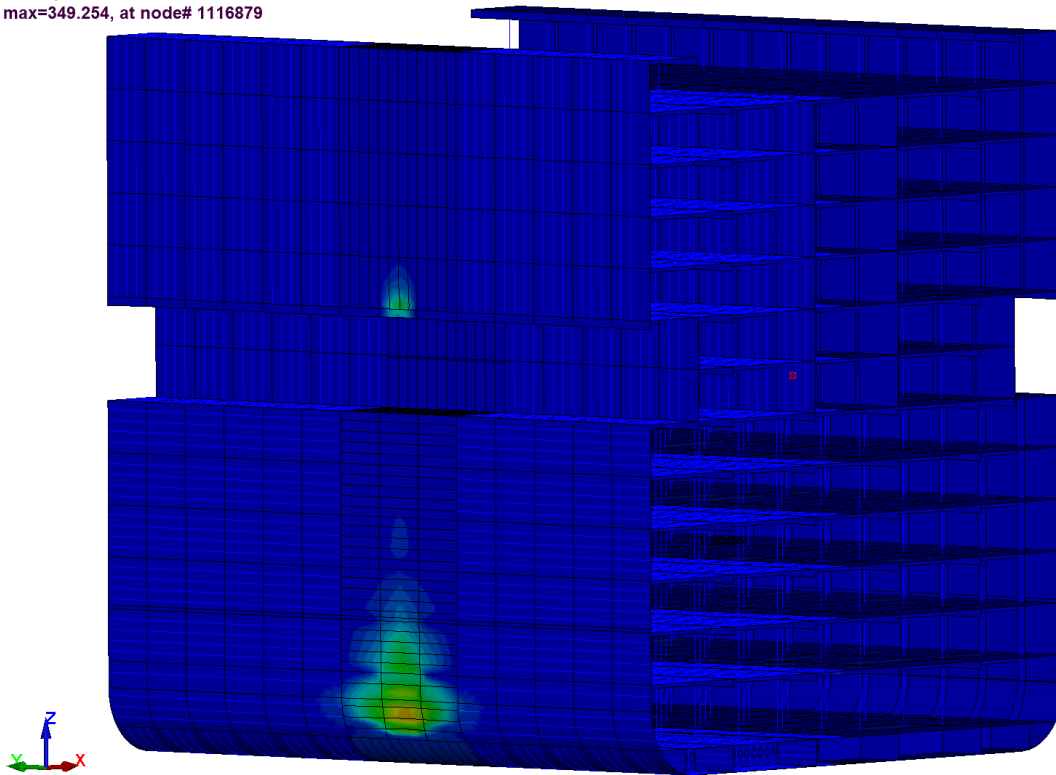
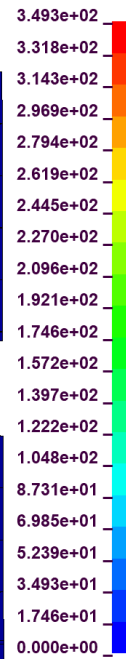


Figure 154. Resultant Displacement SB side [mm]

Figure 155 shows the deformation of the foundation, which indicates a clear buckling failure of the foundation.

**LS-DYNA keyword deck by LS-PrePost**

Time = 6

Contours of Resultant Displacement  
min=7.62903, at node# 1249272  
max=23527.7, at node# 1244908

**Resultant Displacement**

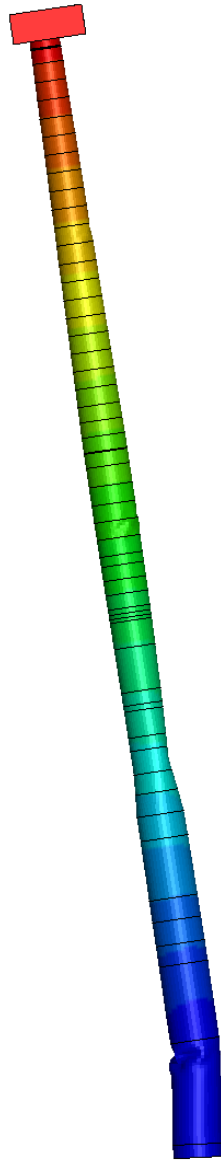
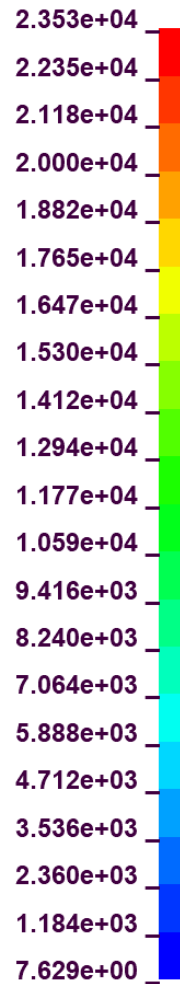
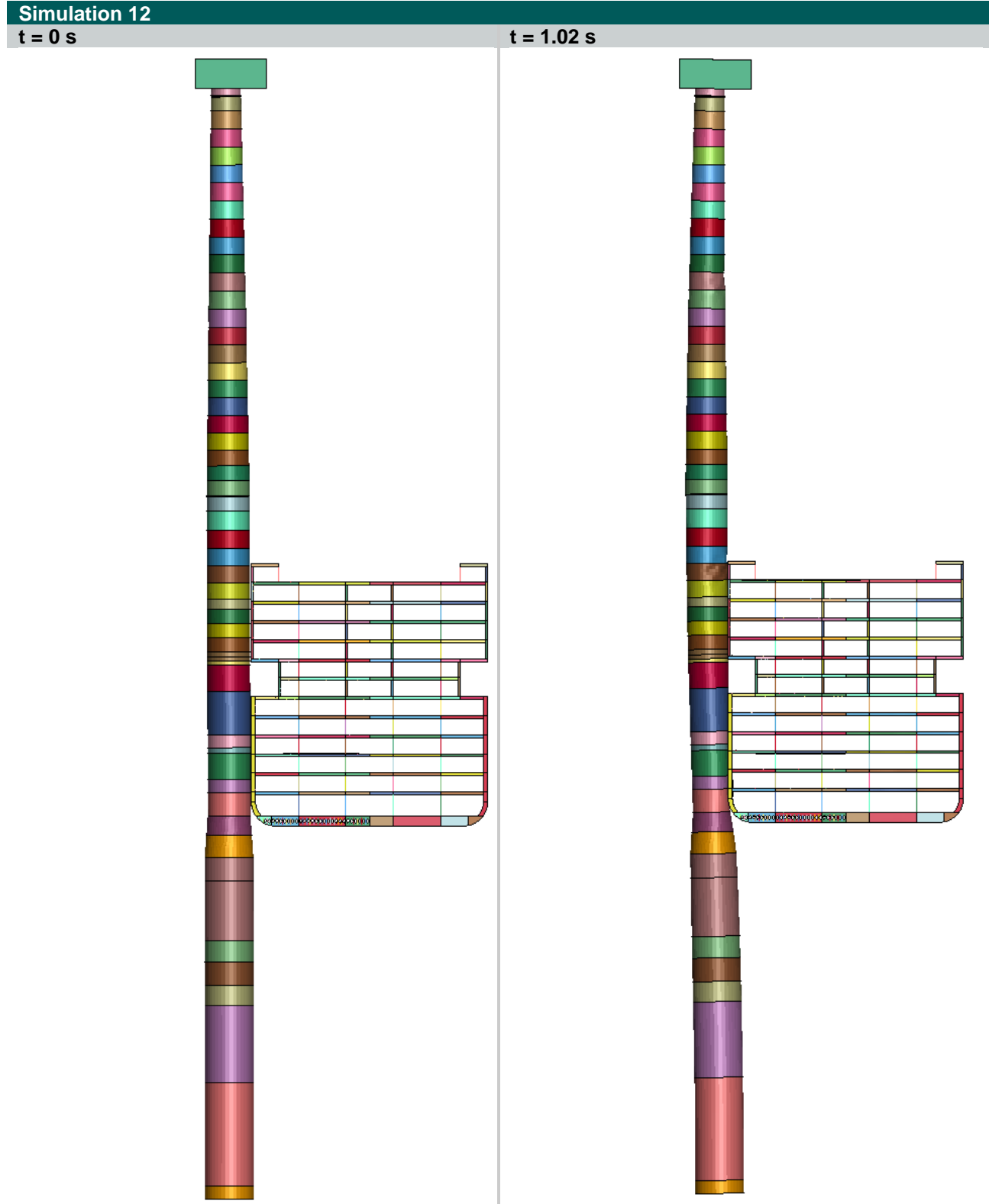


Figure 155. Resultant Displacement Foundation Tower [mm]

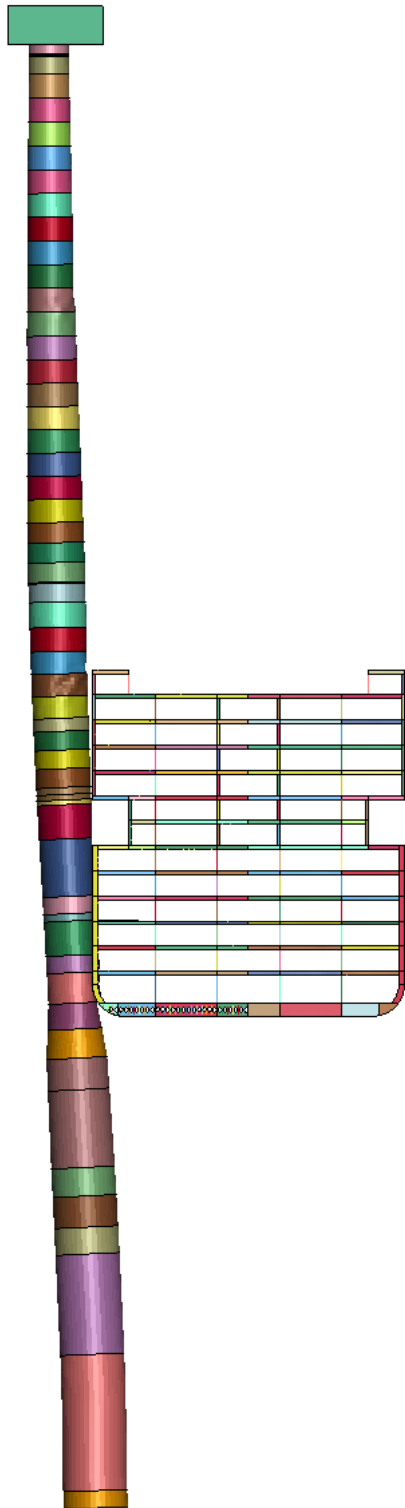


Table 61. Visual timeline simulation 12

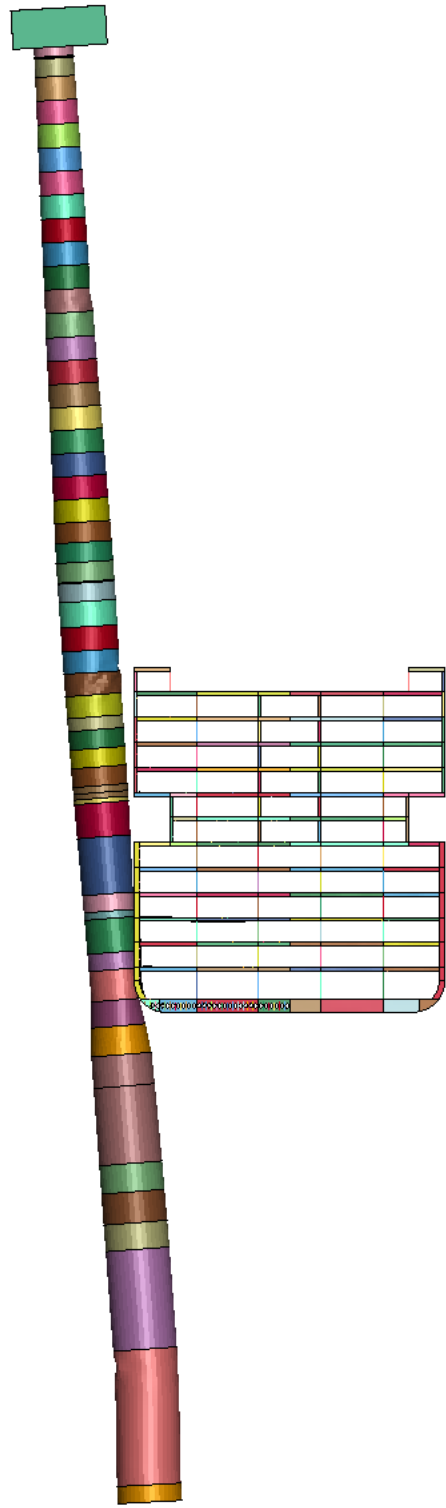




Simulation 12  
t = 1.98 s



t = 3 s

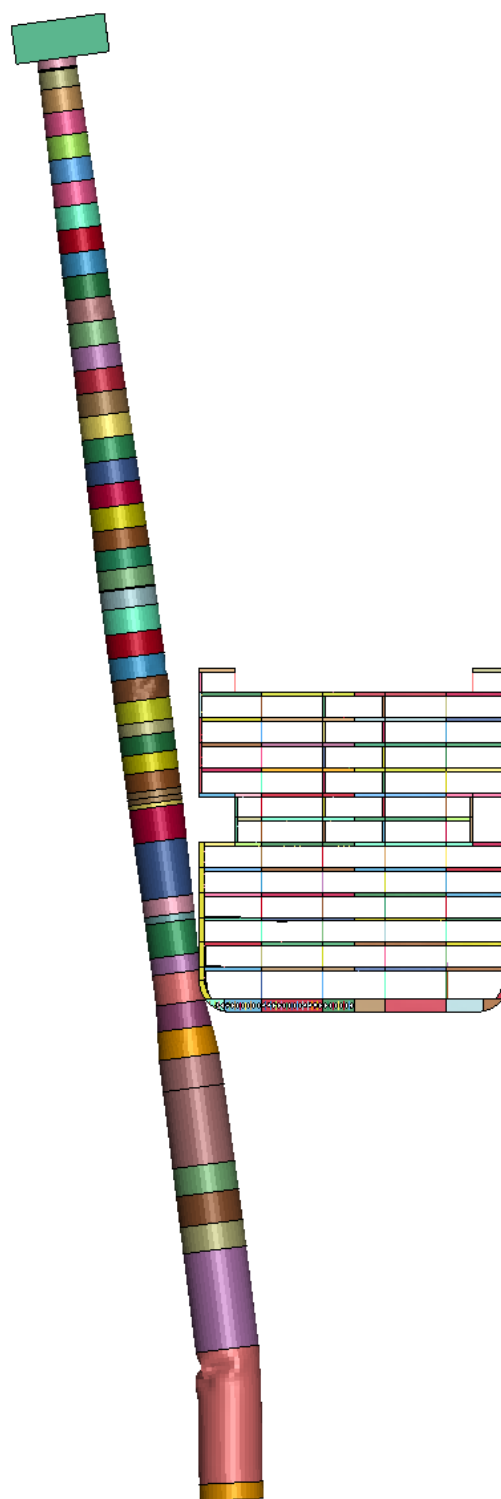
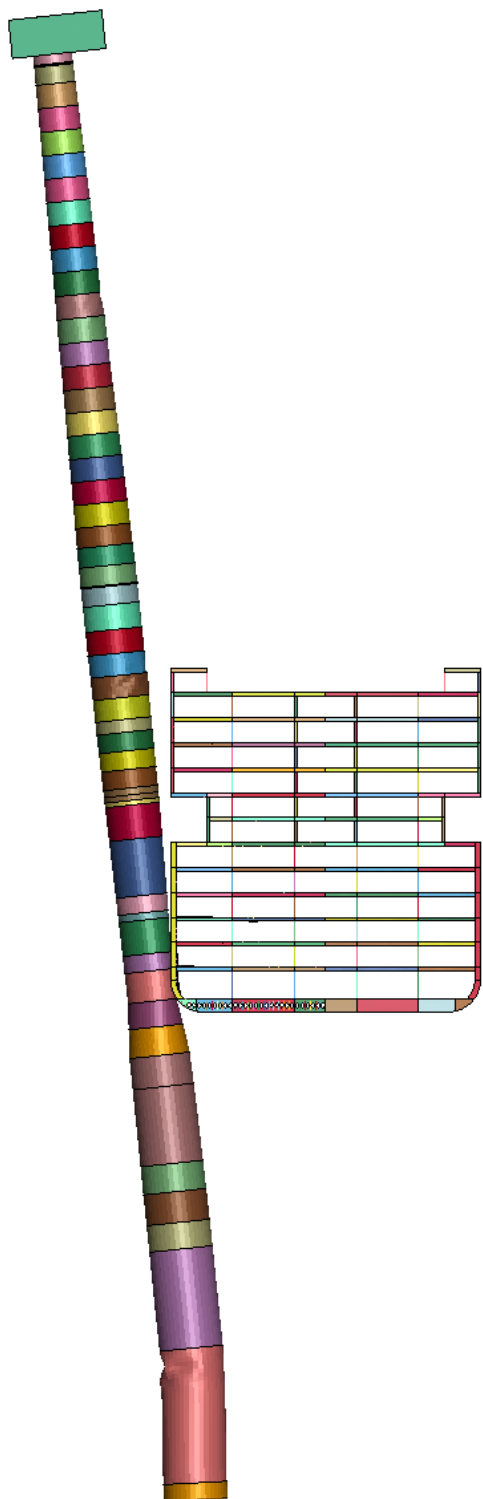




Simulation 12

t = 4.02 s

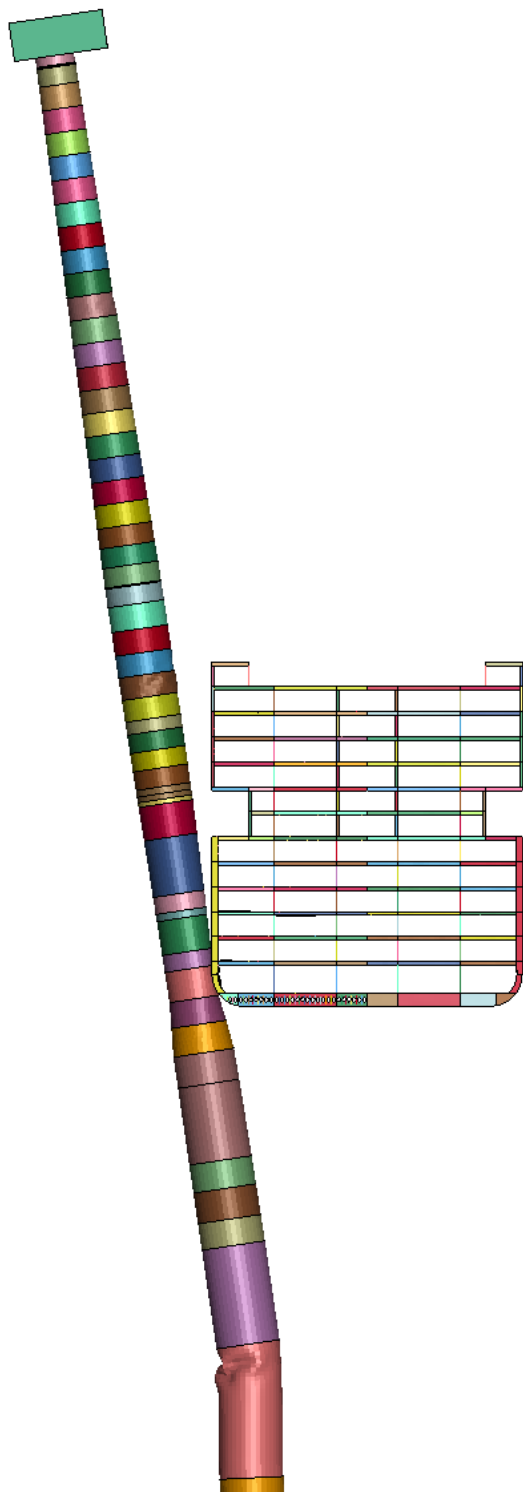
t = 4.98 s





Simulation 12

t = 6.0 s





## J.2. Results Turbine dropping

### J.2.1. Vertical impact

The visual timelapse of the turbine falling vertically onto the passenger vessel is presented in *Table 62*. As shown, the turbine falls through the upper seven decks before becoming lodged and plastically deforming the eighth deck. *Figure 156* depicts the impact force.

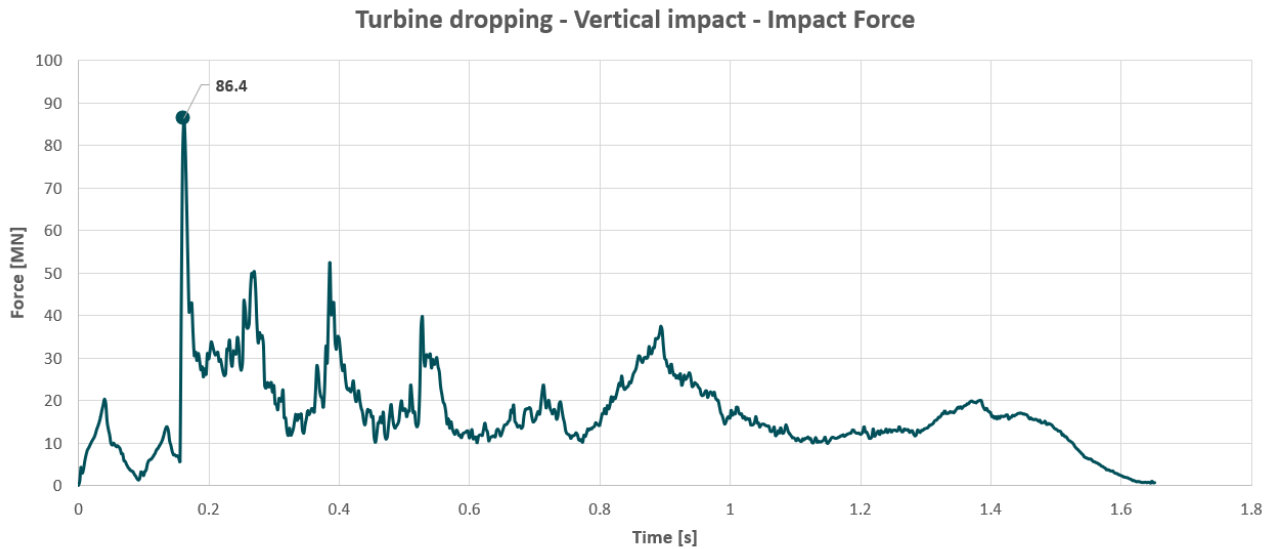


Figure 156. Impact Force over time

*Figure 157* shows the velocity of the nacelle over time. As seen, the velocity becomes negative at 1.5 seconds because the nacelle does not pass through the 8th deck but instead rebounds slightly upward.

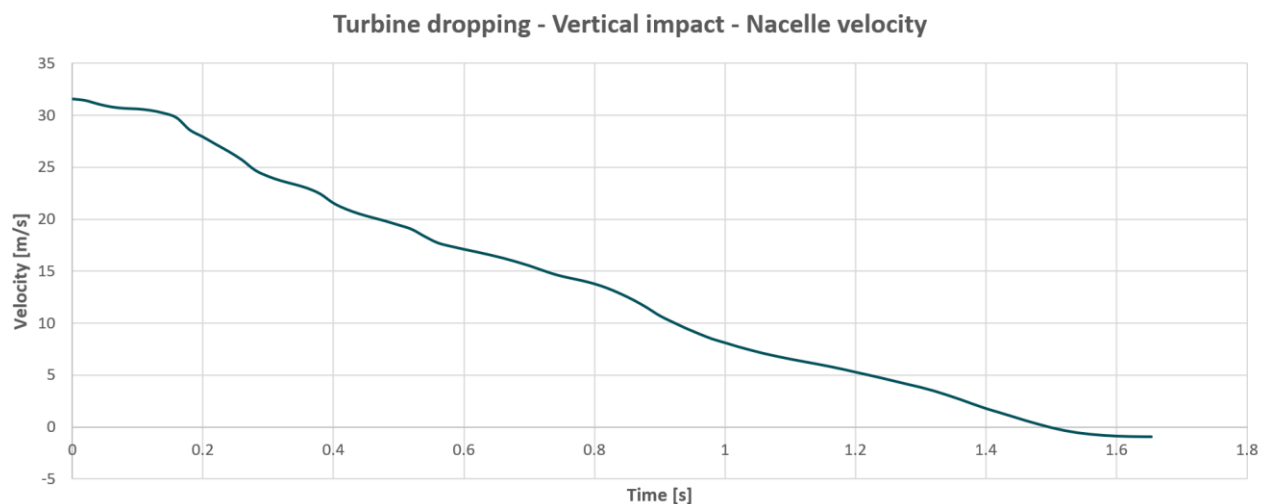


Figure 157. Fall velocity nacelle over time

Figure 158 and Figure 159 illustrate the damage caused by the impact of the turbine.

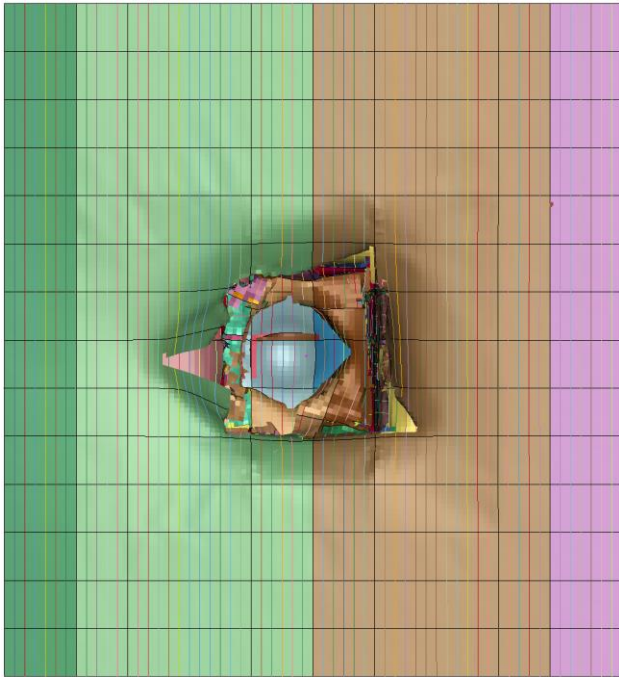


Figure 158. Top view damage at end of simulation

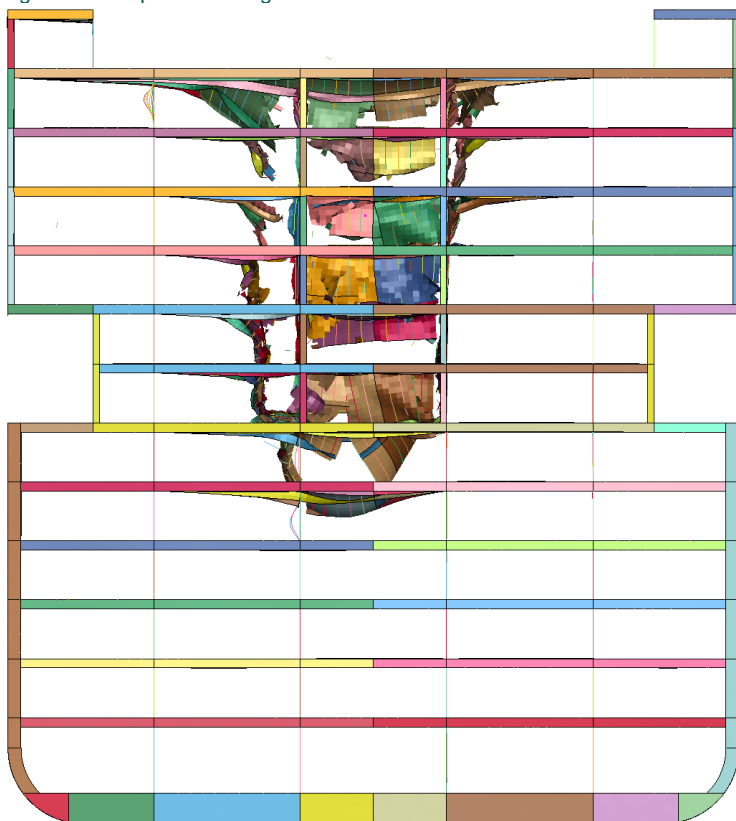
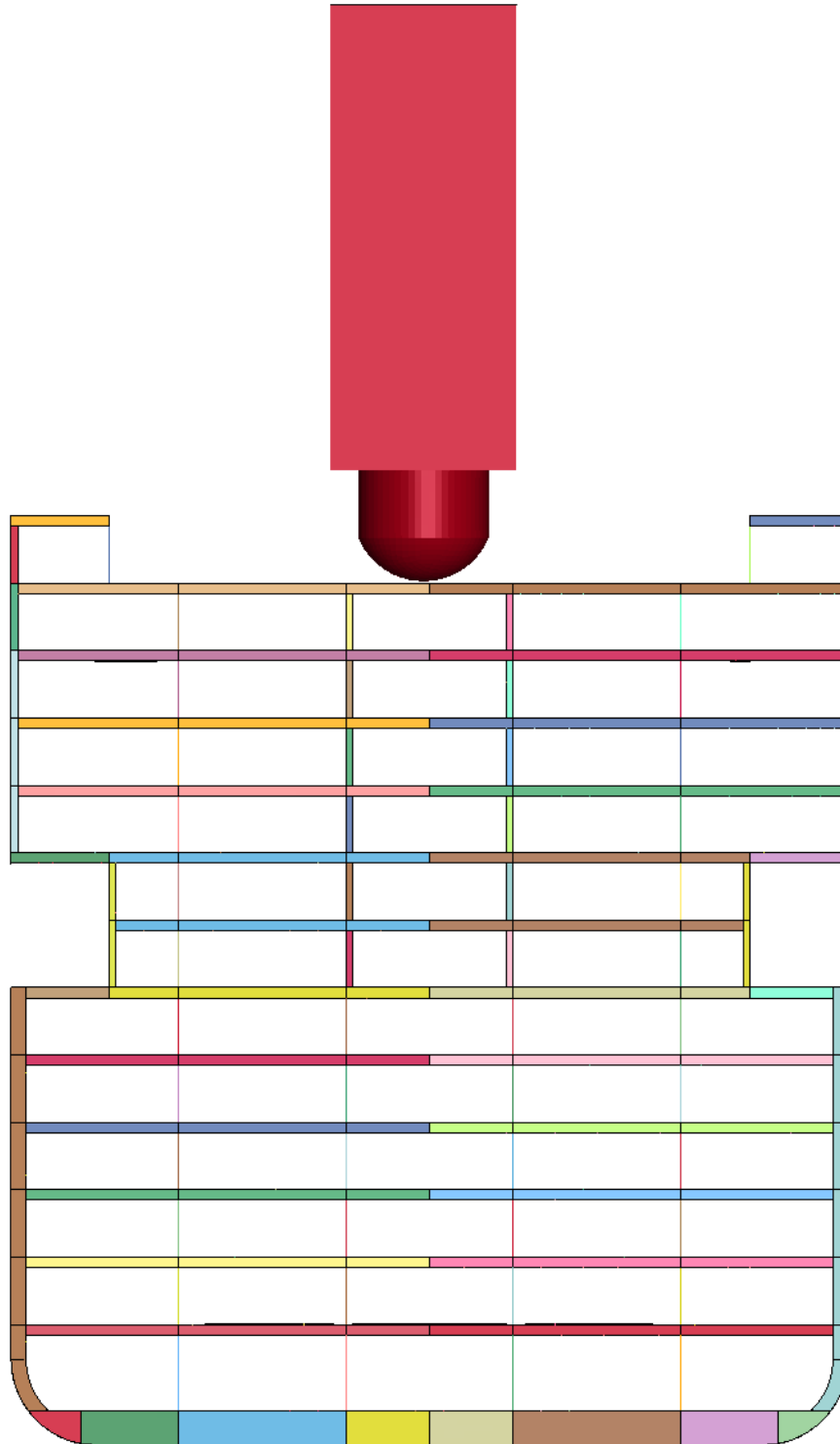


Figure 159. Side view of damage at end of simulation

Table 62. Visual timeline simulation vertical turbine impact

**Simulation vertical turbine impact**

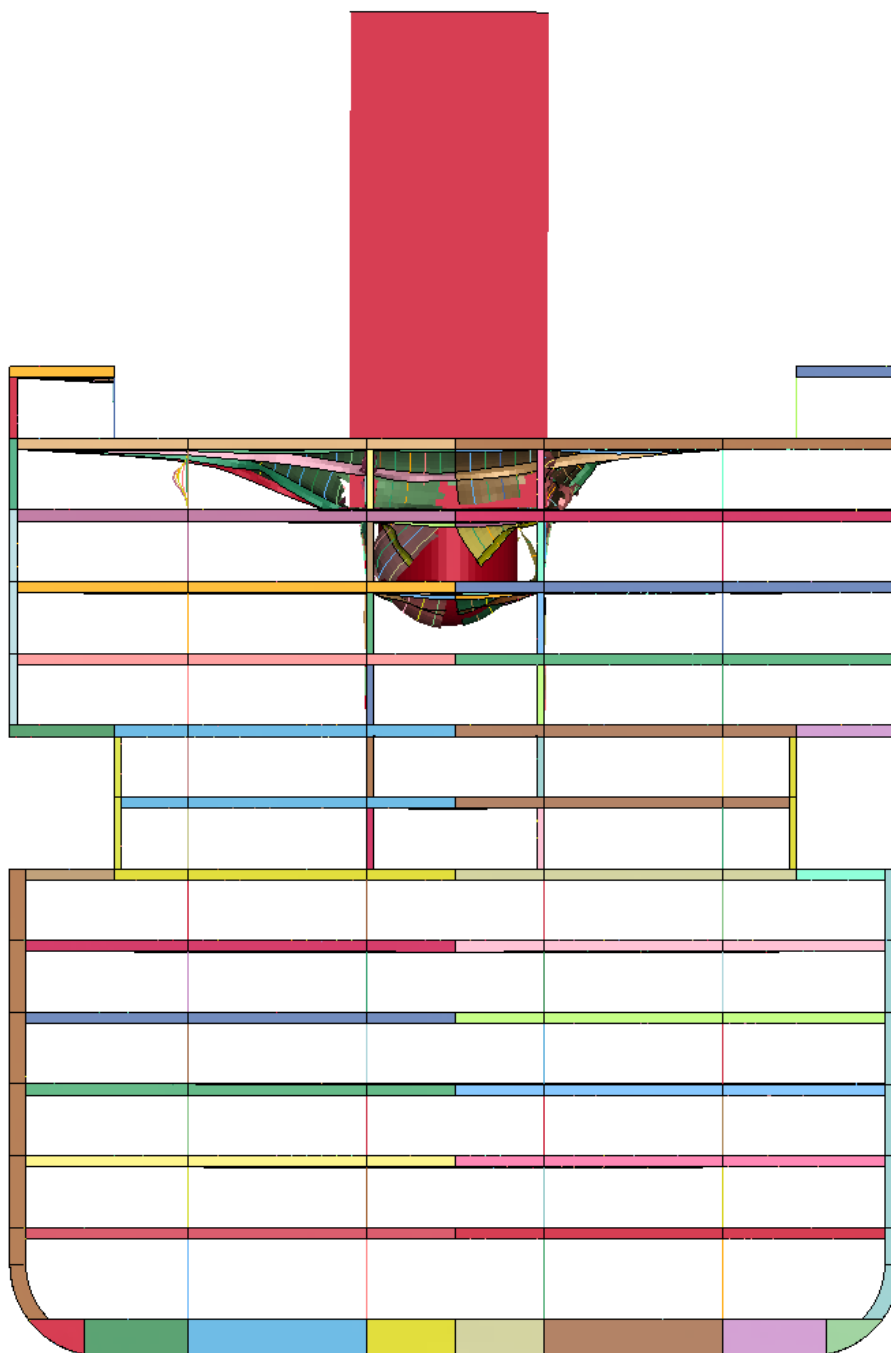
t = 0 s





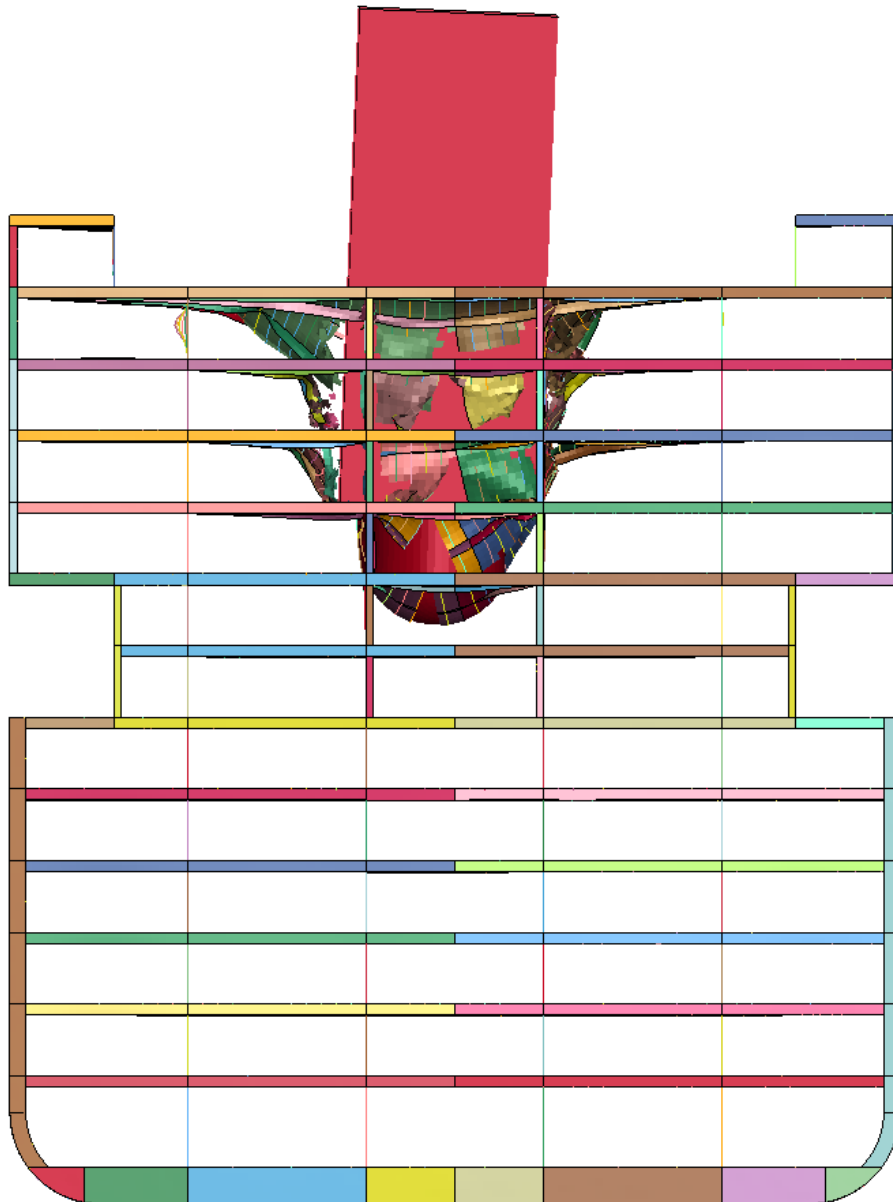
Simulation vertical turbine impact

t = 0.26 s





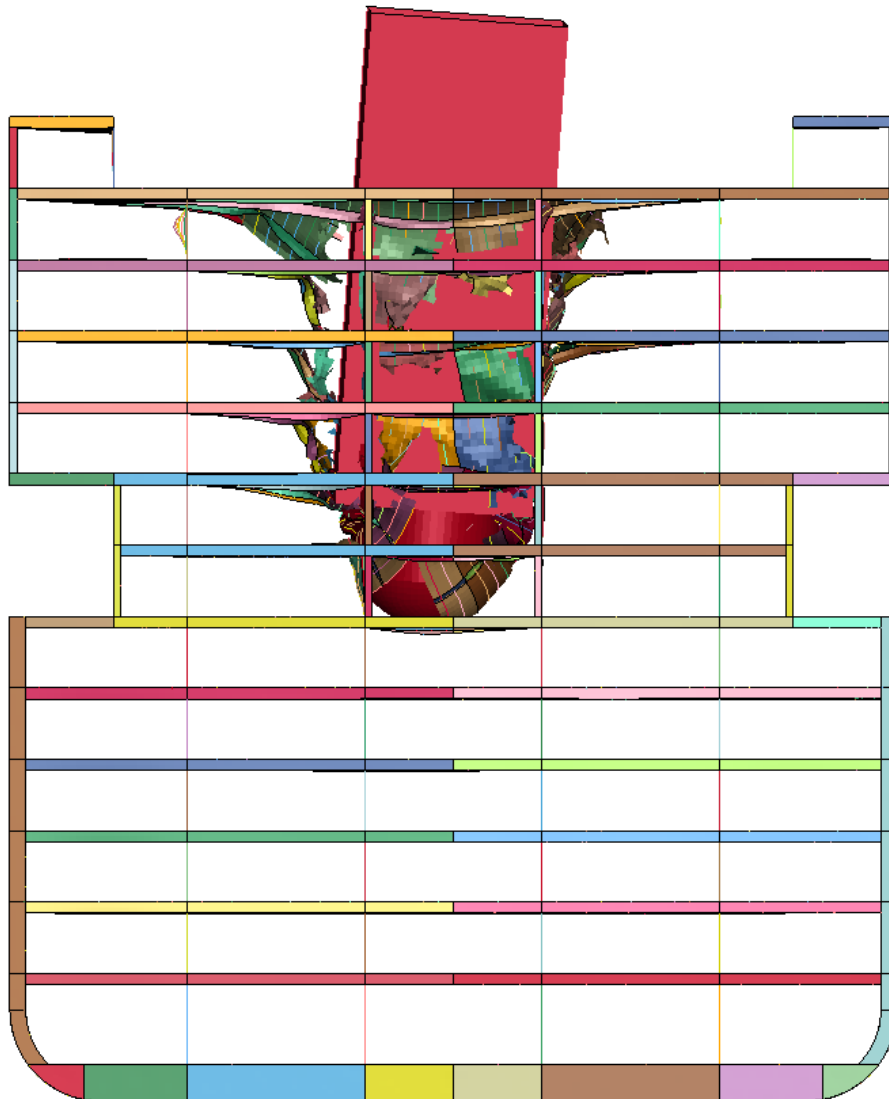
Simulation vertical turbine impact  
 $t = 0.54 \text{ s}$





Simulation vertical turbine impact

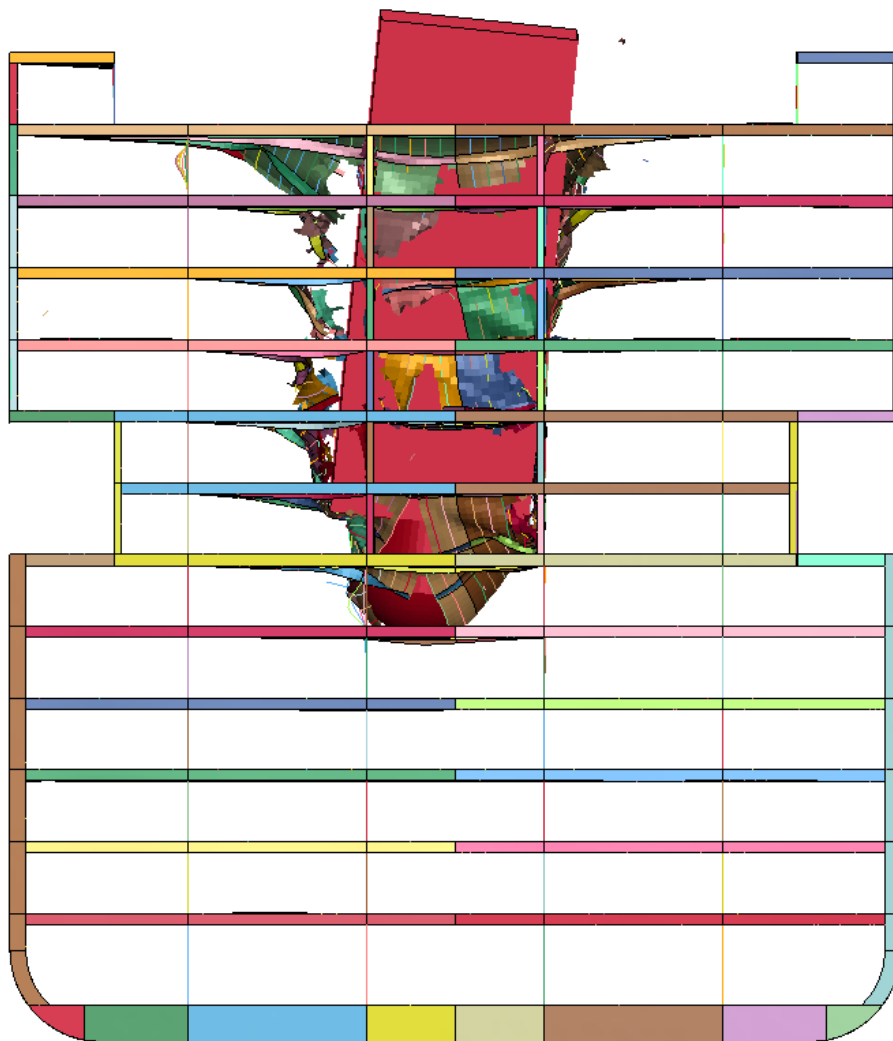
t = 0.8 s





Simulation vertical turbine impact

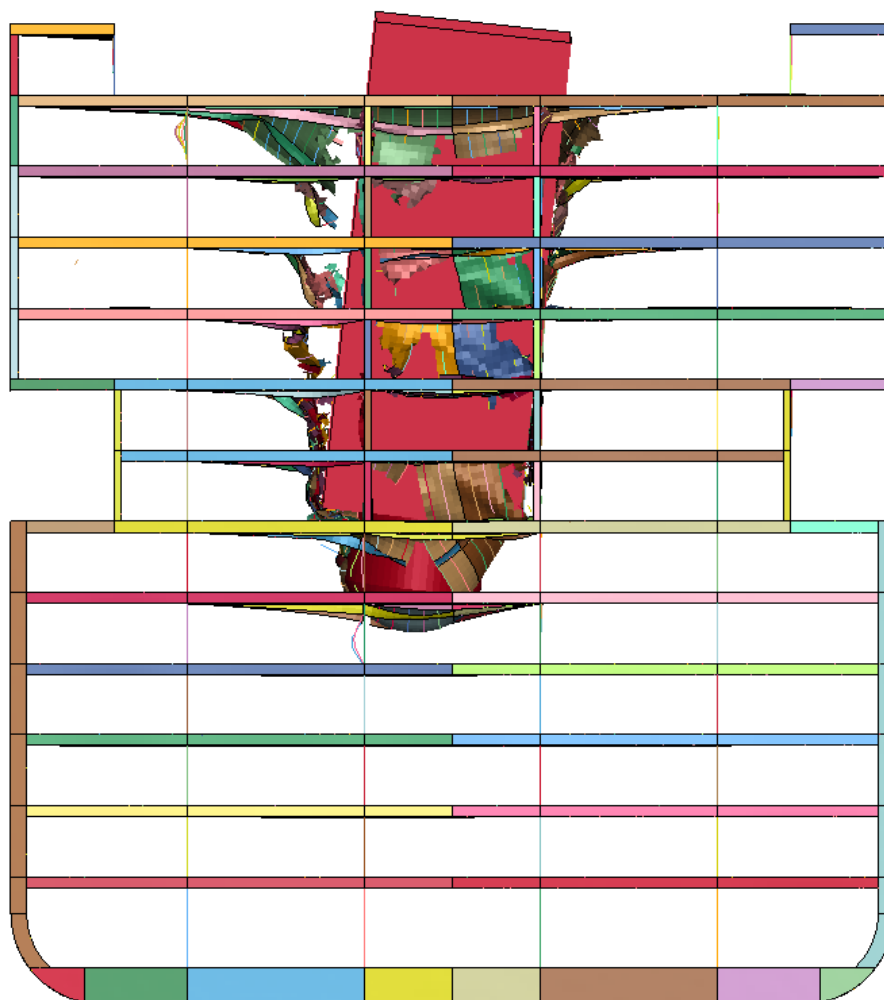
t = 1.1 s





Simulation vertical turbine impact

t = 1.36 s

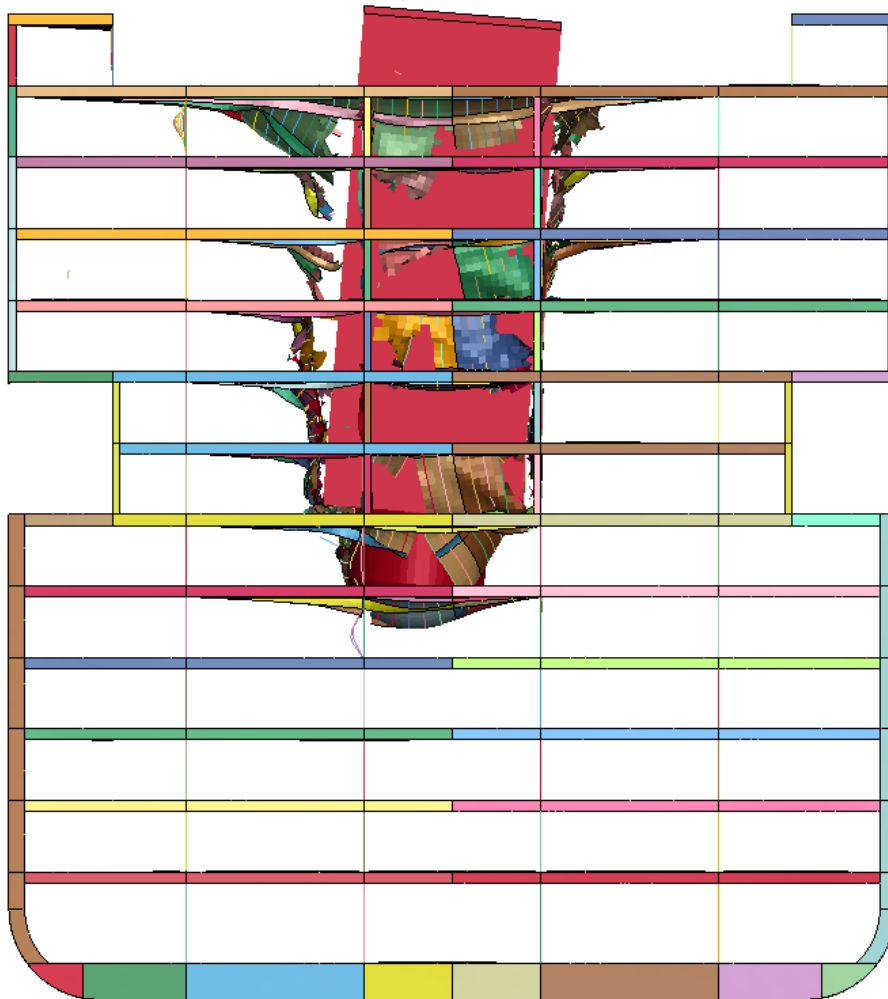






Simulation vertical turbine impact

t = 1.65 s



### J.2.2. Horizontal impact

The impact force over time of the horizontal turbine dropping is shown in *Figure 160*.

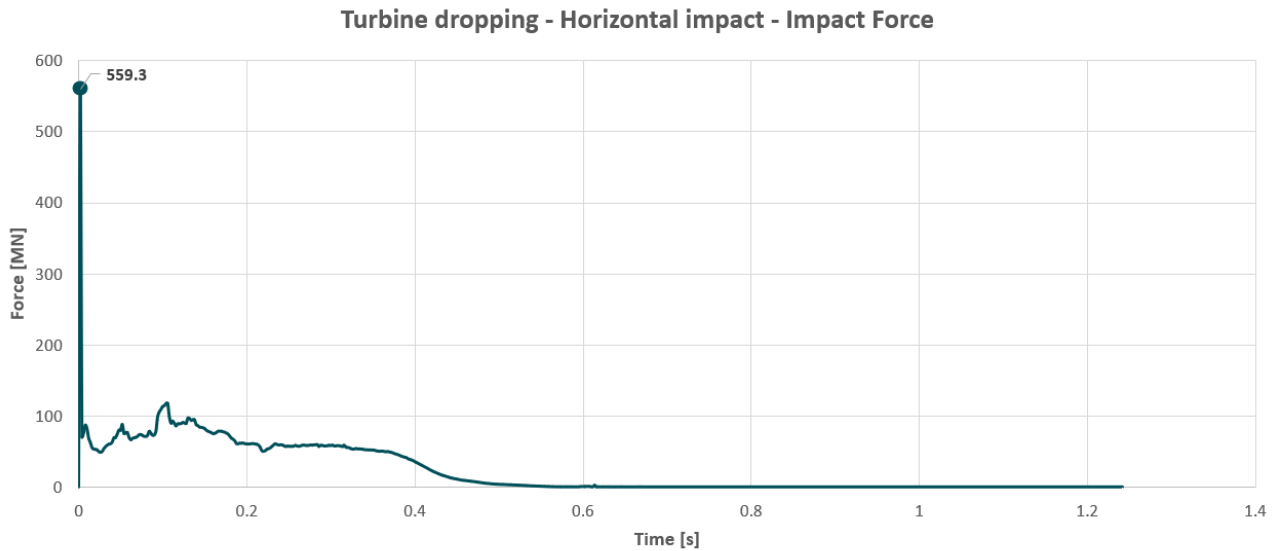


Figure 160. Impact Force over time

As shown in *Figure 161*, the fall velocity decreases when the turbine impacts the upper deck. Due to this impact, the turbine rebounds slightly, causing the velocity to become negative. This marks the end of the simulation.

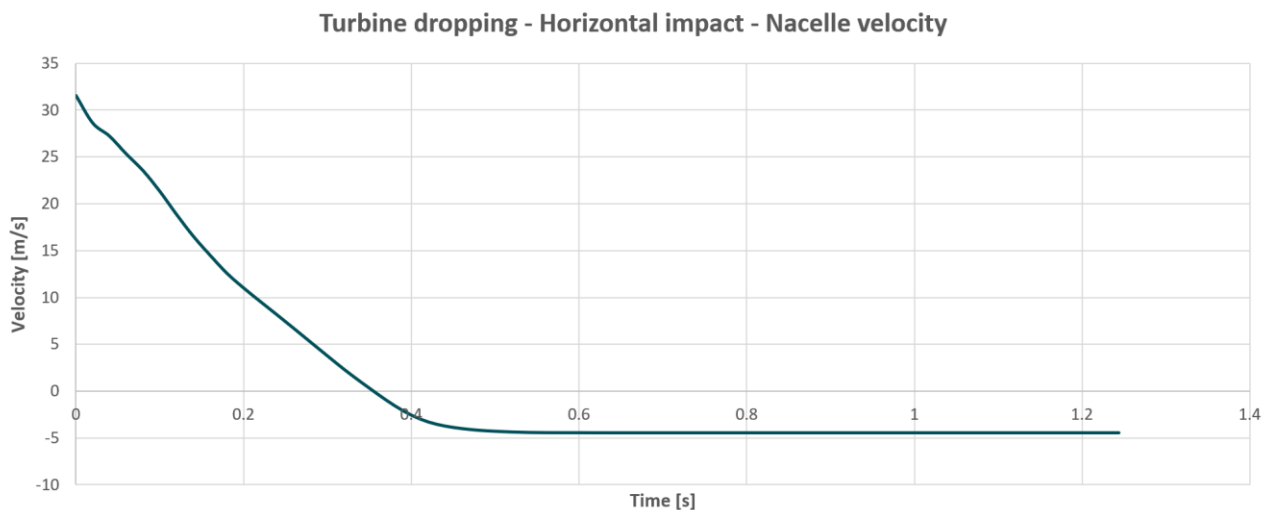
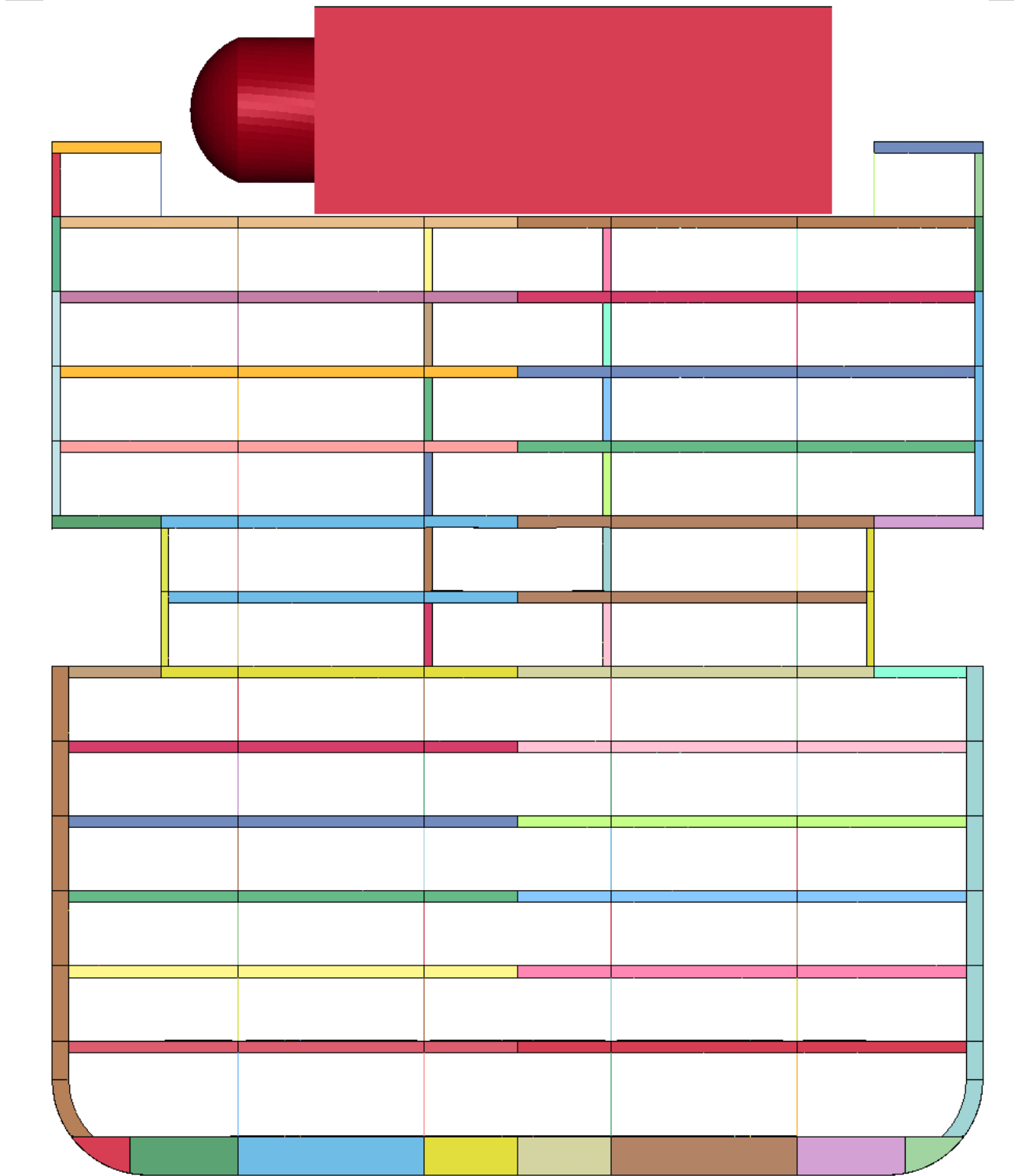


Figure 161. Fall velocity nacelle over time

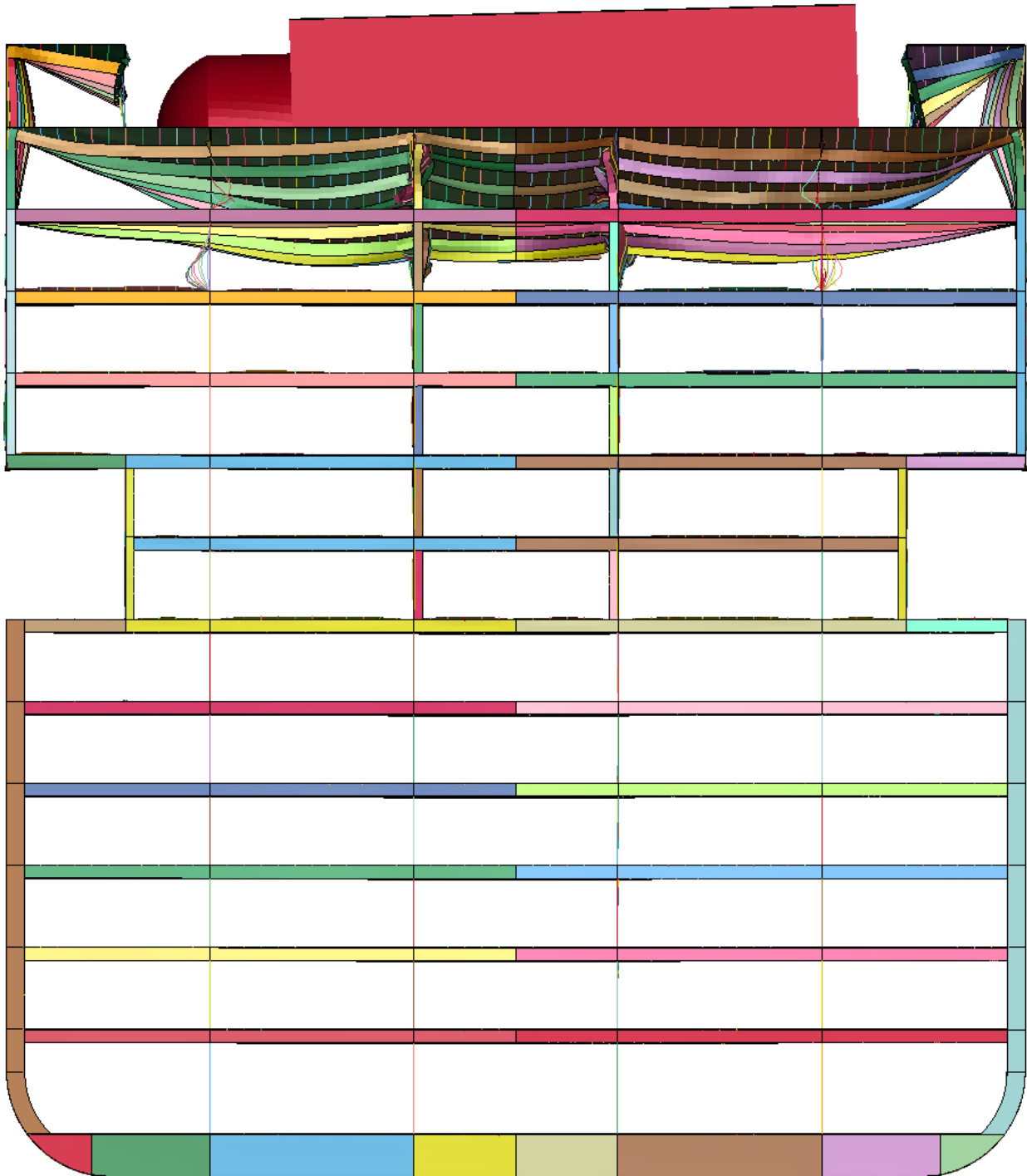
Table 63. Visual timeline simulation vertical turbine impact

**Simulation horizontal turbine impact**



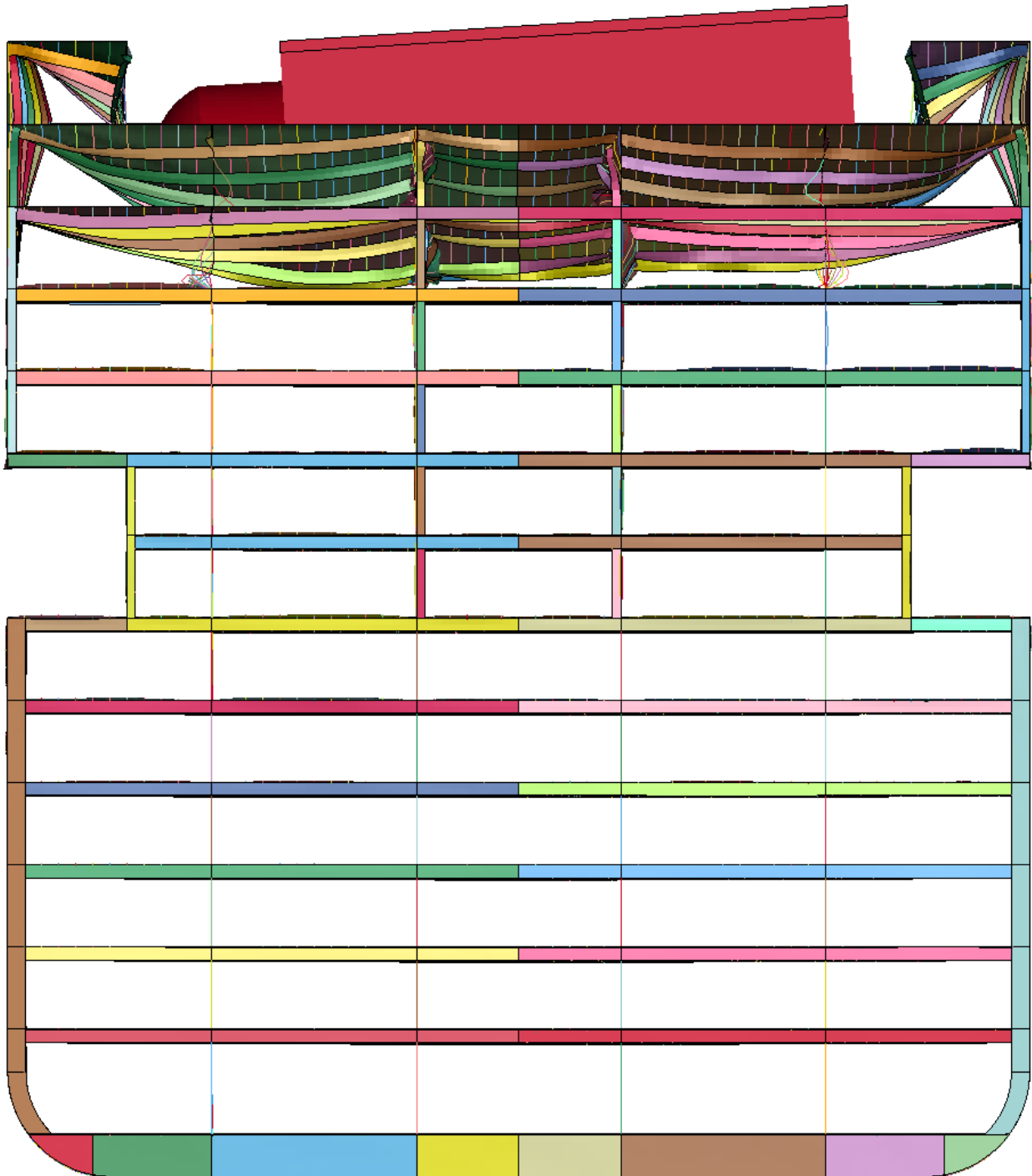


Simulation horizontal turbine impact  
 $t = 0.2$  s





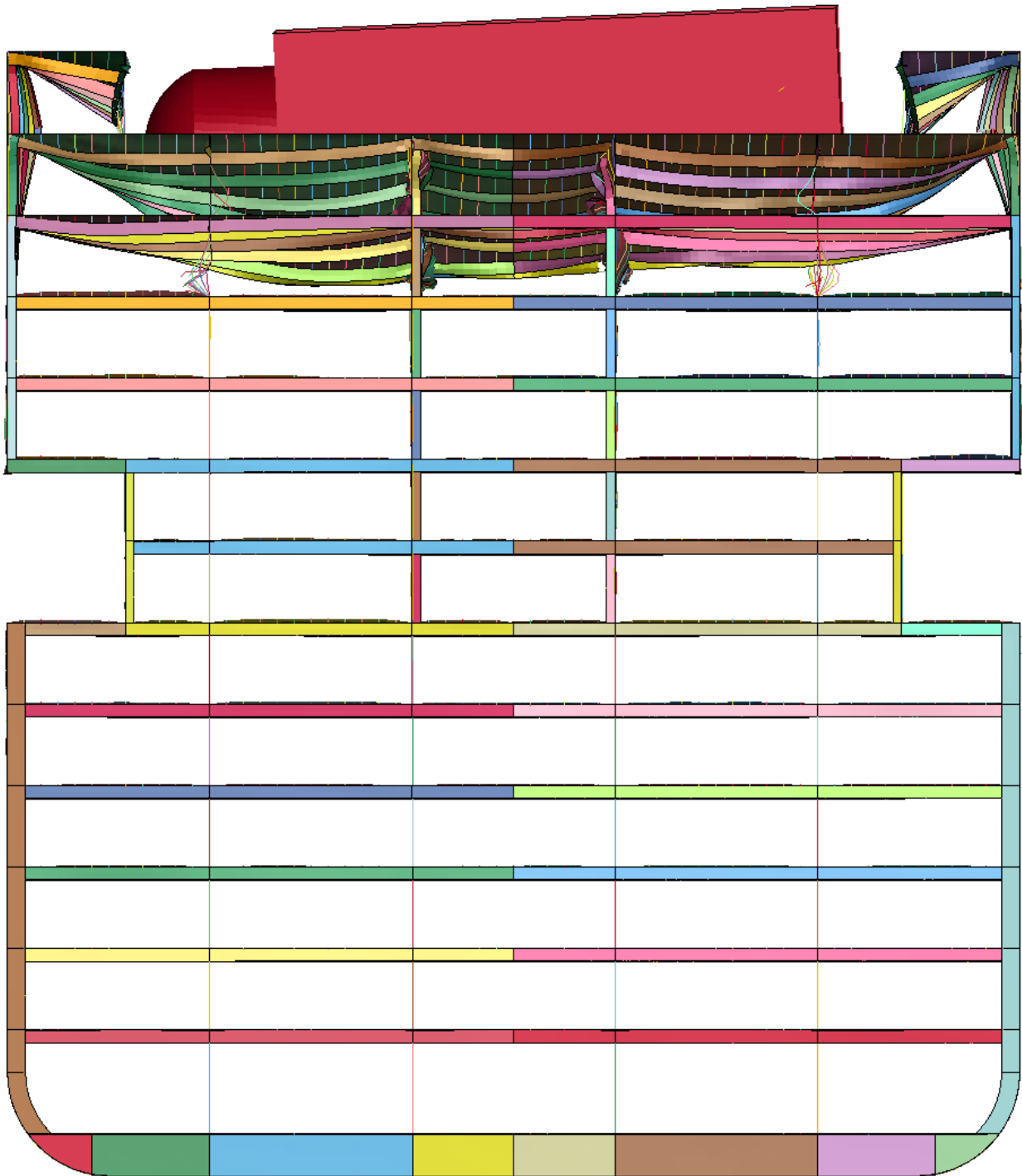
Simulation horizontal turbine impact  
 $t = 0.4 \text{ s}$





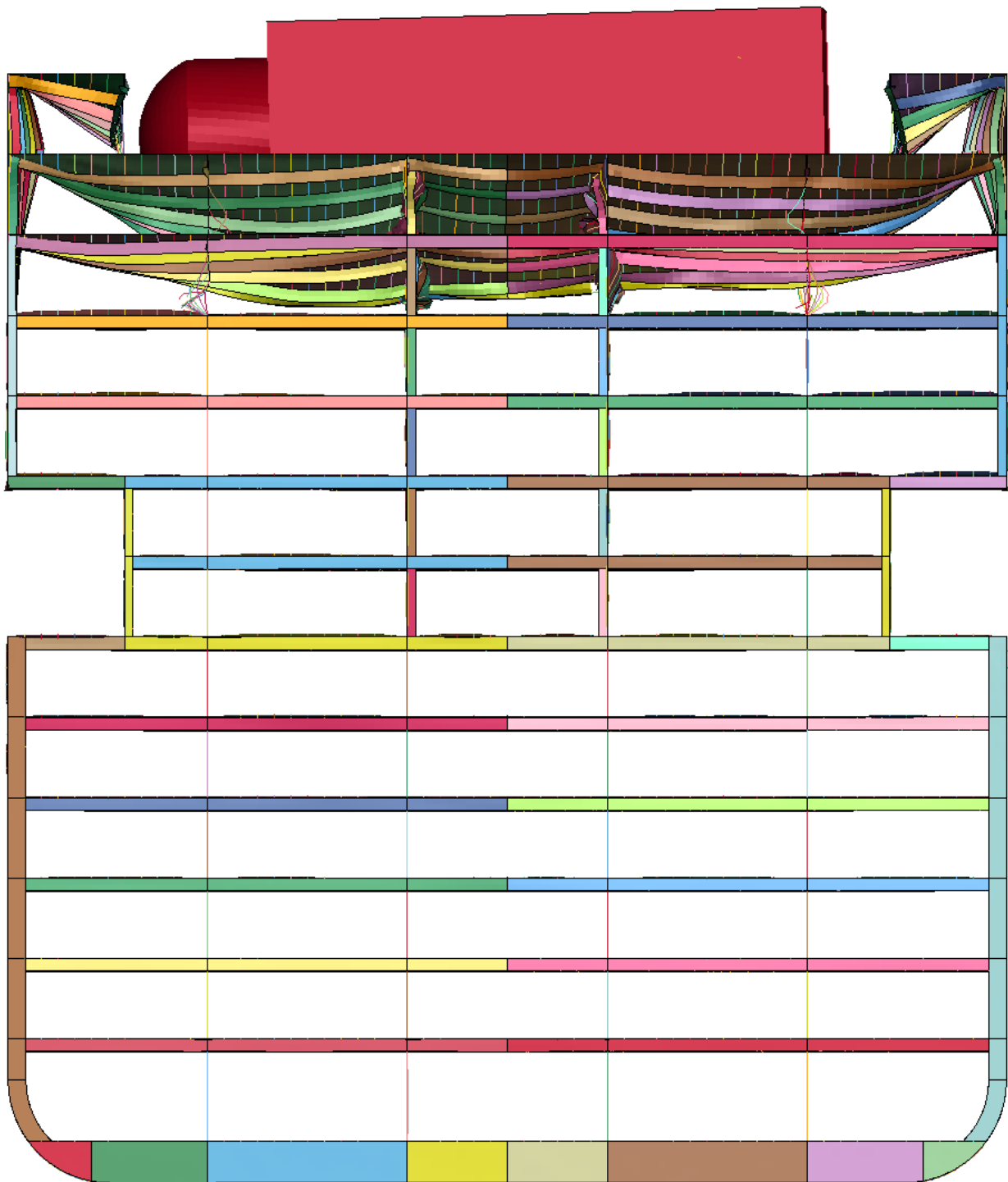
Simulation horizontal turbine impact

t = 0.6 s





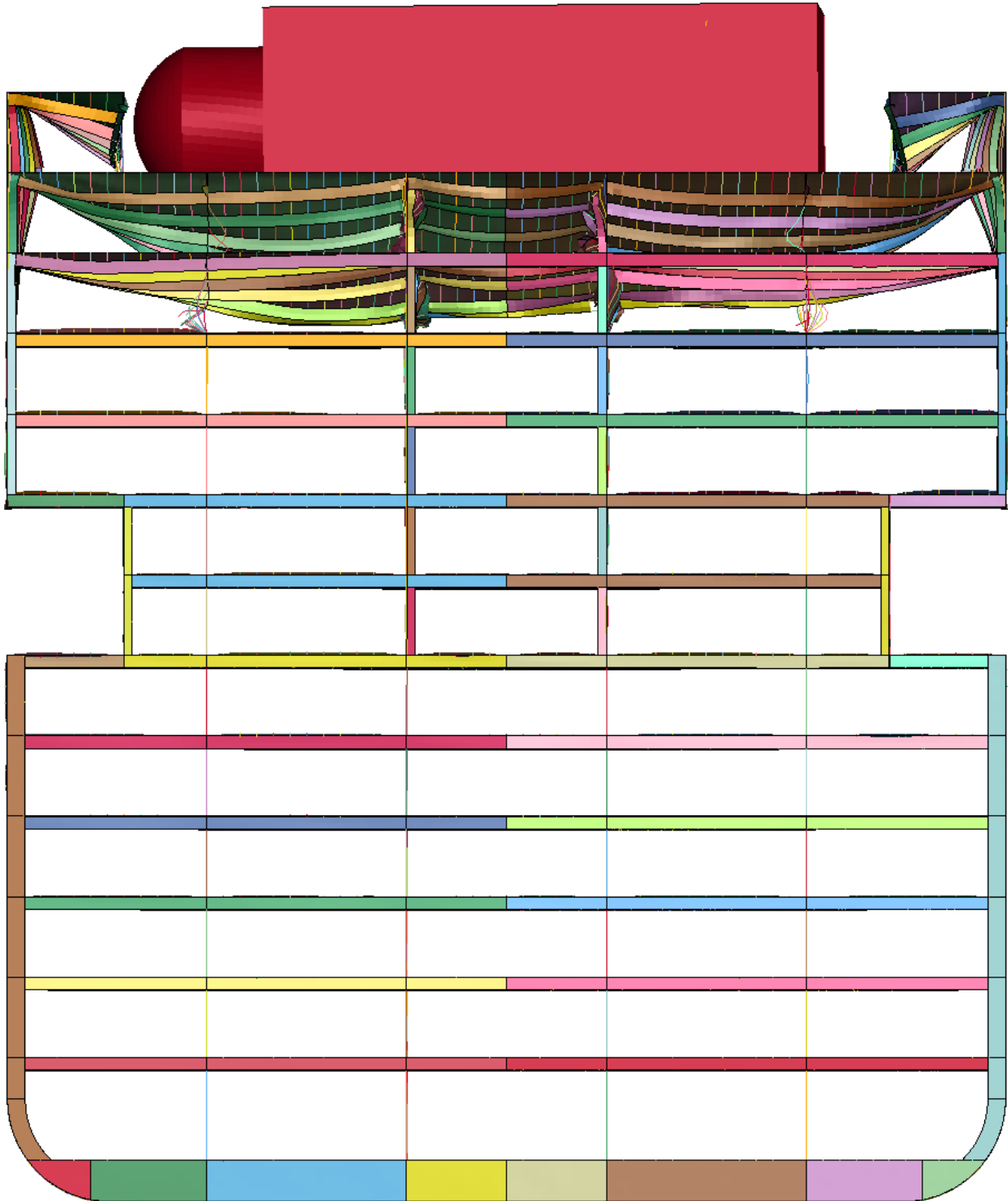
Simulation horizontal turbine impact  
 $t = 0.8$  s





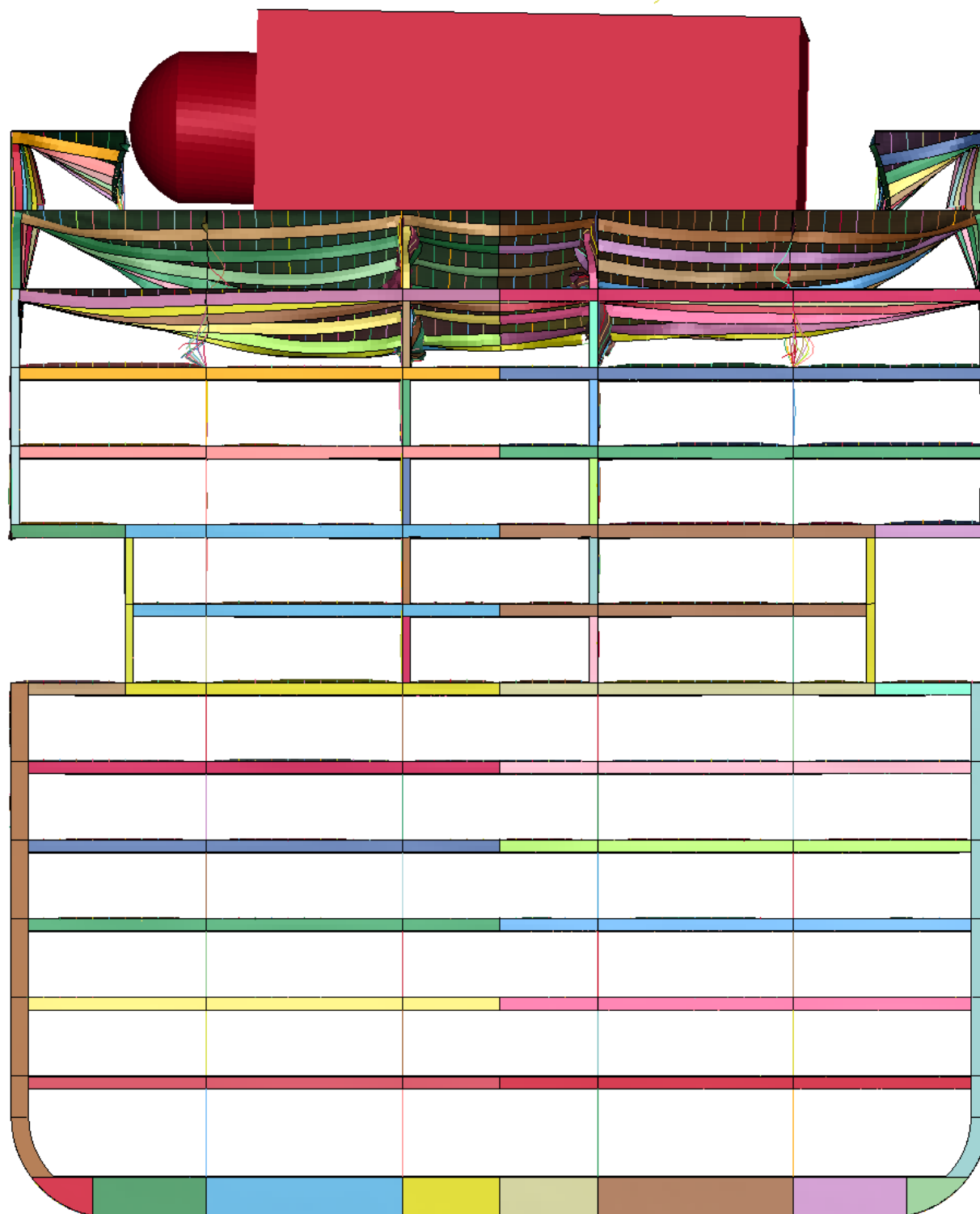
Simulation horizontal turbine impact

t = 1.0 s





Simulation horizontal turbine impact  
 $t = 1.25$  s





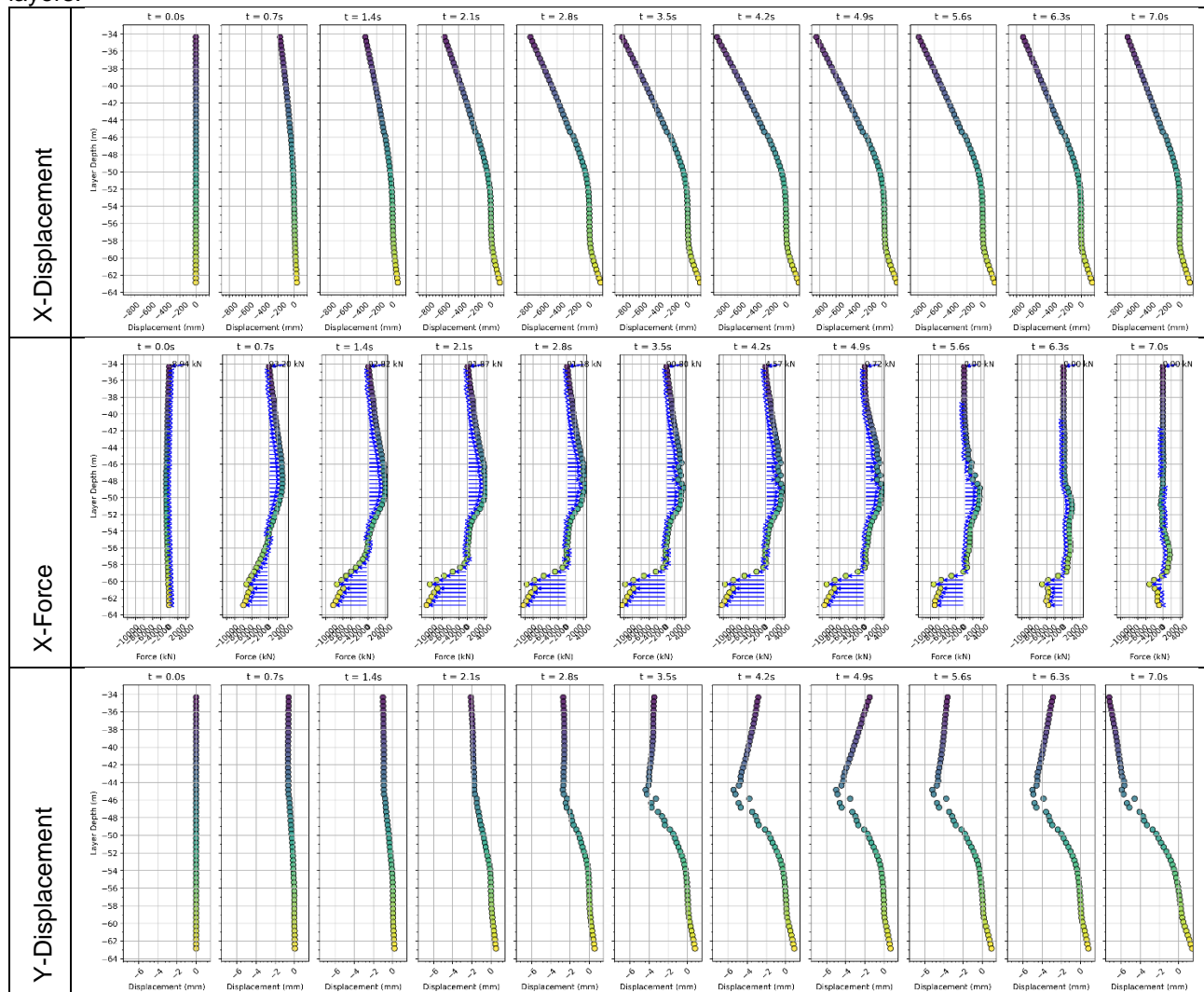
## K. Soil spring results

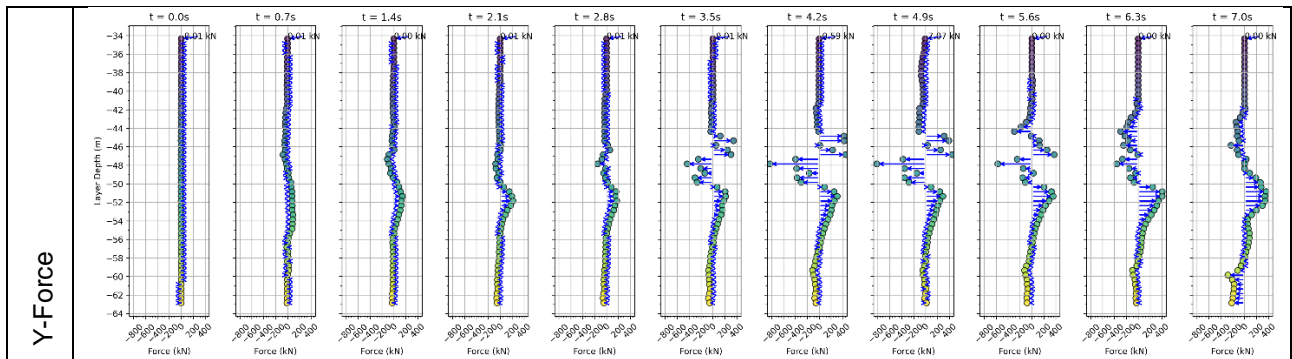
The images in this appendix display the deformations and reaction forces of the non-linear soil spring in the collision direction (X-direction) and perpendicular to the collision direction (Y-direction). These deformations and forces are essential for understanding the structural stability and response of the soil under horizontal turbine impacts. The results are plotted along the soil depth of each layer, providing a profile of how different layers react over time. The results are plotted over 11 time increments, starting from  $t = 0$  seconds up to the end time of the simulation, capturing dynamic changes over these intervals. This temporal resolution allows for an examination of the soil's behavior under impact conditions, highlighting moments of deformation and force application.

## K.1. Chemical tanker

### K.1.1. Mid section 2.06 m/s

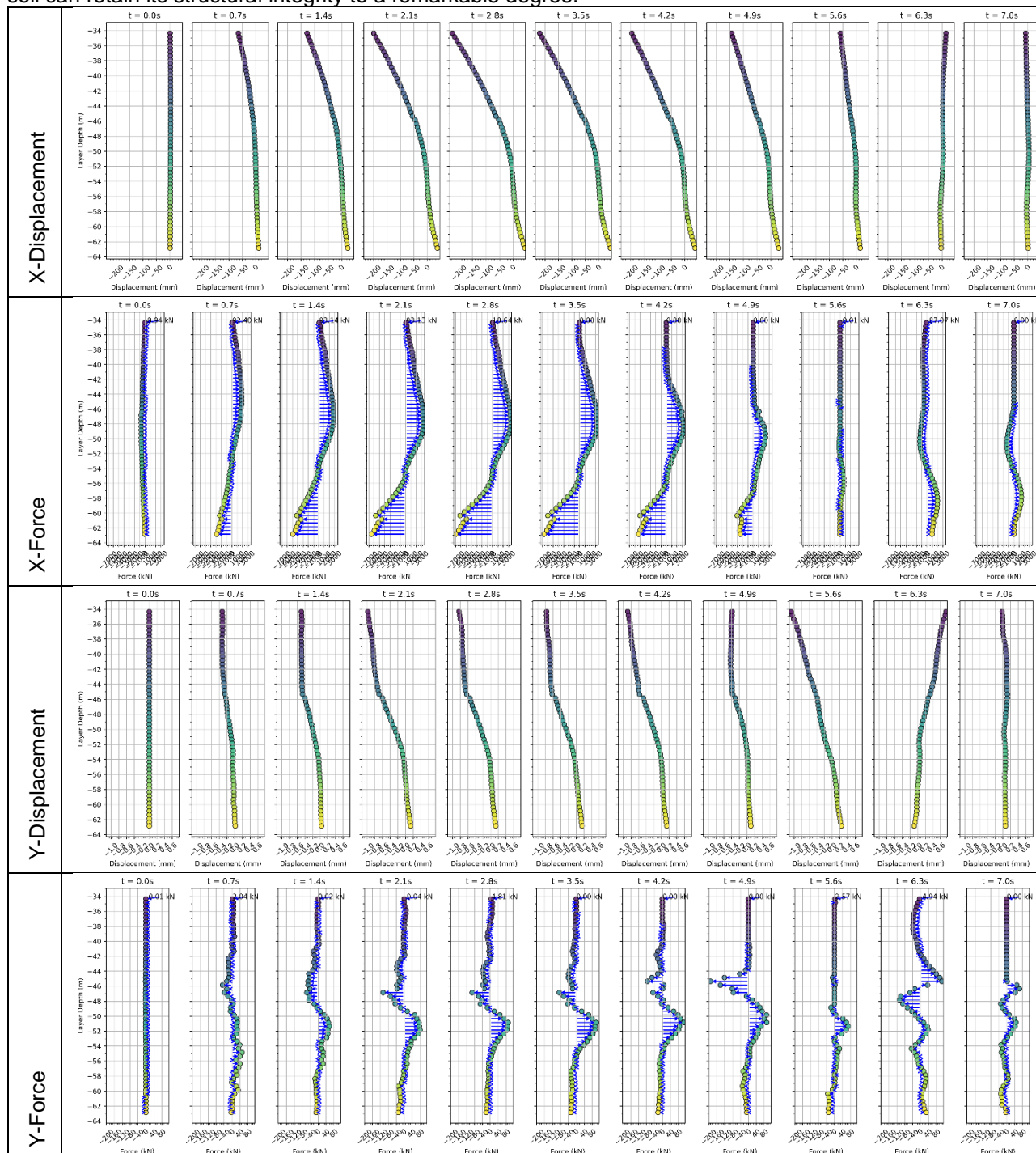
The results below show the top soil layers up to -42 m failing in the collision direction (X-direction). This significant deformation indicates considerable displacement and force application within these upper soil layers.





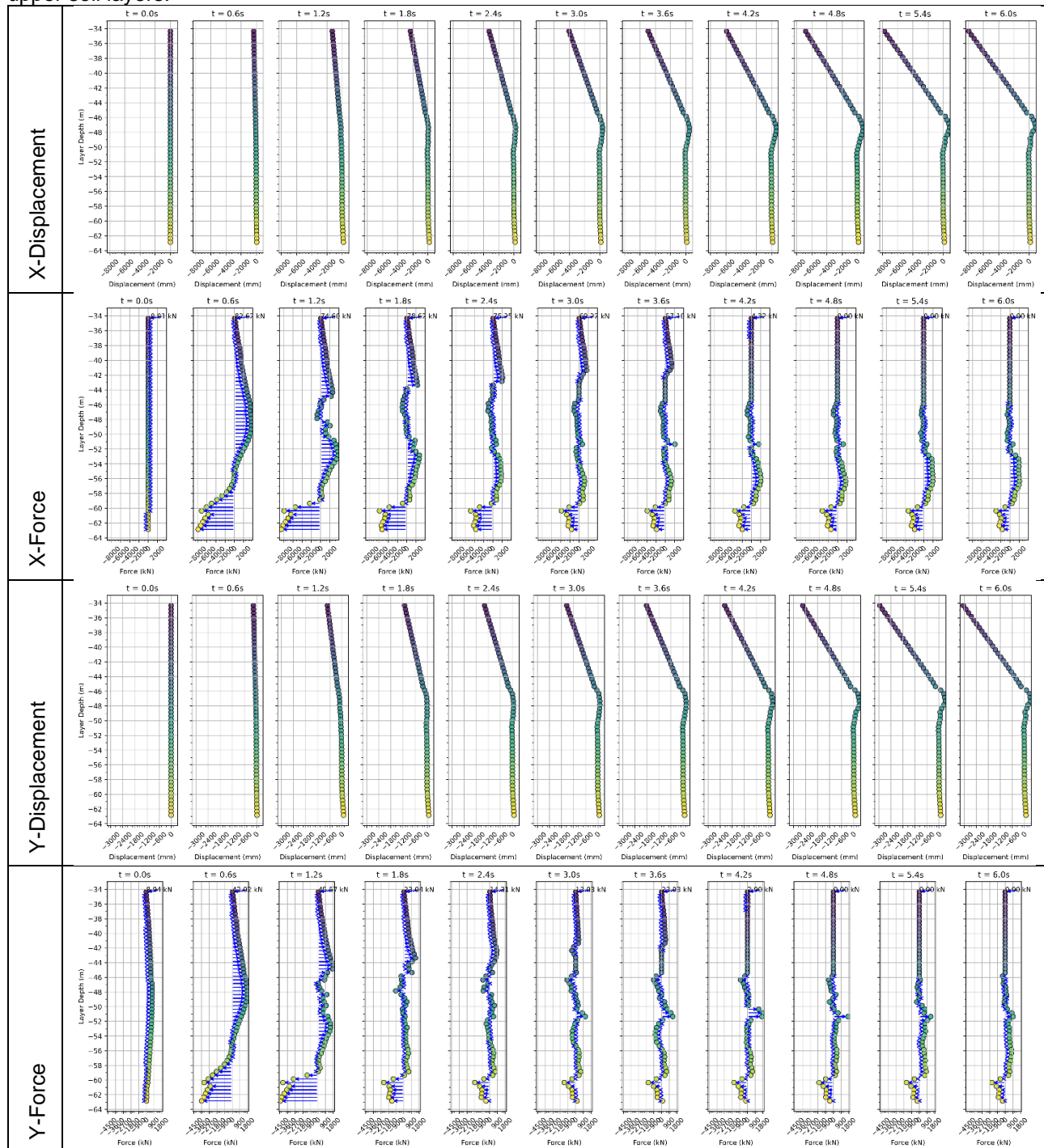
### K.1.2. Mid section 1.03m/s

These results indicate no soil failure. The X-deformation shows a recovery of the deformations almost back to the original position. This resilience in the soil layers suggests that even under significant impact forces, the soil can retain its structural integrity to a remarkable degree.



### K.1.3. Forward section 10.29m/s

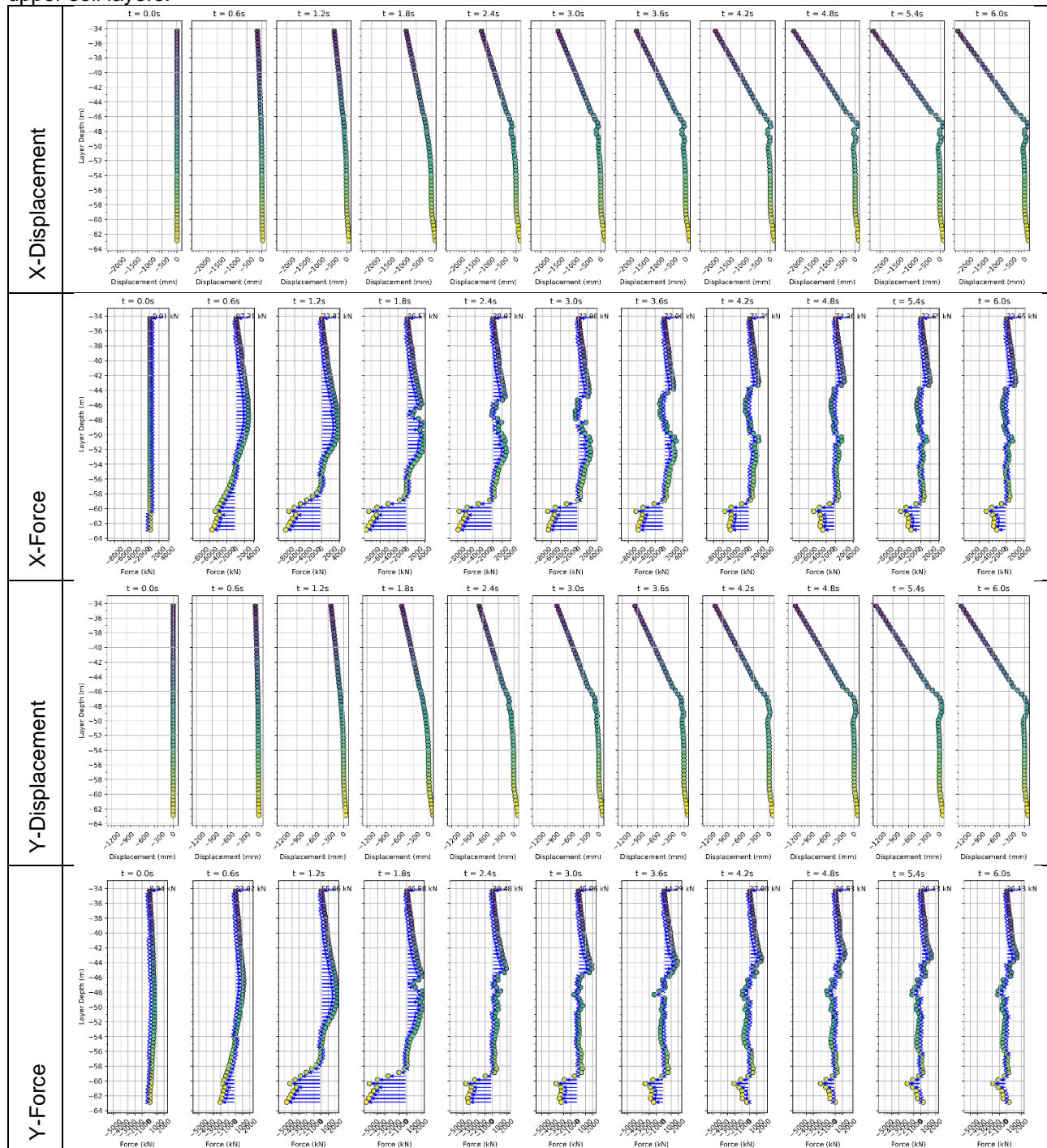
The results below show the top soil layers up to -46 m failing in the collision direction (X-direction and Y-direction). This significant deformation indicates considerable displacement and force application within these upper soil layers.





### K.1.4. Forward section 5.14m/s

The results below show the top soil layers up to -46 m failing in the collision direction (X-direction and Y-direction). This significant deformation indicates considerable displacement and force application within these upper soil layers.

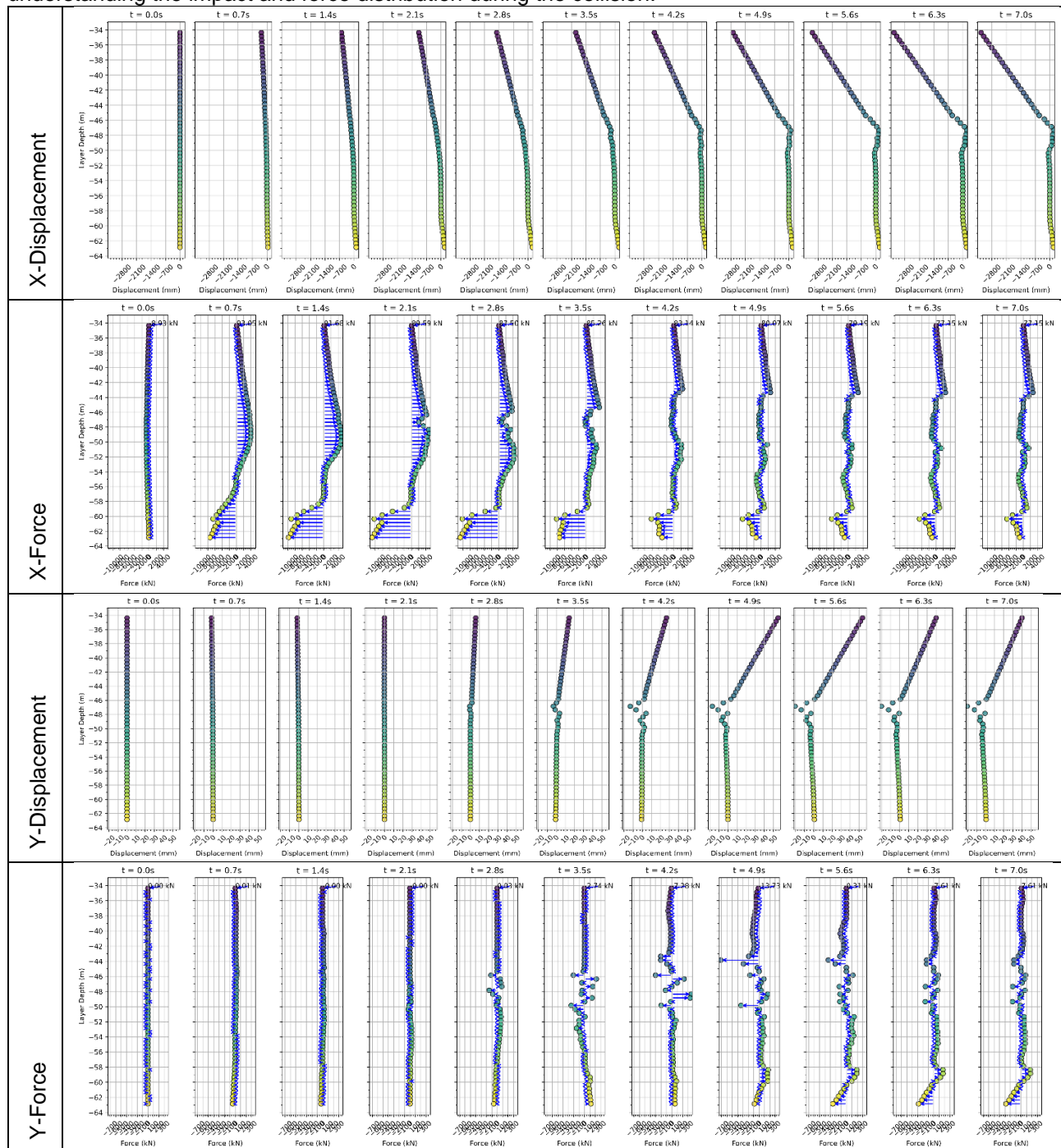




## K.2. Container Ship

### K.2.1. Mid section 2.06 m/s

The results show soil deformations in the X-direction that remain unrecoverable yet retain some resistance, consequently generating a reaction force. The soil's ability to resist despite significant deformation is critical in understanding the impact and force distribution during the collision.

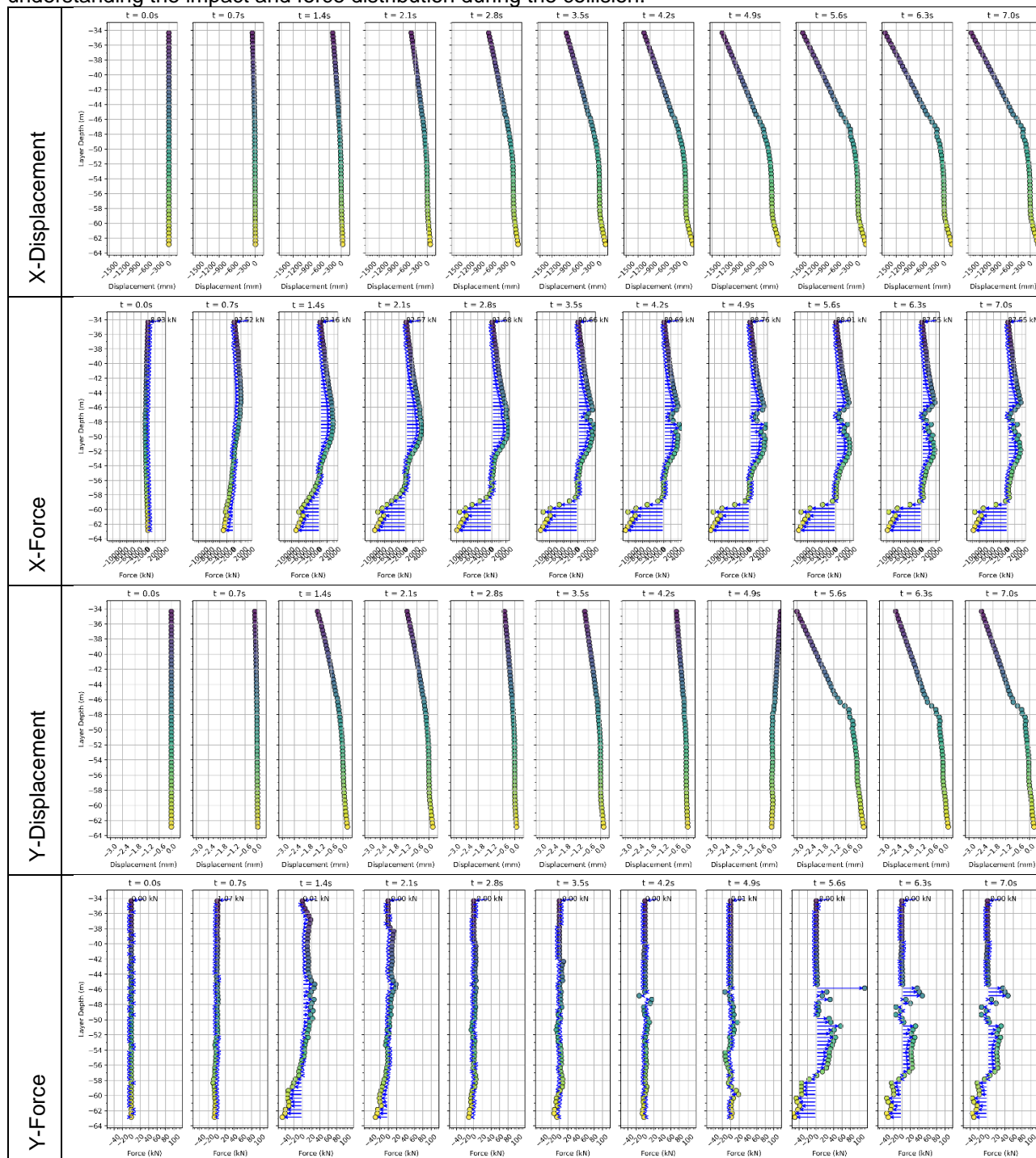






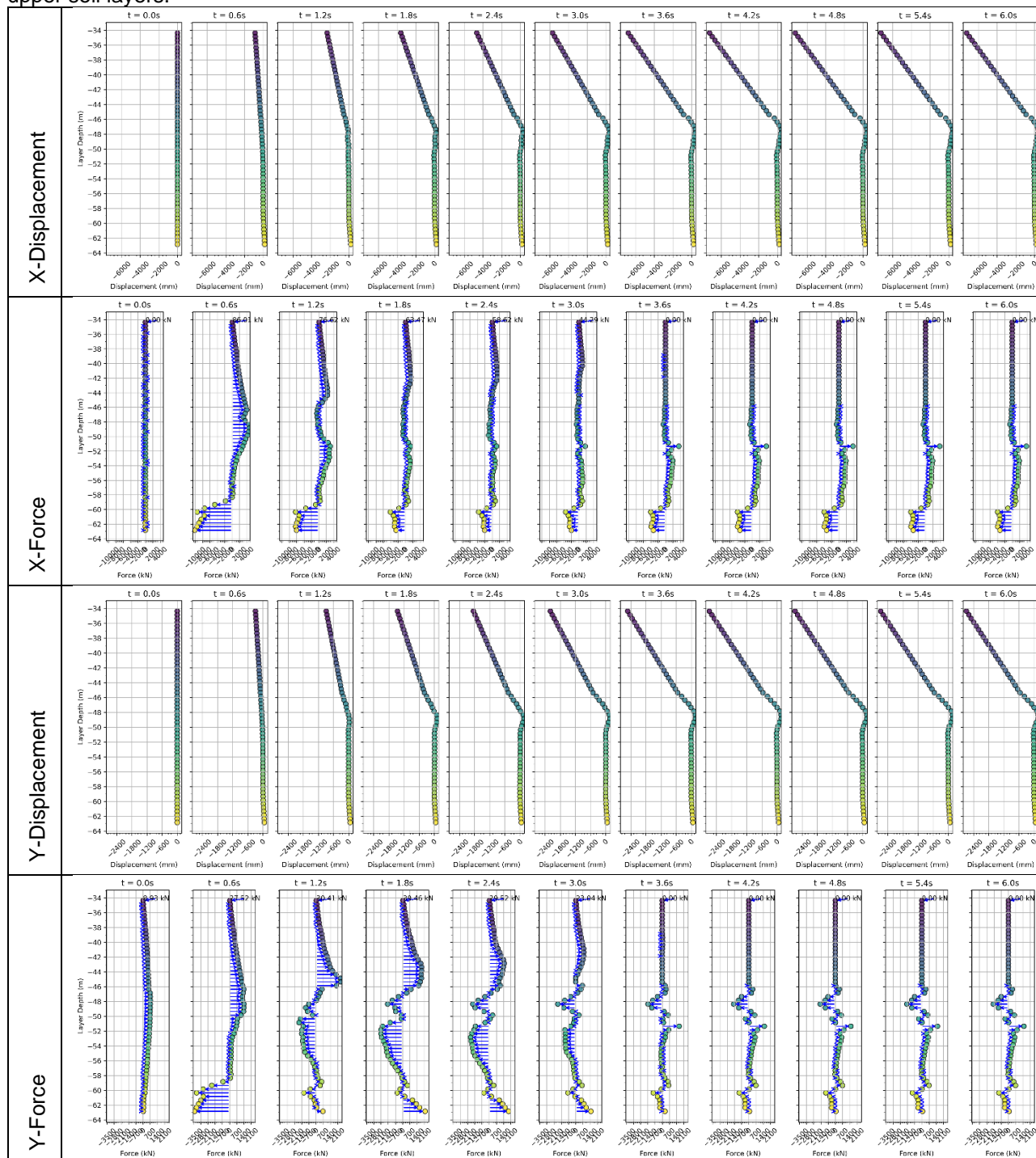
### K.2.2. Mid section 1.03 m/s

The results show soil deformations in the X-direction that remain unrecoverable yet retain some resistance, consequently generating a reaction force. The soil's ability to resist despite significant deformation is critical in understanding the impact and force distribution during the collision.



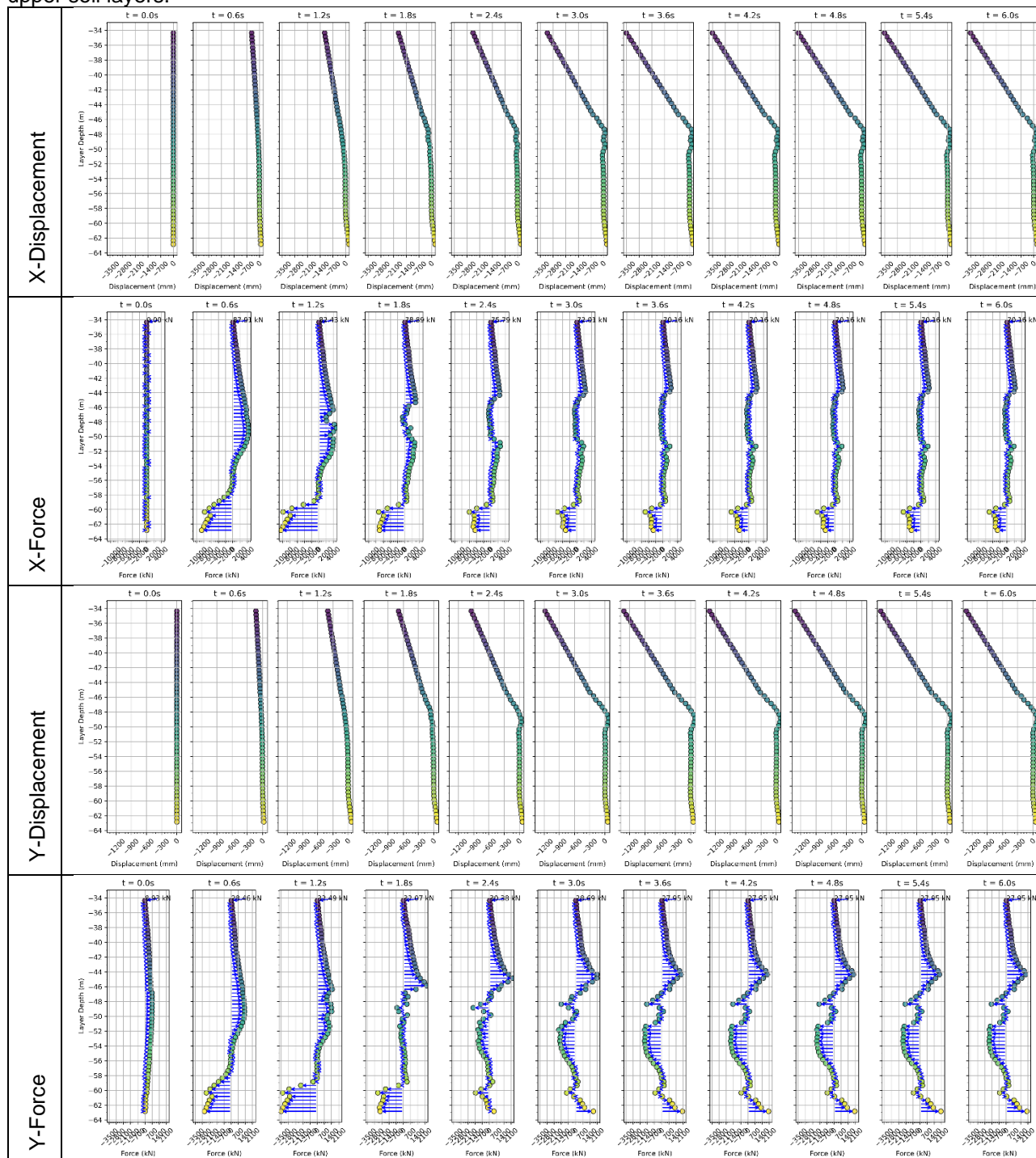
### K.2.3. Forward section 10.29 m/s

The results below show the top soil layers up to -46 m failing in the collision direction (X-direction and Y-direction). This significant deformation indicates considerable displacement and force application within these upper soil layers.



### K.2.4. Forward section 5.14 m/s

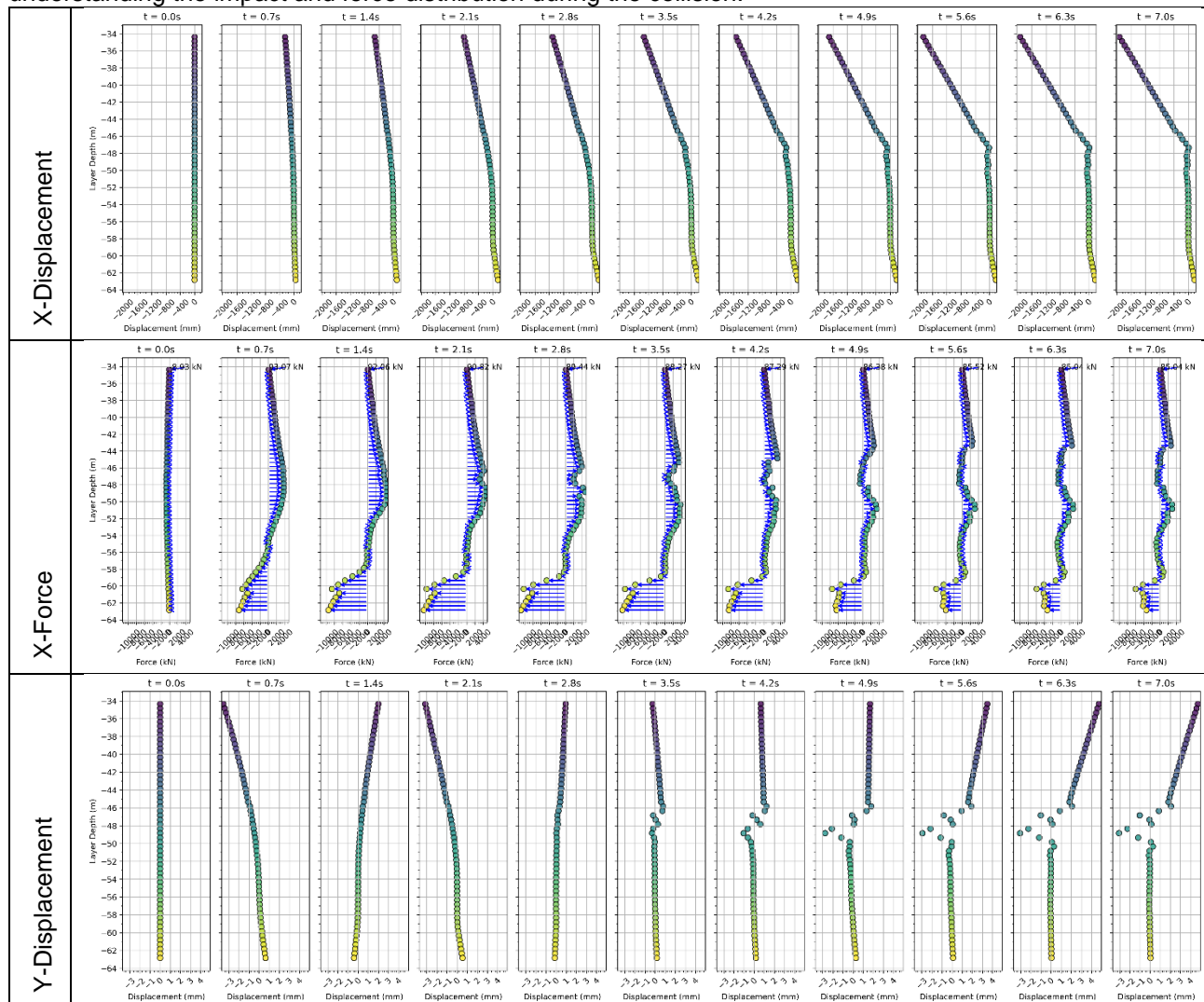
The results below show the top soil layers up to -46 m failing in the collision direction (X-direction and Y-direction). This significant deformation indicates considerable displacement and force application within these upper soil layers.

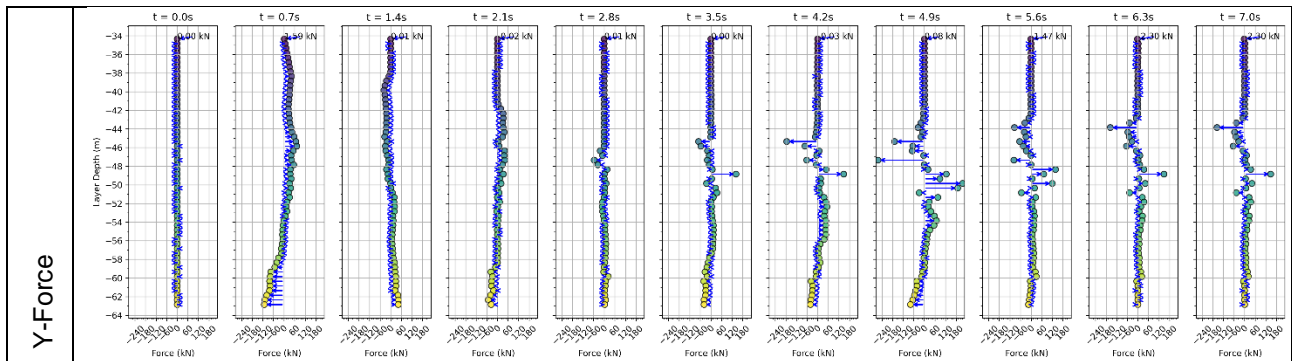


### K.3. Passenger Vessel

#### K.3.1. Mid section 2.06 m/s

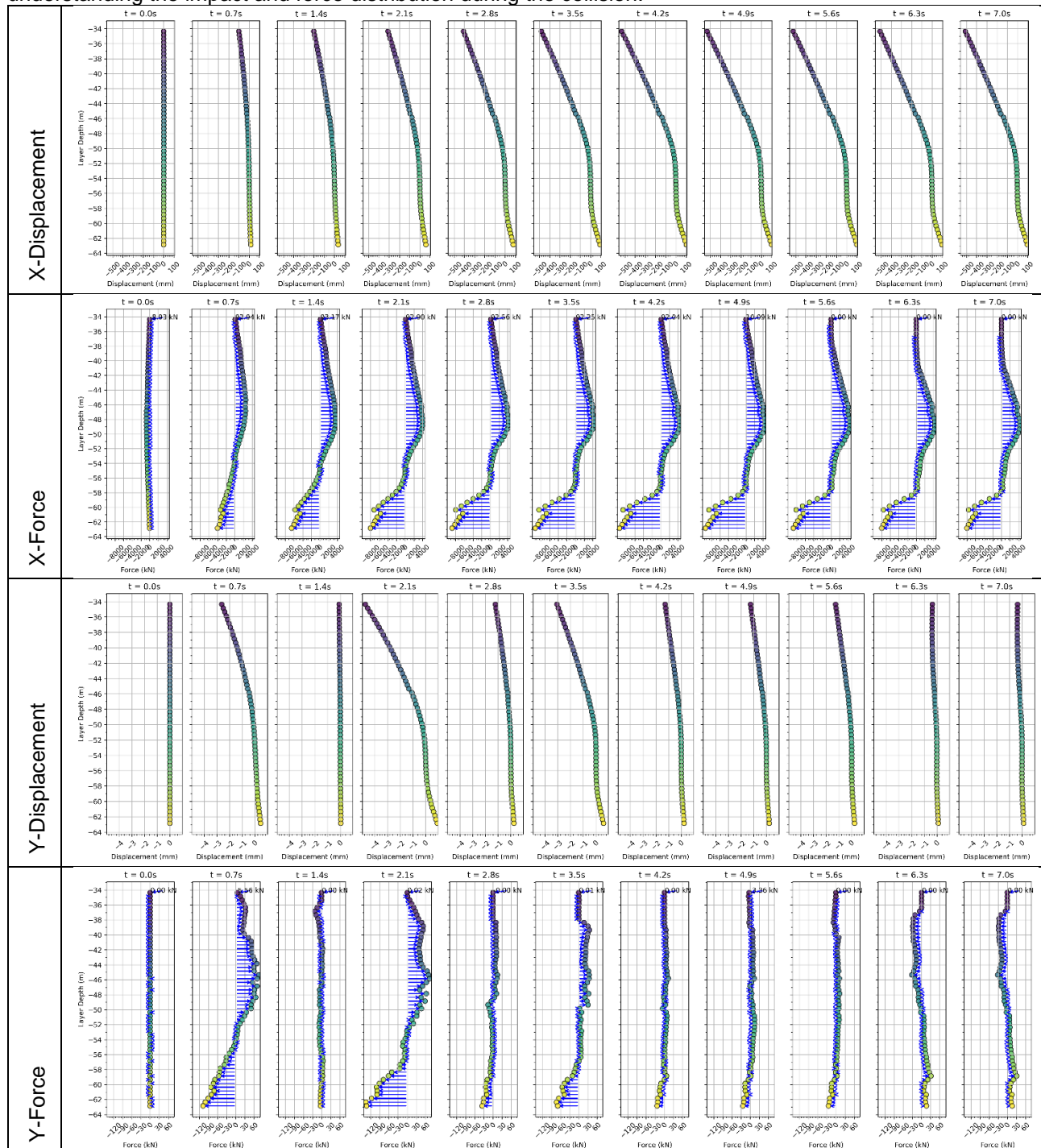
The results show soil deformations in the X-direction that remain unrecoverable yet retain some resistance, consequently generating a reaction force. The soil's ability to resist despite significant deformation is critical in understanding the impact and force distribution during the collision.





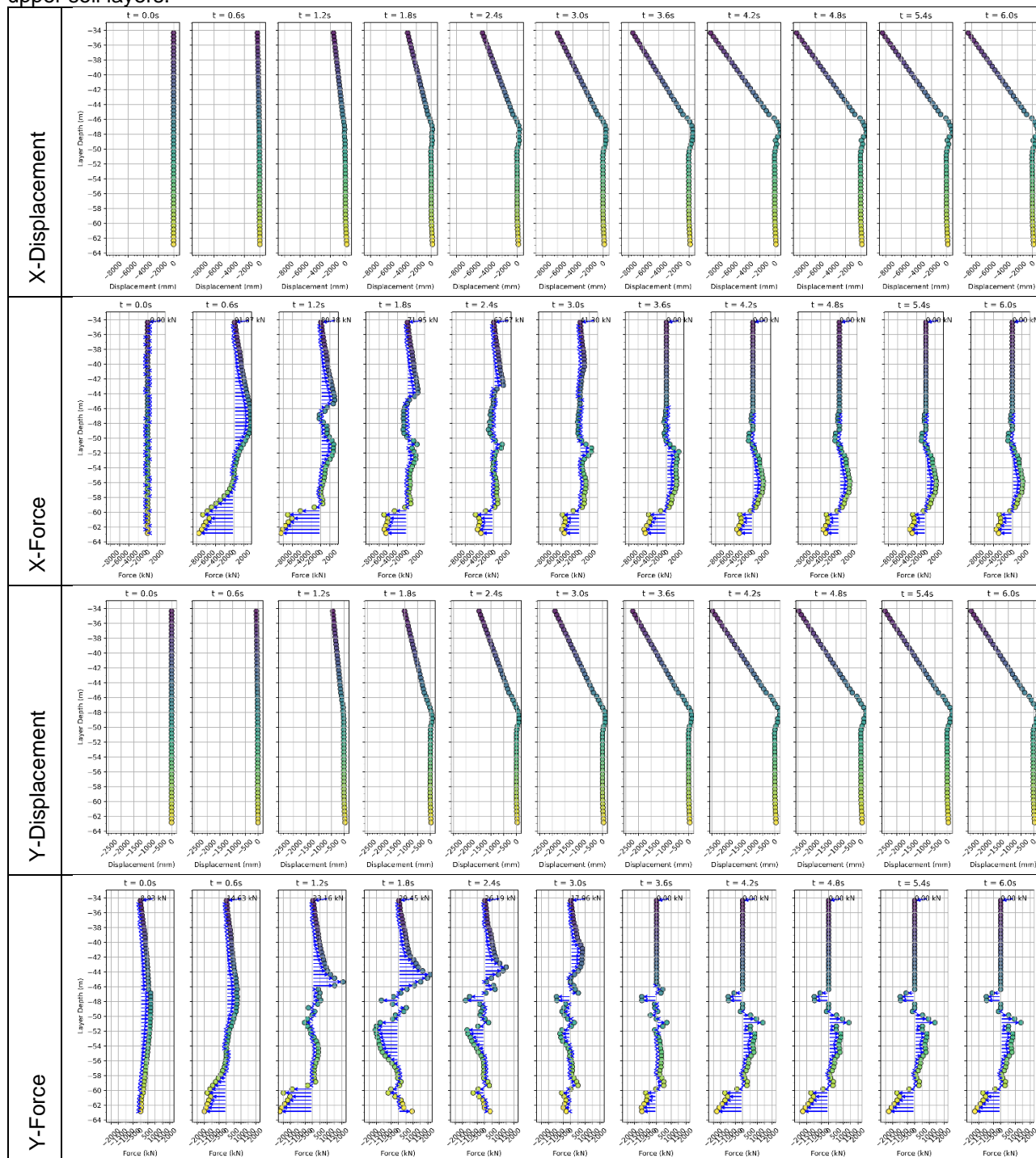
### K.3.2. Mid section 1.03 m/s

The results show soil deformations in the X-direction that remain unrecoverable yet retain some resistance, consequently generating a reaction force. The soil's ability to resist despite significant deformation is critical in understanding the impact and force distribution during the collision.



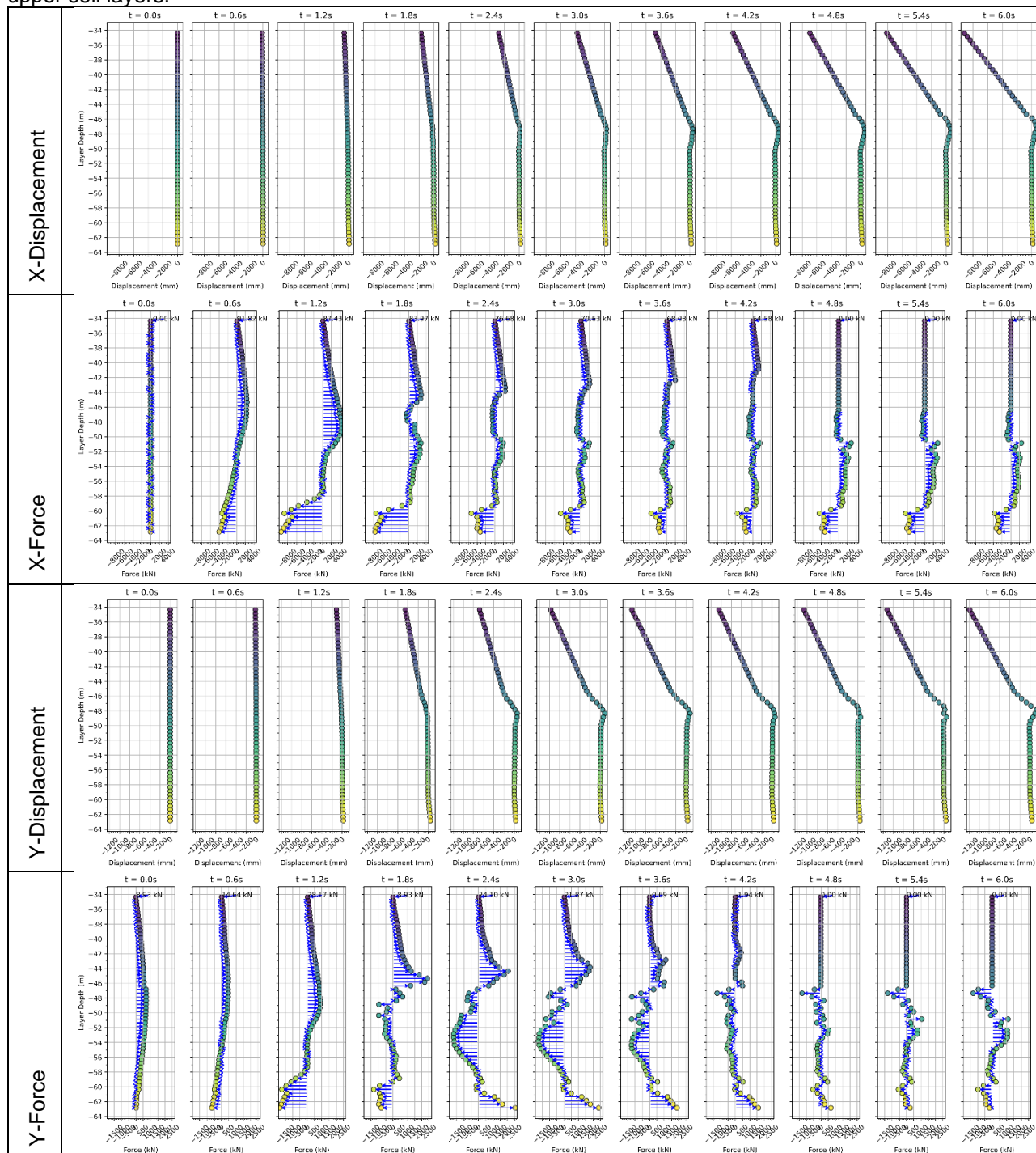
### K.3.3. Forward section 15.43 m/s

The results below show the top soil layers up to -46 m failing in the collision direction (X-direction and Y-direction). This significant deformation indicates considerable displacement and force application within these upper soil layers.



### K.3.4. Forward section 10.29 m/s

The results below show the top soil layers up to -46 m failing in the collision direction (X-direction and Y-direction). This significant deformation indicates considerable displacement and force application within these upper soil layers.







#### **K.4. Conclusion and summary**

The tables presenting the results illustrate the outcomes for the chemical tanker, container ship, and passenger vessel across various sections and velocities. For midsection scenarios, the largest deformations occur in the direction of the collision (X-direction). Due to the symmetrical nature of the collision scenario, the results perpendicular to the collision direction (Y-direction) are minimal. Similarly, for forepart scenarios, the largest deformations are also observed in the direction of the collision (X-direction). Owing to the collision eccentricity, the deformations perpendicular to the collision (Y-direction) amount to approximately 40% of the deformations in the X-direction.

The findings indicate significant displacement and force application in the upper soil layers up to a depth of -46 meters in both the X and Y directions as a result of the collision impact. These deformations are associated with failures in the soil layers, particularly due to monopile buckling, as the initial soil layers exhibit the lowest stiffness according to p-y curves.

The collision impact energy leads to the failure of the initial soil layers, a phenomenon observable in all forepart and midsection simulations. Soil failure progresses in depth during impact, as indicated by reaction forces on the spring becoming zero. However, in certain scenarios, the inertia energy is fully transferred without soil failure, which is evident from the charts where the reaction forces remain on the initial layers.



## L. Declaration validation team (TNO)

) TNO Intern



### Memo

Send to Walter Langedijk (Iv-Infra)  
Copy to Johan Kraus  
Author Lisa Tang  
Subject Review 3D FEM analyses ship-wind turbine collisions

www.tno.nl  
lisa.tang@tno.nl  
+31621368792  
Date  
20 February 2025  
Our reference  
TNO-2025-MEM-100356360

### Introduction

TNO is an independent not-for-profit research organisation. TNO's mission is to create impactful innovations for the sustainable wellbeing and prosperity of society.

The Naval and Offshore Structures (NOS) department, specializes in designing, analysing, and testing an extensive array of mechanical structures for the maritime and offshore industry, as well as defence applications. Our primary focus is ensuring the structural integrity of these constructions under extreme conditions throughout their entire lifecycle.

We combine a strong understanding of materials and structures, expert modelling capabilities, and unique laboratory facilities. Our well-equipped labs for mechanical testing allow practical and theoretical knowledge to go hand in hand, enabling us to solve the most complex problems and validate groundbreaking structural solutions. Examples of our research range from the safe use of alternative fuels on board ships and assessing the structural safety of offshore wind turbines to developing shock and explosion-resistant ship structures. We are actively addressing today's critical challenges: the energy transition and the increasing attention to safety at sea.

Our numerical expertise is mainly focused on non-linear 3D FEM simulations. We have a lot of knowledge about failure- and material models and we validate our models by conducting tests at different scales, ranging from material tests to large scale tests.

### Summary of verification of FEM models and results

Iv-Infra carried out 3D FEM analyses to assess the potential damage from ship-wind turbine collisions at the North Sea. Three ship types were considered: a chemical tanker, a container ship and a passenger vessel. The models and results needed to be verified by an independent institute. TNO (department NOS) was asked by Iv-Infra to execute this verification.

TNO performed a review on the 'Concept Eindrapport (DP4)', which includes the review of the FEM models, the memos on material and soil models, FEM modelling approaches, simulation results, and validation results. Before, intermediate reviews have been performed on drafts. In general, it is concluded that the FEM modelling approach is sufficient for the purpose of this study. Appropriate models and parameters are assumed to ensure accurate and reliable simulation results. Remarks from TNO related to the assumptions and choices made with this FEM modelling approach are adhered to and processed. Therefore, TNO declares to have no objections regarding the presented work in its current form.

L. Tang  
Author

J. Kraus  
Review

S. Alonso Lucas  
Project manager

R.A.C. Dragt  
Research manager  
Naval and Offshore Structures



) TNO Intern

1/1



Waarderweg 40  
2031 BP Haarlem  
The Netherlands

Pettelaarpark 10-15  
5216 PD 's-Hertogenbosch  
The Netherlands

Nevelgaarde 10  
3436 ZZ Nieuwegein  
The Netherlands

**iv-Infra b.v.**  
Trapezium 322  
3364 DL Sliedrecht  
The Netherlands

Trompstraat 36a  
9190 Stekene  
Belgium

Westervoortsedijk 73  
Gebouw CB  
6827 AV Arnhem  
The Netherlands

[www.iv-infra.nl](http://www.iv-infra.nl)  
Telephone +31 88 943 3200  
P.O. Box 135  
3360 AC Sliedrecht  
[officemanagement.infra@iv.nl](mailto:officemanagement.infra@iv.nl)